PHASE 2 INITIAL BOREHOLE DRILLING AND TESTING AT IG BH04/05/06 IGNACE AREA

WP06 Data Report Hydraulic Testing for IG BH04

APM-REP-01332-0280 November 2023

WSP Canada Inc.

NUCLEAR WASTE MANAGEMENT ORGANIZATION SOCIÉTÉ DE GESTION DES DÉCHETS NUCLÉAIRES

Nuclear Waste Management Organization
22 St. Clair Avenue East, 4th Floor
Toronto, Ontario
M4T 2S3
Canada

Tel: 416-934-9814
Web: www.nwmo.ca

REPORT

Phase 2 Initial Borehole Drilling and Testing at IG_BH04/05/06, Ignace Area

WP06 Data Report - Hydraulic Testing for IG_BH04

Submitted to:

Nuclear Waste Management Organization

4th Floor
22 St. Clair Avenue East
Toronto, Ontario M4T 2S3

Submitted by:

WSP Canada Inc.

6925 Century Avenue, Suite #600, Mississauga, Ontario, L5N 7K2, Canada

+1 905 567 4444

20253946 (4060)

NWMO Report: APM-REP-01332-0280

November 3, 2023

Distribution List

e-copy: NWMO

e-copy: WSP Canada Inc.

WP06 DATA REPORT
HYDRAULIC TESTING FOR IG_BH04

CLIENT INFORMATION

Project Name:	Phase 2 Initial Borehole Drilling and Testing at IG_BH04/05/06, Ignace Area		
Project Number:	20253946		
Client PO Number:	2001102		
Document Name:	20253946 (4060) ig_bh04_wp06_report_r2a		
Client:	Nuclear Waste Management Organization (NWMO)		
Address:	22 St. Clair Avenue East, 4th Floor		
City:	Toronto		
Province:	Ontario		
Postal Code:	M4T 2S3		
Client Contact:	Ryan Abrams	Warwick Watt	Natacha Lugo Bizarro
Email:	rabrams@nwmo.ca	wwatt@nwmo.ca	nlugo@nwmo.ca

ISSUE/REVISION INDEX

Issue Code	Revision					Revision Details
	No.	By	Rev'd.	App.	Date	
RR	R0a	STH	MD	JC	02 Sept 2022	Draft released for review and comment
RI	R1a	STH	MD	JC	19 Oct 2022	Final Released for Information
RI	R2a	STH	ML	JC	03 Nov 2023	Final Released for Information

Issue Codes: RR = Released for Review and Comments, RI = Released for Information

SIGNATURES

Prepared by: ____________________

Steve Hales, P.Geo.
Hydrogeologist

Reviewed by: ____________________

Michael Lemon, P.Eng.
Lead Geological Engineer

Approved by: ____________________

Joe Carvalho, Ph.D., P.Eng.
Senior Geotechnical Engineer

Table of Contents

TABLES

FIGURES

APPENDICES

1.0 INTRODUCTION

The Phase 2 Initial Borehole Drilling and Testing at IG_BH04/05/06 project in the Wabigoon Lake Ojibway Nation (WLON) – Ignace area of Ontario, is part of the Phase 2 Geoscientific Preliminary Field Investigations of the Nuclear Waste Management Organization's (NWMO) Adaptive Phased Management (APM) Site Selection Phase.

This project involves testing of deep borehole IG_BH04 and the drilling and testing of deep boreholes IG_BH05 and IG_BH06 in the Revell site within the identified Potential Repository Area (PRA). The work for IG_BH04 comprised of a total of eleven work packages, with involvement from a team led by Golder Associates Ltd. (now WSP Canada Inc.) on behalf of the NWMO in nine of these packages. The IG_BH04 program is described in a Borehole Characterization Plan (BCP) for IG_BH04.

This report describes the methodology, activities and results for Work Package 6 (WP06): Hydraulic Testing for IG_BH04. Borehole IG_BH04 is an inclined hole and all depths referred to in this report are in meters below ground surface along the length of the borehole (mbgs along hole), rather than true vertical depth.

2.0 BACKGROUND INFORMATION

2.1 Geological Setting

The approximately 2.7 billion year old Revell batholith is located in the western part of the Wabigoon Subprovince of the Archean Superior Province. The batholith is roughly elliptical in shape trending northwest, is approximately 40 km in length, 15 km in width, and covers an area of approximately 455 km^2. Based on geophysical modelling, the batholith is approximately 2 km to 3 km thick through the center of the northern portion (SGL, 2015). The batholith is surrounded by supracrustal rocks of the Raleigh Lake (to the north and east) and Bending Lake (to the southwest) greenstone belts (Figure 2).

IG_BH04 is located within an investigation area of approximately 19 km^2 in size, situated in the northern portion of the Revell batholith. Bedrock exposure in the area is generally very good due to minimal overburden, few water bodies, and relatively recent logging activities. Ground elevations generally range from 400 to 450 m above sea level. The ground surface broadly slopes towards the northwest as indicated by the flow direction of the main rivers in the area. Local water courses tend to flow to the southwest towards Mennin Lake (Figure 1).

Four main rock units are identified in the supracrustal rock group: mafic metavolcanic rocks, intermediate to felsic metavolcanic rocks, metasedimentary rocks, and mafic intrusive rocks (Figure 2). Sedimentation within the supracrustal rock assemblage was largely synvolcanic, although sediment deposition in the Bending Lake area may have continued past the volcanic period (Stone, 2009; Stone, 2010a; Stone, 2010b). All supracrustal rocks are affected, to varying degrees, by penetrative brittle-ductile to ductile deformation under greenschist- to amphibolite-facies metamorphic conditions (Blackburn and Hinz, 1996; Stone et al., 1998). In some locations, primary features, such as pillow basalt or bedding in sedimentary rocks are preserved, in other locations, primary relationships are completely masked by penetrative deformation. Uranium-lead (U-Pb) geochronological analysis of the supracrustal rocks produced ages that range between 2734.6 +/-1.1 Ma and 2725 +/-5 Ma (Stone et al. 2010).

Three main suites of plutonic rock are recognized in the Revell batholith, including, from oldest to youngest: a Biotite Tonalite to Granodiorite suite, a Hornblende Tonalite to Granodiorite suite, and a Biotite Granite to Granodiorite suite (Figure 2). Plutonic rocks of the Biotite Tonalite to Granodiorite suite occur along the southwestern and northeastern margins of the Revell batholith. The principal type of rock within this suite is a white to grey, medium-grained, variably massive to foliated or weakly gneissic, biotite tonalite to granodiorite. One sample of foliated and medium-grained biotite tonalite produced a U-Pb age of 2734.2+/-0.8 Ma (Stone et al. 2010). The Hornblende Tonalite to Granodiorite suite occurs in two irregularly-shaped zones surrounding the central core of the Revell batholith. Rocks of the Hornblende Tonalite to Granodiorite suite range compositionally from tonalite through granodiorite to granite and also include significant proportions of quartz diorite and quartz monzodiorite. One sample of coarse-grained grey mesocratic hornblende tonalite produced a U-Pb age of 2732.3+/-0.8 Ma (Stone et al. 2010). Rocks of the Biotite Granite to Granodiorite suite underlie most of the northern, central and southern portions of the Revell batholith. Rocks of this suite are typically coarse-grained, massive to weakly foliated, and white to pink in colour. The Biotite Granite to Granodiorite suite ranges compositionally from granite through granodiorite to tonalite. A distinct potassium (K)-Feldspar Megacrystic Granite phase of the Biotite Granite to Granodiorite suite occurs as an oval-shaped body in the central portion of the Revell batholith (Figure 2). One sample of coarse-grained, pink, massive K-feldspar megacrystic biotite granite produced a U-Pb age of 2694.0+/-0.9 Ma (Stone et al. 2010).

The bedrock surrounding IG_BH04 is composed mainly of massive to weakly foliated felsic intrusive rocks that vary in composition between granodiorite and tonalite, and together form a relatively homogeneous intrusive complex. Bedrock identified as tonalite transitions gradationally into granodiorite and no distinct contact relationships between these two rock types are typically observed (SRK and Golder, 2015; Golder and PGW, 2017). Massive to weakly foliated granite is identified at the ground surface to the northwest of the feldspar-megacrystic granite. The granite is observed to intrude into the granodiorite-tonalite bedrock, indicating it is distinct from, and younger than, the intrusive complex (Golder and PGW 2017).

West-northwest trending mafic dykes interpreted from aeromagnetic data extend across the northern portion of the Revell batholith and into the surrounding greenstone belts. One mafic dyke occurrence, located to the northwest of IG_BH01, is approximately 15-20 m wide (Figure 2). All of these mafic dykes have a similar character and are interpreted to be part of the Wabigoon dyke swarm. One sample from the same Wabigoon swarm produced a U-Pb age of 1887+/-13 Ma (Stone et al., 2010), indicating that these mafic dykes are Proterozoic in age. It is assumed based on surface measurements that these mafic dykes are sub-vertical (Golder and PGW 2017).

Long, narrow valleys are located along the western and southern limits of the investigation area (Figure 1). These local valleys host creeks and small lakes that drain to the southwest and may represent the surface expression of structural features that extend into the bedrock. A broad valley is located along the eastern limits of the investigation area and hosts a more continuous, un-named water body that flows to the south. The linear and segmented nature of this waterbody’s shorelines may also represent the surface expression of structural features that extend into the bedrock.

Regional observations from mapping have indicated that structural features are widely spaced (typical 30 to 500 cm spacing range) and dominantly comprised of sub-vertical joints with two dominant orientations, northeast and northwest trending (Golder and PGW 2017). Interpreted bedrock lineaments generally follow these same dominant orientations in the northern portion of the Revell batholith (Figure 2; DesRoches et al., 2018). Minor sub-horizontal joints have been observed with minimal alteration, suggesting they are younger and perhaps related to glacial unloading. One mapped regional-scale fault, the Washeibemaga Lake fault, trends east and is located to the west of the Revell batholith (Figure 2). Ductile lineaments, also shown on Figure 2, follow the trend of foliation mapped in the surrounding greenstone belts. Additional details of the lithological units and structures found at surface within the investigation area are reported in Golder and PGW (2017).

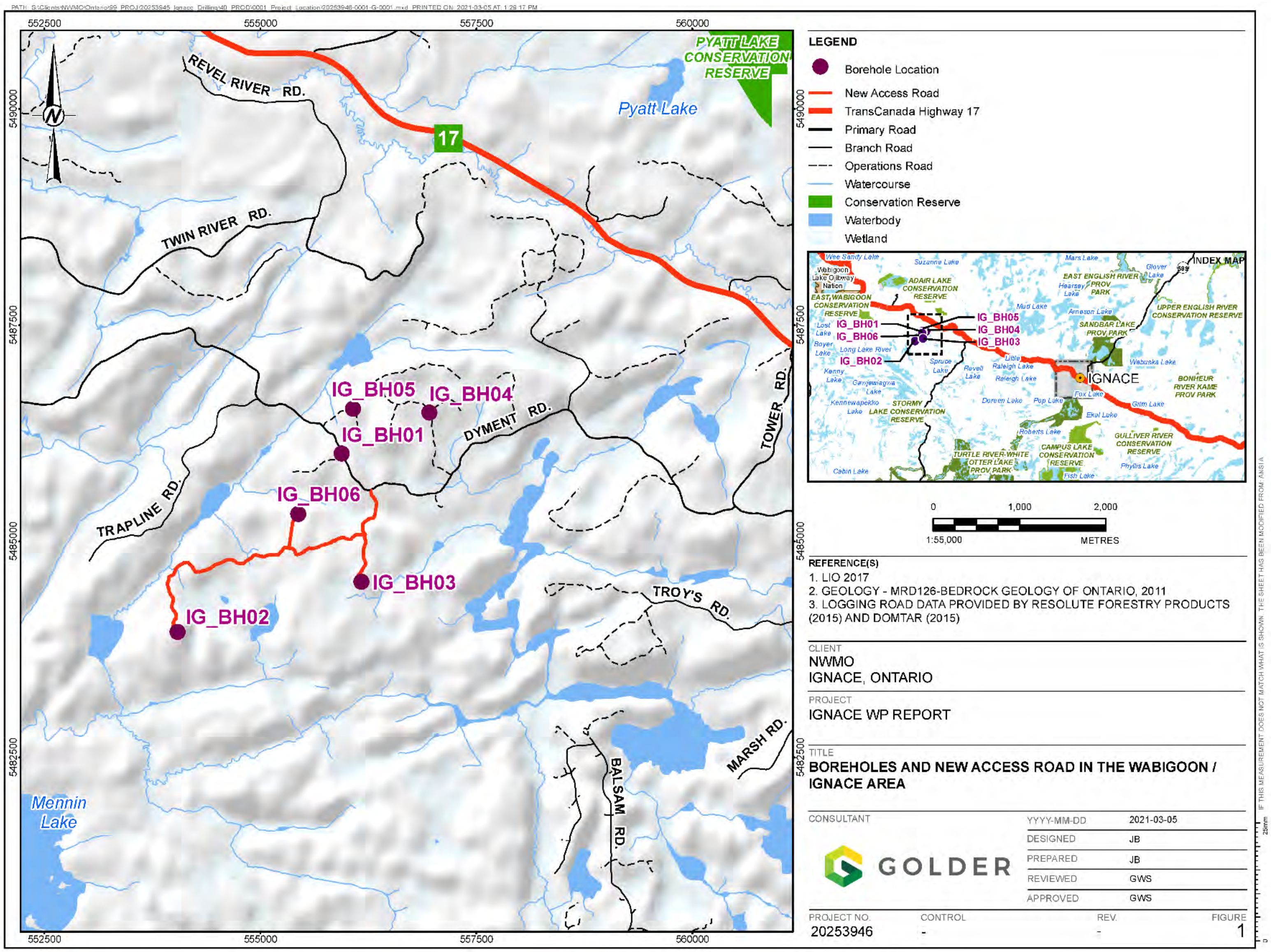

Figure 1: Location of IG_BH04 in relation to the Ignace Area

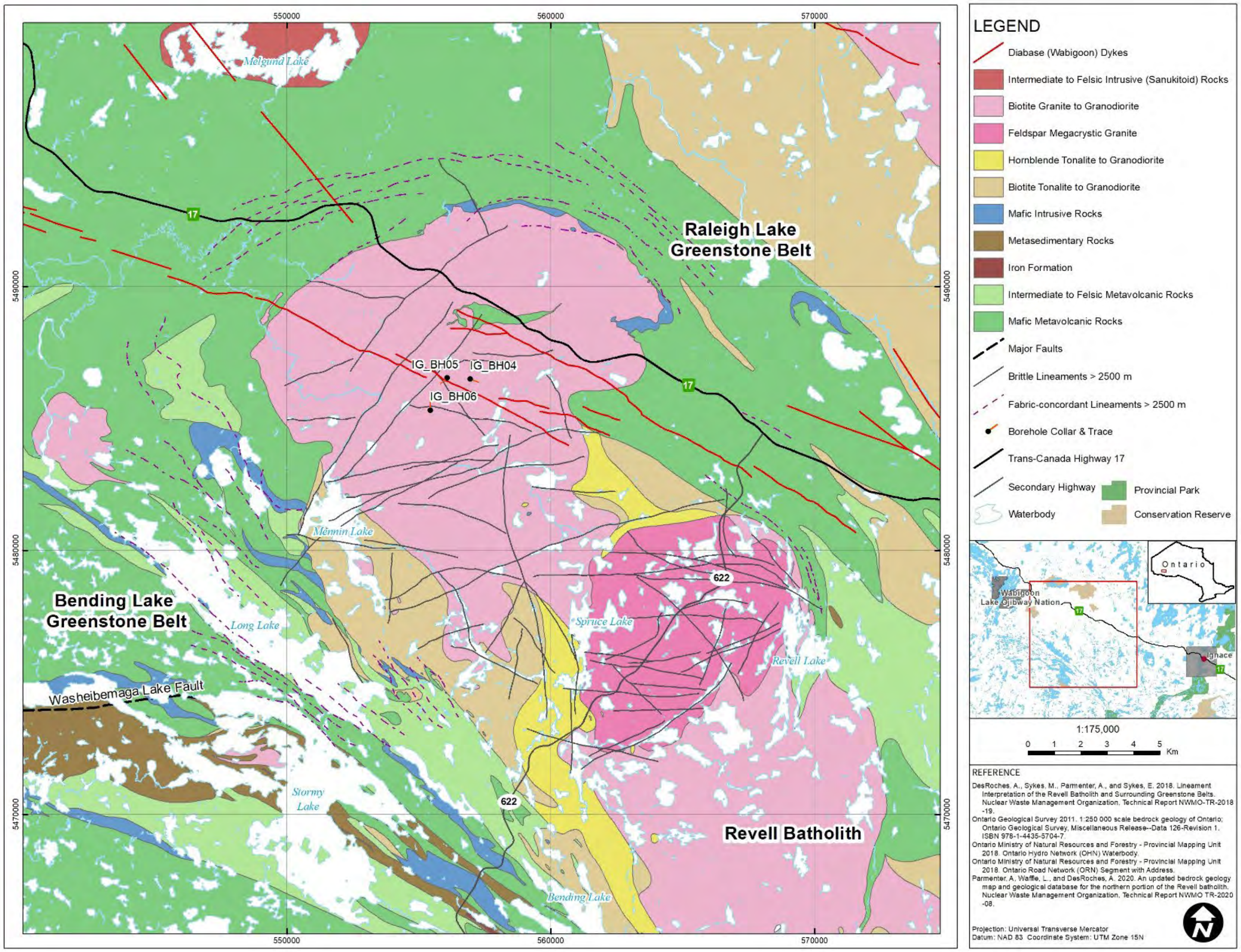

Figure 2: Geological Setting and Location of Boreholes IG_BH04, IG_BH05, and IG_BH06 in the Northern Portion of the Revell Batholith

2.2 Purpose

The purpose of WP06 is to estimate the hydraulic properties of the crystalline rock units at selected depths in the borehole IG_BH04. The borehole was drilled in 96 mm (HQ) diameter at an inclination of 70° from horizontal and an azimuth of 110° to a total depth of 1000.36 m along hole. Additional borehole details are presented in the report WP02 Data Report – Borehole Drilling and Coring for IG_BH04 (Golder, 2021a). Testing occurred after the completion of drilling and logging. Selection of test intervals considered potential water conductive zones based on review of the earlier stages of work that included the following:

- WP02 – Borehole Drilling and Coring;
- WP03 – Geological and Geotechnical Core Logging, Photography, and Sampling;
- WP05 – Geophysical Logging and Interpretation; and
- WP07 – Opportunistic Groundwater Sampling.

The scientific objective is the collection of high quality and reliable test data that will support the estimation of high-confidence hydraulic properties including:

- Hydraulic conductivity (transmissivity / thickness);
- Inferred hydraulic pressure in the rock;
- Test zone compressibility, including the rock within the isolated interval, water within the test zone and the test tool;
- Borehole skin factor; and
- Specific storage (storativity / thickness).

The procedures for the collection, analyses and reporting of the test data were developed by Golder and reviewed by the NWMO. These procedures for data collection are summarized in the following sections.

For the purpose of test analysis, the static formation pressure was estimated by extrapolation of the test interval pressure response.

2.3 Roles and Responsibilities

Testing was carried out by a team of testing specialists from Golder. Drill rig operation support was provided by Rodren Drilling Ltd., based in Winnipeg, Manitoba. Testing was carried out on a 24-hour, 7 days per week basis. Day shifts ran from 7 am to 7 pm, and night shifts from 7 pm to 7 am. A driller and helper were on site for each day and night shift, and a drilling foreman was typically present during the day shifts, or as required. Work was performed under direction and review from Golder’s WP06 lead. Golder’s WP06 lead communicated with the NWMO’s WP06 lead regarding the development of the test plan and decisions during field testing based on preliminary test results.

3.0 TESTING EQUIPMENT

The equipment used for hydrogeological testing of borehole IG_BH04 consisted of a straddle packer tool with a 20 m long test interval, integrated downhole shut-in valve (DHSIV) for isolating the test interval from the test tubing to reduce wellbore storage, and real-time multi-zone pressure and temperature monitoring. Real-time pressure from test tubing, and above, between and below the packers was monitored at surface using DataCan pressure transducers mounted in a gauge carrier directly above the DHSIV. A separate pressure transducer with internal memory, manufactured by Pioneer Petrotech Services (PPS), was positioned within the interval to collect data for test analyses directly from the test interval. A list of equipment used downhole is provided in Table 1, and a list of equipment used at surface is provided in Table 2. Photos of the testing equipment are provided in Appendix A. Pressure transducers were calibrated following manufacturers' instructions, and calibration certificates are provided in Appendix B.

Table 1: List of Downhole Equipment

Item Name	Manufacturer and Model	Item Description
Packers (2x)	Baski MD-2.7, Medium Duty, Sliding-Head Type	Inflatable packers for isolating test zone Uninflated OD = 69 mm Largest recommended hole size = 127 mm Mandrel pipe size = 25 mm Uninflated element length = 1016 mm Max differential pressure rating in 102 mm hole = 5.5 MPa
Test Tubing above tool	Boart Longyear	BQ threaded pipe with O-ring sealed joints OD = 55.7 mm ID = 46.1 mm Length = 3 m
Test Tubing within interval	Boart Longyear	ARQTK threaded perforated pipe between packers OD = 44.7 mm ID = 37.5 mm Length = 1.5 m
Multi-zone pressure transducers (4x)	DataCan Multi-Gauge Piezo Bottom Pressure Gauge, Model 108931	Absolute pressure monitoring in test interval between packers, bottom zone below lower packer, annulus above upper packer and test tubing above DHSIV. Max operating pressure rating = 41.37 MPa Accuracy: Pressure = 0.022% FS Temperature = 0.25°C Resolution: Pressure = 0.0003% FS Temperature = 0.005°C
Multi-zone pressure transducer protective casing	DataCan	Protective metal gauge carrier for Multi-Gauge real-time pressure transducers, installed in-line above the DHSIV
Interval pressure transducer	PPS25 pressure transducer	Absolute pressure monitoring in test interval for data analyses Max operating pressure rating= 41.37 MPa Accuracy: Pressure = 0.03% FS Temperature = 0.5°C Resolution: Pressure = 0.0003% FS Temperature = 0.01°C

Item Name	Manufacturer and Model	Item Description
Swabbing Tool	BQ size, rubber flexible cups on articulated shaft with an attachment for wireline	Used for the removal of water from test tubing for slug/pulse tests Cup diameter = 44.7 mm (unexpanded)
Downhole Shut-in Valve (DHSIV)	IPI Downhole Shut-in Valve (DSHIV)	Hydraulically actuated single line for isolation of the test interval from the test tubing OD = 70mm Zero-volume displacement 100% sealing ball valve Pressure rating up to 68.9 MPa
In-line adapter (ILA) (4x)	Baski	Steel adapter to feed pressure lines from outside of the packer string through the packer OD = 69 mm
Centralizers (6x)	Baski	Positioned above the DataCan gauge carrier, above and below each packer and within the test interval OD = 82.6 mm Length = 300 mm
Flatpack and Spool	Baski	Santoprene encased integrated pressure and electric cable line system 0.0343 m x 0.00104 m x 1400 m 1x 6.35 mm OD x 0.71 mm wall tubing encapsulated single conductor cable 3x 6.35 mm OD x 0.89 mm wall Duplex 2205 stainless steel Motorized metal spool 2 m diameter, 1 m wide 1800 kg weight
Pressure transducer for wellbore storage estimation	Solinst 3001 LT Barologger, M1.5	Lowered inside test tubing during the opening of the DHSIV to measure the volume displacement to estimate the test zone compressibility and wellbore storage Max operating pressure rating= 14.71 kPa Accuracy: Pressure = 0.05 kPa Temperature = 0.05°C Resolution: Pressure = 0.002% FS Temperature = 0.003°C

Table 2: List of Surface Equipment

Item Name	Manufacturer and Model	Item Description
Inflation Pressure Vessel	Misc.	20-liter capacity, 8.0 MPa pressure rating. Filled with water and pressurized using nitrogen to inflate packers.
Packer Inflation Control Manifold and Hoses	Misc.	A manifold to control nitrogen flow for packer inflation,

Item Name	Manufacturer and Model	Item Description
		8.0 MPa pressure rating
Nitrogen Pressure Regulator	Misc.	High pressure regulator for controlling pressure outflow from nitrogen cylinder used for packer inflation.
Nitrogen Cylinders	Praxair Canada Inc., Dryden, Ontario	Compressed nitrogen gas cylinder for pressurizing the packer inflation pressure vessel.
DHSIV Activation Pump	CVS Controls Ltd.	Manual high-pressure pump for DHSIV operation. Maximum Injection Pressure = 20.68 MPa
Barometric Pressure Transducer	Solinst 3001 LT Barologger, M1.5	Barometric pressure monitoring for correcting absolute pressure downhole gauges Max operating pressure rating= 14.71 kPa Accuracy: Pressure = 0.05 kPa Temperature = 0.05°C Resolution: Pressure = 0.002% FS Temperature = 0.003°C
Master Pressure Gauge, Packer Pressure Monitoring	Omega DPG4000-2K	Digital pressure gauge for field calibration check of pressure transducers and monitoring of packer inflation pressure Max pressure = 13.79 MPa Accuracy = ±0.05%
Data Acquisition System	DataCan Surface Readout Box, Model 105421	Data logger with real-time communication, collection and storing of downhole and surface sensor data with 20M sample capacity, USB set-up/ download

3.1 Packer Inflation

Water was used for packer inflation instead of gas to reduce the required packer inflation pressure, and the compressibility of the packers and the inflation lines which contribute to the test interval compressibility. A surface pressure vessel filled with water was pressurized using compressed nitrogen to achieve the desired packer inflation pressure.

Packer inflation pressure is calculated following the manufacturer's recommendations and recorded in the Field Data tab of the Data Quality Confirmation workbook. The inflation pressure at surface was set at 2.05 MPa, which is the summation of several criteria:

a) *Hydrostatic Pressure* – Pressure exerted on the external surface of the packers. When inflating packers with water, the external pressure on the packer is balanced by the equivalent internal hydrostatic pressure in the inflation line resulting in an assumed net pressure of zero.

b) *Packer stretch (or packer seating pressure)* – Pressure required to expand and seat the packer to the borehole wall. This pressure is dependent on the borehole diameter and provided in the manufacturer's user manual (equals 0.7 MPa for HQ borehole).

c) *Test Differential Pressure (or packer sealing pressure)* – Packer pressure required to prevent leakage across the packer when maximum differential pressure is exerted at the test interval during the test execution. A maximum test pressure of 1.0 MPa was applied for the inflation pressure calculation as the maximum test differential pressure was limited to 0.83 MPa due to the maximum lift capacity of the pump; however, the target minimum differential pressure as defined in the Test Plan was 100 kPa.

d) *Factor of Safety* – Extra applied pressure to ensure the required packer inflation pressure is maintained through the entire test. The factor of safety accounts for any slow leakage in the system, temperature variations at surface, and fluid density variation between the water within the inflation system and the borehole fluid. A factor of safety of 0.35 MPa was applied for all tests.

The required packer inflation pressure is first set at the nitrogen cylinder using the pressure regulator. This pressure is then transferred to the packer inflation manifold, where a more precise adjustment of the required inflation pressure can be achieved using an Omega analog pressure gauge. The pressure from the packer inflation manifold is then diverted to the pressure vessel where it pressurizes the water within, forcing it into the packer inflation line in the flatpack to inflate the packers. The two packers were inflated using two separate inflation lines allowing for individual inflating and deflating of the packers.

3.2 Data Acquisition

In order to collect accurate pressure and temperature data, the following instruments were used:

- **Real-time Multi-zone Downhole Pressure Measurements -** Downhole pressure is monitored in four isolated zones using transducers manufactured by DataCan, Model Part Number 108931. Pressure readings are communicated in real-time to the surface via dedicated cable in the flatpack. Data are recorded with a DataCan surface readout box (Figure 3) connected to a field laptop via USB. The real-time pressure readings are used to monitor the test progress, verify packer seal of the test zone and allow for estimation of preliminary transmissivity values during testing. The DataCan transducers are housed within a protective carrier mounted above the DHSIV as shown in Figure 3 and Figure 4. The zones monitored during testing include:
  - Test interval between the packers;
  - Open borehole below the lower packer to confirm adequate seal at the bottom of the test interval;
  - Annular space above the upper packer between the test tubing and borehole wall to confirm adequate seal at the top of the test interval; and
  - Test tubing above the DHSIV to measure the magnitude of the induced slug or pulse.
- **Test Interval Pressure Data (for analyses)** - Pressure and temperature data were recorded directly in the test interval with a single pressure transducer manufactured by Pioneer Petrotech Services Inc. (PPS), Model PPS25. The PPS transducer is self-contained with integrated internal memory and battery. The transducer was positioned inside a perforated pipe below the upper packer and the recorded pressures from this transducer were used for the final test analyses since it provided a complete borehole pressure history from the start of testing.
- **Packer Pressure -** Packer pressures were monitored at surface with the Omega DPG4000-2K pressure gauge connected to the packer inflation vessel. Packer pressures were monitored during the testing to ensure no leakage in the packer inflation system occurred. Packer pressures at the start and end of each test were

recorded in the Field Data tab of the Data Quality Confirmation (DQC) workbook included in the electronic deliverable under separate cover.

- **Barometric Pressure** – Barometric pressure was recorded at the drill rig during testing using a Solinst 3001 LT Barologger, M1.5. Barometric pressure and air temperature were recorded every minute for barometric pressure correction of the downhole absolute pressure transducers. Barometric pressure was used to compensate the downhole transducer pressures by subtracting the barometric pressure from the downhole transducer absolute pressure reading to provide gauge pressure at depth. The range of barometric pressure recorded over the duration of each test was included in the Field Data tab of the DQC workbook.

All electronic instruments were calibrated following the manufacturer's instructions prior to arrival on site. Calibration checks are recorded in the Tool Assembly tab of the DQC workbook. Calibration certificates are provided in Appendix B.

Figure 3: DataCan Surface Readout Box, Model 105421

Figure 4: DataCan Gauge Carrier and Transducers with Outer Protective Casing Removed

3.3 Tool Assembly

The tool configuration as shown in Figure 5 was used for all tests.

Due to its length, the testing tool was mobilized in modules and assembled on site from bottom-up as it was lowered into the borehole. The tool assemble sequence was as follows:

- The bottom packer was threaded to the AQTK interval test tubing which was threaded to the perforated transducer carrier.
- The pre-programmed, battery powered, interval pressure transducer (PPS25) with internal memory was threaded inside the transducer carrier. The recording frequency was set to 5 second intervals allowing for several weeks of data recording and storage.
- The perforated transducer carrier was threaded to the bottom of the top packer with the DHSIV positioned above the upper packer.
- The DataCan multi-zone pressure transducer protective casing is positioned above the DHSIV.

Prior to lowering the tool down the borehole, the packers and the inflation lines were filled with water to remove the air from the system.

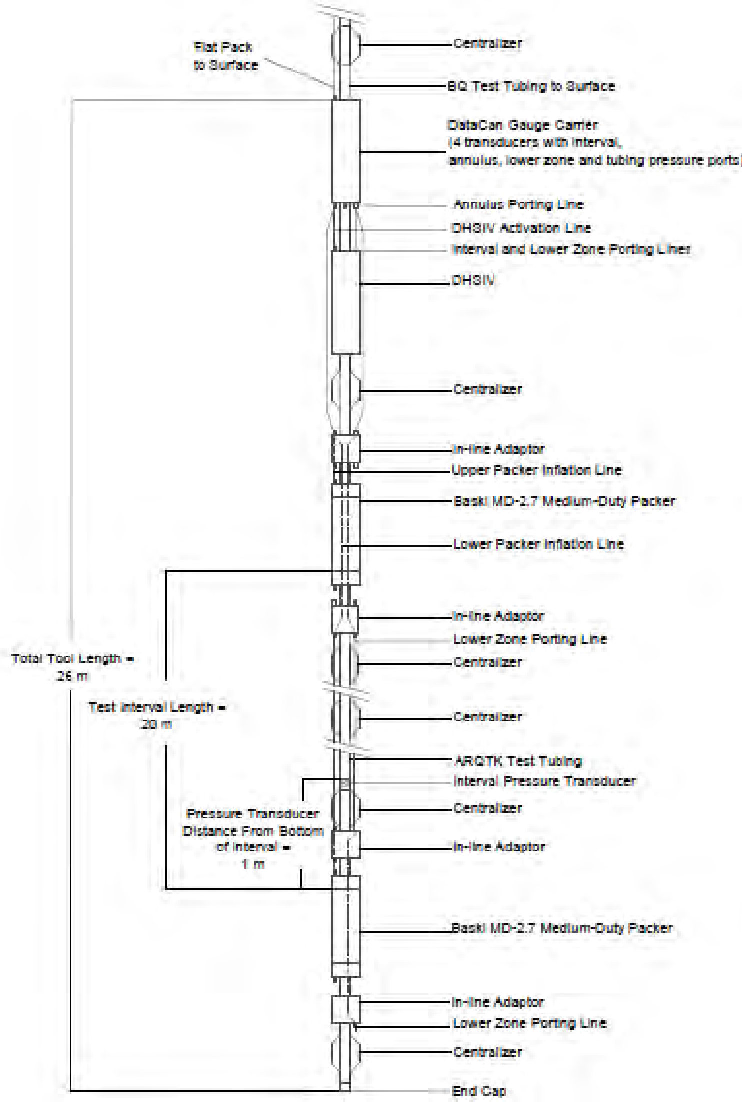

Figure 5: Tool Schematic

The end of the flatpack was positioned directly above the multi-zone pressure transducer carrier and the three stainless steel lines in the flatpack were connected to the upper packer, the lower packer, and the DHSIV. The electrical cable was connected to the common lead (cable head) from the pressure transducers.

BQ drill rods were used to lower the tool to the selected test depths and the flatpack was secured to the outside of the test tubing with duct tape. The joints of the drill rods were sealed with a rubber O-ring and tightened using pipe wrenches. Rod joint leakage less than the measured magnitude of the interval transmissivity observed during testing had no impact on the pulse test results because the fluid in the tubing is isolated from the test interval by the closed DHSIV.

The pressure required to inflate the packers was supplied from a compressed nitrogen gas cylinder at the surface. A high-pressure regulator was directly attached to the cylinder and connected to packer inflation control manifold. The control manifold was used to inflate packers by pressurizing the water-filled inflation pressure vessel. A manual activation pump was used to operate the DHSIV (Figures 6, 7 and 8).

Figure 6: Work area tent with flatpack and pressure vessel (packer inflation manifold with pressure gauge on right side of cage) (see Figure 8)

Figure 7: Work area tent with flatpack and pressure vessel (packer inflation manifold with pressure gauge on right side of cage (see Figure 8), red DHSIV activation pump below flatpack at center

Figure 8: Pressure vessel (front) and packer inflation manifold with pressure gauge and nitrogen bottle on side of flatpack cage

3.4 Tool Operation Checks

Quality assurance (QA) testing of the tool operation was performed on the packer inflation lines and DHSIV activation line inside the surface casing to check for leaks in the system. Data from the quality assurance testing is documented in the DQC workbook.

Four QA tests (Leak Tests) were performed inside the surface casing. Leak tests were performed at the start of testing prior to test HT001, removal of the tool to inspect tool for damage after completing test HT004a, after completing tool inspection prior to lower the tool for test HT010, and at the end of the testing program. The leak tests measure the leakage of the testing system at the maximum anticipated test differential pressures and allow for the estimation of an equivalent transmissivity of the cased interval to confirm the testing tool met the project's requirement of accurately measuring test interval hydraulic conductivity to 10^{-13} m/sec.

The leak tests performed are summarized in the following subsections. Details on each test are provided in the DQC workbook.

3.4.1 Leak Test #1 – Start of Testing Prior to Test HT001

Leak Test #1 was performed on May 16, 2021 at the start of testing prior to test HT001. The pressure data collected during the test are presented in Figure 9. The testing tool with a test interval length of 20.03 m was lowered into the surface casing below the water level. The packers were inflated to 2.48 MPa surface pressure

(20% above the anticipated inflation pressure during testing) and monitored for leakage. No leakage was observed from the testing system. With the packers inflated, the DHSIV was closed to simulate the PSR phase and the water level in the test tubing was lowered by 0.229 MPa in preparation for a slug withdrawal (SW) phase. No hydraulic connection was observed between the annulus, tubing, and test interval. The DHSIV was then opened introducing the pressure change to the test interval, and the interval pressure was monitored for 30 minutes. Following the SW phase, the DHSIV was closed for 30 minutes for a shut-in recovery phase (SWS) with no observable hydraulic connection above and below the test interval.

With the DHSIV open, transmissivity of 8E-11 m^2/sec and an equivalent hydraulic conductivity of 4E-12 m/sec for the 20.03 m test interval length was derived for the testing tool from the slug withdrawal phase (SW) data. These values can be considered the lower limit of the testing tool for the slug test at HT001. The analyses of the data from shut-in recovery phase (SWS) resulted in a transmissivity of 3E-13 m^2/sec or an equivalent hydraulic conductivity of 2E-14 m/sec for the 20.03 m test interval length. Leak Test #1 confirmed the tool performance met the project's requirement of accurately measuring test interval hydraulic conductivity down to 10^{-13} m/sec.

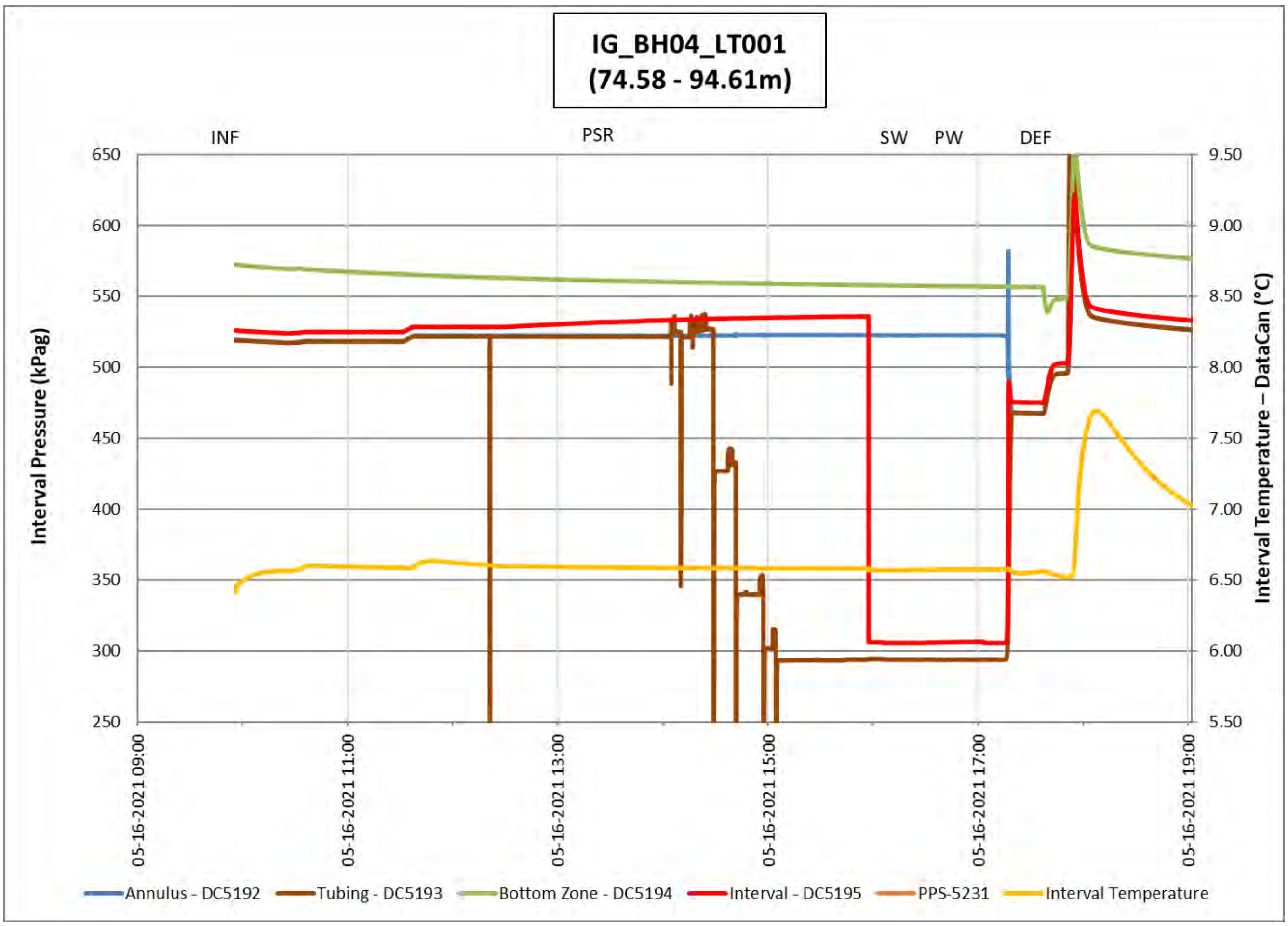

Figure 9: Leak Test #1 Pressure Plot

3.4.2 Leak Test #2 – Removal of Tool for Inspection Following Test HT004a

Leak Test #2 was performed on May 30, 2021 during removal of the tool for damage inspection following abnormal test responses observed during HT007, HT008, HT009, and HT004a. The pressure data collected during the test are presented in Figure 10. The testing tool with a test interval length of 20.03 m was pulled into the surface casing below the water level. The packers were inflated to 2.46 MPa surface pressure (20% above the anticipated inflation pressure during testing) and monitored for leakage. No leakage was observed from the testing system. With the packers inflated, the DHSIV was closed to simulate the PSR phase and the water level in the test tubing was lowered by 0.332 MPa in preparation for a slug withdraw (SW) phase. No hydraulic connection was observed between the annulus, tubing, and test interval. The DHSIV was then opened introducing the pressure change to the test interval and the interval pressure was monitored for 30 minutes. Following the SW phase, the DHSIV was closed for 30 minutes for a shut-in recovery phase (SWS) with no observable hydraulic connection above and below the test interval.

With the DHSIV open, transmissivity of 2E-11m^2/sec and an equivalent hydraulic conductivity of 1E-12 m/sec for the 20.03 m test interval length was derived for the testing tool from the slug withdrawal phase (SW) data. These values can be considered the lower limit of the testing tool for slug tests with the DHSIV open. The analyses of the data from shut-in recovery phase (SWS) resulted in a transmissivity of 1E-13 m^2/sec or an equivalent hydraulic conductivity of 7E-15 m/sec for the 20.03 m test interval length. Leak Test #2 confirmed the tool performance met the project's requirement of accurately measuring test interval hydraulic conductivity down to 10^{-13} m/sec.

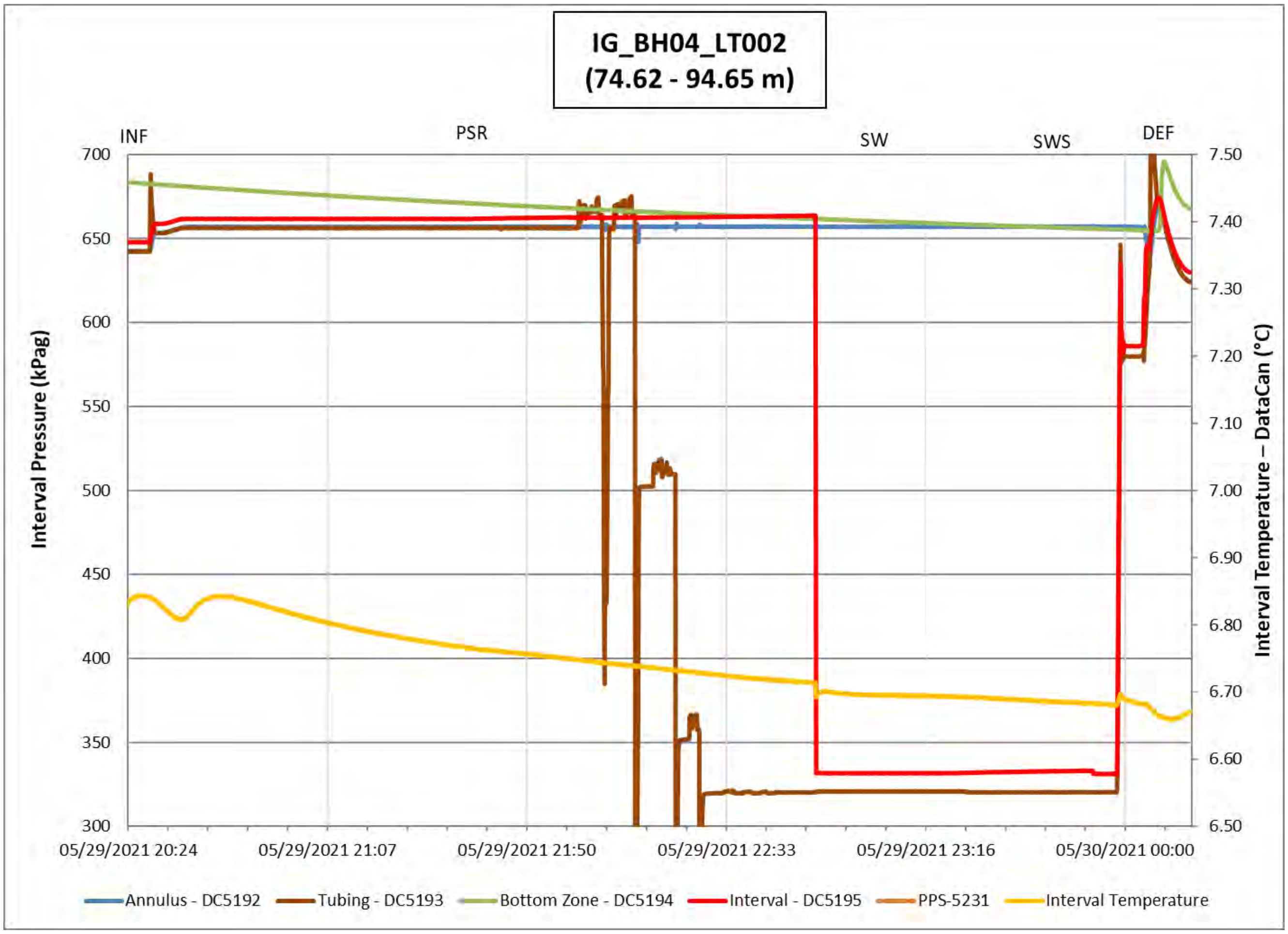

Figure 10: Leak Test #2 Pressure Plot

3.4.3 Leak Test #3 – Lowering of Tool Prior to Test HT010

Leak Test #3 was performed on May 31 and June 1, 2021 during lowering of the tool prior to the resumption of testing activities at the HT010 interval. The pressure data collected during the test are presented in Figure 11. The testing tool with a test interval length of 20.03 m was lowered into the surface casing below the water level. The packers were inflated to 2.46 MPa surface pressure (20% above the anticipated inflation pressure during testing) and monitored for leakage. No leakage was observed from the testing system. With the packers inflated, the DHSIV was closed to simulate the PSR phase and the water level in the test tubing was lowered by 0.338 MPa in preparation for a slug withdrawal (SW) phase. No hydraulic connection was observed between the annulus, tubing and test interval. The DHSIV was then opened introducing the pressure change to the test interval, and the interval pressure was monitored for 30 minutes. Following the SW phase, the DHSIV was closed for 55 minutes for a shut-in recovery phase (SWS) with no observable hydraulic connection above and below the test interval.

With the DHSIV open, transmissivity of 1E-11 m^2/sec and an equivalent hydraulic conductivity of 5E-13 m/sec for the 20.03 m test interval length was derived for the testing tool from the slug withdrawal phase (SW) data. The analyses of the data from shut-in recovery phase (SWS) resulted in a transmissivity of 5E-14 m^2/sec or an equivalent hydraulic conductivity of 3E-15 m/sec for the 20.03 m test interval length. Leak Test #3 confirmed the tool performance met the project's requirement of accurately measuring test interval hydraulic conductivity down to 10^{-13} m/sec.

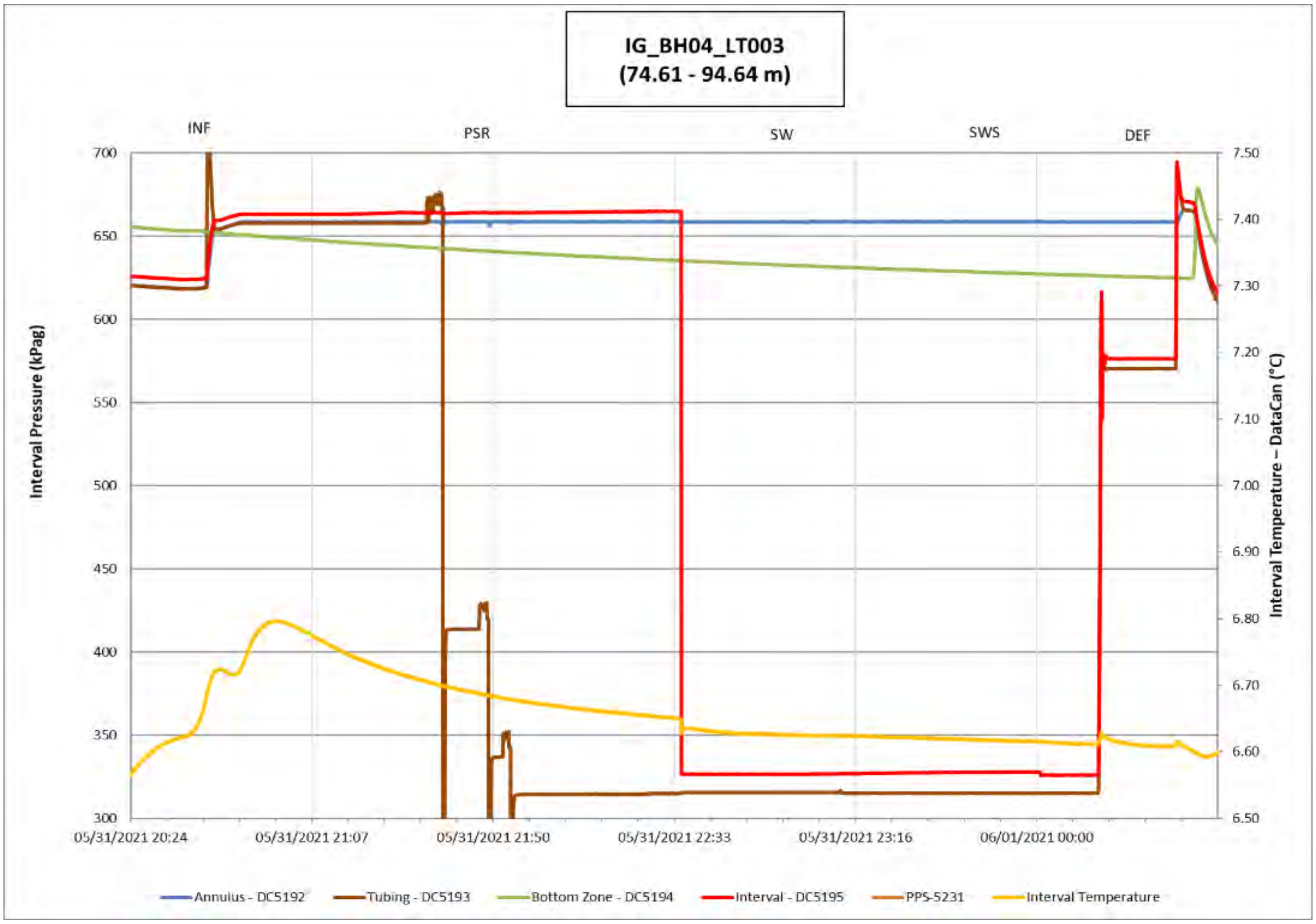

Figure 11: Leak Test #3 Pressure Plot

3.4.4 Leak Test #4 - End of Testing

Leak Test #4 was performed on June 24, 2021 after the completion of test HT007a. The pressure data collected during the test are presented in Figure 12. The testing tool with a test interval length of 20.03 m was pulled into the surface casing below the water level. The packers were inflated to 2.46 MPa surface pressure (20% above the anticipated inflation pressure during testing) and monitored for leakage. No leakage was observed from the testing system. With the packers inflated, the DHSIV was closed to simulate the PSR phase and the water level in the test tubing was lowered by 0.220 MPa in preparation for a slug withdrawal (SW) phase. No hydraulic connection was observed between the annulus, tubing, and test interval. The DHSIV was then opened introducing the pressure change to the test interval, and the interval pressure was monitored for 30 minutes. Following the SW phase, the DHSIV was closed for 35 minutes for a shut-in recovery phase (SWS) with no observable hydraulic connection above and below the test interval.

With the DHSIV open, transmissivity of 4E-11 m^2/sec and an equivalent hydraulic conductivity of 2E-12 m/sec for the 20.03 m test interval length was derived for the testing tool from the slug withdrawal phase (SW) data. The analyses of the data from shut-in recovery phase (SWS) resulted in a transmissivity of 5E-13 m^2/sec or an equivalent hydraulic conductivity of 3E-14 m/sec for the 20.03 m test interval length. Leak Test #4 confirmed the tool performance met the project's requirement of accurately measuring test interval hydraulic conductivity down to 10^{-13} m/sec.

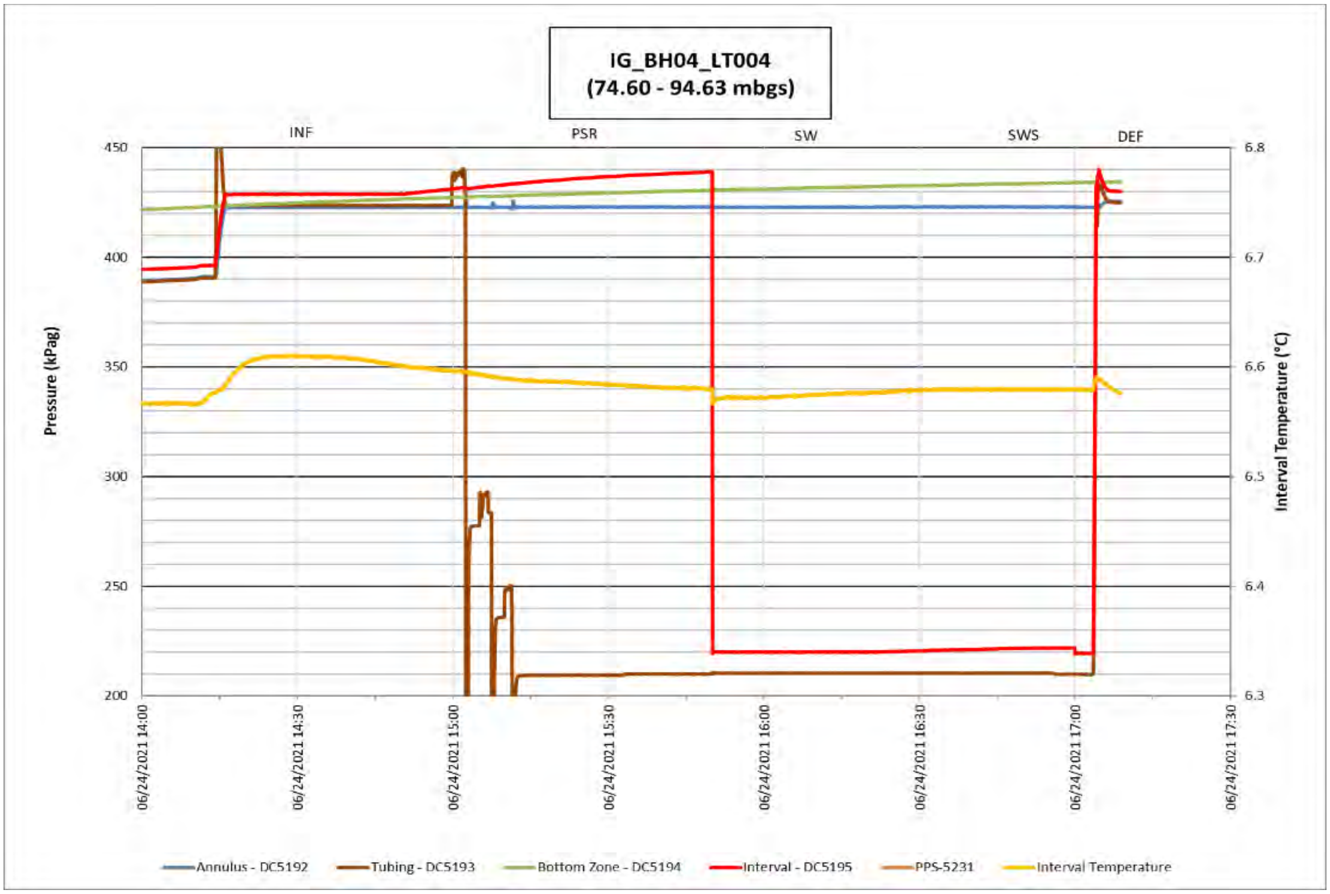

Figure 12: Leak Test #4 Pressure Plot

4.0 TEST INTERVAL SELECTION

The selection of test intervals was determined in a collaborative workshop with the NWMO and Golder technical leads based on the findings from drilling, core logging, and geophysical logging. The objectives for test interval selection consisted of:

- Confirm low rock mass hydraulic conductivity in potential repository depths (below 500 m below ground surface (mbgs)) and directly above potential repository depths (above 500 mbgs);
- Determine hydraulic conductivity of identified higher fracture frequency intervals within and in proximity to the repository horizon; and
- Develop an initial understanding of the general trend in hydraulic properties with depth.

The final selection of the test intervals considered the following criteria:

- **Acceptable packer element placement**. Packer element placement is based on the borehole condition. Geophysical caliper logs (WP05) were reviewed to confirm the borehole had a consistent diameter (no washouts) to ensure the differential pressure rating of the packers would apply. Acoustic televiewer imagery (WP05) and core photos (WP03) were reviewed to ensure the packers were seated in sections of the borehole free of fractures to ensure no packer bypass.
- **Location of hydrogeologic features.** The presence of broken fractures, and zones of increased porosity or weathering can influence the hydraulic response of the bulk rock mass. These features were identified and incorporated into the test interval selection decision to ensure that low hydraulic conductivity intervals as well as intervals containing potentially conductive features are tested to assess the range of hydraulic conductivities within the borehole. Flow logging was performed under static (non-pumping) and dynamic (pumping) conditions to identify the potentially water conductive fractures. The selection of potentially water conductive fractures was carried out during Drilling and Coring (WP02), Geological and Geotechnical Core Logging, Photography and Sampling (WP03), and Fluid Temperature and Resistivity Log and Flowing Fluid Electrical Conductivity Log (WP05).

Observations from these data are summarized in the Cover Page of the DQC workbook.

A total of thirty (30) intervals were identified based on the testing objectives and the test interval selection criteria. The intervals were tested in sequence as the tool was being lowered downhole, with the exception of tests HT011, HT023, and HT029, which were omitted in favour of tool diagnostic retests at intervals HT004a, HT007a, HT008a, and HT009a. The remaining testing sequence was selected to limit the amount of time moving the tool between tests. This sequence of testing is reflected in the test identification numbers (HT001, HT002, HT003, etc.). The testing was carried out from May 16, 2021 through June 24, 2021.

5.0 TESTING METHODOLOGY

The planned hydraulic testing methodology is illustrated in Figure 13. However, due to the overall low to very low hydraulic conductivity of the selected test intervals in borehole IG_BH04, only two test types were performed:

1) Pulse withdrawal tests in all intervals;

2) Slug tests in three intervals HT001, HT008, and HT012 (in addition to pulse test).

The individual test sequences are described in detail in the following sections.

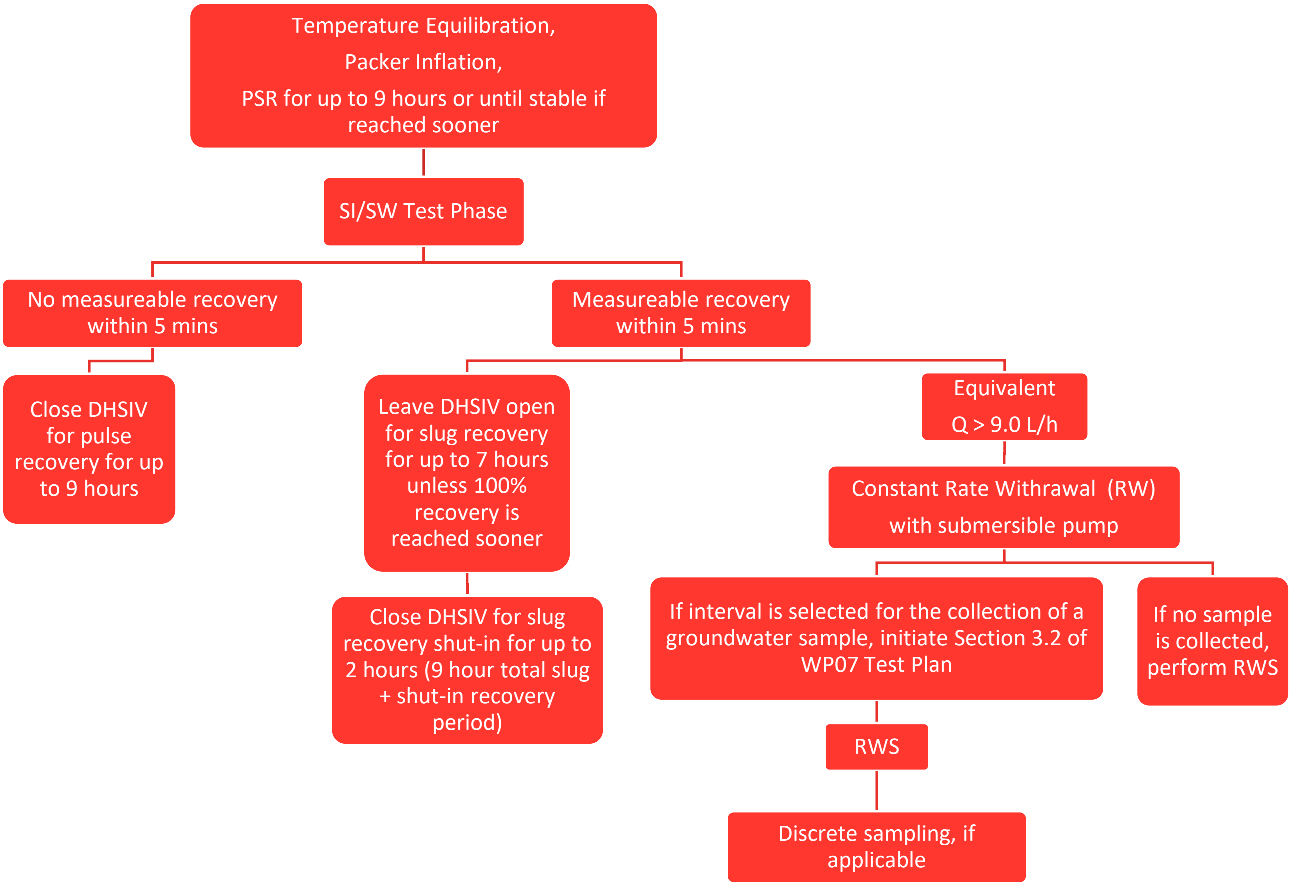

Figure 13: IG_BH04 WP06 Test Plan Flow Chart

A graphical representation of a typical pulse test as demonstrated in Test HT002 is shown in Figure 14. The test included a PSR phase, pulse withdrawal phase, and recovery phase. The hydraulic isolation of the test interval is demonstrated by the different pressure responses from the borehole annulus (blue), tubing (brown), bottom zone (green), and test interval (red and orange). The figure also shows a relative stabilization in the interval temperature that occurs prior to the initiation of the pulse.

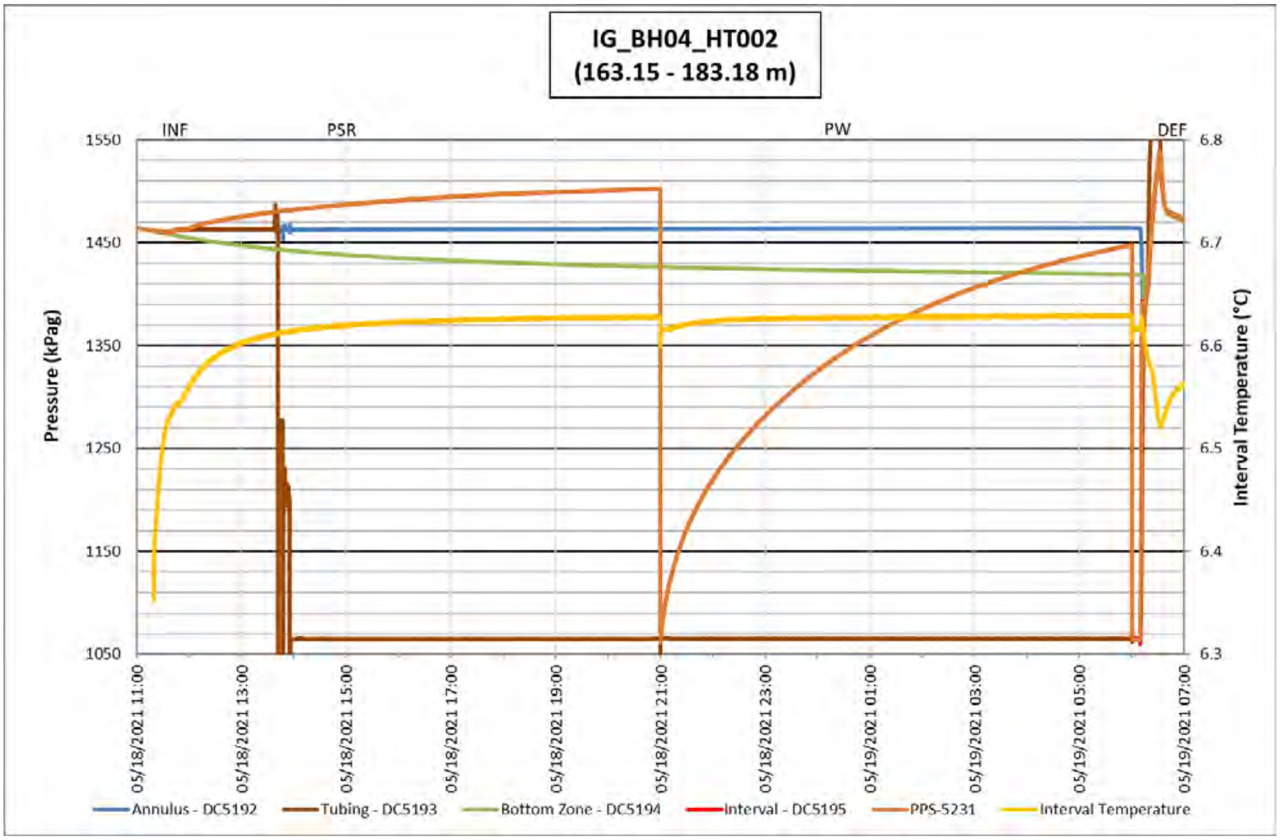

Figure 14: Typical Pulse Test Procedure, IG_BH04_HT002

Packer Inflation

The required packer inflation pressure was first set at the nitrogen cylinder using a pressure regulator. This pressure was then directed through the packer inflation manifold to the pressure vessel that pressurized the water within the flatpack inflation lines and the packers. The packer inflation pressure was monitored at the pressure vessel with a digital pressure gauge. The nitrogen pressure was applied to the pressure vessel until the water level in the vessel remained stable, indicating the packers have inflated to their full size against the borehole wall. The typical duration of the packer inflation was approximately 45 minutes.

After the packers were inflated, the packer seals were confirmed by monitoring the real-time pressure responses in the bottom zone below the lower packer and the borehole annulus above the upper packer (see zone pressure responses during the INF phase in Figure 14). If the expected pressure responses were not discernable (i.e., enough to raise the water column at least one meter), several litres of drilling supply water were poured between the surface casing and the test tubing while monitoring the interval transducer for any change in pressure. The interval temperature was monitored until it stabilized before initiating the pressure static recovery phase. The packer pressure (start and end of test) was recorded in the Field Data tab in the DQC workbook.

Pressure Static Recovery (PSR) Phase

The PSR phase is intended to assess the initial pressure within the test interval prior to testing. After the packers were inflated at the selected depth interval, the PSR phase was initiated by closing the DHSIV. The DHSIV pressure was adjusted and controlled manually using a 4-litre water-filled high-pressure pump, and from there diverted to the DHSIV via the flatpack.

Closing and opening the DHSIV was completed within a relatively short period of time (a few seconds). The PSR phase was initiated by closing the DHSIV, effectively separating the hydrostatic pressure within the test section from the rest of the test tubing while the pressure in the test interval starts equilibrating. The PSR phase was monitored in real-time by the interval transducer and continued until the rate of pressure change stabilized relative to the transducer resolution or could be extrapolated with confidence by examining the semi-log Horner plot in Golder's analysis software HydroBench. The semi-log Horner plot for test HT012 is shown as Figure 15 below as an example.

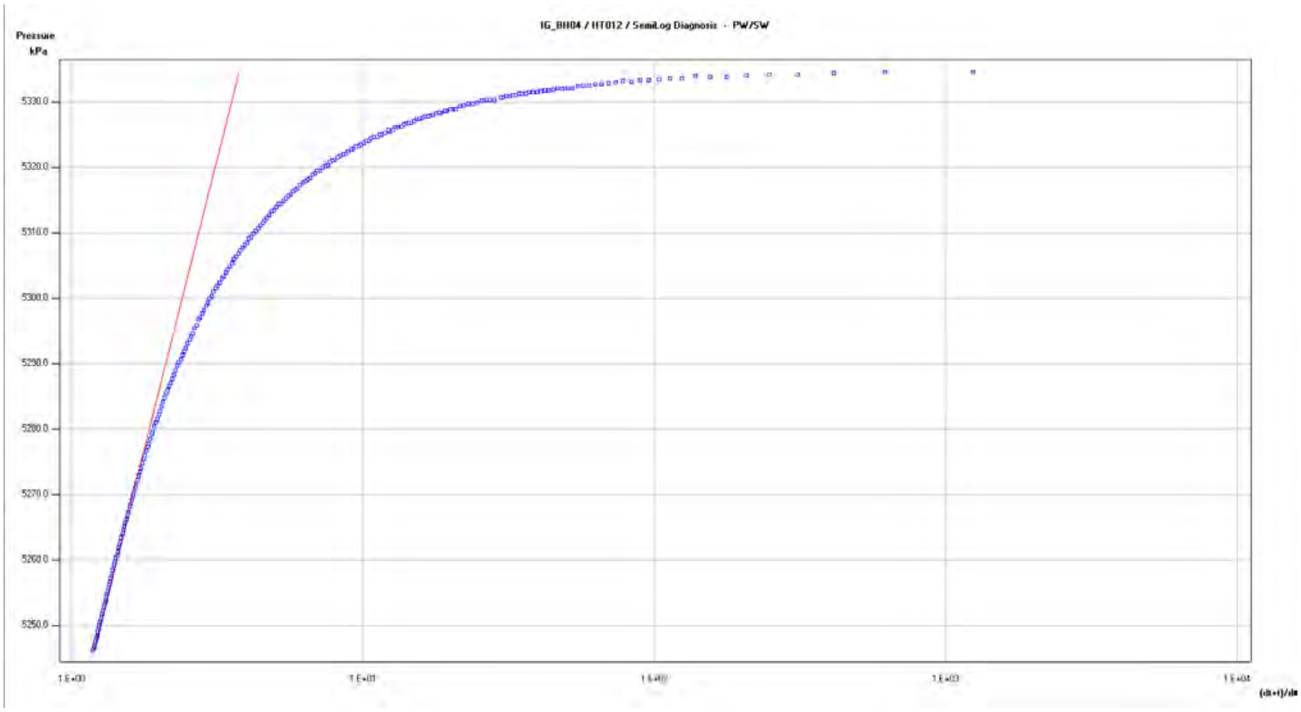

Figure 15: Semi-log Plot of IG_BH04_HT012 analyses showing the pressure recovery of the PSR phase (dark blue) and extrapolated static pressure fit line (red)

The PSR phase details including start time, end time, and stabilized pressure were recorded in the Field Data tab of the DQC workbook. In addition to assessing the initial test interval pressure prior to testing, the PSR Phase served to dissipate a portion of the borehole pressure and temperature history effects to minimize their influence on the derivation of hydraulic parameters for the test interval.

Creating Test Differential Pressure

The water level within the test tubing was typically within 20 m of the ground surface, which allowed for the differential pressure for each test to be created by withdrawing water from the test tubing with the exception of tests HT009 that showed water level in the test interval at approximately 90 meters below ground surface. To create the pressure differential for Test HT009, the water level was raised by adding water to the test tubing with the DHSIV closed. This anomalous water table depth however was not present for the retest of this interval as HT009a.

For the other tests, the pressure differential was created using a swabbing tool lowered on the rig wireline inside the test tubing (HQ drill pipe) to various depths ranging from 19 to 84 metres with the DHSIV closed. The swabbing tool was raised to surface, removing the column of water and inducing a differential pressure in the test interval. Pressure differentials achieved for the tests ranged from approximately 0.181 MPa to 0.804 MPa. After removing water from the test tubing, the DHSIV was opened, introducing the pressure change to the test interval for several seconds. The DHSIV was then closed to begin the pulse recovery phase (PW).

Test Pressure Recovery for Very Low Conductivity Test Intervals

For 28 out of 31 test intervals with very low transmissivity (i.e., < 1E-10 m^2/s) the interval pressure did not recover from the PW within the pre-determined recovery duration of 9 hours. The interval pressure recovery was monitored in real-time with the DataCan interval pressure transducer and assessed in the field using Golder's analysis software HydroBench. This field assessment of real-time data was used to ensure a high level of confidence was achieved for the derived formation parameters prior to terminating each interval test.

Test Pressure Recovery for Low Conductivity Test Intervals

Three test intervals (HT001, HT008, HT012) had sufficient transmissivity for the interval pressure to nearly recover within 9 hours. For these three intervals, a slug withdrawal (SW) was performed at the end of the PW phase by opening the DHSIV. The interval pressure during the SW phase was monitored with the DHSIV open. The length of the slug recovery phase depended on the remaining pre-determined recovery time.

The interval pressure recovery was monitored in real-time with the interval pressure transducer and assessed in the field using Golder's analysis software HydroBench. This field assessment of real-time data was used to determine the duration of the interval pressure recovery phases (SW) to ensure a high level of confidence has been achieved for the derived formation parameters prior to terminating each interval test.

The observed pressure recovery curves indicated that none of the tested intervals demonstrated sufficiently high transmissivity values to warrant constant-rate withdrawal testing.

Packer Deflation

At the termination of each test, the packers were deflated by releasing the nitrogen pressure from the pressure vessel. The pressures in the bottom, interval, and annulus zones were monitored in real-time for pressure equilibration to confirm the packers had unseated from the borehole wall. The tool was moved to the next test interval when the level of water in the pressure vessel had returned to the pre-inflation level, which indicated the packers were fully deflated.

6.0 TEST ANALYSIS

In fractured crystalline rock settings, it is expected that the rock mass would have low bulk hydraulic conductivity, and main contribution to hydraulic conductivity and total porosity comes from localized conductive fractures. Under these conditions, the volume of rock actually influenced during a borehole hydraulic test can be quite limited. For relatively short duration test that were completed for this program, it is expected that near borehole conditions dominate the test response with only limited transition to the undisturbed formation response further away from the borehole. The approach was to apply wellbore storage with a composite flow model (i.e., inner skin zone with outer formation zone) was applied to try matching the test interval pressure responses.

The final analyses of the hydraulic tests were carried out using nSIGHTS (n-dimensional Stochastic Inverse Graphical Hydraulic Test Simulator) version 2.50 freely available online (Geofirma and INTERA, 2011). nSIGHTS is a well-test code developed for Sandia National Laboratories by Geofirma. Non-linear parameter-estimation methods are used in nSIGHTS to find the optimal values of the model fitting parameters (formation hydraulic conductivity (K), formation specific storage (S_S), inferred formation pressure, flow dimension, skin K, and skin thickness) that provide the best statistical match to the observed test data.

A comparison of the best fit and median value for each model fitting parameter was performed to identify which was the best statistical match to the field data. In general, the difference between the best fit and median values was less than an order of magnitude for each parameter, however, there were several instances (up to 25% of the tests) where the difference was slightly greater than an order of magnitude. There was no significant trend, some parameters were higher in some tests while lower in others. There was no indication that the median value produced a more representative value than the best fit. For this reason, the best fit results will be reported.

Input parameters used for each test analysis are listed in Appendix C. The parameters are defined in the following subsections.

6.1 Input Parameters

6.1.1 Test Pressure

Final analyses were completed at the end of the WP06 testing program using the interval pressure data from the PPS transducer positioned inside the test interval. The recorded pressures from this transducer were used for the final test analyses since it is positioned directly inside the test interval and the data do not require depth correction. The pressure measured with the PPS transducer was corrected for barometric pressure by subtracting the barometric pressure measured at the surface (drill rig) using a Solinst Barologger.

6.1.2 Wellbore Storage

Wellbore storage is the response of the test zone to the change in pressure as a result of the compressibility of the fluid in the system (test interval + test tubing), the packer tool, and the rock formation within the interval. For test interval sections of low hydraulic conductivity, the phase of the pressure response dominated by wellbore storage can mask the pressure response of the rock. Wellbore storage is identified with an early unit slope of the pressure change derivative plotted on the log-log plot. nSIGHTS produces this graph for assessing the wellbore storage phase during testing.

Wellbore storage is a sensitive parameter in the estimation of hydraulic parameters in low transmissivity rock. There are two types; open tubing wellbore storage where the fluid level is changing in the tubing with the DHSIV open, and shut-in wellbore storage where pressure is recovering within the test interval with the DHSIV closed. For slug tests, the open tubing wellbore storage coefficient is determined by the test tubing radius where the fluid column change is measured.

Open Tubing Wellbore Storage

For slug tests, wellbore storage C (m^3/Pa) is calculated by the equation below

$$C(DHSIV\ open) = \frac{\pi * r_u^2}{\rho * g}$$

where:

- r_u is the equivalent test tubing radius = SQRT((tubing radius)^2/sin(borehole inclination)) = 0.02378 m
  - where tubing radius = 0.02305 m and borehole inclination = 70 degrees
- ρ is the density of water at 10°C = 999.7 kg/m^3
- g is the earth gravity acceleration = 9.81 m/s^2

Applying these values, C (SI open) = 1.8E-07 m^3/Pa, which was applied for all slug test analyses.

Shut-in Wellbore Storage

For test phases where the DHSIV is closed, C (m^3/Pa) is determined by the change in volume required to produce the corresponding change in pressure for the pulse test, which is determined by the compressibility of the system (drill fluid column + interval rock matrix + packer tool). This compressibility is estimated during the pulse phase of the test by measuring the change in water level within the test tubing using a datalogger (Solinst Barologger). The datalogger was lowered into the test tubing from the surface after lowering the water level in the tubing in preparation for the pulse to measure the change in volume induced from the pulse activation (opening and closing the DHSIV) then removed from the test tubing for the recovery phase.

Wellbore Storage was calculated using the following equation:

$$C\ (DHSIV\ closed) = \frac{(dP_{tubing}) * \pi * r_u^2}{\rho * g} * \frac{1}{(dP_{interval})}$$

where:

- ρ is the density of the fluid (kg/m^3)
- g is the earth gravity acceleration (m/s^2)
- r_u is the equivalent test tubing radius = SQRT((tubing radius)^2/sin(borehole inclination)) = 0.02378 m
- where tubing radius = 0. 02305 m and borehole inclination = 70 degrees
- dP_{tubing} is the change in pressure measured in the test tubing as a result of the pulse (Pa)
- $dP_{interval}$ is the change in pressure measured in the test interval as a result of the pulse (Pa)

The wellbore storage measurements ranged from 4E-11 m^3/Pa (HT016) to 1E-09 m^3/Pa (HT012).

Dividing the wellbore storage by the test interval volume, a total test zone compressibility ranged from of 3E-10 1/Pa (HT016) to 8E-09 1/Pa (HT012) with an average value of 1E-09 1/Pa. Casing tests carried out for the Swiss National Cooperative for the Disposal of Radioactive Waste (NAGRA) report water and test tool compressibility values that typically approach 2E-09 1/Pa to 6E-10 1/Pa (Kennedy and Davidson 1989). Total test zone compressibility typically averages 2E-09 1/Pa (Ostrowski et al. 1992).

6.2 Output Parameters

The input parameters applied to the test analysis have different degrees of uncertainty that impact the uncertainty of the transmissivity estimates (output parameters) from the test analyses. The analysis approach follows a systematic, hierarchical workflow to minimize uncertainty:

- Tests were performed to minimize factors that increase uncertainty such as borehole history and temperature effects.
- Establish a conceptual model using pressure data input and defining test sequences.

- Diagnostic analyses by generating pressure-derivative plots to determine base case of fitting parameters (hydraulic conductivity, skin, storativity, inferred formation pressure, and flow model). The flow model and parameter estimates from the diagnostic analysis were used as input in the forward simulation in nSIGHTS.
- Inverse parameter estimation was performed by using the flow model and parameter estimates using non-linear regression techniques. The result gave best-fit parameters to match the well test behavior and statistical information on model errors. The first (forward simulation) and the second (optimization) of these two analysis steps were completed. The parameters (also known as model constraints) including flow dimension, formation hydraulic conductivity, formation specific storage, skin hydraulic conductivity, skin thickness, and static formation pressure were used as fitting parameters for the optimization. Flow dimension and static formation pressure were varied in a linear scale while the other constraints will be varied in a logarithmic scale.
- Residual analyses applied the model errors to determine their distribution to statistically verify the inferred flow model;
- Perturbation analysis to evaluate the uniqueness of the base case parameters (i.e., check for parametric correlations). This process was repeated a number of times to determine if the non-linear regression algorithm was converging to a unique global minimum or if local minima were obscuring the results. Typically, 200 perturbations with perturbation span of 0.40 is performed. The subsequent perturbation analysis used the last optimization value for its initial estimate of parameters. The final number of perturbations is dependant on the best-fit parameter values for each test.

A summary of the test results is provided in Appendix C. Appendix C presents a brief summary of each test interval, plot of pressures and temperature from all monitored zones, test tubing pressure during the DHSIV activation for WBS calculation, table with nSIGHTS fitted parameter output ranges, and the following analyses plots produced by nSIGHTS:

- Pressure plot showing best fit simulation and best fit results. Test data is shown as red points, best fit simulation is shown as a green line;
- Deconvolved pressure change (red points) and pressure derivative plot (blue points) showing the best fit simulation (magenta line);
- XY scatter plot of each fitted parameter vs the fit value (to check the uniqueness of the best fit value); and
- XY scatter plot showing the relation between selected pairs of fitted parameters, using symbols colored according to the corresponding fit value. (to check the degree of correlation between fitted parameters).

Data Quality Confirmation forms are provided within the Data Deliverable package.

The analysis includes the following main steps:

- Define fitting parameters using results of the preliminary HydroBench analyses;
- Define minimum and maximum values for each fitting parameter (approximately two orders of magnitude below and above the initially assumed values for conductivity and specific storage, ± 200 kPa around the initial value of the static formation pressure, 0.001 m and 1 m for the radial thickness of the skin-zone, 1 and 3 for flow dimension);

- Define the test phases to be included in fitting (typically Pulse and / or Slug);
- Define fit types for each selected test phase (typically normalized pressure vs. time, deconvolved pressure and derivative vs. time, and cartesian plot of pressure vs. time.)
- Define a composite fit using a proper combination of individual fits;
- Define the number of perturbations (200 in each case) and the perturbation span (0.4, i.e., 40% of the domain defined by min and max values, centered around the initial guess value);
- Perform perturbation run; and
- Analyze the results by creating appropriate tables (e.g., best fit parameter values, statistics of fitted parameter values) and plots (pressure plot showing best fit simulation, cumulative distribution function plot of each fitting parameter, XY scatter plot of selected pairs of fitted parameters, XY scatter plot of each fitted parameter vs the fit value).

6.2.1 Transmissivity and Hydraulic Conductivity

The nSIGHTS analysis produces the test interval transmissivity. Hydraulic conductivity is derived from transmissivity by applying the measured transmissivity over the length of the test interval contributing to that transmissivity. It was assumed for all tests that the test interval is homogeneous (i.e., the entire test interval contributes equally to the measured transmissivity). Thus, hydraulic conductivity was calculated by dividing the measured transmissivity by the interval length.

6.2.2 Storativity

Storativity is a fitting parameter in nSIGHTS, which is directly correlated with skin effect and cannot be uniquely determined from a single hole test. While storativity directly impacts skin, it has less of an impact on the determination of transmissivity.

Storativity is calculated using the following equation:

$$S = \rho * g * \emptyset * c_t * h$$

Where

- ρ is the density of water
- g is the acceleration of gravity
- $\emptyset$ is the formation effective porosity
- c_t is the formation compressibility in 1/Pa
- h is the length of the test interval in m

The formation compressibility and effective porosity were varied to produce the best fit storativity parameter.

6.2.3 Formation Pressure

It should be noted that the accuracy of the derived initial formation pressure is strongly dependent on the borehole pressure history. Generally, the longer and more complicated is the borehole pressure history period, the greater are the uncertainties in the analysis. Lower transmissivities are more strongly influenced by uncertainties in the borehole pressure history. To reduce the influence of borehole pressure history on the derivation of transmissivity, a PSR phase was included at the start of each test to dissipate a portion of the borehole pressure history prior to initiation of the active phases, and each test was completed with a relatively long duration shut-in recovery phase when borehole pressure history effects will be minimal compared to the early portion of the test.

Formation pressure is a fitting parameter in nSIGHTS.

6.2.4 Skin Zone

Skin is a dimensionless term that is used to quantify the hydraulic properties of the rock around a borehole which may be enhanced by an increased fracturing caused by drilling or reduced by drilling debris and/or mud invasion. The skin magnitude correlates to the ratio of the change in permeability as a factor to the thickness of the skin relative to the borehole diameter. Diagnostic tools are used to identify the hydraulic properties (transmissivity and radial thickness) of the “skin zone” based on the shape and the slopes of the semi-log derivative of the specific drawdown on the log-log plot produced in nSIGHTS. A negative skin value corresponds to an increase in transmissivity within the skin zone. A positive skin value corresponds to a decrease in transmissivity within the skin zone. The effects of the skin are then separated from the portion of the data that is primarily influenced by the undisturbed rock properties. nSIGHTS apply skin thickness and magnitude as fitting parameters to the simulation match which influences the shape of the pressure derivative.

6.2.5 Flow Dimension

nSIGHTS can apply multi-dimensional flow models. If there is a slope in the derivative data that is characteristic for a flow geometry other than two-dimensional radial flow such as one dimensional linear (positive half slope) or three-dimensional spherical flow (negative half slope), alternative non-radial flow geometry produces a better match to the test response. The slope of derivative data is equal to 1-n/2 where n is the flow dimension; therefore, for linear flow which has a flow dimension of one (1) as flow area does not increase with distance from well results in a positive half slope in the derivative data. Inputting a flow dimension of 1 into the equation above yields a derivative slope of 1/2 on the log-log plot.

In low permeability setting, a composite flow response is often observed that is consistent with a near well zone of higher transmissivity with a flow dimension of 2 and outer zone of lower transmissivity more representative of the undisturbed formation. Allowing flow geometry to be a fitted parameter in manual or automated matching would provide an improved match because there are more parameters applied to the fit but would result in a flow model that is not consistent with the measured data and conceptual geologic understanding. Therefore, the additional fitted parameters would only be used to compensate for inaccuracies in representing the borehole history effects and results in more uncertainty (although improving the match).

7.0 SUMMARY OF RESULTS

Hydraulic testing was completed in 27 intervals in borehole IG_BH04. Due to abnormal pressure responses observed in intervals HT007, HT008 and HT009 these intervals were subsequently retested as HT007a, HT008a and HT009a. The retest of these intervals did not show abnormal pressure responses. Test HT004 was considered a successful test but was repeated to confirm the abnormal pressure responses observed during the previous tests HT007, HT008 and HT009. Test HT004a (retest of HT004) showed similar abnormal pressure responses as HT007, HT008 and HT009 confirming the abnormal pressure were likely caused by tool behavior during those tests.

Test intervals HT011, HT023 and HT029 were omitted from the testing program because, according to inputs from other work packages, they did not contain notably transmissive features. These tests were replaced by retesting intervals HT007, HT008 and HT009. The analyses results from the retests, designated as HT007a, HT008a, and HT009a are included in this report in lieu of results from the original tests at intervals HT007, HT008, and HT009.

Transmissivity values were estimated to be in the range of 9E-13 to 2E-08 m^2/s with hydraulic conductivities in the range of 5E-14 to 1E-09 m/s.

All tests showed a very minor hydraulic connection between the borehole annulus and the test tubing (likely caused by minor leakage at threaded tubing joints), but this connection did not impact the analyses of the pulse test as the test tubing is not hydraulically connected to the test interval when the DHSIV is closed during the test. The leakage from the test tubing also did not impact the slug test recoveries of tests HT001 and HT012 as the magnitude of the leakage was less than the fluid loss to the formation during each of the slug test recoveries.

The primary uncertainties in estimation of transmissivity are the uncertainty in the input parameters, inherent uncertainties due to borehole pressure history effects and, to a lesser degree, temperature transients. Uncertainty in hydraulic conductivity also stems from the assumption of formation length across which flow occurs.

There were several steps taken to minimize the uncertainty as summarized below:

- Test tool included a downhole shut-in valve to minimize wellbore storage and pressure gauges with a relatively high degree of accuracy.
- Leak tests within casing and the tool function checks were performed during the testing program to estimate the lower transmissivity limit of the tool and confirm that the packer seals were adequate.
- Measurement of the change in the interval volume during the pulse induction to estimate test zone compressibility.
- Test design and performance included the following:
  - PSR phase to dissipate part of the borehole pressure history and temperature history effects; and
  - Test phases optimal to the magnitude of transmissivity with slug phases for higher transmissivity and pulse phases for lower transmissivity.

Based on Golder's experience with hydraulic testing and sensitivity analyses for nuclear repository programs (e.g., Enachescu et al., 1997), for test intervals with transmissivity in the magnitude of 1E-11 m^2/s to 1E-09 m^2/s, the inherent uncertainty in hydraulic parameters is considered to range between plus/minus a factor of 5 to plus or minus a factor of 10 as borehole pressure history and temperature history effects become more material in this transmissivity range and difficult to accurately replicate in the analysis.

Test results are presented in Appendix C and shown on Figure 16 and Figure 17.

Table 3: Summary of Test Results

TEST ID	Top of Interval along Borehole (mbgs)	Bottom of Interval along Borehole (mbgs)	Interval Length (m)	Inferred Formation Pressure (kPa)	WBS (m^3/Pa)		Transmissivity (m^2/sec)	Bulk Hydraulic Conductivity[1] (m/sec)
					DHSIV Open - Tubing Related	DHSIV Closed		
HT001	117.75	137.78	20.03	1162	2E-07	2E-10	2E-08	1E-09
HT002	163.15	183.18	20.03	1509	2E-07	2E-10	3E-11	2E-12
HT003	223.07	243.10	20.03	2072	2E-07	1E-10	2E-11	9E-13
HT004	263.44	283.47	20.03	2382	2E-07	1E-10	9E-13	5E-14
HT005	335.61	355.64	20.03	3028	2E-07	9E-11	2E-12	1E-13
HT006	401.21	421.24	20.03	3606	2E-07	8E-11	3E-12	1E-13
HT007a	429.99	450.02	20.03	3827	2E-07	7E-11	1E-11	6E-13
HT008a	477.70	497.73	20.03	4257	2E-07	5E-11	1E-09	5E-11
HT009a	497.17	517.20	20.03	4449	2E-07	5E-11	3E-12	1E-13
HT010	530.59	550.62	20.03	4752	2E-07	7E-11	2E-12	9E-14
HT011	594.50	614.53	20.03	--[2]	--[2]	--[2]	--[2]	--[2]
HT012	605.63	625.66	20.03	5338	2E-07	1E-09	3E-10	1E-11
HT013	625.11	645.14	20.03	5523	2E-07	7E-11	2E-08	1E-09
HT014	644.63	664.66	20.03	5725	2E-07	7E-11	6E-12	3E-13
HT015	664.13	684.16	20.03	5874	2E-07	7E-11	2E-12	1E-13
HT016	683.64	703.67	20.03	6060	2E-07	4E-11	1E-10	7E-12
HT017	699.50	719.53	20.03	6173	2E-07	8E-11	2E-11	9E-13
HT018	715.00	735.03	20.03	6303	2E-07	8E-11	2E-11	1E-12
HT019	734.50	754.53	20.03	6531	2E-07	9E-11	3E-12	2E-13

TEST ID	Top of Interval along Borehole (mbgs)	Bottom of Interval along Borehole (mbgs)	Interval Length (m)	Inferred Formation Pressure (kPa)	WBS (m^3/Pa)		Transmissivity (m^2/sec)	Bulk Hydraulic Conductivity[1] (m/sec)
					DHSIV Open - Tubing Related	DHSIV Closed		
HT020	754.25	774.28	20.03	6685	2E-07	9E-11	4E-12	2E-13
HT021	774.00	794.03	20.03	7124	2E-07	1E-10	1E-12	5E-14
HT022	793.14	813.17	20.03	7104	2E-07	9E-11	3E-11	1E-12
HT023	829.00	849.03	20.03	--[2]	--[2]	--[2]	--[2]	--[2]
HT024	849.93	869.96	20.03	7856	2E-07	7E-11	7E-10	3E-11
HT025	881.24	901.27	20.03	7879	2E-07	1E-10	4E-12	2E-13
HT026	902.64	922.67	20.03	7978	2E-07	7E-11	9E-11	5E-12
HT027	923.00	943.03	20.03	8754	2E-07	1E-10	1E-12	5E-14
HT028	938.50	958.53	20.03	8596	2E-07	1E-10	5E-11	3E-12
HT029	959.65	979.68	20.03	--[2]	--[2]	--[2]	--[2]	--[2]
HT030	959.65	1000.2	40.55	8477	2E-07	3E-10	1E-10	4E-12

Notes:

1) Bulk hydraulic conductivity is calculated by transmissivity / interval length.
2) Interval not tested.

Transmissivity and hydraulic conductivity results are plotted relative to depth on Figure 16 and Figure 17.

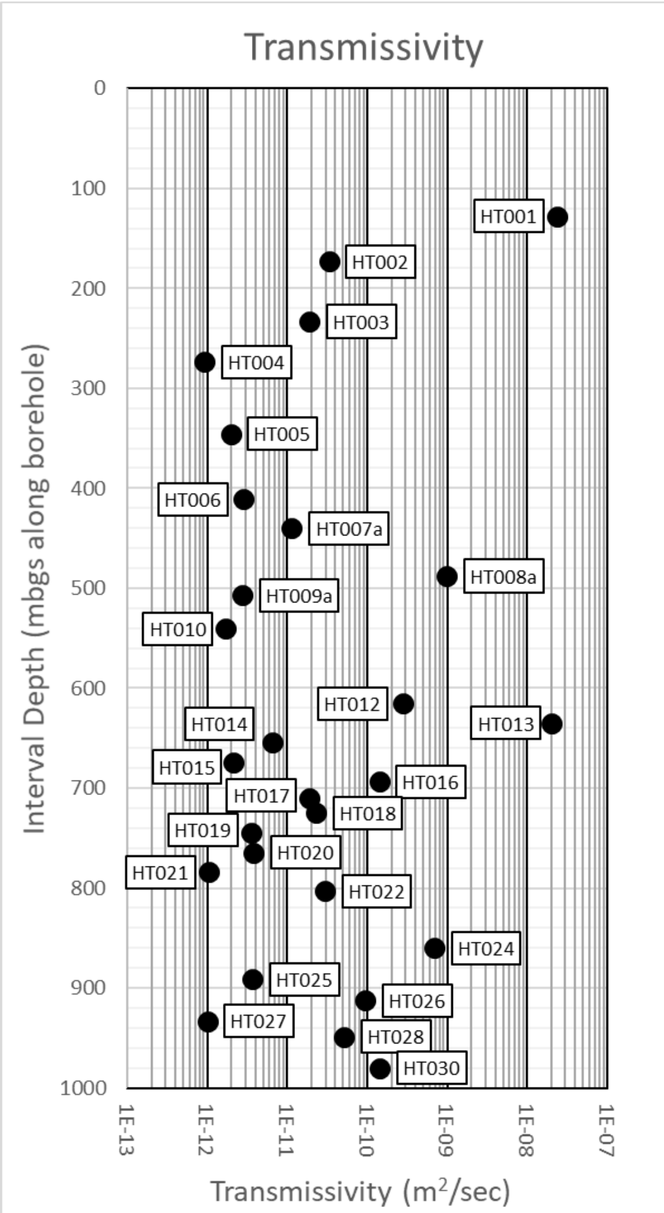

Figure 16: Transmissivity

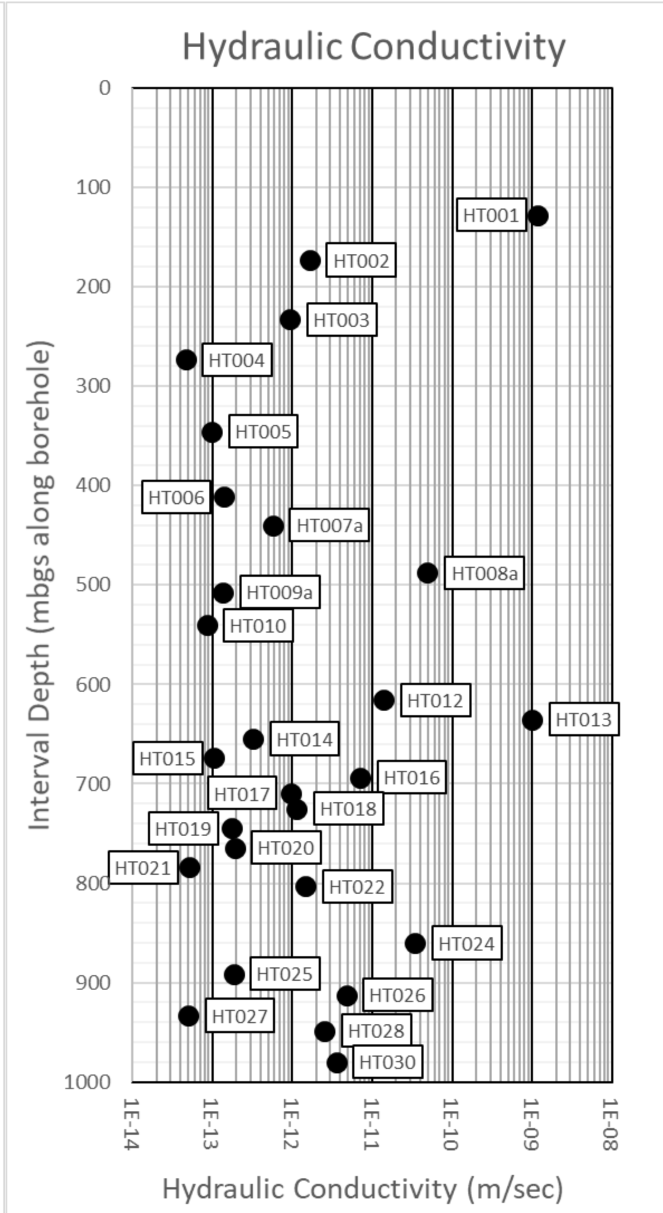

Figure 17: Hydraulic Conductivity

8.0 REFERENCES

Blackburn, C.E. and Hinz, P., 1996. Gold and base metal potential of the northwest part of the Raleigh Lake greenstone belt, northwestern Ontario-Kenora Resident Geologist's District; in Summary of Field Work and Other Activities 1996, Ontario Geological Survey, Miscellaneous Paper 166, p.113-115.

DesRoches, A., Sykes, M., Parmenter, A. and Sykes, E., 2018. Lineament Interpretation of the Revell Batholith and Surrounding Greenstone Belts (Nuclear Waste Management Organization. No. NWMO-TR-2018-19).

Enachescu, C., J-M Lavanchy, L. Ostrowski, R. Senger and J. Wozniewicz, 1997. Hydrological Investigations at Wellenberg: Hydraulic Packer Testing in Boreholes SB4a/v and SB4a/s. Methods and Field Results. NAGRA Technical Report 95-02.

Geofirma Engineering Ltd. and INTERA Inc., 2011. nSIGHTS Version 2.50 User Manual.

Golder and PGW (Paterson Grant and Watson Ltd.), 2017. Phase 2 Geoscientific Preliminary Assessment, Geological Mapping, Township of Ignace and Area, Ontario: APM-REP-01332-0225.

Golder, 2021a. Phase 2 Initial Borehole Drilling and Testing at IG_BH04/05/06, Ignace Area, WP02 Data Report – Borehole Drilling and Flushing for IG_BH04. NWMO Report Number: APM-REP-01332-0278.

Kennedy, K.G. and Davidson, L.M., 1989. Oberbauenstock (OBS) 1987: Results of the hydrogeological testing program OBS-1. – Nagra Technical Report, NTB 88-03, Nagra, Baden.

OGS (Ontario Geological Survey), 2011. 1:250 000 scale bedrock geology of Ontario, Ontario Geological Survey, Miscellaneous Release Data 126 - Revision 1.

Ostrowski, L.P., Enachescu, C., Haborth, B. and Kloska, M.B, 1992. Hydrological Investigations at Wellenberg: Hydraulic Packer Testing in Boreholes SB3, SB4 and SB6, Methods and Field Results. Nagra Technical Report, NTB 92-05; Nagra, Wettingen.

Parmenter, A., Waffle, L. and DesRoches, A., 2020. An updated bedrock geology map and geological database for the northern portion of the Revell batholith (No. NWMO-TR-2020-08). Nuclear Waste Management Organization.

SGL (Sander Geophysics Limited), 2015. Phase 2 Geoscientific Preliminary Assessment, Acquisition, Processing and Interpretation of High-Resolution Airborne Geophysical Data, Township of Ignace, Ontario. Prepared for Nuclear Waste Management Organization (NWMO). NWMO Report Number: APM-REP-06145-0002.

SRK (SRK Consulting, Inc). and Golder, 2015. Phase 2 Geoscientific Preliminary Assessment, Observation of General Geological Features, Township of Ignace, Ontario. Prepared for Nuclear Waste Management Organization. NWMO Report Number: APM-REP-06145-0004.

Stone, D., 2009. Geology of the Bending Lake Area, Northwestern Ontario; *in* Summary of Field Work and Other Activities 2009. Ontario Geological Survey. Open File Report 6240.

Stone, D., 2010a. Geology of the Stormy Lake Area, Northwestern Ontario; *in* Summary of Field Work and Other Activities 2010. Ontario Geological Survey, Open File Report 6260.

Stone, D., 2010b. Precambrian geology of the central Wabigoon Subprovince area, northwestern Ontario. Ontario Geological Survey, Open File Report 5422.

Stone, D., Halle, J. and Chaloux, E., 1998. Geology of the Ignace and Pekagoning Lake Areas, Central Wabigoon Subprovince; *in* Summary of Field Work and Other Activities 1998, Ontario Geological Survey, Misc. Paper 169.

Stone, D., Davis, D.W., Hamilton, M.A. and Falcon, A., 2010. Interpretation of 2009 Geochronology in the Central Wabigoon Subprovince and Bending Lake Areas, Northwestern Ontario, *in* Summary of Field Work and Other Activities 2010, Ontario Geological Survey, Open File Report 6260.

APPENDIX A

Equipment Photographs

Photo 1 – Packer testing tool with lower packer shown on left. Datalogger, DHSIV and upper packer shown on right.

Photo 2 – Datalogger, DHSIV and upper packer shown assembled at drill rig.

Photo 3 – Stitched photograph showing entire tool. Top of tool is shown in upper right, bottom of tool shown on lower left.

APPENDIX B

Calibration Certificates

DataCan

"The Next Generation of Down Hole Tools"

Calibration Date:	29-Mar-21	**Calibration System:**	CALIBRATION04
Max Pressure Error:	0.009% F.S.	**Batch Number:**	20210325.160414
Max Temperature Error:	0.132 °C		
Part Number:	108931		
Serial Number:	DC5192		

0.75 OD_Multi-Gauge_Piezo_Bottom_1/4 Wire_SS			
Max Pressure		Max Temperature	
psi	kPa	ºF	ºC
6,000	41,369	185	85

Accuracy: As shown in the graph below, this DataCan Pressure gauge conforms to within +/- 0.030% F.S. of the pressure standard used in calibration, which is accurate to within +/- 0.01% of reading.

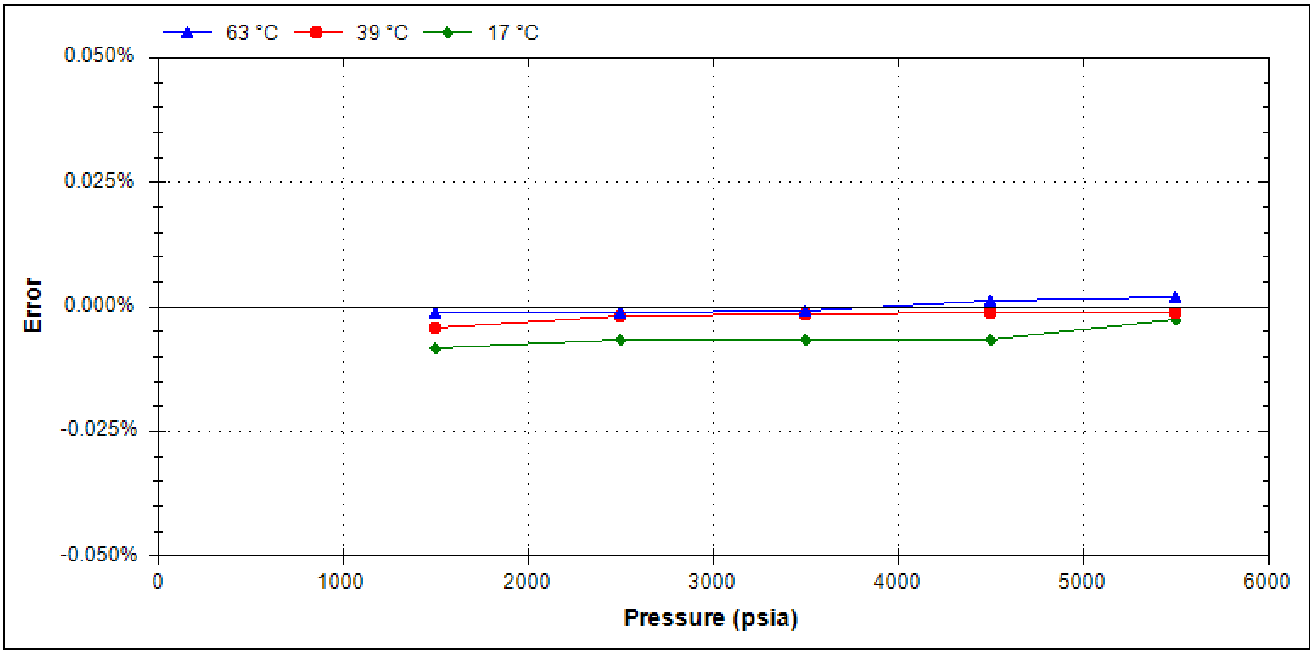

Working Standards

Sun Electronic Systems Environmental Chamber, Model: EC127, Serial: EC0180

DHI Instruments Pressure Controller, Model: PPCH-200M (30,000psi Reference), Serial: 3171

Traceability Statement

All working standards are traceable to nationally or internationally recognized standards.

Approved By:	Calibrated By:
DataCan Services Corp.	Angelo Pulido

DataCan

"The Next Generation of Down Hole Tools"

Calibration Date:	29-Mar-21	**Calibration System:**	CALIBRATION04
Max Pressure Error:	0.007% F.S.	**Batch Number:**	20210325.160414
Max Temperature Error:	0.135 °C		
Part Number:	108931		
Serial Number:	DC5193		

0.75 OD_Multi-Gauge_Piezo_Bottom_1/4 Wire_SS			
Max Pressure		Max Temperature	
psi	kPa	ºF	ºC
6,000	41,369	185	85

Accuracy: As shown in the graph below, this DataCan Pressure gauge conforms to within +/- 0.030% F.S. of the pressure standard used in calibration, which is accurate to within +/- 0.01% of reading.

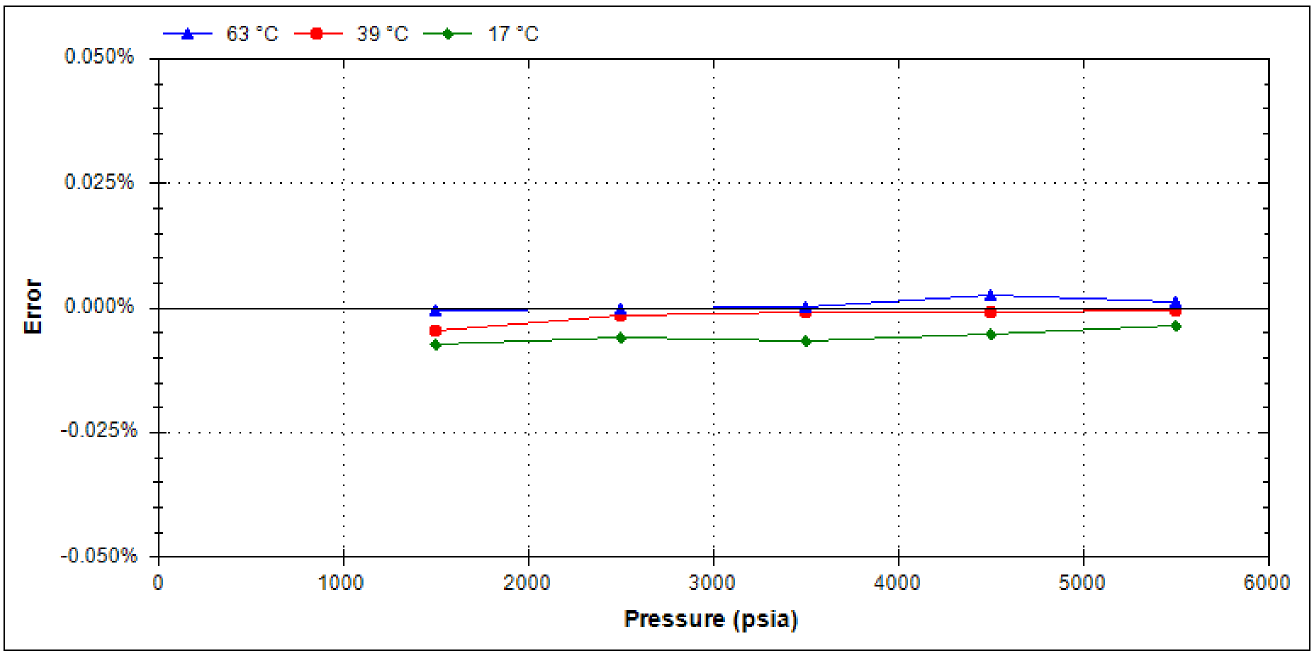

Working Standards

Sun Electronic Systems Environmental Chamber, Model: EC127, Serial: EC0180

DHI Instruments Pressure Controller, Model: PPCH-200M (30,000psi Reference), Serial: 3171

Traceability Statement

All working standards are traceable to nationally or internationally recognized standards.

Approved By:	Calibrated By:
DataCan Services Corp.	Angelo Pulido

DataCan

"The Next Generation of Down Hole Tools"

Calibration Date:	29-Mar-21	**Calibration System:**	CALIBRATION04
Max Pressure Error:	0.011% F.S.	**Batch Number:**	20210325.160414
Max Temperature Error:	0.126 °C		
Part Number:	108931		
Serial Number:	DC5194		

0.75 OD_Multi-Gauge_Piezo_Bottom_1/4 Wire_SS			
Max Pressure		Max Temperature	
psi	kPa	ºF	ºC
6,000	41,369	185	85

Accuracy: As shown in the graph below, this DataCan Pressure gauge conforms to within +/- 0.030% F.S. of the pressure standard used in calibration, which is accurate to within +/- 0.01% of reading.

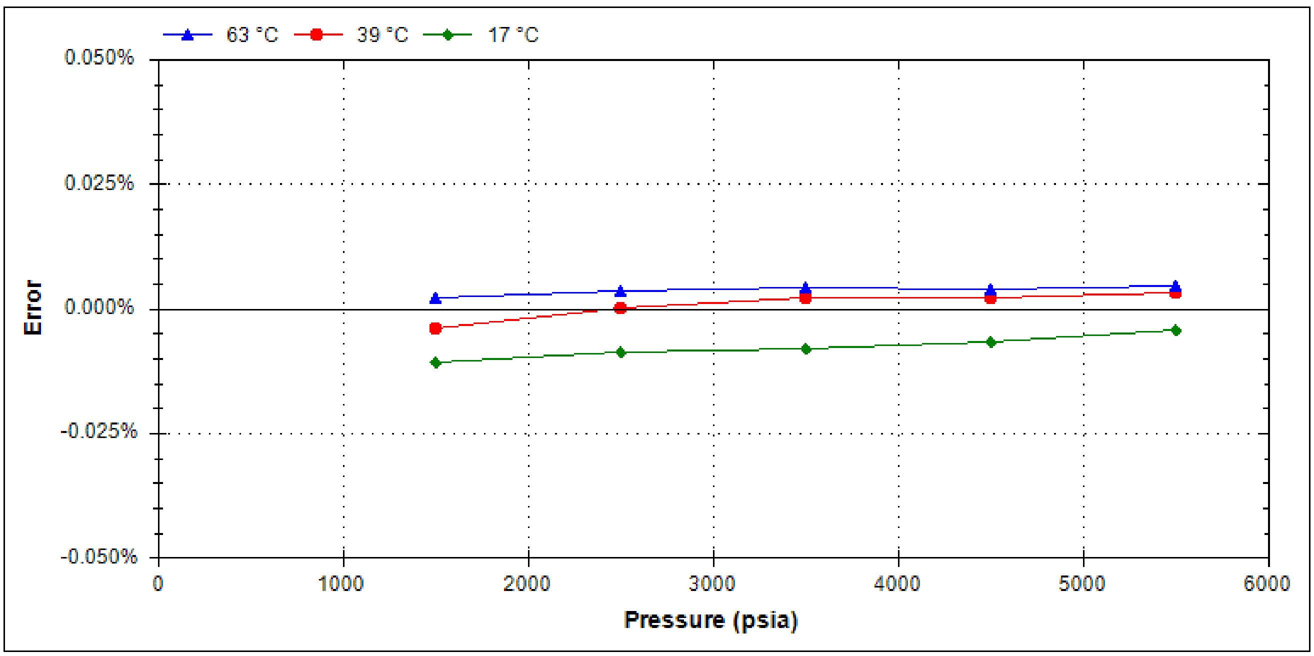

Working Standards

Sun Electronic Systems Environmental Chamber, Model: EC127, Serial: EC0180

DHI Instruments Pressure Controller, Model: PPCH-200M (30,000psi Reference), Serial: 3171

Traceability Statement

All working standards are traceable to nationally or internationally recognized standards.

Approved By:	Calibrated By:
DataCan Services Corp.	Angelo Pulido

DataCan

“The Next Generation of Down Hole Tools”

Calibration Date:	29-Mar-21	**Calibration System:**	CALIBRATION04
Max Pressure Error:	0.006% F.S.	**Batch Number:**	20210325.160414
Max Temperature Error:	0.129 °C		
Part Number:	108931		
Serial Number:	DC5195		

0.75 OD_Multi-Gauge_Piezo_Bottom_1/4 Wire_SS			
Max Pressure		Max Temperature	
psi	kPa	ºF	ºC
6,000	41,369	185	85

Accuracy: As shown in the graph below, this DataCan Pressure gauge conforms to within +/- 0.030% F.S. of the pressure standard used in calibration, which is accurate to within +/- 0.01% of reading.

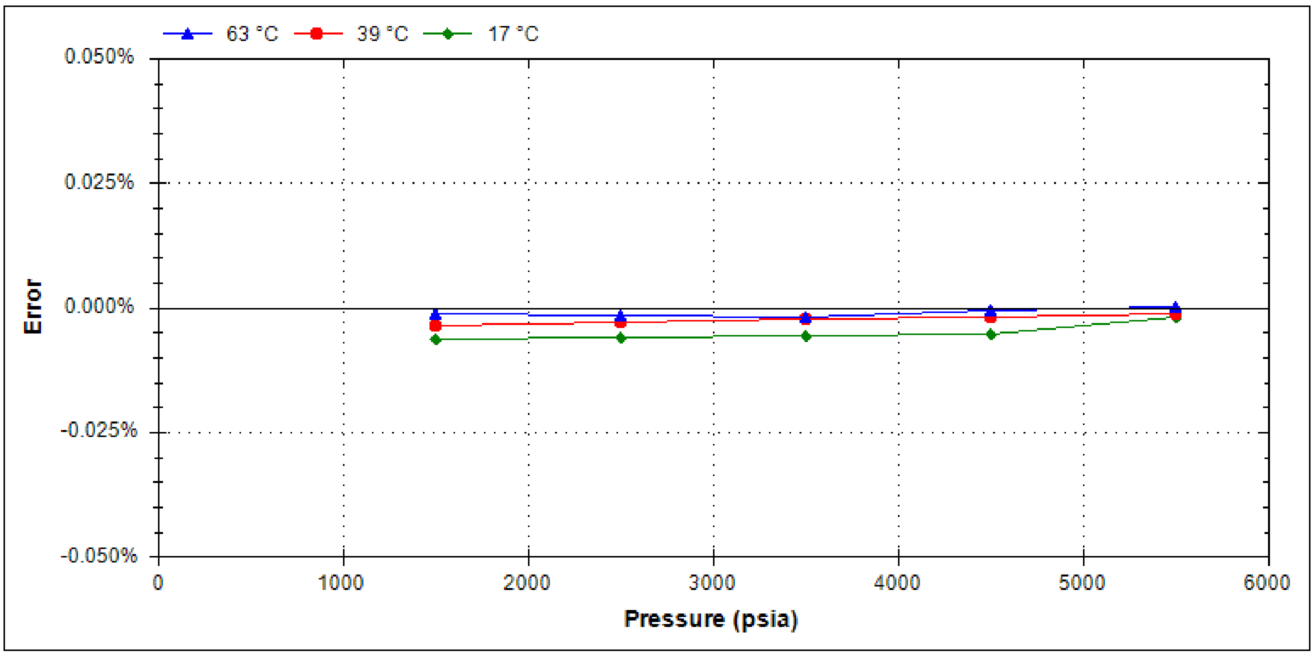

Working Standards

Sun Electronic Systems Environmental Chamber, Model: EC127, Serial: EC0180

DHI Instruments Pressure Controller, Model: PPCH-200M (30,000psi Reference), Serial: 3171

Traceability Statement

All working standards are traceable to nationally or internationally recognized standards.

Approved By:
DataCan Services Corp.

Calibrated By:
Angelo Pulido

www.wescancal.com

Wescan calibration

Wescan Calibration
9-12240 Horseshoe Way
Richmond, BC V7A 4X9

Cert # 1500.02

CERTIFICATE OF CALIBRATION

Description	PRESSURE GAUGE, DIGITAL	**Work Order**	R0920140
Model Number	DPG4000	**Serial Number**	4645403
Instrument Id	N/A	**Cal Procedure**	33K6-4-314-1
Manufacturer	OMEGA	**Cal Date**	26 Mar 2021
Customer Name	GOLDER ASSOCIATES LTD.	**Recall Cycle**	52 Weeks
	300 - 3811 NORTH FRASER WAY	**Next Cal Date**	26 Mar 2022
	BURNABY, BC V5J 5J2	**Purchase Order**	PENDING

Calibration Environment: Temperature 21.0 °C Relative Humidity 35.0 %RH

Received Condition: Not Within Tolerance

Completed Condition: Within Tolerance

Remarks: Adjusted

Standards Used to Establish Traceability

Instrument Type	Model	Asset #	Cal Due Date
PRESSURE CALIBRATOR	6270A/PM600-A7M/P	102018	28 Feb 2022

Wescan certifies that, at the time of calibration, the above listed instrument meets or exceeds all of the specifications defined on the Test Data Sheet (TDS), otherwise indicated. The Certificate received and completed conditions and the TDS specifications are based on the procedure(s) and/or specification(s) referenced on the TDS unless otherwise indicated. Any statement of compliance is made without taking measurement uncertainty into account and is based on the instrument's performance against the test limits documented on the test data sheet.

Wescan has been independently assessed and accredited to ISO/IEC 17025:2017. The above listed instrument has been calibrated using standards that are traceable to the International System of Units (SI) through a National Metrological Institute (such as NRC or NIST) and in compliance with ISO/IEC 17025:2017. The reported expanded uncertainty is a normal distribution with a coverage factor of K=2, corresponding to a coverage of approximately 95% and conforms with the recommendations of the ISO Guide to the Expression of Uncertainty in Measurement. This certificate may contain data that is not included in the Scope of Accreditation or where measurement uncertainty is not applicable. Unaccredited results, including uncertainties reported as N/A, and functional or binary (such as Pass / Fail, True / False) are clearly defined within the test data.

Test data As Found and Final (as left) results are the same unless reported otherwise. Certificate remarks identify if adjustments were performed.

Metrologist : *R007* Quality Assurance: *R001* Date of Issue: 26 Mar 2021

Wescan calibration

Calibration procedure	**33K6-4-314-1**
Item type	**Pressure gauge**
Range	**2000.0 psi**
Accuracy	**0.05 % of full scale**
Test item resolution	**0.1 psi**

Note: this data sheet applies to calibrations where the standard is set to an exact gauge marking

As found

	Nominal	Standard	Lower limit	Test item	Upper limit	% limits used	Uncertainty	TUR if<4:1
	% of range	psi	psi	psi	psi		psi	
increasing	10%	200.000	199.000	199.7	201.000	-30.0%	0.065	
	20%	400.000	399.000	399.6	401.000	-40.0%	0.070	
	30%	600.000	599.000	599.4	601.000	-60.0%	0.083	
	40%	800.000	799.000	799.3	801.000	-70.0%	0.099	
	50%	1000.000	999.000	999.3	1001.000	-70.0%	0.12	
	60%	1200.000	1199.000	1199.2	1201.000	-80.0%	0.13	
	70%	1400.000	1399.000	1399.2	1401.000	-80.0%	0.15	
	80%	1600.000	1599.000	1599.1	1601.000	-90.0%	0.17	
	90%	1800.000	1799.000	1798.9	1801.000	-110.0%	0.19	
	100%	2000.000	1999.000	1998.8	2001.000	-120.0%	0.21	
decreasing	90%	1800.000	1799.000	1799.0	1801.000	-100.0%	0.19	
	80%	1600.000	1599.000	1599.2	1601.000	-80.0%	0.17	
	70%	1400.000	1399.000	1399.3	1401.000	-70.0%	0.15	
	60%	1200.000	1199.000	1199.3	1201.000	-70.0%	0.13	
	50%	1000.000	999.000	999.4	1001.000	-60.0%	0.12	
	40%	800.000	799.000	799.3	801.000	-70.0%	0.099	
	30%	600.000	599.000	599.4	601.000	-60.0%	0.083	
	20%	400.000	399.000	399.6	401.000	-40.0%	0.070	
	10%	200.000	199.000	199.8	201.000	-20.0%	0.065	

As left

	Nominal	Standard	Lower limit	Test item	Upper limit	% limits used	Uncertainty	TUR if<4:1
	% of range	psi	psi	psi	psi		psi	
increasing	10%	200.000	199.000	200.0	201.000	0.0%	0.065	
	20%	400.000	399.000	399.9	401.000	-10.0%	0.070	
	30%	600.000	599.000	599.9	601.000	-10.0%	0.083	
	40%	800.000	799.000	799.9	801.000	-10.0%	0.099	
	50%	1000.000	999.000	1000.0	1001.000	0.0%	0.12	
	60%	1200.000	1199.000	1199.9	1201.000	-10.0%	0.13	
	70%	1400.000	1399.000	1399.9	1401.000	-10.0%	0.15	
	80%	1600.000	1599.000	1599.9	1601.000	-10.0%	0.17	
	90%	1800.000	1799.000	1799.9	1801.000	-10.0%	0.19	
	100%	2000.000	1999.000	2000.0	2001.000	0.0%	0.21	
decreasing	90%	1800.000	1799.000	1800.0	1801.000	0.0%	0.19	
	80%	1600.000	1599.000	1599.9	1601.000	-10.0%	0.17	
	70%	1400.000	1399.000	1399.9	1401.000	-10.0%	0.15	
	60%	1200.000	1199.000	1199.9	1201.000	-10.0%	0.13	
	50%	1000.000	999.000	1000.0	1001.000	0.0%	0.12	
	40%	800.000	799.000	800.0	801.000	0.0%	0.099	
	30%	600.000	599.000	600.0	601.000	0.0%	0.083	
	20%	400.000	399.000	400.0	401.000	0.0%	0.070	
	10%	200.000	199.000	200.0	201.000	0.0%	0.065	

End of calibration data

Highlighted data are outside acceptance limits

CALIBRATION REPORT

Instrument type	Memory Gauge		
Calibration Date	2020-09-02	Due date:	2021-09-02
Model Number	LevelTroll 700		
Pressure Range	1000 PSI		
Manufacturer	In-Situ Inc.		
Serial number	373153		

Pressure Test Data Sheet

Applied Pressure (PSI)	Reported Pressure (PSI)	Deviation (PSI)	FS Error %
0.5	0.503	0.0	0.00
103.5	103.600	0.1	0.01
202.4	202.300	-0.1	-0.01
307.1	307.200	0.1	0.01
405.0	405.200	0.2	0.02
502.0	502.500	0.5	0.05
599.0	599.600	0.6	0.06
700.0	700.800	0.8	0.08
816.4	817.200	0.8	0.08
903.0	903.770	0.8	0.08
998.3	999.400	1.1	0.11
	Maximum Value:	1.10	0.11

End of calibration data

Performed by	A.Brugger

Calibration and Equipment used:

Instrument type	DPG4000-2K
Calibration Date	2019-06-24
Manufacturer	Omega

Equipment used is traceable to the National Institute of Standards and Technology

Pressure Range:	0-2000 psi
Accuracy	+/- 0.1%
Serial Number	4645403

Pioneer Petrotech Services Inc.
#1, 1431 - 40 Ave. NE
Calgary, AB, Canada, T2E 8N6
Tel: +1 (403)282-7669
Fax: +1 (403)282-0509
www.pioneerps.com

Calibration Certificate

Model:	**PPS25**	**Pressure Range:**	**6,000 psi**
Serial Number:	**5231**	**Calibration Date:**	**Apr 07, 2021**

Specifications

Pressure Range:	Minimum:	13 psia	Maximum:	6,000 psia
Temperature Range:	Minimum:	0 °C	Maximum:	150 °C
Pressure Accuracy:			±	0.03 %F.S.
Temperature Accuracy:			±	0.5 °C
Housing Material:				SS 17-4
Housing OD				0.75"

Calibration Summary

Calibration Pressure Range:	Minimum:	15.03 psia	Maximum:	6,001 psia
Calibration Temperature Range:	Minimum:	0.77 °C	Maximum:	151 °C
Pressure Accuracy (Maximum Error):			–	1.70 psi
Temperature Accuracy (Maximum Error):			–	0.26 °C

Working Standards

Pressure: Fluke DH Instruments piston-cylinder, 30kpsi (±0.01% of reading)
Temperature: Fluke Hart Scientific RTD (±0.05°C)

Traceability Statement

All working standards are traceable to nationally or internationally recognized standards.

Lucy

Pioneer Petrotech Services Inc.

Apr 30, 2021
Date

Instrument:

Manufacturer:	Solinst Canada
Product:	3001 LT Barologger
Model Number:	M1.5
Serial Number:	2110133
Pressure Range:	0-1.5 m H20
Resolution:	0.03 mm H20
Temperature Range:	-20 - +80 °C
Temperature Resolution:	0.003 °C

Method of Calibration:

The Levelogger is calibrated against a range of set reference points, with units of pressure in pounds per square inch. The conversion factor for pounds per square inch relates to pressure in bars and meters of water column is as follows: 1 pound per square inch = 0.0689476 bar = 0.703070 m H20 @ 4°C.

During the calibration procedure, the Levelogger is fully submerged in a highly accurate water bath, set to 6°C. The pressure is then calibrated to six separate pressure points covering the entire range for that particular Levelogger, to check for any non-linearity. This process is repeated at 18°C and then 36°C to check for temperature effects. The Levelogger is approved after all specifications for accuracy, precision, stability and hysteresis have been met.

Traceability:

Pressure standard: ISO/IEC 17025:2005, ANSI/NCSL Z540-1-1994, NIST
Temperature standard: ISO/IEC 17025:2005, NVLAP LAB CODE: 200348-0

Uncertainty:

The standard deviation of the temperature was calculated from the contributions of uncertainties originating from the measurement standard, the bath homogeneity, and from any short term contribution from the instrument being calibrated. The standard deviation of the pressure was calculated from the contributions of the uncertainties originating from the measurement standard, any short term contribution from the instrument, and the uncertainty resulting from the uncertainty in temperature compensation. The reported uncertainty is stated as the standard deviation mutliplied by a factor of two.

For further information, please contact: Solinst Canada Ltd.
35 Todd Road, Georgetown, Ontario, Canada L7G 4R8 E-mail: instruments@solinst.com
Fax: +1 (905) 873-1992; (800) 516-9081 Tel: +1 (905) 873-2255; (800) 661-2023 Web Site: www.solinst.com

Serial Number: 2110133 Model Number: M1.5

Test Results:

Calibration Date: 8/2/2019

Pressure Tests

Pressure	Reading (6 °C)	Level	Reading	Error (%FS)
12.5 psi	12.4995 psi	-0.7116 m	-0.7120 m	0.003%
13.2 psi	13.1496 psi	-0.2546 m	-0.2549 m	0.003%
13.8 psi	13.8005 psi	0.2024 m	0.2027 m	-0.003%
14.5 psi	14.4496 psi	0.6594 m	0.6591 m	0.003%
15.1 psi	15.0996 psi	1.1164 m	1.1161 m	0.003%
15.8 psi	15.7503 psi	1.5734 m	1.5736 m	-0.002%

Hysteresis:

Standard Deviation: 0.0028%

Temperature Tests

Temperature	Reading	Error (%FS)
6 ºC	5.9997 ºC	0.000%
18 ºC	17.9998 ºC	0.000%
36 ºC	35.9998 ºC	0.000%

Standard Deviation: 0.0001%

Conclusion: This instrument fulfils the specifications

Uncertainty temperature standard: 0.003 ºC

Overall uncertainty temperature: ±1.002

Uncertainty pressure standard: <0.003%

Overall uncertainty pressure: 0.01%

Calibration Manager: Ken Shah

For further information, please contact: Solinst Canada Ltd.
35 Todd Road, Georgetown, Ontario, Canada L7G 4R8 E-mail: instruments@solinst.com
Fax: +1 (905) 873-1992; (800) 516-9081 Tel: +1 (905) 873-2255; (800) 661-2023 Web Site: www.solinst.com

Solinst®

Levelogger Edge Calibration Report

Instrument:

Manufacturer:	Solinst Canada
Product:	3001 LT Barologger
Model Number:	M1.5
Serial Number:	2110146
Pressure Range:	0-1.5 m H20
Resolution:	0.03 mm H20
Temperature Range:	-20 - +80 °C
Temperature Resolution:	0.003 °C

Method of Calibration:

The Levelogger is calibrated against a range of set reference points, with units of pressure in pounds per square inch. The conversion factor for pounds per square inch relates to pressure in bars and meters of water column is as follows: 1 pound per square inch = 0.0689476 bar = 0.703070 m H20 @ 4°C.

During the calibration procedure, the Levelogger is fully submerged in a highly accurate water bath, set to 6°C. The pressure is then calibrated to six separate pressure points covering the entire range for that particular Levelogger, to check for any non-linearity. This process is repeated at 18°C and then 36°C to check for temperature effects. The Levelogger is approved after all specifications for accuracy, precision, stability and hysteresis have been met.

Traceability:

Pressure standard: ISO/IEC 17025:2005, ANSI/NCSL Z540-1-1994, NIST
Temperature standard: ISO/IEC 17025:2005, NVLAP LAB CODE: 200348-0

Uncertainty:

The standard deviation of the temperature was calculated from the contributions of uncertainties originating from the measurement standard, the bath homogeneity, and from any short term contribution from the instrument being calibrated. The standard deviation of the pressure was calculated from the contributions of the uncertainties originating from the measurement standard, any short term contribution from the instrument, and the uncertainty resulting from the uncertainty in temperature compensation. The reported uncertainty is stated as the standard deviation mutliplied by a factor of two.

For further information, please contact: Solinst Canada Ltd.
35 Todd Road, Georgetown, Ontario, Canada L7G 4R8 E-mail: instruments@solinst.com
Fax: +1 (905) 873-1992; (800) 516-9081 Tel: +1 (905) 873-2255; (800) 661-2023 Web Site: www.solinst.com

Serial Number: 2110146 Model Number: M1.5

Test Results:

Calibration Date: 8/2/2019

Pressure Tests

Pressure	Reading (6 ºC)	Level	Reading	Error (%FS)
12.5 psi	12.5006 psi	-0.7116 m	-0.7112 m	-0.004%
13.2 psi	13.1506 psi	-0.2546 m	-0.2542 m	-0.004%
13.8 psi	13.8005 psi	0.2024 m	0.2027 m	-0.003%
14.5 psi	14.4504 psi	0.6594 m	0.6596 m	-0.002%
15.1 psi	15.0995 psi	1.1164 m	1.1160 m	0.003%
15.8 psi	15.7502 psi	1.5734 m	1.5735 m	-0.002%

Hysteresis:

Standard Deviation: 0.0027%

Temperature Tests

Temperature	Reading	Error (%FS)
6 ºC	5.9997 ºC	0.000%
18 ºC	17.9997 ºC	0.000%
36 ºC	35.9998 ºC	0.000%

Standard Deviation: 0.0001%

Conclusion: This instrument fulfils the specifications

Uncertainty temperature standard: 0.003 ºC

Overall uncertainty temperature: ±1.002

Uncertainty pressure standard: <0.003%

Overall uncertainty pressure: 0.01%

Calibration Manager: Ken Shah

For further information, please contact: Solinst Canada Ltd.
35 Todd Road, Georgetown, Ontario, Canada L7G 4R8 E-mail: instruments@solinst.com
Fax: +1 (905) 873-1992; (800) 516-9081 Tel: +1 (905) 873-2255; (800) 661-2023 Web Site: www.solinst.com

Solinst®

APPENDIX C

Test Results

1.0 HT001 (117.75 – 137.78 M)

HT001 was selected to test a shallow fractured interval. 37 broken fractures were observed in the core. No drill fluid parameter triggers were reached during drilling. No indication of flow was recorded during FFEC logging post-drilling.

The test was initiated with a shut-in pressure recovery phase (PSR). A pulse withdrawal test (PW) with a shut-in recovery followed by a slug withdrawal (SW) phase was completed after the PSR phase.

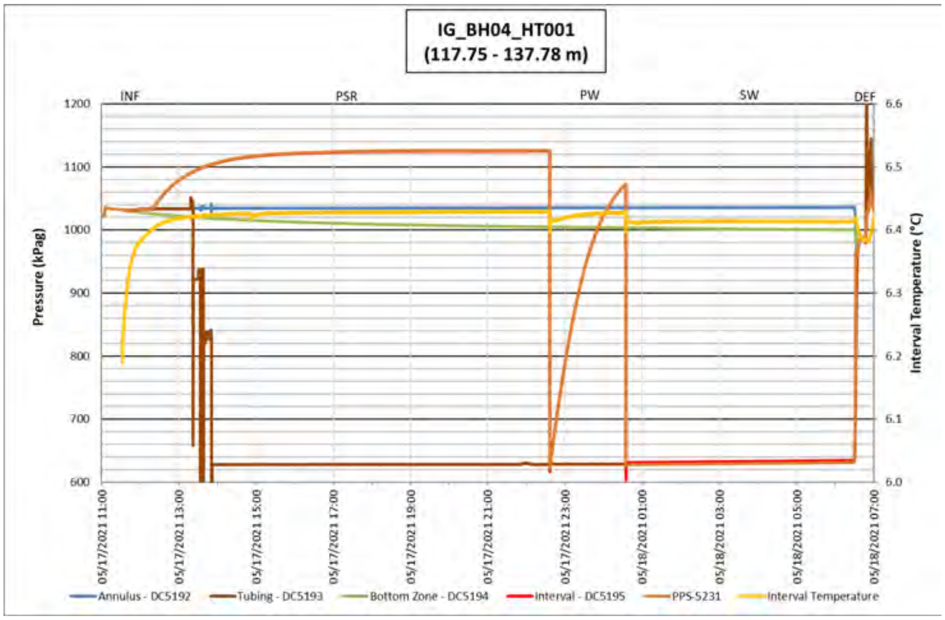

Figure 1: HT001 Annotated test plot showing monitored zone pressure and interval temperature.

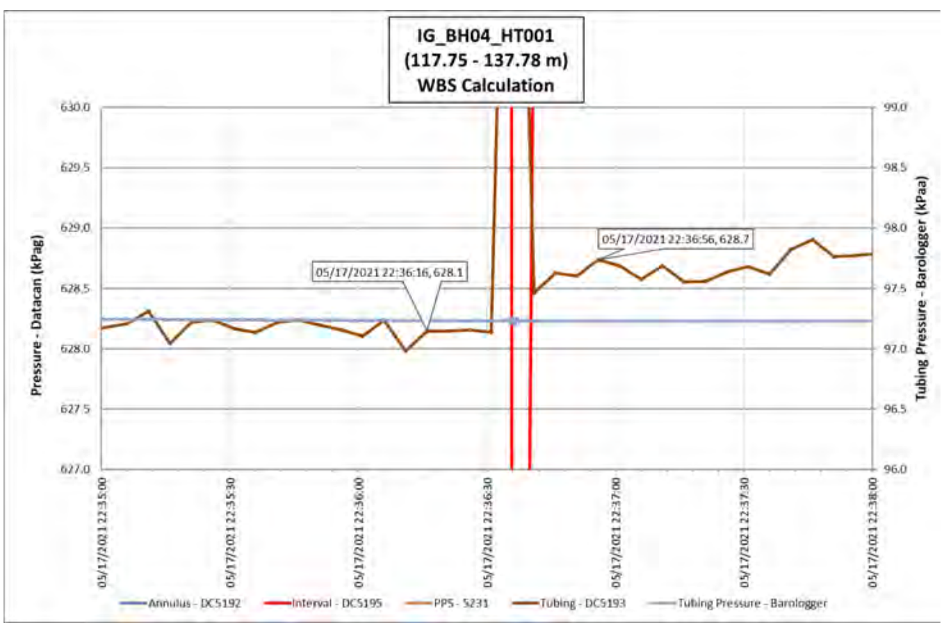

Figure 2: HT001 Tubing pressure during DHSIV activation. DHSIV Closed Wellbore Storage Estimate = 2E-10 m3/Pa

Table 1: Summary of Analysis Results – HT001

	Formation conductivity	Skin zone conductivity	Static formation pressure	Formation specific storage	Radial thickness of skin	Flow dimension
	[m/s]	[m/s]	[kPa]	[1/m]	[m]	[–]
Best Fit	1.2E-09	3.7E-14	1162	4.1E-08	3.8E-04	2.9
Minimum	4.2E-12	1.0E-14	1107	1.0E-09	1.0E-04	1.0
Maximum	9.0E-09	1.9E-12	1198	9.3E-06	3.0E-02	3.0
Mean	1.2E-09	4.1E-13	1163	5.6E-07	4.3E-03	2.2
Median	3.4E-10	2.9E-13	1164	4.5E-08	2.8E-03	2.2
Geometric mean	3.6E-10	2.4E-13	1163	4.3E-08	2.4E-03	2.2

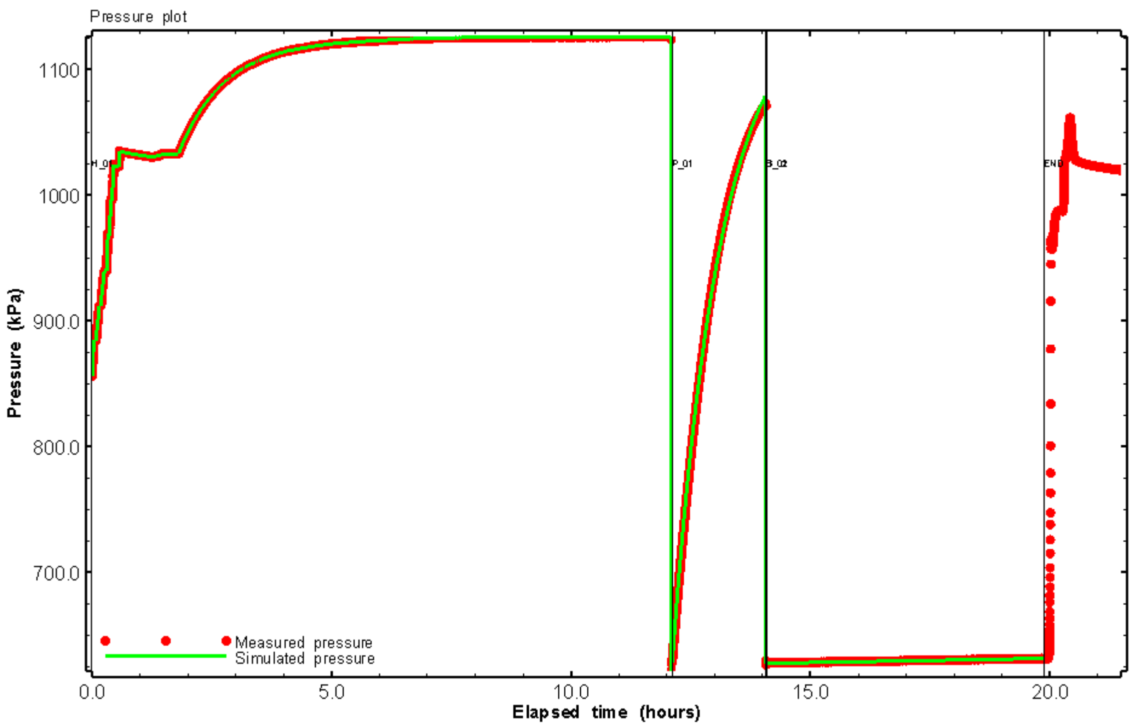

Figure 3: HT001 Pressure plot showing best-fit simulation and best fit results

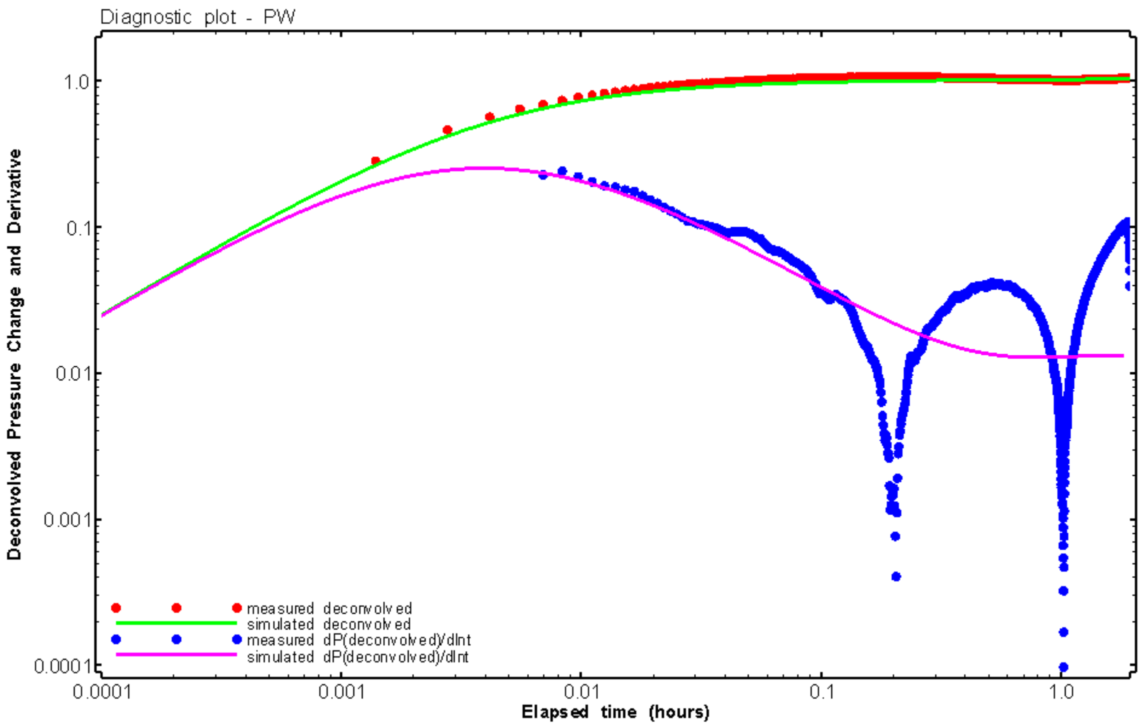

Figure 4: HT001 Deconvolved pressure change and derivative plot of the PW sequence showing best-fit simulation

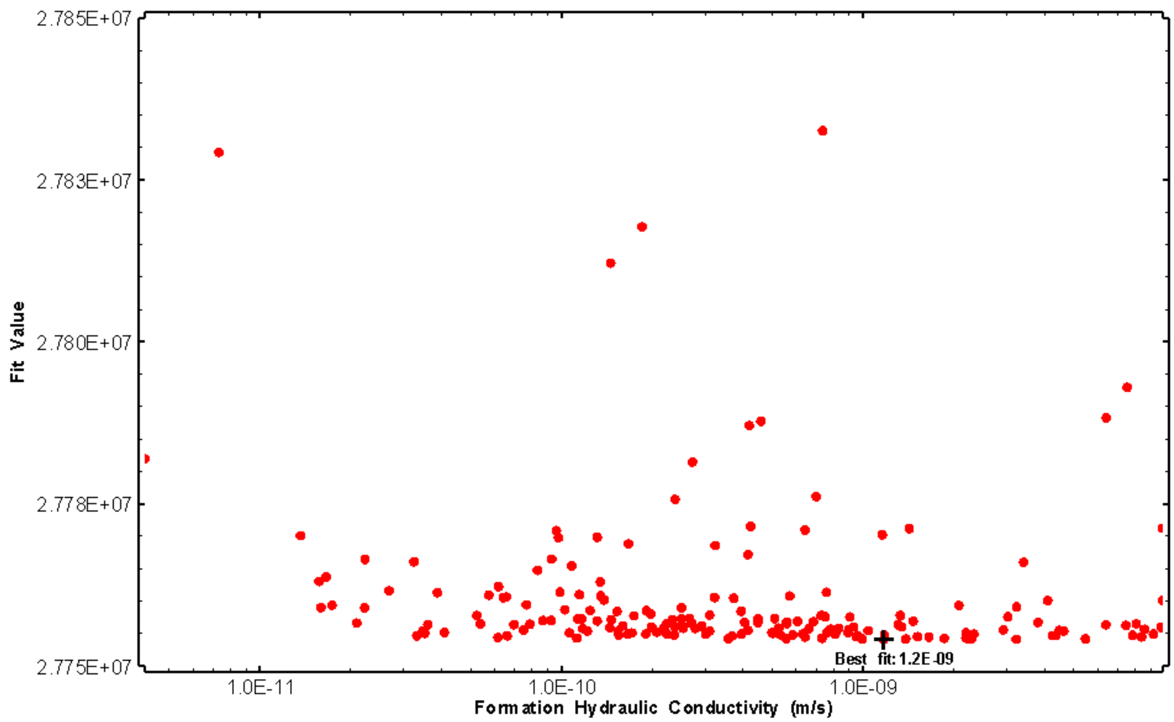

Figure 5: HT001 XY-scatter plot of formation hydraulic conductivity vs. fit value

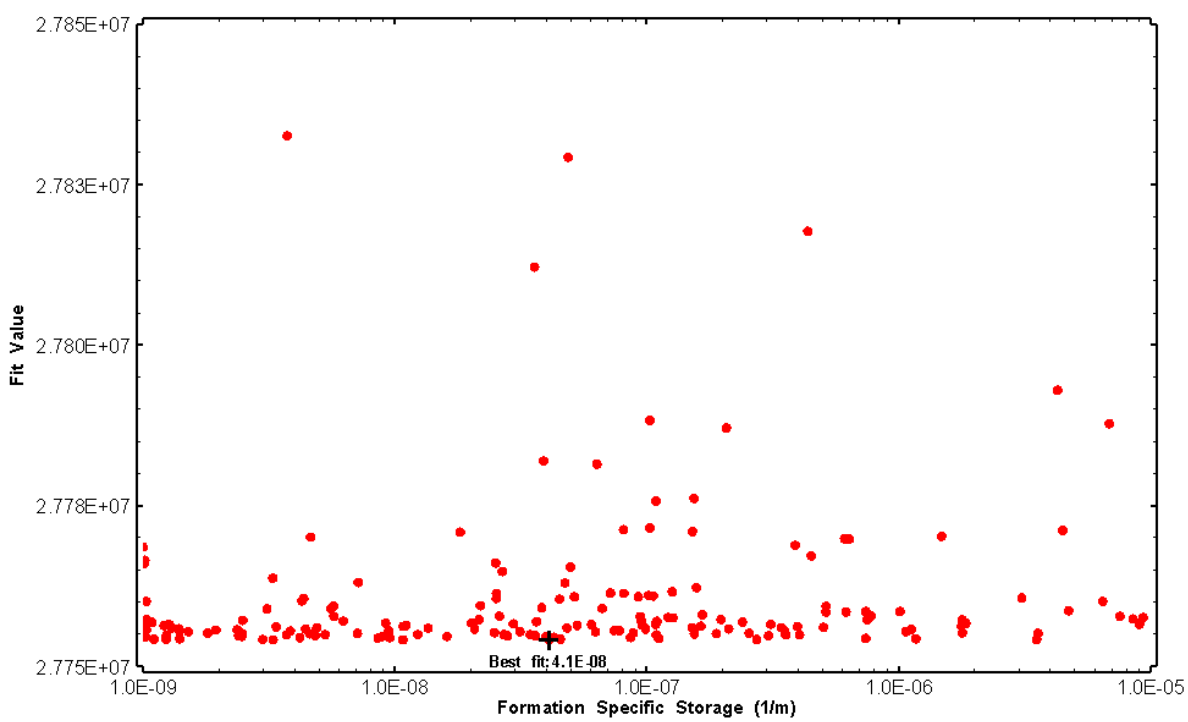

Figure 6: HT001 XY-scatter plot of formation specific storage vs. fit value

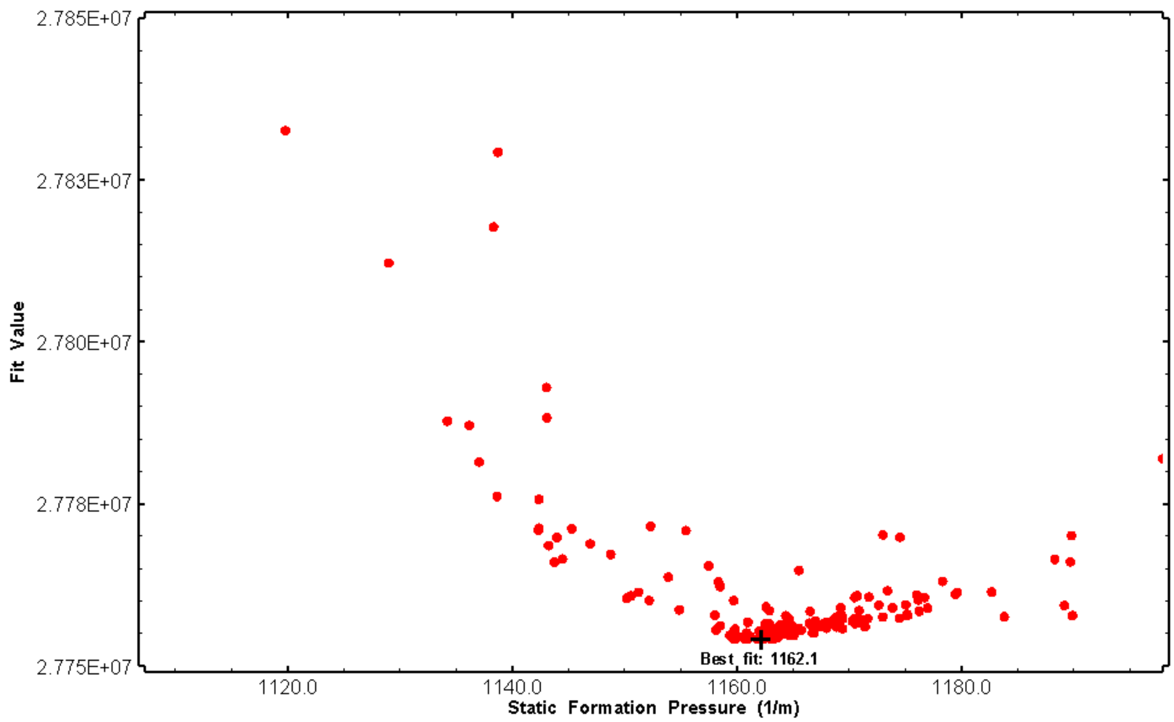

Figure 7: HT001 XY-scatter plot of static formation pressure vs. fit value

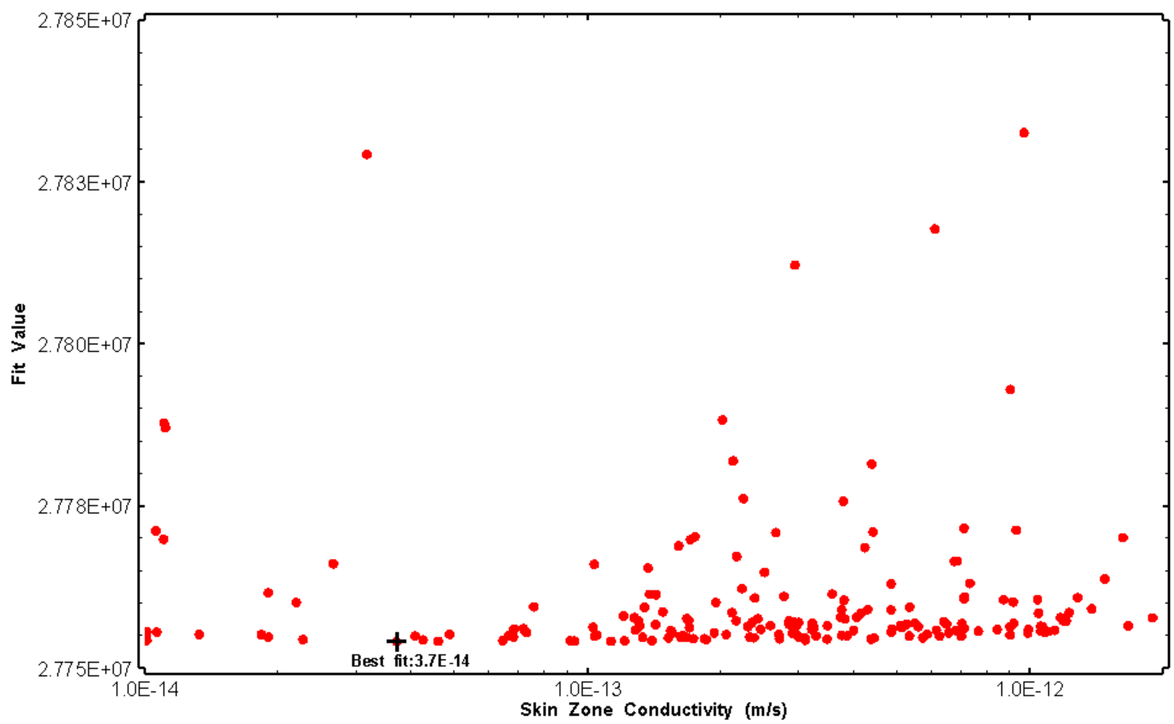

Figure 8: HT001 XY-scatter plot of skin zone conductivity vs. fit value

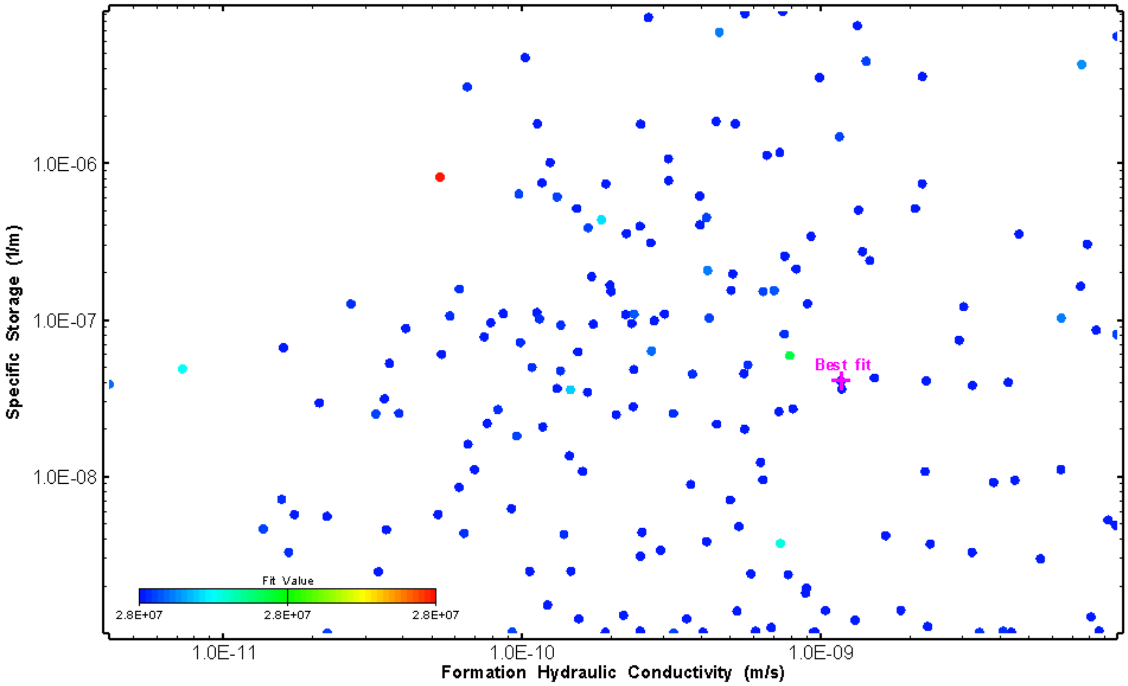

Figure 9: HT001 XY-scatter plot showing estimates of formation hydraulic conductivity and specific storage from perturbation analysis

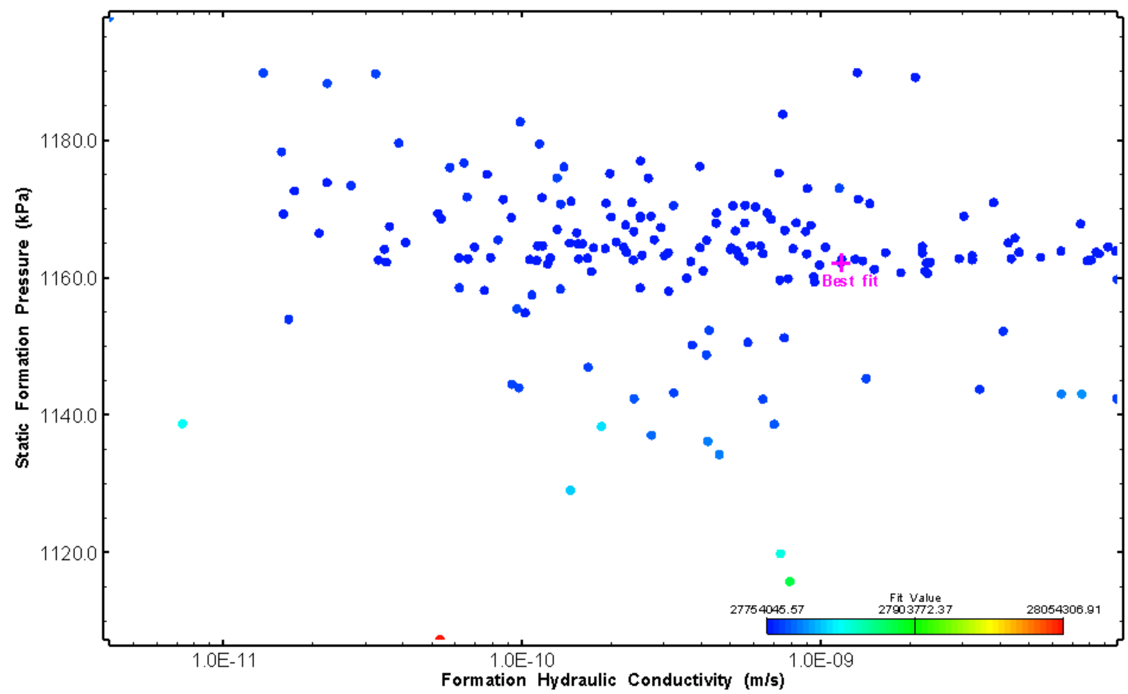

Figure 10: HT001 XY-scatter plot showing estimates of formation hydraulic conductivity and static formation pressure from perturbation analysis

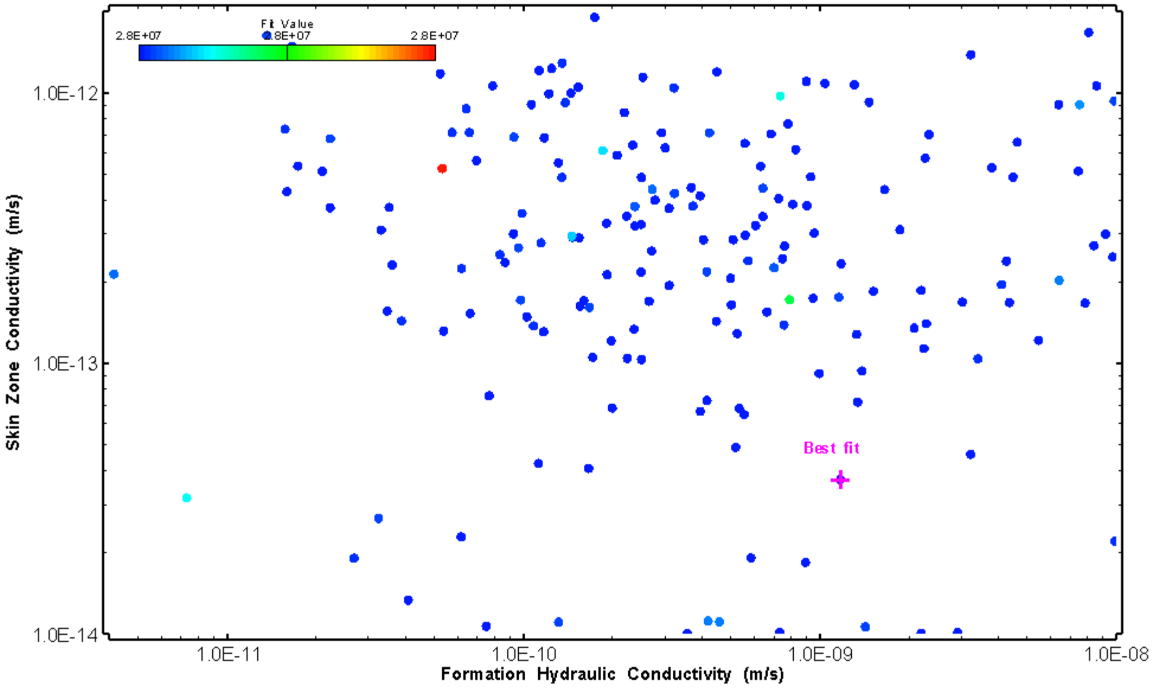

Figure 11: HT001 XY-scatter plot showing estimates of formation hydraulic conductivity and skin zone conductivity from perturbation analysis

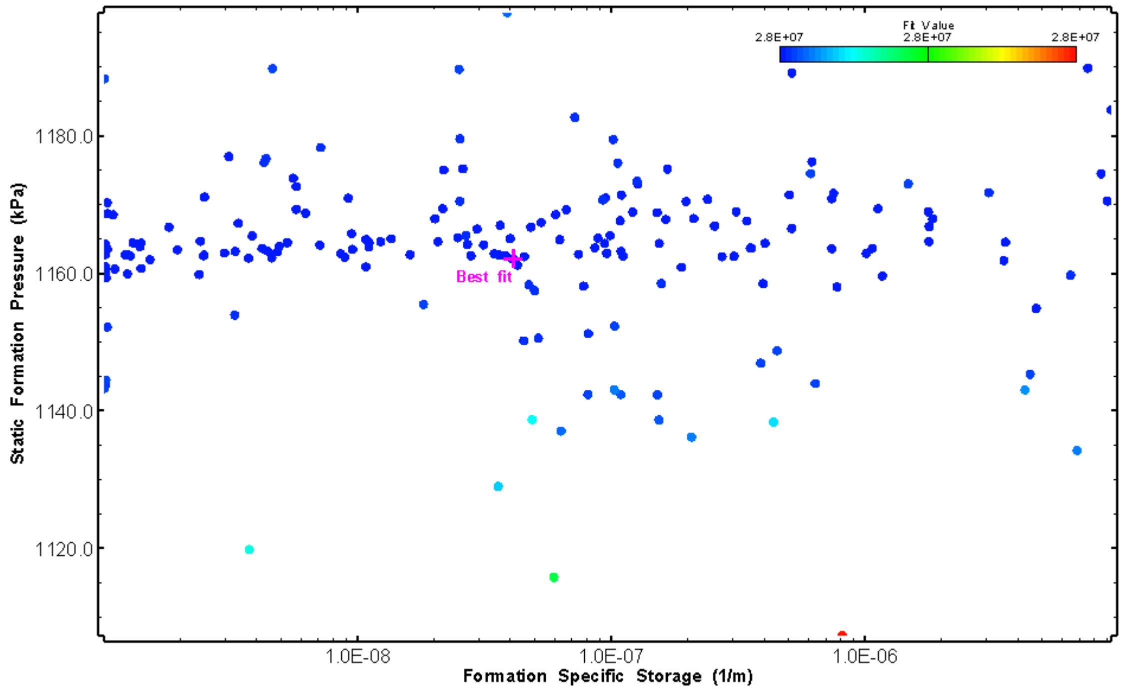

Figure 12: HT001 XY-scatter plot showing estimates of specific storage and static formation pressure from perturbation analysis

2.0 HT002 (163.15 – 183.18 M)

HT002 was selected to test a shallow fractured interval. Nine broken fractures were observed in the core. No drill fluid parameter triggers were reached during drilling. A slight indication of flow was recorded during FFEC logging post-drilling.

The test was initiated with a shut-in pressure recovery phase (PSR). A pulse withdrawal test (PW) with a shut-in recovery was completed after the PSR phase.

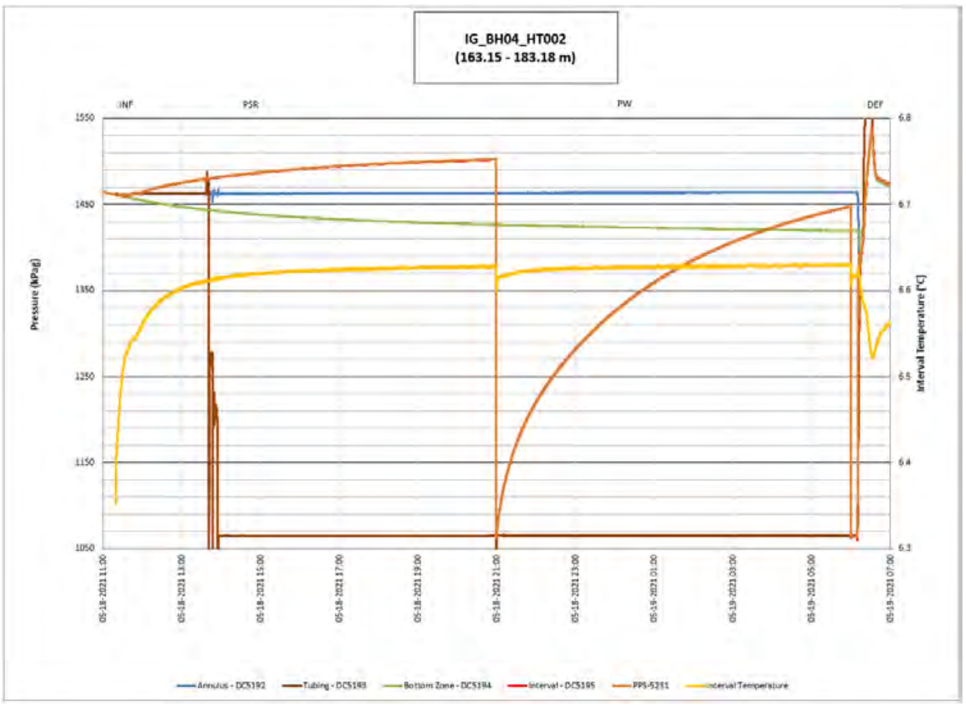

Figure 13: HT002 Annotated test plot showing monitored zone pressure and interval temperature.

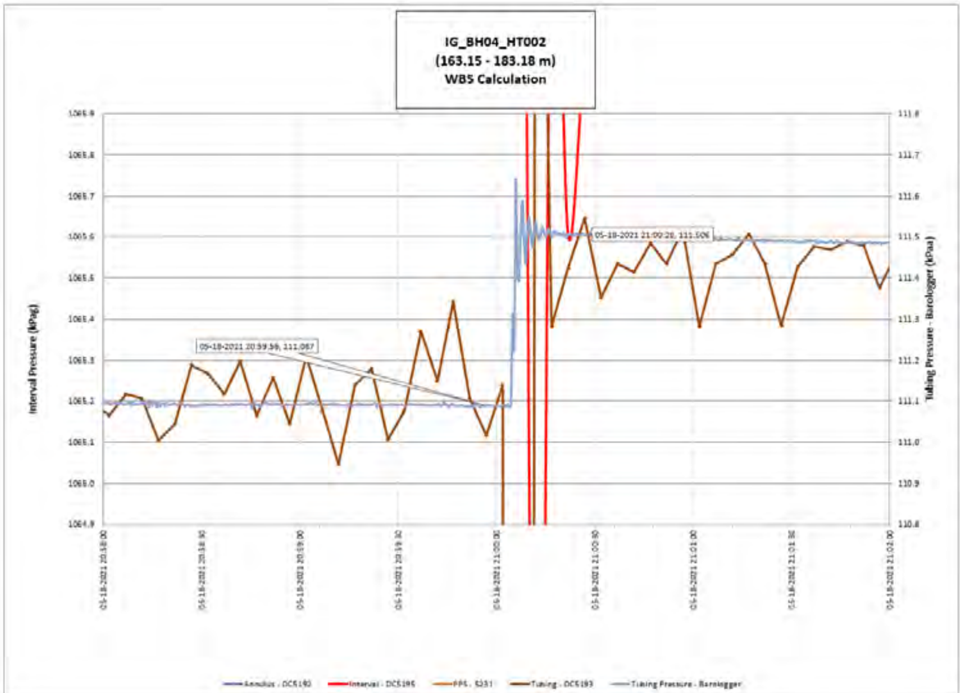

Figure 14: HT002 Tubing pressure during DHSIV activation. DHSIV Closed Wellbore Storage Estimate = 2E-10 m^3/Pa

Table 2: Summary of Analysis Results – HT002

	Formation conductivity	Skin zone conductivity	Static formation pressure	Formation specific storage	Radial thickness of skin	Flow dimension
	[m/s]	[m/s]	[kPa]	[1/m]	[m]	[–]
Best Fit	1.7E-12	2.7E-12	1509	4.2E-09	2.0E-01	2.4
Minimum	3.2E-13	1.7E-13	1496	1.0E-09	1.0E-03	1.3
Maximum	9.9E-11	9.9E-11	1600	8.4E-06	9.8E-01	3.0
Mean	7.9E-12	1.6E-11	1554	5.9E-07	1.8E-01	2.0
Median	2.2E-12	5.8E-12	1555	1.5E-07	6.2E-02	1.9
Geometric mean	2.9E-12	6.6E-12	1554	1.3E-07	4.0E-02	2.0

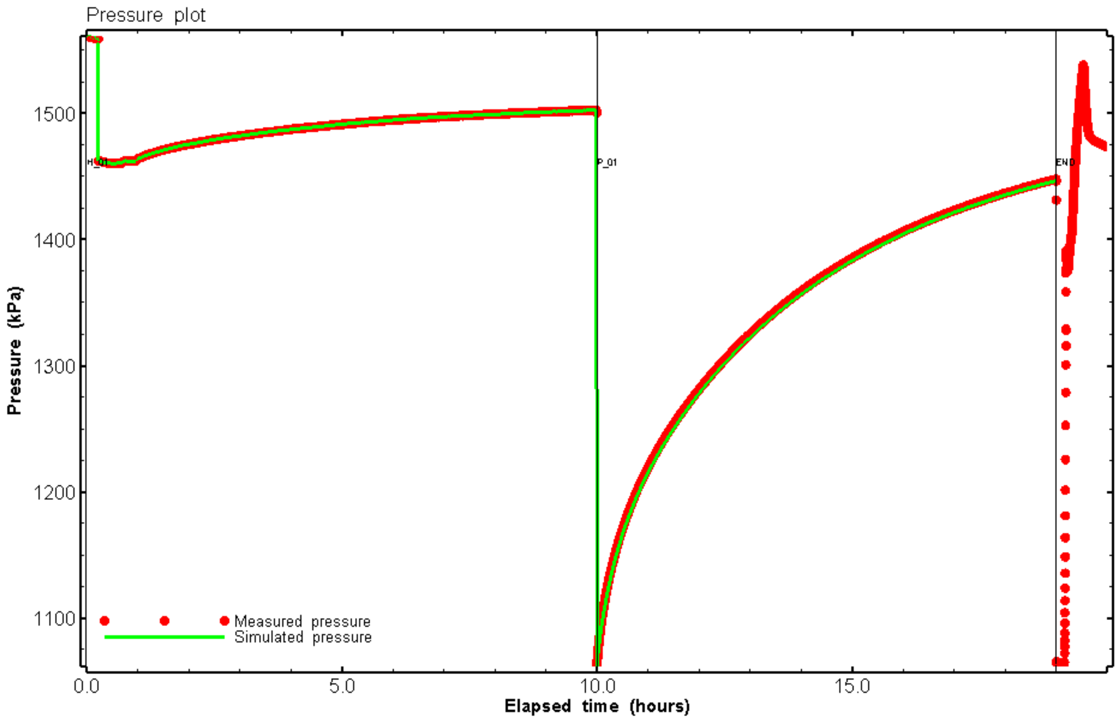

Figure 15: HT002 Pressure plot showing best-fit simulation and best fit results

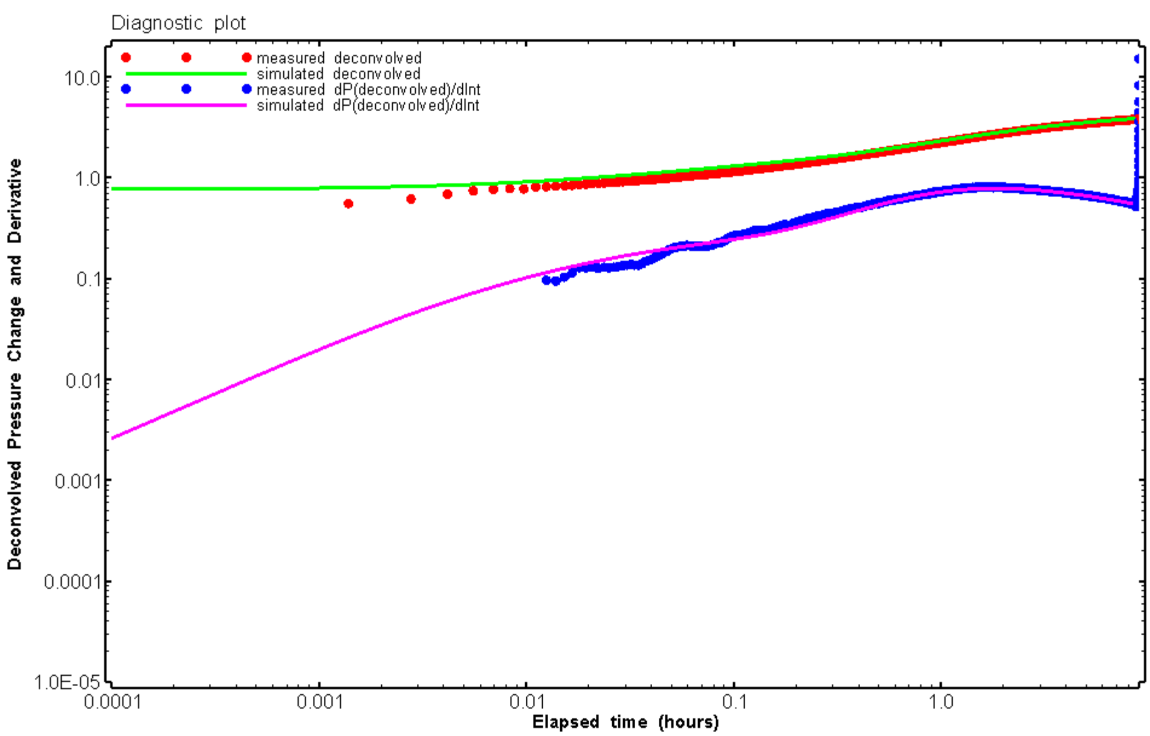

Figure 16: HT002 Deconvolved pressure change and derivative plot of the PW sequence showing best-fit simulation

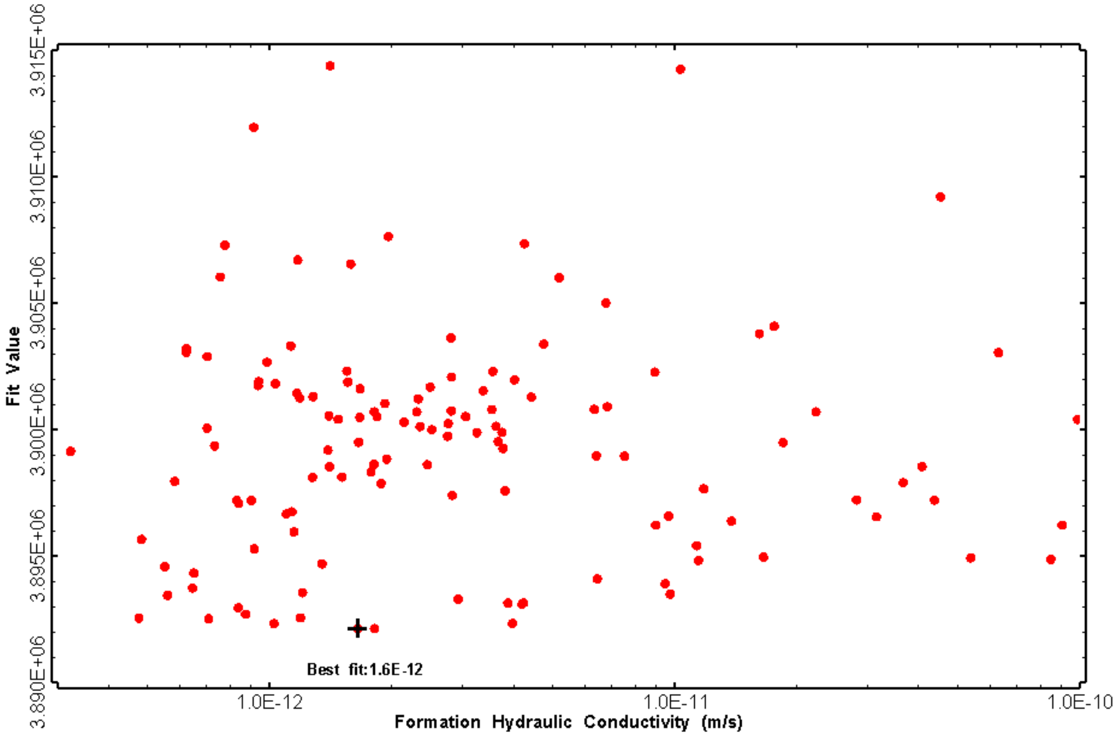

Figure 17: HT002 XY-scatter plot of formation hydraulic conductivity vs. fit value

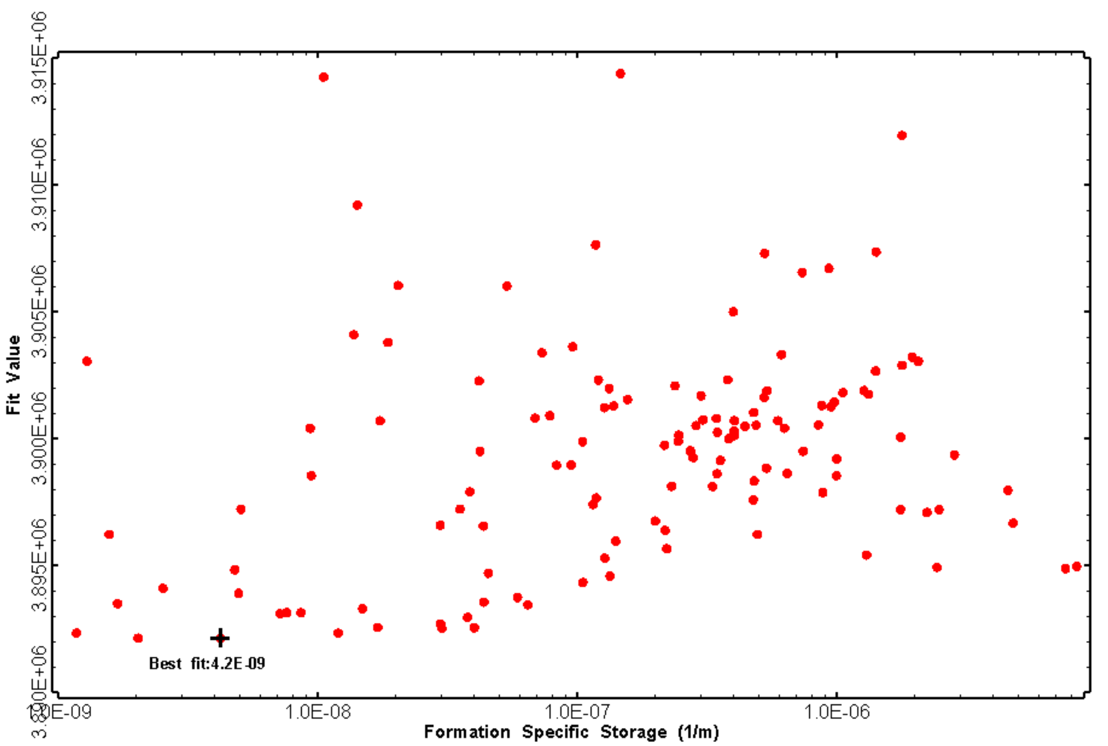

Figure 18: HT002 XY-scatter plot of formation specific storage vs. fit value

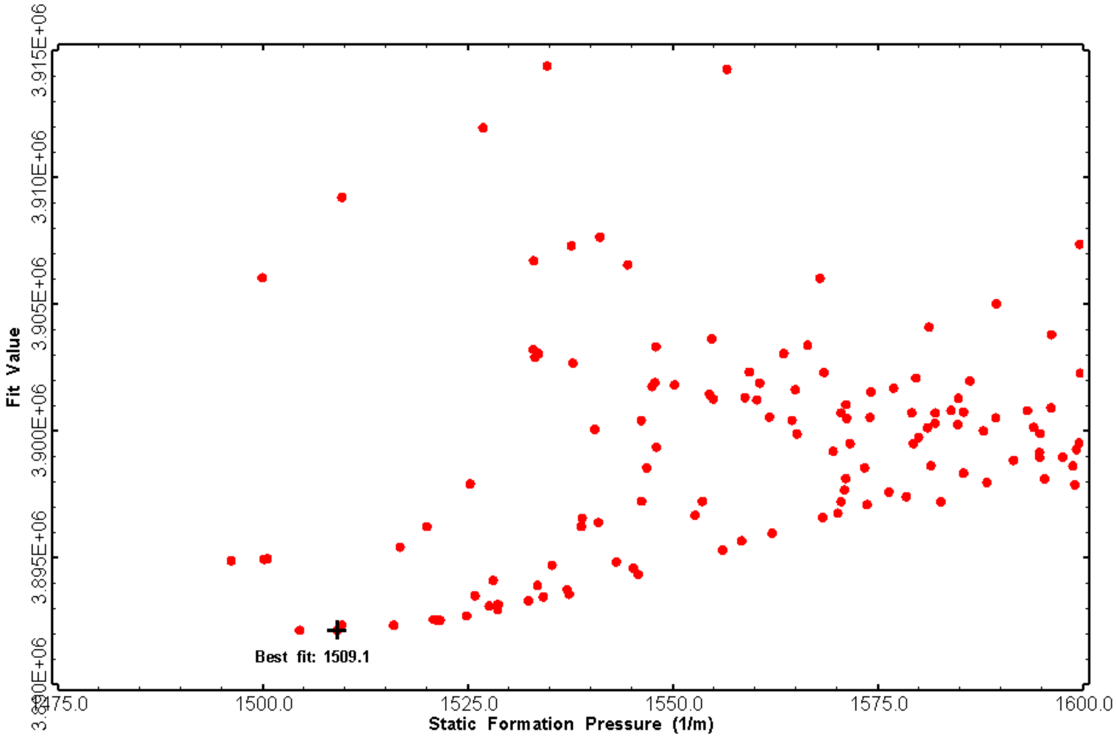

Figure 19: HT002 XY-scatter plot of static formation pressure vs. fit value

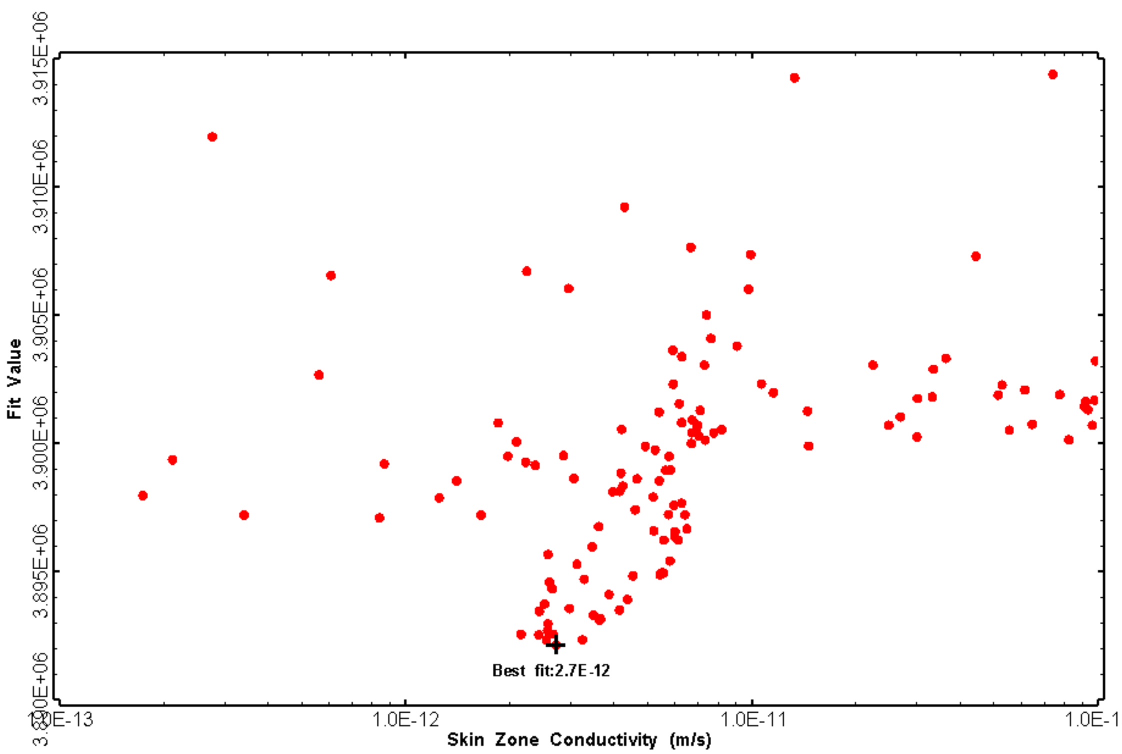

Figure 20: HT002 XY-scatter plot of skin zone conductivity vs. fit value

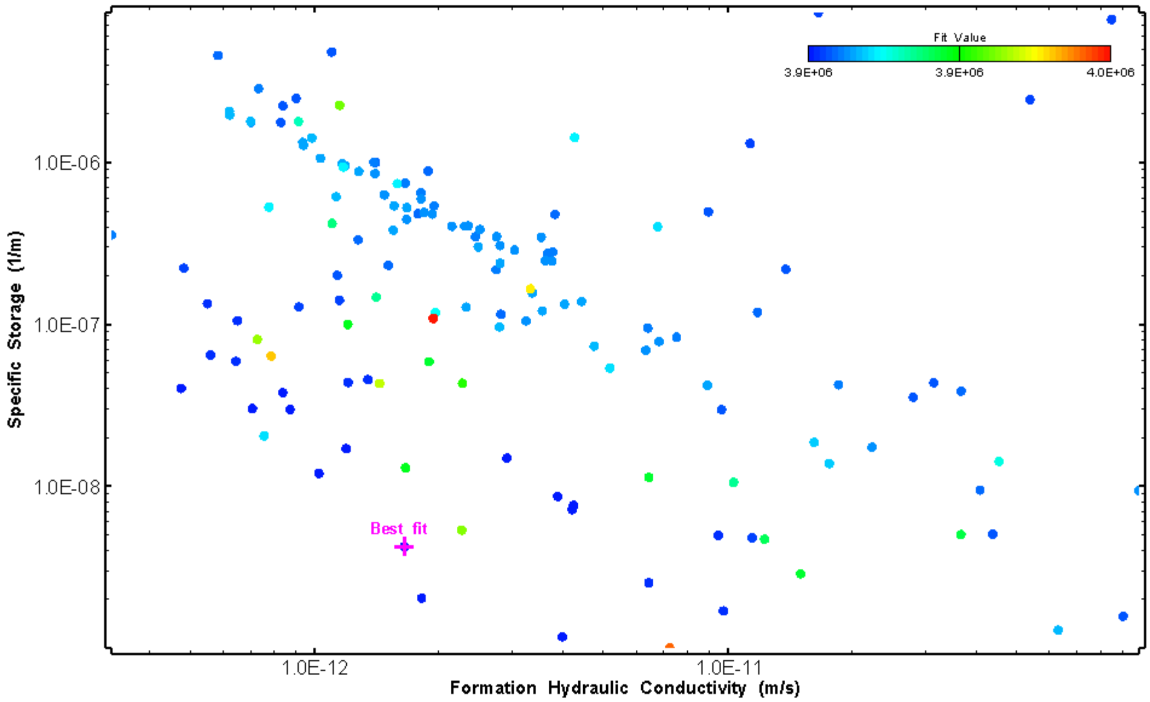

Figure 21: HT002 XY-scatter plot showing estimates of formation hydraulic conductivity and specific storage from perturbation analysis

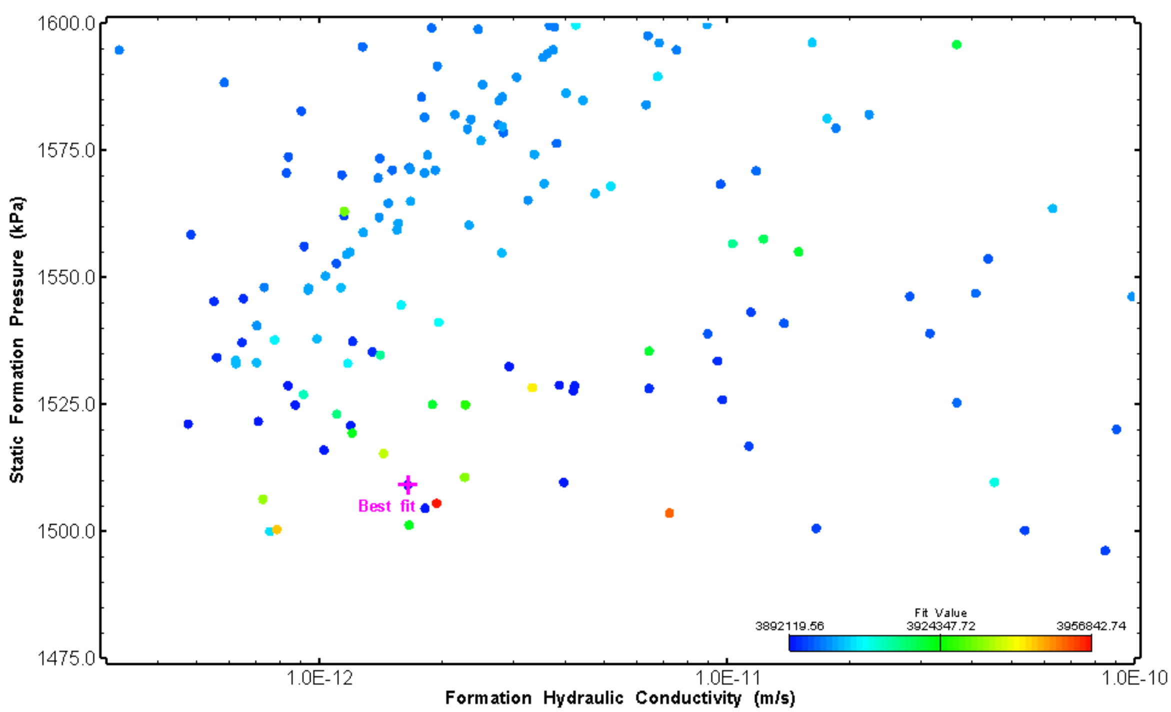

Figure 22: HT002 XY-scatter plot showing estimates of formation hydraulic conductivity and static formation pressure from perturbation analysis

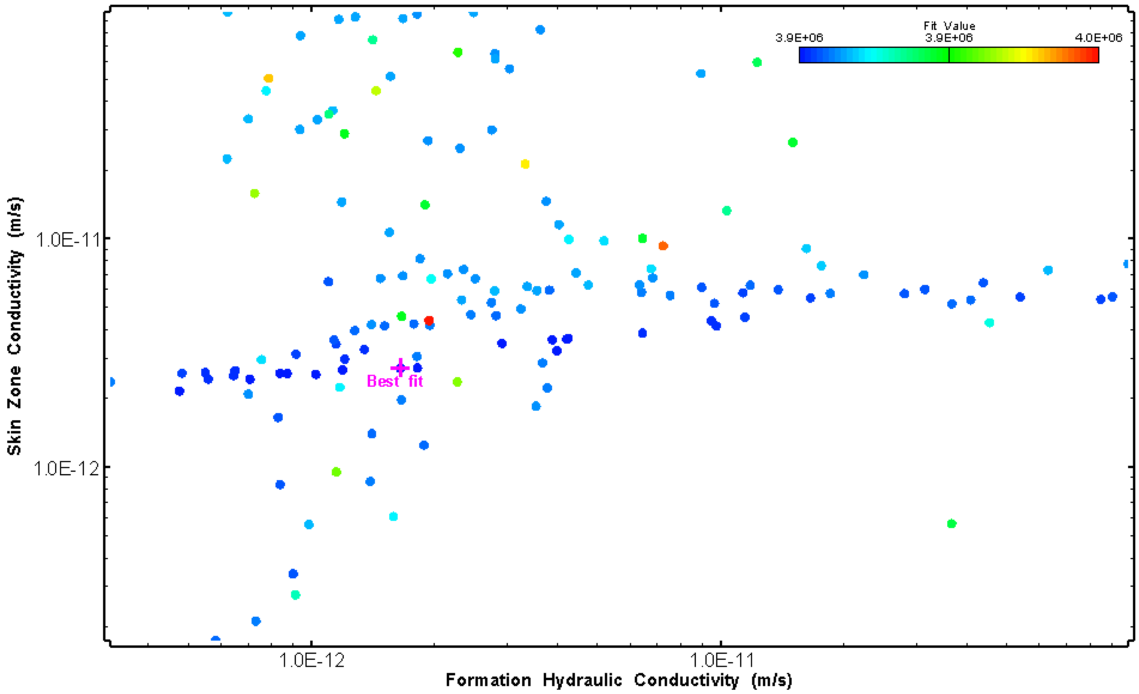

Figure 23: HT002 XY-scatter plot showing estimates of formation hydraulic conductivity and skin zone conductivity from perturbation analysis

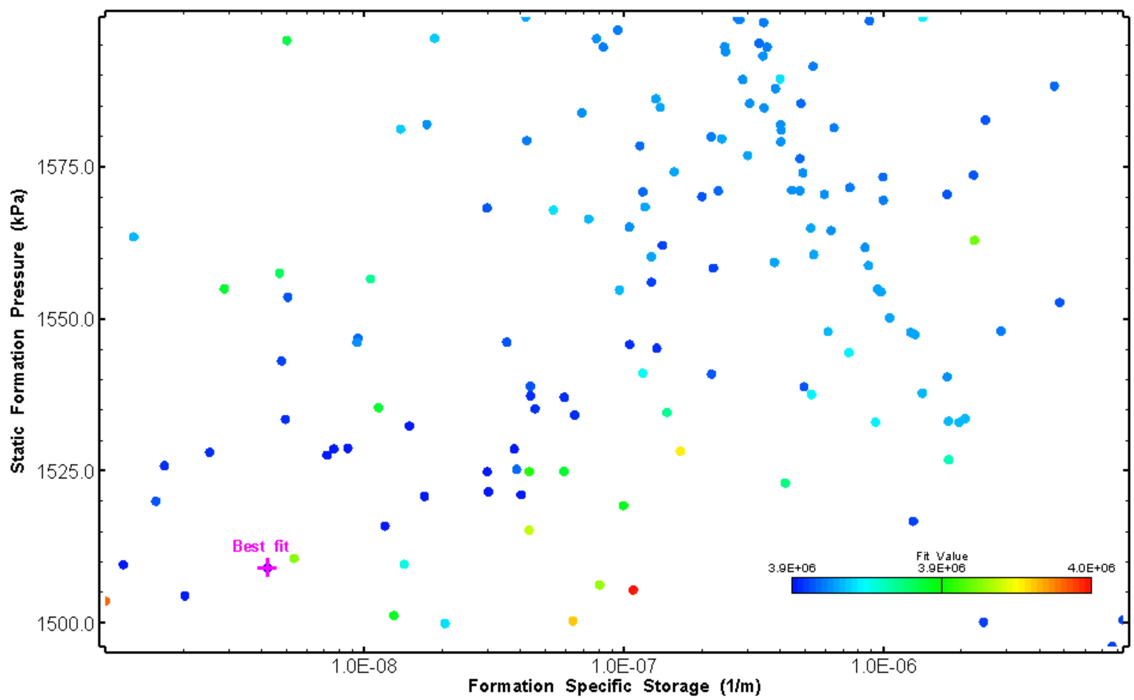

Figure 24: HT002 XY-scatter plot showing estimates of specific storage and static formation pressure from perturbation analysis

3.0 HT003 (223.07 – 243.10 M)

HT003 was selected to test a shallow fractured interval. 16 broken fractures were observed in the core. No drill fluid parameter triggers were reached during drilling. A slight indication of flow was recorded during FFEC logging post-drilling.

The test was initiated with a shut-in pressure recovery phase (PSR). A pulse withdrawal test (PW) with a shut-in recovery was completed after the PSR phase.

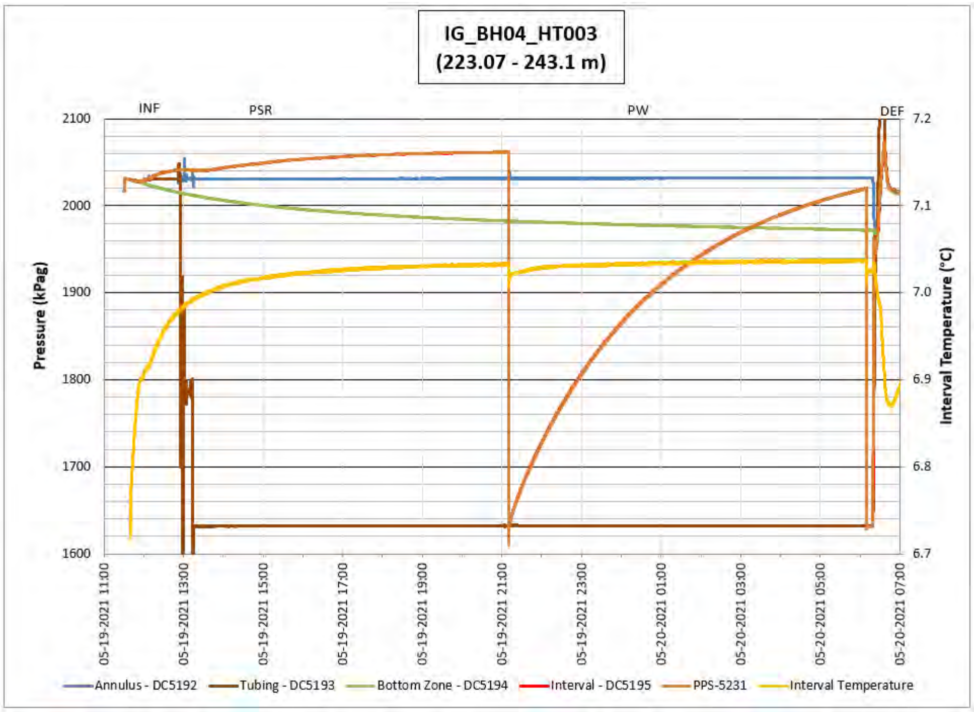

Figure 25: HT003 Annotated test plot showing monitored zone pressure and interval temperature.

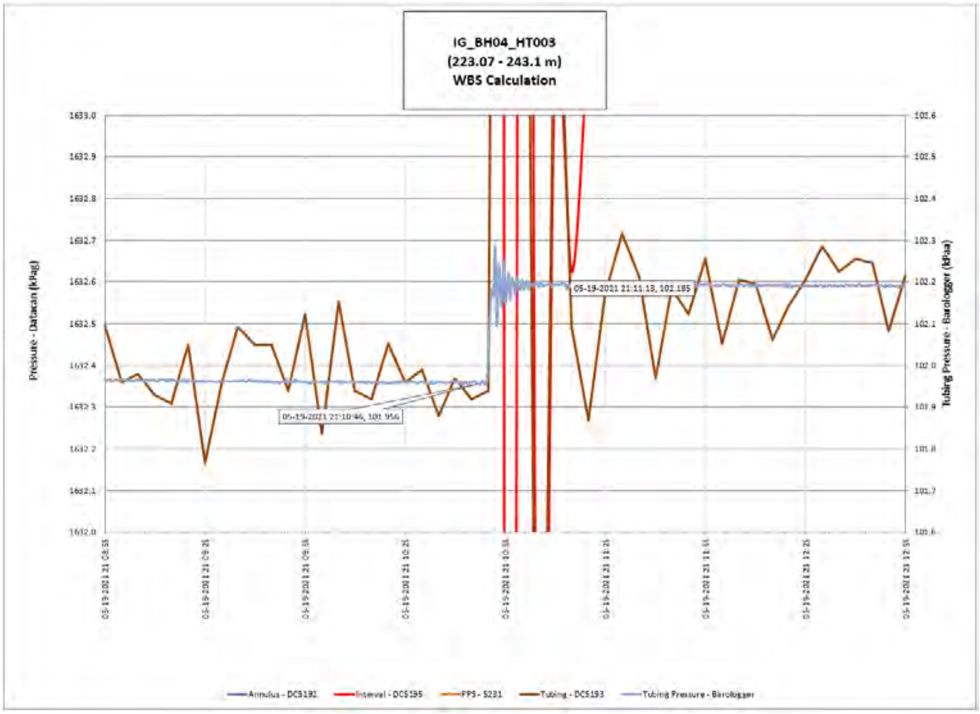

Figure 26: HT003 Tubing pressure during DHSIV activation. DHSIV Closed Wellbore Storage Estimate = 1E-10 m^3/Pa

Table 3: Summary of Analysis Results – HT003

	Formation conductivity	Skin zone conductivity	Static formation pressure	Formation specific storage	Radial thickness of skin	Flow dimension
	[m/s]	[m/s]	[kPa]	[1/m]	[m]	[–]
Best Fit	9.4E-13	1.23E-14	2072	2.0E-08	2.0E-03	2.6
Minimum	1.0E-15	7.7E-13	2050	1.0E-09	9.0E-04	1.1
Maximum	9.7E-11	4.3E-13	2154	7.8E-06	6.8E-01	3.0
Mean	2.0E-11	4.6E-13	2073	6.2E-07	5.4E-02	2.0
Median	9.7E-12	3.9E-13	2072	1.4E-07	5.0E-02	2.0
Geometric mean	9.9E-12	1.3E-14	2073	1.3E-07	4.0E-02	2.0

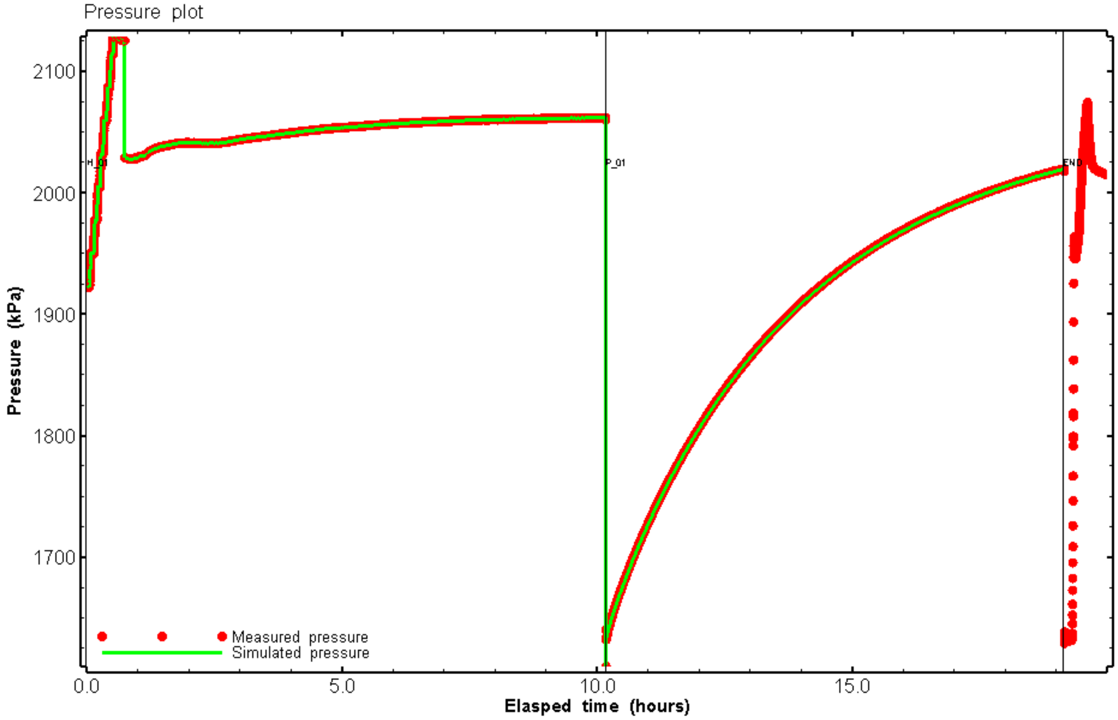

Figure 27: HT003 Pressure plot showing best-fit simulation and best fit results

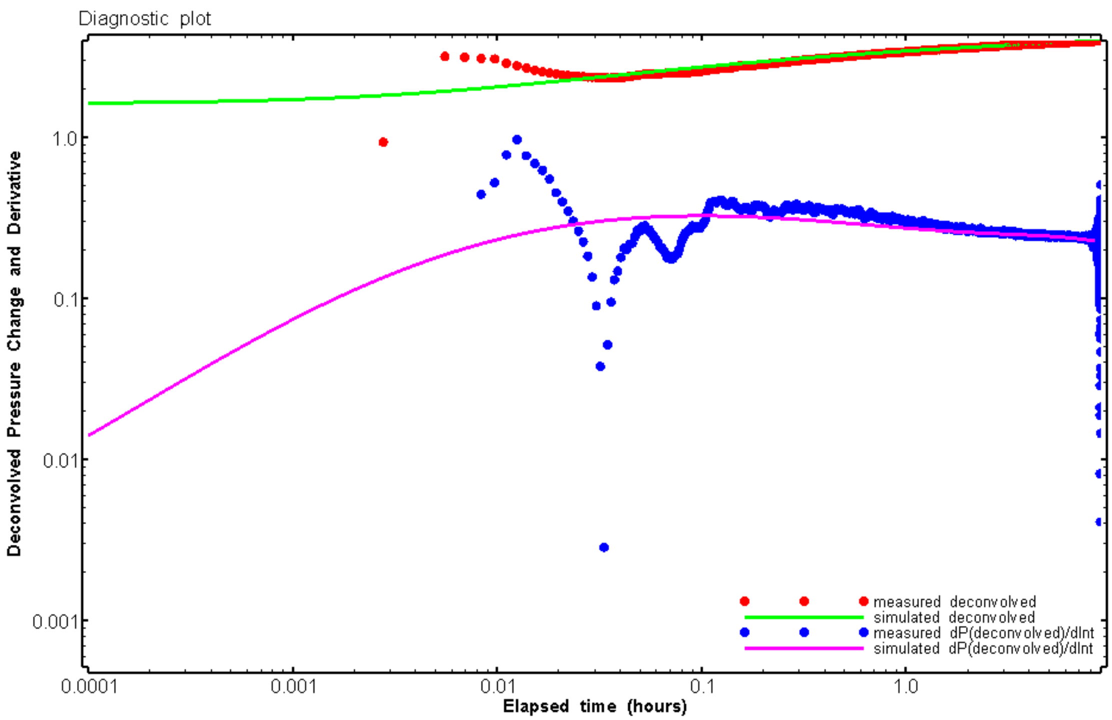

Figure 28: HT003 Deconvolved pressure change and derivative plot of the PW sequence showing best-fit simulation

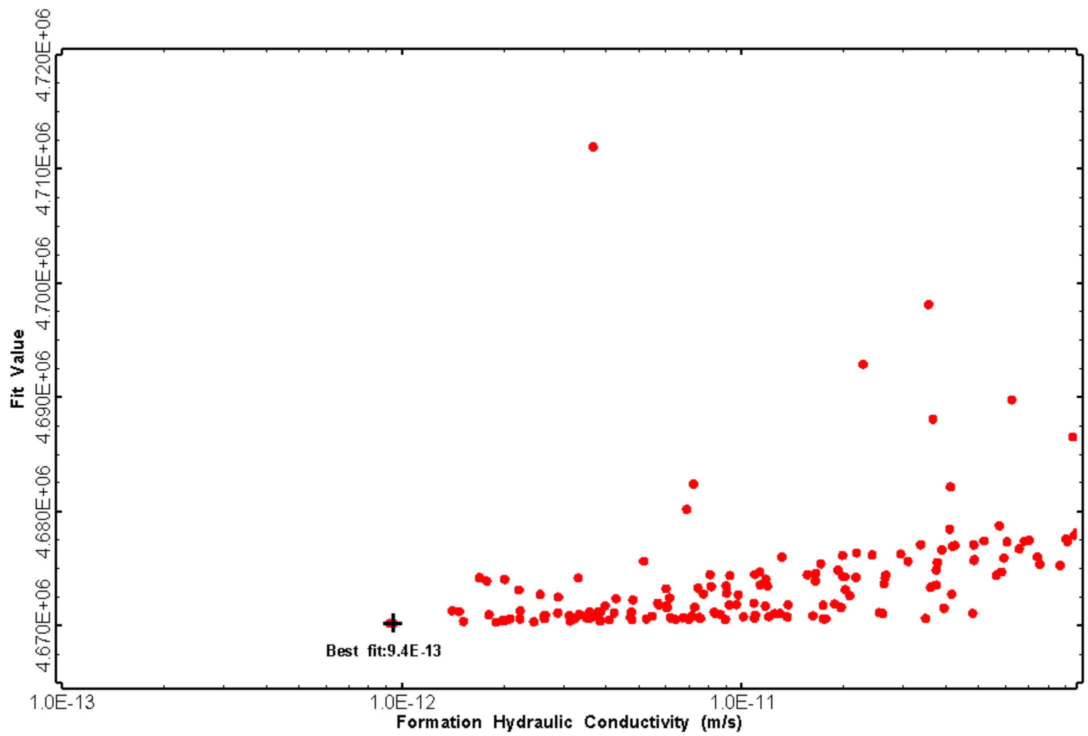

Figure 29: HT003 XY-scatter plot of formation hydraulic conductivity vs. fit value

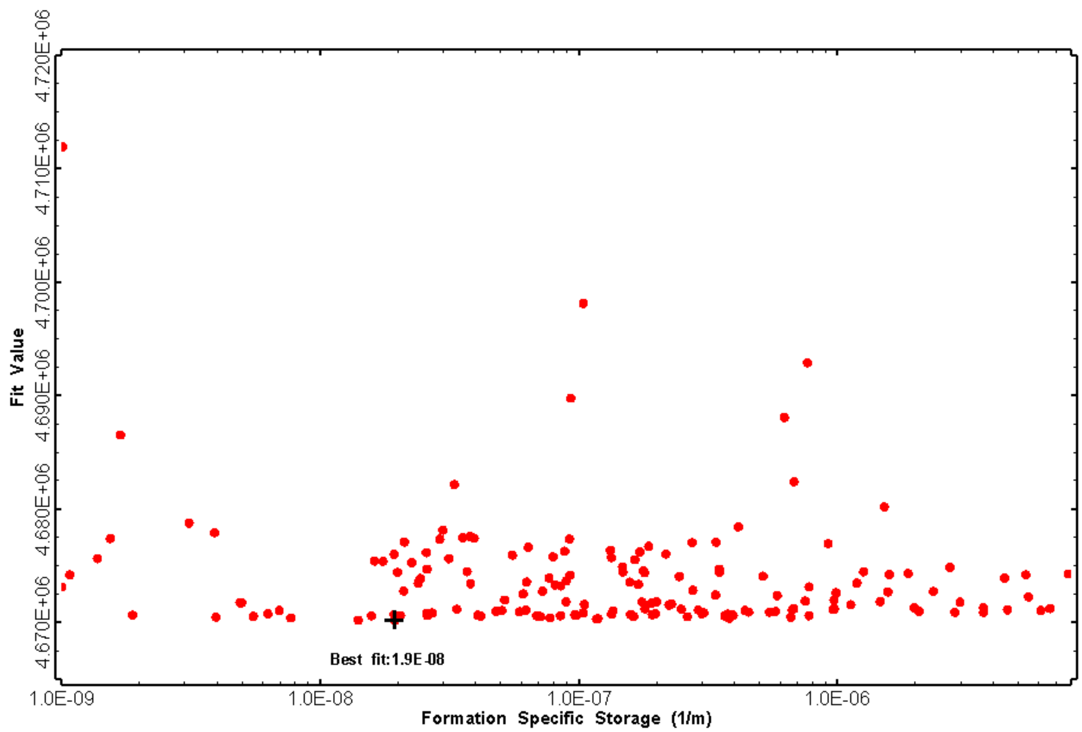

Figure 30: HT003 XY-scatter plot of formation specific storage vs. fit value

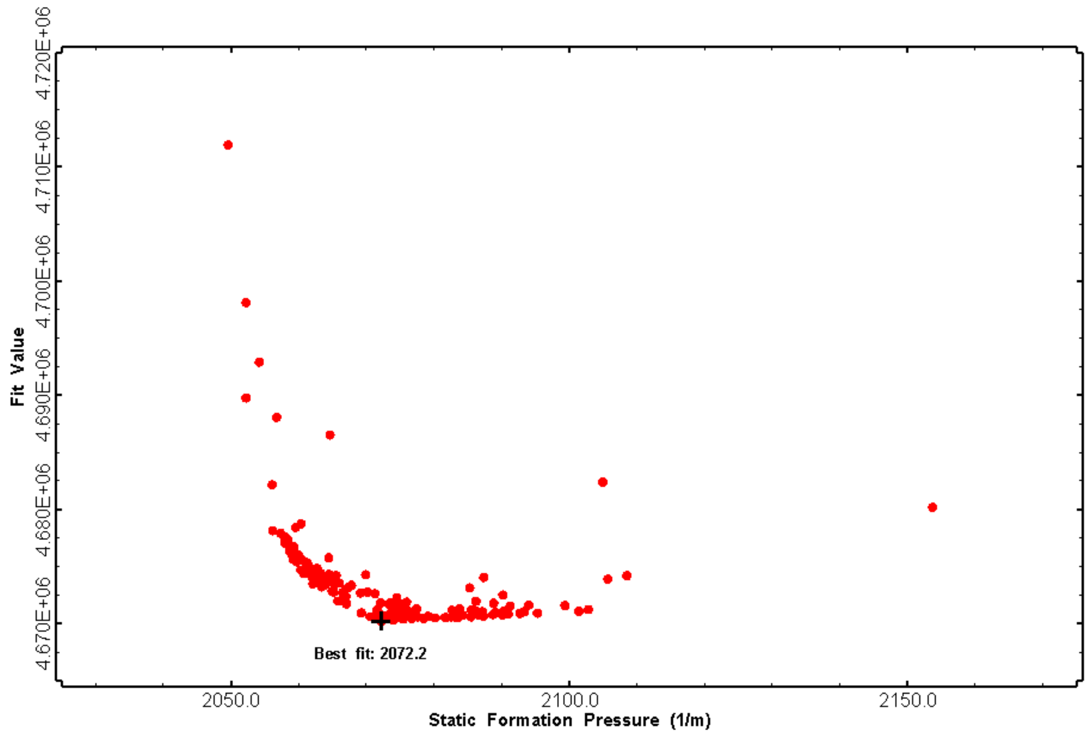

Figure 31: HT003 XY-scatter plot of static formation pressure vs. fit value

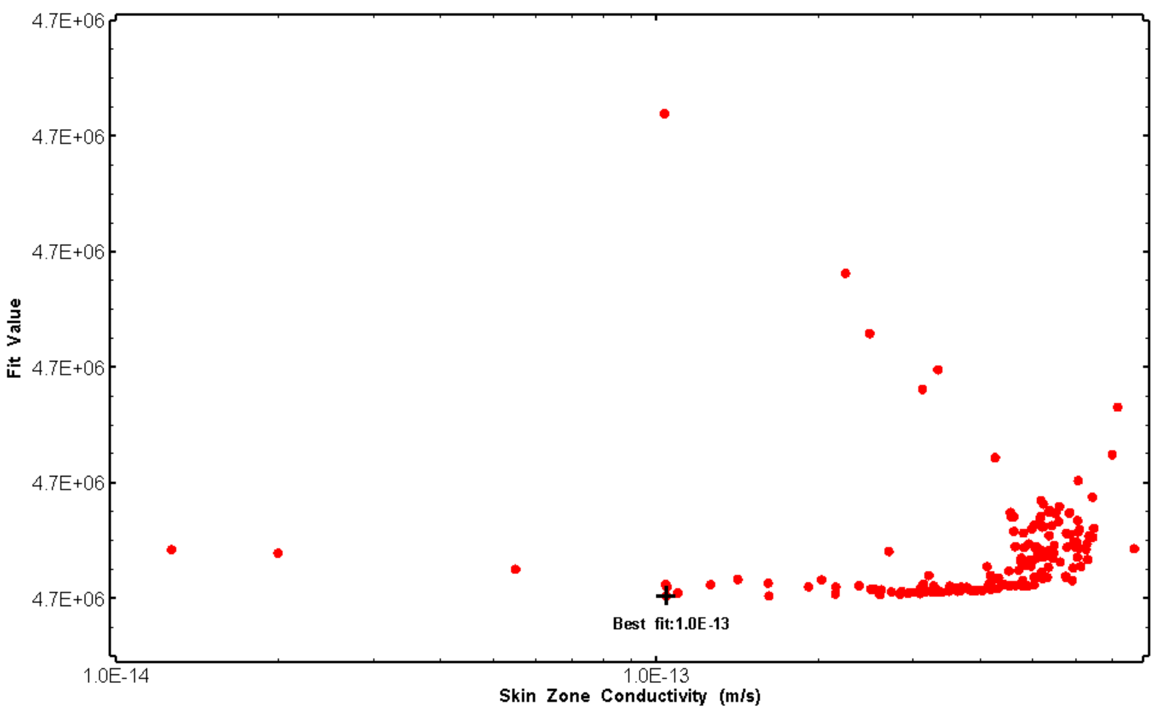

Figure 32: HT003 XY-scatter plot of skin zone conductivity vs. fit value

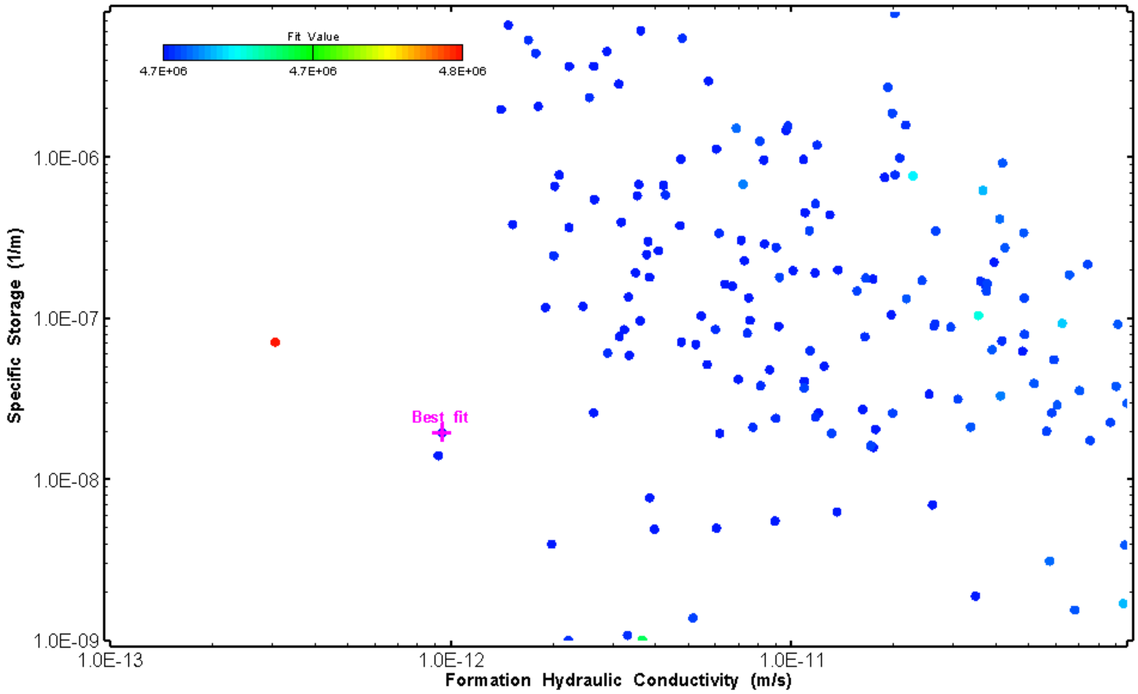

Figure 33: HT003 XY-scatter plot showing estimates of formation hydraulic conductivity and specific storage from perturbation analysis

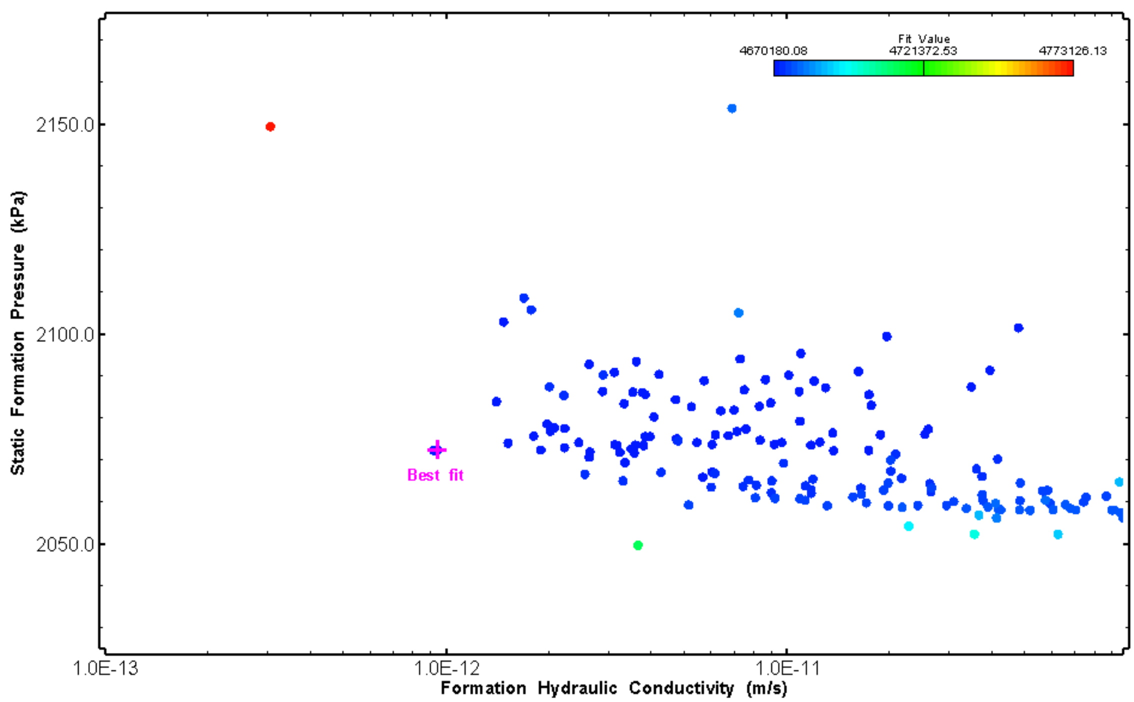

Figure 34: HT003 XY-scatter plot showing estimates of formation hydraulic conductivity and static formation pressure from perturbation analysis

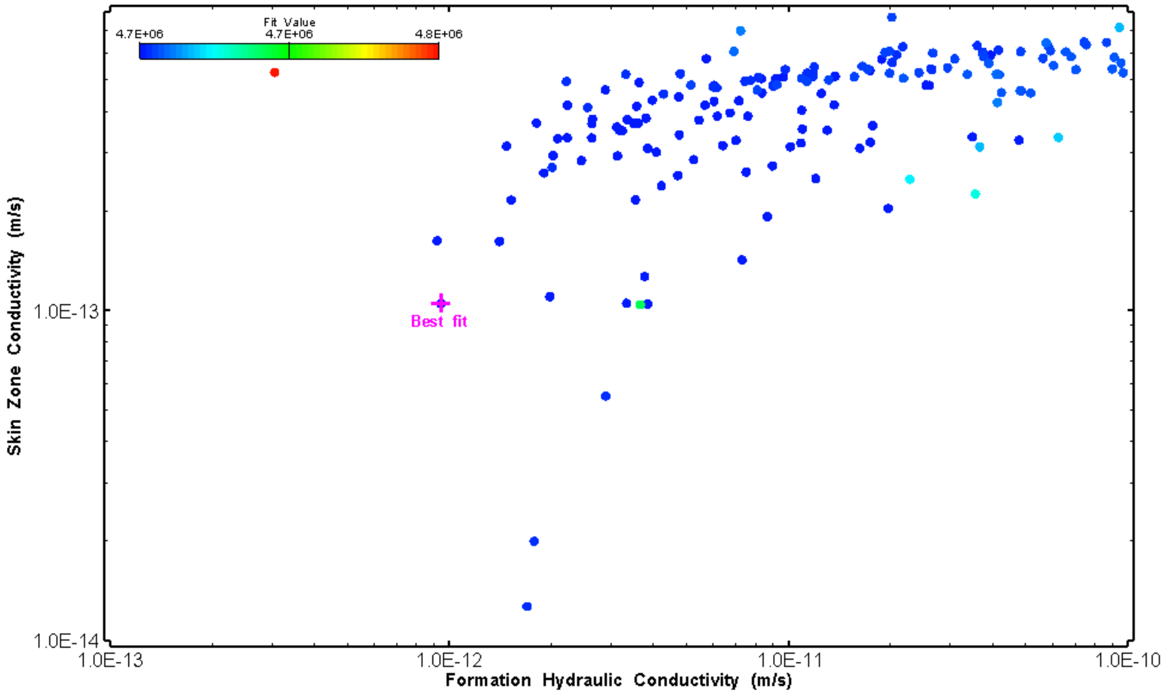

Figure 35: HT003 XY-scatter plot showing estimates of formation hydraulic conductivity and skin zone conductivity from perturbation analysis

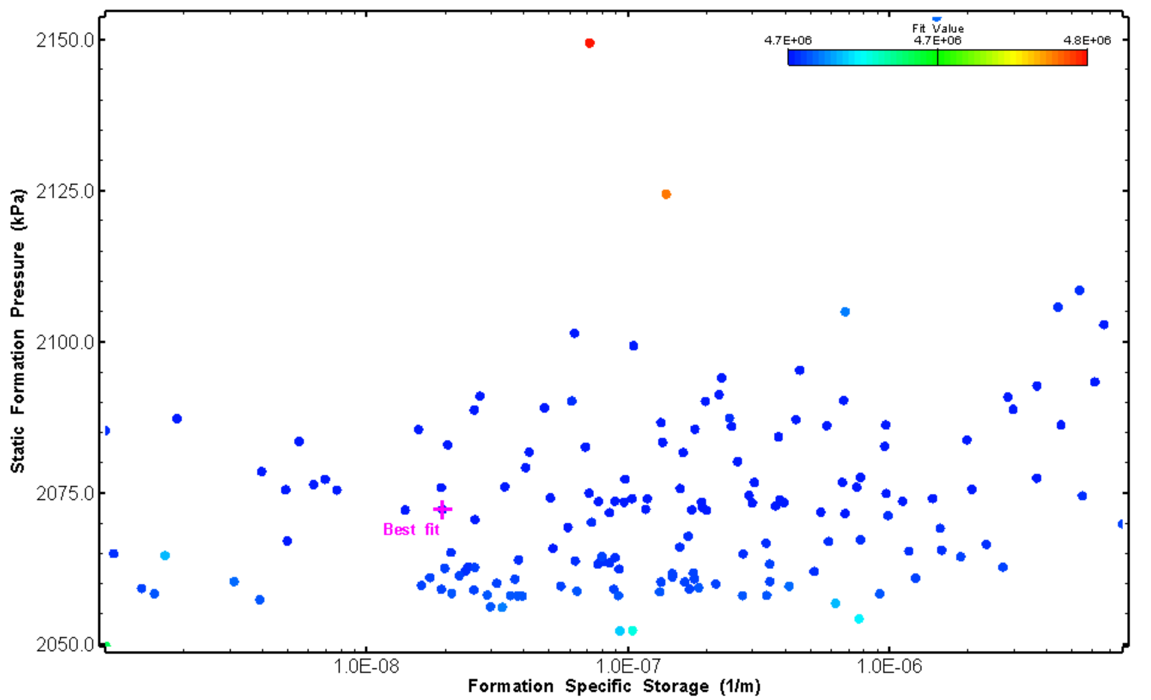

Figure 36: HT003 XY-scatter plot showing estimates of specific storage and static formation pressure from perturbation analysis

4.0 HT004 (263.44 – 283.47 M)

HT004 was selected to test a shallow fractured interval. 21 broken fractures were observed in the core. No drill fluid parameter triggers were reached during drilling. No indication of flow was recorded during FFEC logging post-drilling.

The test was initiated with a shut-in pressure recovery phase (PSR). A pulse withdrawal test (PW) with a shut-in recovery was completed after the PSR phase.

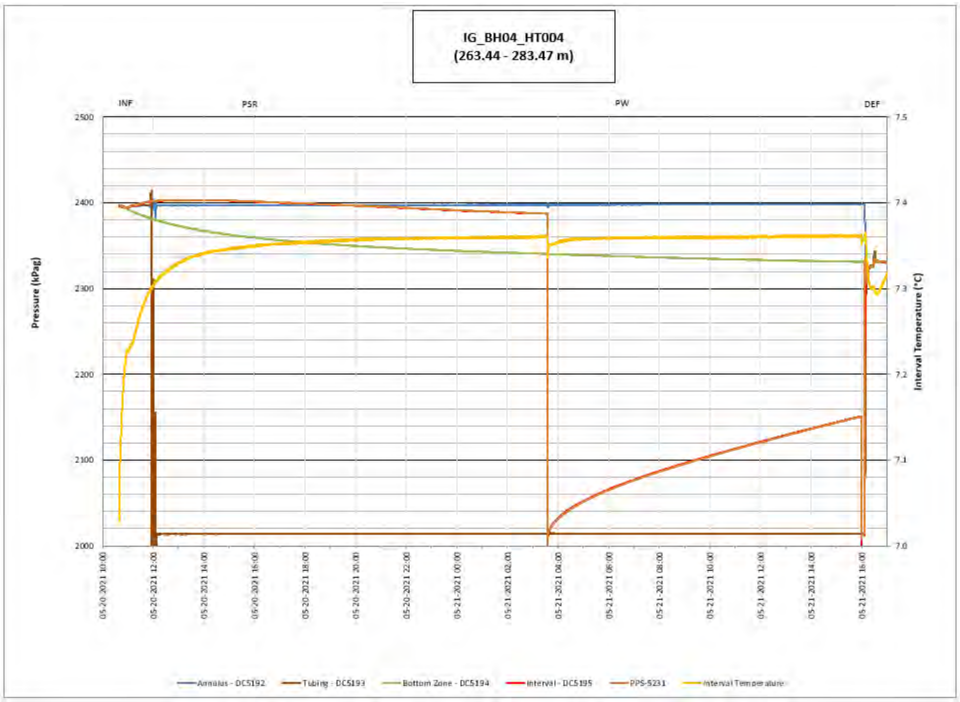

Figure 37: HT004 Annotated test plot showing monitored zone pressure and interval temperature.

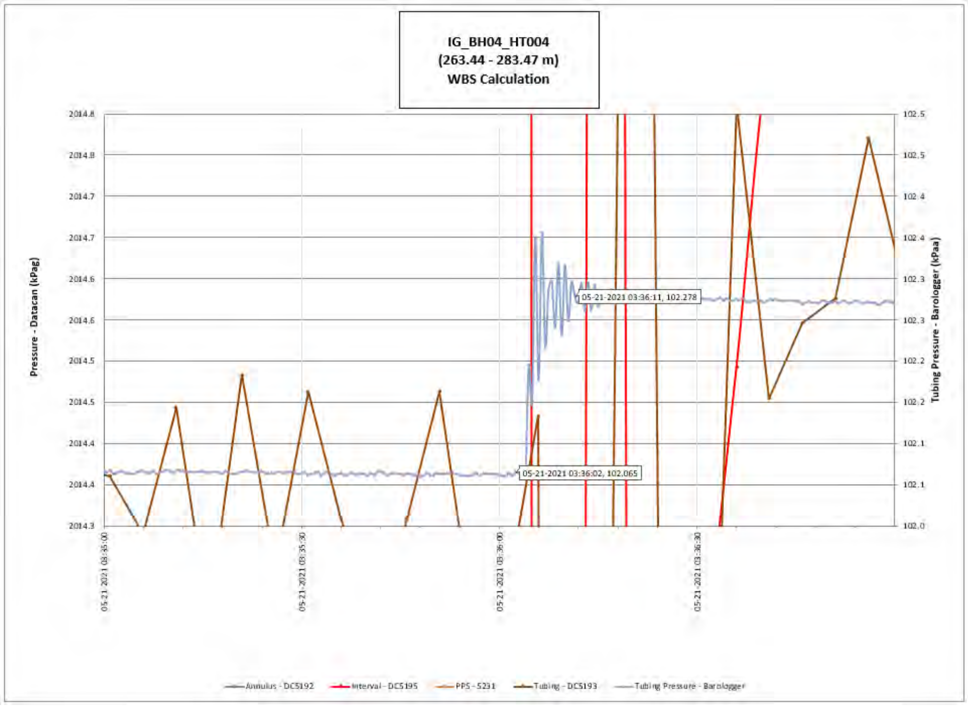

Figure 38: HT004 Tubing pressure during DHSIV activation. DHSIV Closed Wellbore Storage Estimate = 1E-10 m^3/Pa

Table 4: Summary of Analysis Results – HT004

	Formation conductivity	Skin zone conductivity	Static formation pressure	Formation specific storage	Radial thickness of skin	Flow dimension
	[m/s]	[m/s]	[kPa]	[1/m]	[m]	[–]
Best Fit	4.6E-14	1.2E-13	2382	2.0E-08	5.5E-02	3.0
Minimum	3.3E-15	1.1E-13	2264	5.4E-10	1.0E-03	1.2
Maximum	9.8E-11	9.8E-12	2400	9.9E-07	9.4E-01	3.0
Mean	2.5E-12	1.1E-12	2364	1.7E-07	1.8E-01	2.1
Median	1.9E-13	2.1E-13	2368	9.7E-08	1.0E-01	2.1
Geometric mean	2.9E-13	3.5E-13	2364	7.7E-08	6.9E-02	2.1

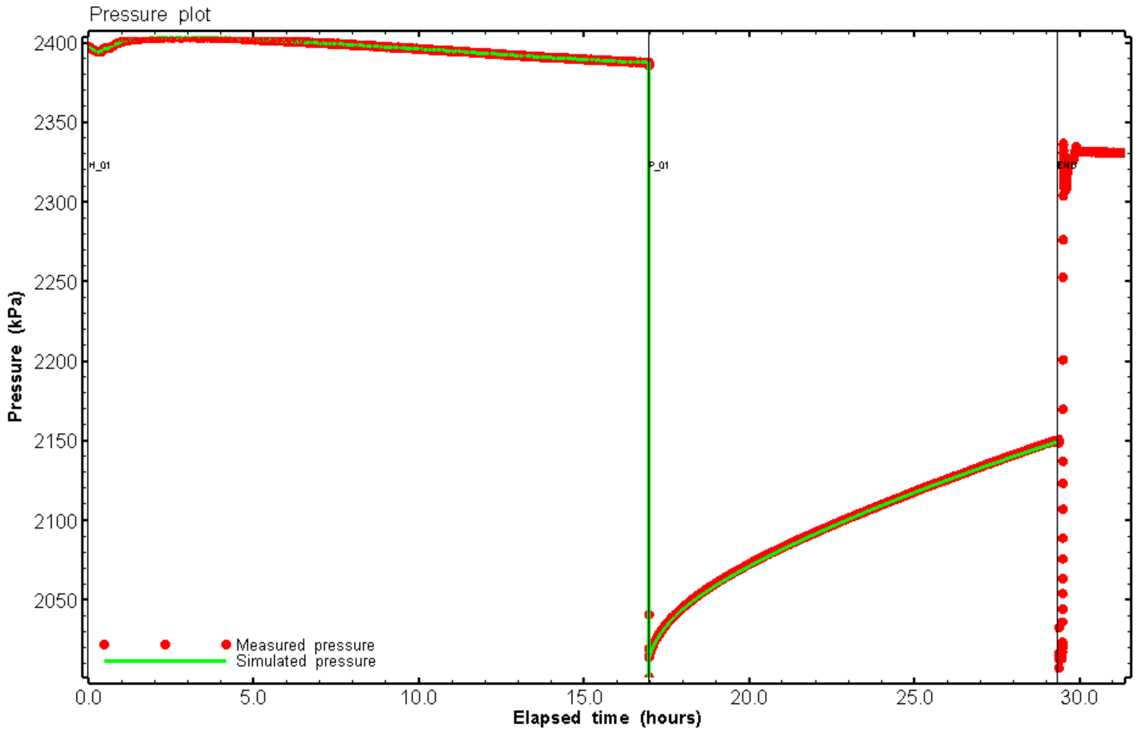

Figure 39: HT004 Pressure plot showing best-fit simulation and best fit results

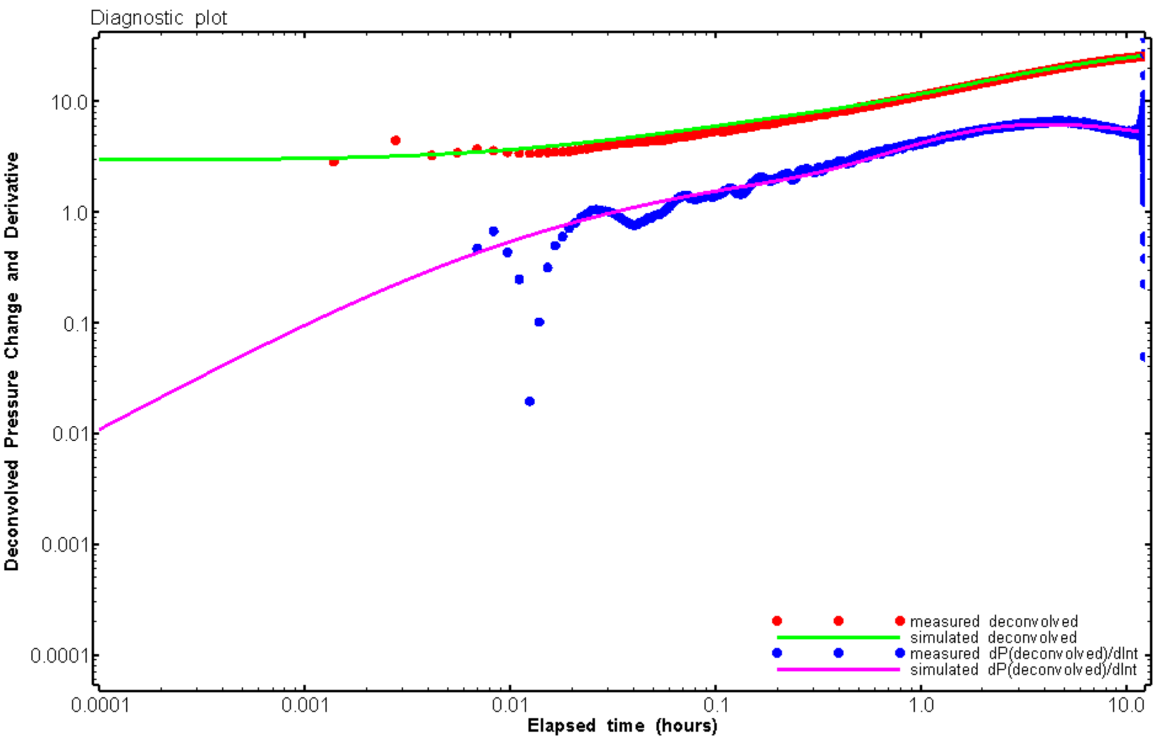

Figure 40: HT004 Deconvolved pressure change and derivative plot of the PW sequence showing best-fit simulation

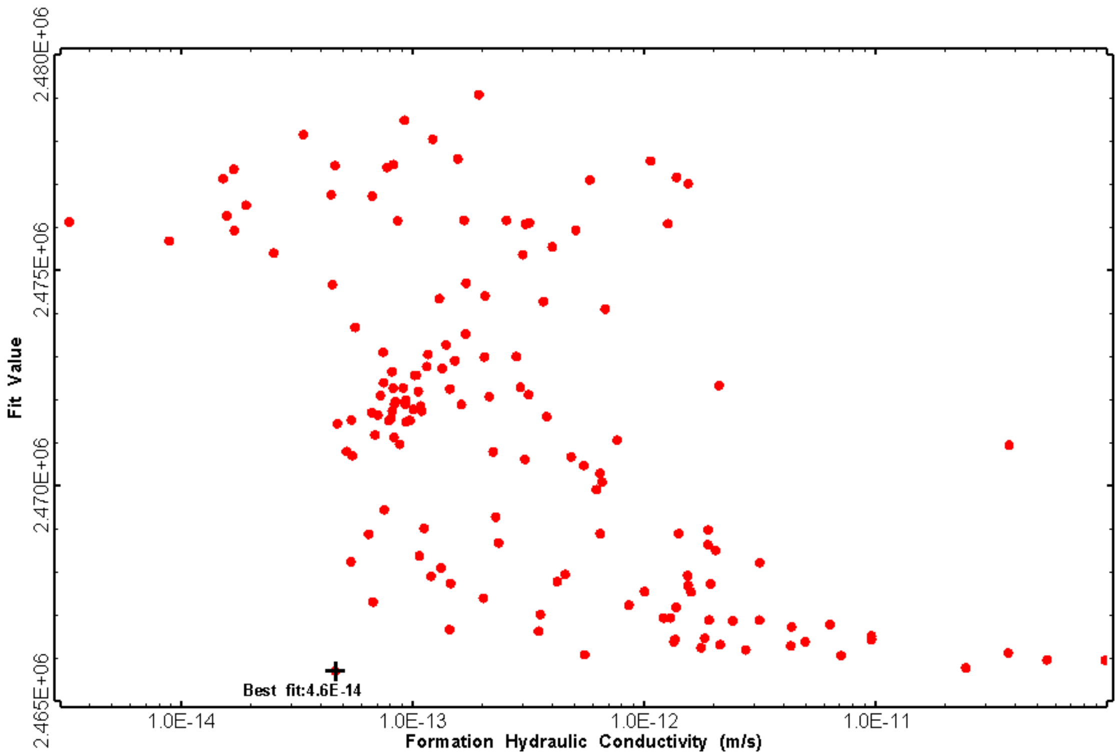

Figure 41: HT004 XY-scatter plot of formation hydraulic conductivity vs. fit value

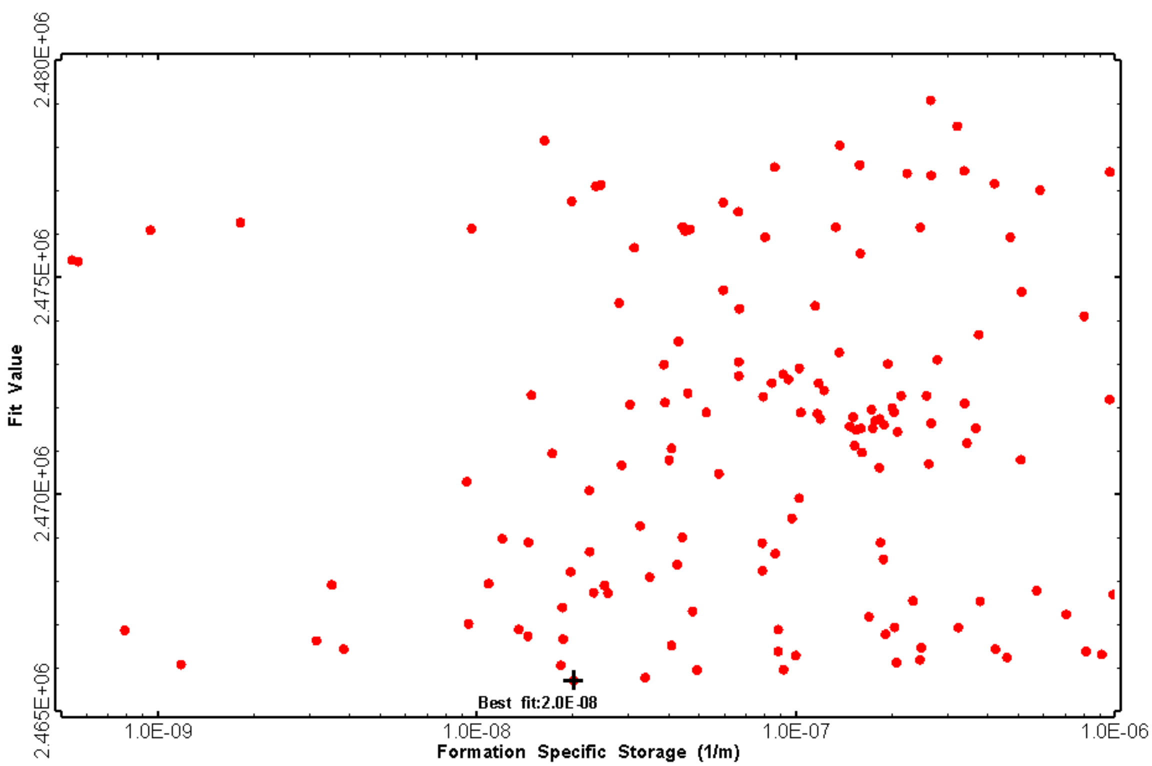

Figure 42: HT004 XY-scatter plot of formation specific storage vs. fit value

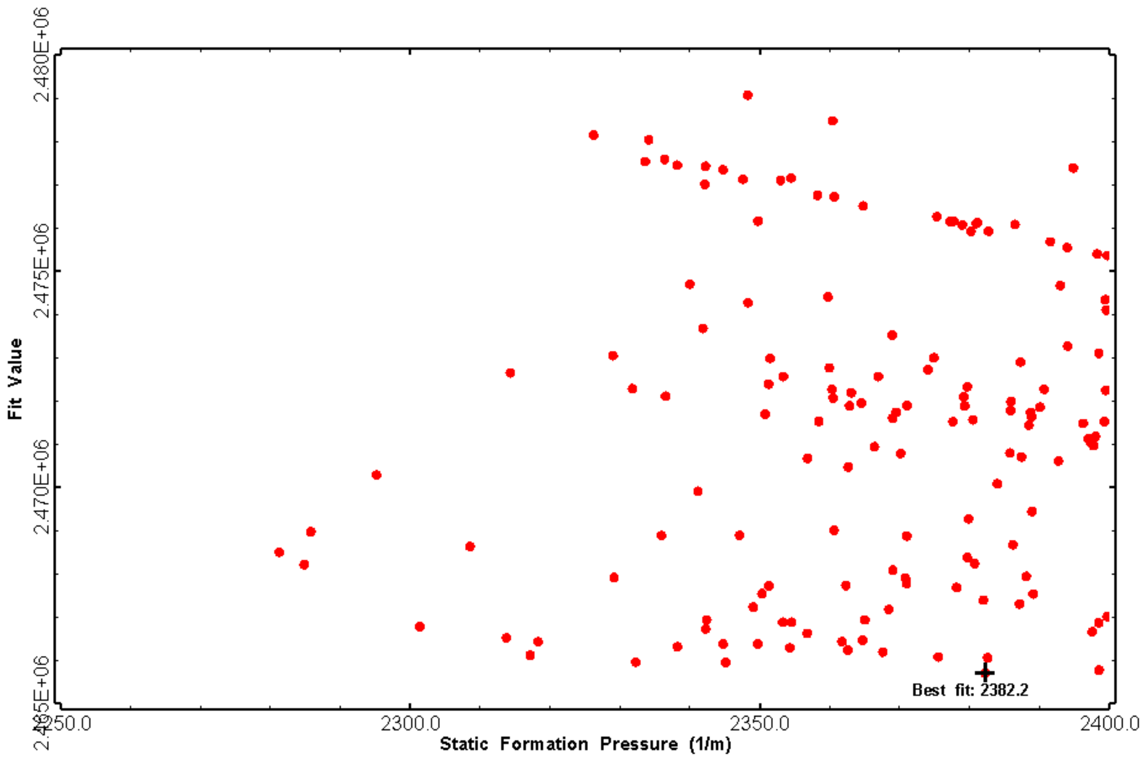

Figure 43: HT004 XY-scatter plot of static formation pressure vs. fit value

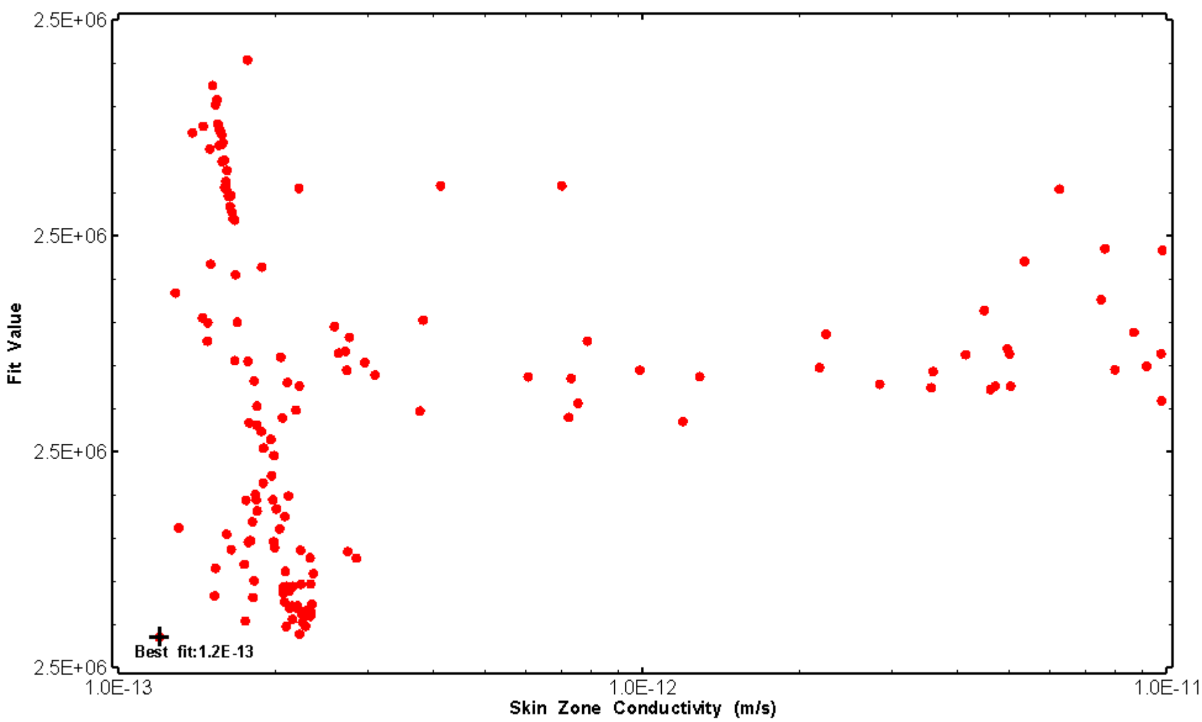

Figure 44: HT004 XY-scatter plot of skin zone conductivity vs. fit value

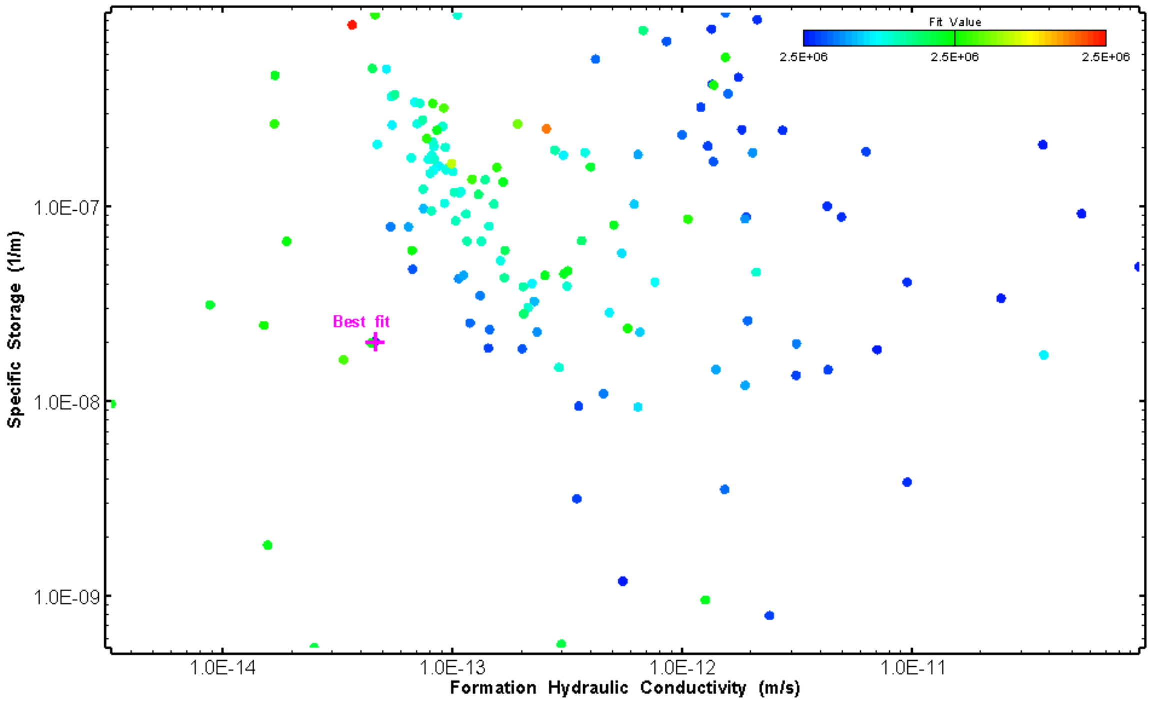

Figure 45: HT004 XY-scatter plot showing estimates of formation hydraulic conductivity and specific storage from perturbation analysis

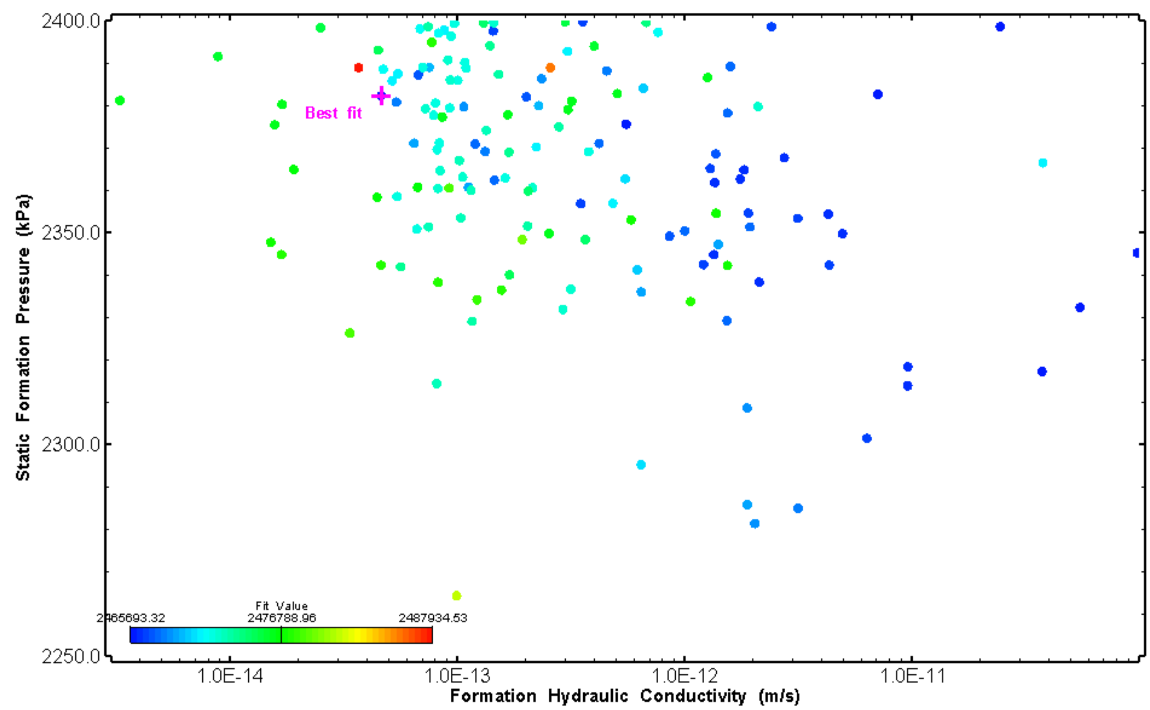

Figure 46: HT004 XY-scatter plot showing estimates of formation hydraulic conductivity and static formation pressure from perturbation analysis

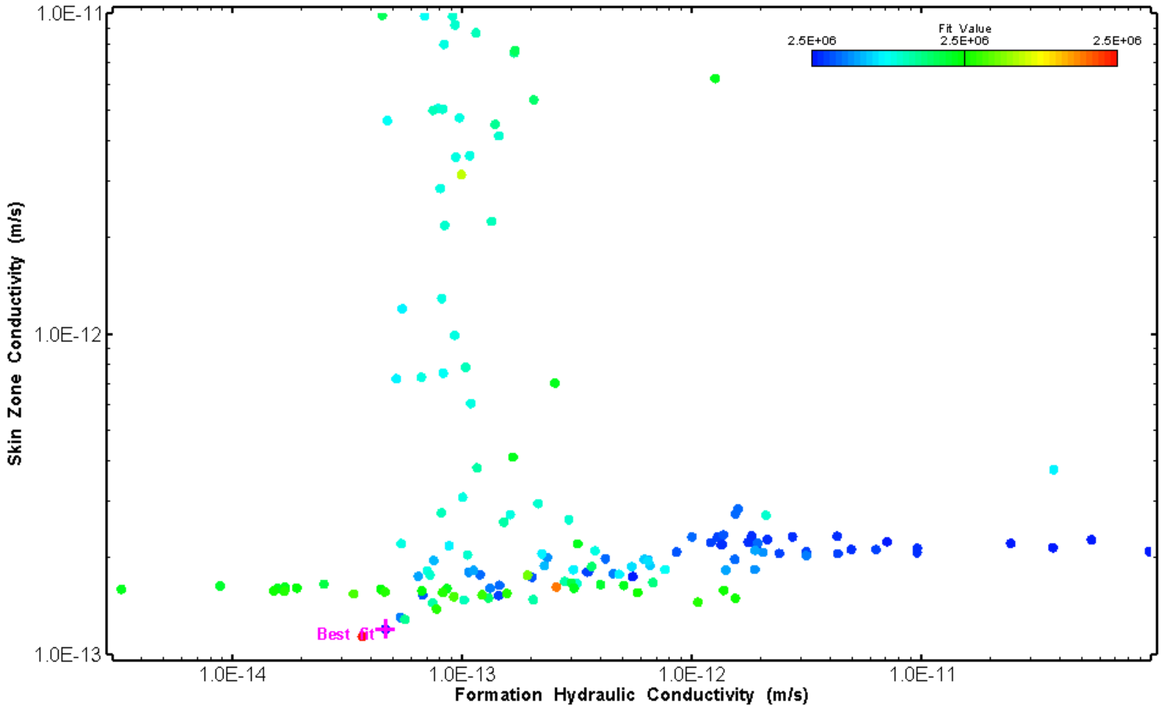

Figure 47: HT004 XY-scatter plot showing estimates of formation hydraulic conductivity and skin zone conductivity from perturbation analysis

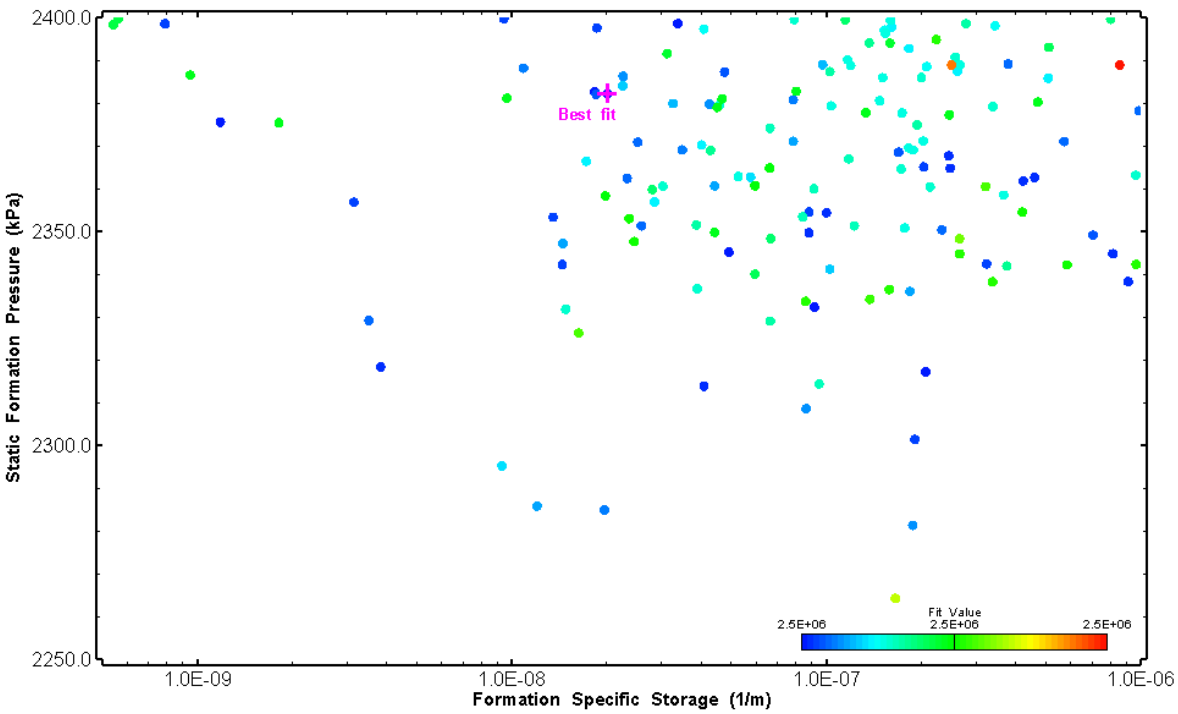

Figure 48: HT004 XY-scatter plot showing estimates of specific storage and static formation pressure from perturbation analysis

5.0 HT005 (335.61 – 355.64 M)

HT005 was selected to test a shallow slightly fractured interval. Ten broken fractures were observed in the core. No drill fluid parameter triggers were reached during drilling. No indication of flow was recorded during FFEC logging post-drilling.

The test was initiated with a shut-in pressure recovery phase (PSR). A pulse withdrawal test (PW) with a shut-in recovery was completed after the PSR phase.

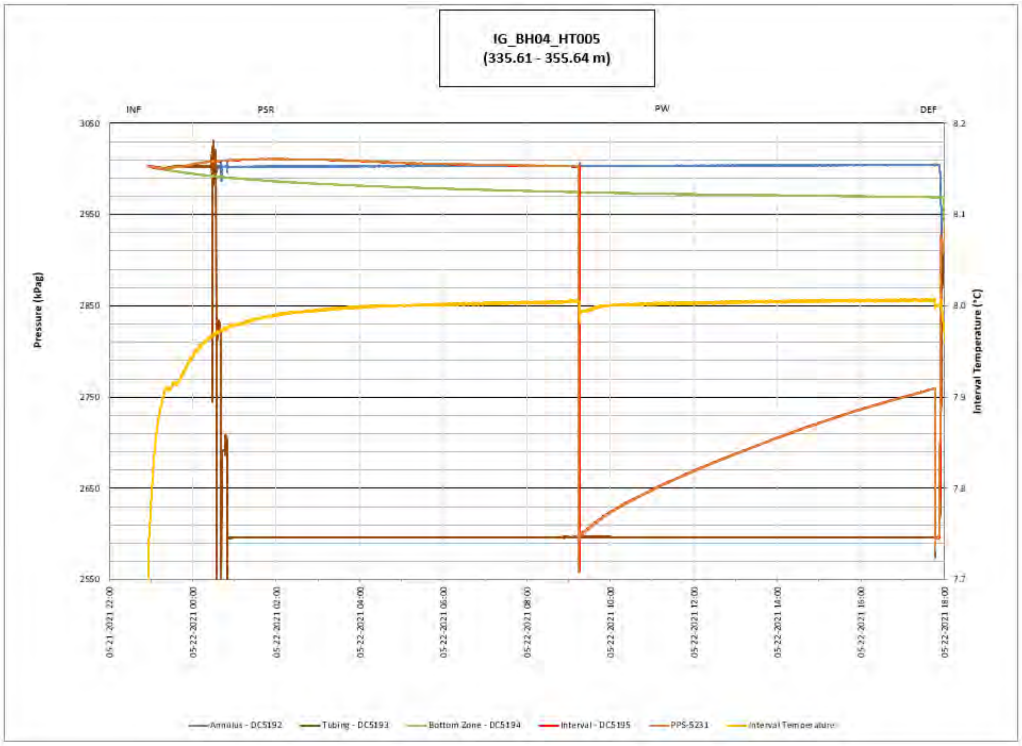

Figure 49: HT005 Annotated test plot showing monitored zone pressure and interval temperature.

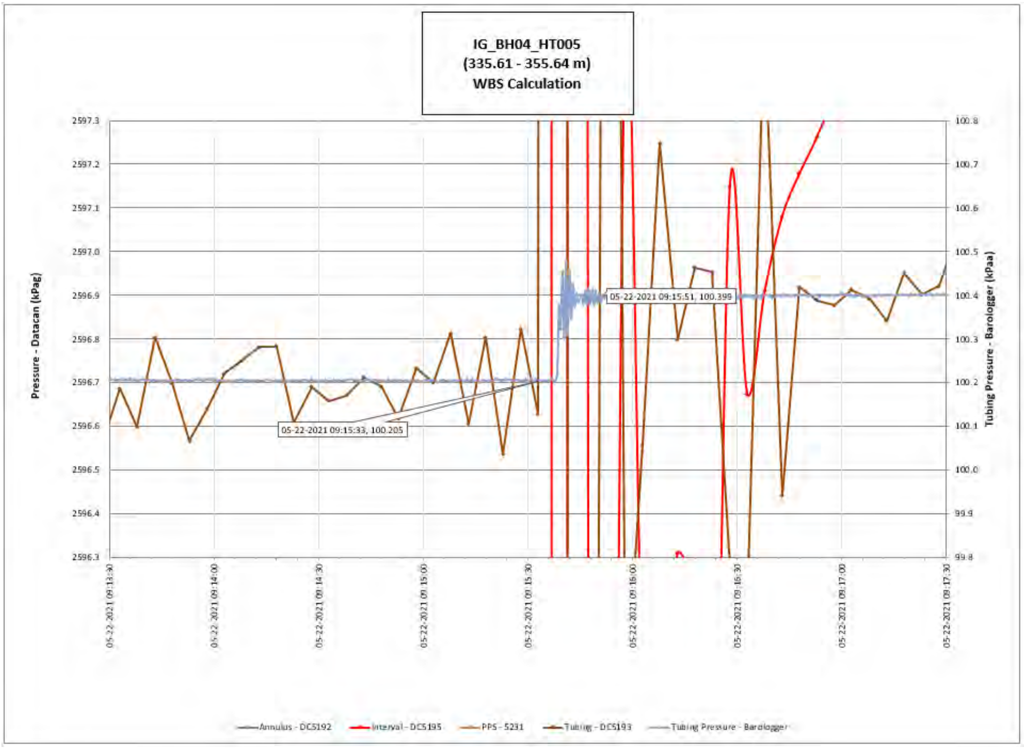

Figure 50: HT005 Tubing pressure during DHSIV activation. DHSIV Closed Wellbore Storage Estimate = 9E-11 m^3/Pa

Table 5: Summary of Analysis Results – HT005

	Formation conductivity	Skin zone conductivity	Static formation pressure	Formation specific storage	Radial thickness of skin	Flow dimension
	[m/s]	[m/s]	[kPa]	[1/m]	[m]	[–]
Best Fit	9.8E-14	2.5E-14	3028	1.4E-07	1.5E-03	2.9
Minimum	1.0E-15	2.5E-14	2928	1.0E-09	1.1E-03	1.2
Maximum	3.0E-11	6.9E-11	3099	4.6E-06	7.5E-01	3.0
Mean	1.8E-12	1.2E-12	3027	3.8E-07	9.1E-02	2.2
Median	6.3E-13	1.4E-13	3032	1.4E-07	7.6E-02	2.2
Geometric mean	5.9E-13	1.6E-13	3027	1.3E-07	5.5E-02	2.2

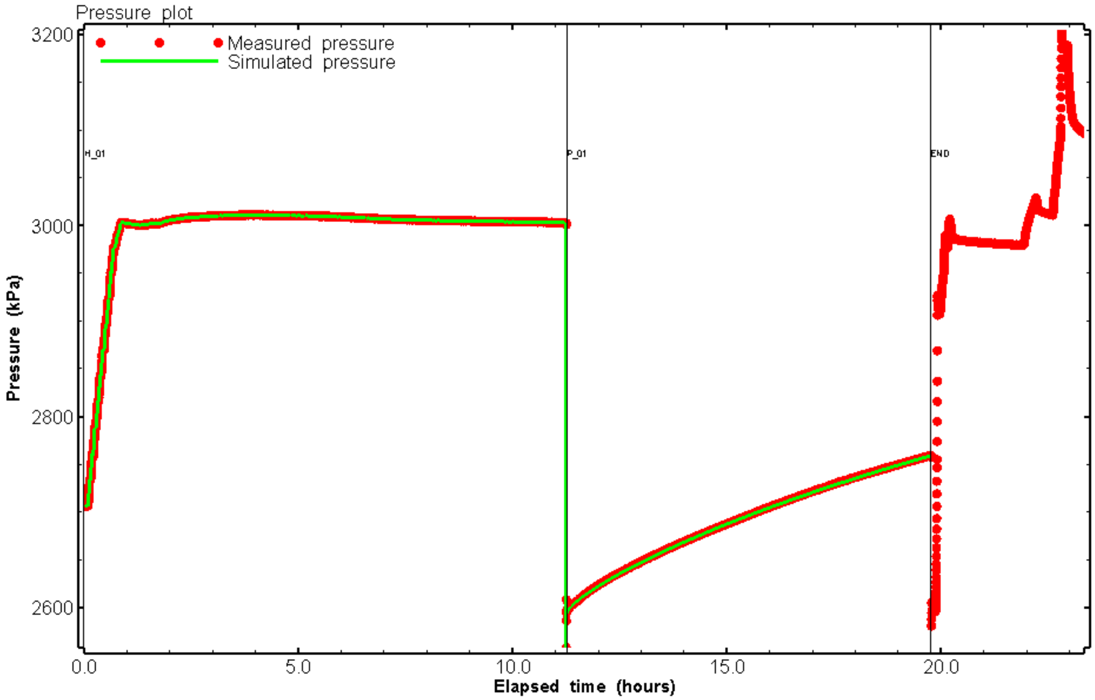

Figure 51: HT005 Pressure plot showing best-fit simulation and best fit results

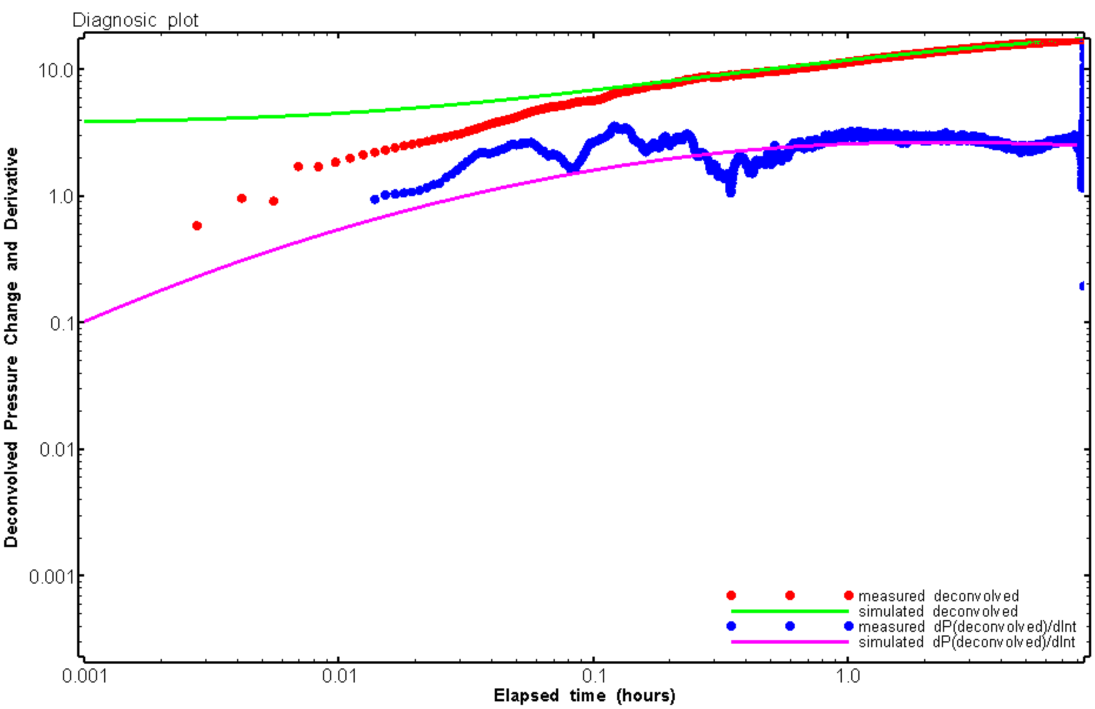

Figure 52: HT005 Deconvolved pressure change and derivative plot of the PW sequence showing best-fit simulation

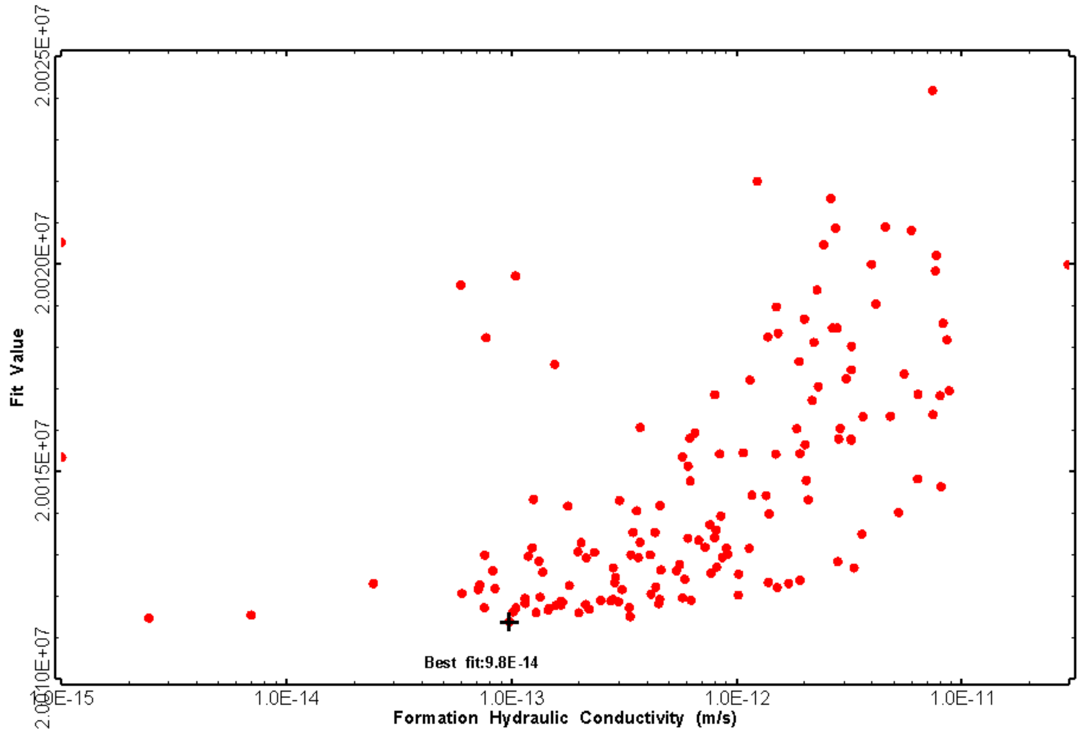

Figure 53: HT005 XY-scatter plot of formation hydraulic conductivity vs. fit value

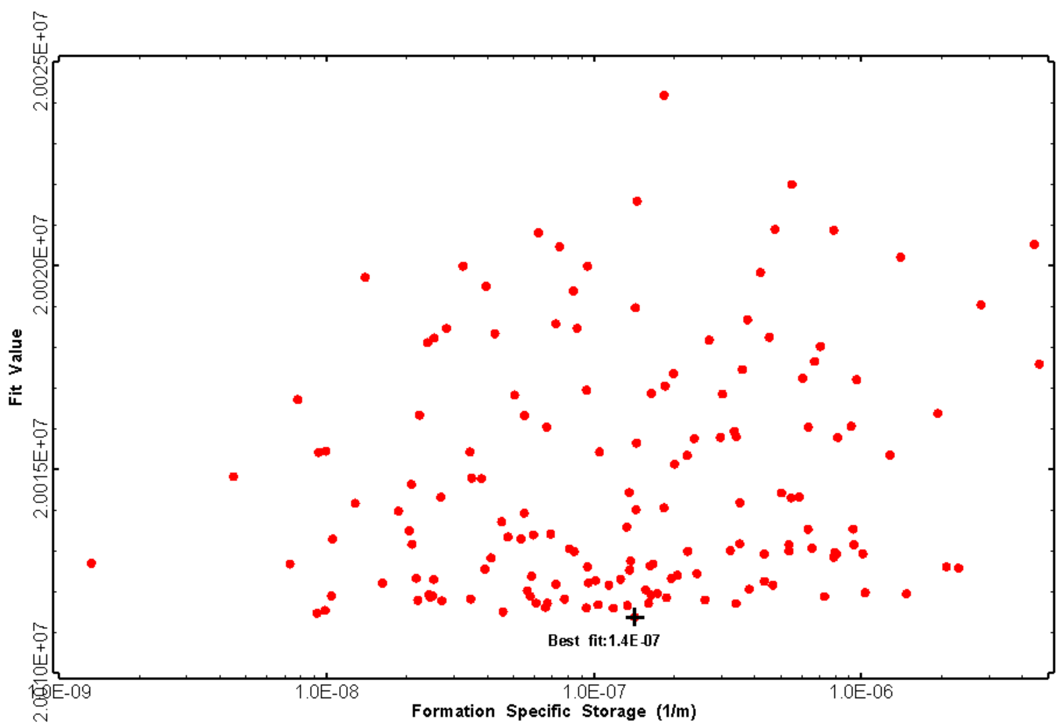

Figure 54: HT005 XY-scatter plot of formation specific storage vs. fit value

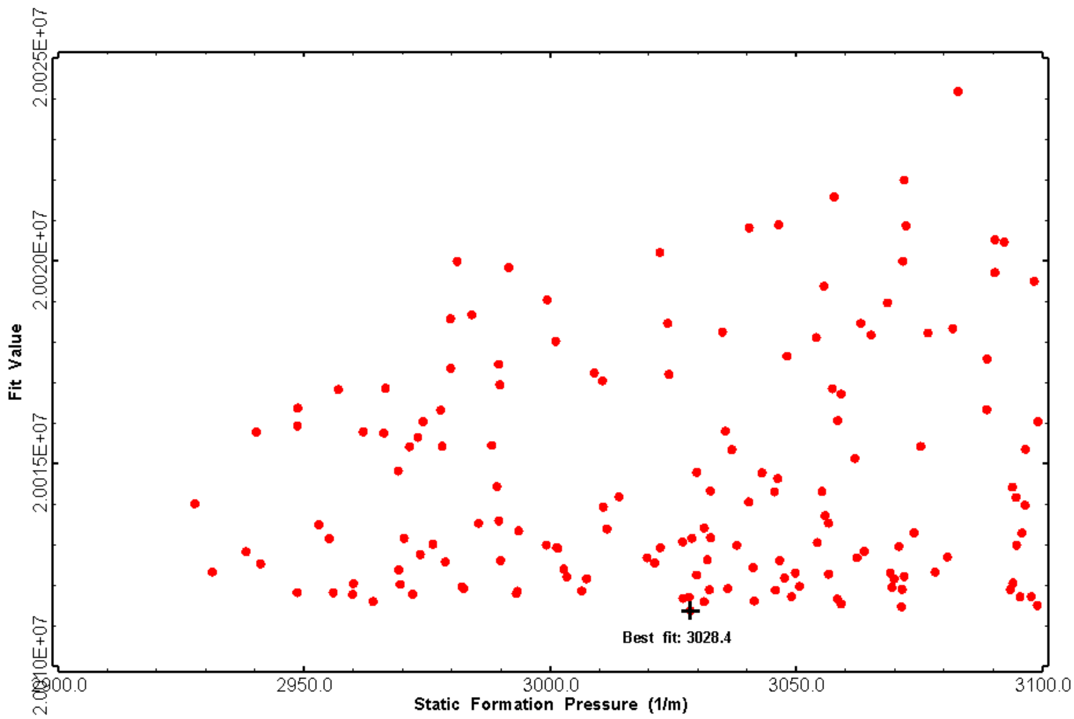

Figure 55: HT005 XY-scatter plot of static formation pressure vs. fit value

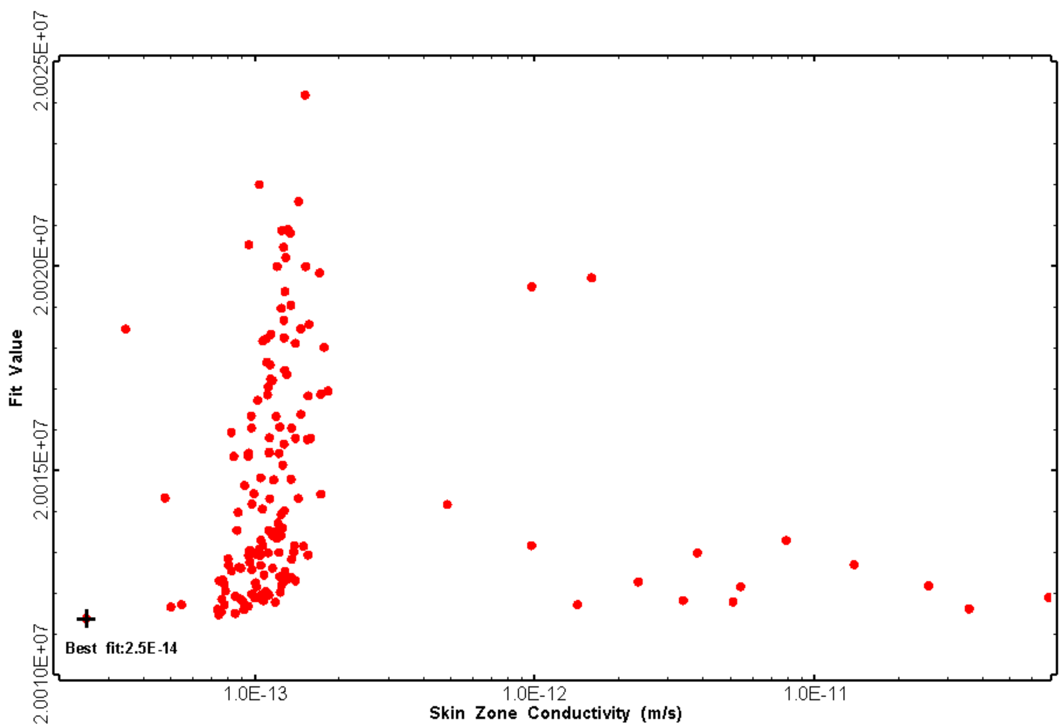

Figure 56: HT005 XY-scatter plot of skin zone conductivity vs. fit value

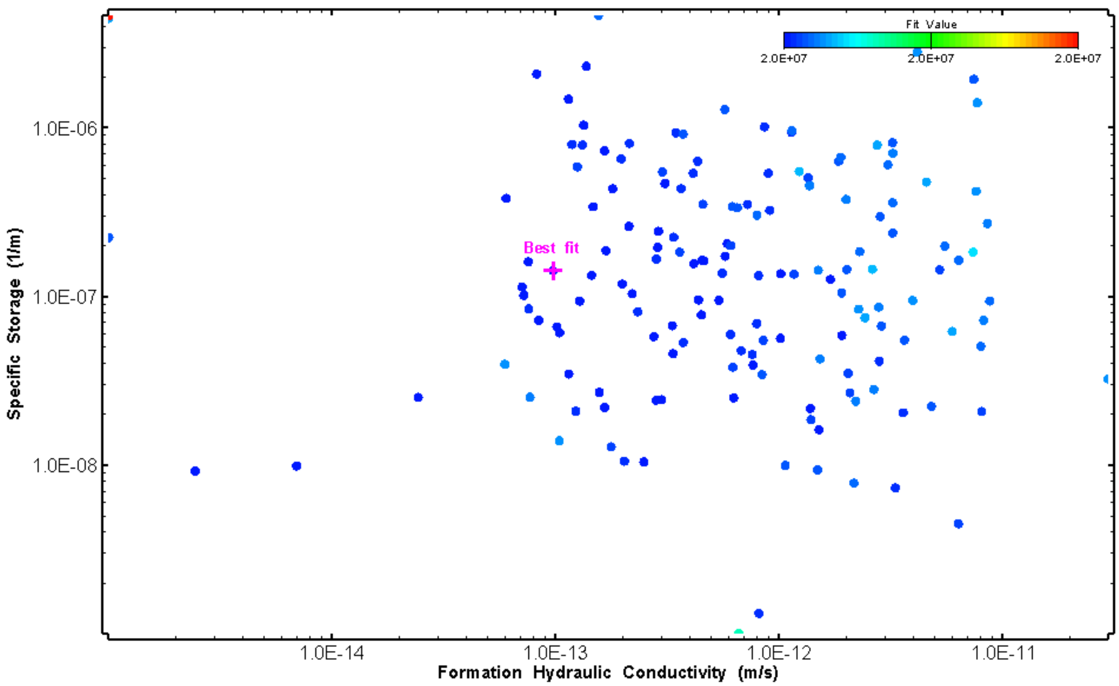

Figure 57: HT005 XY-scatter plot showing estimates of formation hydraulic conductivity and specific storage from perturbation analysis

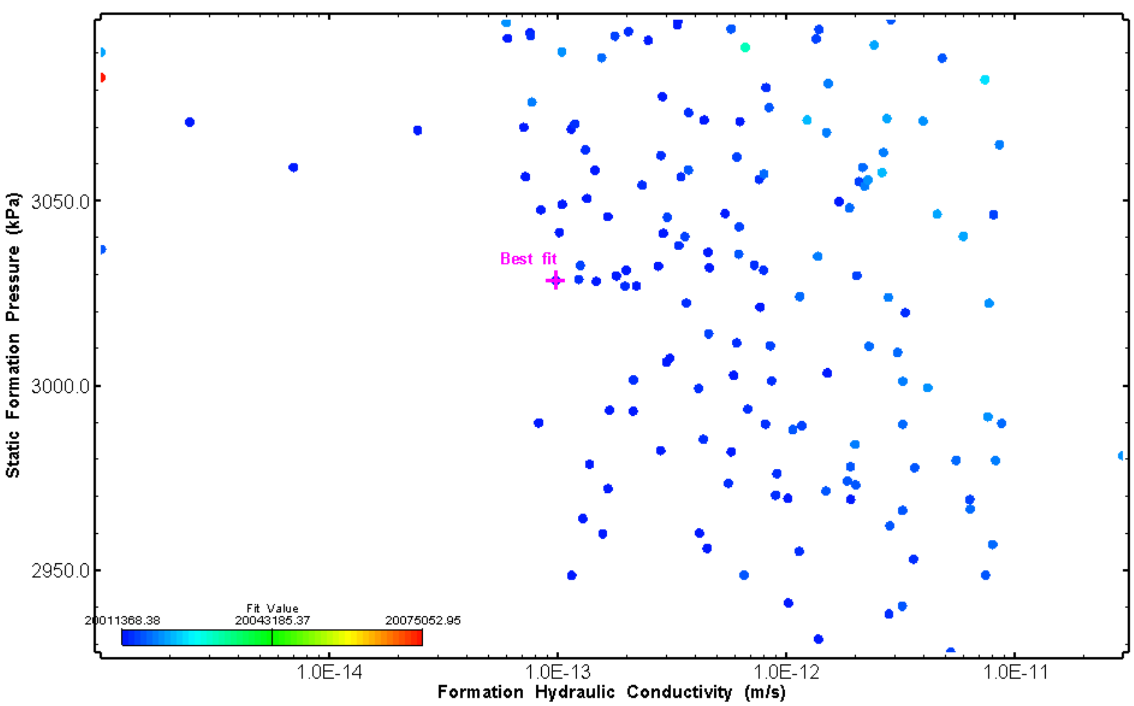

Figure 58: HT005 XY-scatter plot showing estimates of formation hydraulic conductivity and static formation pressure from perturbation analysis

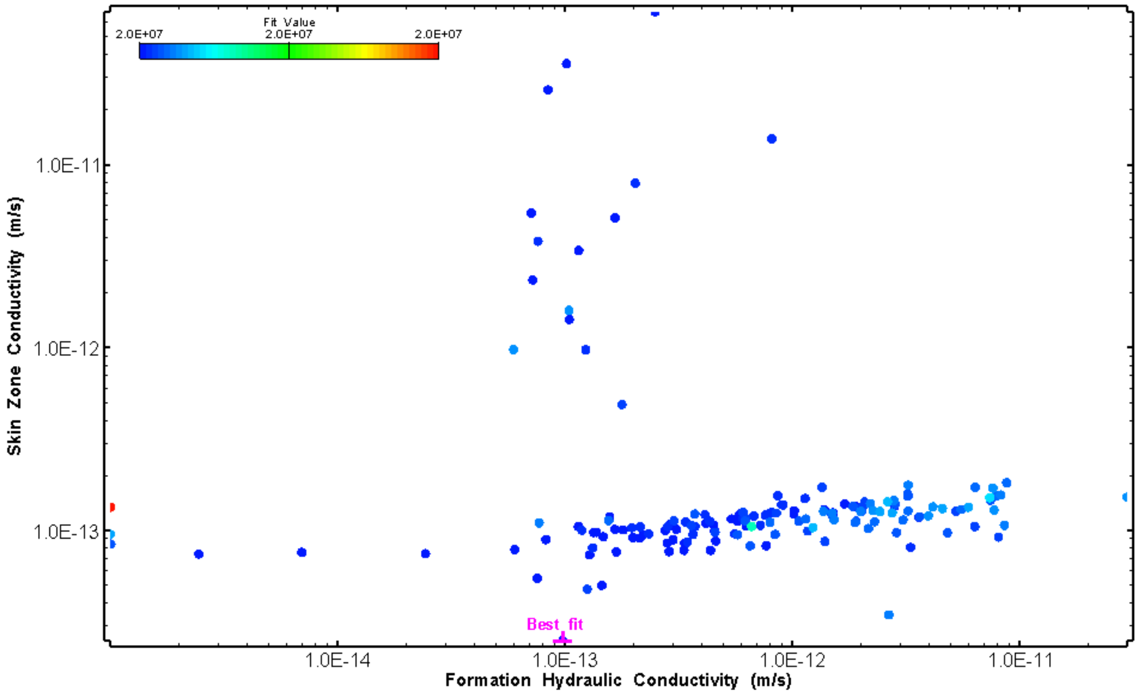

Figure 59: HT005 XY-scatter plot showing estimates of formation hydraulic conductivity and skin zone conductivity from perturbation analysis

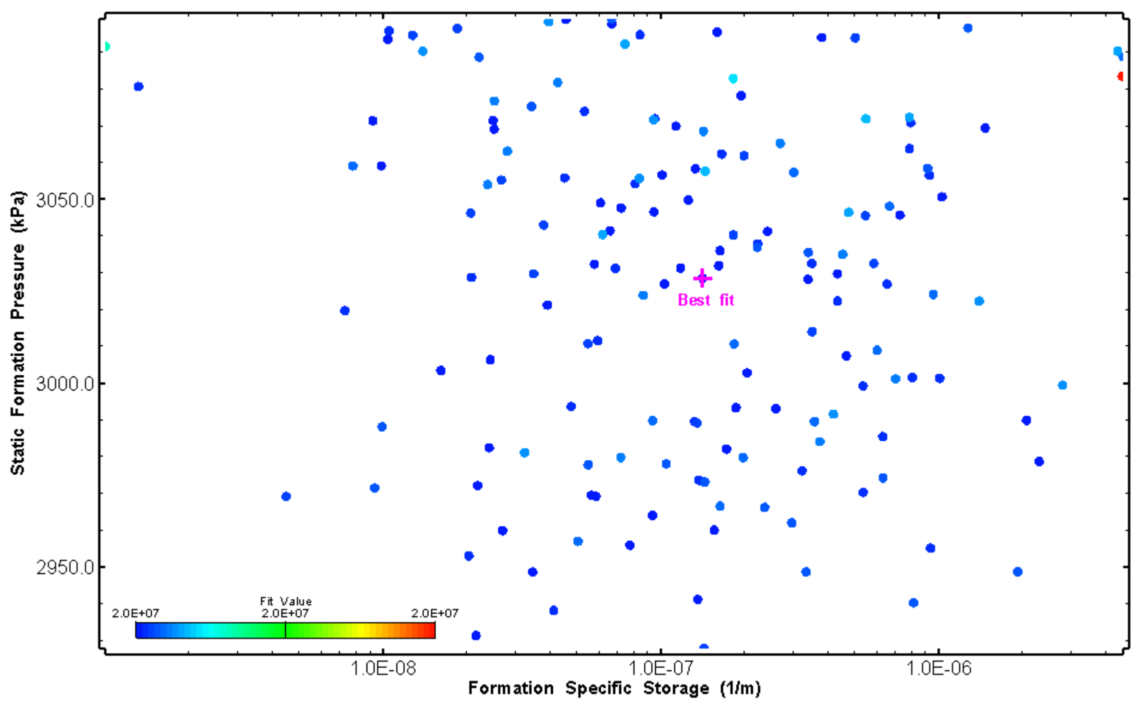

Figure 60: HT005 XY-scatter plot showing estimates of specific storage and static formation pressure from perturbation analysis

6.0 HT006 (401.21 – 421.24 M)

HT006 was selected to test a shallow slightly fractured interval. Six broken fractures were observed in the core. A change in electrical conductivity of drilling fluid was observed in this interval. An indication of flow was recorded during FFEC logging post-drilling.

The test was initiated with a shut-in pressure recovery phase (PSR). A pulse withdrawal test (PW) with a shut-in recovery was completed after the PSR phase.

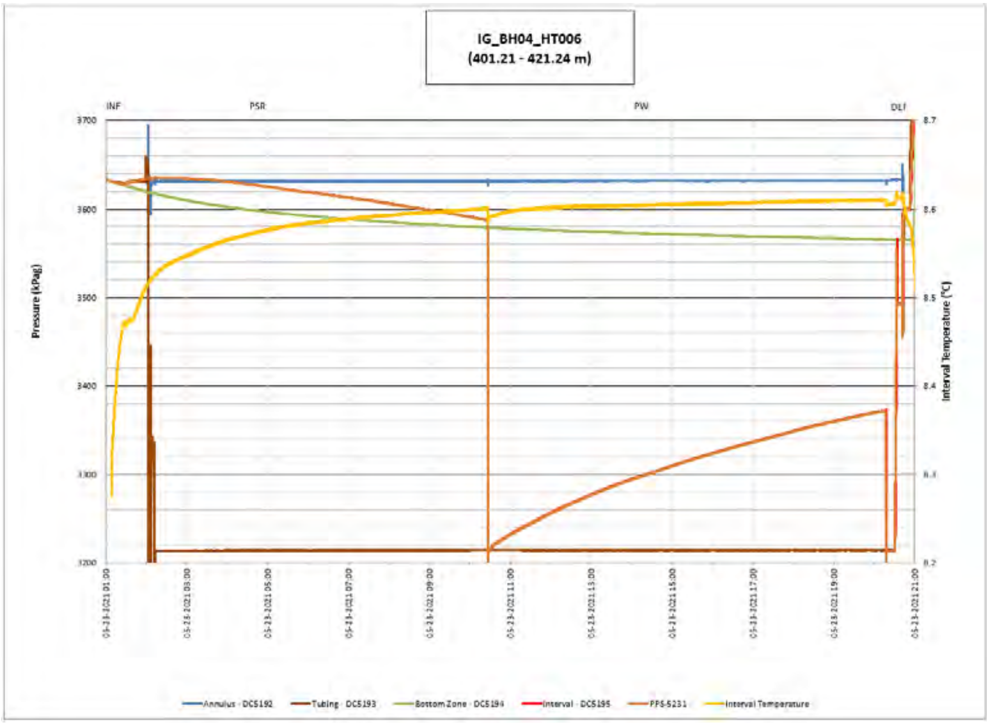

Figure 61: HT006 Annotated test plot showing monitored zone pressure and interval temperature.

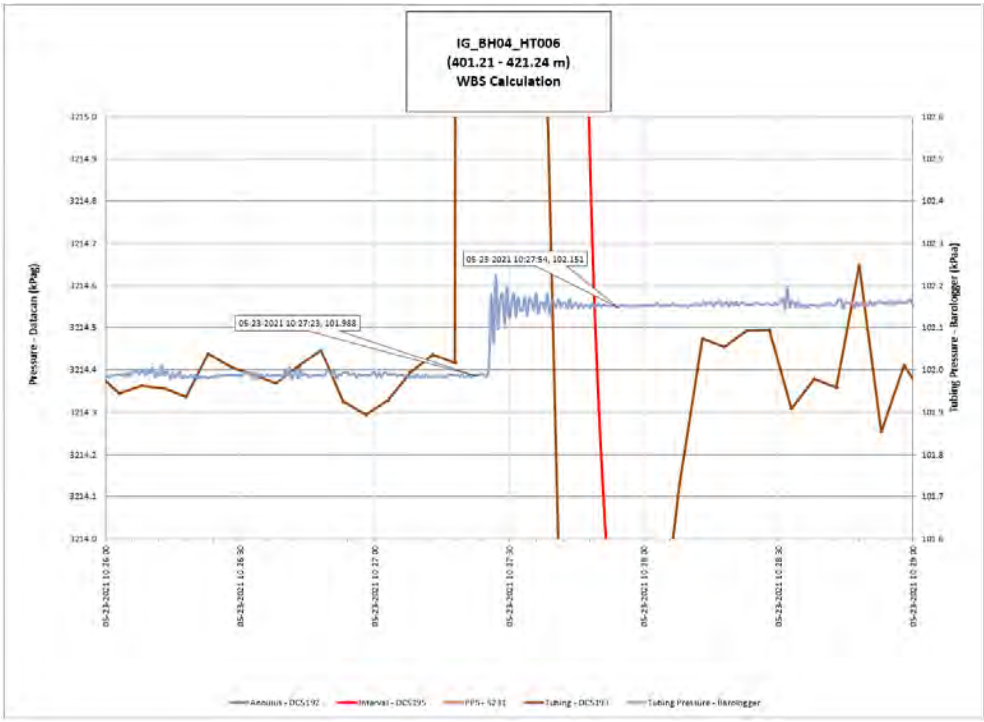

Figure 62: HT006 Tubing pressure during DHSIV activation. DHSIV Closed Wellbore Storage Estimate = 8E-11 m^3/Pa

Table 6: Summary of Analysis Results – HT006

	Formation conductivity	Skin zone conductivity	Static formation pressure	Formation specific storage	Radial thickness of skin	Flow dimension
	[m/s]	[m/s]	[kPa]	[1/m]	[m]	[–]
Best Fit	1.4E-13	3.2E-14	3606	7.5E-07	9.4E-03	2.2
Minimum	1.0E-14	3.0E-14	3448	1.0E-09	1.9E-03	1.0
Maximum	9.8E-11	1.8E-13	3699	9.8E-06	8.9E-01	3.0
Mean	6.5E-12	9.5E-14	3539	1.2E-06	6.9E-02	2.1
Median	9.7E-13	9.6E-14	3518	2.3E-07	4.0E-02	2.1
Geometric mean	1.2E-12	9.0E-14	3538	2.1E-07	4.4E-02	2.0

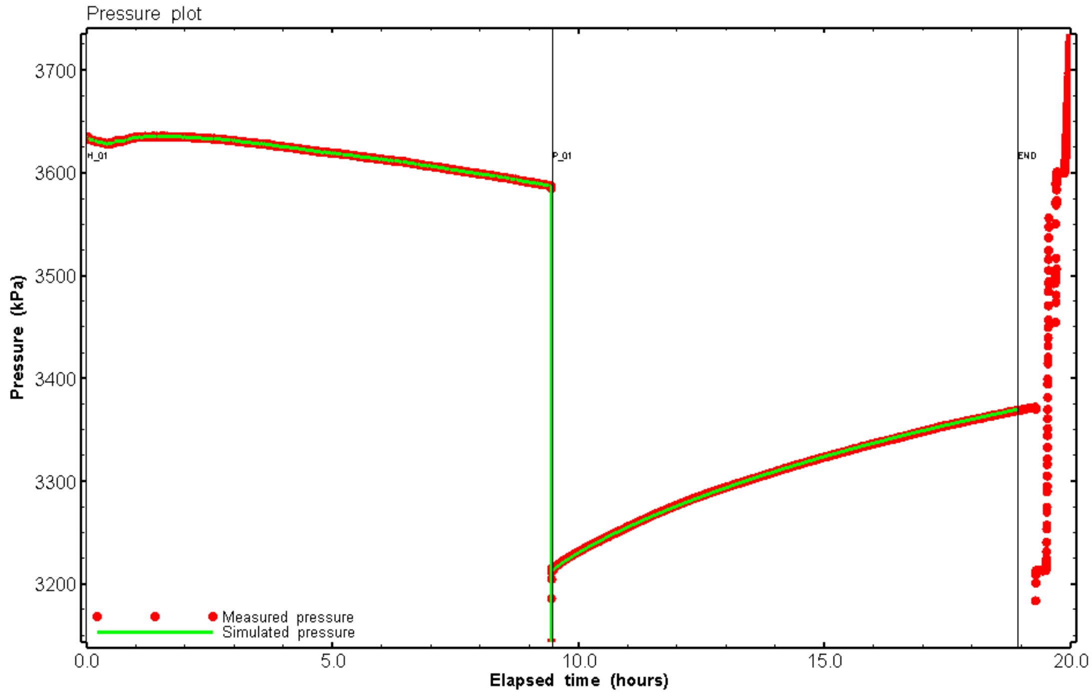

Figure 63: HT006 Pressure plot showing best-fit simulation and best fit results

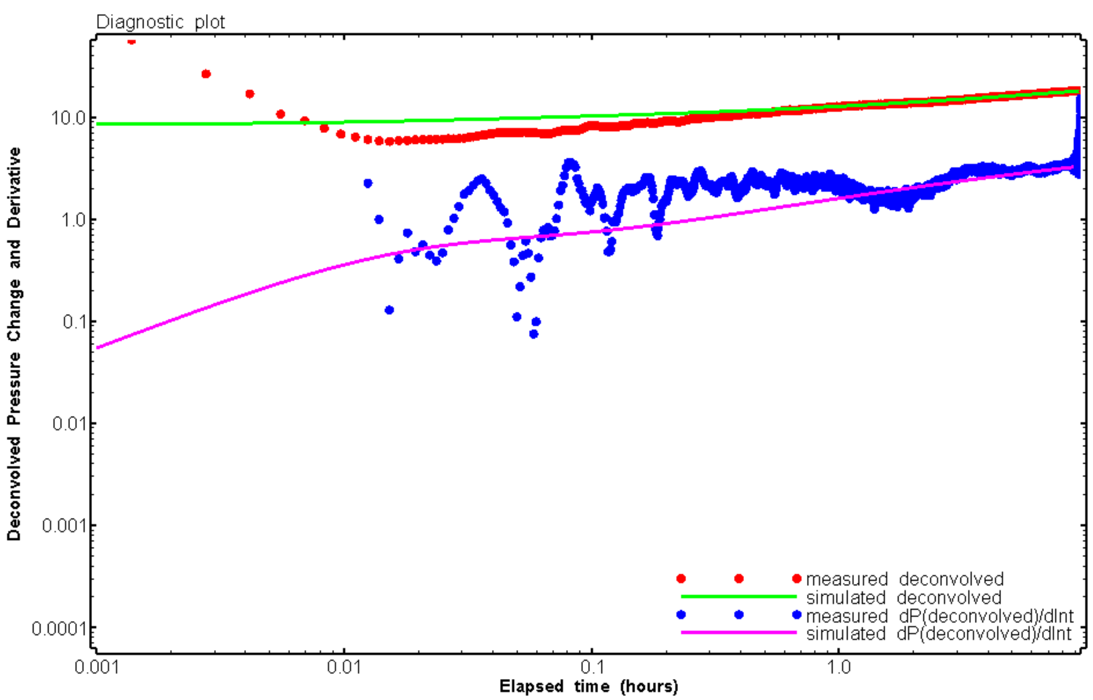

Figure 64: HT006 Deconvolved pressure change and derivative plot of the PW sequence showing best-fit simulation

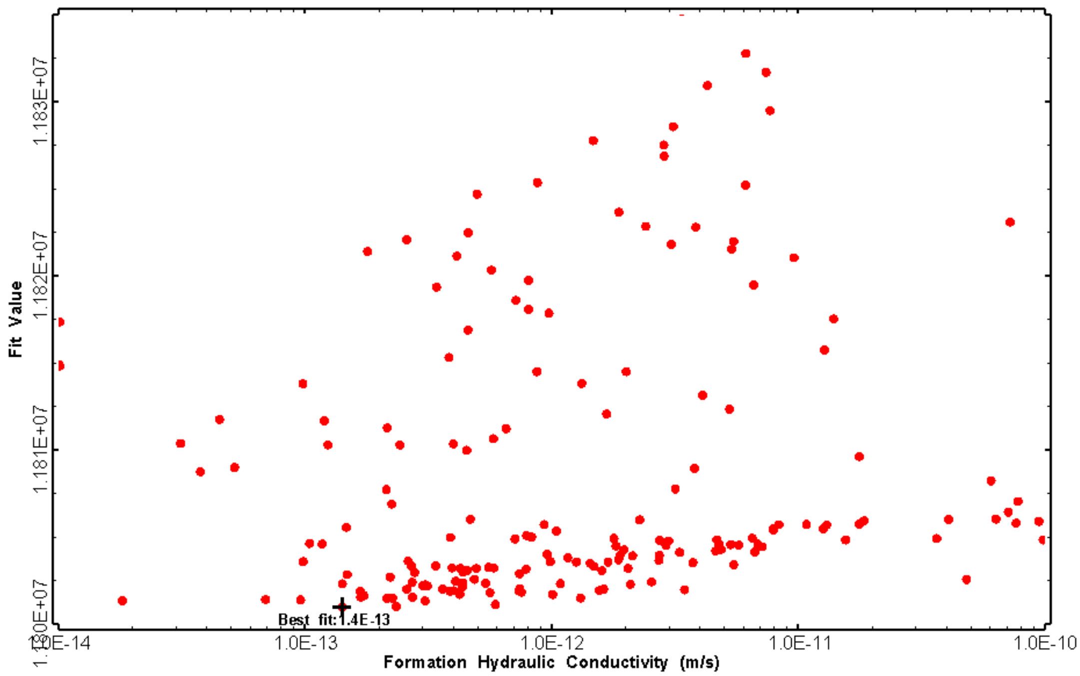

Figure 65: HT006 XY-scatter plot of formation hydraulic conductivity vs. fit value

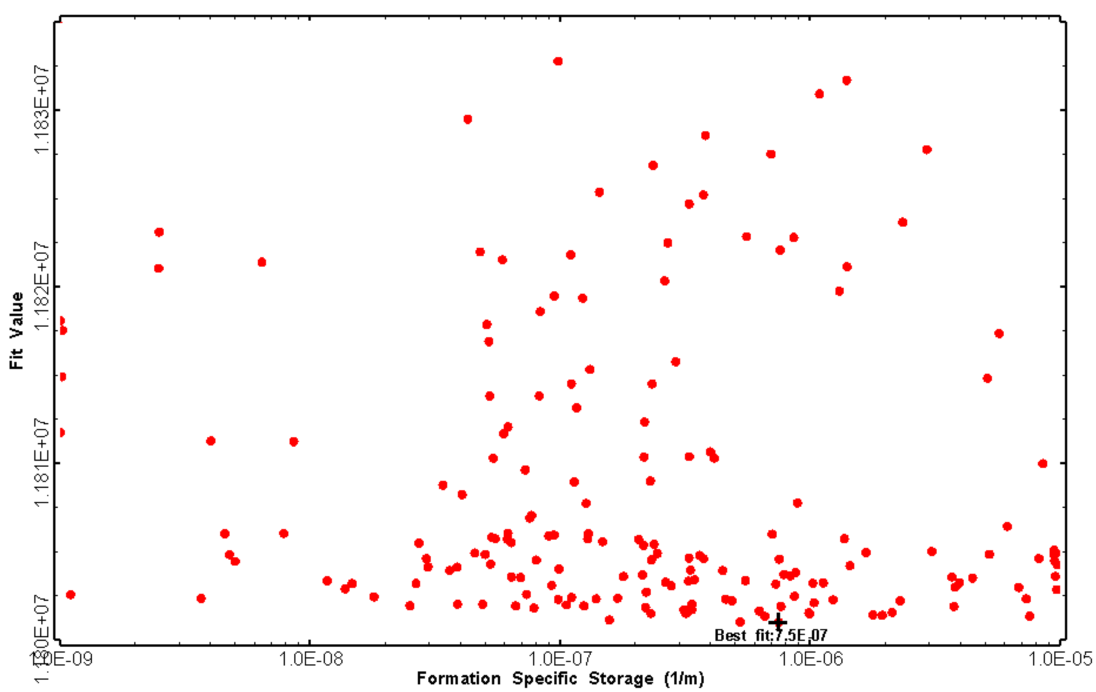

Figure 66: HT006 XY-scatter plot of formation specific storage vs. fit value

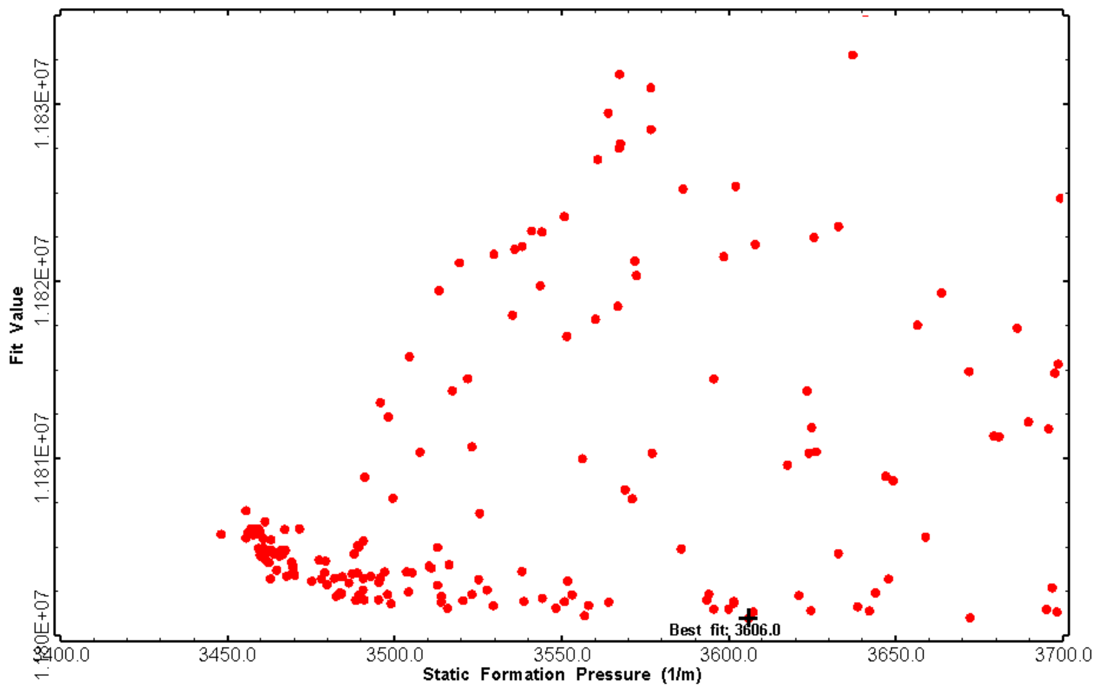

Figure 67: HT006 XY-scatter plot of static formation pressure vs. fit value

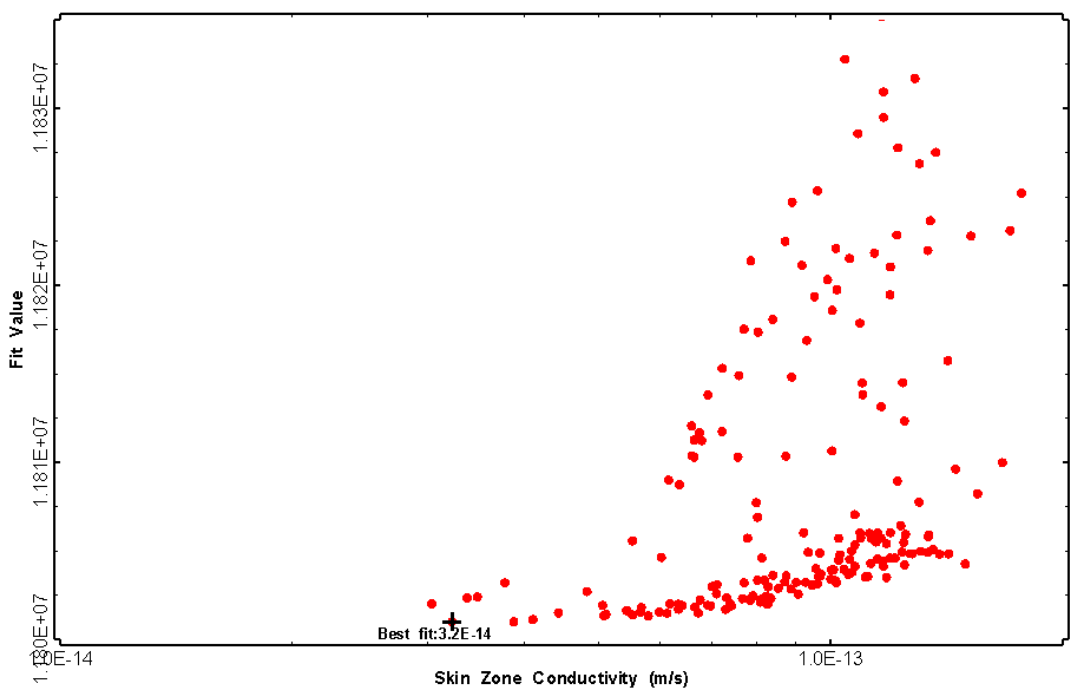

Figure 68: HT006 XY-scatter plot of skin zone conductivity vs. fit value

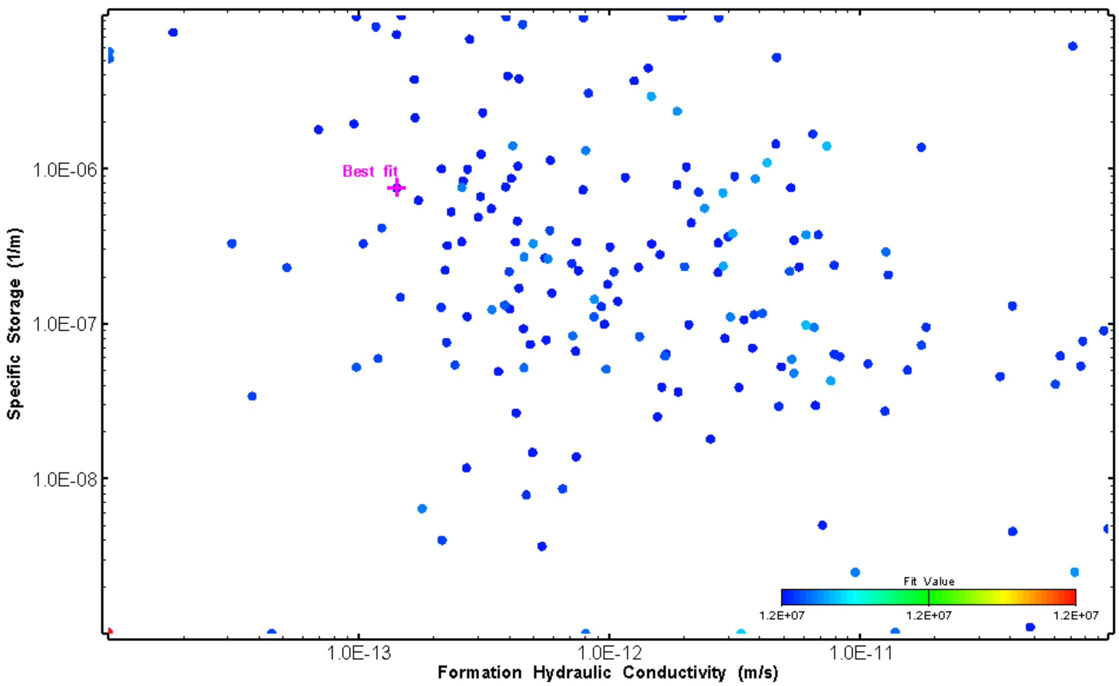

Figure 69: HT006 XY-scatter plot showing estimates of formation hydraulic conductivity and specific storage from perturbation analysis

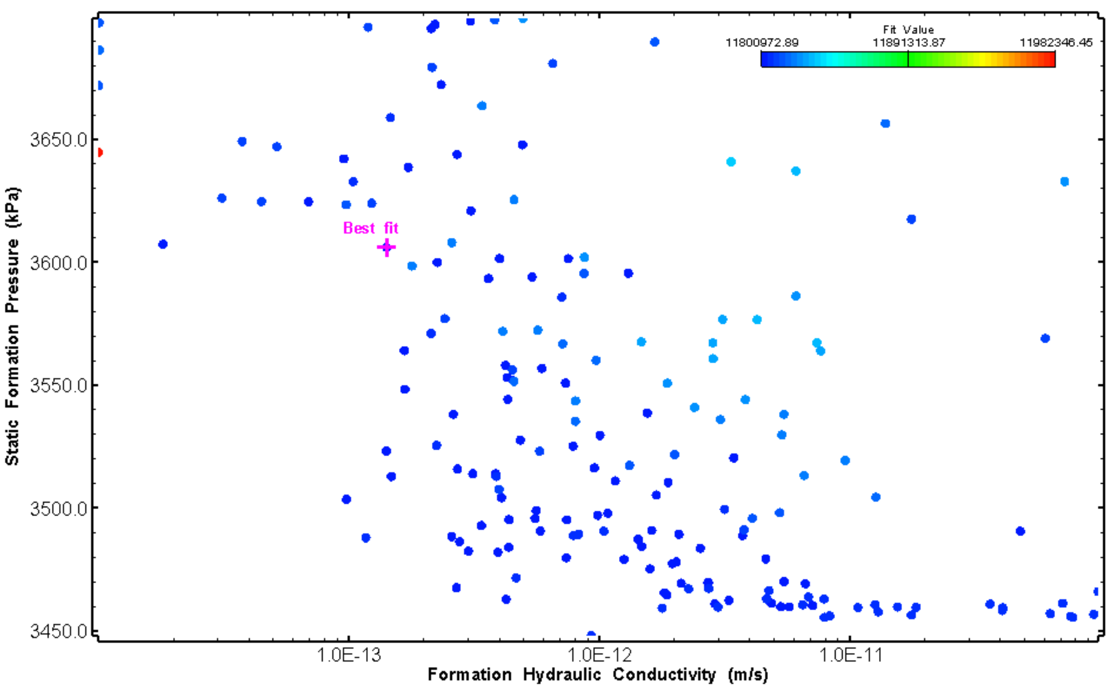

Figure 70: HT006 XY-scatter plot showing estimates of formation hydraulic conductivity and static formation pressure from perturbation analysis

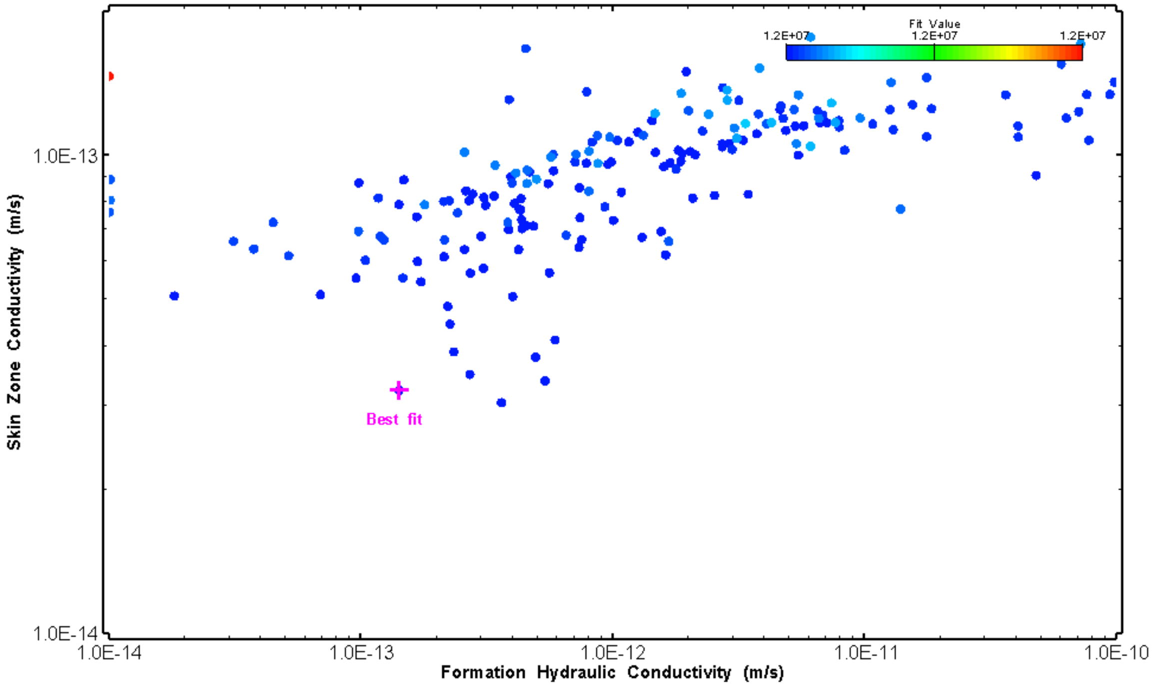

Figure 71: HT006 XY-scatter plot showing estimates of formation hydraulic conductivity and skin zone conductivity from perturbation analysis

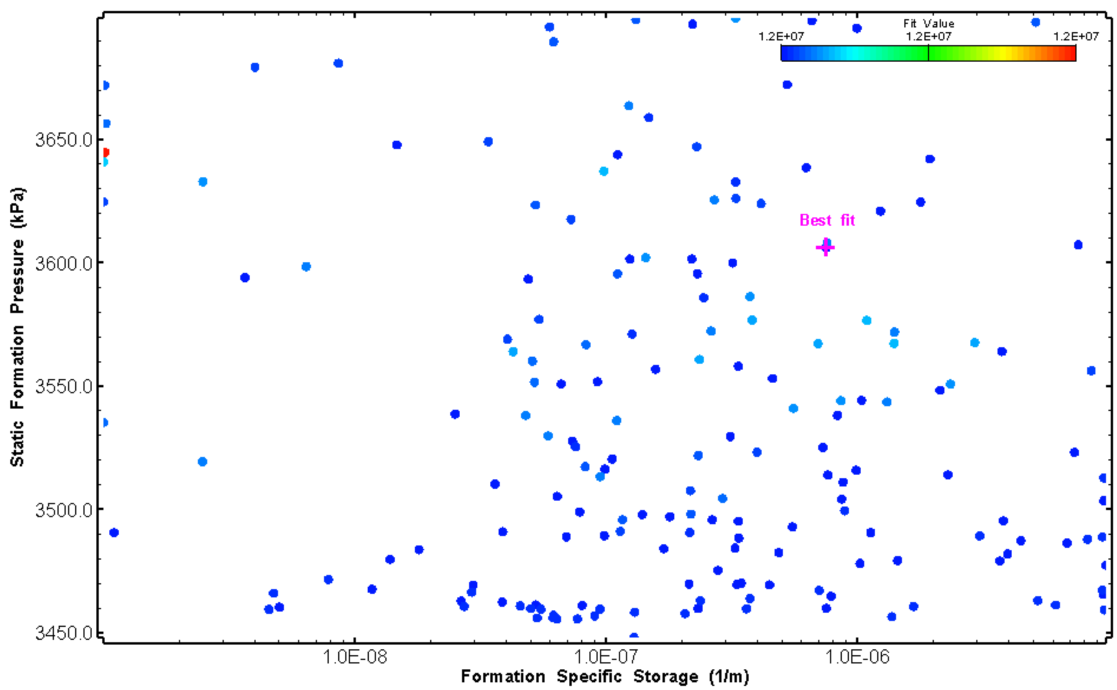

Figure 72: HT006 XY-scatter plot showing estimates of specific storage and static formation pressure from perturbation analysis

7.0 HT007A (429.99 – 450.02 M)

HT007a was selected to test a fractured interval with a dyke. Three broken fractures were observed in the core. No drill fluid parameter triggers were reached during drilling. An indication of flow was recorded during FFEC logging post-drilling.

The test was initiated with a shut-in pressure recovery phase (PSR). A pulse withdrawal test (PW) with a shut-in recovery was completed after the PSR phase.

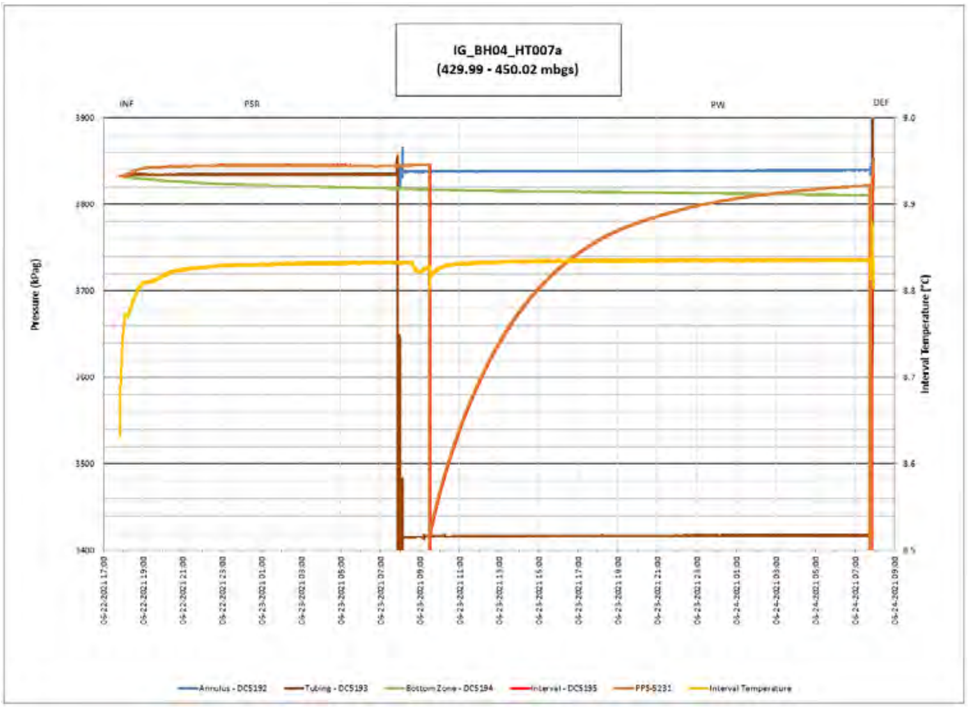

Figure 73: HT007A Annotated test plot showing monitored zone pressure and interval temperature.

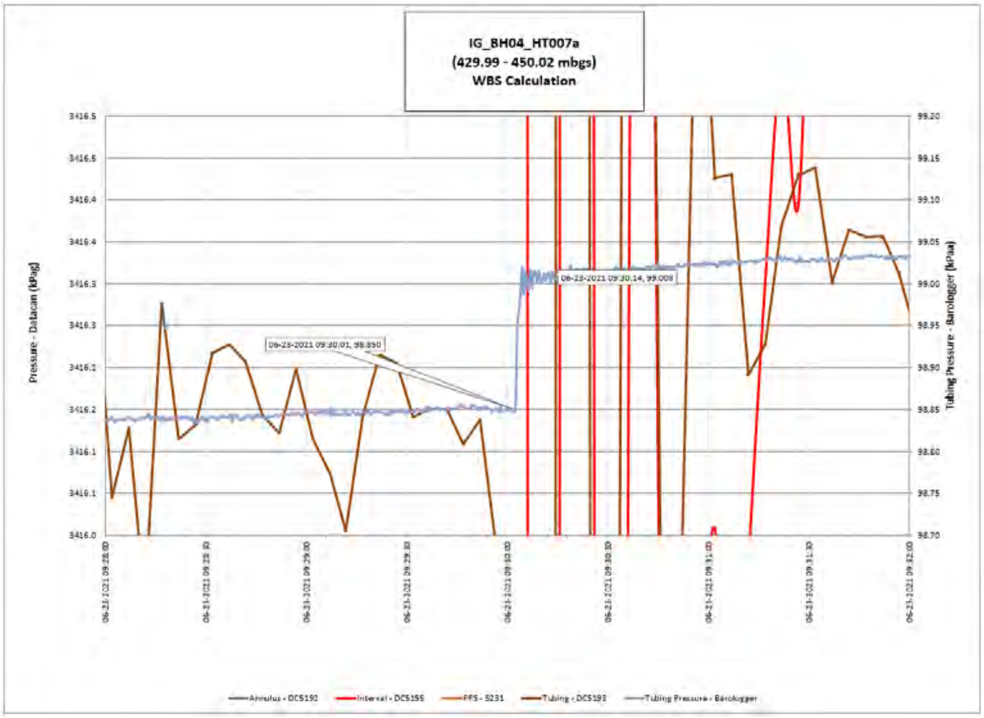

Figure 74: HT007A Tubing pressure during DHSIV activation. DHSIV Closed Wellbore Storage Estimate = 7E-11 m^3/Pa

Table 7: Summary of Analysis Results – HT007A

	Formation conductivity	Skin zone conductivity	Static formation pressure	Formation specific storage	Radial thickness of skin	Flow dimension
	[m/s]	[m/s]	[kPa]	[1/m]	[m]	[–]
Best Fit	5.7E-13	6.7E-14	3827	2.2E-08	4.5E-03	2.8
Minimum	1.6E-13	1.6E-14	3801	1.0E-09	1.0E-03	1.2
Maximum	3.1E-11	1.0E-10	3900	8.9E-06	3.6E-02	3.0
Mean	1.4E-12	2.1E-11	3857	1.4E-07	9.9E-03	2.5
Median	5.8E-13	2.1E-13	3857	1.6E-08	8.1E-03	2.5
Geometric mean	7.4E-13	1.1E-12	3857	1.9E-08	7.2E-03	2.4

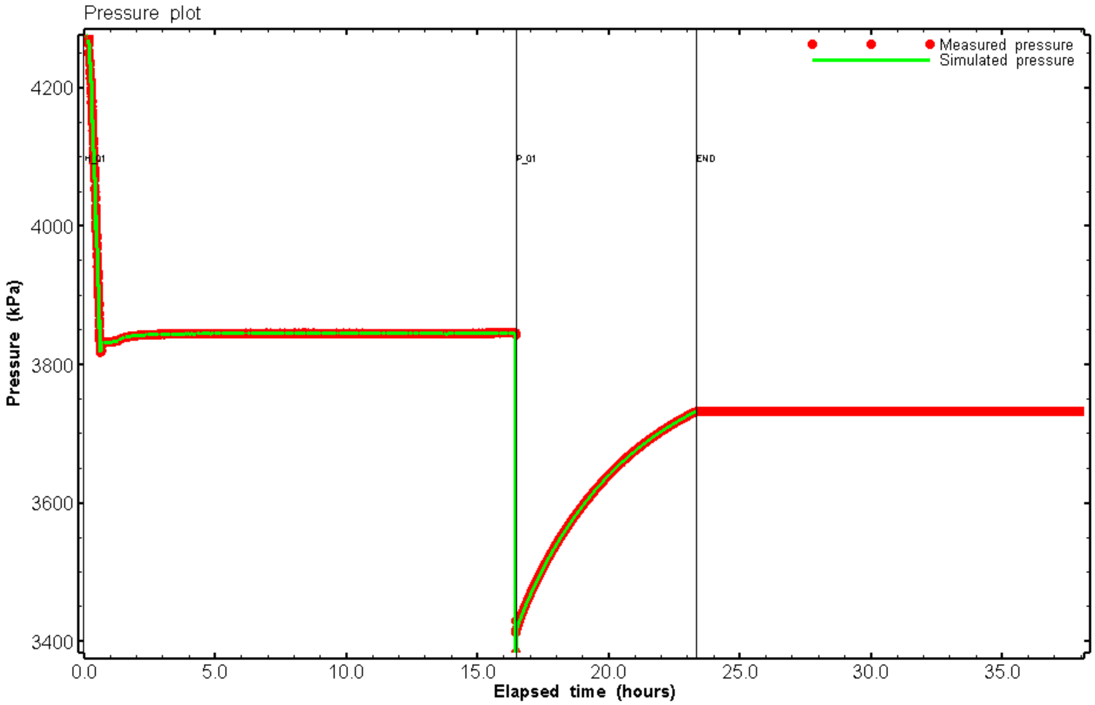

Figure 75: HT007A Pressure plot showing best-fit simulation and best fit results

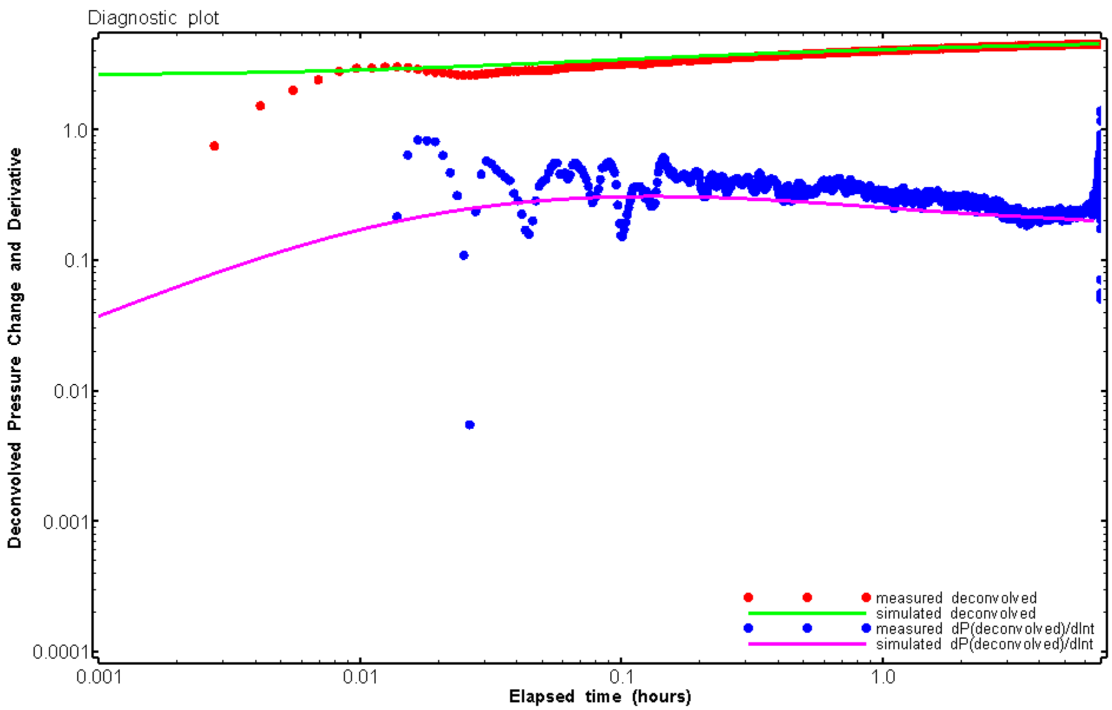

Figure 76: HT007A Deconvolved pressure change and derivative plot of the PW sequence showing best-fit simulation

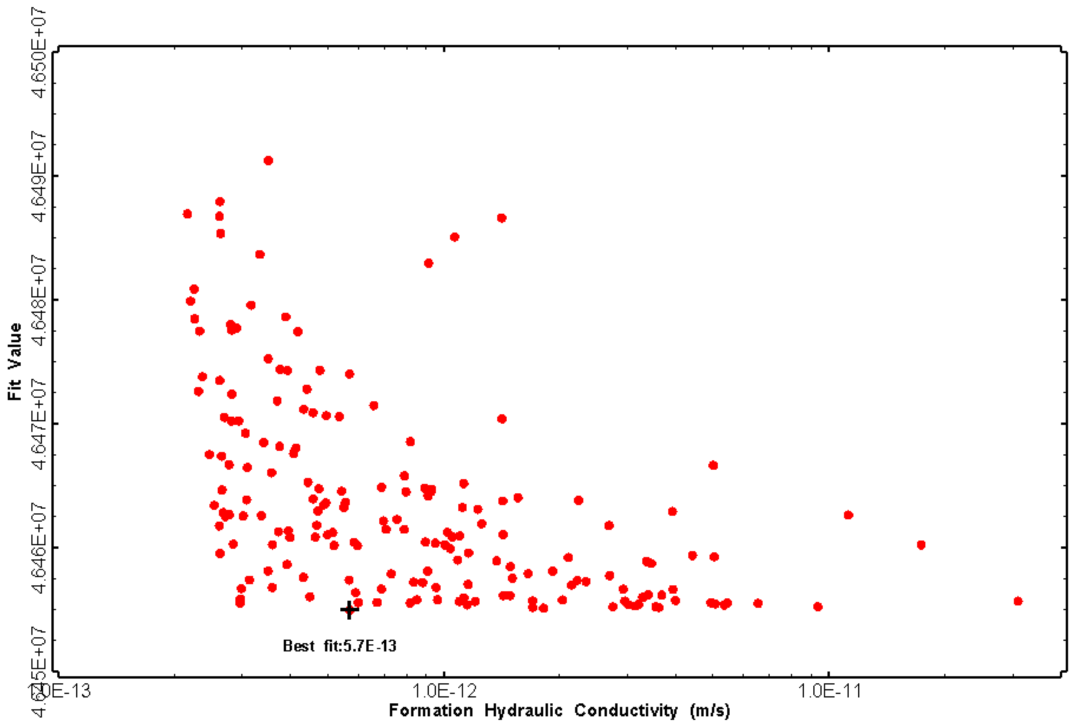

Figure 77: HT007A XY-scatter plot of formation hydraulic conductivity vs. fit value

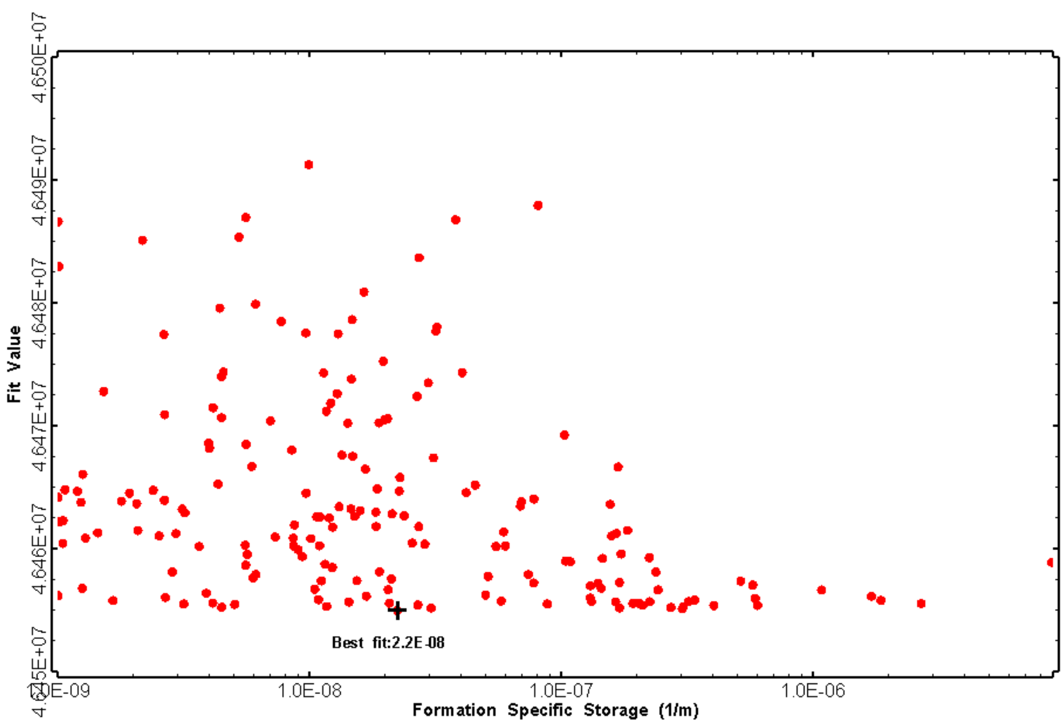

Figure 78: HT007A XY-scatter plot of formation specific storage vs. fit value

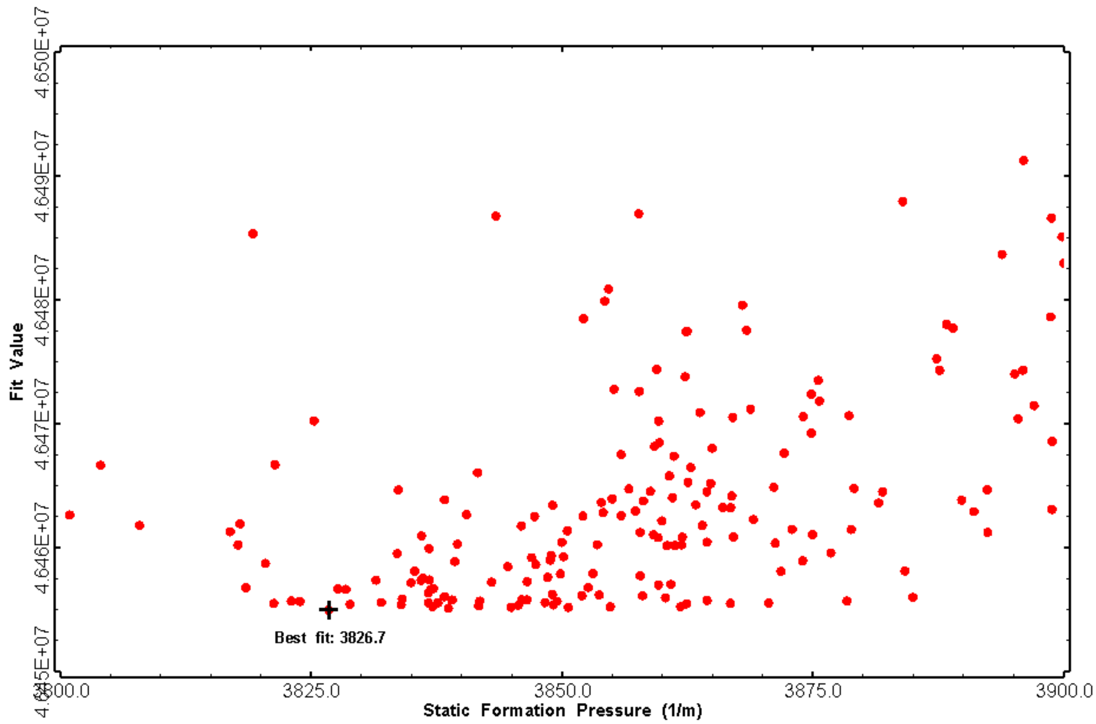

Figure 79: HT007A XY-scatter plot of static formation pressure vs. fit value

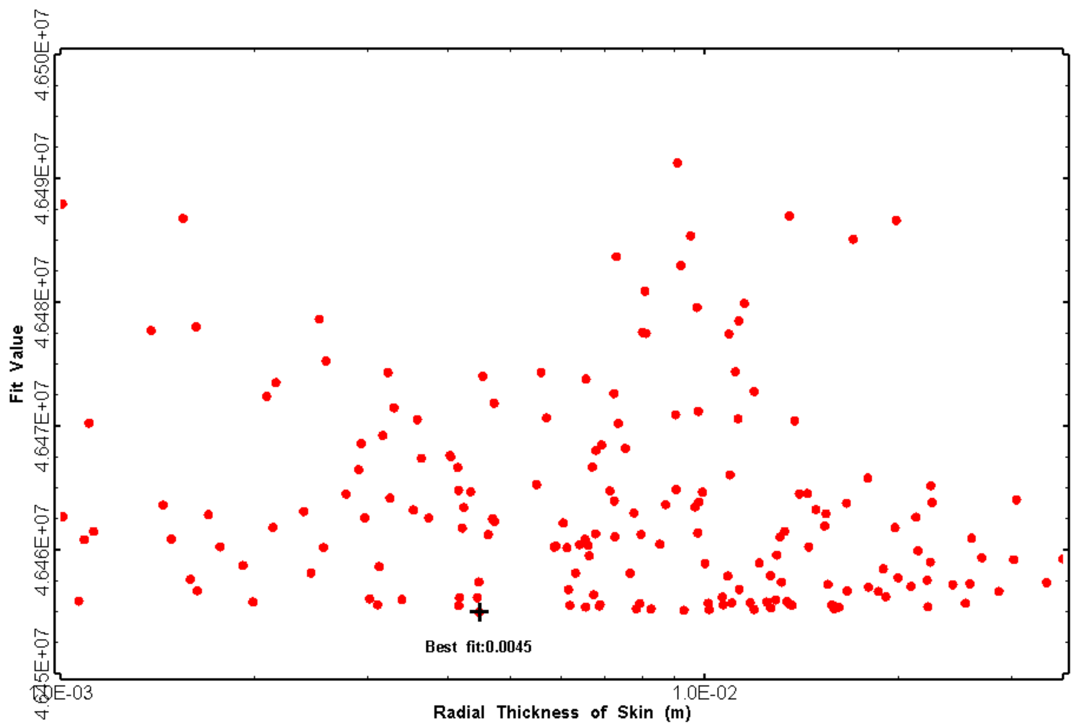

Figure 80: HT007A XY-scatter plot of skin zone conductivity vs. fit value

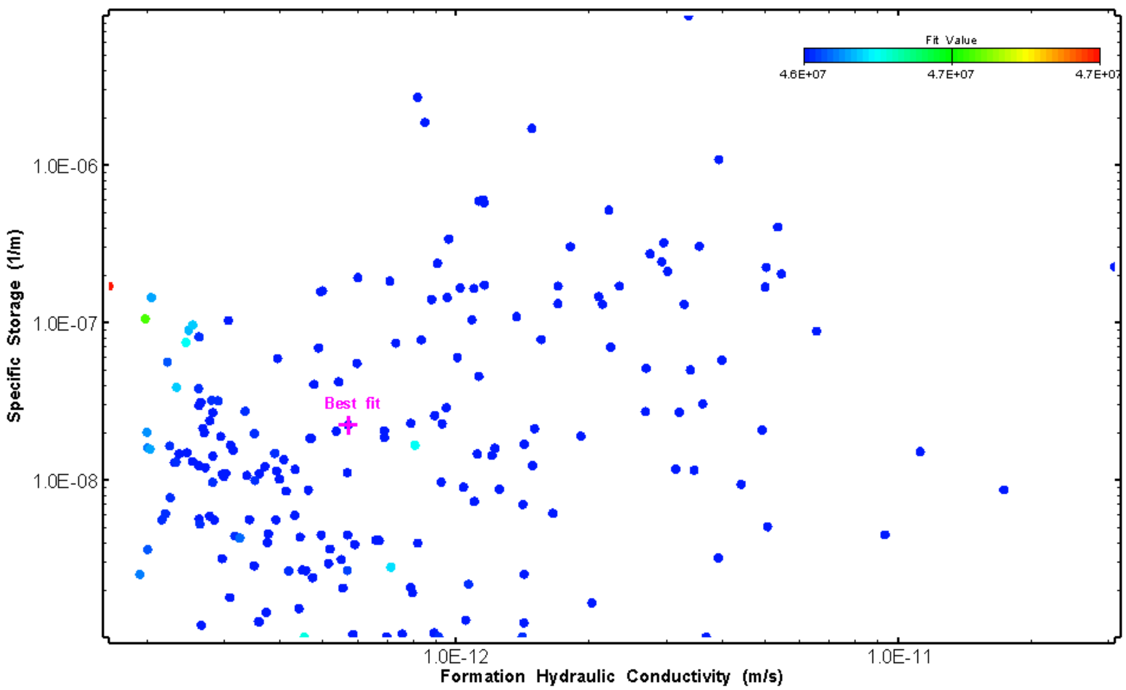

Figure 81: HT007A XY-scatter plot showing estimates of formation hydraulic conductivity and specific storage from perturbation analysis

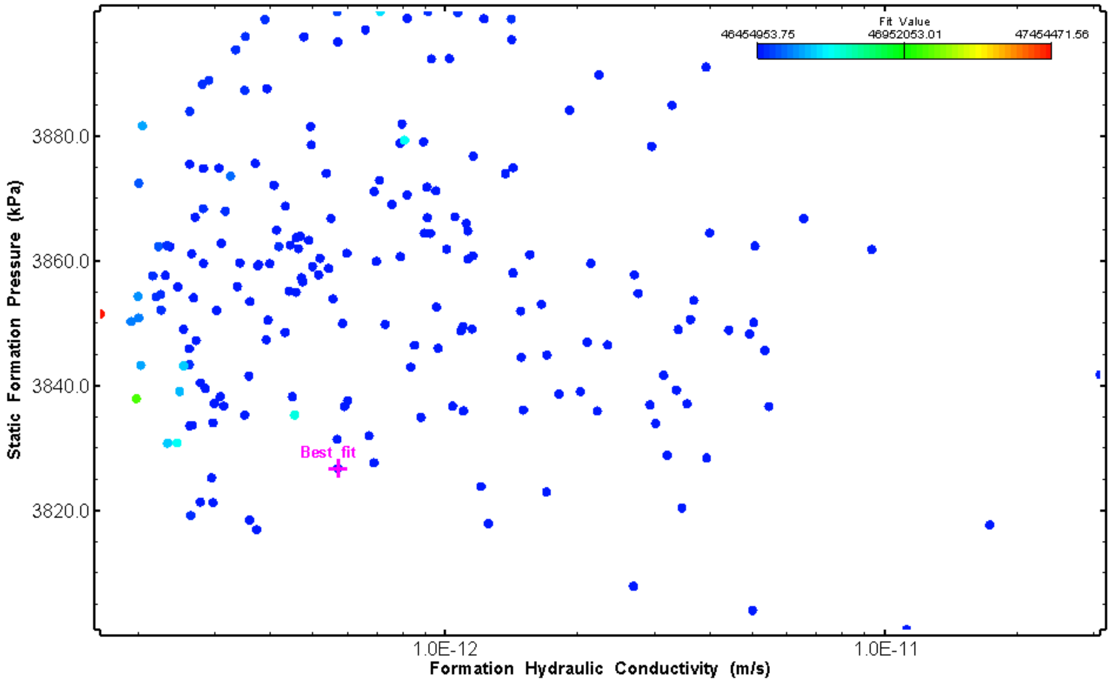

Figure 82: HT007A XY-scatter plot showing estimates of formation hydraulic conductivity and static formation pressure from perturbation analysis

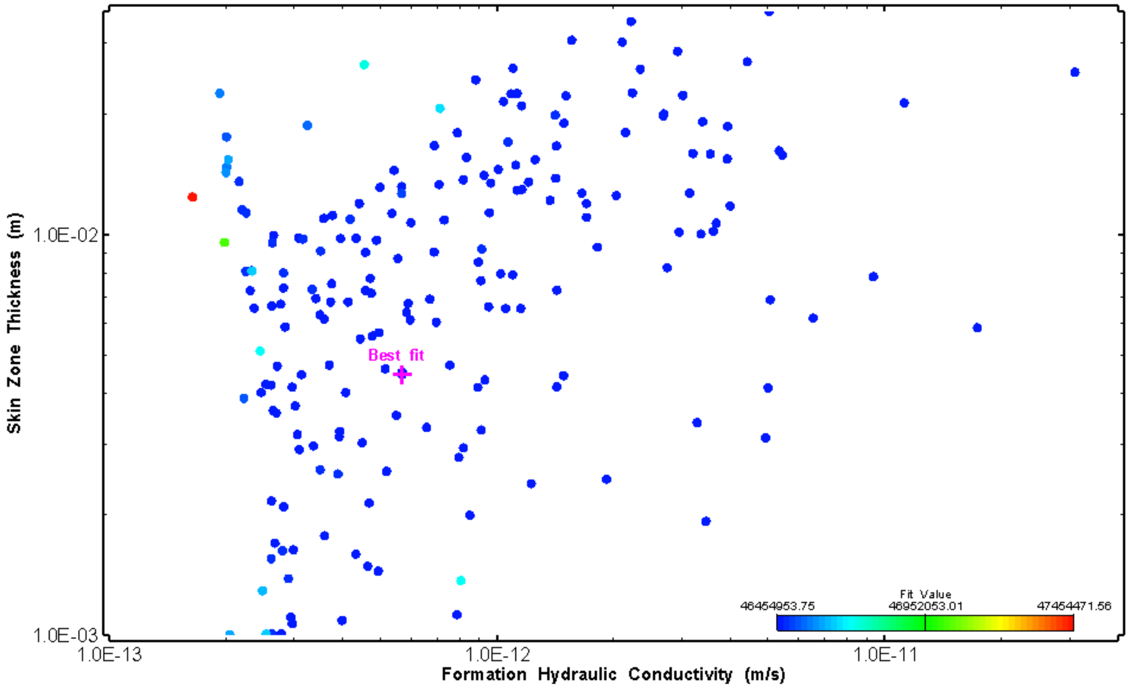

Figure 83: HT007A XY-scatter plot showing estimates of formation hydraulic conductivity and skin zone conductivity from perturbation analysis

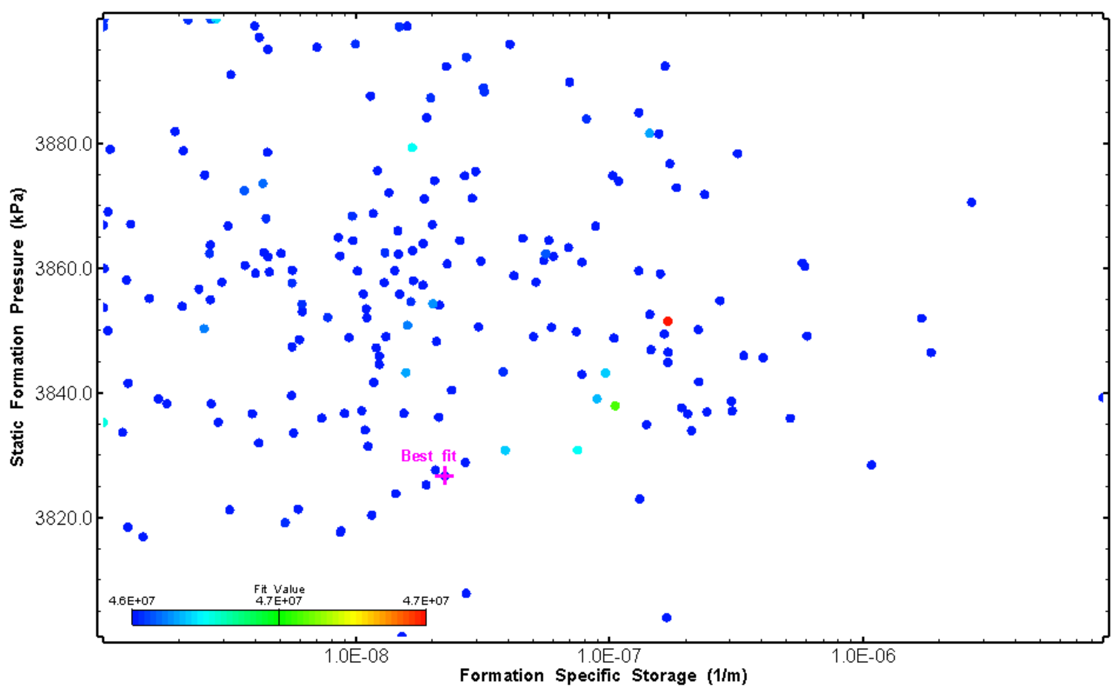

Figure 84: HT007A XY-scatter plot showing estimates of specific storage and static formation pressure from perturbation analysis

8.0 HT008A (477.70 – 497.73 M)

HT008a was selected to test a fractured interval with a dyke. Four broken fractures were observed in the core. No drill fluid parameter triggers were reached during drilling. An indication of flow was recorded during FFEC logging post-drilling.

The test was initiated with a shut-in pressure recovery phase (PSR). A pulse withdrawal test (PW) with a shut-in recovery was completed after the PSR phase.

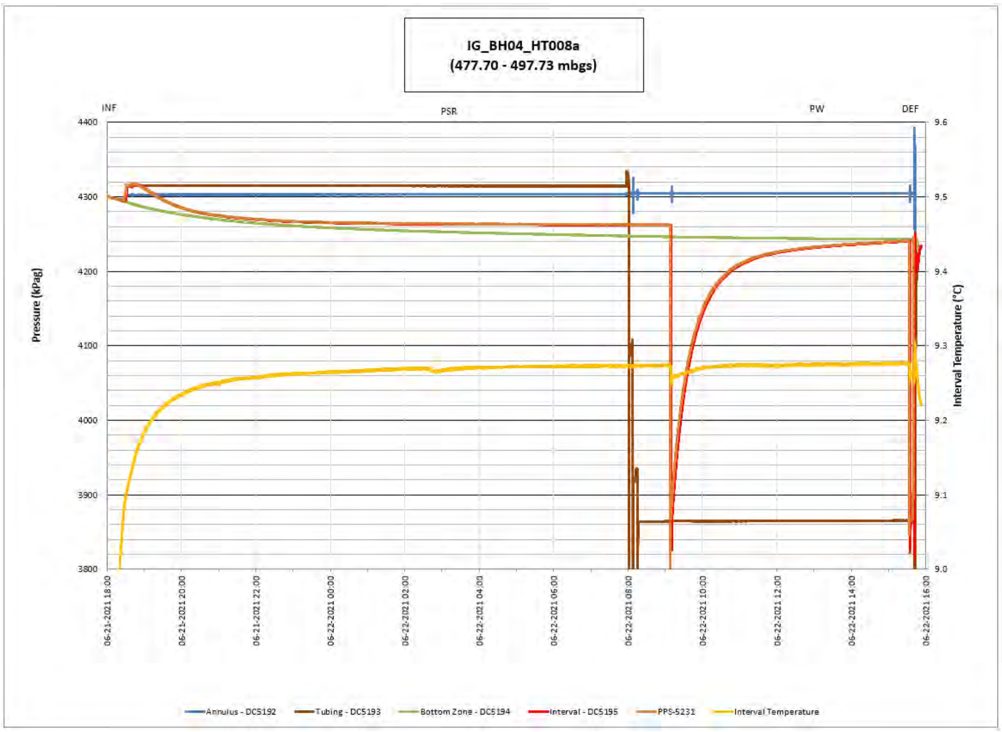

Figure 85: HT008A Annotated test plot showing monitored zone pressure and interval temperature.

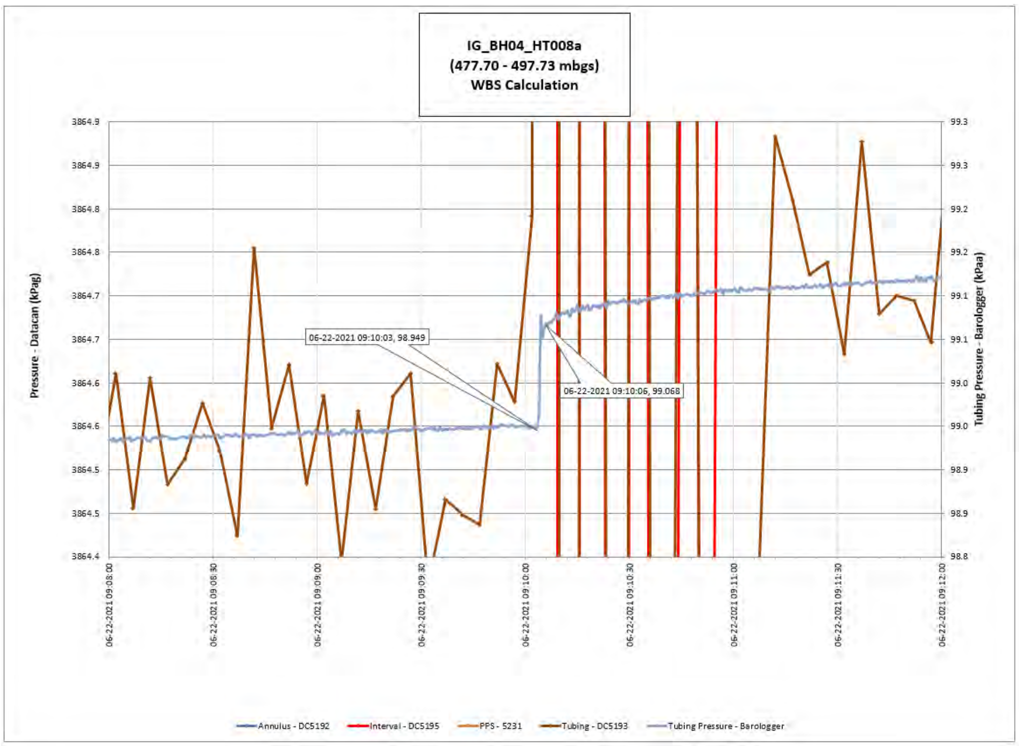

Figure 86: HT008A Tubing pressure during DHSIV activation. DHSIV Closed Wellbore Storage Estimate = 5E-11 m^3/Pa

Table 8: Summary of Analysis Results – HT008A

	Formation conductivity	Skin zone conductivity	Static formation pressure	Formation specific storage	Radial thickness of skin	Flow dimension
	[m/s]	[m/s]	[kPa]	[1/m]	[m]	[–]
Best Fit	4.9E-11	1.4E-13	4257	1.2E-06	2.8E-03	1.0
Minimum	1.0E-15	6.7E-14	4000	1.0E-09	1.0E-03	1.0
Maximum	8.4E-09	9.2E-11	4498	9.9E-06	9.9E-01	2.9
Mean	9.1E-10	7.0E-12	4234	2.3E-06	2.9E-01	1.6
Median	1.8E-11	1.9E-12	4255	5.7E-07	1.9E-01	1.4
Geometric mean	9.5E-12	1.3E-12	4231	2.7E-07	7.3E-02	1.5

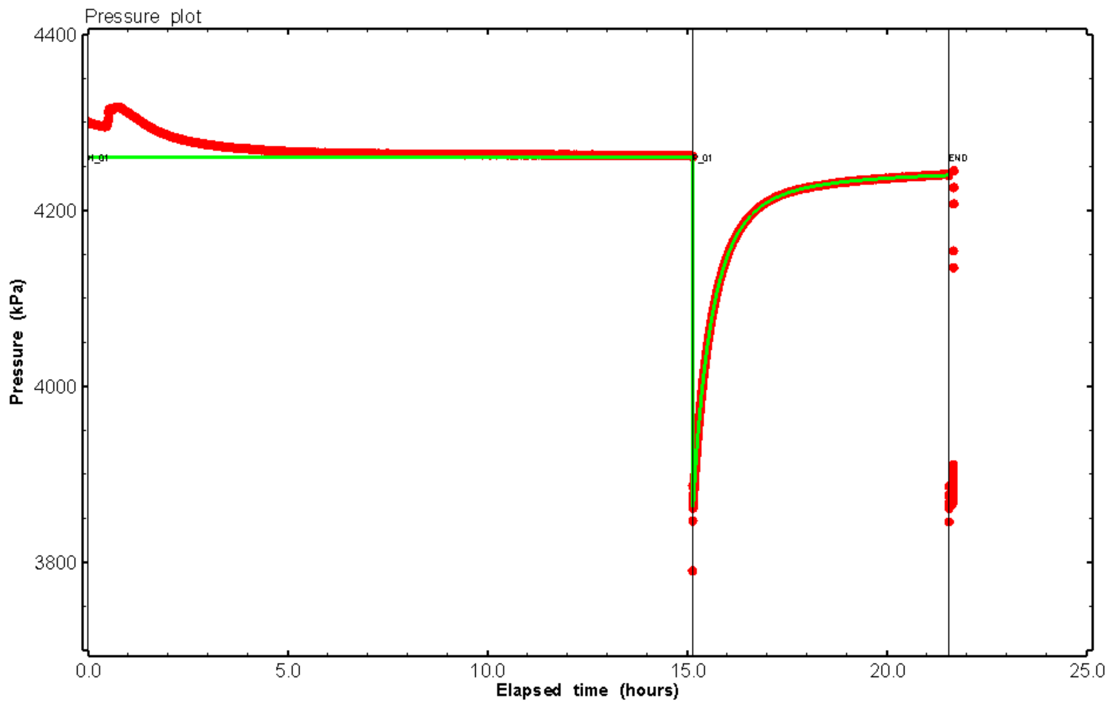

Figure 87: HT008A Pressure plot showing best-fit simulation and best fit results

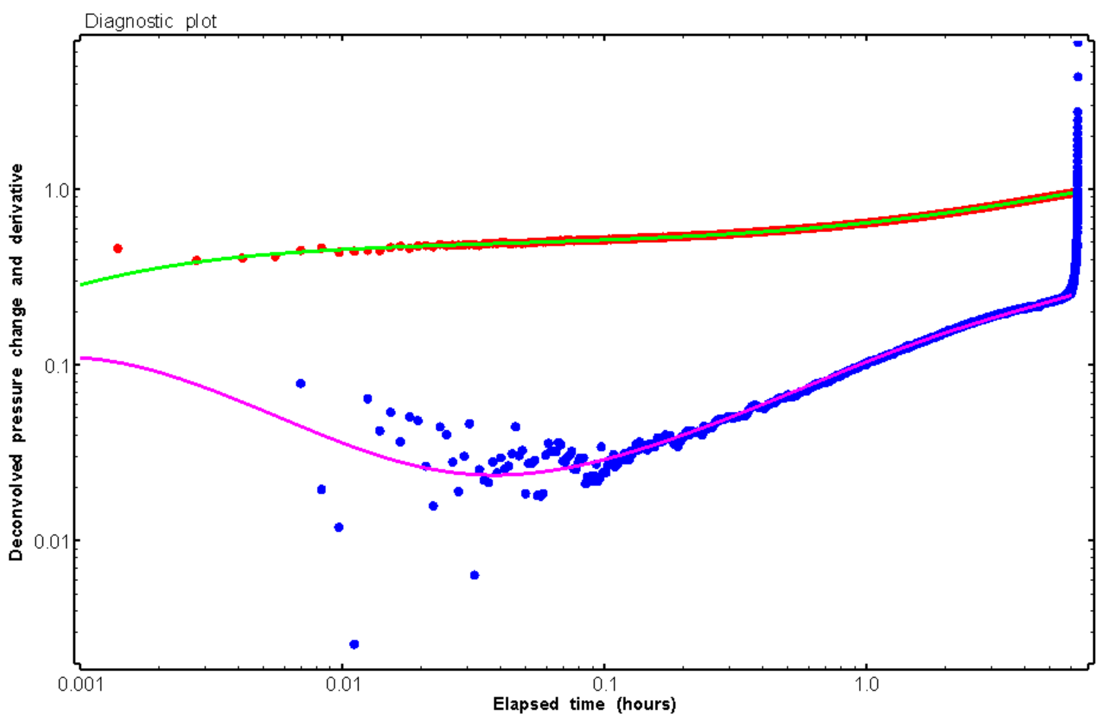

Figure 88: HT008A Deconvolved pressure change and derivative plot of the PW sequence showing best-fit simulation

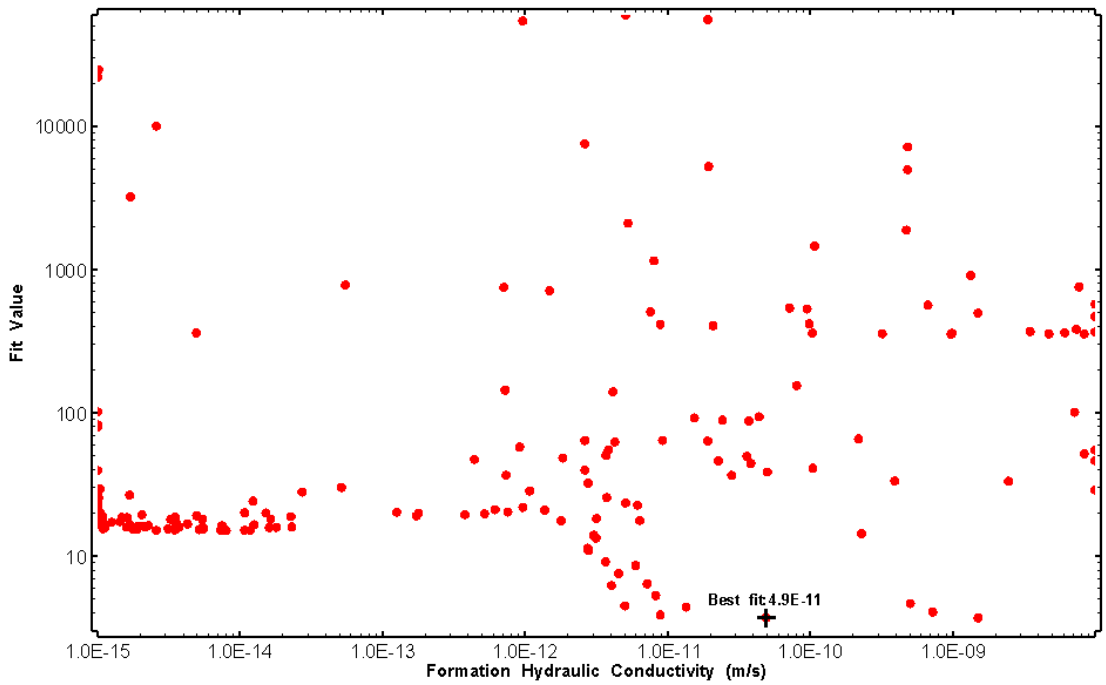

Figure 89: HT008A XY-scatter plot of formation hydraulic conductivity vs. fit value

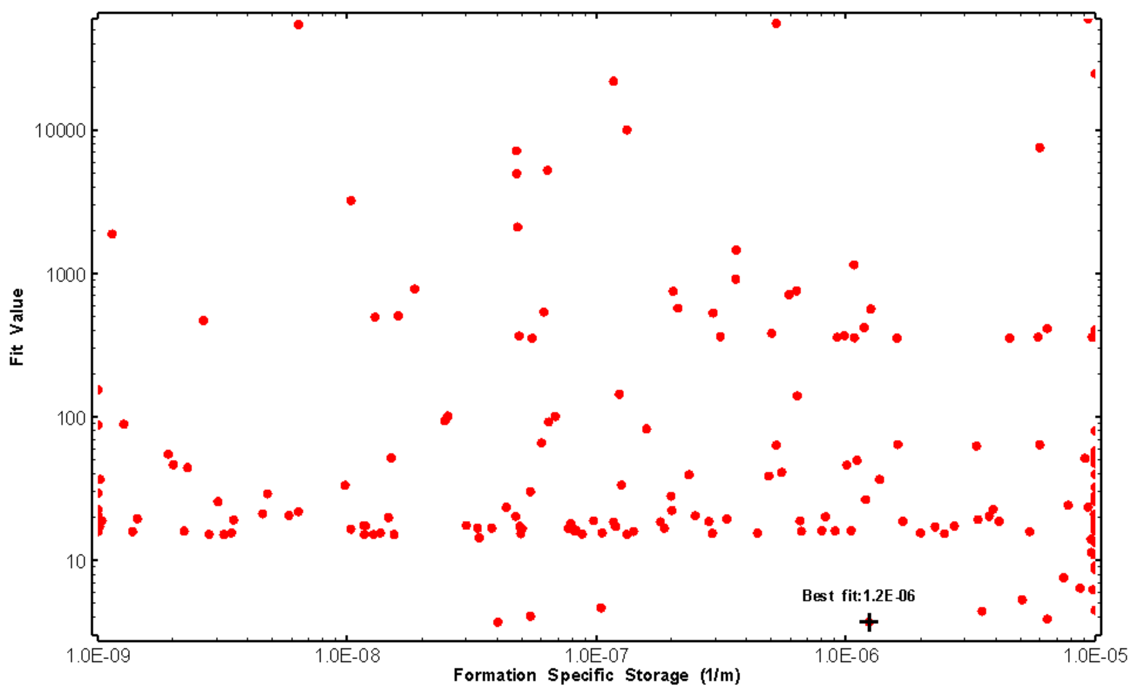

Figure 90: HT008A XY-scatter plot of formation specific storage vs. fit value

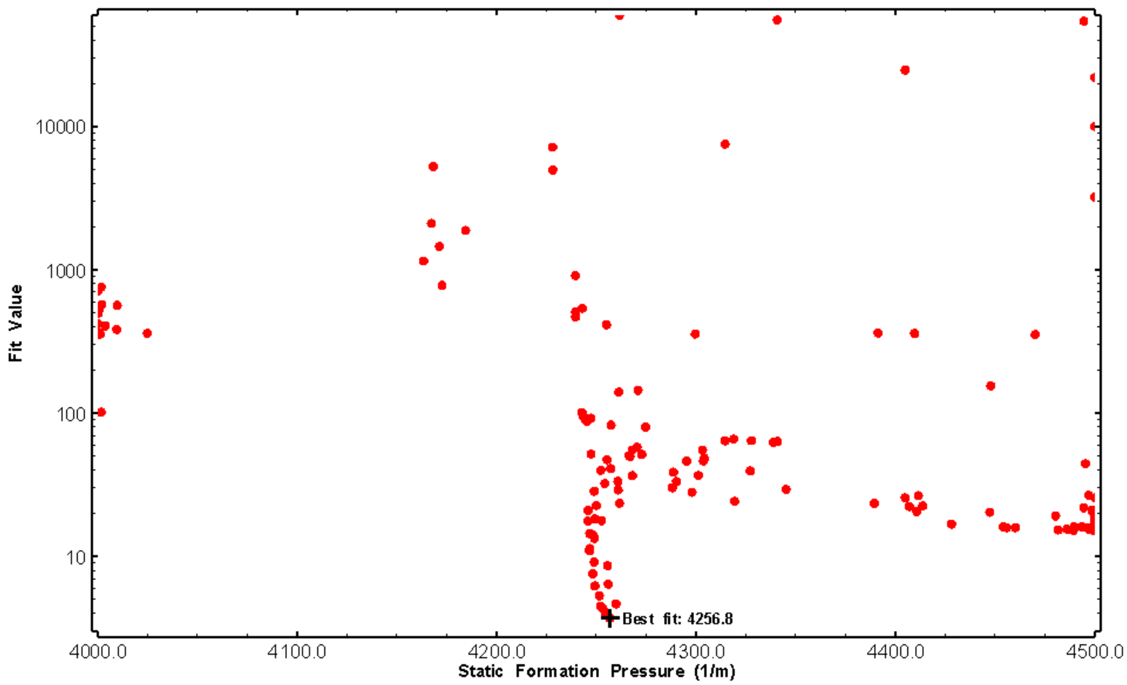

Figure 91: HT008A XY-scatter plot of static formation pressure vs. fit value

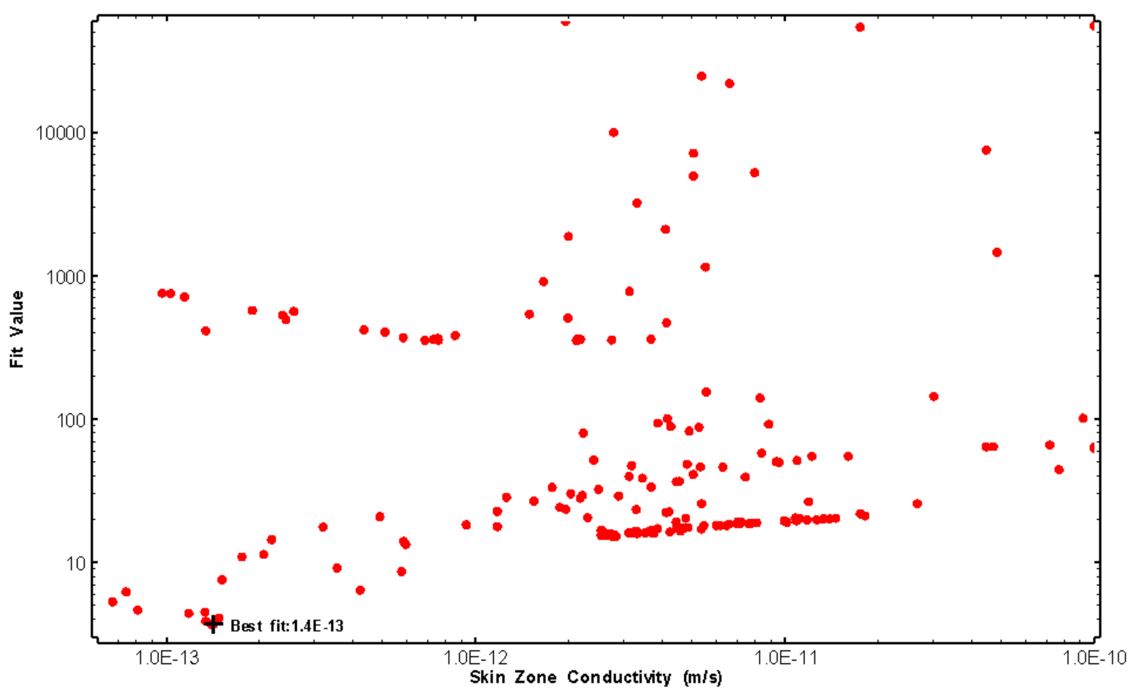

Figure 92: HT008A XY-scatter plot of skin zone conductivity vs. fit value

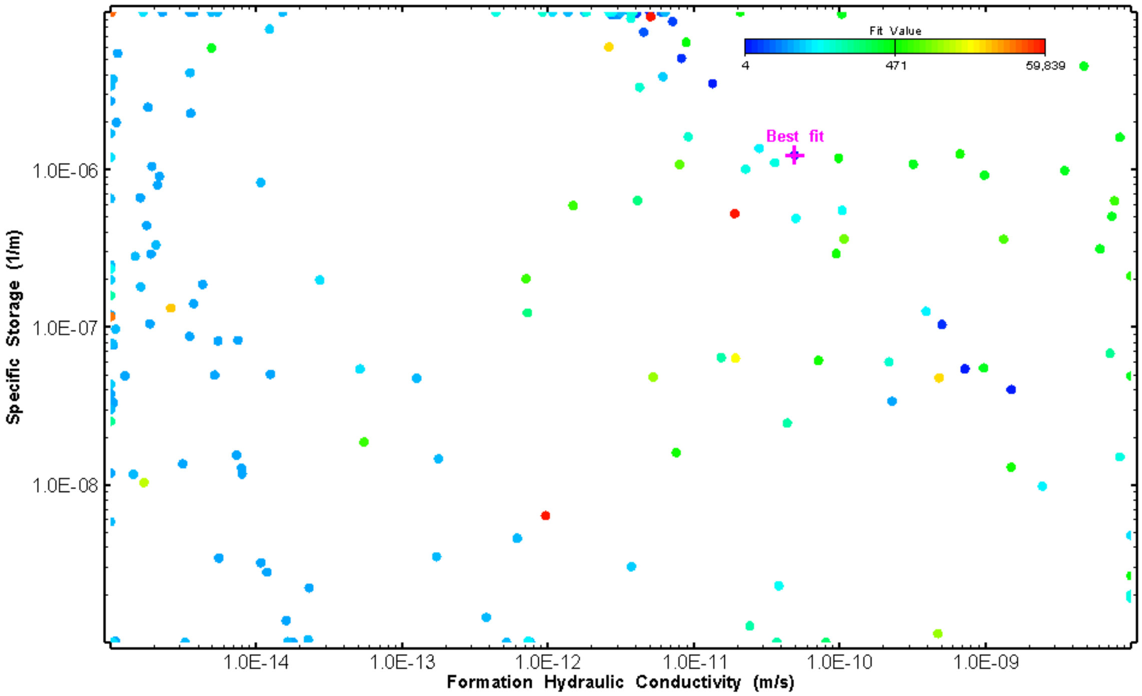

Figure 93: HT008A XY-scatter plot showing estimates of formation hydraulic conductivity and specific storage from perturbation analysis

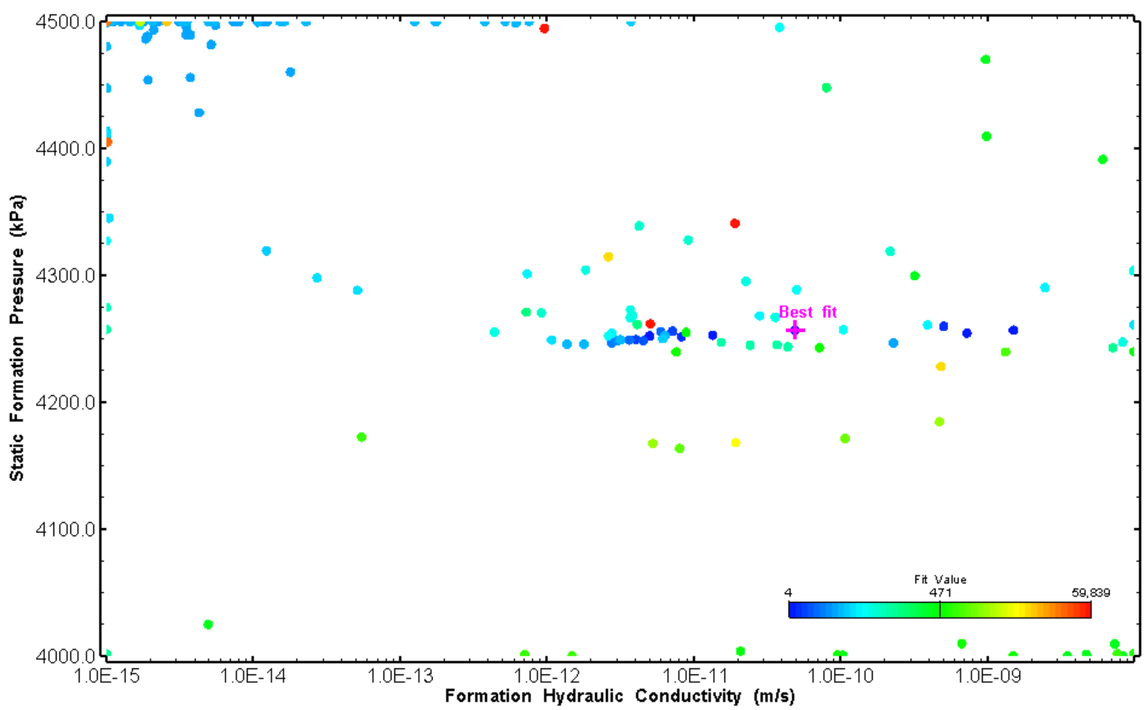

Figure 94: HT008A XY-scatter plot showing estimates of formation hydraulic conductivity and static formation pressure from perturbation analysis

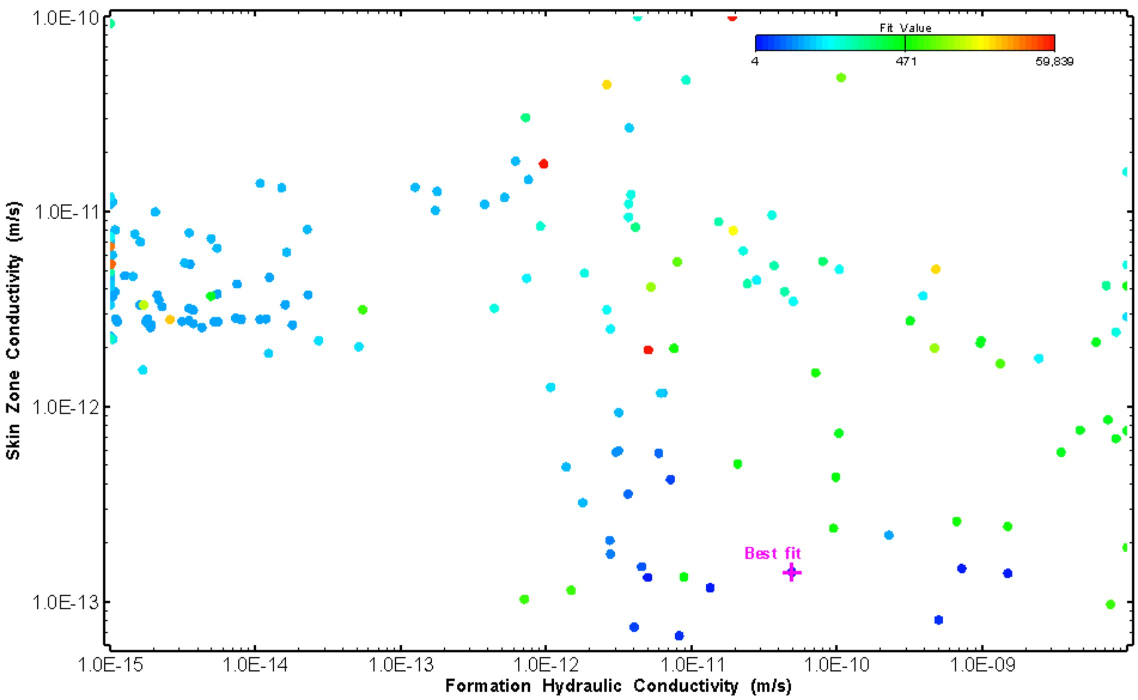

Figure 95: HT008A XY-scatter plot showing estimates of formation hydraulic conductivity and skin zone conductivity from perturbation analysis

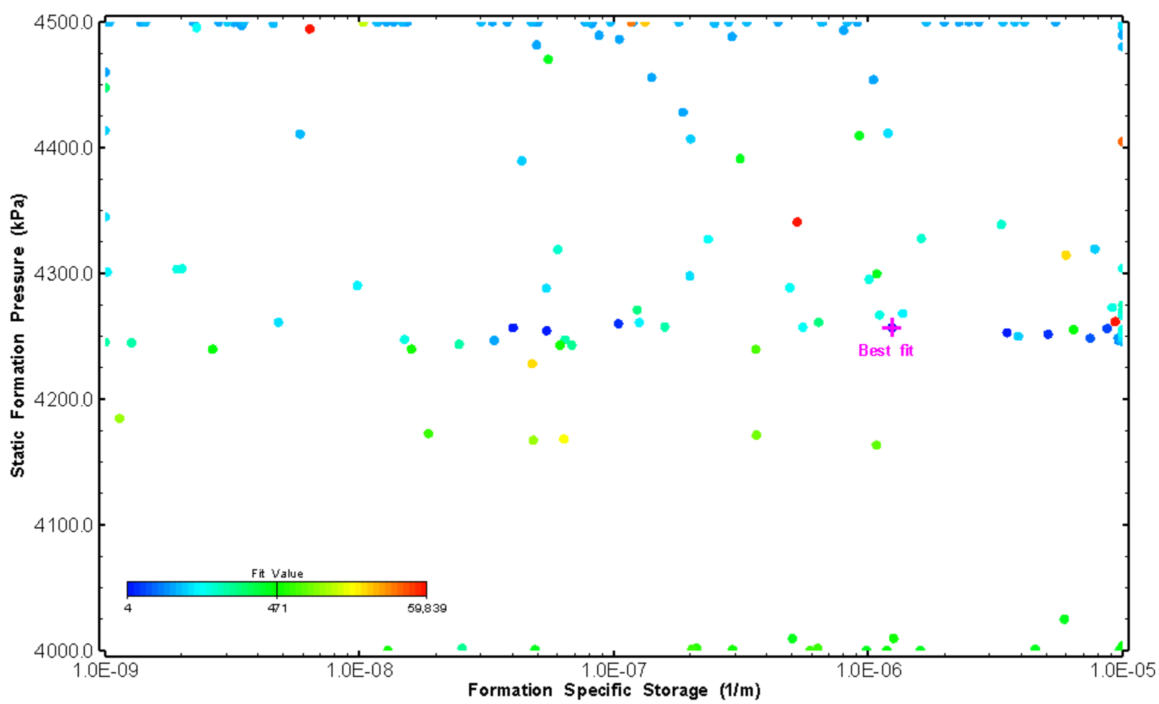

Figure 96: HT008A XY-scatter plot showing estimates of specific storage and static formation pressure from perturbation analysis

9.0 HT009A (497.17 – 517.20 M)

HT009a was selected to test an intact interval with a single broken fracture and a caliper kick from geophysical surveying. A change in electrical conductivity of drilling fluid was observed in this interval. An indication of flow was recorded during FFEC logging post-drilling.

The test was initiated with a shut-in pressure recovery phase (PSR). A pulse withdrawal test (PW) with a shut-in recovery was completed after the PSR phase.

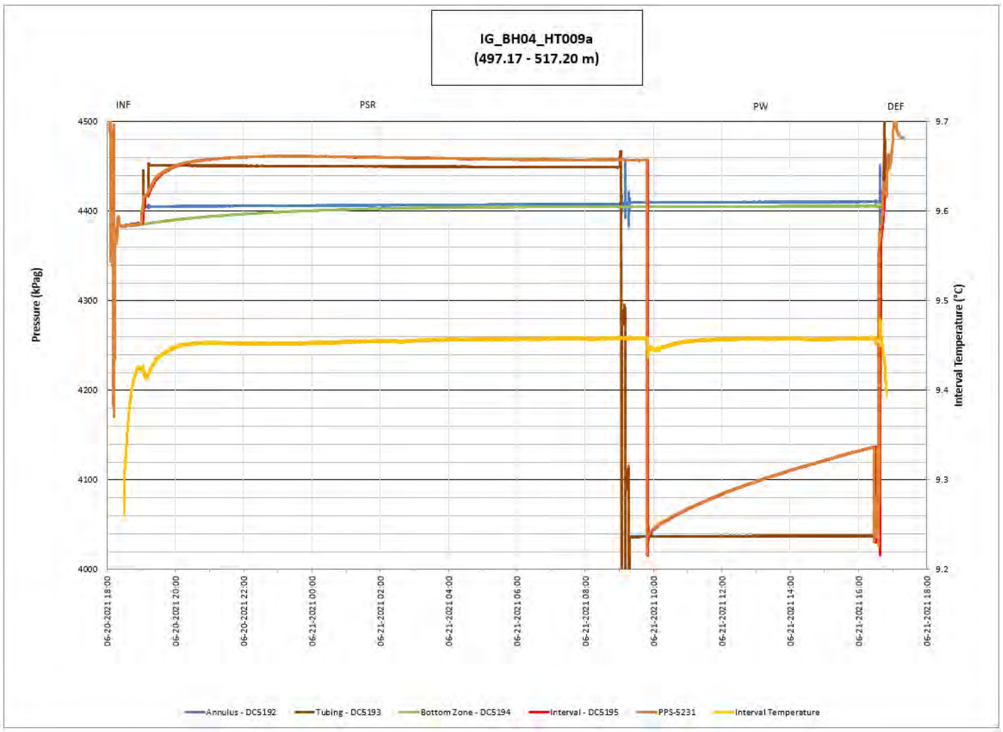

Figure 97: HT009A Annotated test plot showing monitored zone pressure and interval temperature.

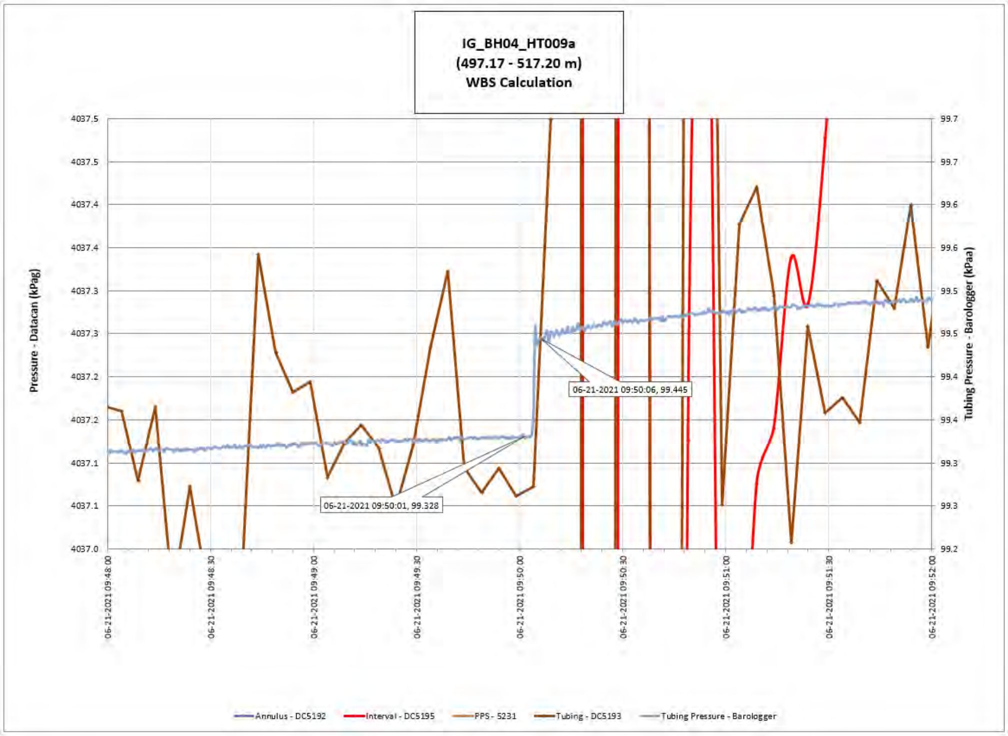

Figure 98: HT009A Tubing pressure during DHSIV activation. DHSIV Closed Wellbore Storage Estimate = 5E-11 m^3/Pa

Table 9: Summary of Analysis Results – HT009A

	Formation conductivity	Skin zone conductivity	Static formation pressure	Formation specific storage	Radial thickness of skin	Flow dimension
	[m/s]	[m/s]	[kPa]	[1/m]	[m]	[–]
Best Fit	1.4E-13	1.5E-14	4449	3.7E-08	3.8E-03	1.8
Minimum	2.6E-14	3.2E-15	4244	2.5E-09	1.0E-03	1.0
Maximum	4.3E-13	1.0E-10	4460	9.9E-07	5.2E-02	3.0
Mean	1.1E-13	2.4E-12	4398	1.8E-07	1.1E-02	2.1
Median	9.5E-14	2.6E-14	4407	9.8E-08	9.3E-03	2.1
Geometric mean	9.4E-14	3.7E-14	4398	9.4E-08	8.1E-03	2.1

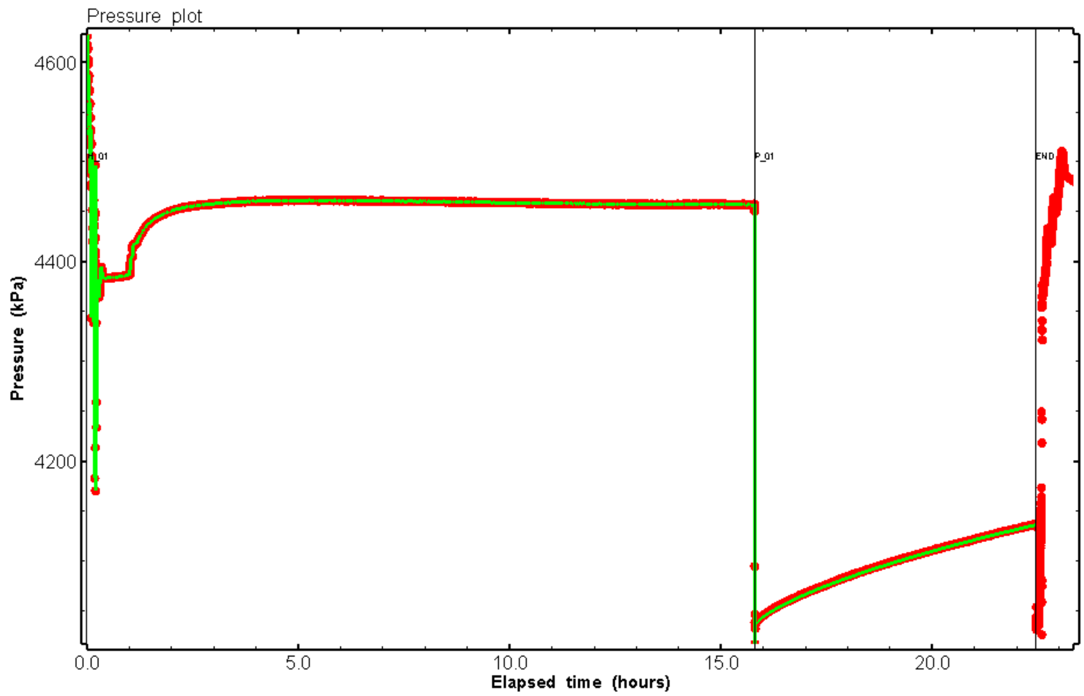

Figure 99: HT009A Pressure plot showing best-fit simulation and best fit results

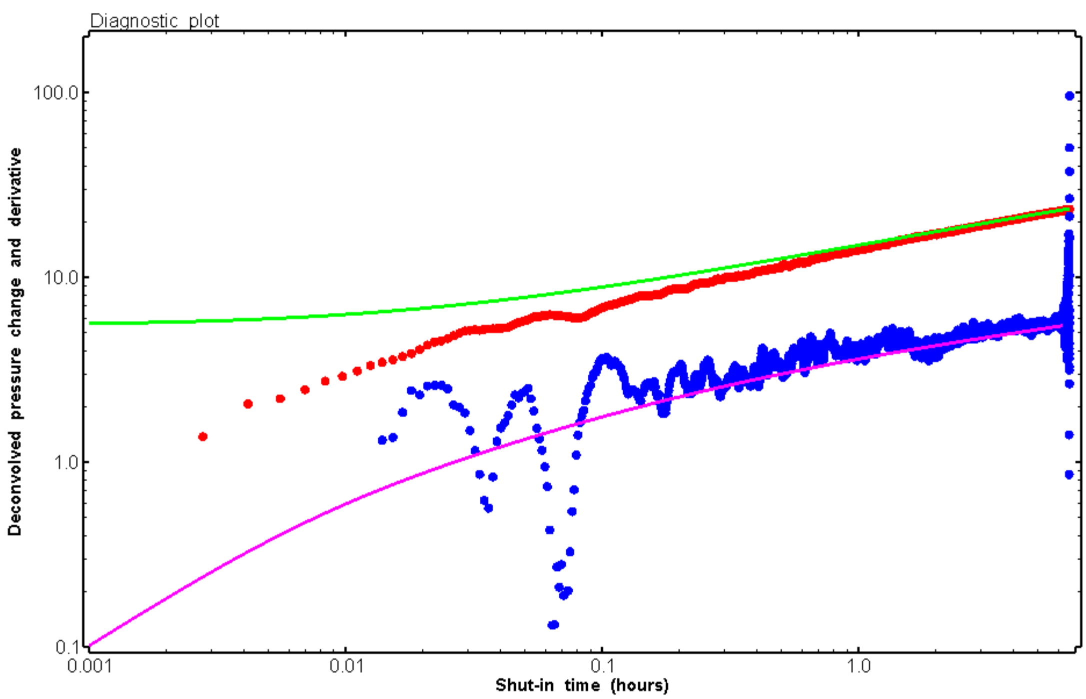

Figure 100: HT009A Deconvolved pressure change and derivative plot of the PW sequence showing best-fit simulation

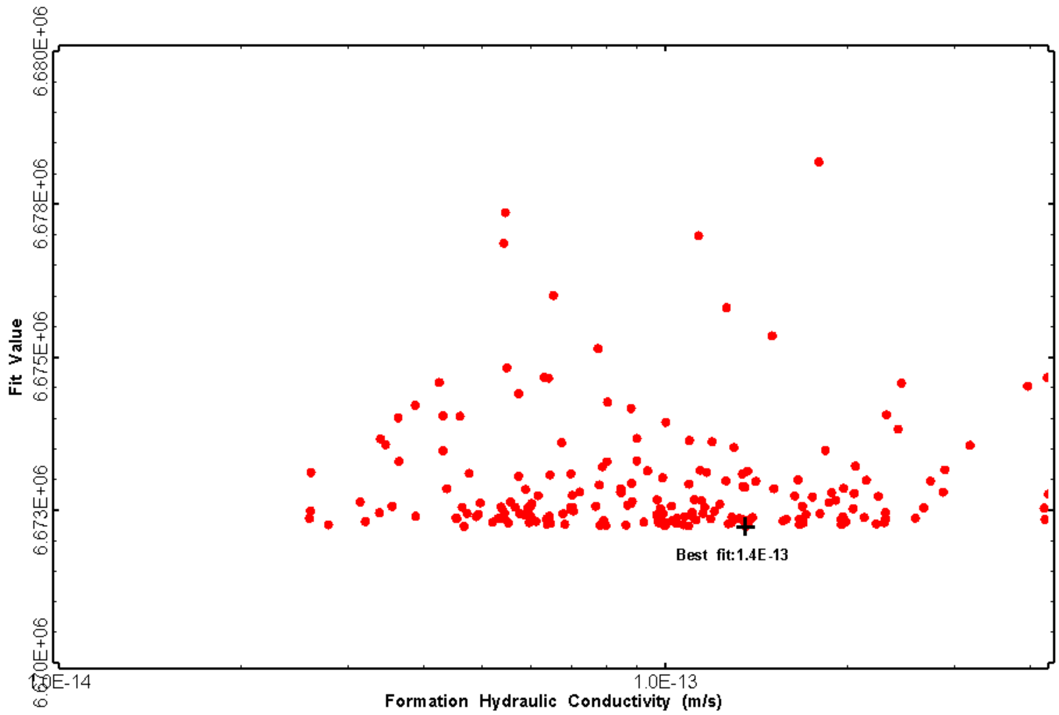

Figure 101: HT009A XY-scatter plot of formation hydraulic conductivity vs. fit value

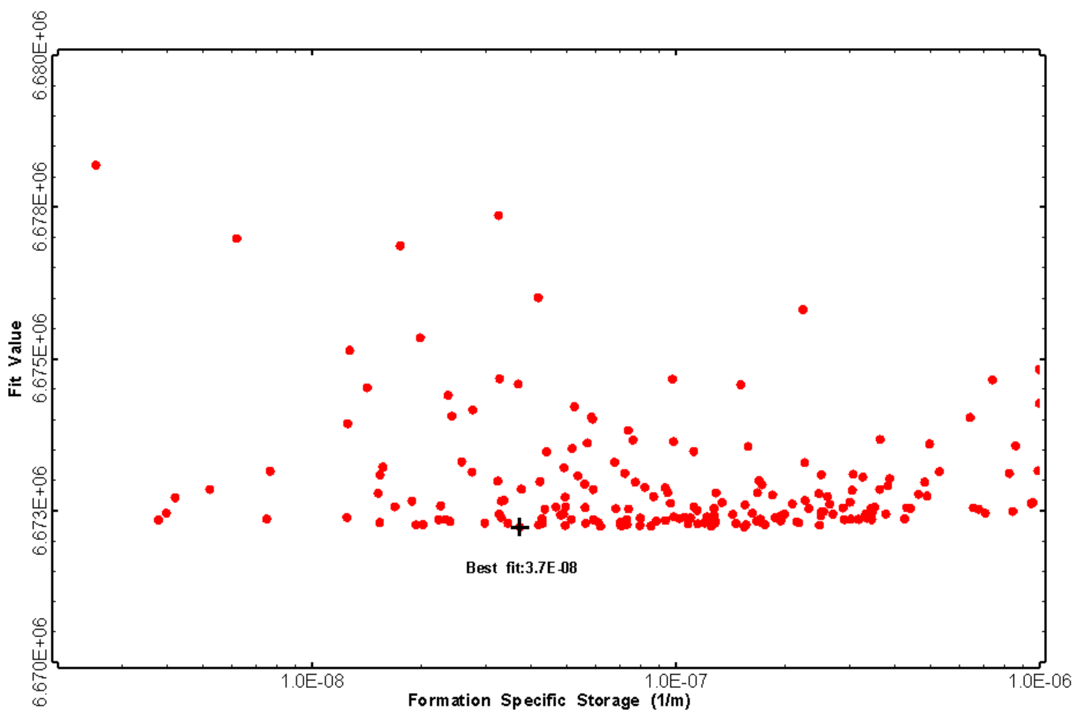

Figure 102: HT009A XY-scatter plot of formation specific storage vs. fit value

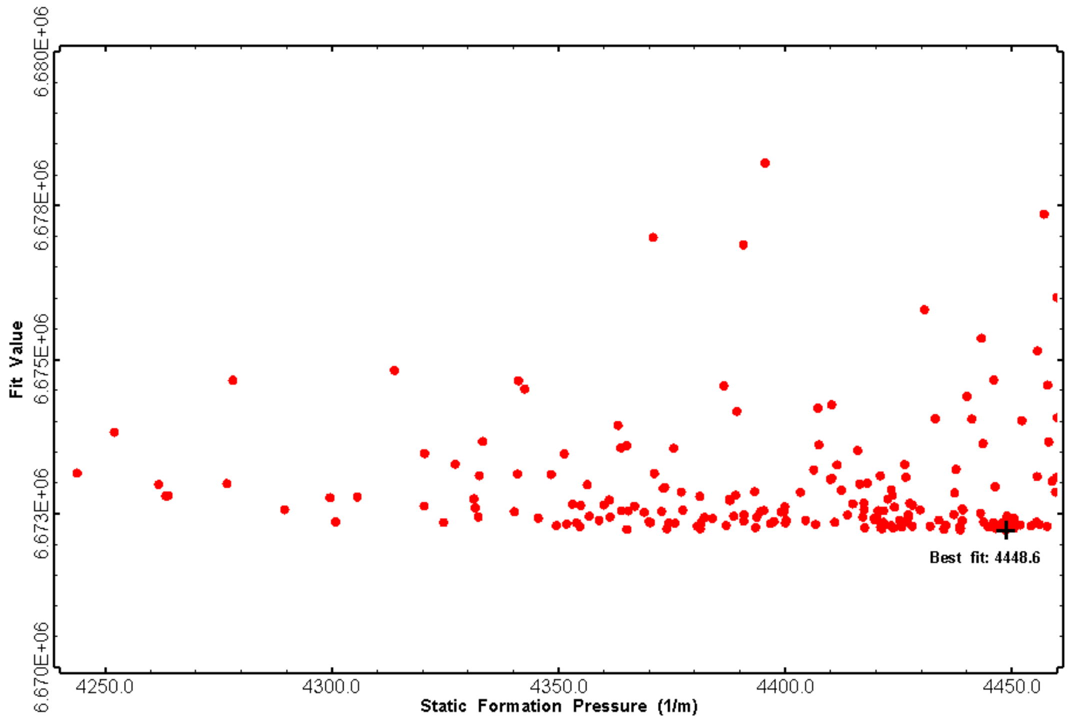

Figure 103: HT009A XY-scatter plot of static formation pressure vs. fit value

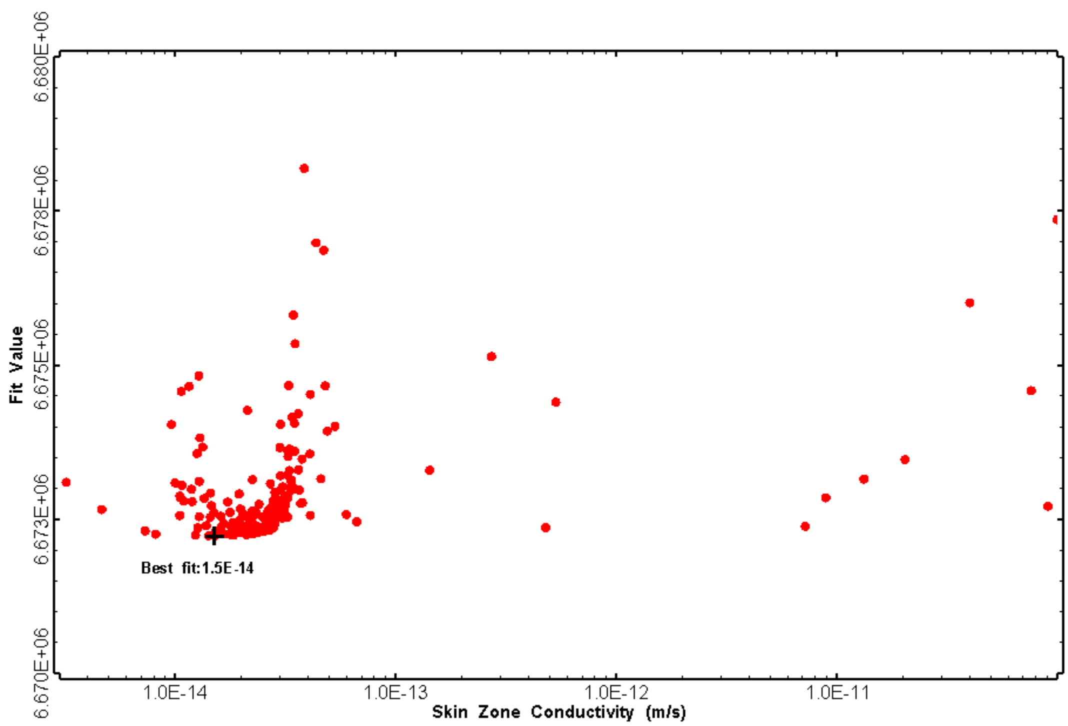

Figure 104: HT009A XY-scatter plot of skin zone conductivity vs. fit value

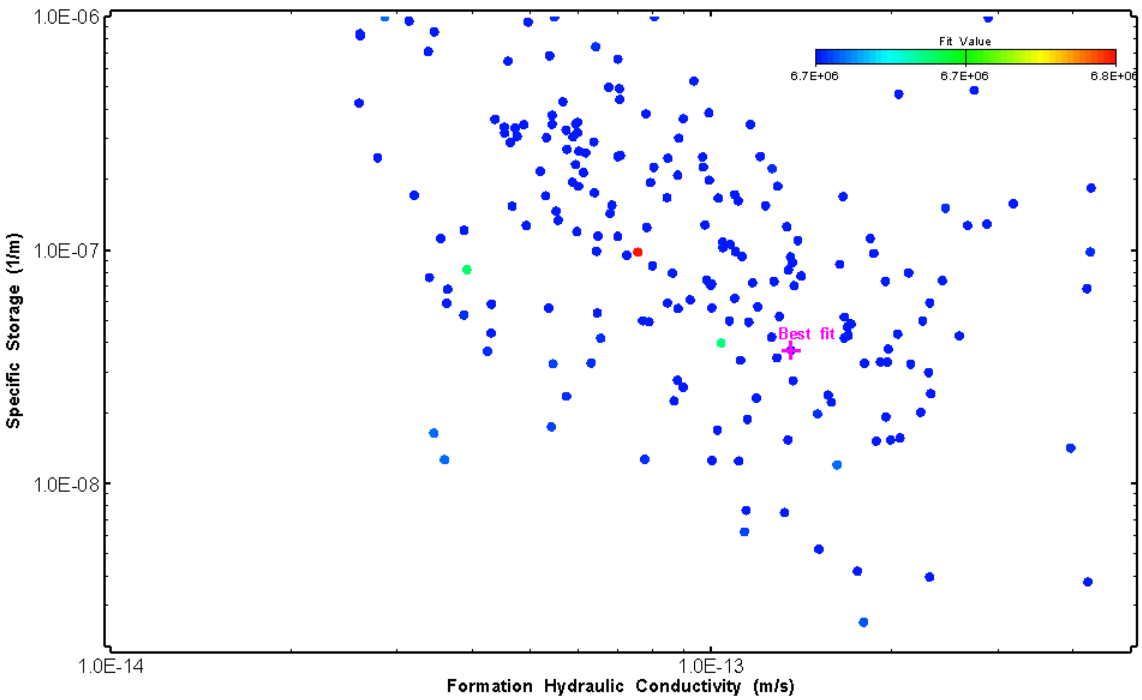

Figure 105: HT009A XY-scatter plot showing estimates of formation hydraulic conductivity and specific storage from perturbation analysis

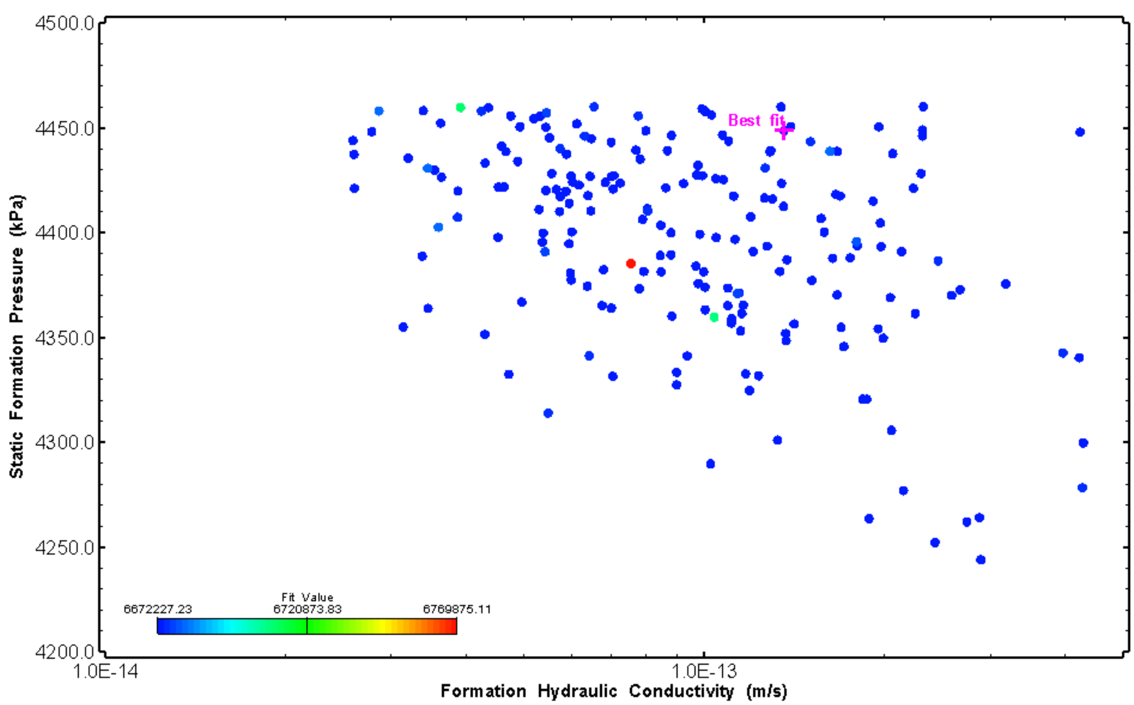

Figure 106: HT009A XY-scatter plot showing estimates of formation hydraulic conductivity and static formation pressure from perturbation analysis

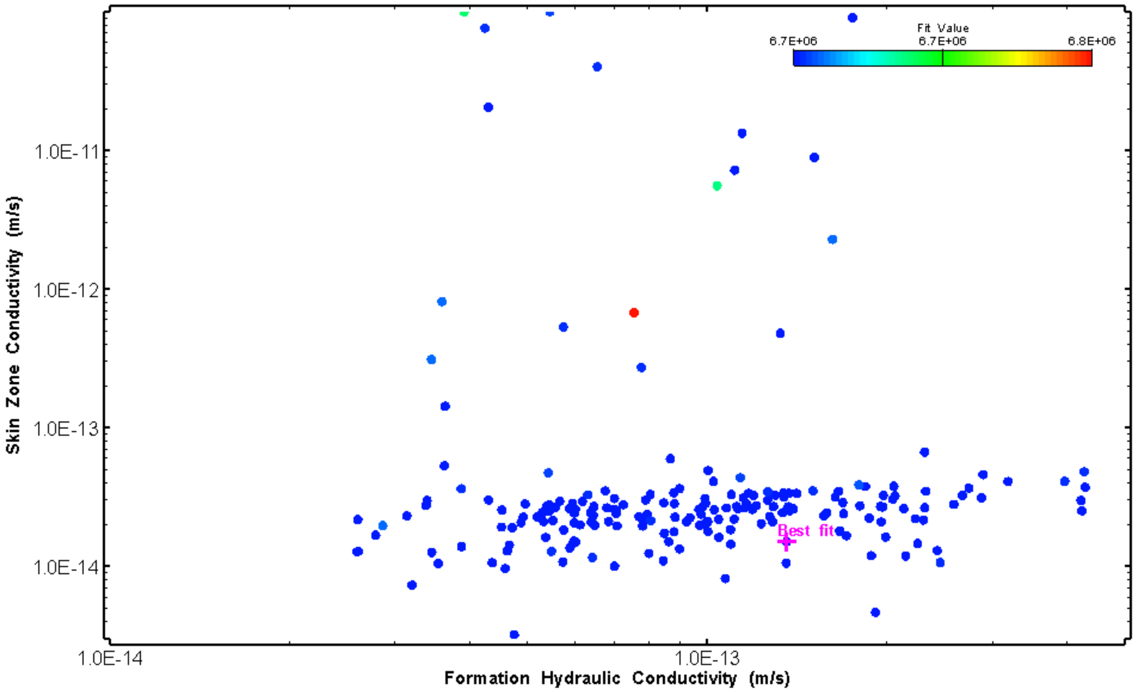

Figure 107: HT009A XY-scatter plot showing estimates of formation hydraulic conductivity and skin zone conductivity from perturbation analysis

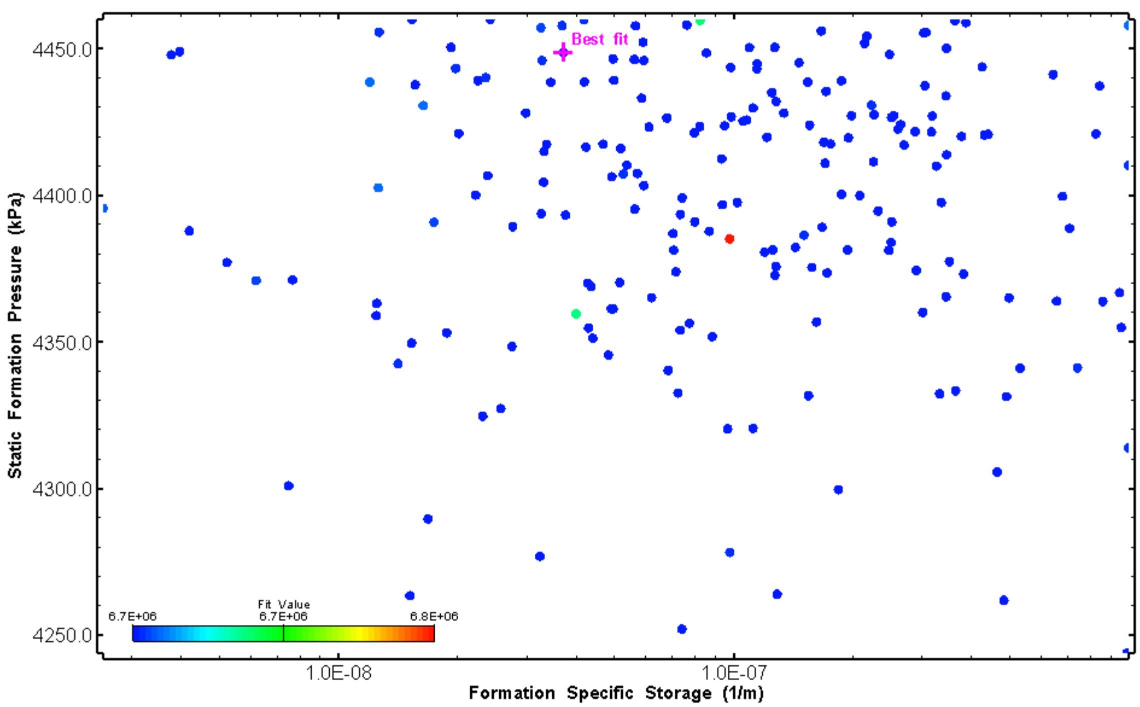

Figure 108: HT009A XY-scatter plot showing estimates of specific storage and static formation pressure from perturbation analysis

10.0 HT010 (530.59 – 550.62 M)

HT010 was selected to test an intact interval. Zero broken fractures were observed in the core. No drill fluid parameter triggers were reached during drilling. No indication of flow was recorded during FFEC logging post-drilling.

The test was initiated with a shut-in pressure recovery phase (PSR). A pulse withdrawal test (PW) with a shut-in recovery was completed after the PSR phase.

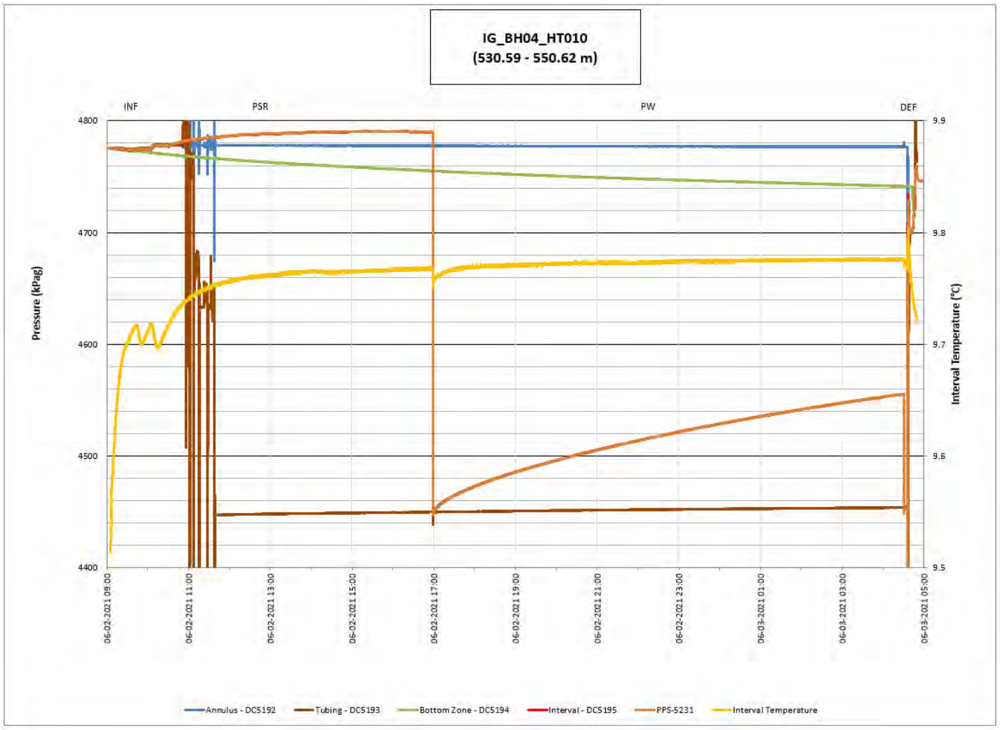

Figure 109: HT010 Annotated test plot showing monitored zone pressure and interval temperature.

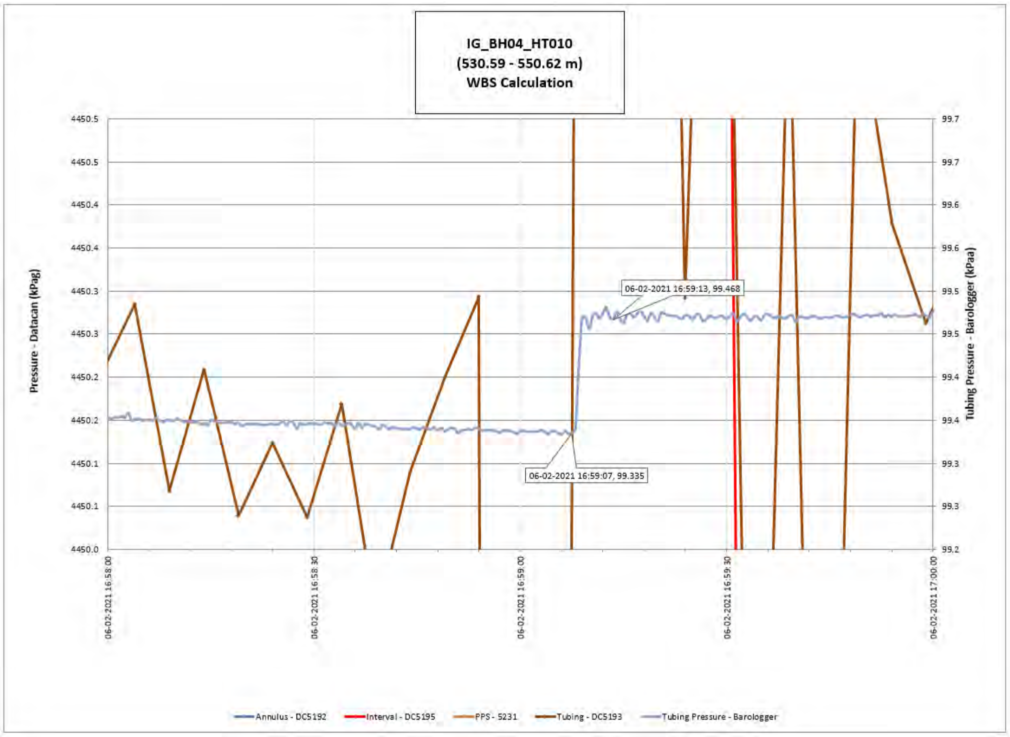

Figure 110: HT010 Tubing pressure during DHSIV activation. DHSIV Closed Wellbore Storage Estimate = 7E-11 m^3/Pa

Table 10: Summary of Analysis Results – HT010

	Formation conductivity	Skin zone conductivity	Static formation pressure	Formation specific storage	Radial thickness of skin	Flow dimension
	[m/s]	[m/s]	[kPa]	[1/m]	[m]	[–]
Best Fit	8.5E-14	4.7E-14	4752	1.1E-07	6.1E-03	2.2
Minimum	2.9E-14	6.7E-15	4580	2.6E-10	1.0E-03	1.0
Maximum	2.9E-11	9.8E-11	4799	8.3E-07	9.2E-02	3.0
Mean	7.8E-13	1.8E-12	4715	1.2E-07	1.9E-02	2.1
Median	1.5E-13	7.1E-14	4724	6.8E-08	1.2E-02	2.1
Geometric mean	2.0E-13	1.3E-13	4714	6.7E-08	1.2E-02	2.0

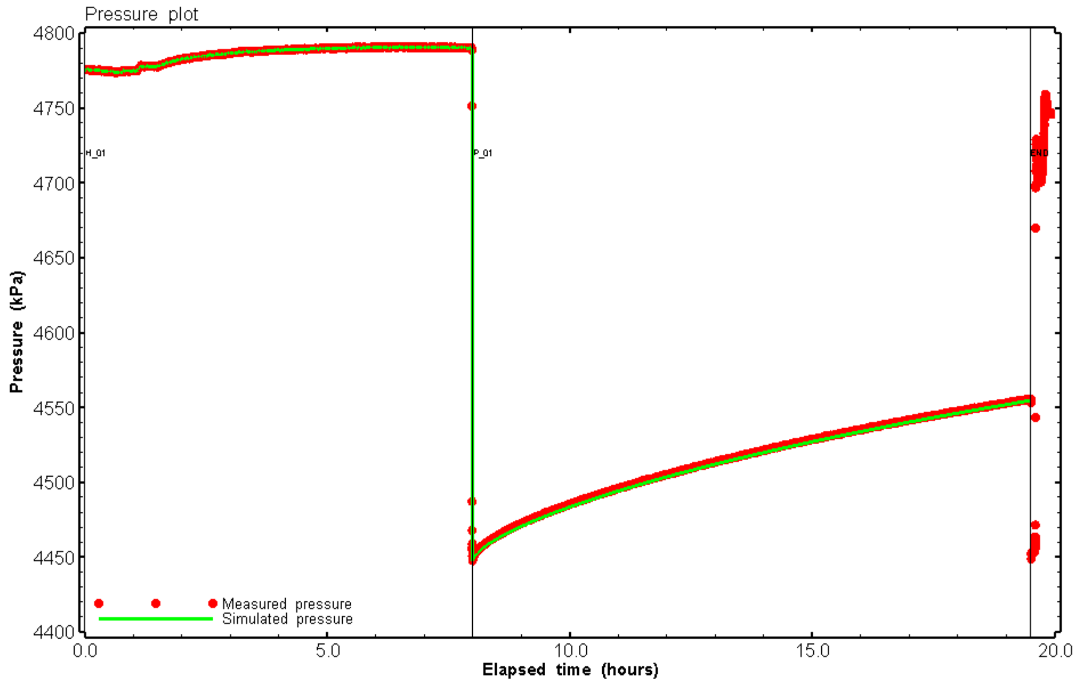

Figure 111: HT010 Pressure plot showing best-fit simulation and best fit results

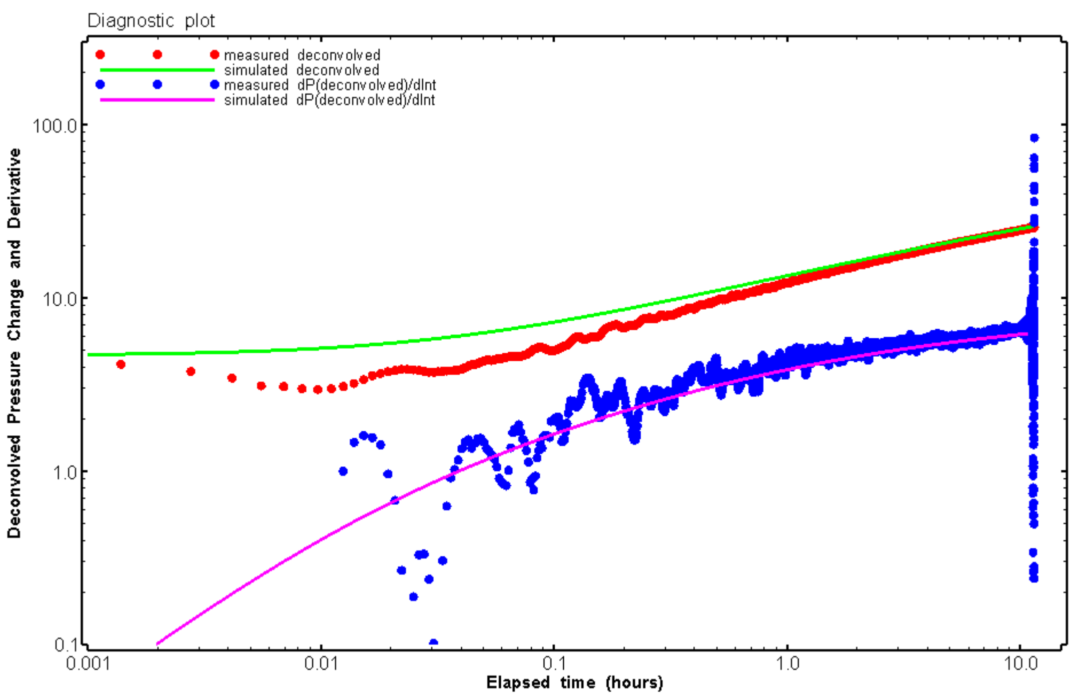

Figure 112: HT010 Deconvolved pressure change and derivative plot of the PW sequence showing best-fit simulation

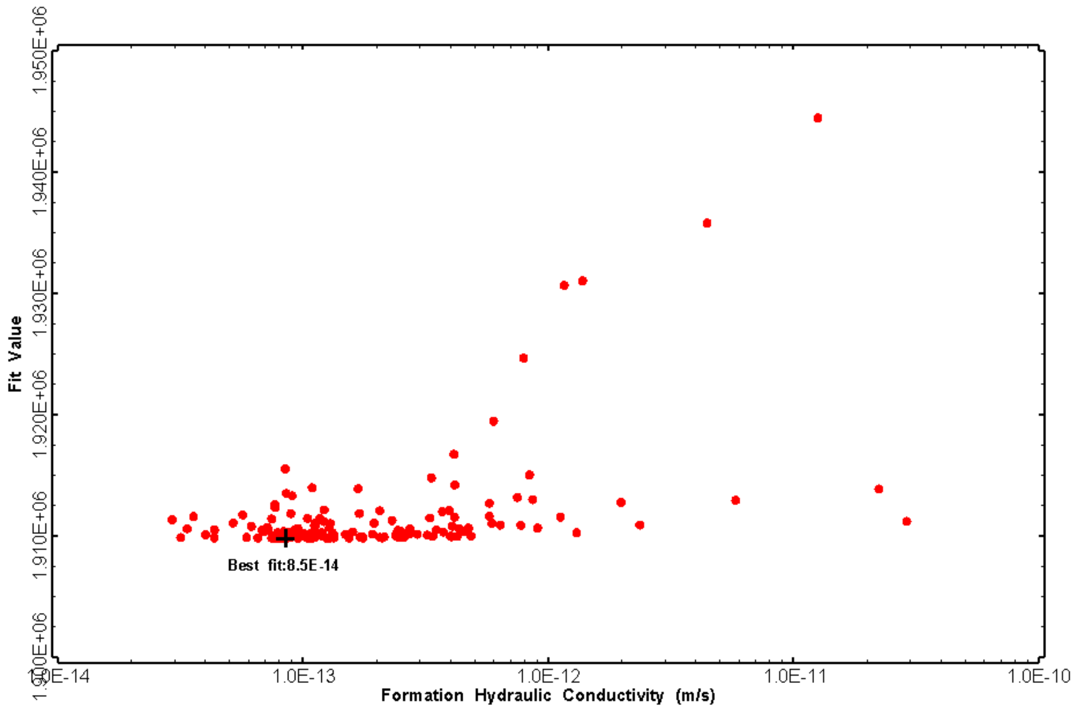

Figure 113: HT010 XY-scatter plot of formation hydraulic conductivity vs. fit value

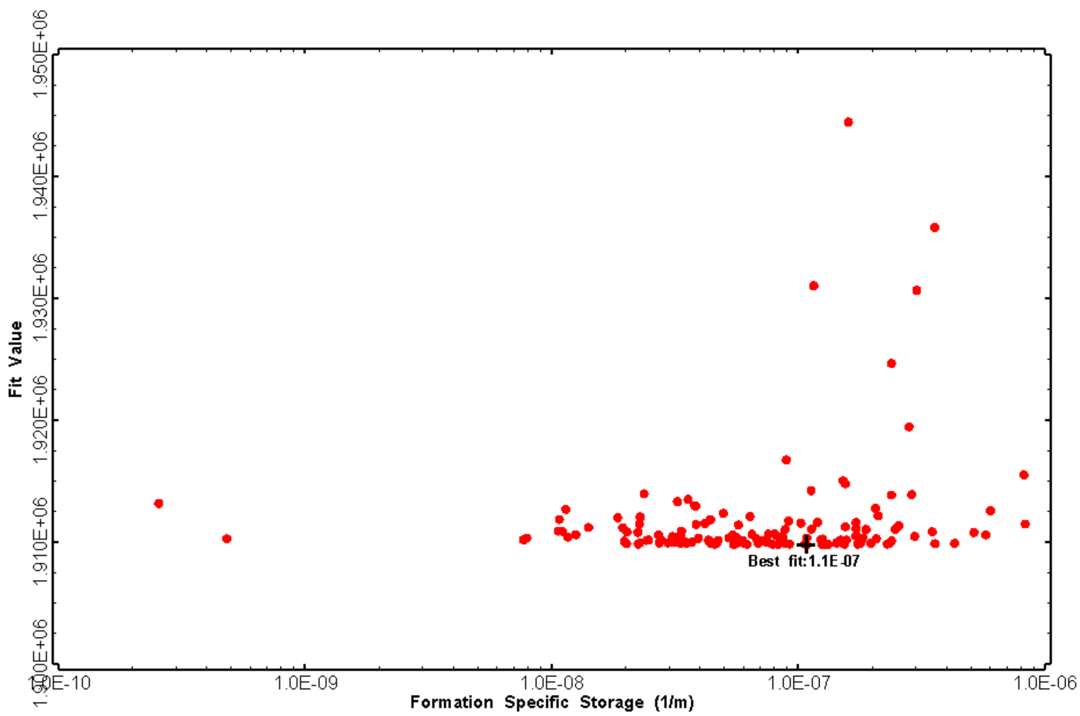

Figure 114: HT010 XY-scatter plot of formation specific storage vs. fit value

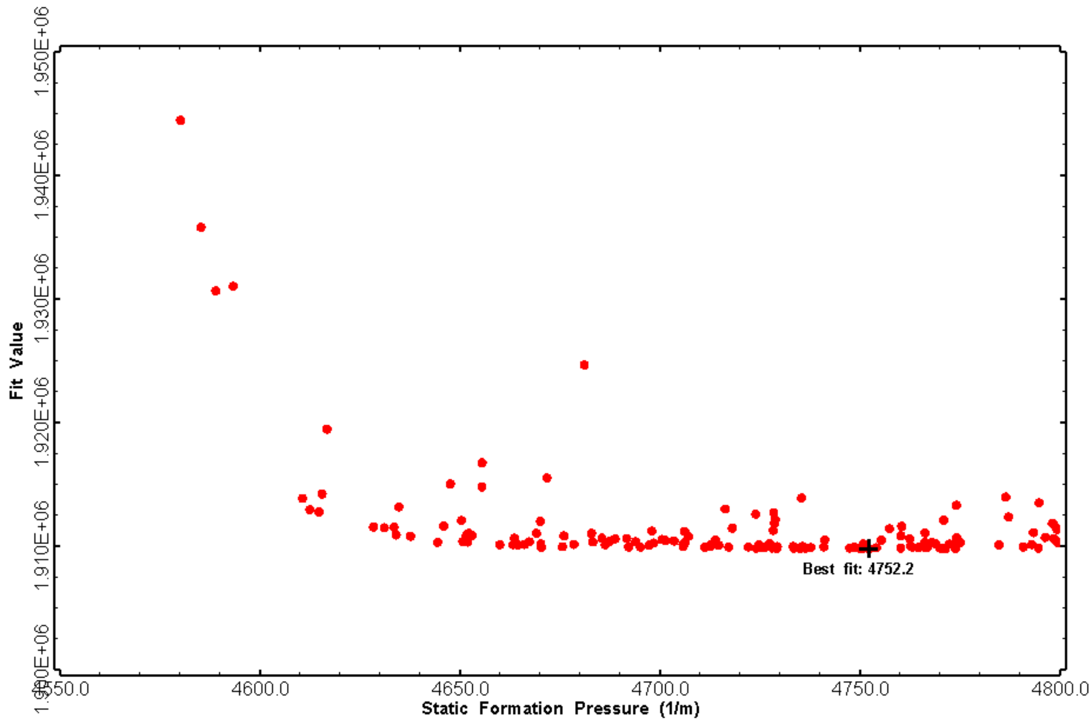

Figure 115: HT010 XY-scatter plot of static formation pressure vs. fit value

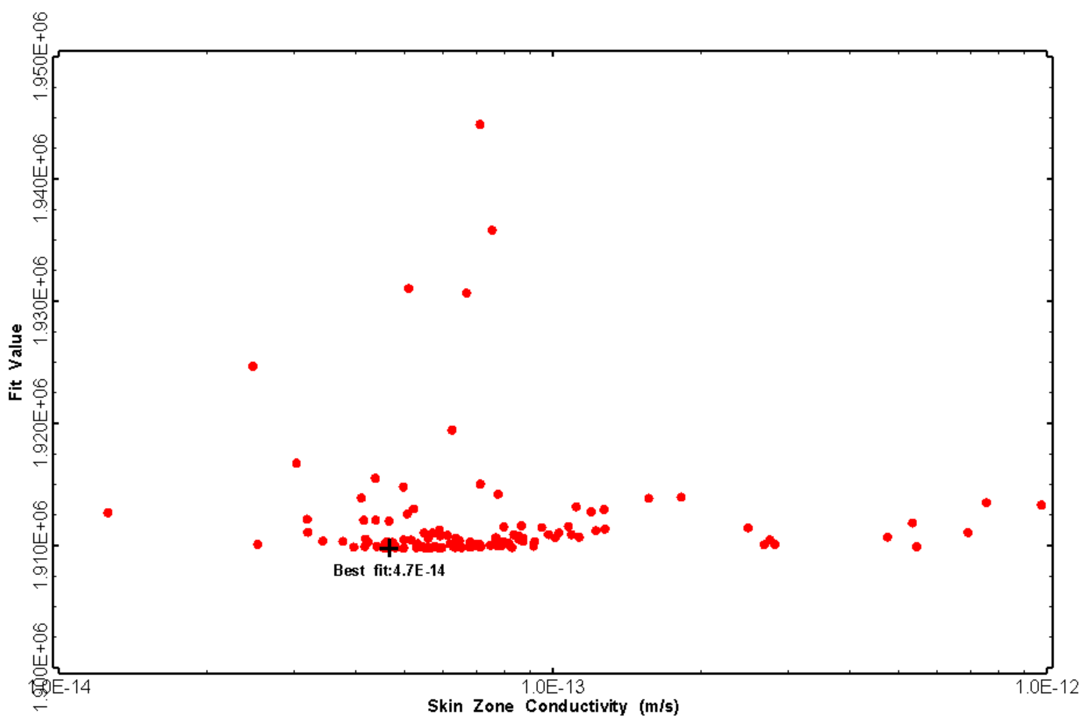

Figure 116: HT010 XY-scatter plot of skin zone conductivity vs. fit value

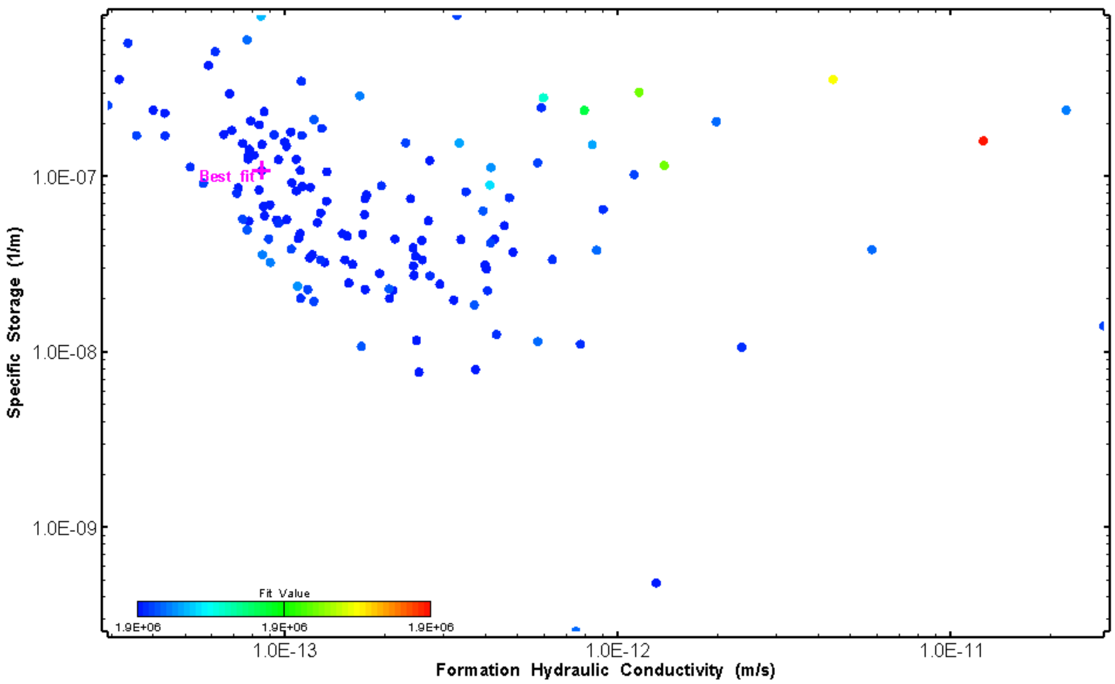

Figure 117: HT010 XY-scatter plot showing estimates of formation hydraulic conductivity and specific storage from perturbation analysis

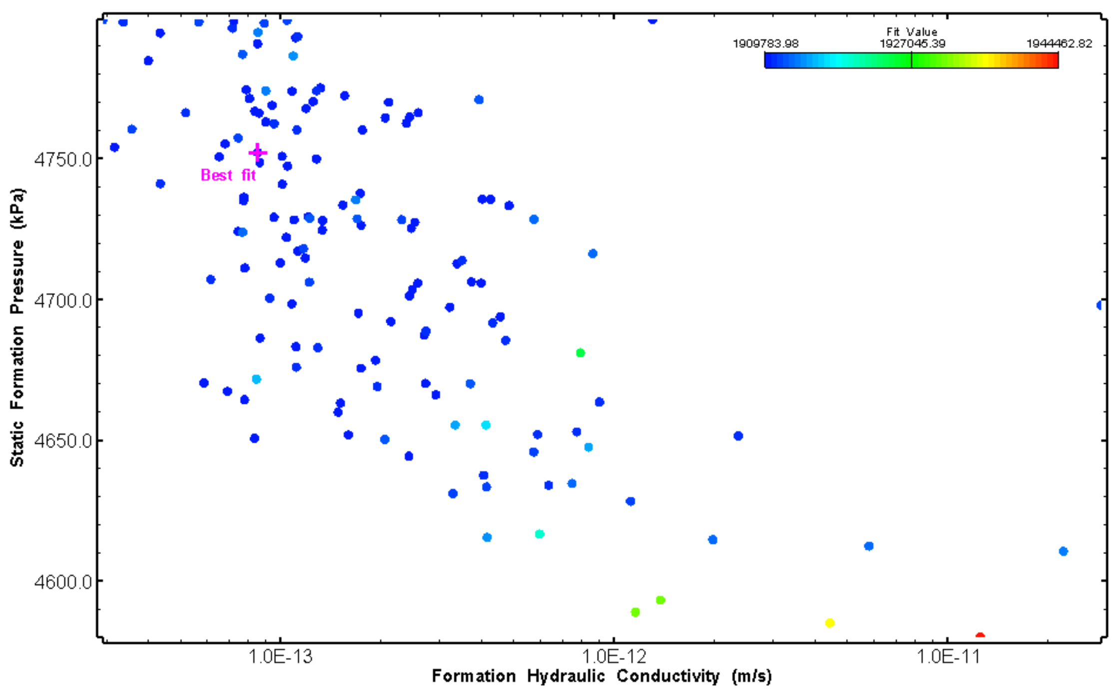

Figure 118: HT010 XY-scatter plot showing estimates of formation hydraulic conductivity and static formation pressure from perturbation analysis

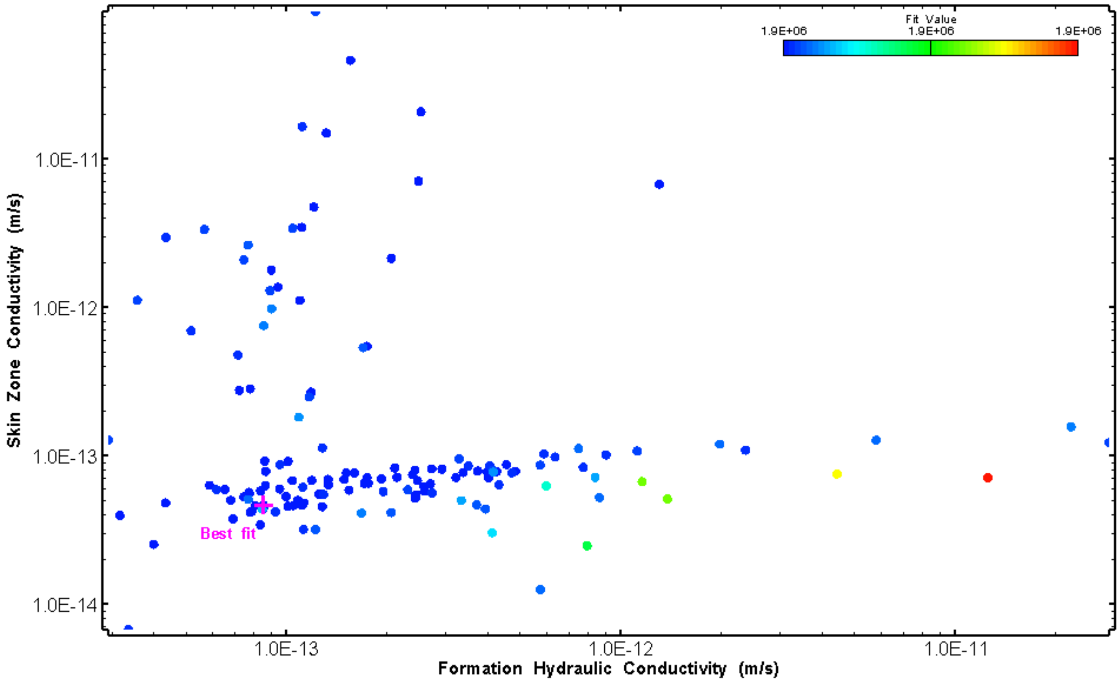

Figure 119: HT010 XY-scatter plot showing estimates of formation hydraulic conductivity and skin zone conductivity from perturbation analysis

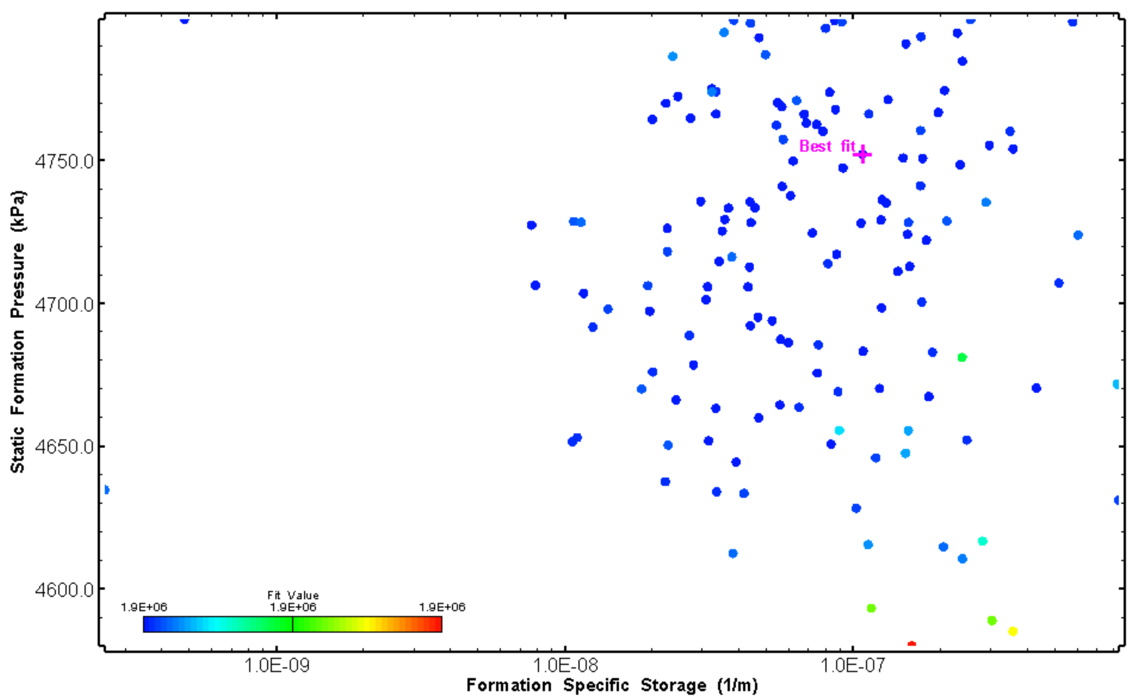

Figure 120: HT010 XY-scatter plot showing estimates of specific storage and static formation pressure from perturbation analysis

11.0 HT012 (605.63 – 625.66 M)

HT012 was selected to obtain continuous testing coverage from 600 to 800 m along hole. 19 broken fractures were observed in the core. No drill fluid parameter triggers were reached during drilling. An indication of flow was recorded during FFEC logging post-drilling.

The test was initiated with a shut-in pressure recovery phase (PSR). A pulse withdrawal test (PW) with a shut-in recovery followed by a slug withdrawal (SW) phase was completed after the PSR phase.

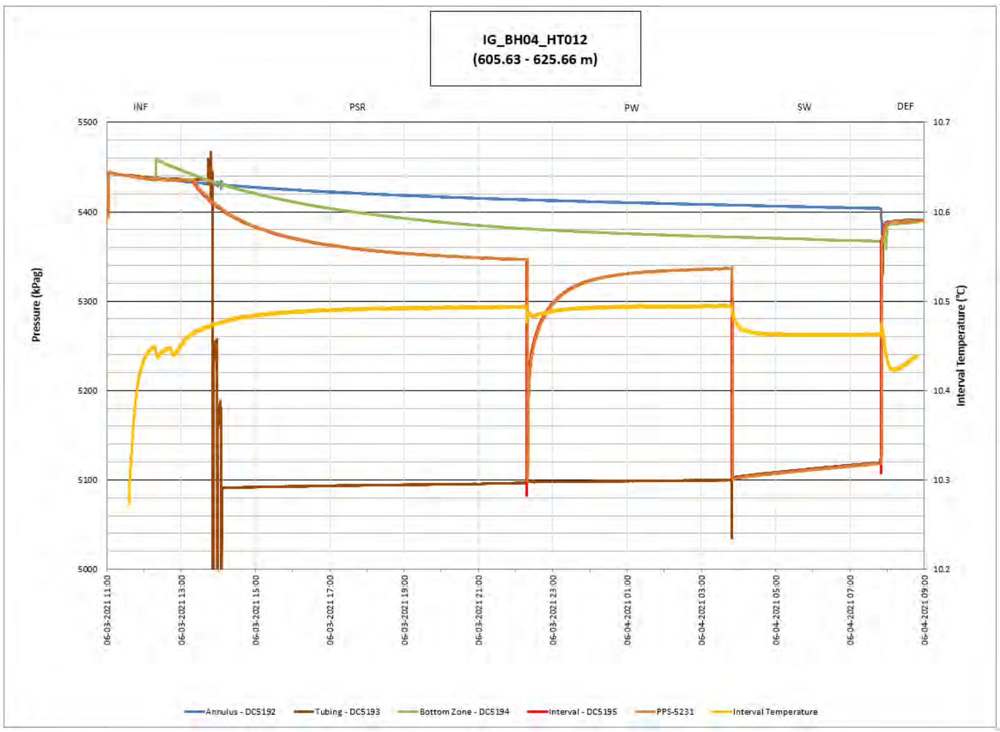

Figure 121: HT012 Annotated test plot showing monitored zone pressure and interval temperature.

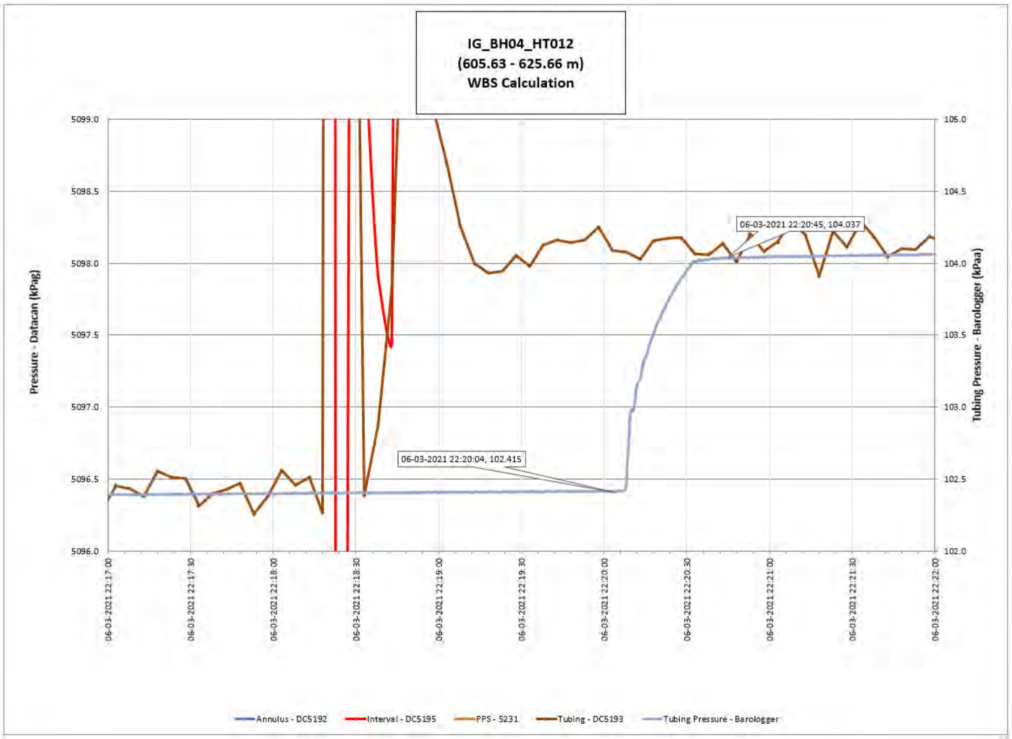

Figure 122: HT012 Tubing pressure during DHSIV activation. DHSIV Closed Wellbore Storage Estimate =1E-9 m^3/Pa

Table 11: Summary of Analysis Results – HT012

	Formation conductivity	Skin zone conductivity	Static formation pressure	Formation specific storage	Radial thickness of skin	Flow dimension
	[m/s]	[m/s]	[kPa]	[1/m]	[m]	[–]
Best Fit	1.4E-11	1.1E-09	5338	4.1E-08	4.5E-01	2.7
Minimum	6.2E-12	6.4E-10	5330	1.0E-10	2.1E-01	1.3
Maximum	9.6E-09	9.5E-08	5350	9.9E-07	6.9E+00	3.0
Mean	4.6E-10	8.9E-09	5339	1.5E-07	7.0E-01	2.2
Median	4.8E-11	3.8E-09	5339	5.9E-08	5.4E-01	2.3
Geometric mean	7.2E-11	4.5E-09	5339	4.9E-08	5.8E-01	2.2

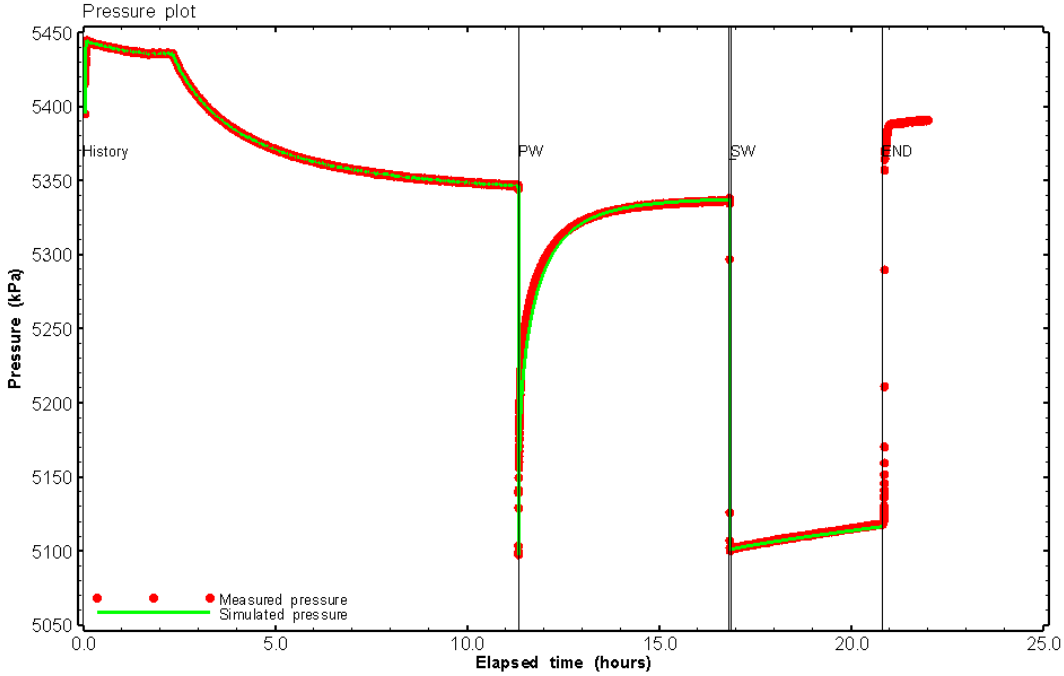

Figure 123: HT012 Pressure plot showing best-fit simulation and best fit results

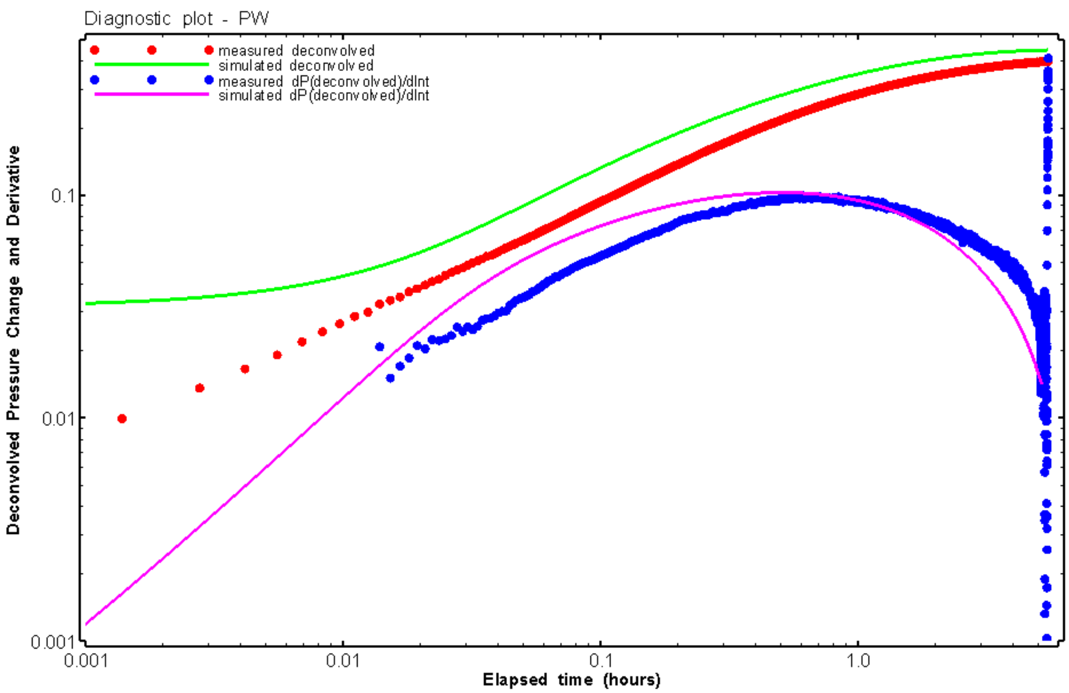

Figure 124: HT012 Deconvolved pressure change and derivative plot of the PW sequence showing best-fit simulation

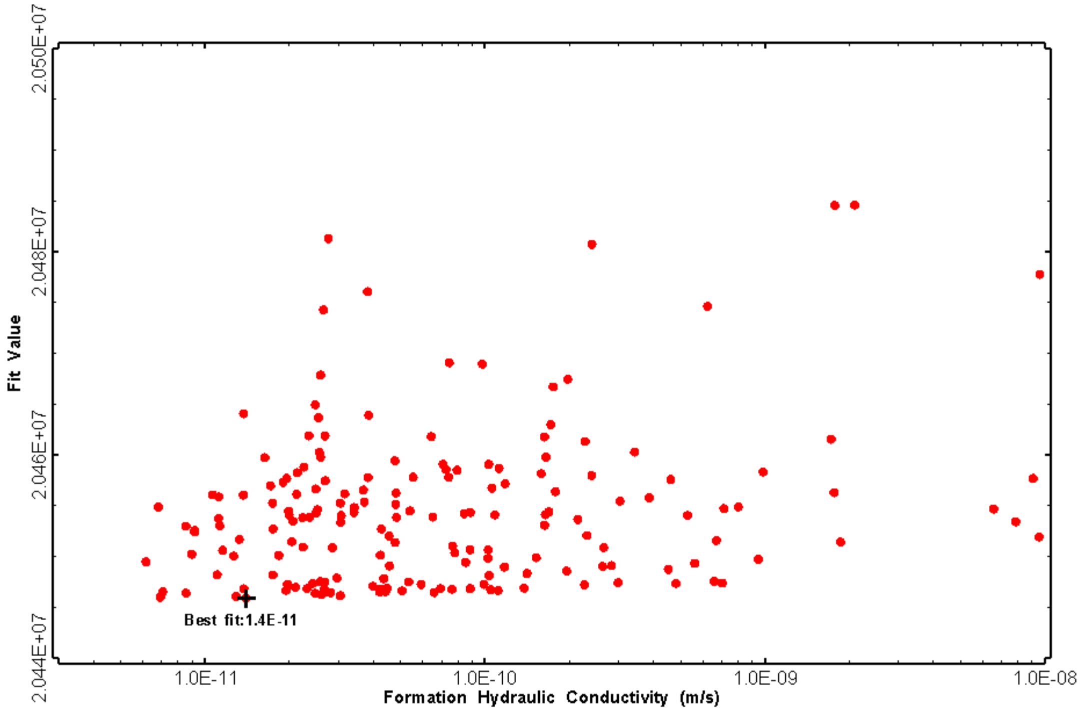

Figure 125: HT012 XY-scatter plot of formation hydraulic conductivity vs. fit value

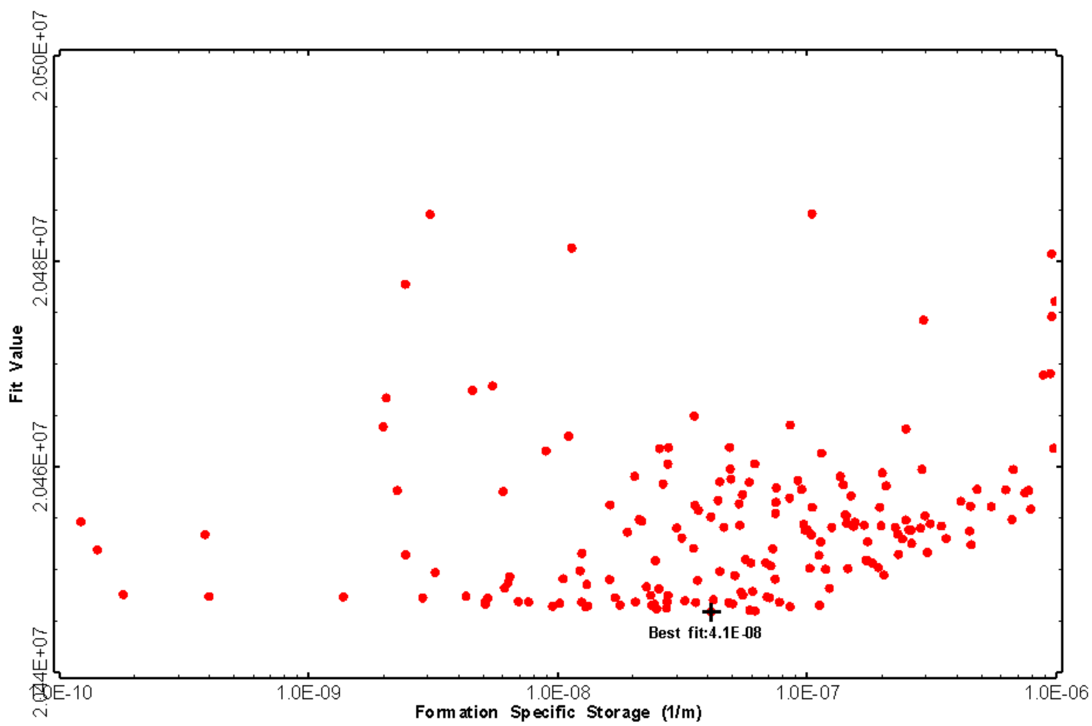

Figure 126: HT012 XY-scatter plot of formation specific storage vs. fit value

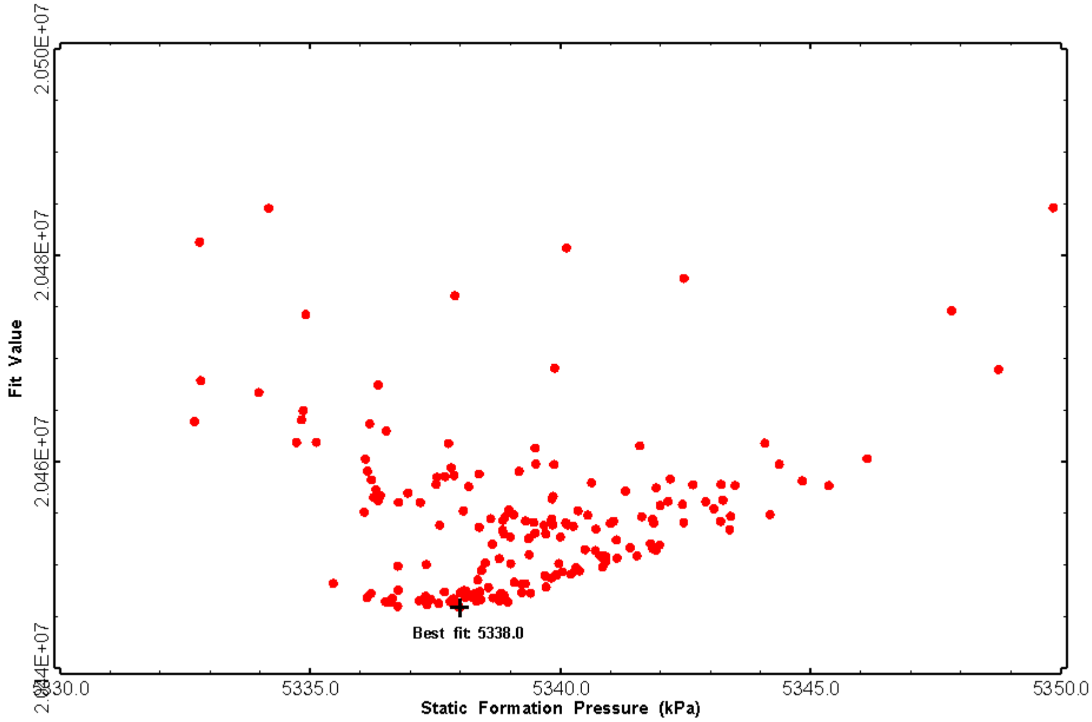

Figure 127: HT012 XY-scatter plot of static formation pressure vs. fit value

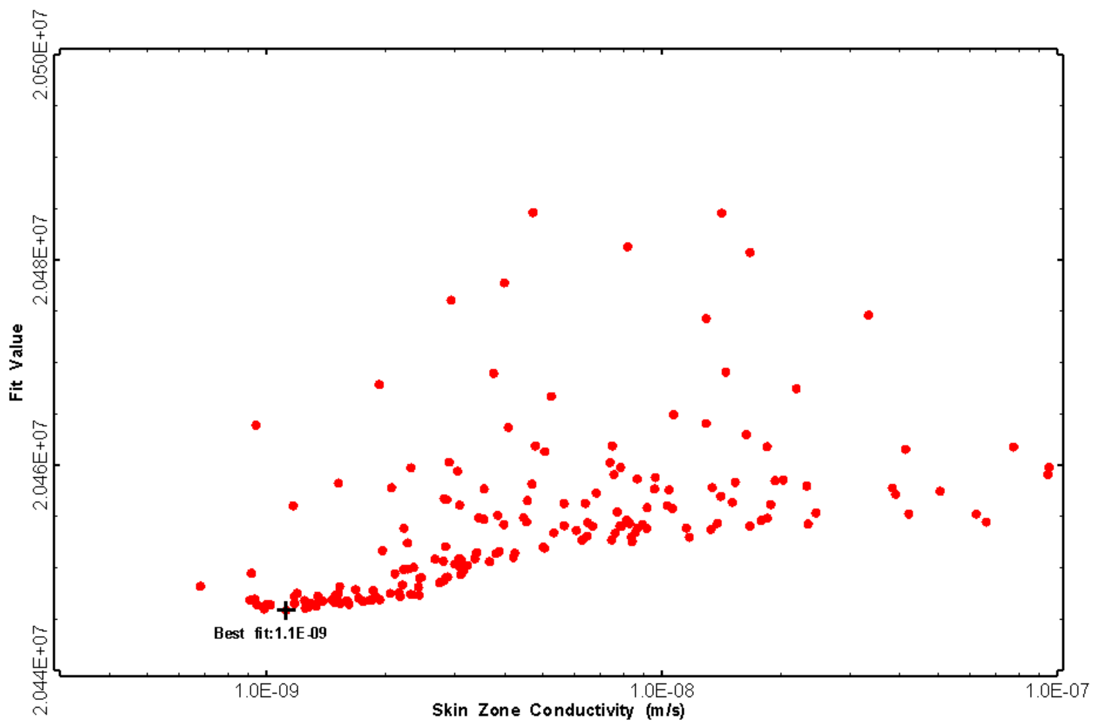

Figure 128: HT012 XY-scatter plot of skin zone conductivity vs. fit value

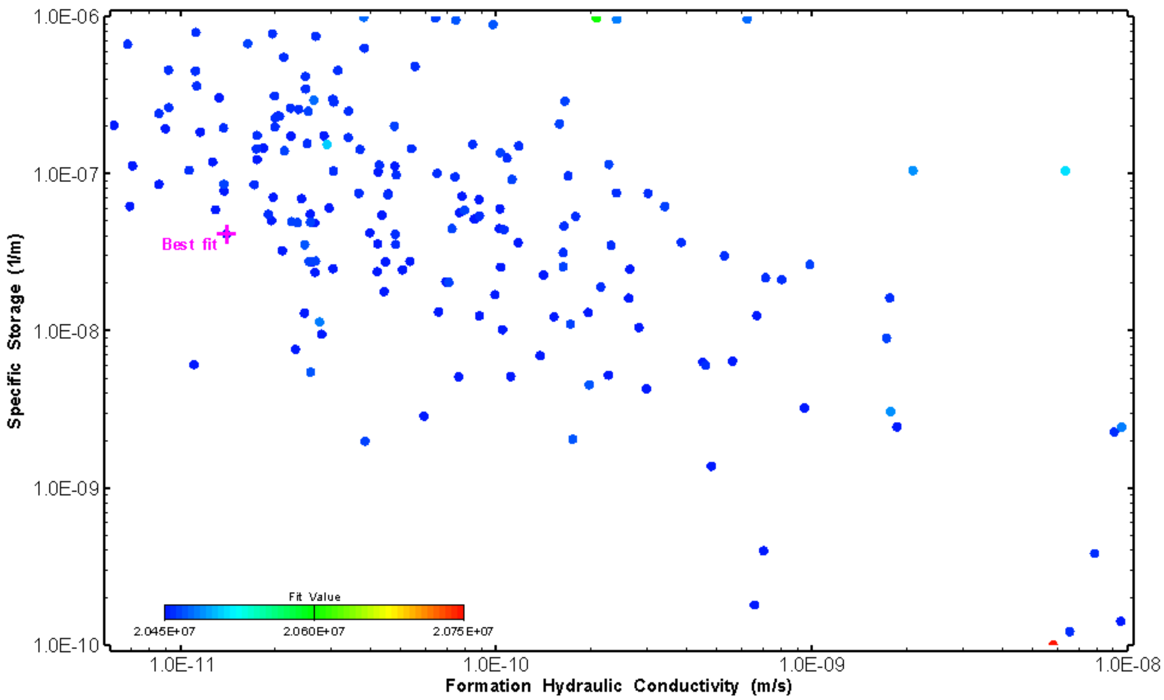

Figure 129: HT012 XY-scatter plot showing estimates of formation hydraulic conductivity and specific storage from perturbation analysis

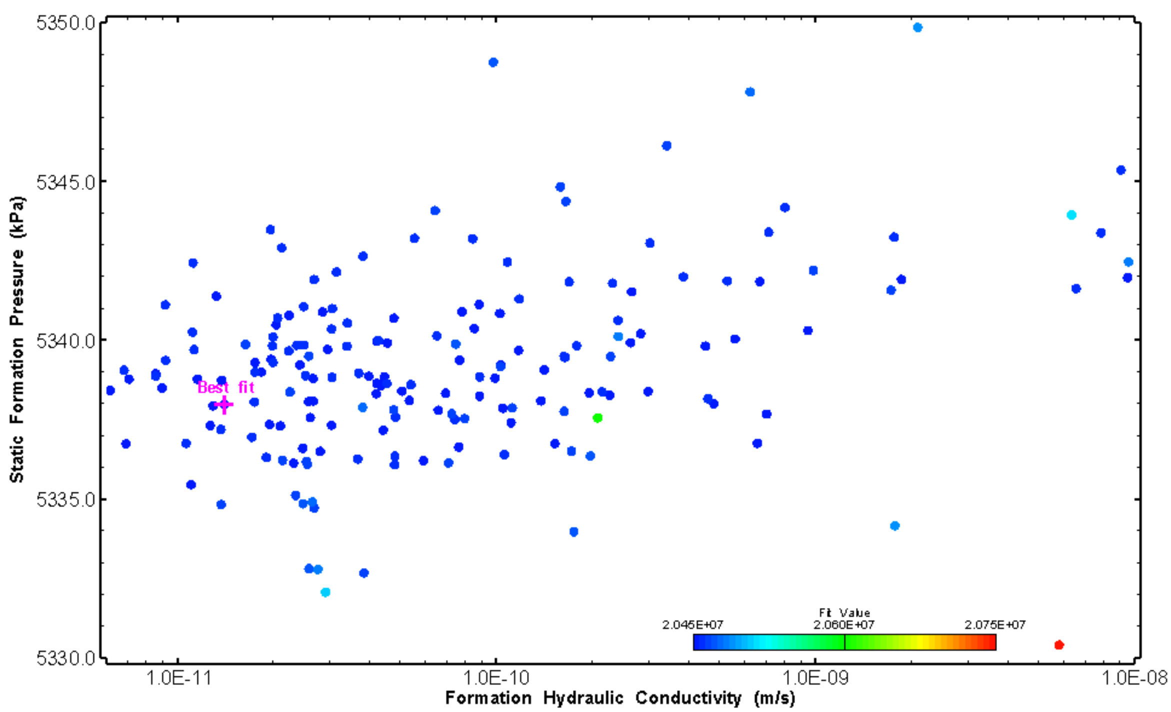

Figure 130: HT012 XY-scatter plot showing estimates of formation hydraulic conductivity and static formation pressure from perturbation analysis

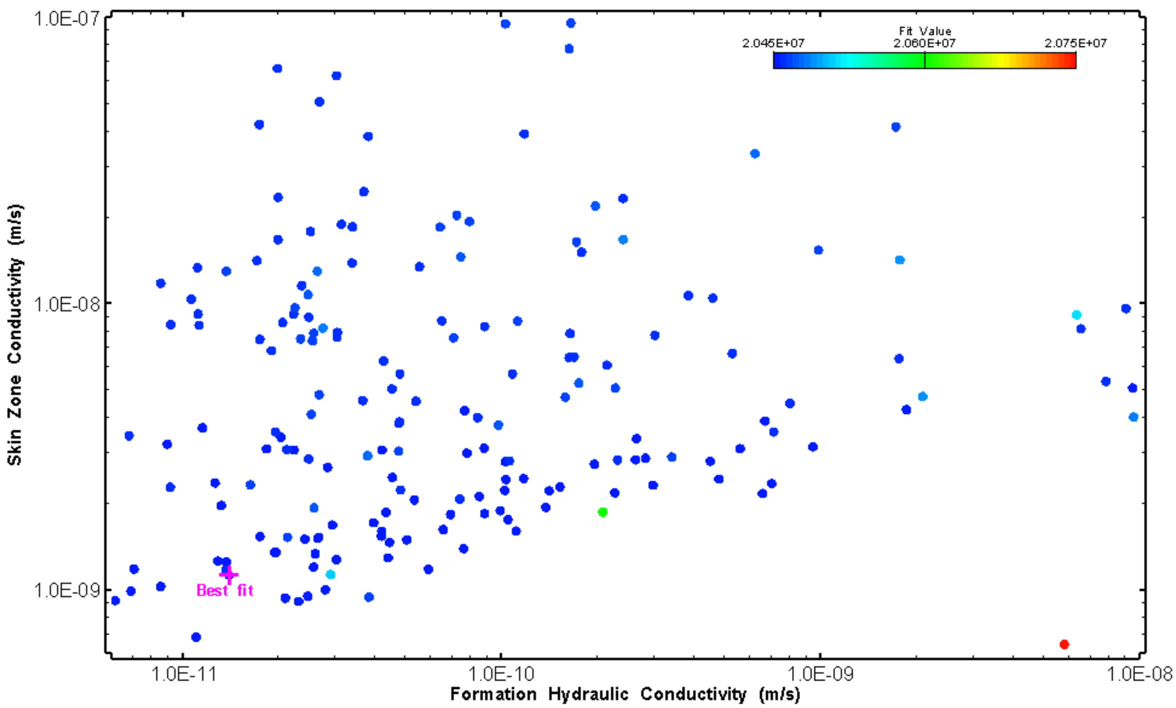

Figure 131: HT012 XY-scatter plot showing estimates of formation hydraulic conductivity and skin zone conductivity from perturbation analysis

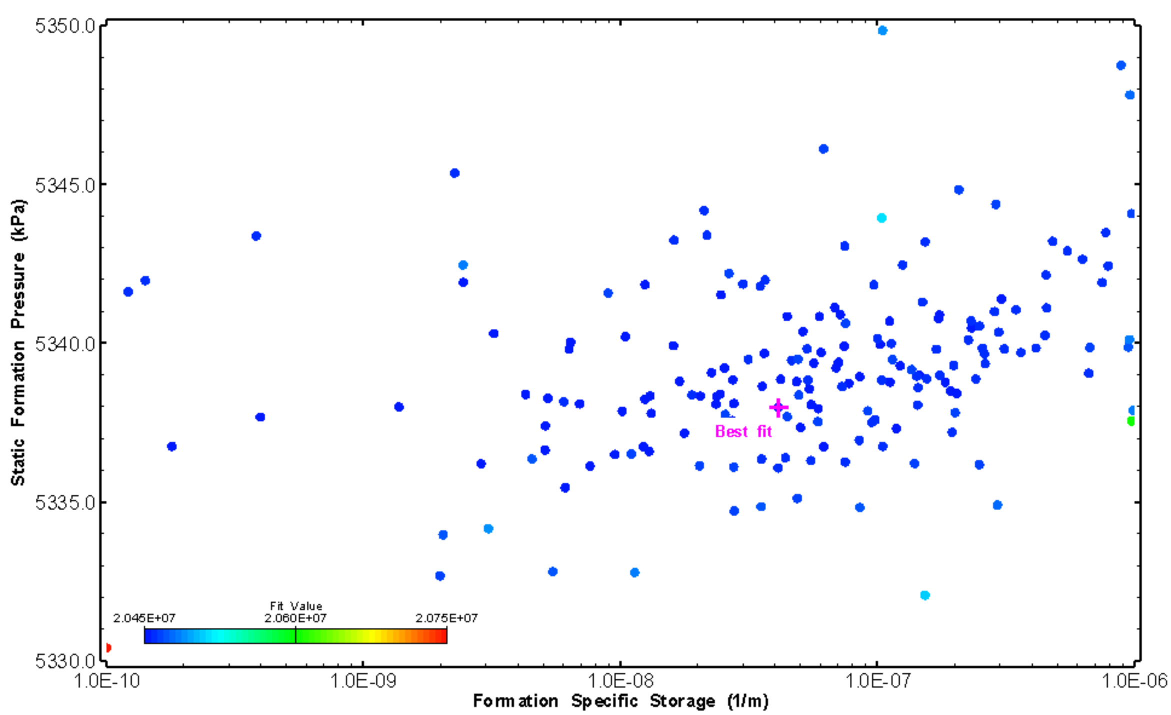

Figure 132: HT012 XY-scatter plot showing estimates of specific storage and static formation pressure from perturbation analysis

12.0 HT013 (625.11 – 645.14 M)

HT013 was selected to obtain continuous testing coverage from 600 to 800 m along hole. 14 broken fractures were observed in the core. No drill fluid parameter triggers were reached during drilling. An indication of flow was recorded during FFEC logging post-drilling.

The test was initiated with a shut-in pressure recovery phase (PSR). A pulse withdrawal test (PW) with a shut-in recovery followed by a slug withdrawal (SW) phase was completed after the PSR phase.

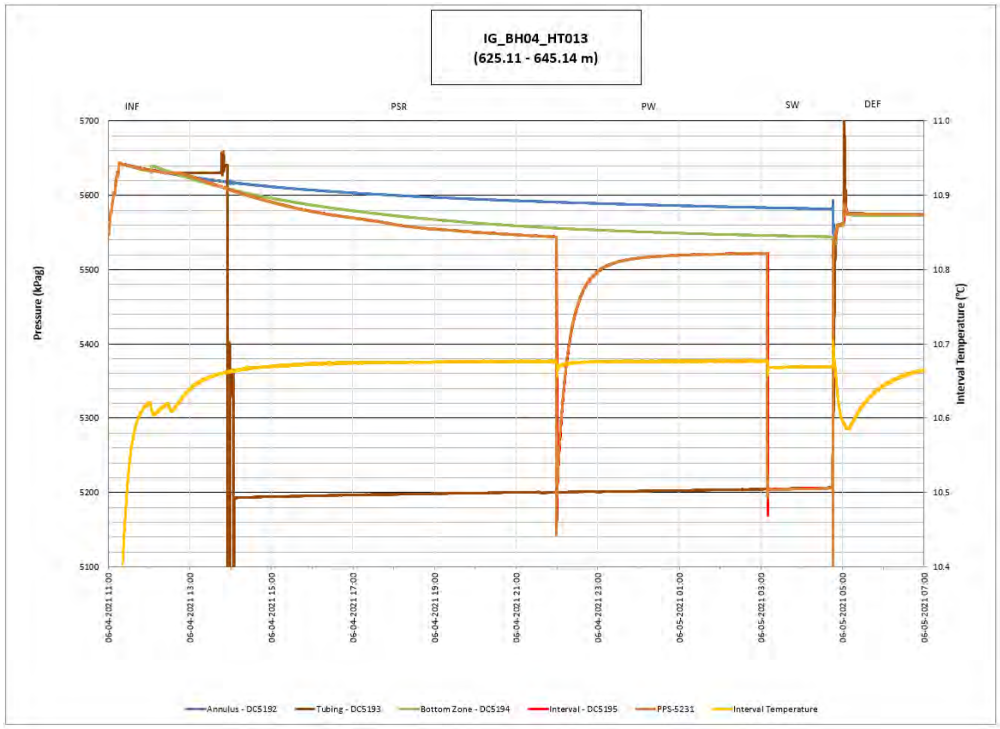

Figure 133: HT013 Annotated test plot showing monitored zone pressure and interval temperature.

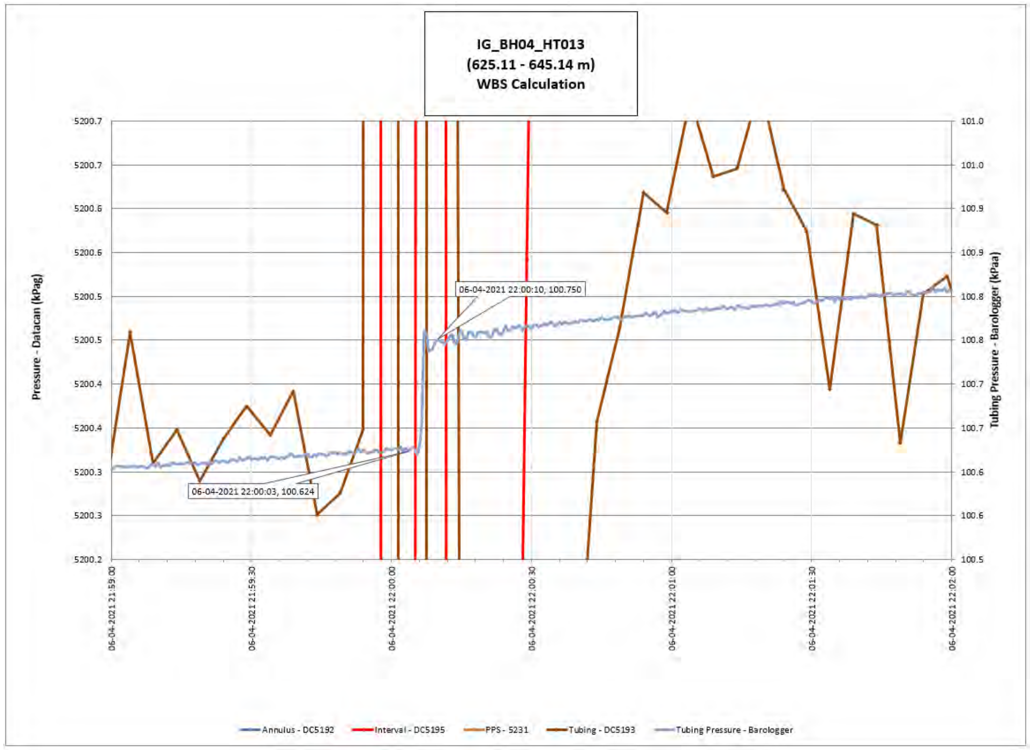

Figure 134: HT013 Tubing pressure during DHSIV activation. DHSIV Closed Wellbore Storage Estimate = 7E-11 m^3/Pa

Table 12: Summary of Analysis Results – HT013

	Formation conductivity	Skin zone conductivity	Static formation pressure	Formation specific storage	Radial thickness of skin	Flow dimension
	[m/s]	[m/s]	[kPa]	[1/m]	[m]	[–]
Best Fit	1.0E-09	8.6E-14	5523	3.4E-08	7.4E-04	1.2
Minimum	1.0E-13	1.4E-14	5500	1.0E-08	1.0E-04	1.0
Maximum	9.9E-09	1.0E-10	5534	1.0E-04	1.0E+00	3.0
Mean	5.8E-10	5.3E-12	5520	4.4E-06	1.8E-01	1.9
Median	4.2E-11	1.5E-12	5521	1.2E-07	4.7E-03	1.8
Geometric mean	3.2E-11	1.0E-12	5520	1.6E-07	7.6E-03	1.8

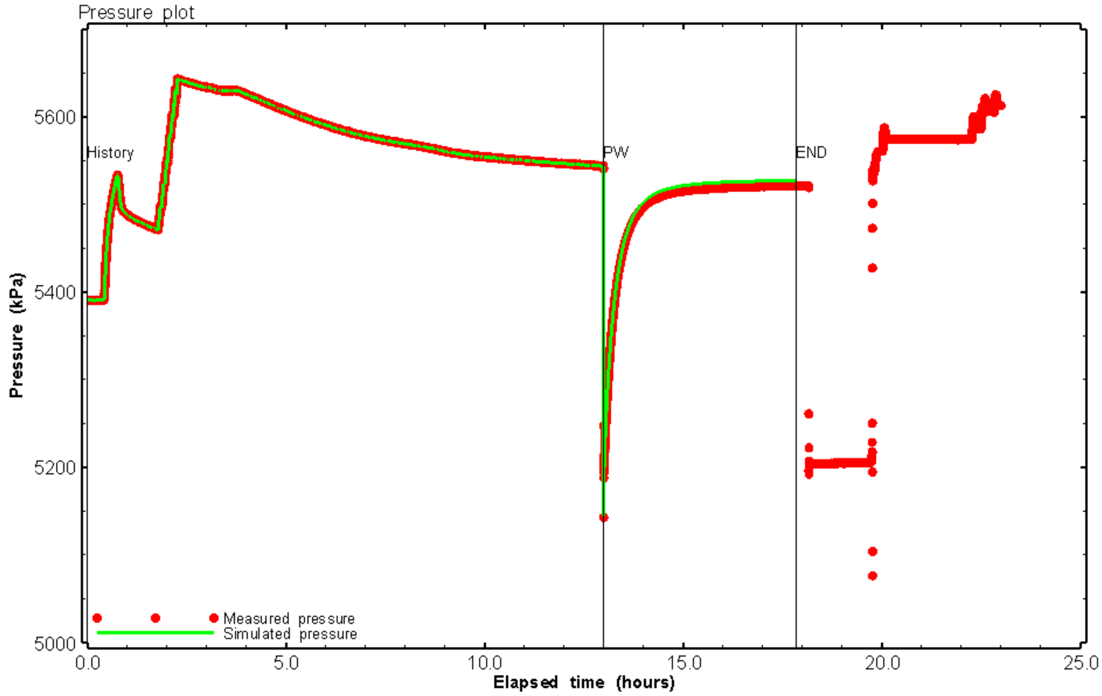

Figure 135: HT013 Pressure plot showing best-fit simulation and best fit results

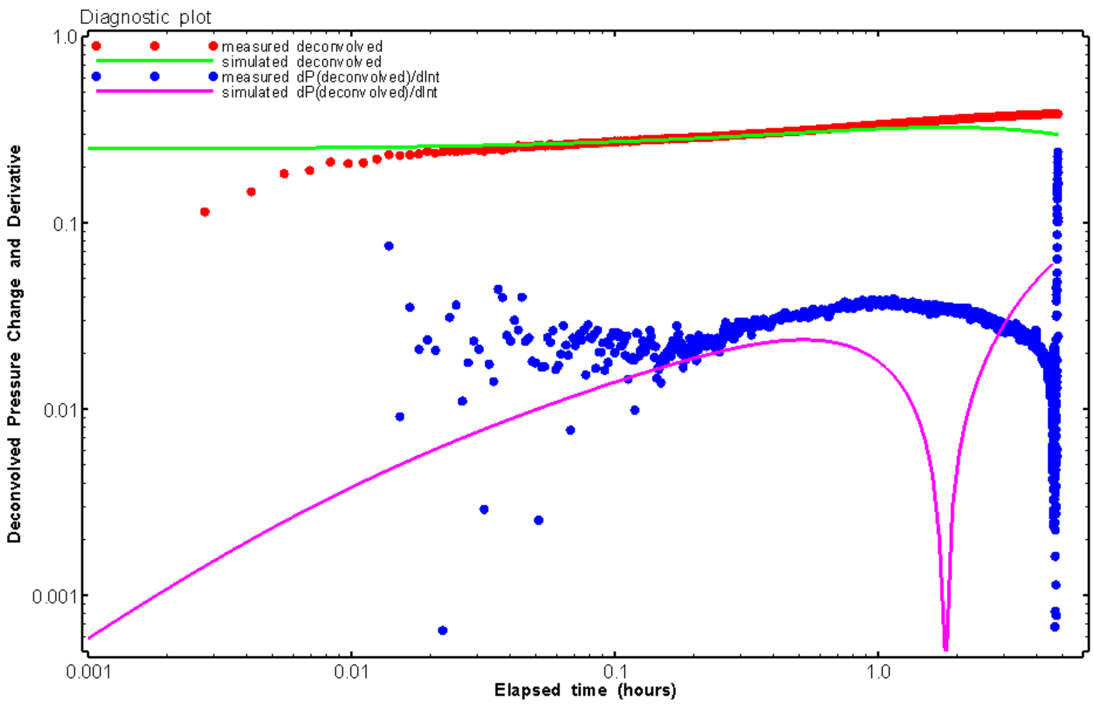

Figure 136: HT013 Deconvolved pressure change and derivative plot of the PW sequence showing best-fit simulation

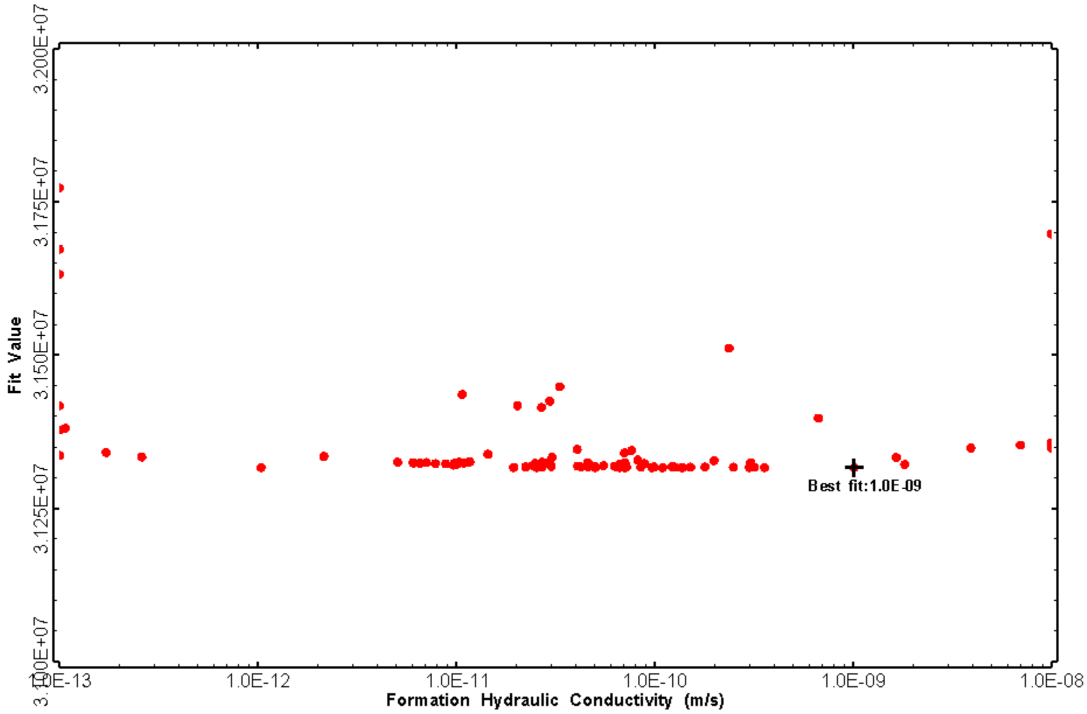

Figure 137: HT013 XY-scatter plot of formation hydraulic conductivity vs. fit value

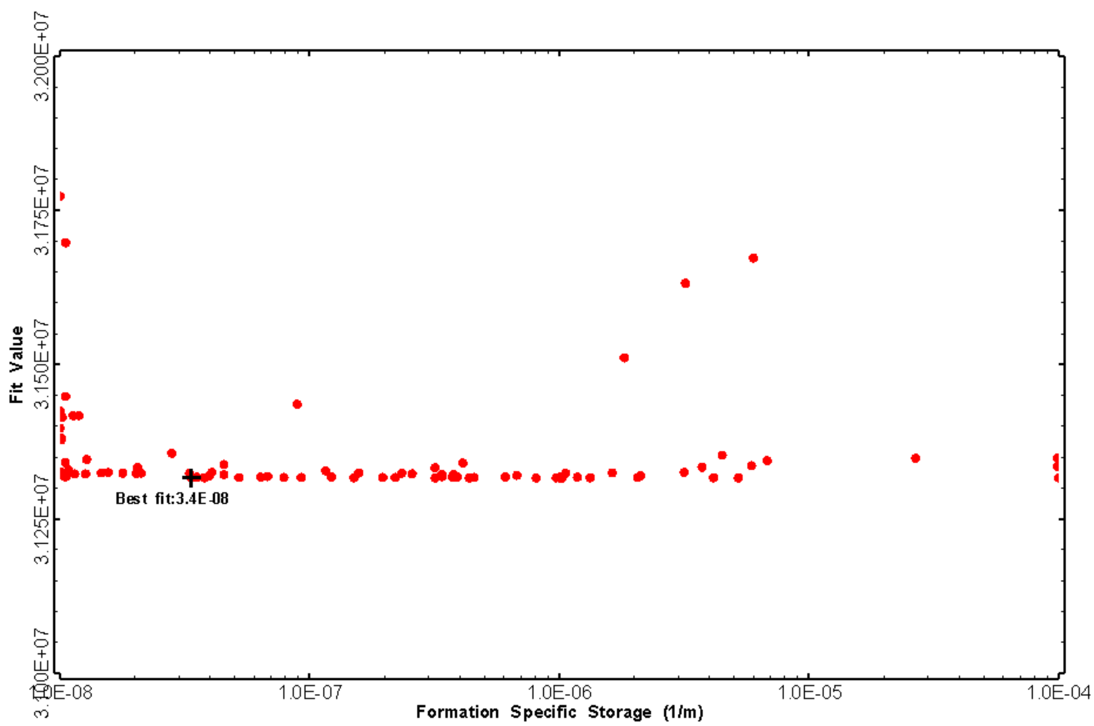

Figure 138: HT013 XY-scatter plot of formation specific storage vs. fit value

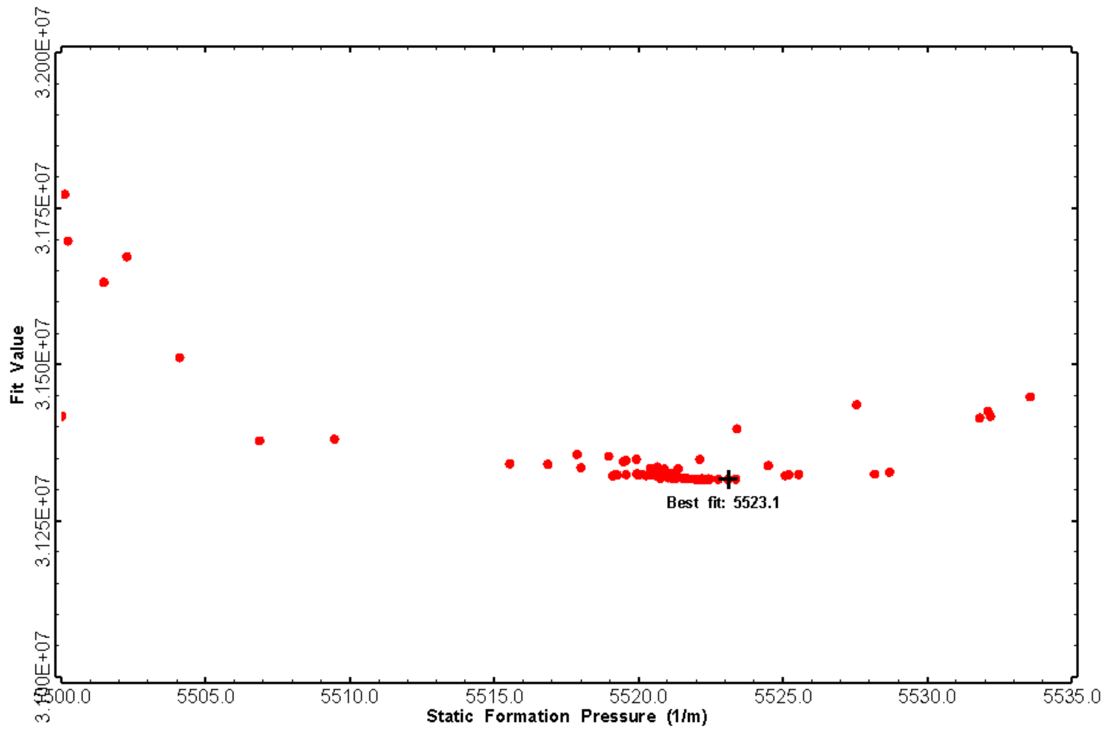

Figure 139: HT013 XY-scatter plot of static formation pressure vs. fit value

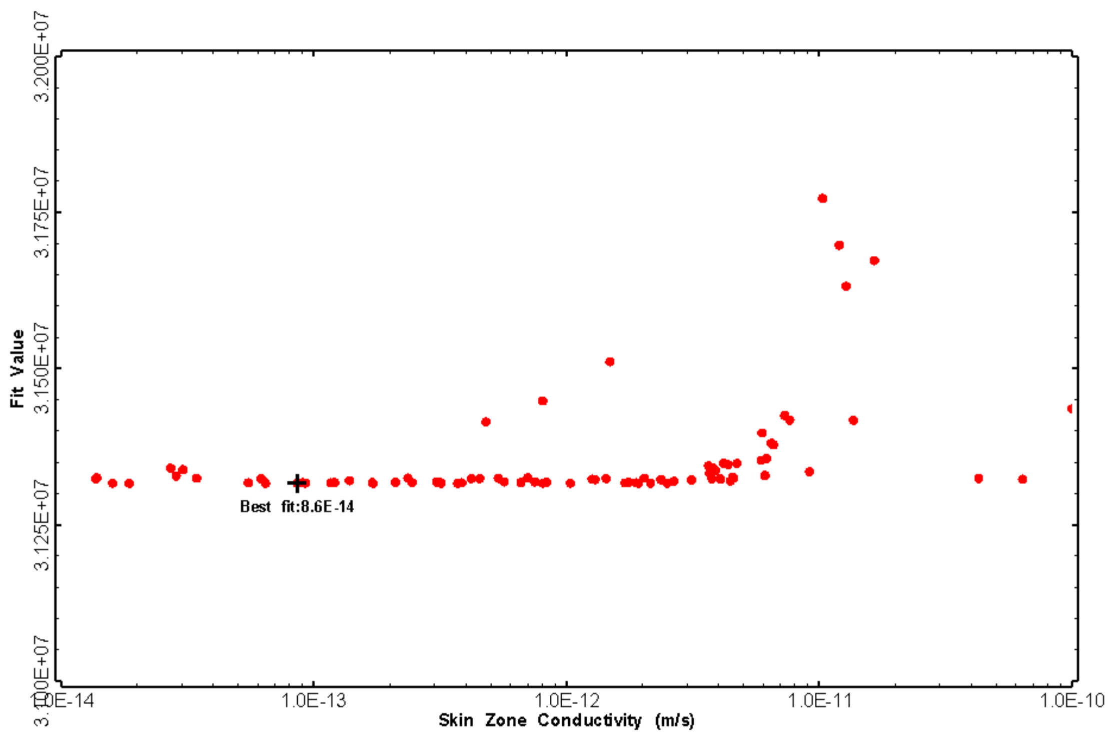

Figure 140: HT013 XY-scatter plot of skin zone conductivity vs. fit value

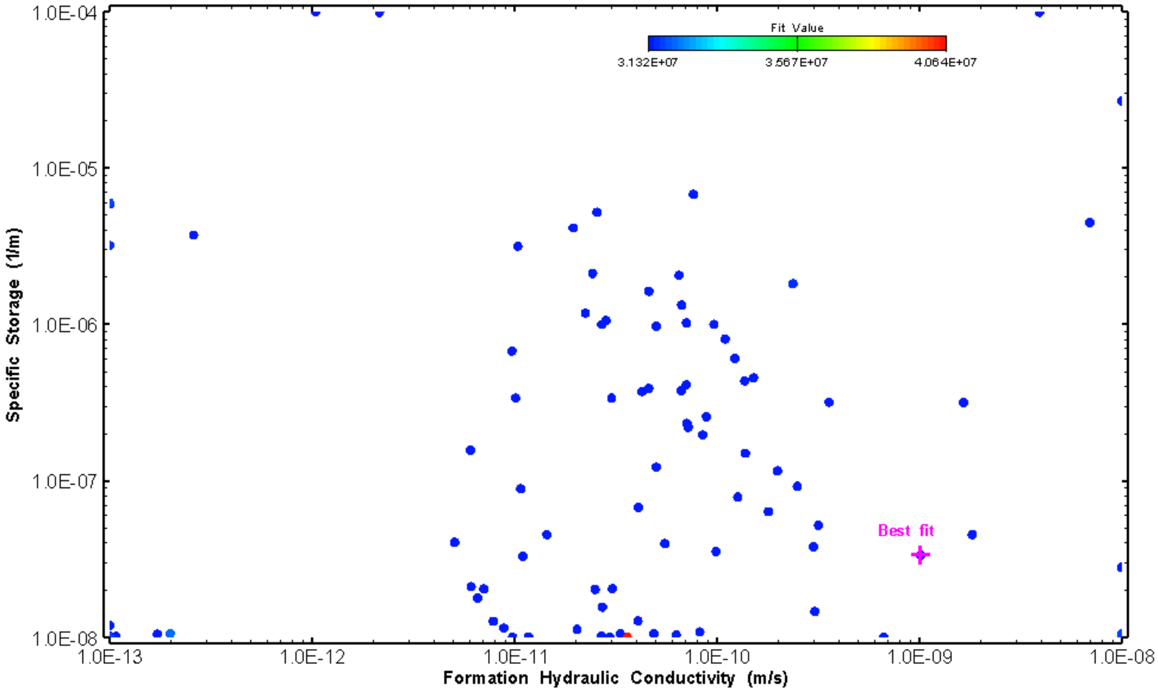

Figure 141: HT013 XY-scatter plot showing estimates of formation hydraulic conductivity and specific storage from perturbation analysis

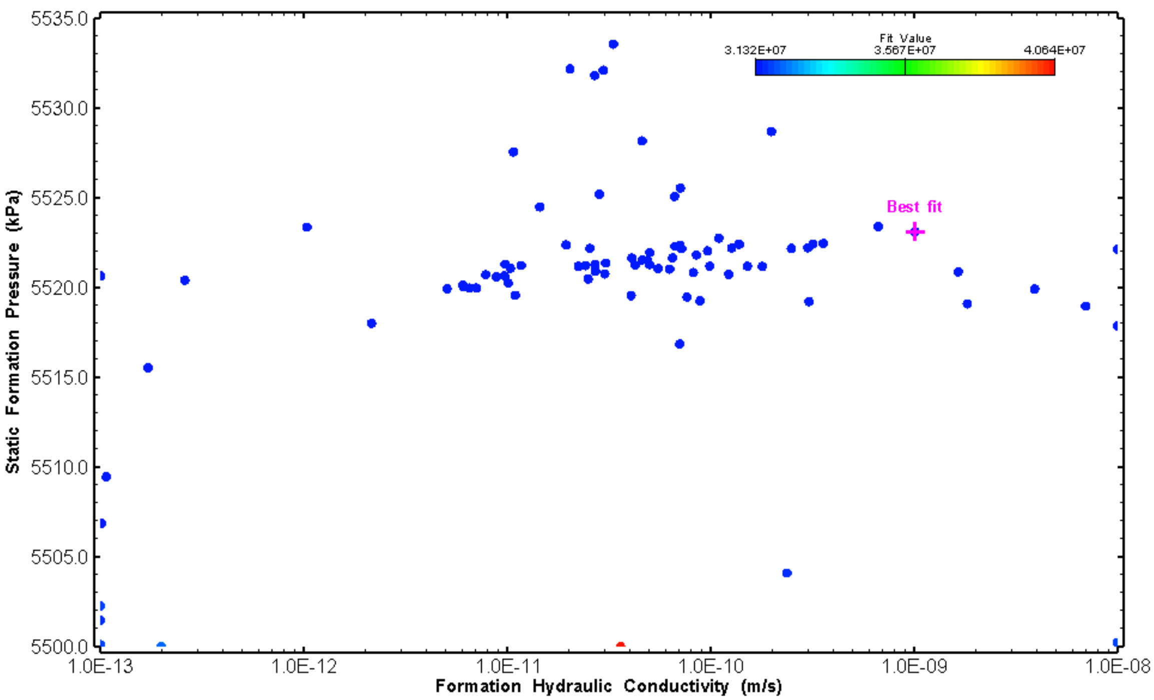

Figure 142: HT013 XY-scatter plot showing estimates of formation hydraulic conductivity and static formation pressure from perturbation analysis

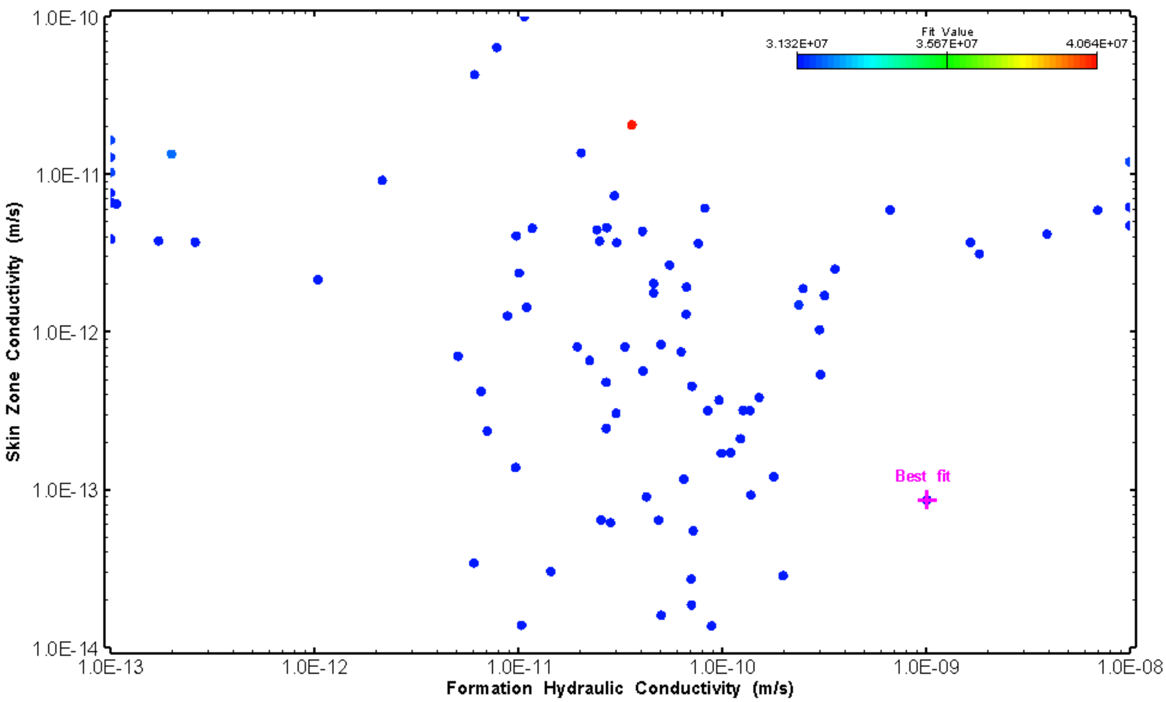

Figure 143: HT013 XY-scatter plot showing estimates of formation hydraulic conductivity and skin zone conductivity from perturbation analysis

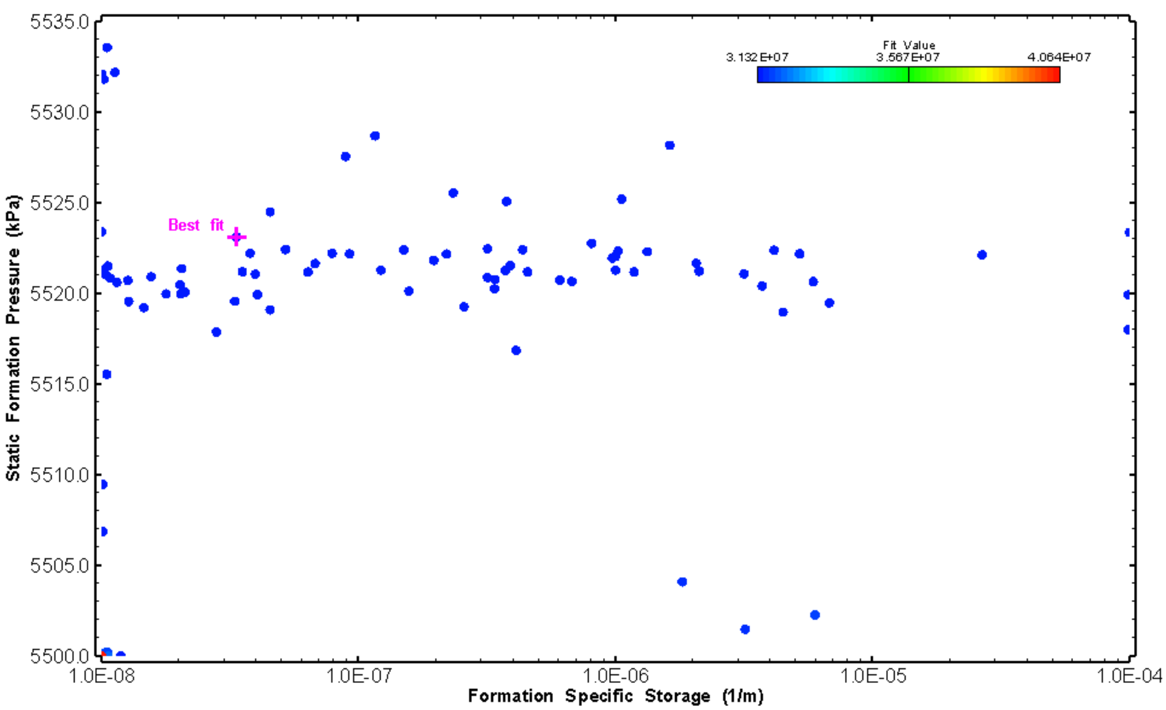

Figure 144: HT013 XY-scatter plot showing estimates of specific storage and static formation pressure from perturbation analysis

13.0 HT014 (644.63 – 664.66 M)

HT014 was selected to obtain continuous testing coverage from 600 to 800 m along hole. 14 broken fractures were observed in the core. A loss of drilling fluid was observed in this interval during drilling. An indication of flow was recorded during FFEC logging post-drilling.

The test was initiated with a shut-in pressure recovery phase (PSR). A pulse withdrawal test (PW) with a shut-in recovery was completed after the PSR phase.

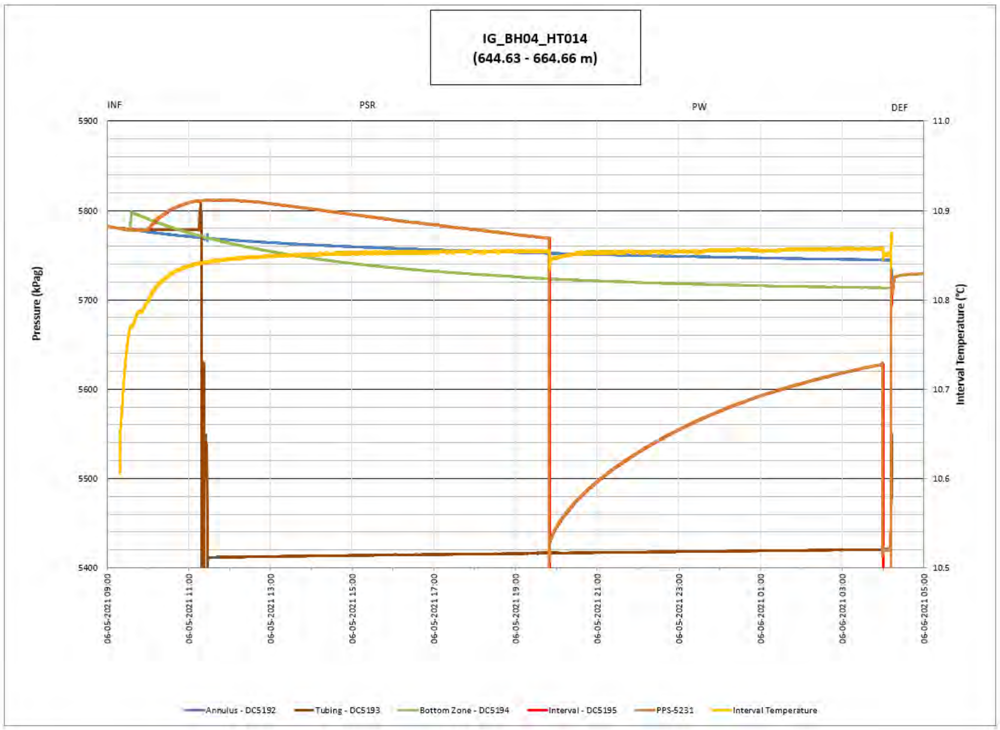

Figure 145: HT014 Annotated test plot showing monitored zone pressure and interval temperature.

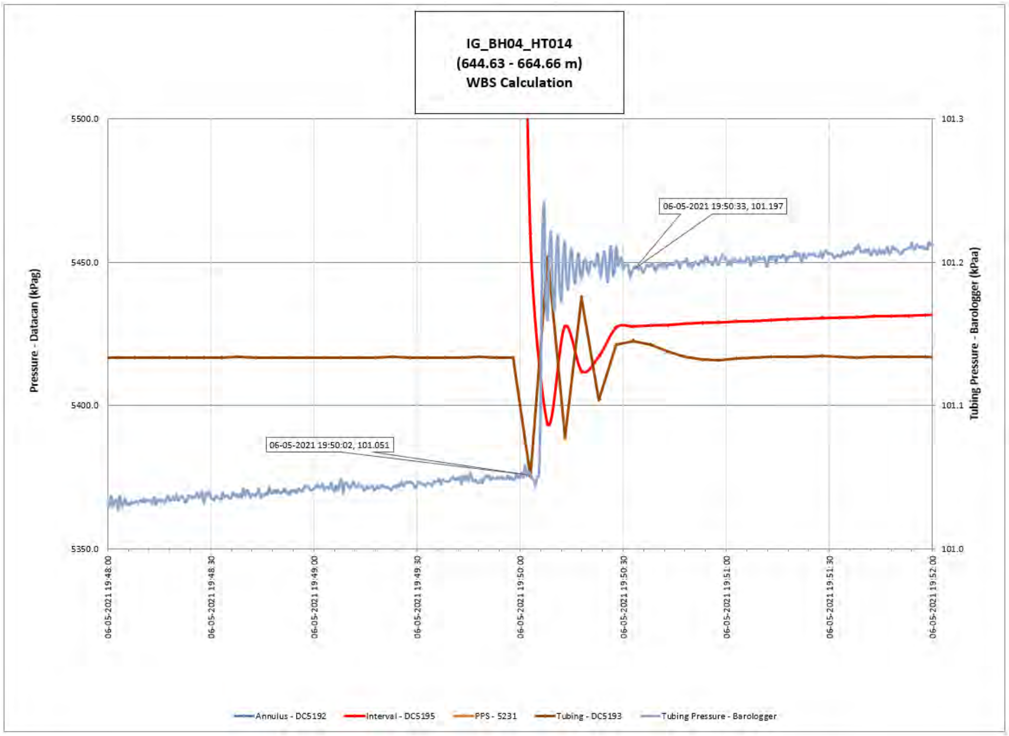

Figure 146: HT014 Tubing pressure during DHSIV activation. DHSIV Closed Wellbore Storage Estimate = 7E-11 m^3/Pa

Table 13: Summary of Analysis Results – HT014

	Formation conductivity	Skin zone conductivity	Static formation pressure	Formation specific storage	Radial thickness of skin	Flow dimension
	[m/s]	[m/s]	[kPa]	[1/m]	[m]	[–]
Best Fit	3.2E-13	2.1E-14	5725	3.6E-07	1.1E-3	2.4
Minimum	1.0E-15	1.3E-14	5589	1.0E-09	1.0E-3	1.0
Maximum	1.0E-11	7.5E-11	6199	8.8E-06	0.98	2.9
Mean	5.8E-13	3.3E-12	5913	1.5E-06	0.18	1.7
Median	6.3E-14	3.7E-13	5901	9.3E-07	0.075	1.6
Geometric mean	7.1E-14	3.7E-13	5912	3.5E-07	0.043	1.6

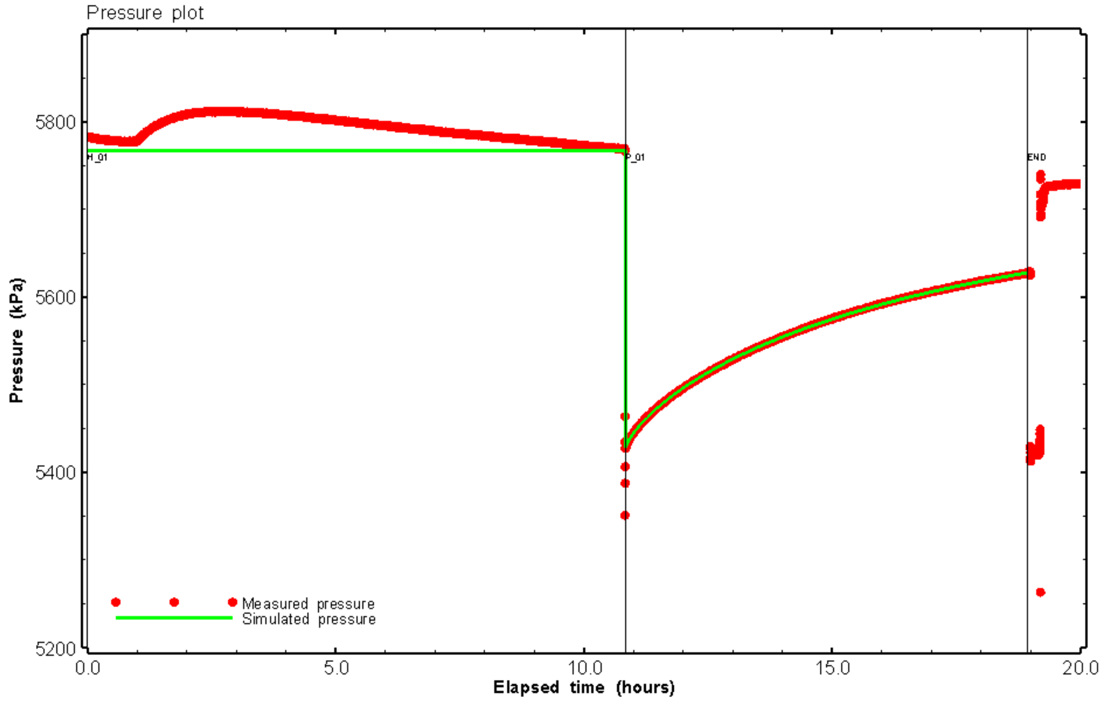

Figure 147: HT014 Pressure plot showing best-fit simulation and best fit results

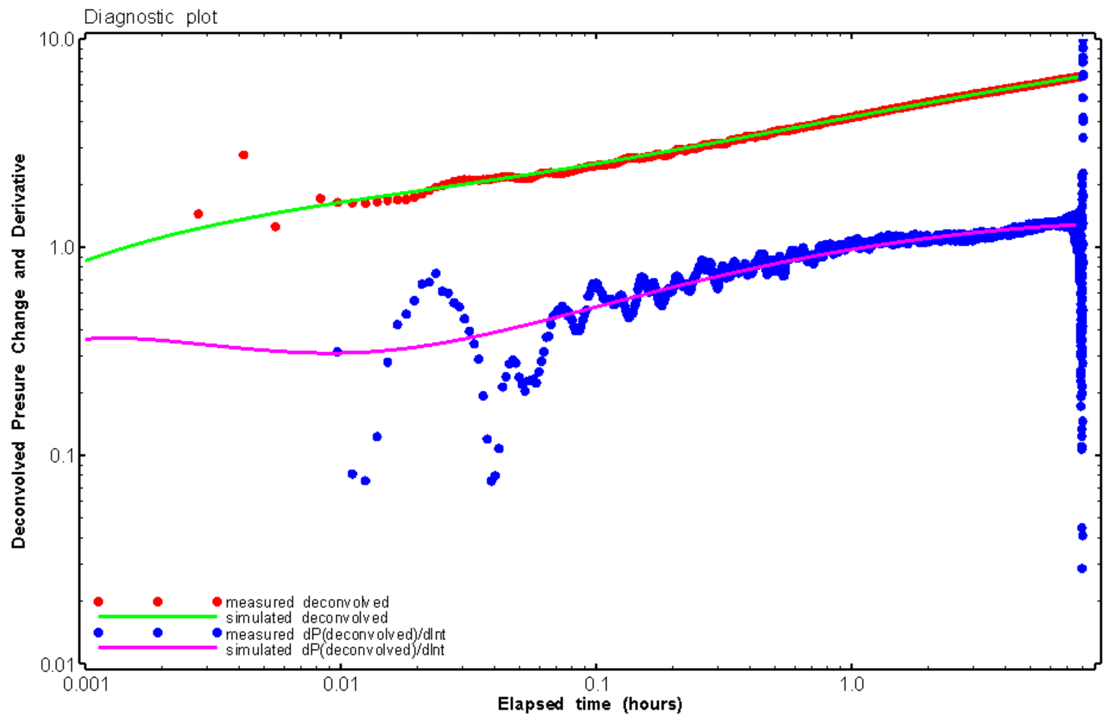

Figure 148: HT014 Deconvolved pressure change and derivative plot of the PW sequence showing best-fit simulation

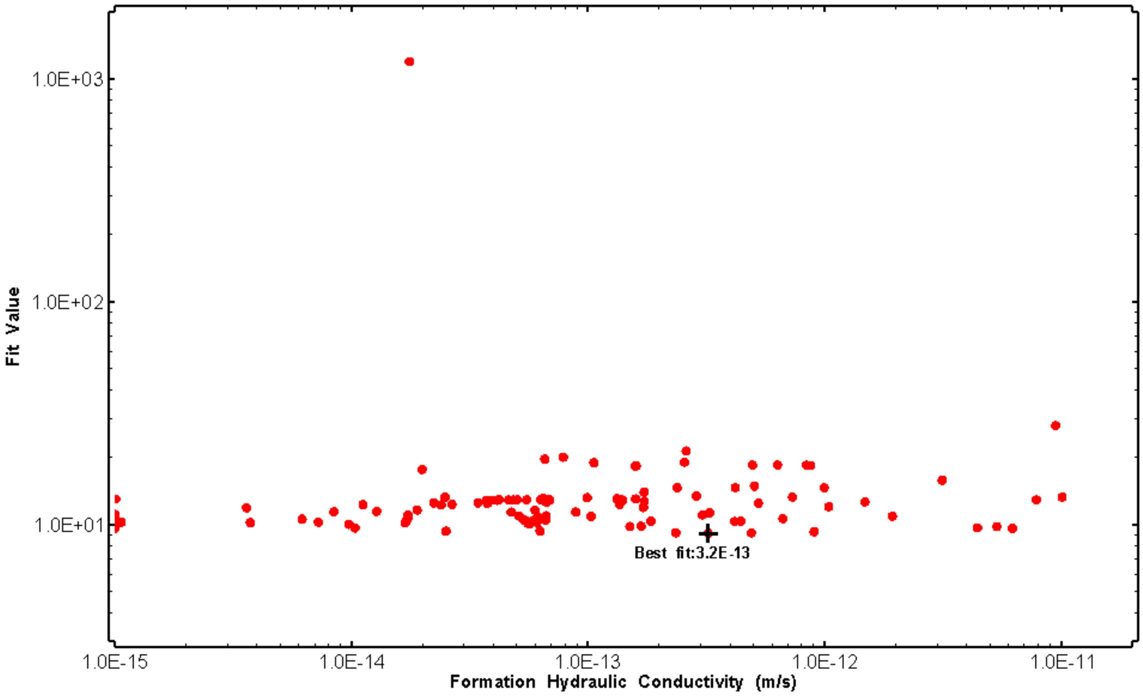

Figure 149: HT014 XY-scatter plot of formation hydraulic conductivity vs. fit value

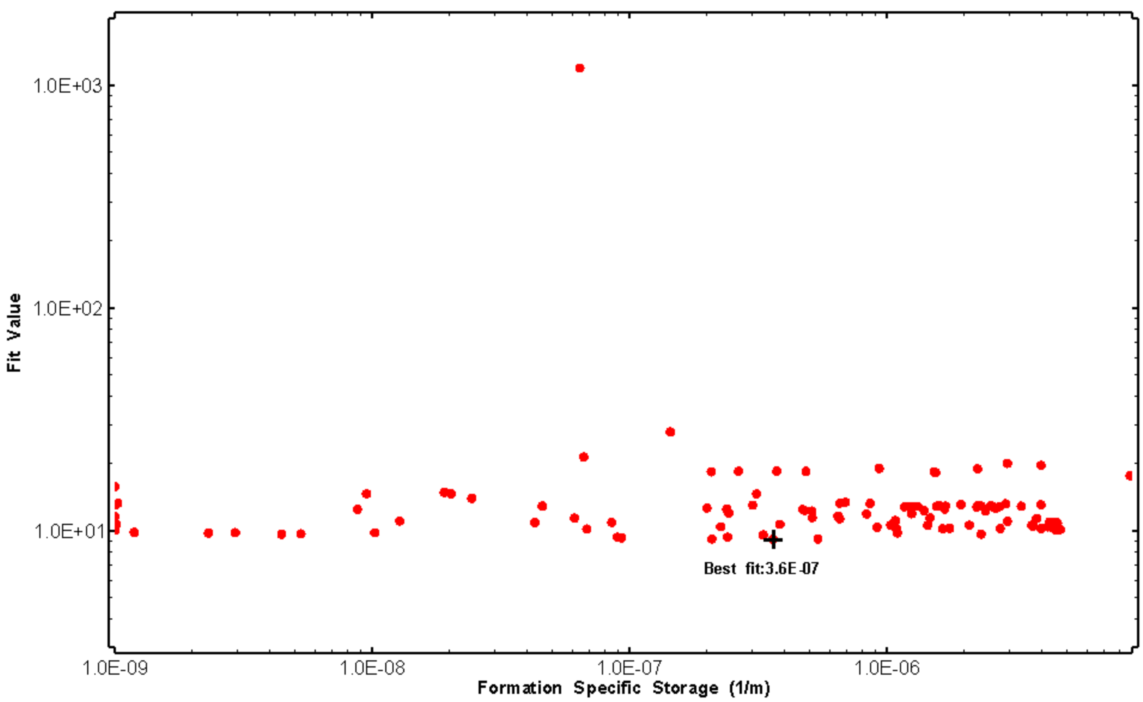

Figure 150: HT014 XY-scatter plot of formation specific storage vs. fit value

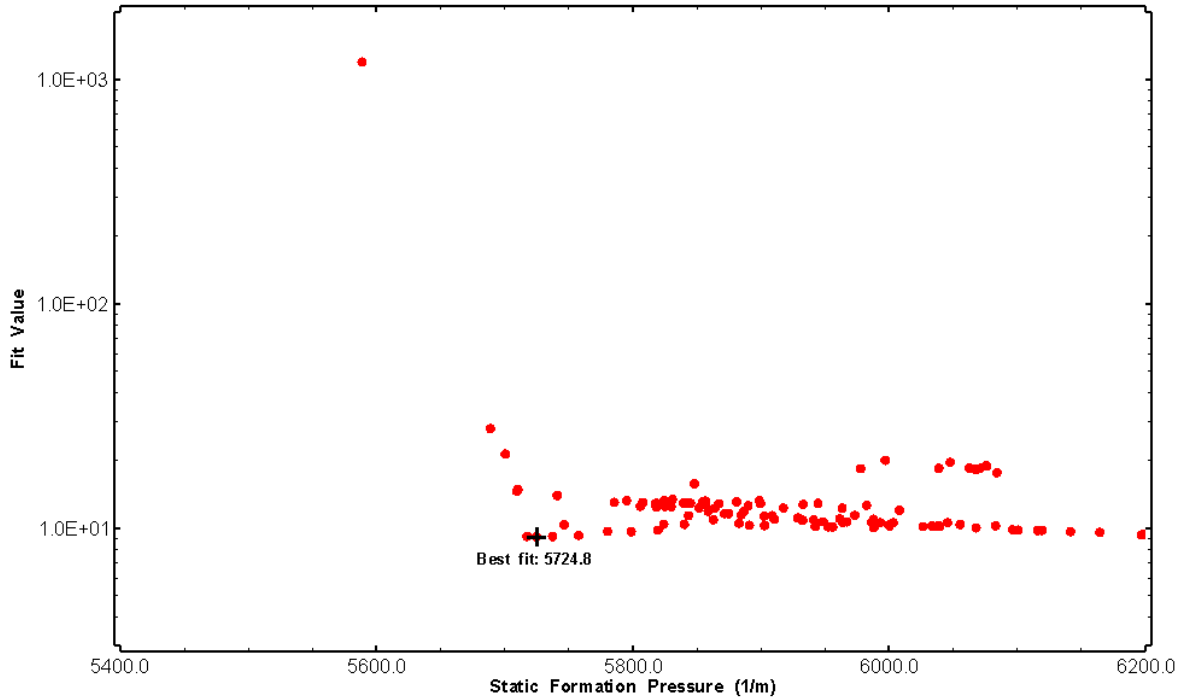

Figure 151: HT014 XY-scatter plot of static formation pressure vs. fit value

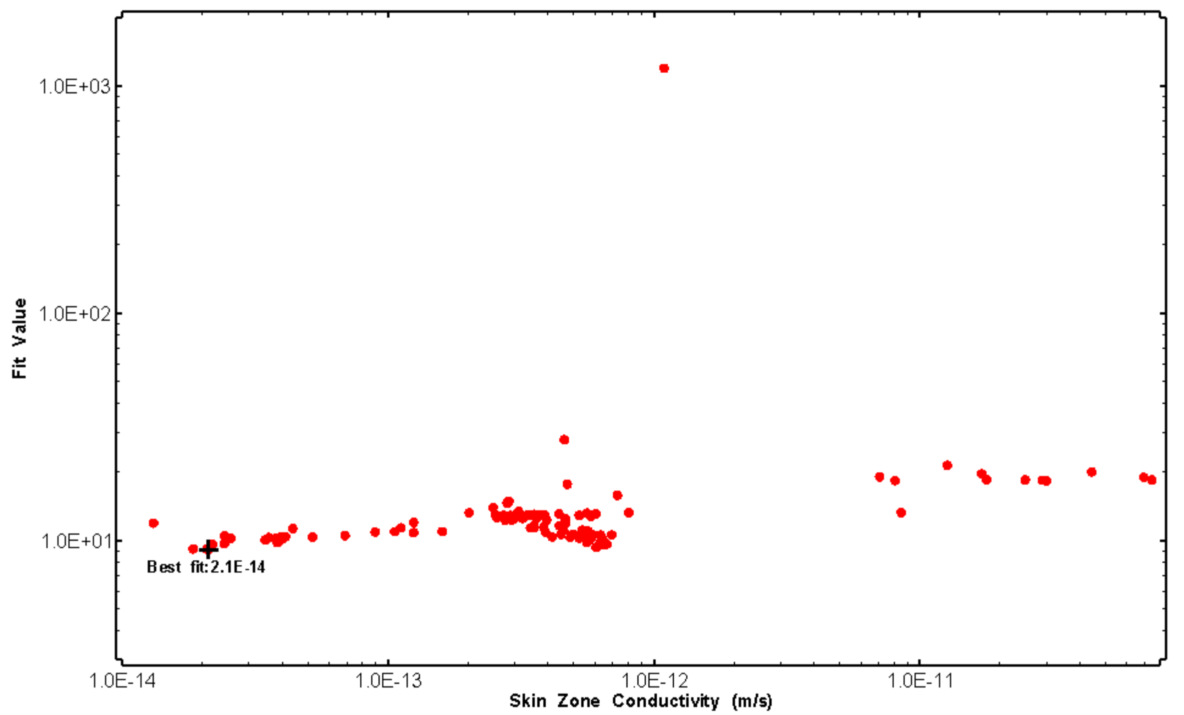

Figure 152: HT014 XY-scatter plot of skin zone conductivity vs. fit value

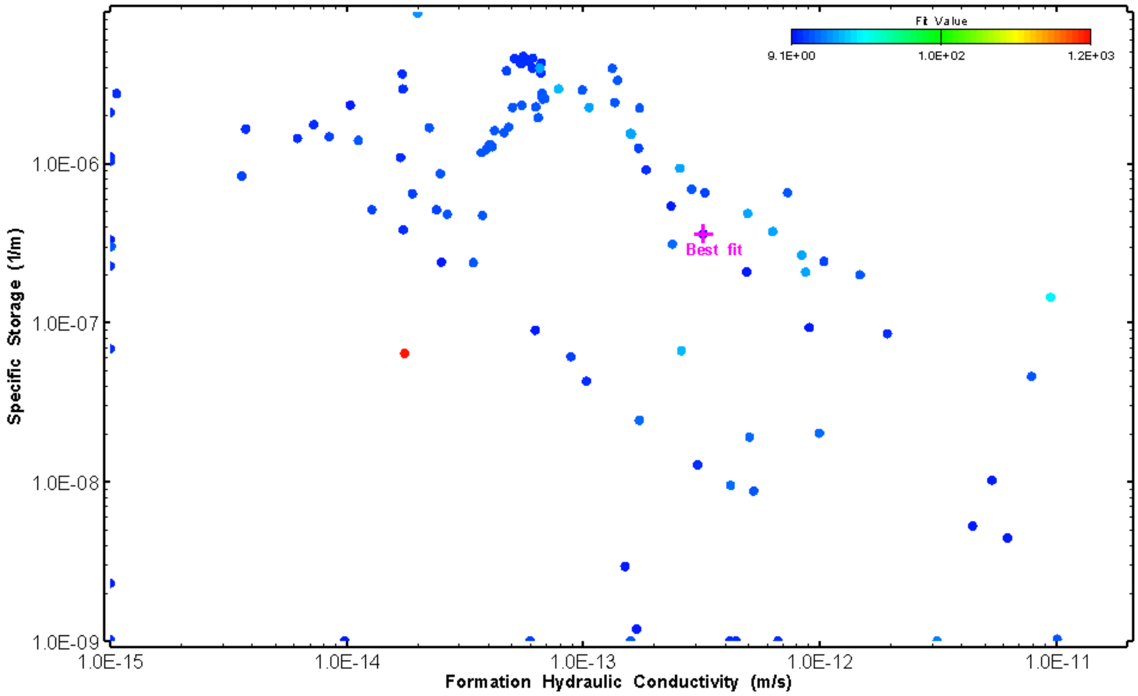

Figure 153: HT014 XY-scatter plot showing estimates of formation hydraulic conductivity and specific storage from perturbation analysis

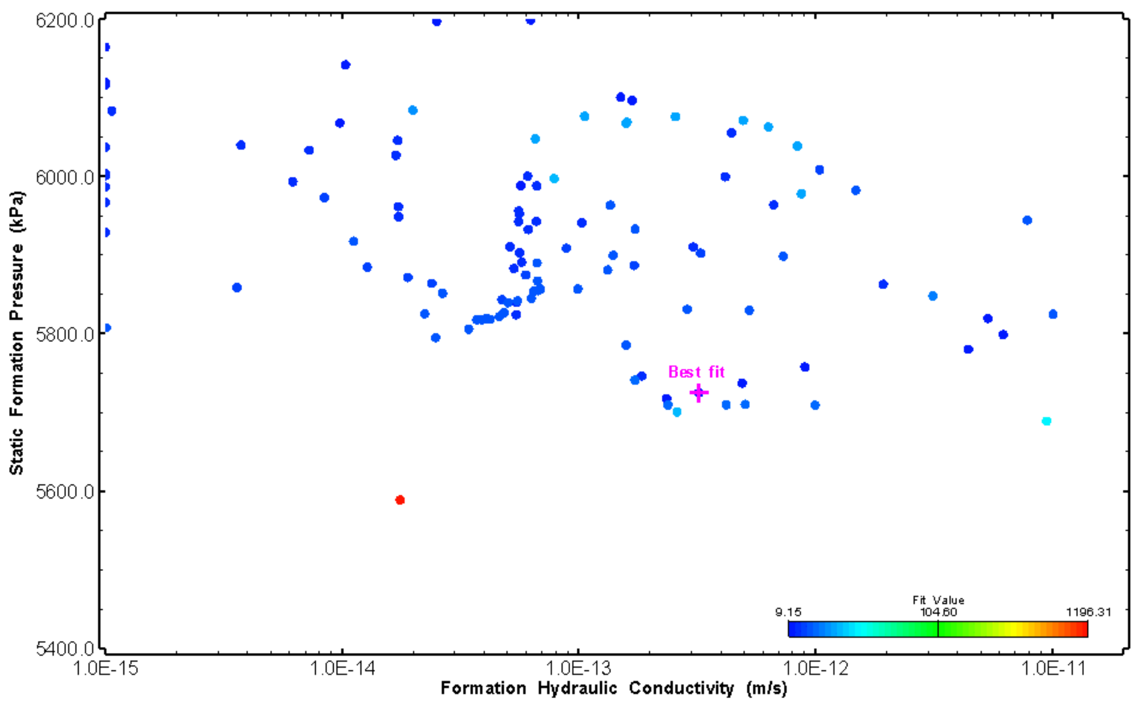

Figure 154: HT014 XY-scatter plot showing estimates of formation hydraulic conductivity and static formation pressure from perturbation analysis

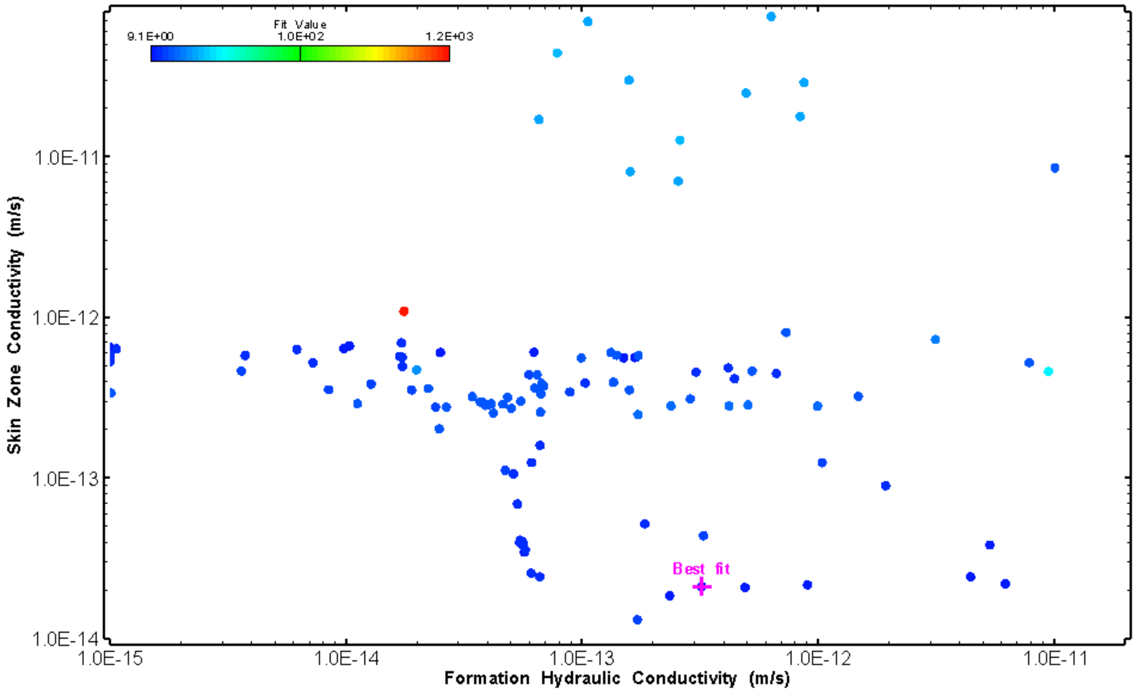

Figure 155: HT014 XY-scatter plot showing estimates of formation hydraulic conductivity and skin zone conductivity from perturbation analysis

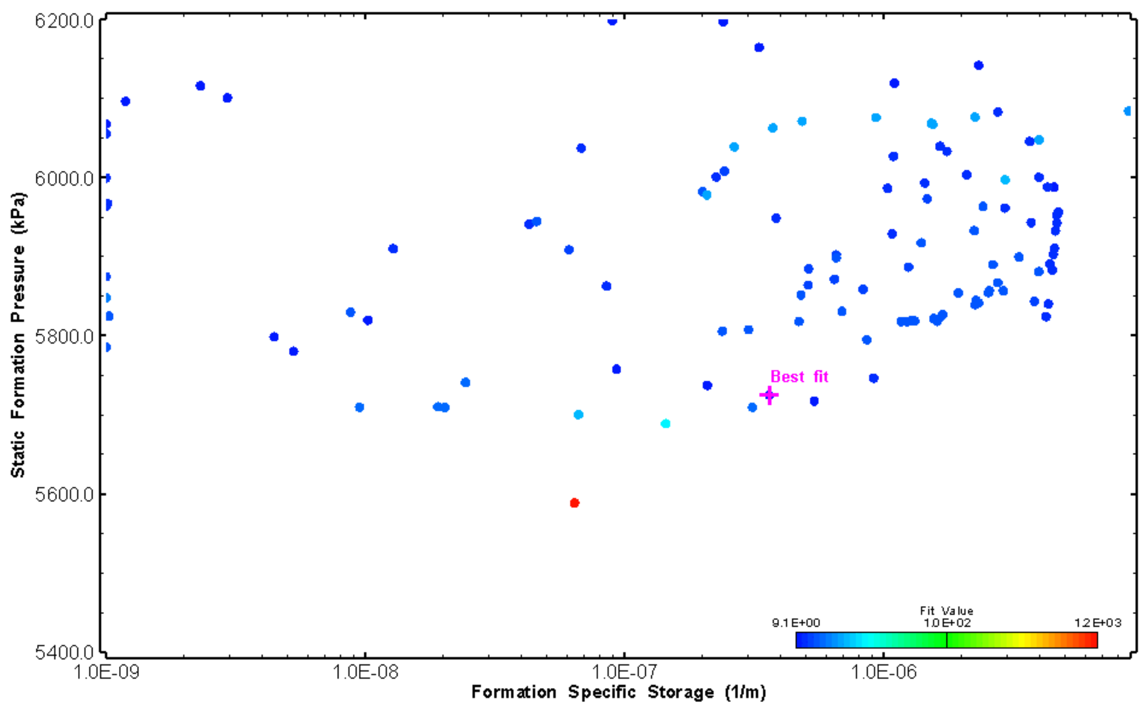

Figure 156: HT014 XY-scatter plot showing estimates of specific storage and static formation pressure from perturbation analysis

14.0 HT015 (664.13 – 684.16 M)

HT015 was selected to obtain continuous testing coverage from 600 to 800 m along hole. Zero broken fractures were observed in the core. No drill fluid parameter triggers were reached during drilling. A slight indication of flow was recorded during FFEC logging post-drilling.

The test was initiated with a shut-in pressure recovery phase (PSR). A pulse withdrawal test (PW) with a shut-in recovery was completed after the PSR phase.

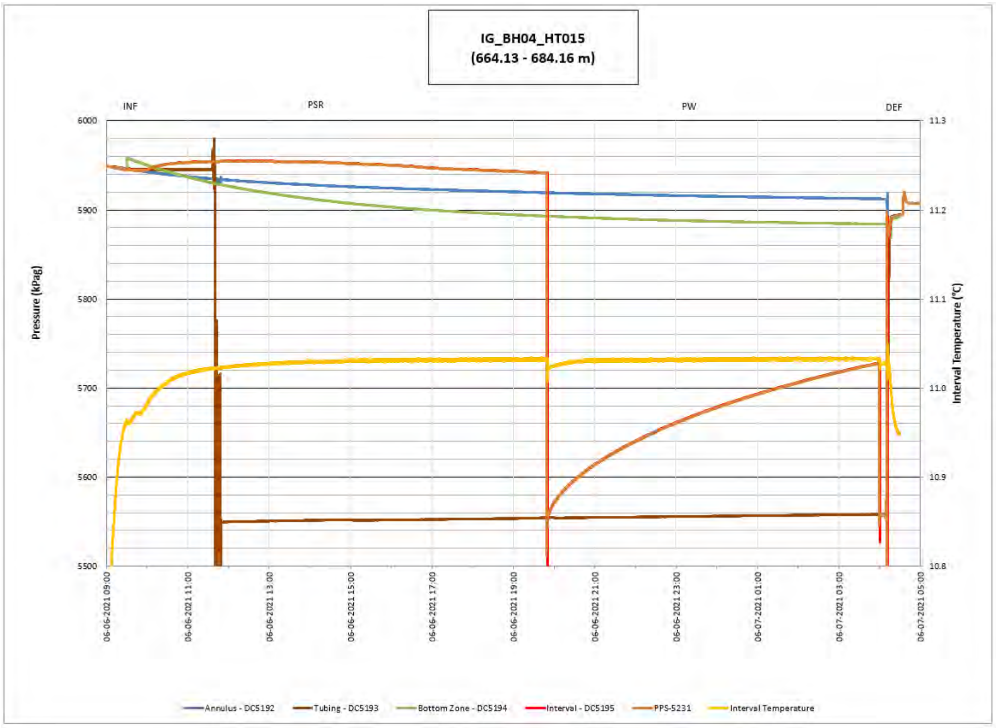

Figure 157: HT015 Annotated test plot showing monitored zone pressure and interval temperature.

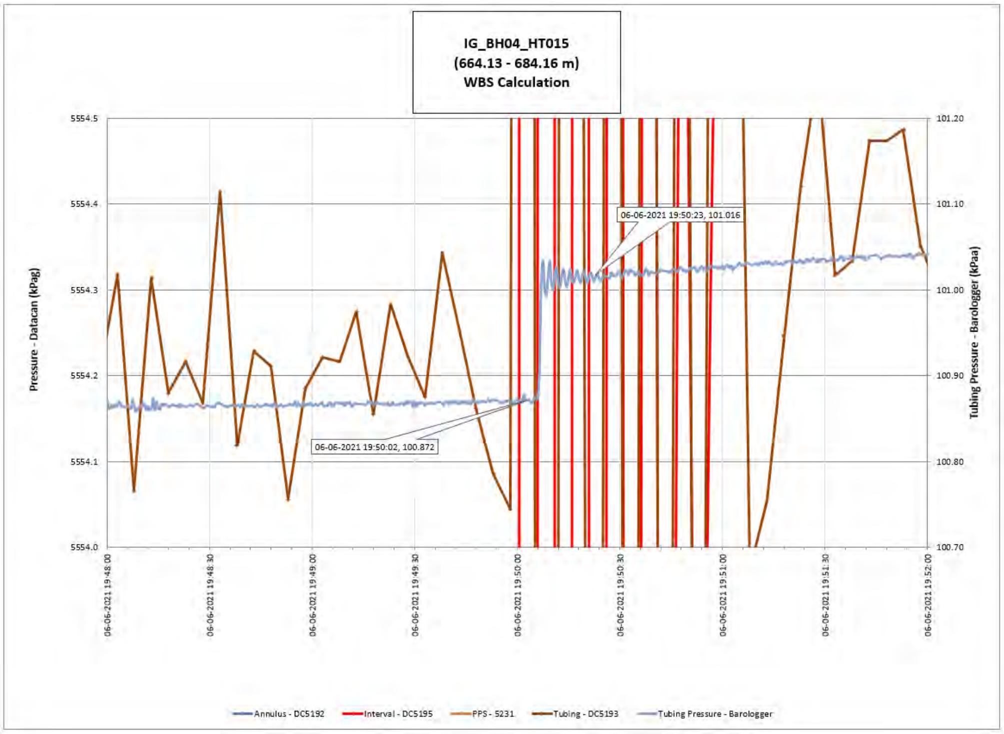

Figure 158: HT015 Tubing pressure during DHSIV activation. DHSIV Closed Wellbore Storage Estimate = 7E-11 m^3/Pa

Table 14: Summary of Analysis Results – HT015

	Formation conductivity	Skin zone conductivity	Static formation pressure	Formation specific storage	Radial thickness of skin	Flow dimension
	[m/s]	[m/s]	[kPa]	[1/m]	[m]	[–]
Best Fit	4.0E-13	2.8E-14	5985	1.1E-07	1.0E-3	1.5
Minimum	1.7E-14	1.8E-14	5879	9.7E-08	1.0E-3	1.0
Maximum	4.0E-13	1.0E-09	6309	2.3E-06	0.041	3.0
Mean	6.8E-14	9.1E-12	5973	1.2E-06	0.0042	2.6
Median	6.2E-14	6.0E-14	5964	9.8E-07	0.0029	2.7
Geometric mean	5.6E-14	9.7E-14	5972	9.9E-07	0.0028	2.5

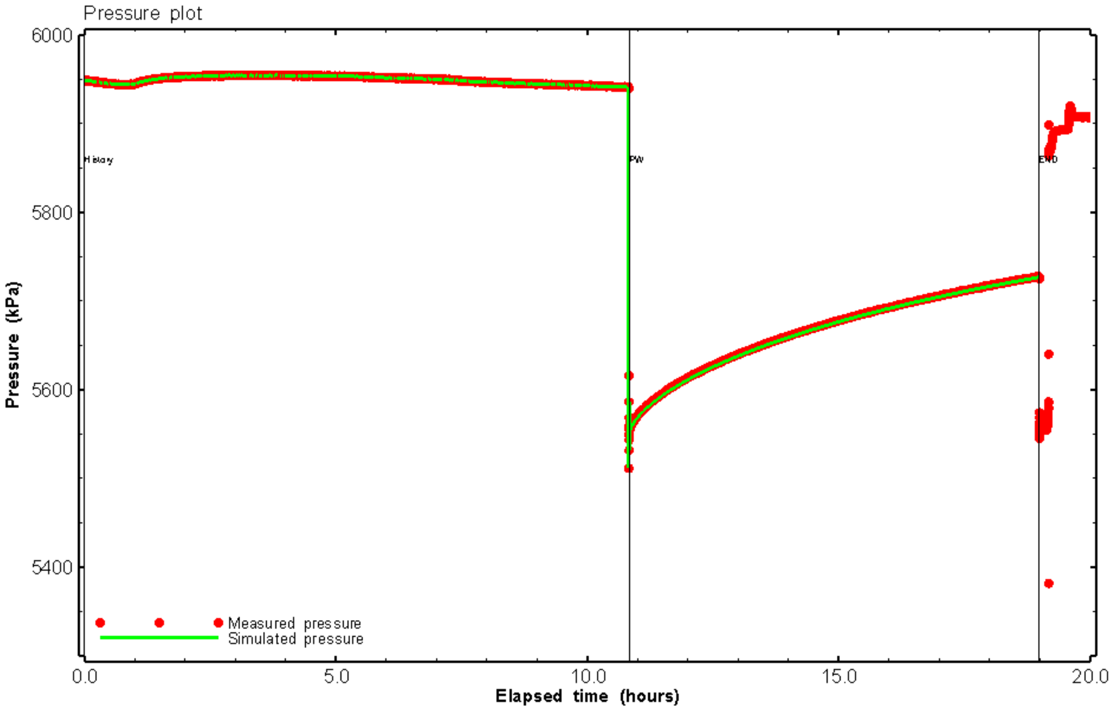

Figure 159: HT015 Pressure plot showing best-fit simulation and best fit results

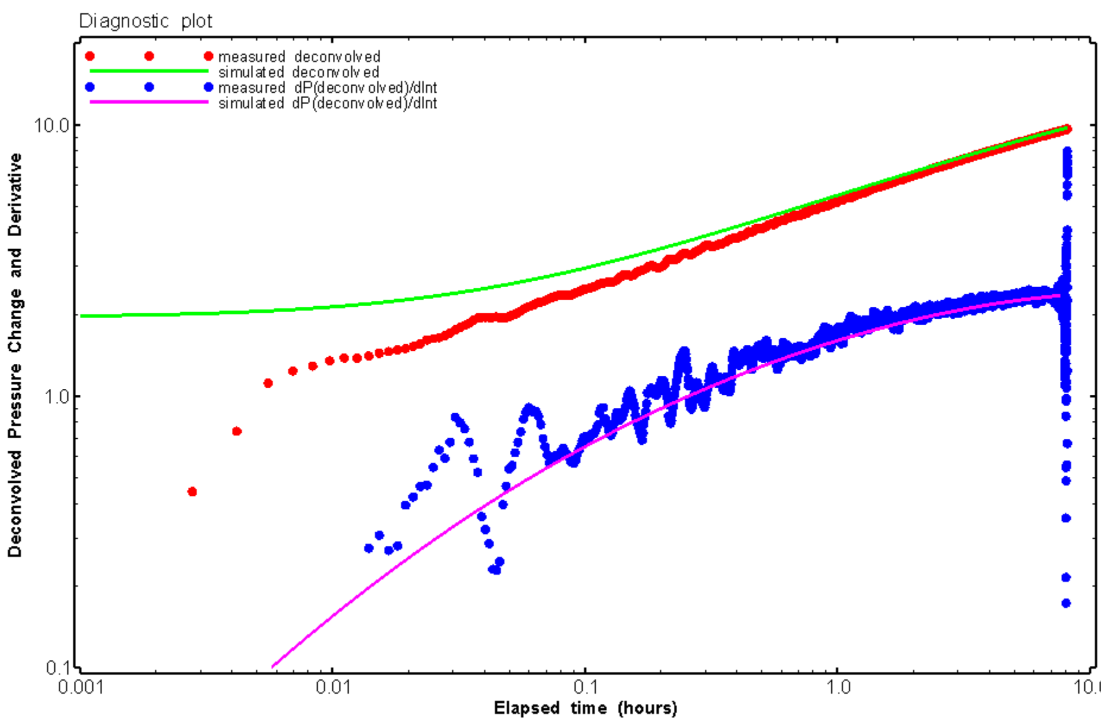

Figure 160: HT015 Deconvolved pressure change and derivative plot of the PW sequence showing best-fit simulation

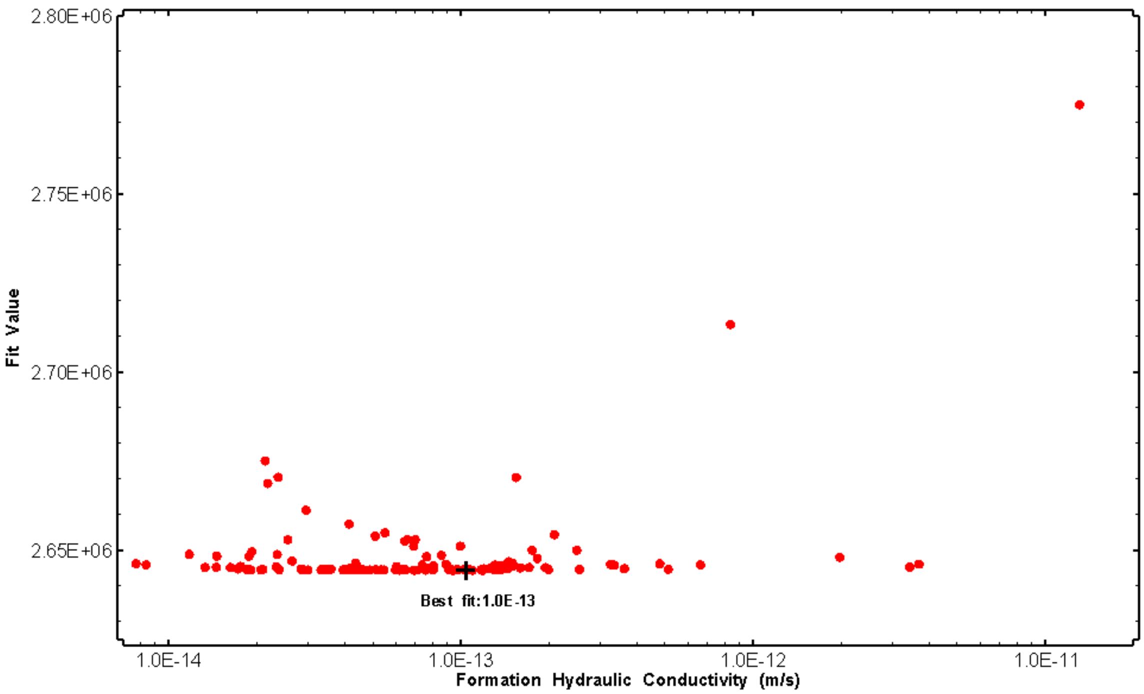

Figure 161: HT015 XY-scatter plot of formation hydraulic conductivity vs. fit value

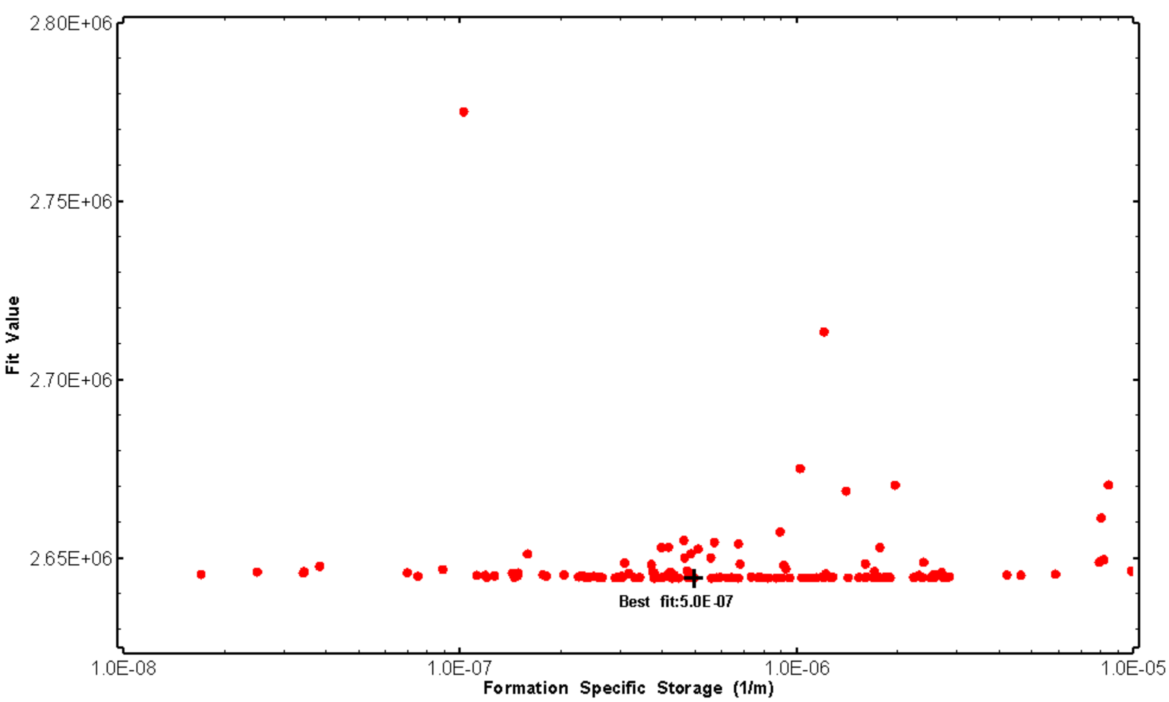

Figure 162: HT015 XY-scatter plot of formation specific storage vs. fit value

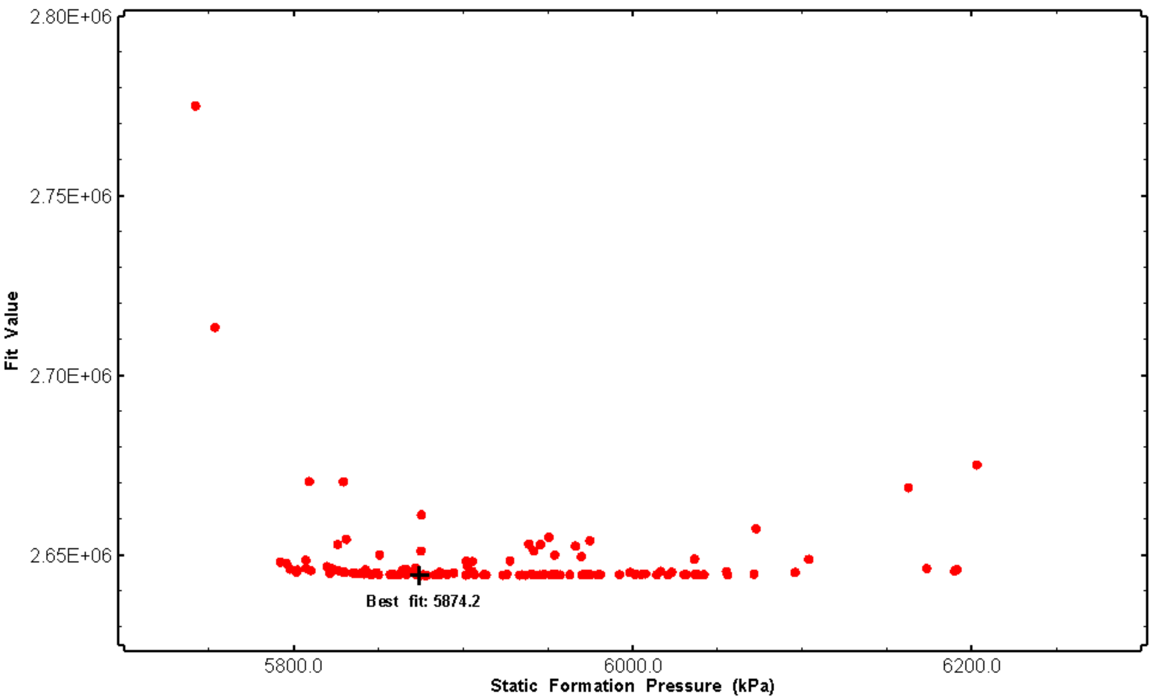

Figure 163: HT015 XY-scatter plot of static formation pressure vs. fit value

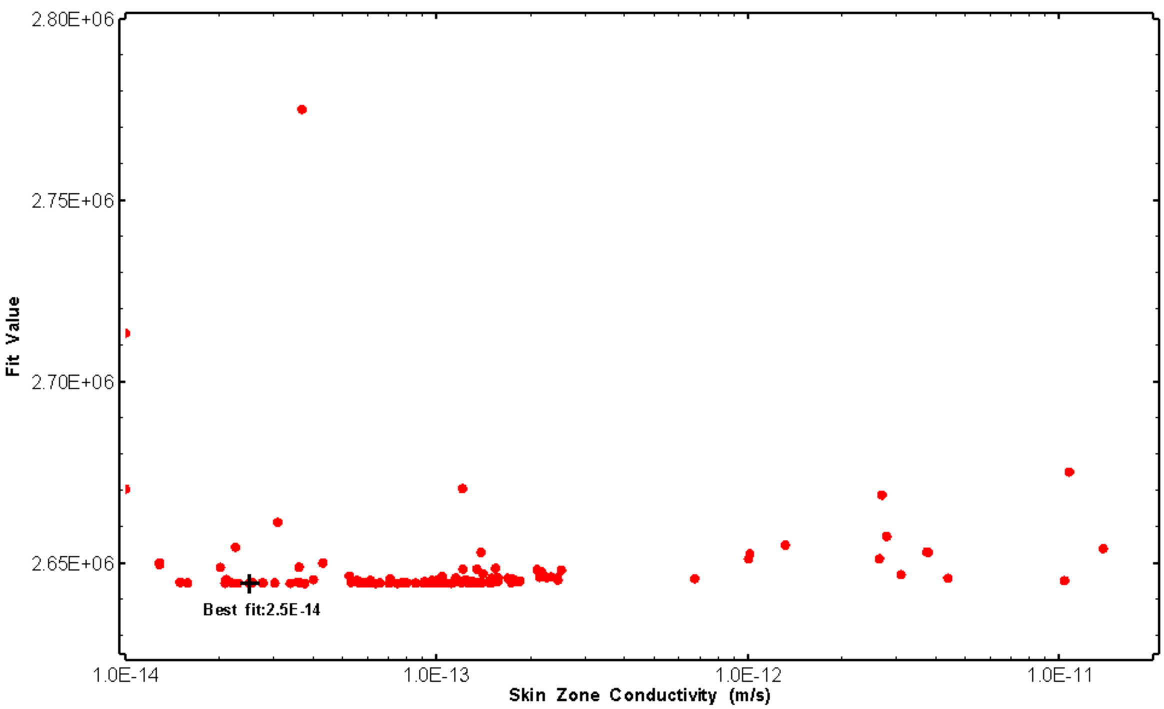

Figure 164: HT015 XY-scatter plot of skin zone conductivity vs. fit value

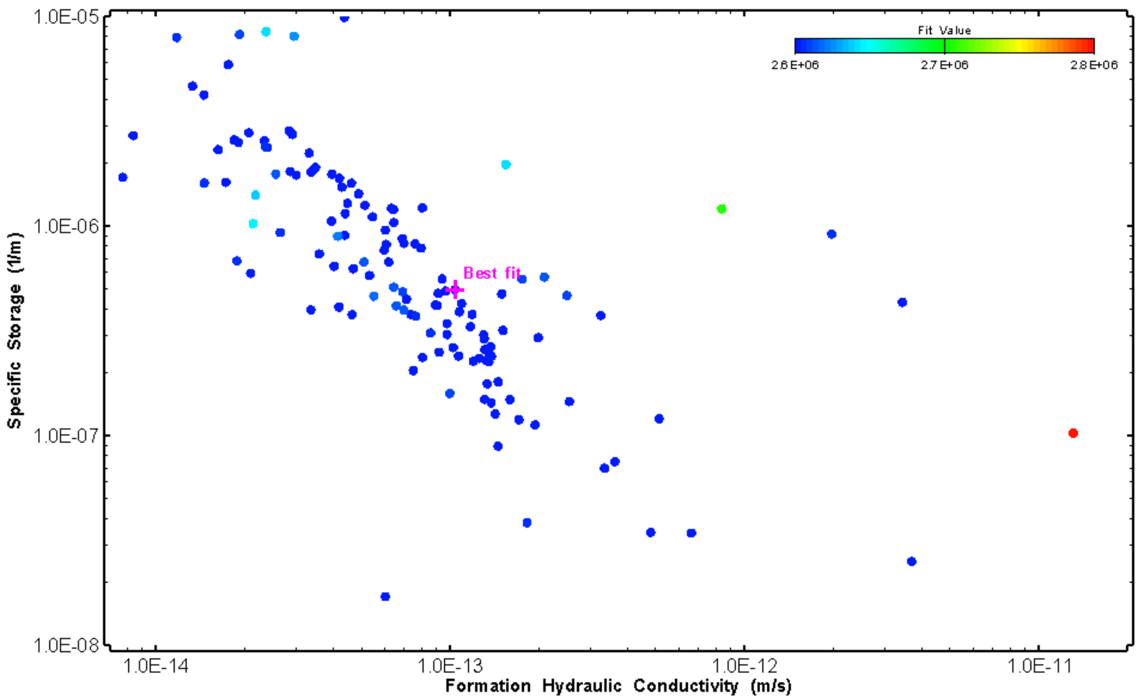

Figure 165: HT015 XY-scatter plot showing estimates of formation hydraulic conductivity and specific storage from perturbation analysis

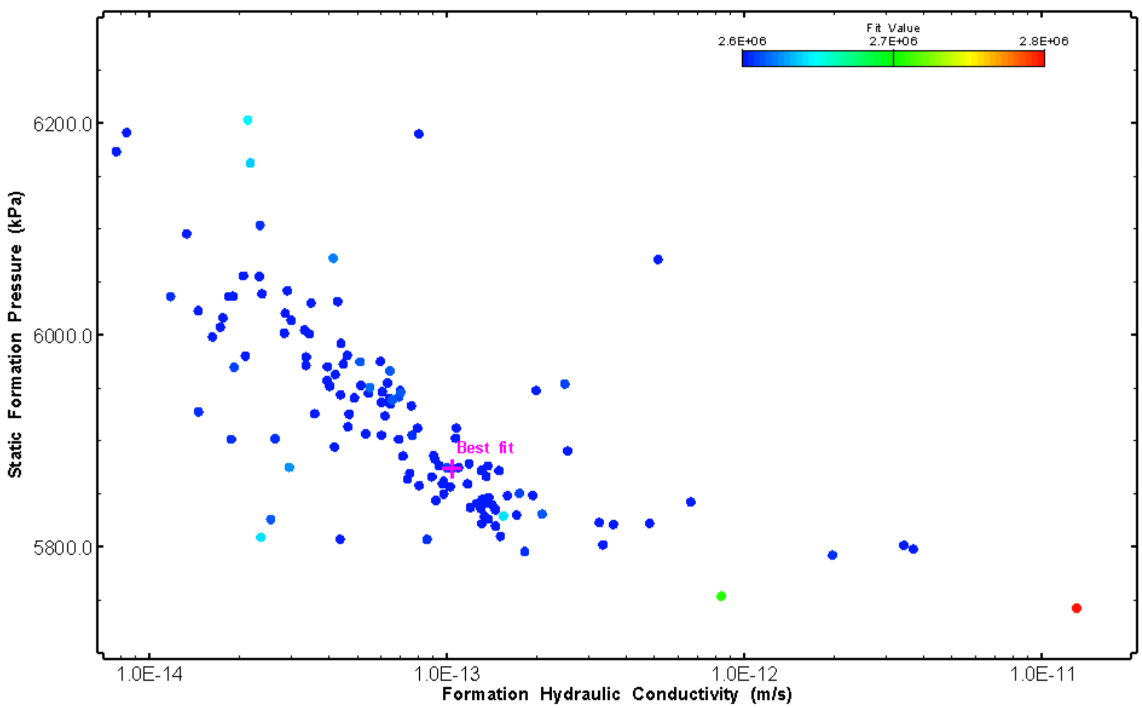

Figure 166: HT015 XY-scatter plot showing estimates of formation hydraulic conductivity and static formation pressure from perturbation analysis

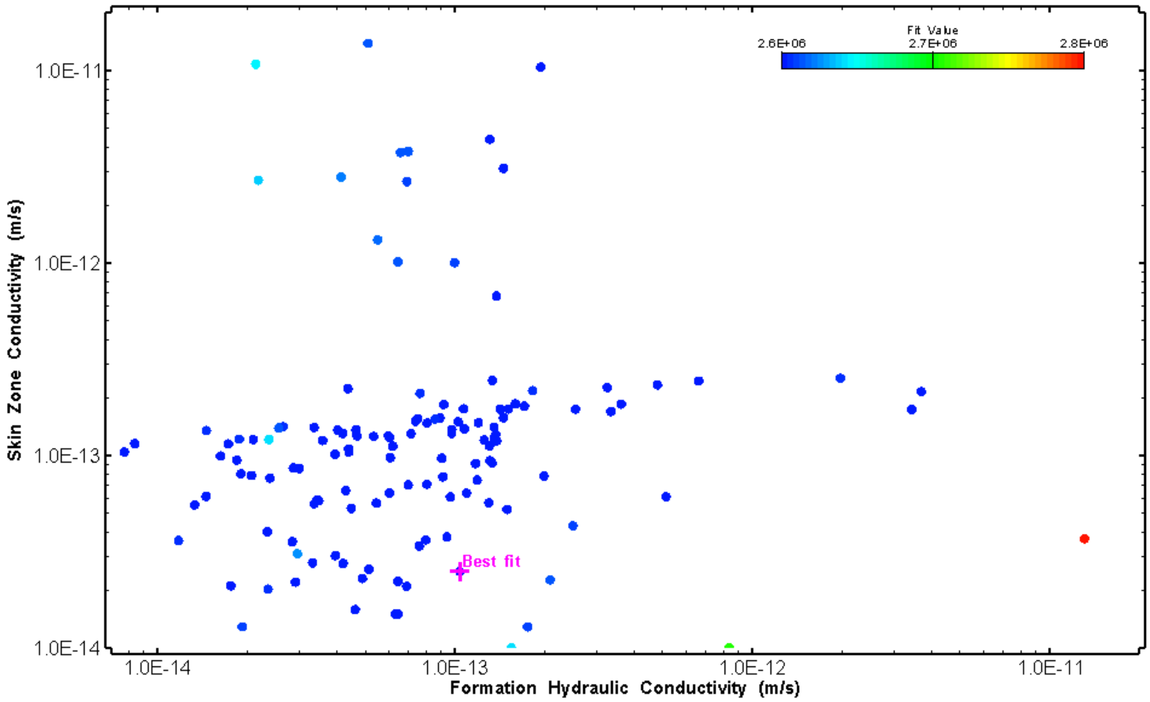

Figure 167: HT015 XY-scatter plot showing estimates of formation hydraulic conductivity and skin zone conductivity from perturbation analysis

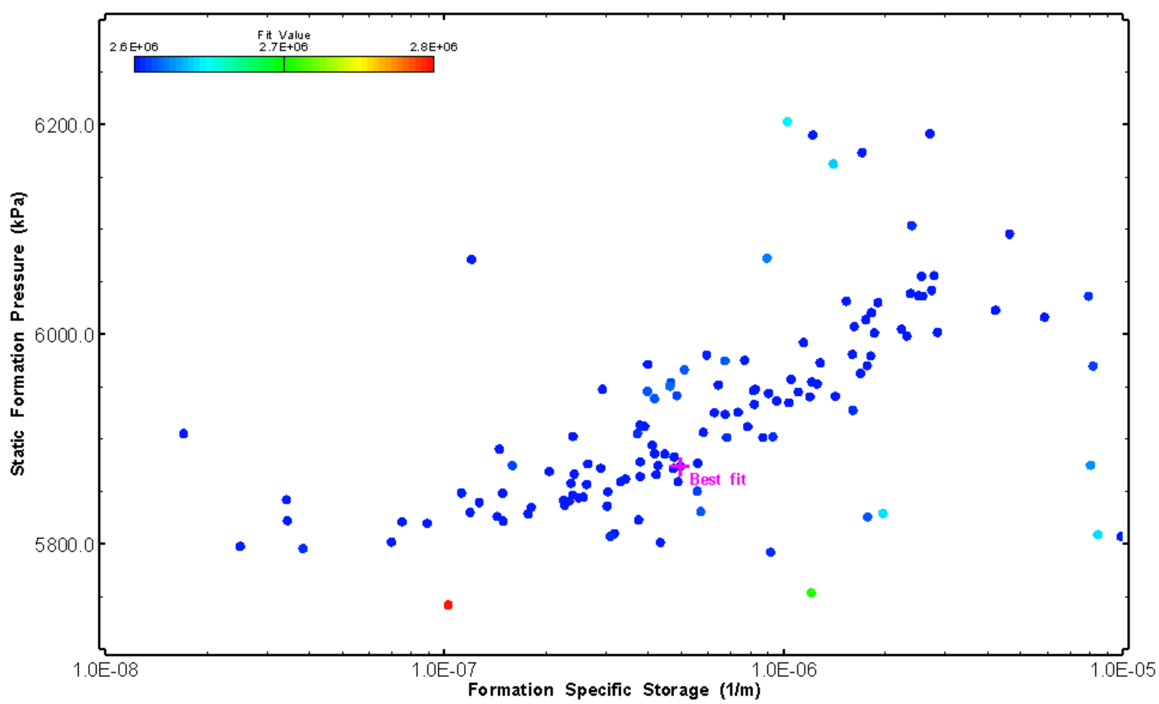

Figure 168: HT015 XY-scatter plot showing estimates of specific storage and static formation pressure from perturbation analysis

15.0 HT016 (683.64 – 703.67 M)

HT016 was selected to obtain continuous testing coverage from 600 to 800 m along hole. One broken fracture was observed in the core. No drill fluid parameter triggers were reached during drilling. A slight indication of flow was recorded during FFEC logging post-drilling.

The test was initiated with a shut-in pressure recovery phase (PSR). A pulse withdrawal test (PW) with a shut-in recovery was completed after the PSR phase.

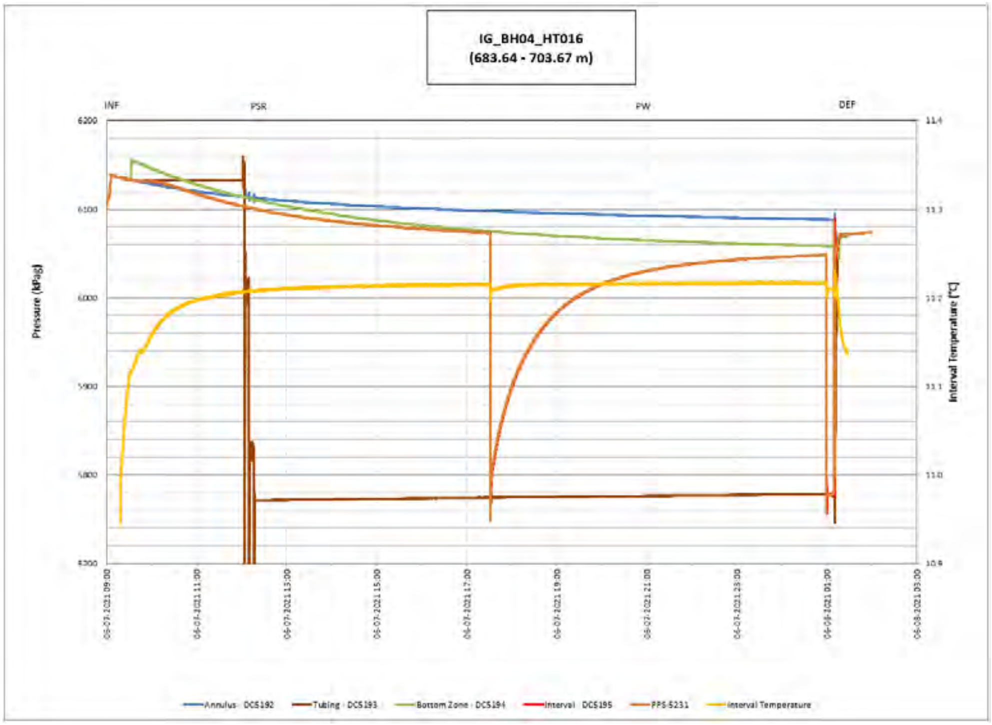

Figure 169: HT016 Annotated test plot showing monitored zone pressure and interval temperature.

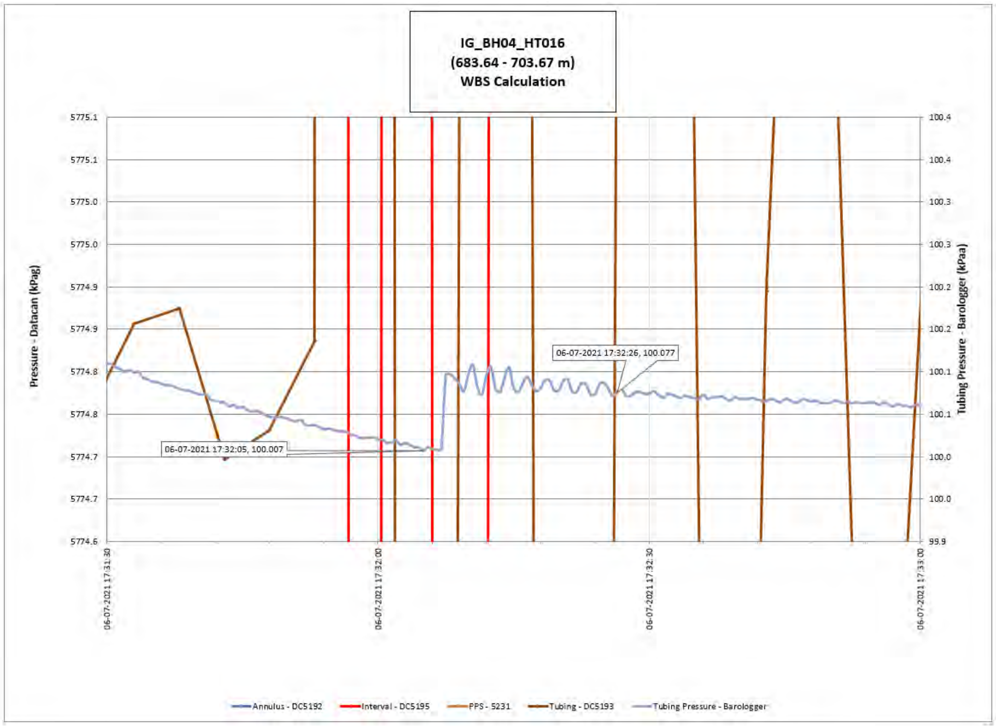

Figure 170: HT016 Tubing pressure during DHSIV activation. DHSIV Closed Wellbore Storage Estimate = 4E-11 m^3/Pa

Table 15: Summary of Analysis Results – HT016

	Formation conductivity	Skin zone conductivity	Static formation pressure	Formation specific storage	Radial thickness of skin	Flow dimension
	[m/s]	[m/s]	[kPa]	[1/m]	[m]	[–]
Best Fit	7.0E-12	1.9E-13	6060	2.0E-07	5.9E-03	1.6
Minimum	1.3E-13	8.9E-14	6048	1.0E-09	1.6E-04	1.0
Maximum	9.5E-11	3.6E-11	6065	9.9E-06	9.5E-01	3.0
Mean	6.5E-12	1.0E-12	6056	7.4E-07	7.9E-02	2.0
Median	3.2E-12	7.2E-13	6055	2.3E-07	2.5E-02	2.0
Geometric mean	3.5E-12	6.6E-13	6056	1.8E-07	2.7E-02	2.0

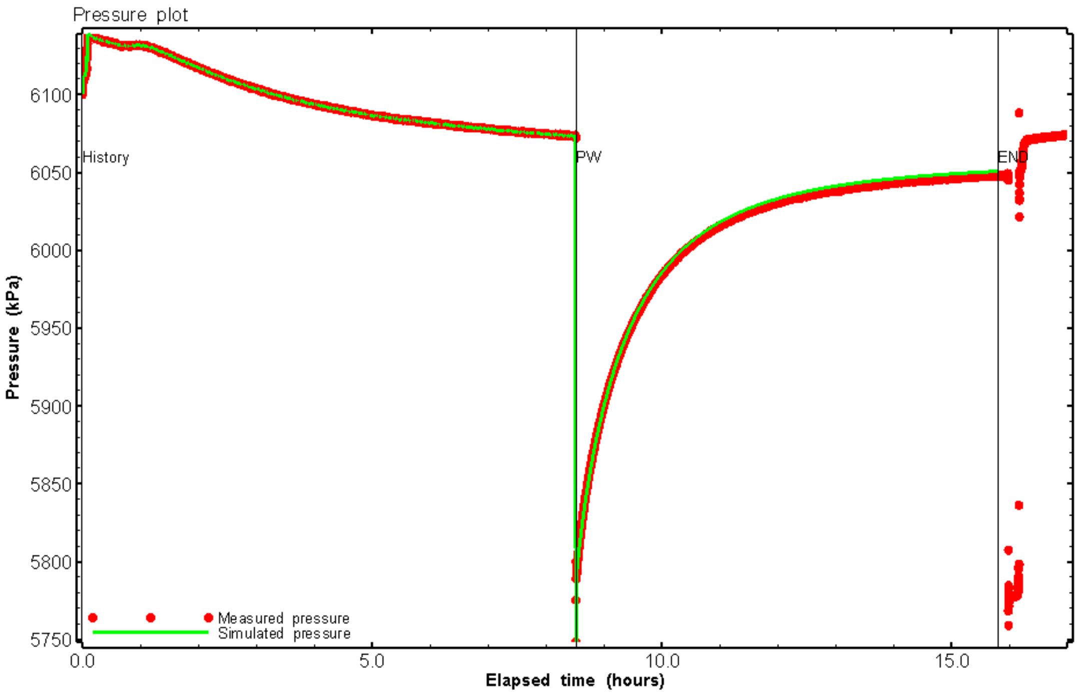

Figure 171: HT016 Pressure plot showing best-fit simulation and best fit results

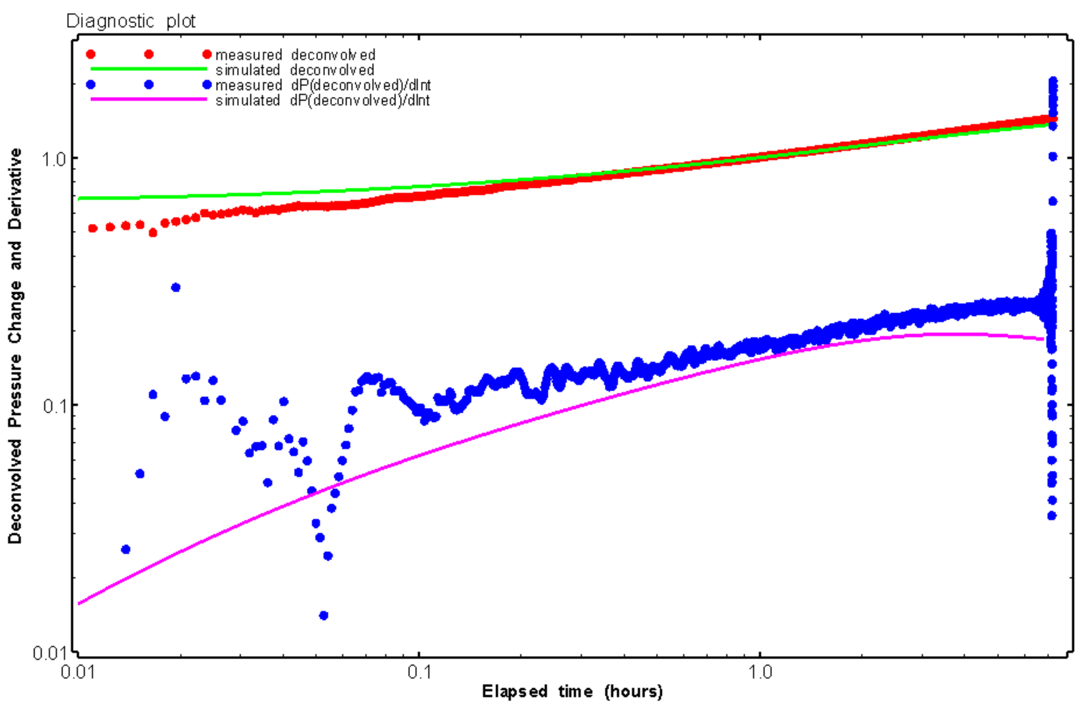

Figure 172: HT016 Deconvolved pressure change and derivative plot of the PW sequence showing best-fit simulation

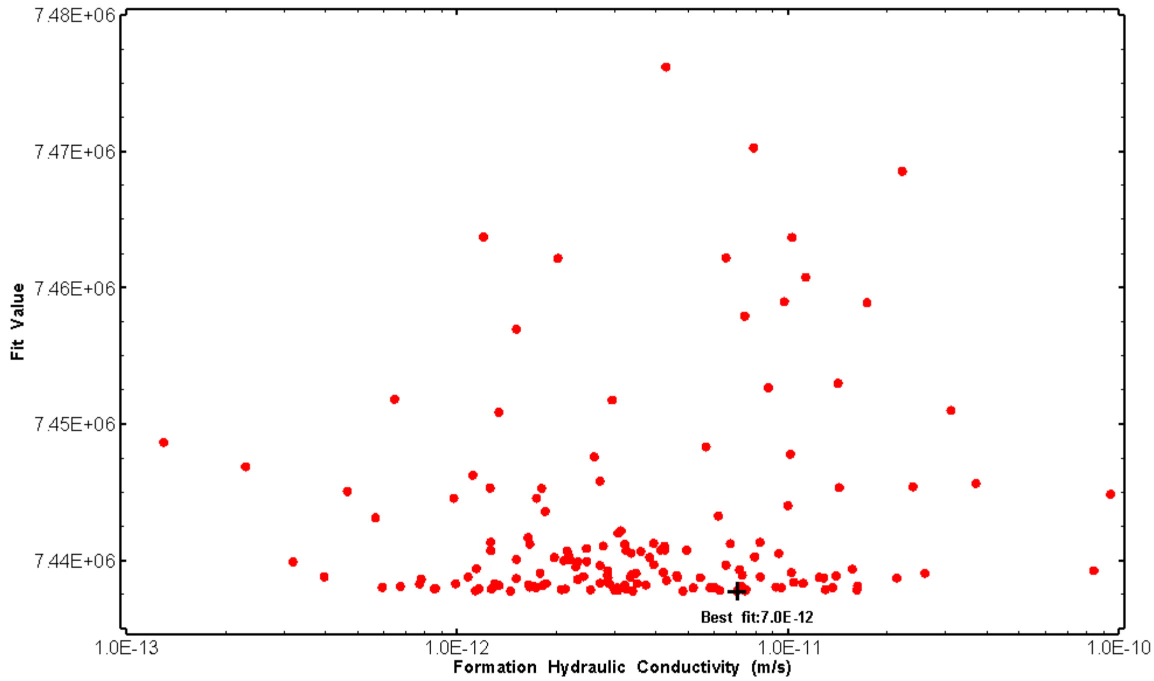

Figure 173: HT016 XY-scatter plot of formation hydraulic conductivity vs. fit value

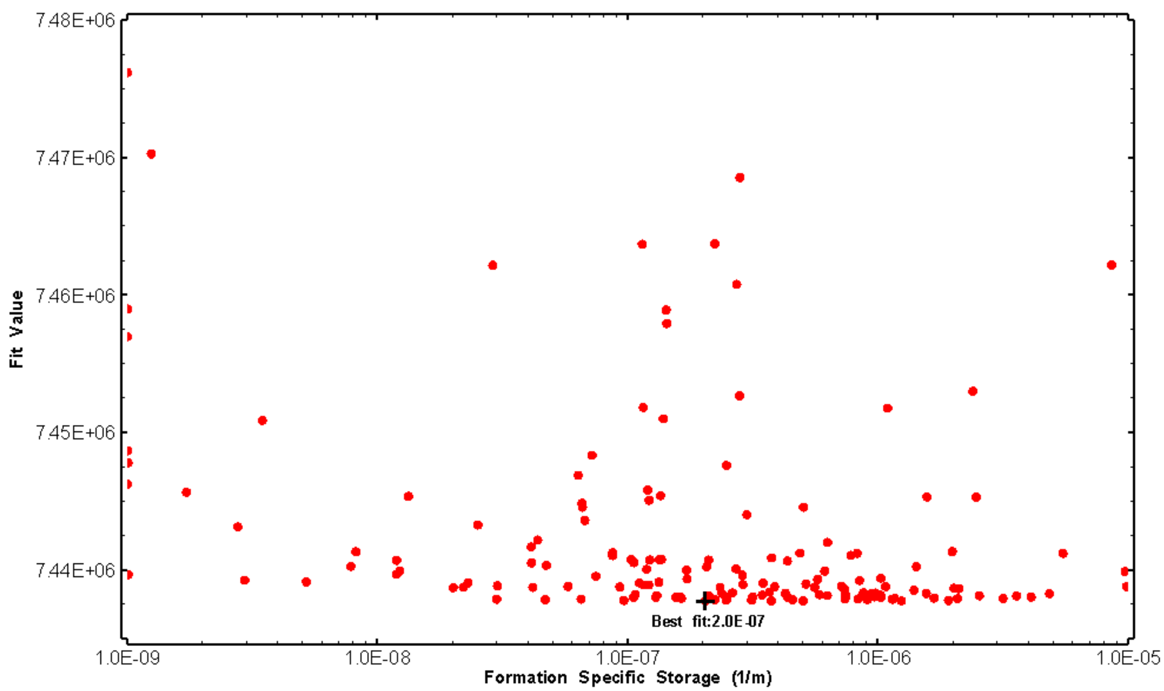

Figure 174: HT016 XY-scatter plot of formation specific storage vs. fit value

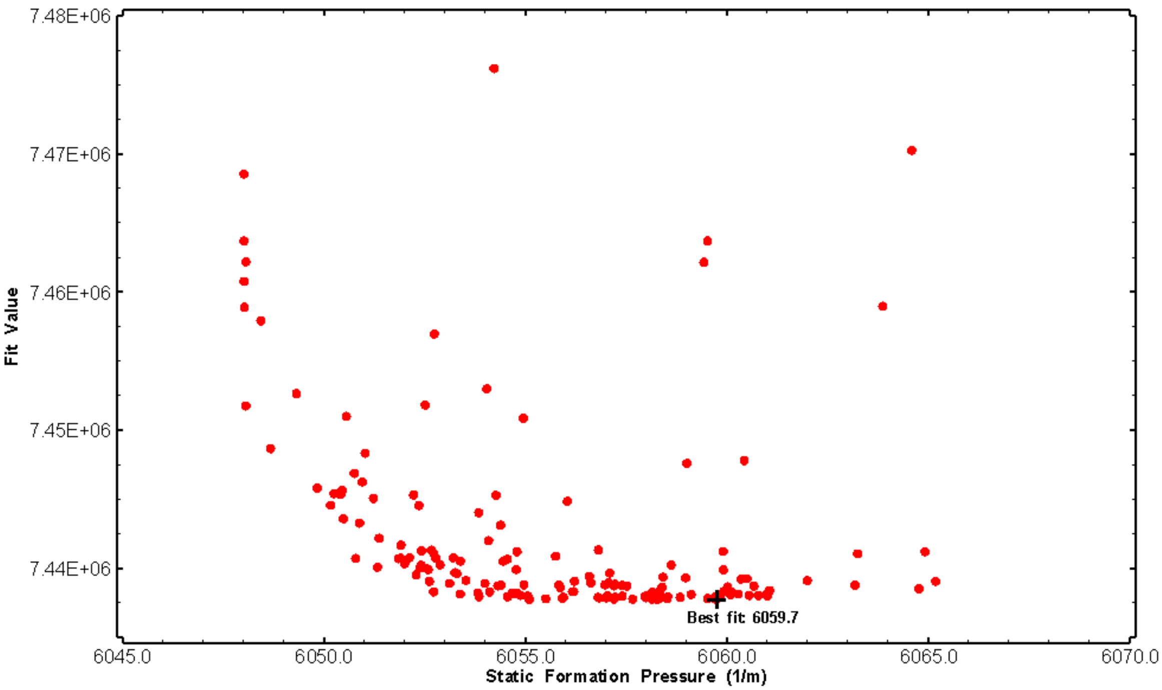

Figure 175: HT016 XY-scatter plot of static formation pressure vs. fit value

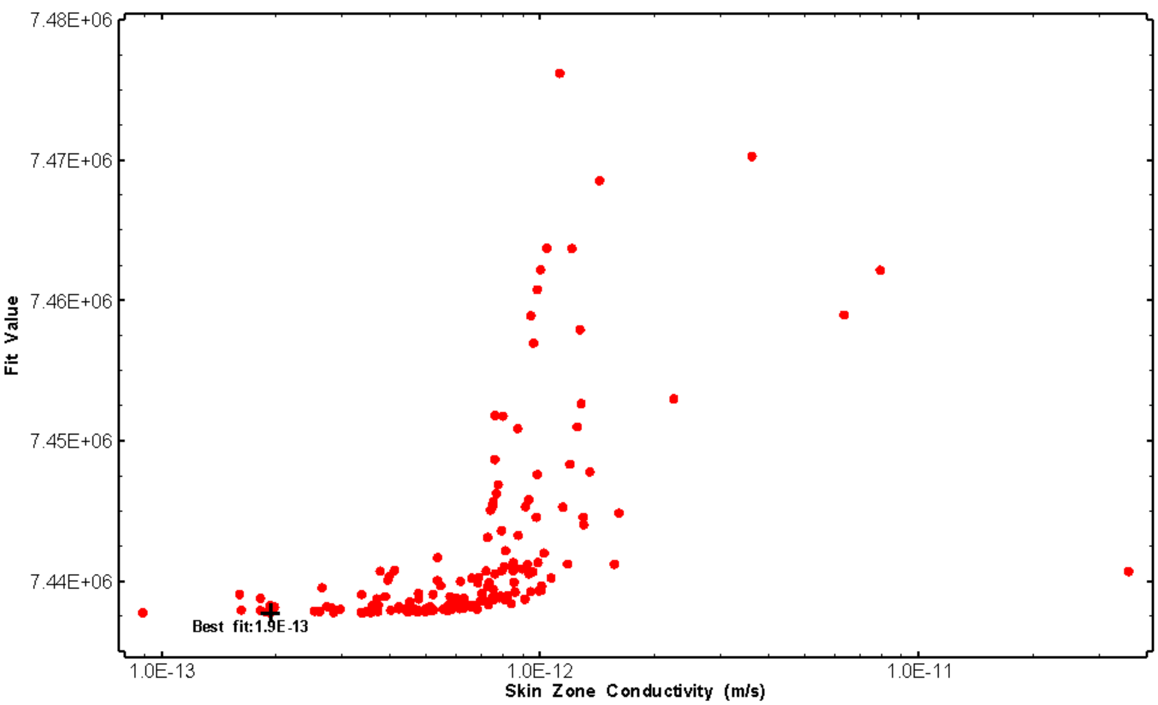

Figure 176: HT016 XY-scatter plot of skin zone conductivity vs. fit value

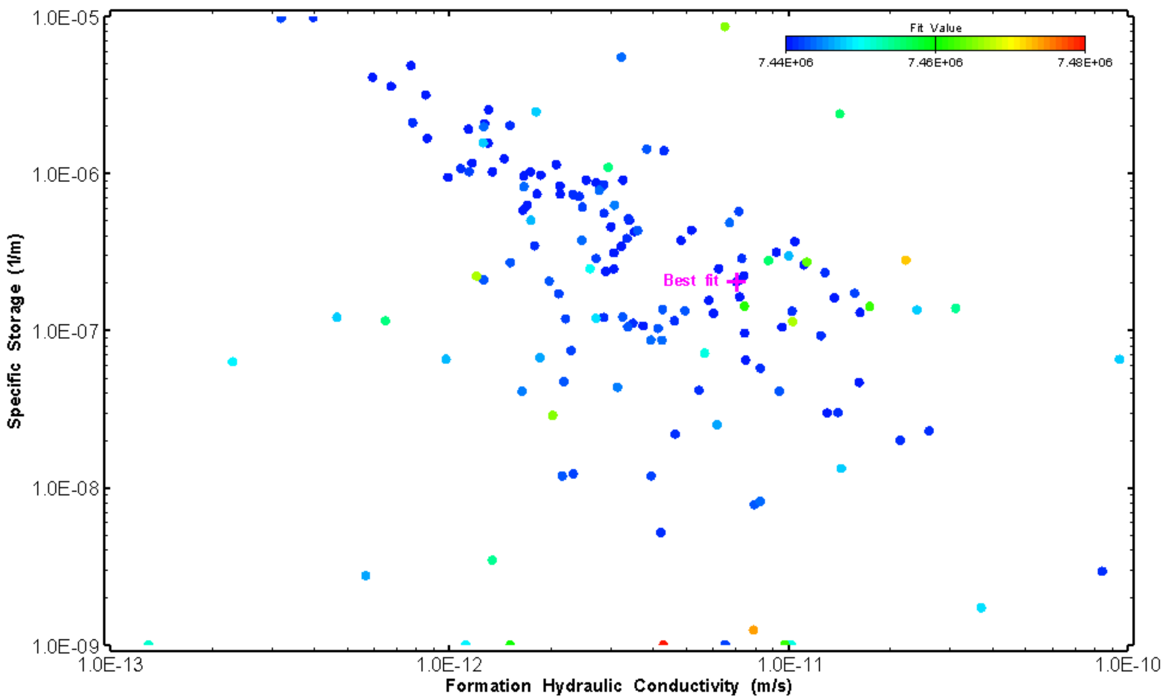

Figure 177: HT016 XY-scatter plot showing estimates of formation hydraulic conductivity and specific storage from perturbation analysis

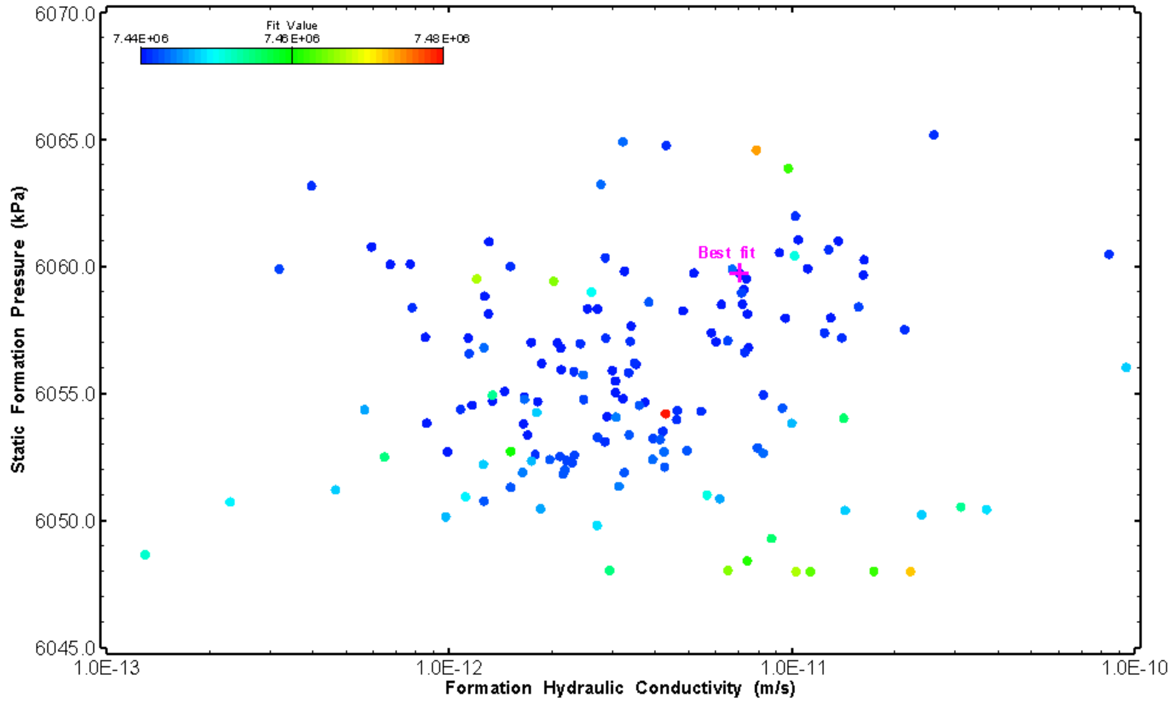

Figure 178: HT016 XY-scatter plot showing estimates of formation hydraulic conductivity and static formation pressure from perturbation analysis

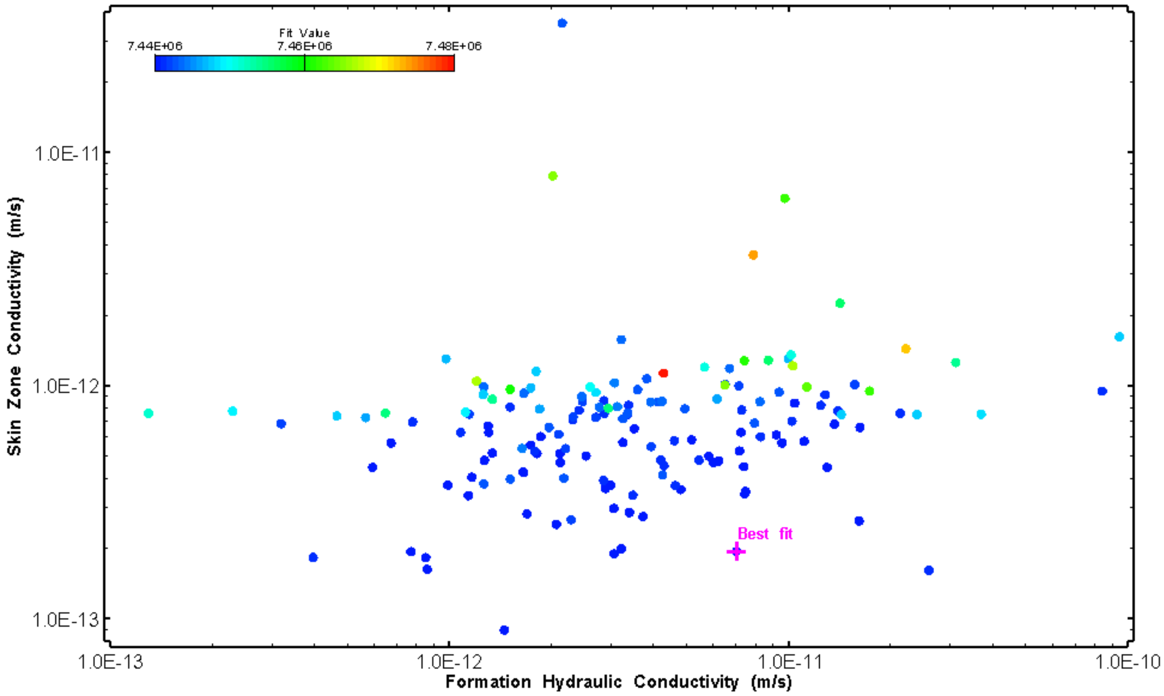

Figure 179: HT016 XY-scatter plot showing estimates of formation hydraulic conductivity and skin zone conductivity from perturbation analysis

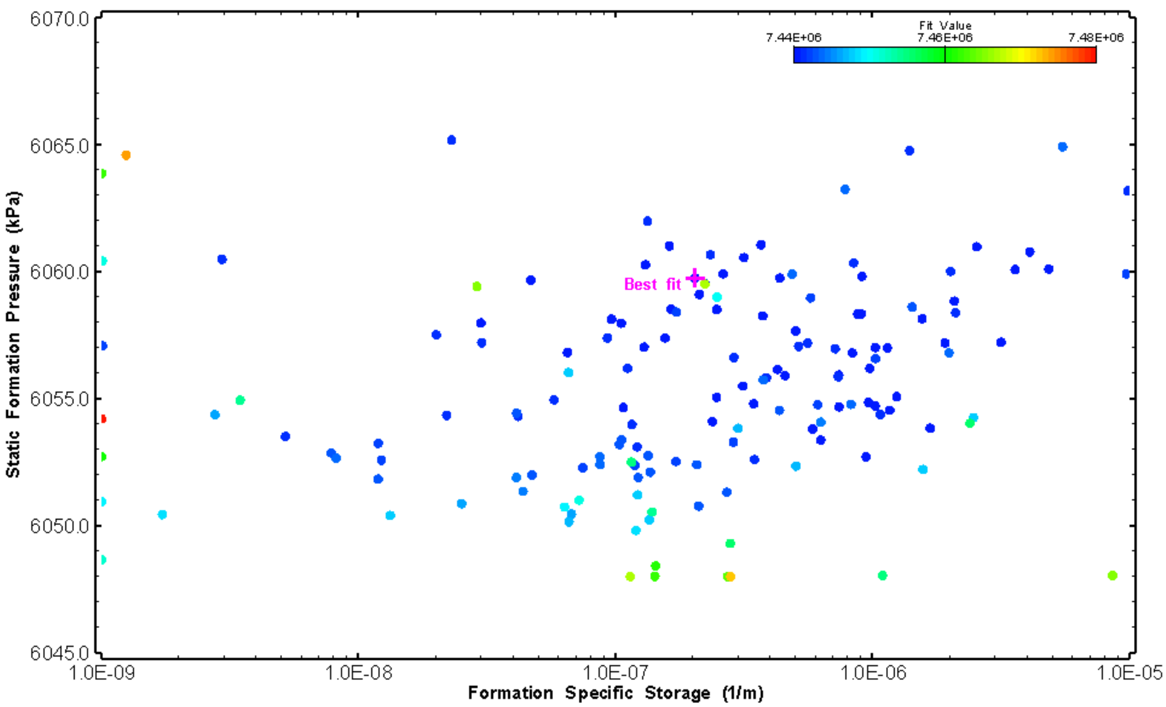

Figure 180: HT016 XY-scatter plot showing estimates of specific storage and static formation pressure from perturbation analysis

16.0 HT017 (699.50 – 719.53 M)

HT017 was selected to obtain continuous testing coverage from 600 to 800 m along hole. One broken fracture was observed in the core. No drill fluid parameter triggers were reached during drilling. A slight indication of flow was recorded during FFEC logging post-drilling.

The test was initiated with a shut-in pressure recovery phase (PSR). A pulse withdrawal test (PW) with a shut-in recovery was completed after the PSR phase.

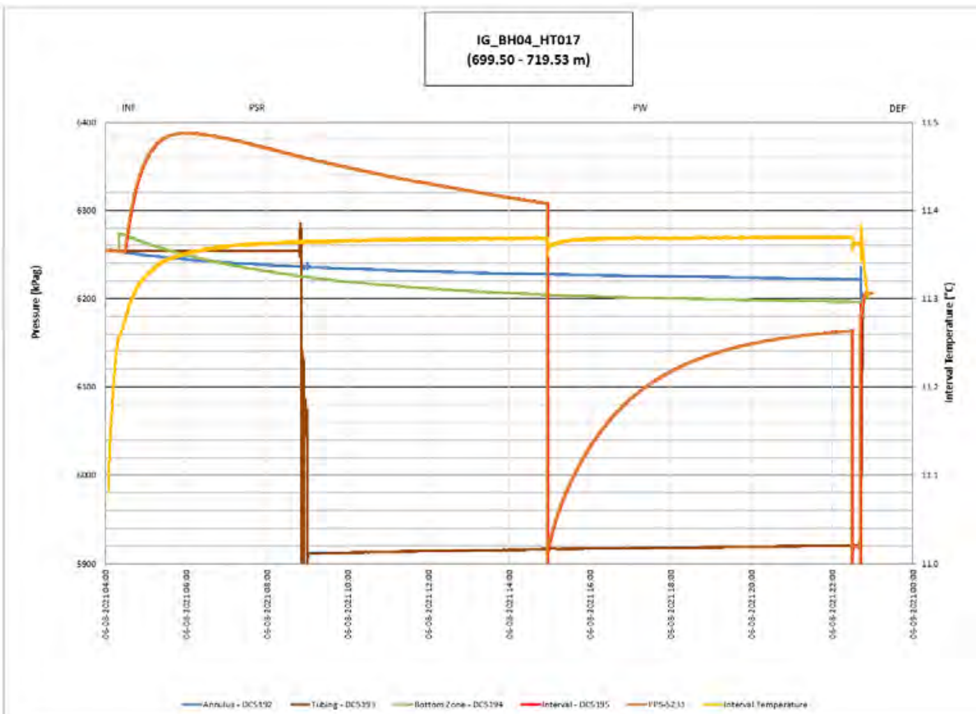

Figure 181: HT017 Annotated test plot showing monitored zone pressure and interval temperature.

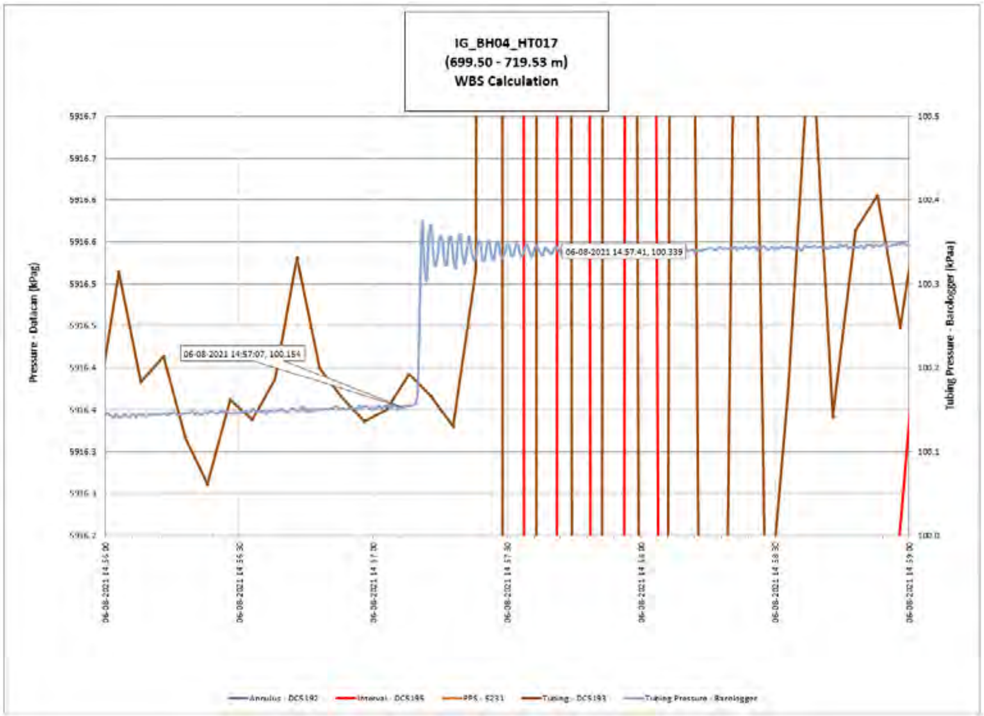

Figure 182: HT017 Tubing pressure during DHSIV activation. DHSIV Closed Wellbore Storage Estimate = 8E-11 m^3/Pa

Table 16: Summary of Analysis Results – HT017

	Formation conductivity	Skin zone conductivity	Static formation pressure	Formation specific storage	Radial thickness of skin	Flow dimension
	[m/s]	[m/s]	[kPa]	[1/m]	[m]	[–]
Best Fit	9.5E-13	4.4E-13	6173	1.2E-06	2.6E-02	3.0
Minimum	1.0E-15	9.4E-14	6163	1.0E-09	1.1E-04	1.2
Maximum	1.0E-10	8.9E-11	6310	1.0E-05	1.0E+00	3.0
Mean	3.8E-12	1.7E-12	6223	1.3E-06	1.9E-01	2.0
Median	8.5E-13	7.7E-13	6229	2.7E-07	7.7E-02	2.0
Geometric mean	6.3E-13	8.0E-13	6223	1.9E-07	8.0E-02	2.0

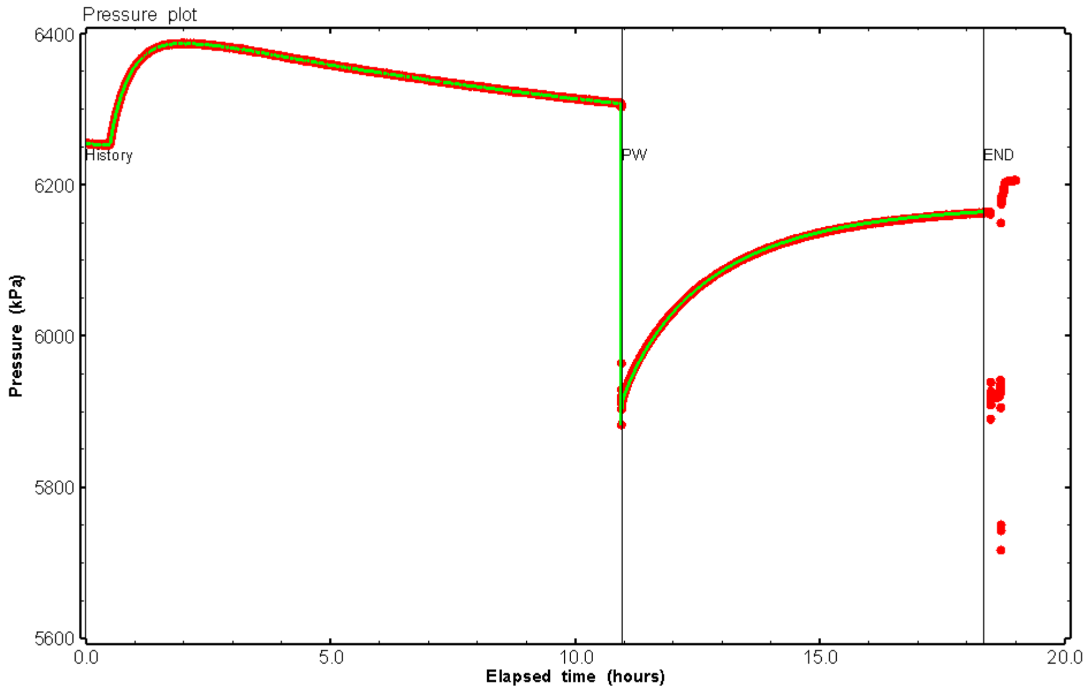

Figure 183: HT017 Pressure plot showing best-fit simulation and best fit results

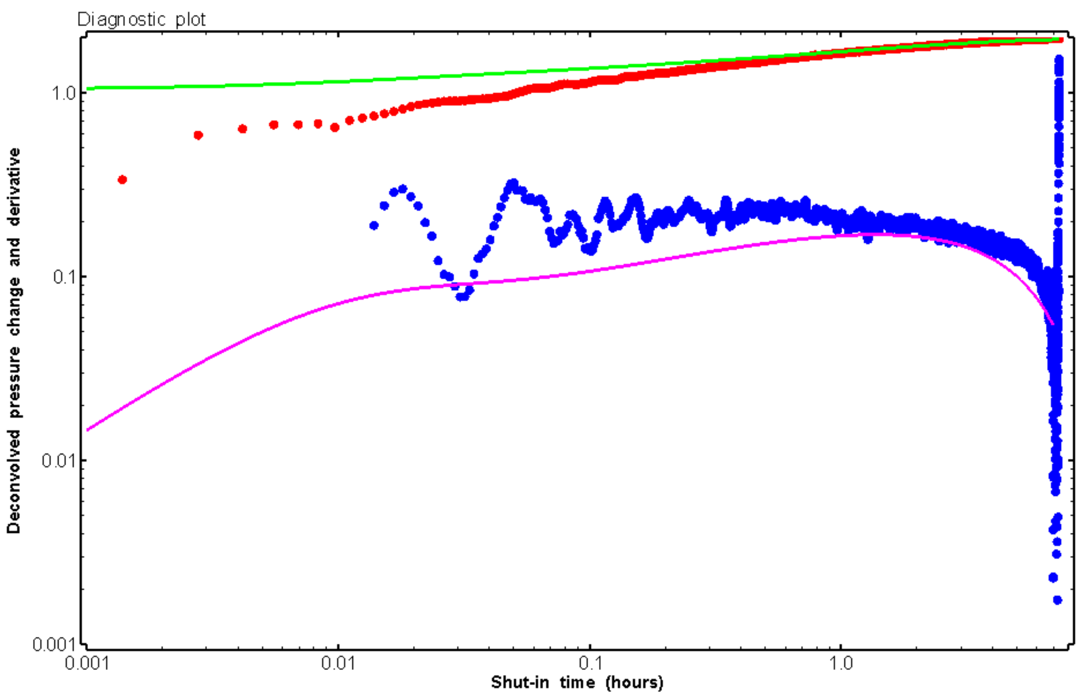

Figure 184: HT017 Deconvolved pressure change and derivative plot of the PW sequence showing best-fit simulation

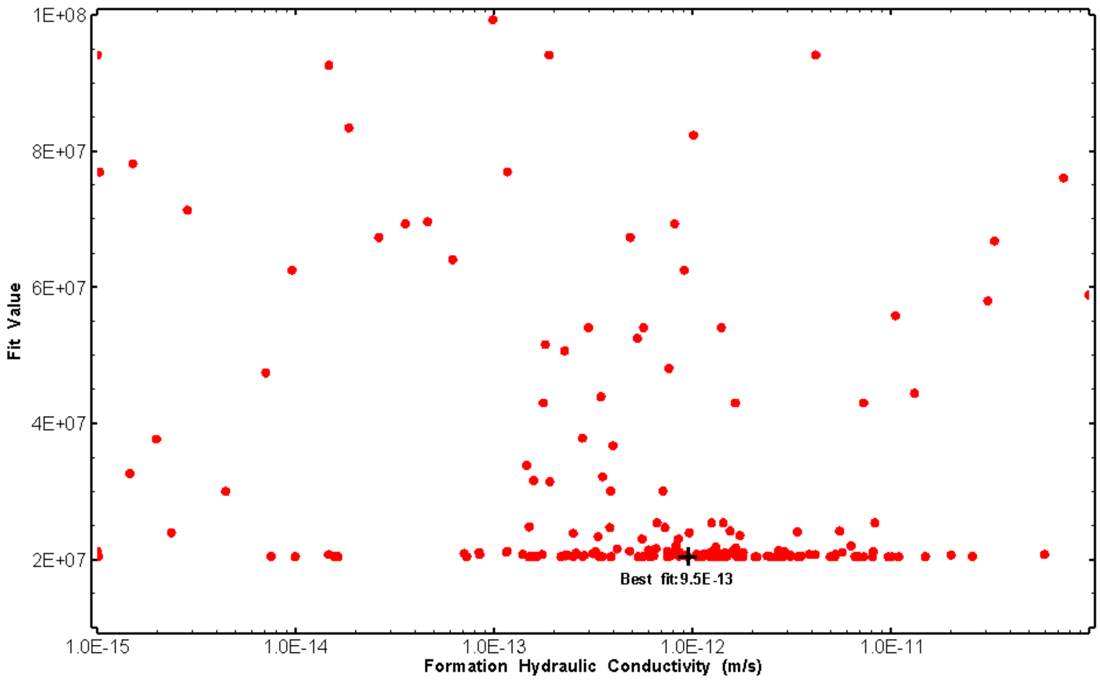

Figure 185: HT017 XY-scatter plot of formation hydraulic conductivity vs. fit value

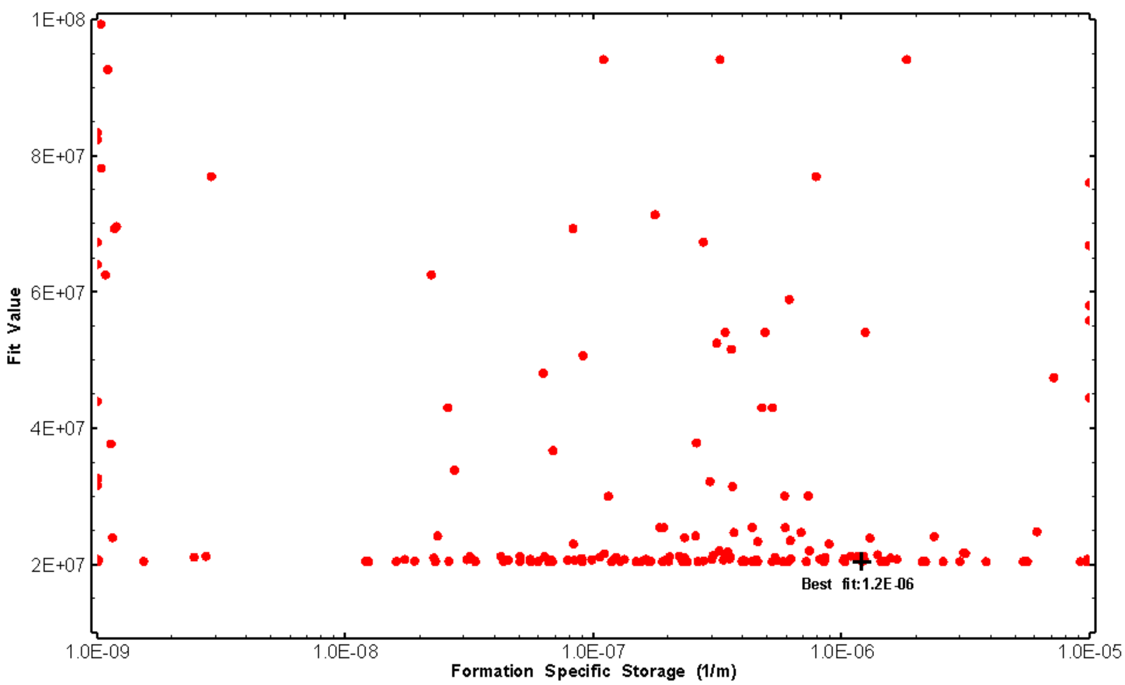

Figure 186: HT017 XY-scatter plot of formation specific storage vs. fit value

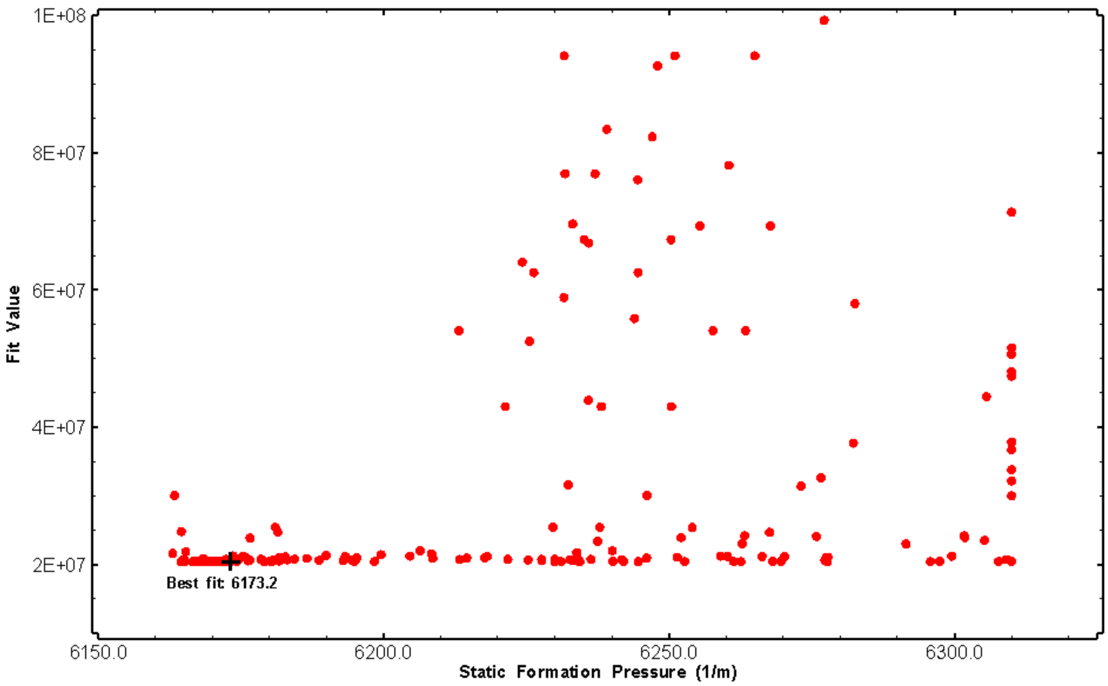

Figure 187: HT017 XY-scatter plot of static formation pressure vs. fit value

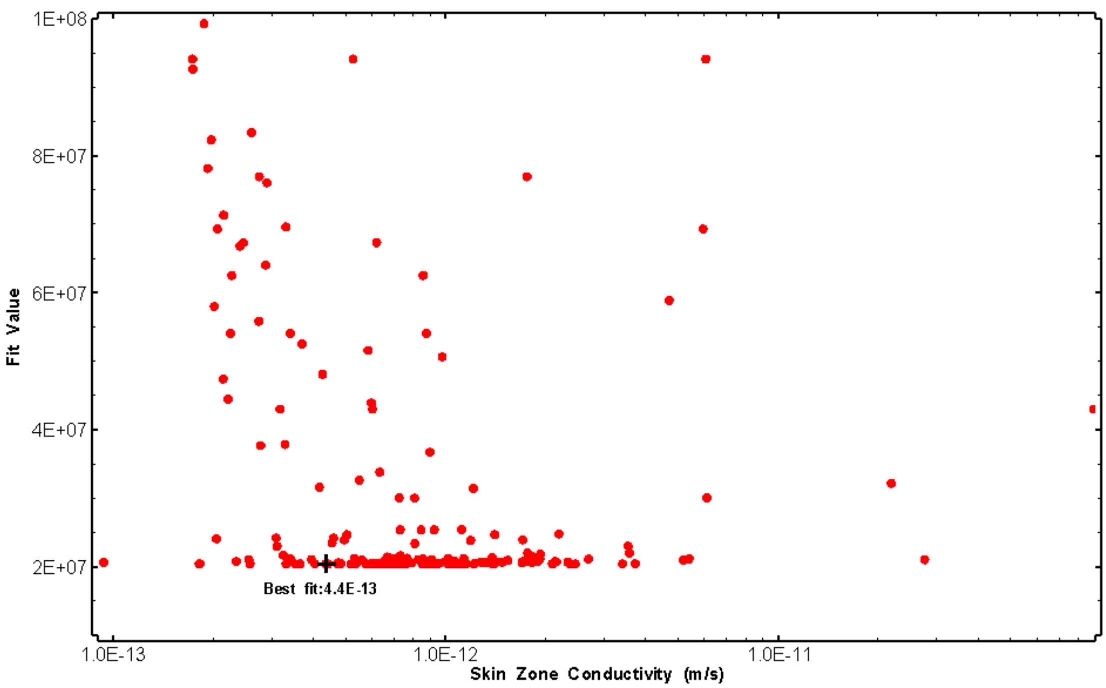

Figure 188: HT017 XY-scatter plot of skin zone conductivity vs. fit value

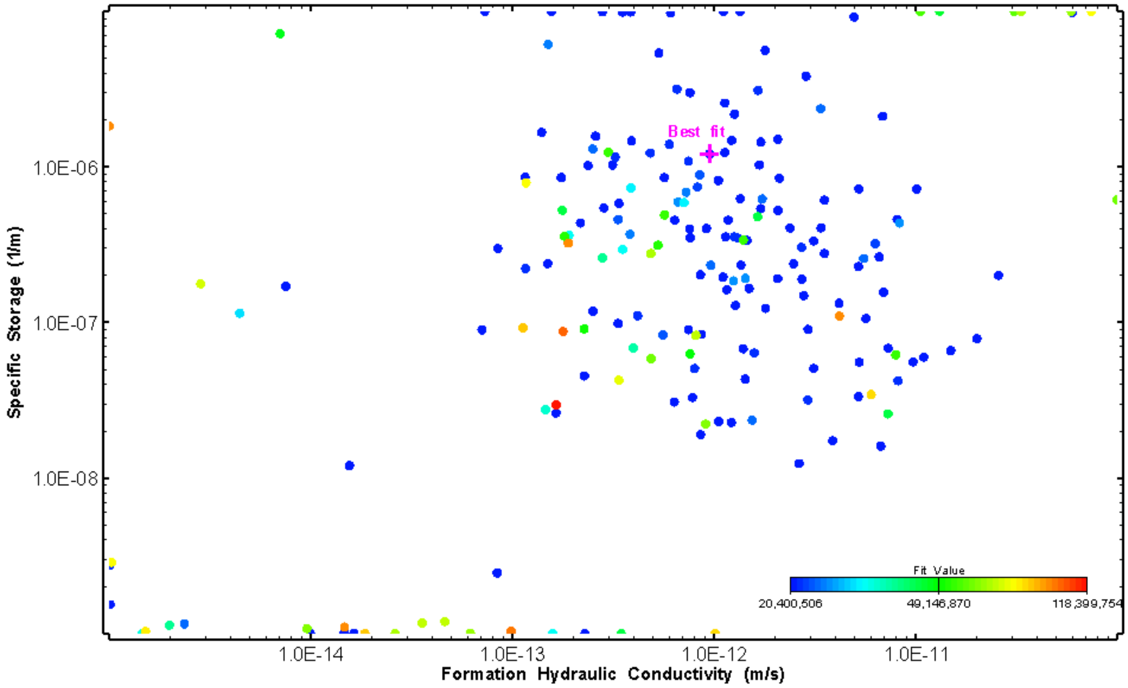

Figure 189: HT017 XY-scatter plot showing estimates of formation hydraulic conductivity and specific storage from perturbation analysis

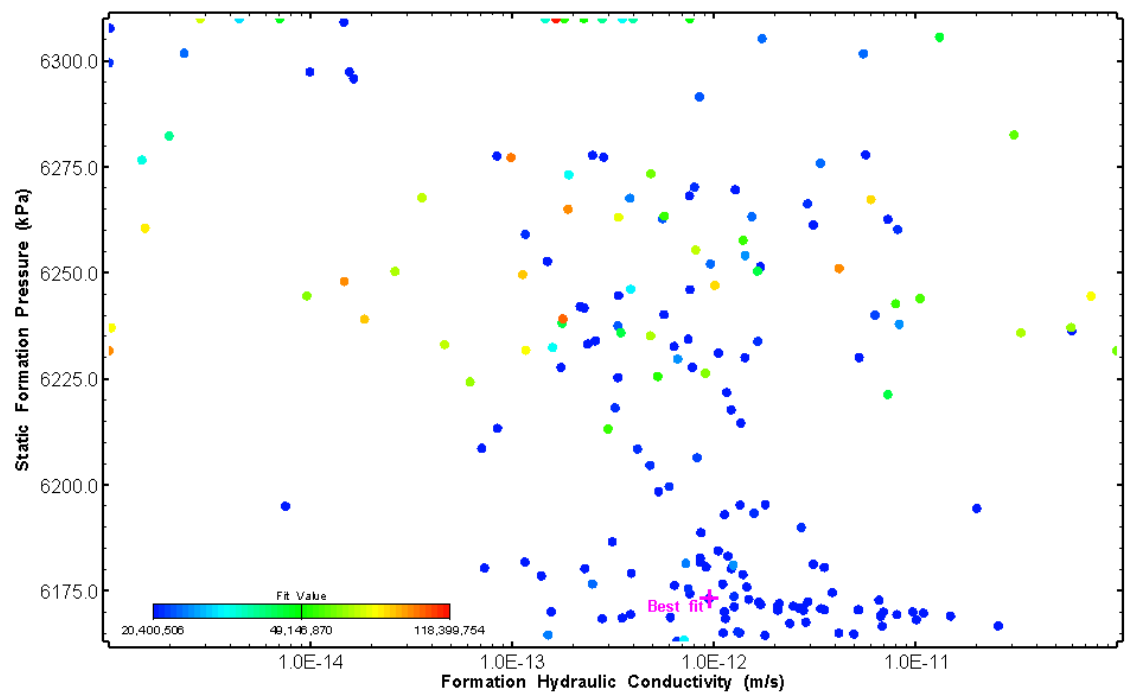

Figure 190: HT017 XY-scatter plot showing estimates of formation hydraulic conductivity and static formation pressure from perturbation analysis

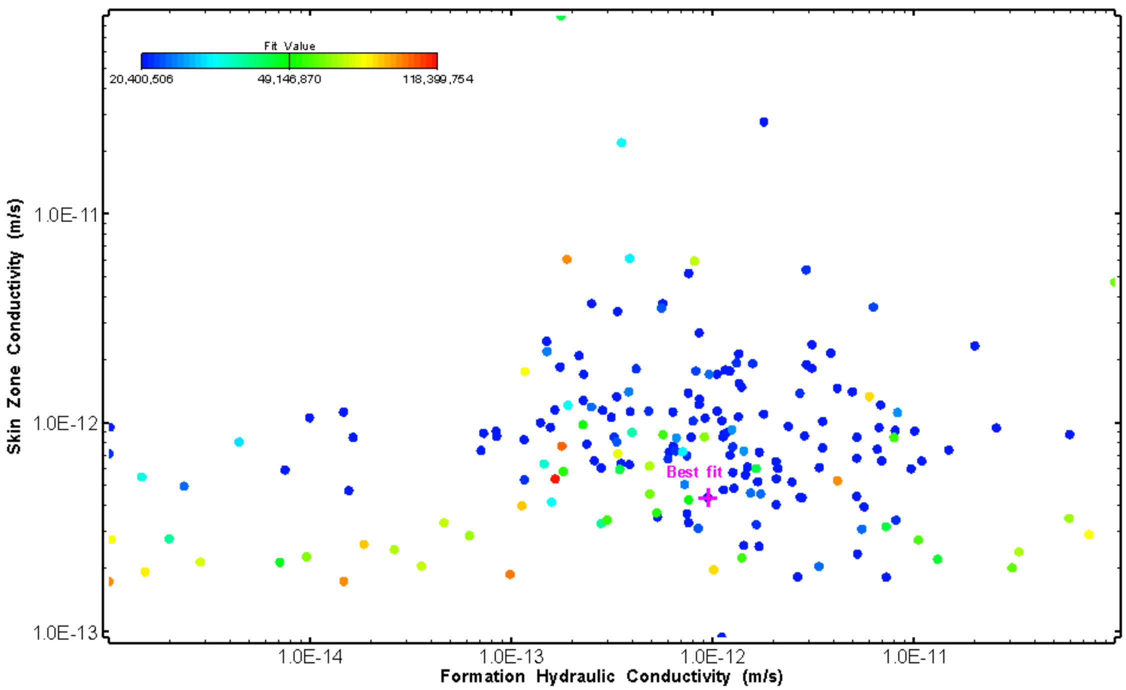

Figure 191: HT017 XY-scatter plot showing estimates of formation hydraulic conductivity and skin zone conductivity from perturbation analysis

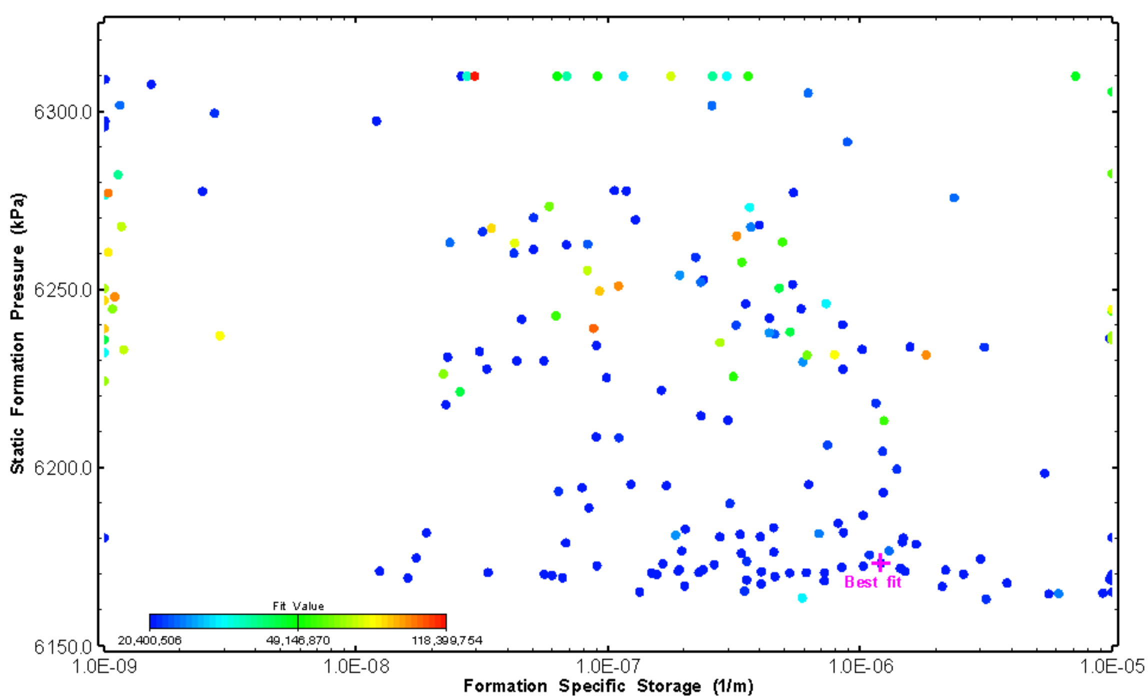

Figure 192: HT017 XY-scatter plot showing estimates of specific storage and static formation pressure from perturbation analysis

17.0 HT018 (715.00 – 735.03 M)

HT018 was selected to obtain continuous testing coverage from 600 to 800 m along hole. Three broken fractures were observed in the core. A loss of drilling fluid was observed in this interval during drilling. An indication of flow was recorded during FFEC logging post-drilling.

The test was initiated with a shut-in pressure recovery phase (PSR). A pulse withdrawal test (PW) with a shut-in recovery was completed after the PSR phase.

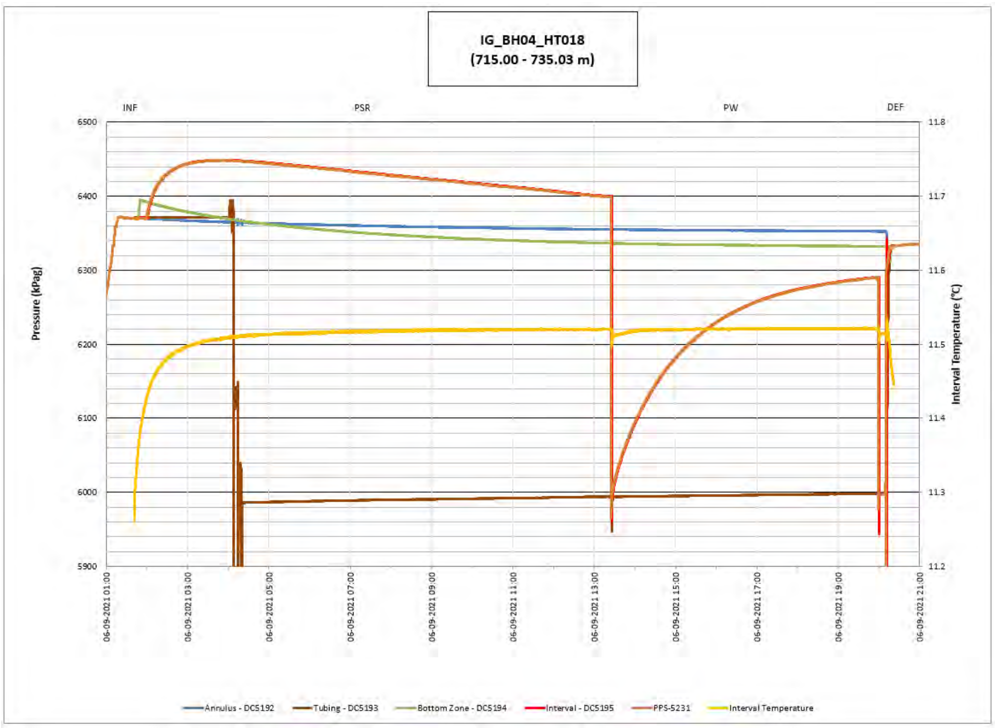

Figure 193: HT018 Annotated test plot showing monitored zone pressure and interval temperature.

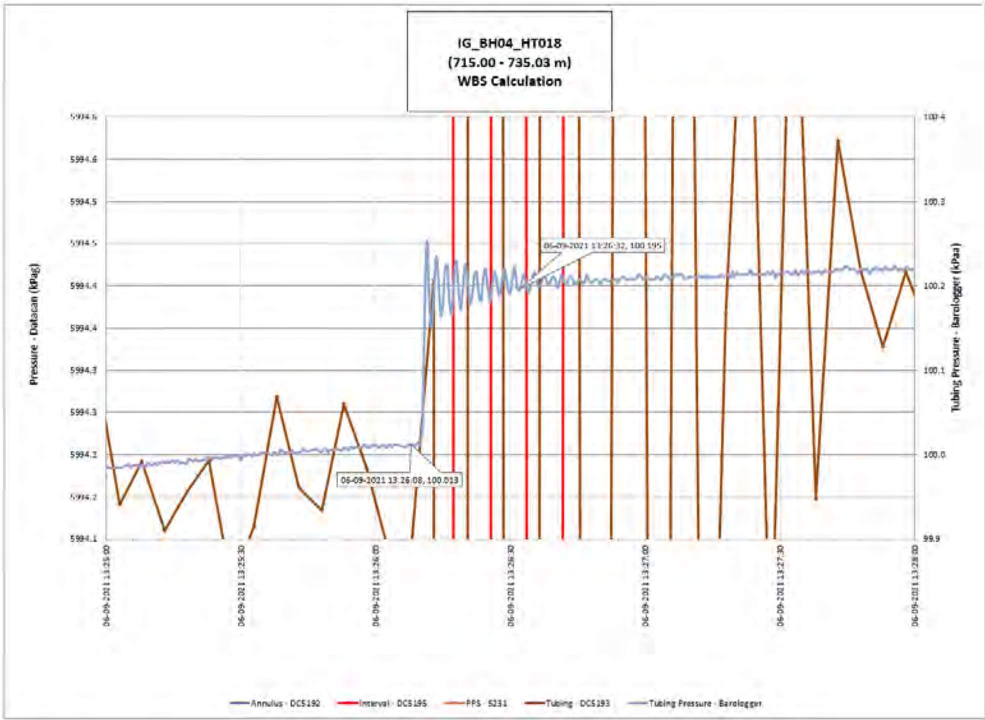

Figure 194: HT018 Tubing pressure during DHSIV activation. DHSIV Closed Wellbore Storage Estimate = 8E-11 m^3/Pa

Table 17: Summary of Analysis Results – HT018

	Formation conductivity	Skin zone conductivity	Static formation pressure	Formation specific storage	Radial thickness of skin	Flow dimension
	[m/s]	[m/s]	[kPa]	[1/m]	[m]	[–]
Best Fit	1.1E-12	3.5E-13	6303	1.6E-07	7.0E-03	3.0
Minimum	1.0E-15	1.4E-13	6293	1.0E-09	1.0E-03	1.5
Maximum	1.0E-10	6.0E-11	6400	1.0E-05	1.0E+00	3.0
Mean	5.4E-12	1.4E-12	6329	2.2E-06	1.5E-01	2.2
Median	2.1E-12	7.7E-13	6306	2.9E-07	6.1E-02	2.1
Geometric mean	1.2E-12	7.0E-13	6329	2.4E-07	6.9E-02	2.2

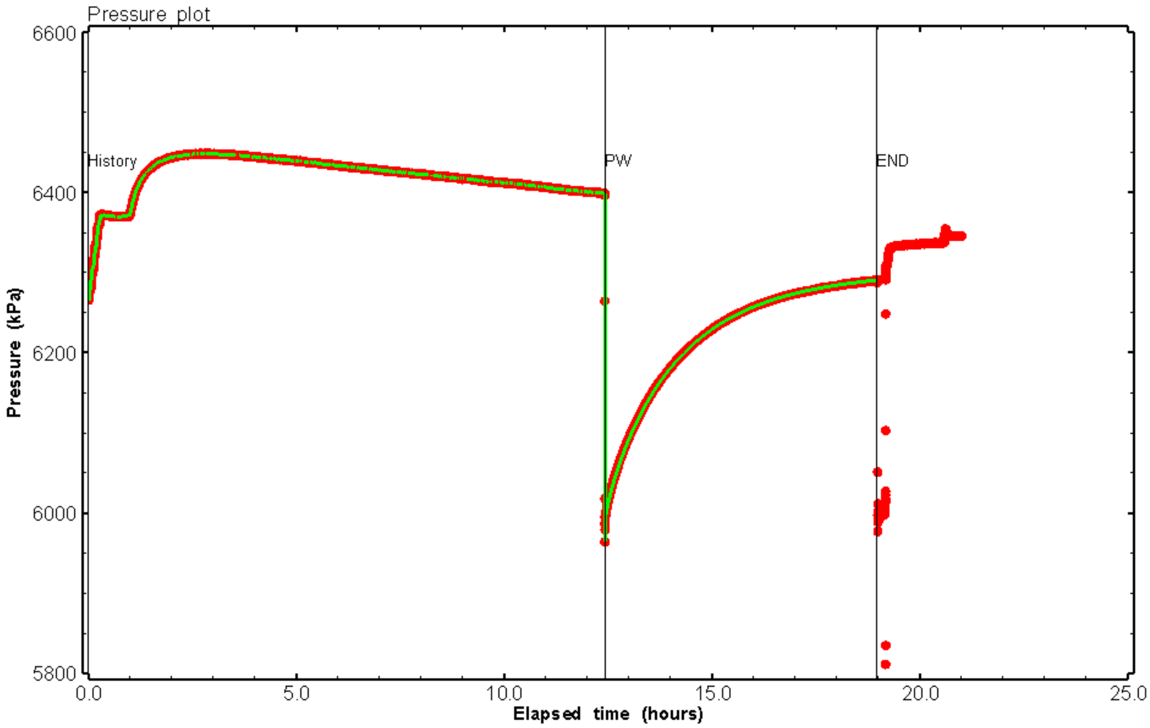

Figure 195: HT018 Pressure plot showing best-fit simulation and best fit results

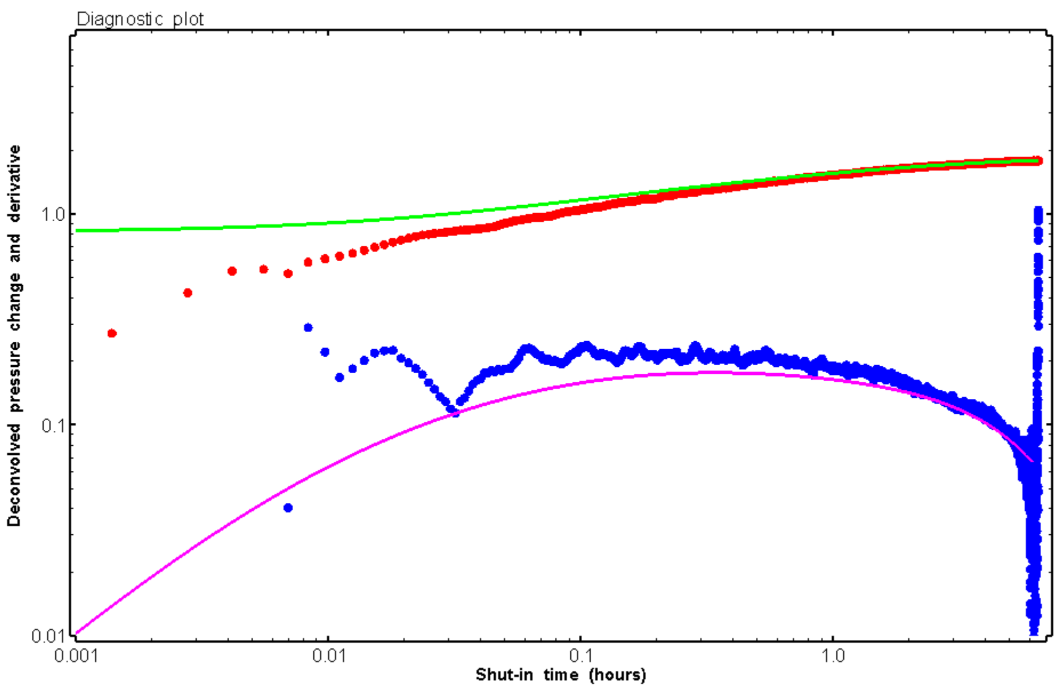

Figure 196: HT018 Deconvolved pressure change and derivative plot of the PW sequence showing best-fit simulation

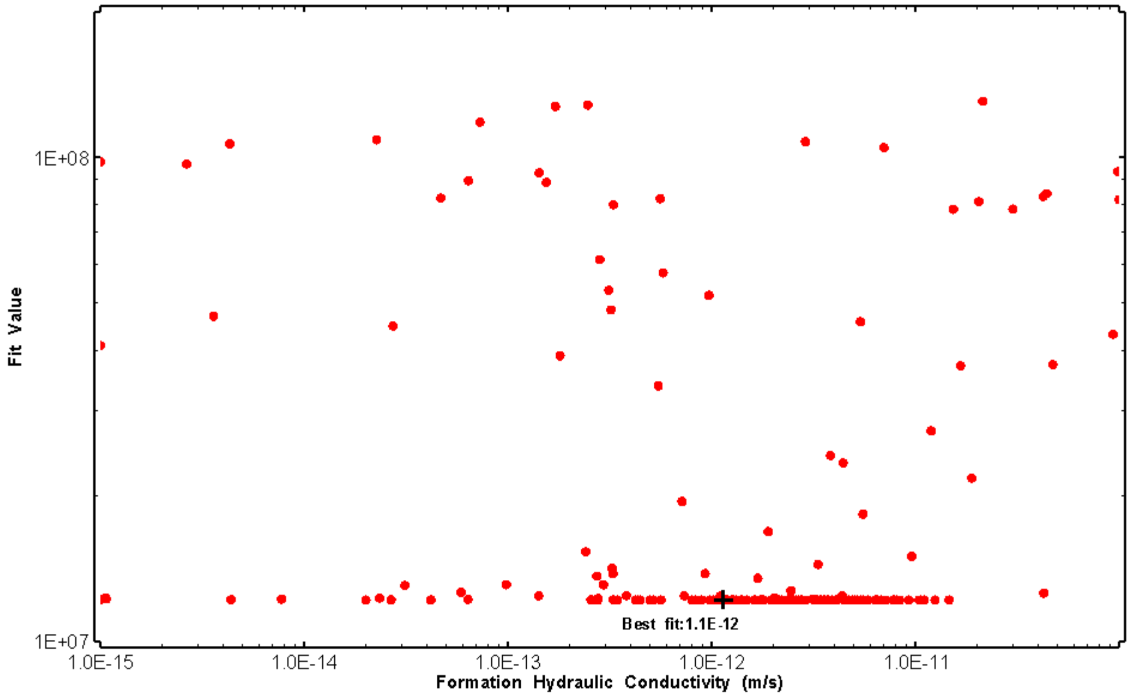

Figure 197: HT018 XY-scatter plot of formation hydraulic conductivity vs. fit value

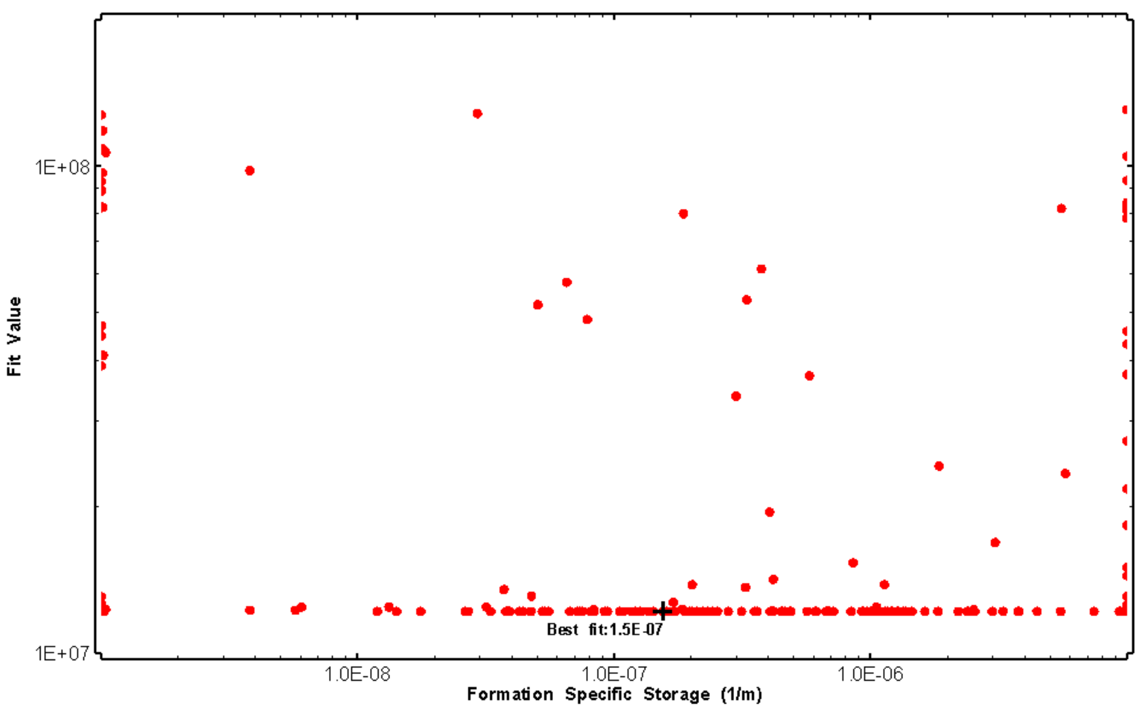

Figure 198: HT018 XY-scatter plot of formation specific storage vs. fit value

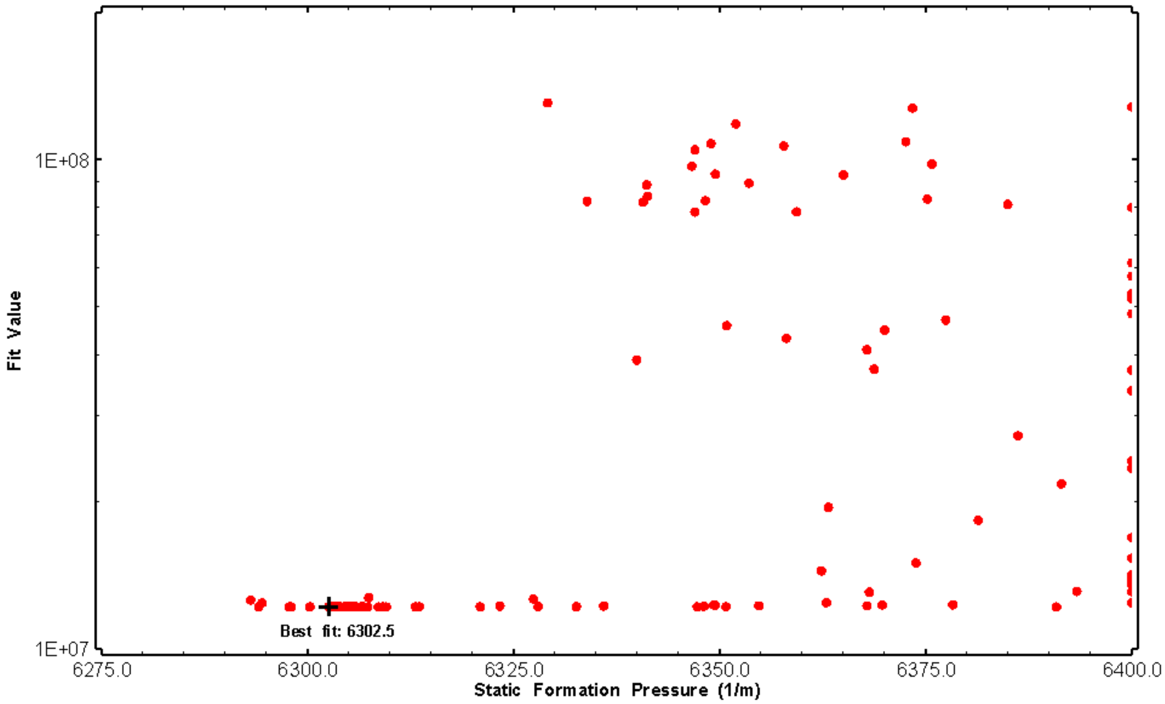

Figure 199: HT018 XY-scatter plot of static formation pressure vs. fit value

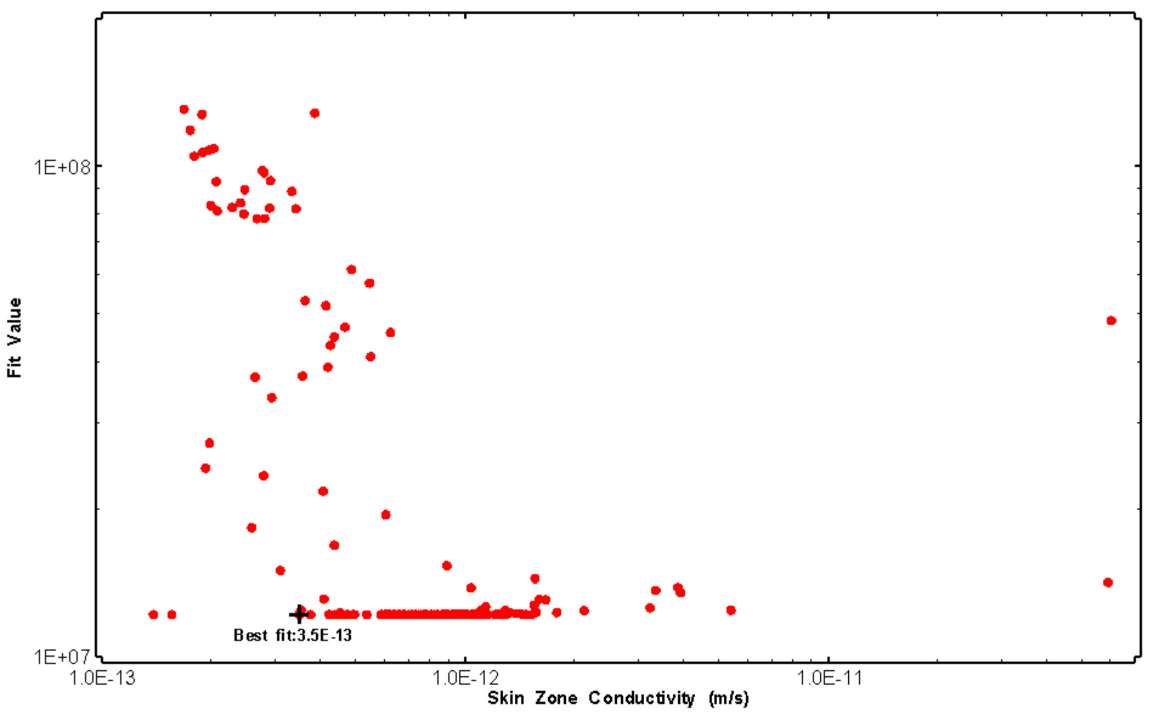

Figure 200: HT018 XY-scatter plot of skin zone conductivity vs. fit value

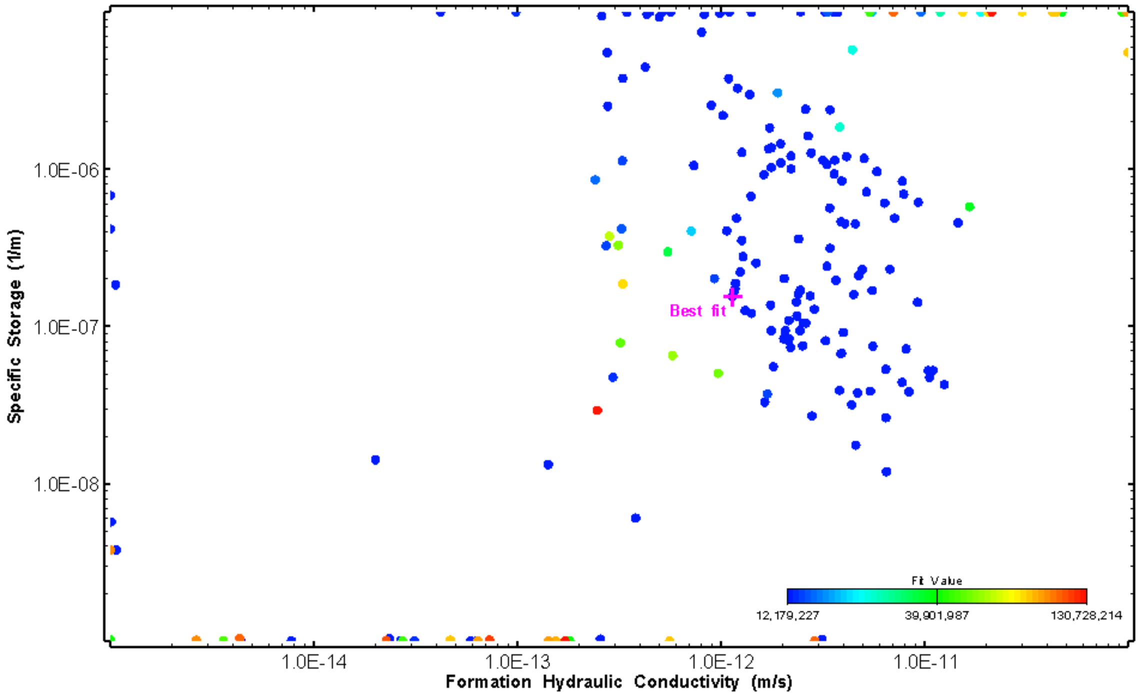

Figure 201: HT018 XY-scatter plot showing estimates of formation hydraulic conductivity and specific storage from perturbation analysis

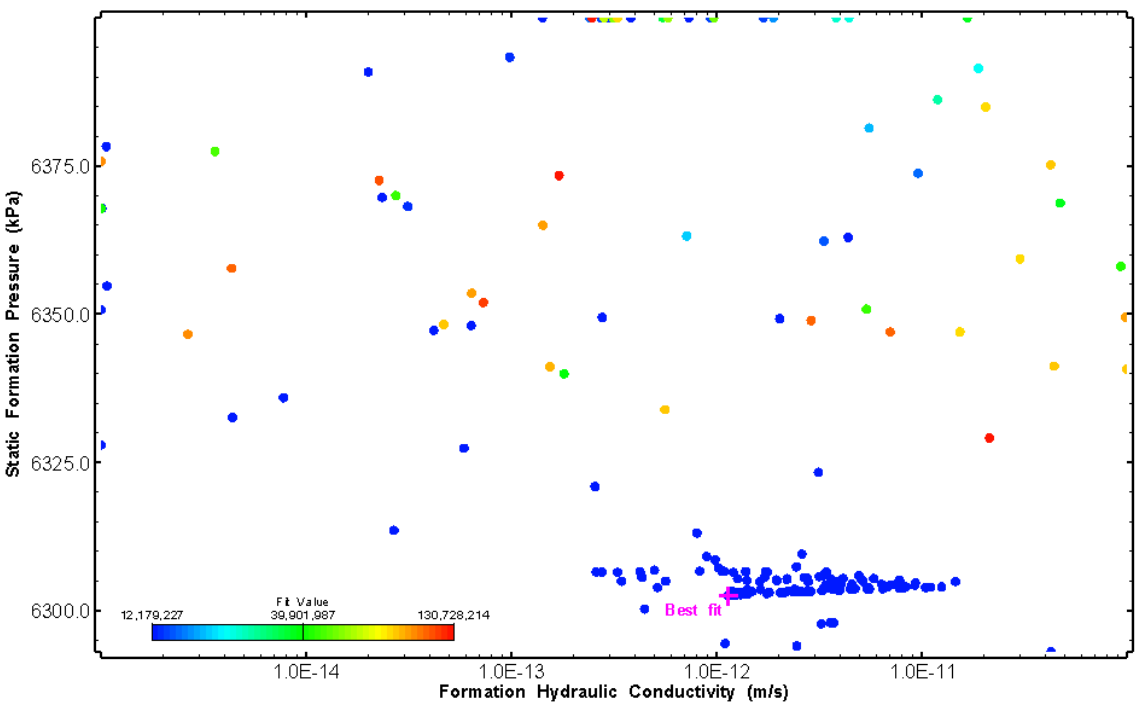

Figure 202: HT018 XY-scatter plot showing estimates of formation hydraulic conductivity and static formation pressure from perturbation analysis

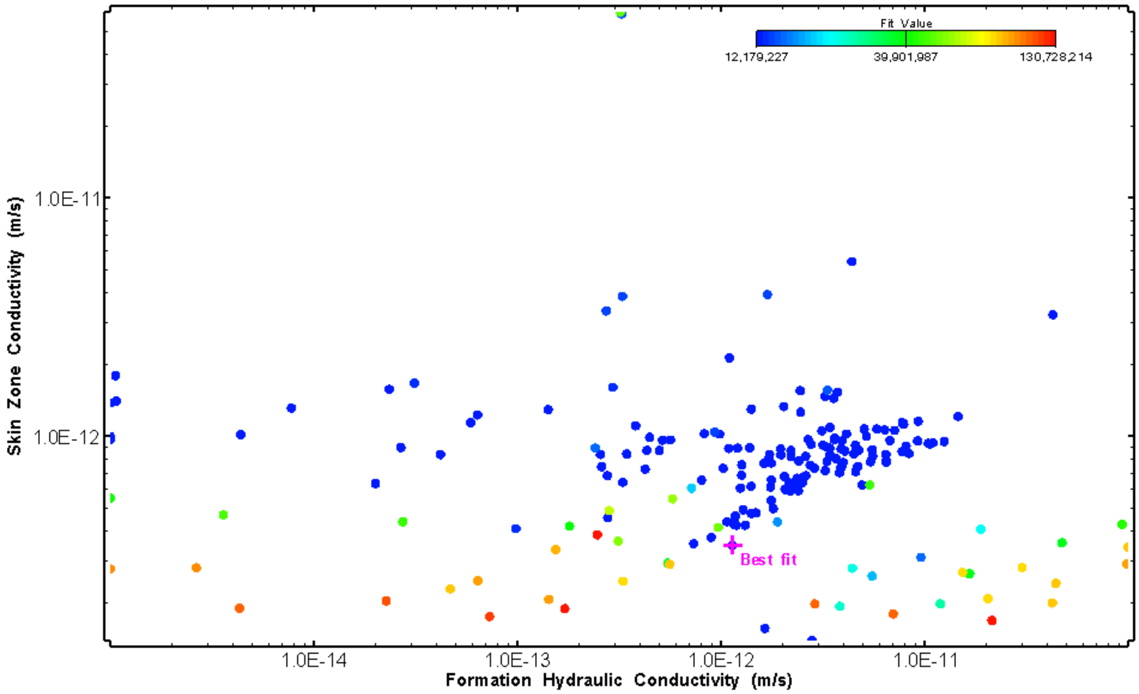

Figure 203: HT018 XY-scatter plot showing estimates of formation hydraulic conductivity and skin zone conductivity from perturbation analysis

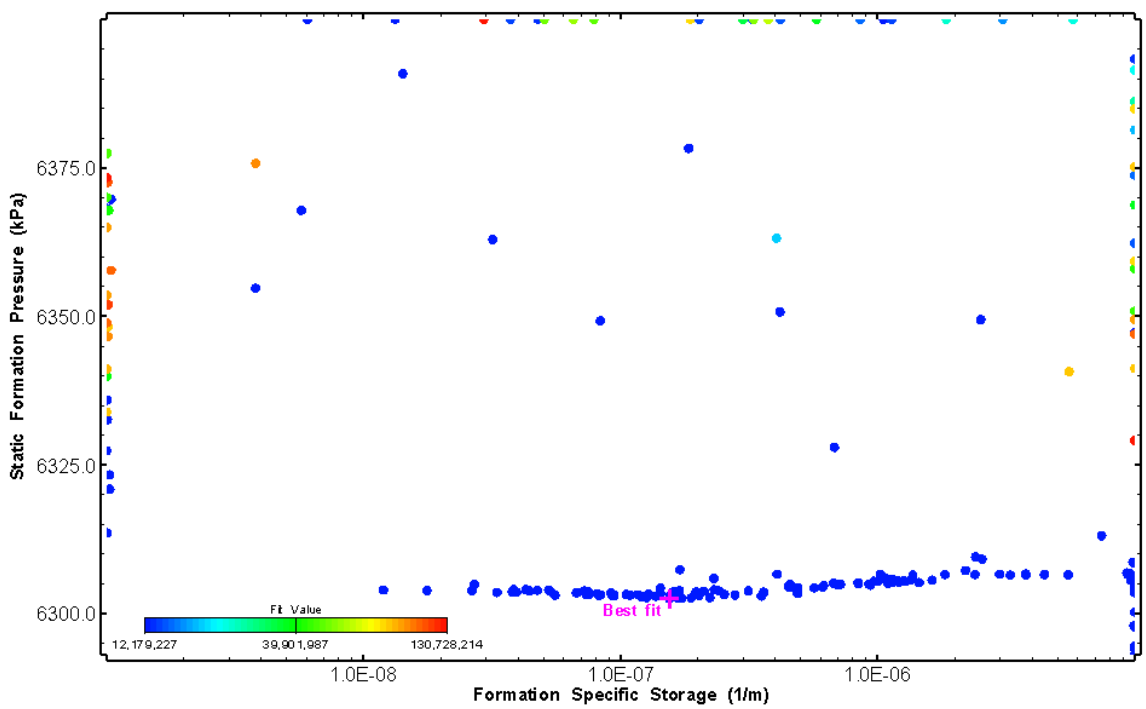

Figure 204: HT018 XY-scatter plot showing estimates of specific storage and static formation pressure from perturbation analysis

18.0 HT019 (734.50 – 754.53 M)

HT019 was selected to obtain continuous testing coverage from 600 to 800 m along hole. Zero broken fractures were observed in the core. A change in electrical conductivity of drilling fluid was observed in this interval. A slight indication of flow was recorded during FFEC logging post-drilling.

The test was initiated with a shut-in pressure recovery phase (PSR). A pulse withdrawal test (PW) with a shut-in recovery was completed after the PSR phase.

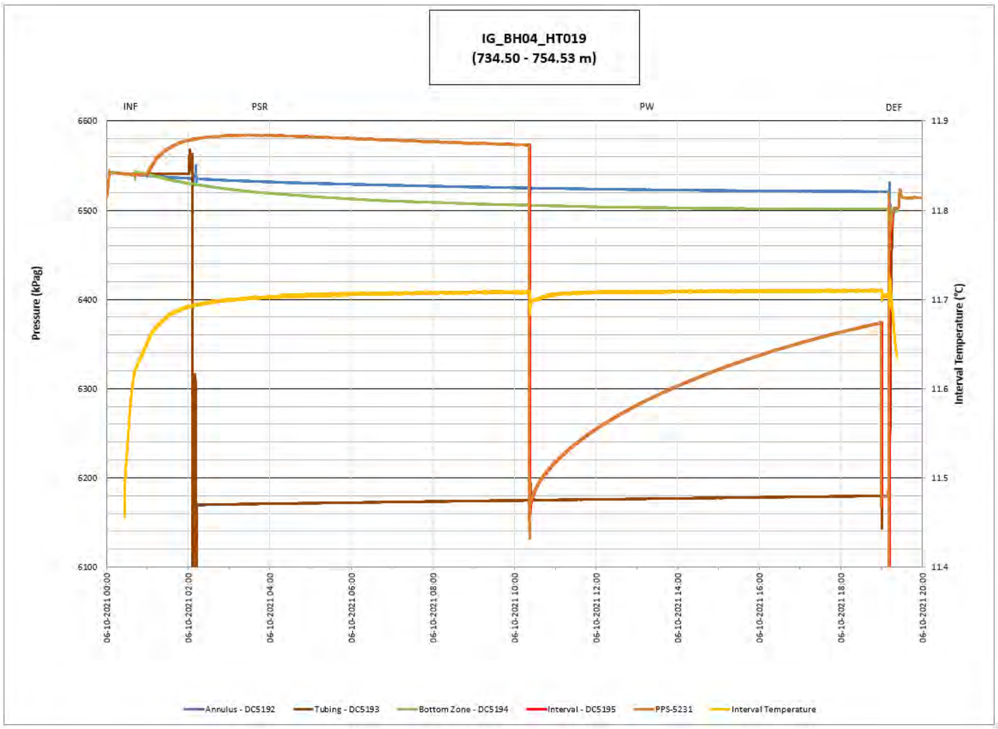

Figure 205: HT019 Annotated test plot showing monitored zone pressure and interval temperature.

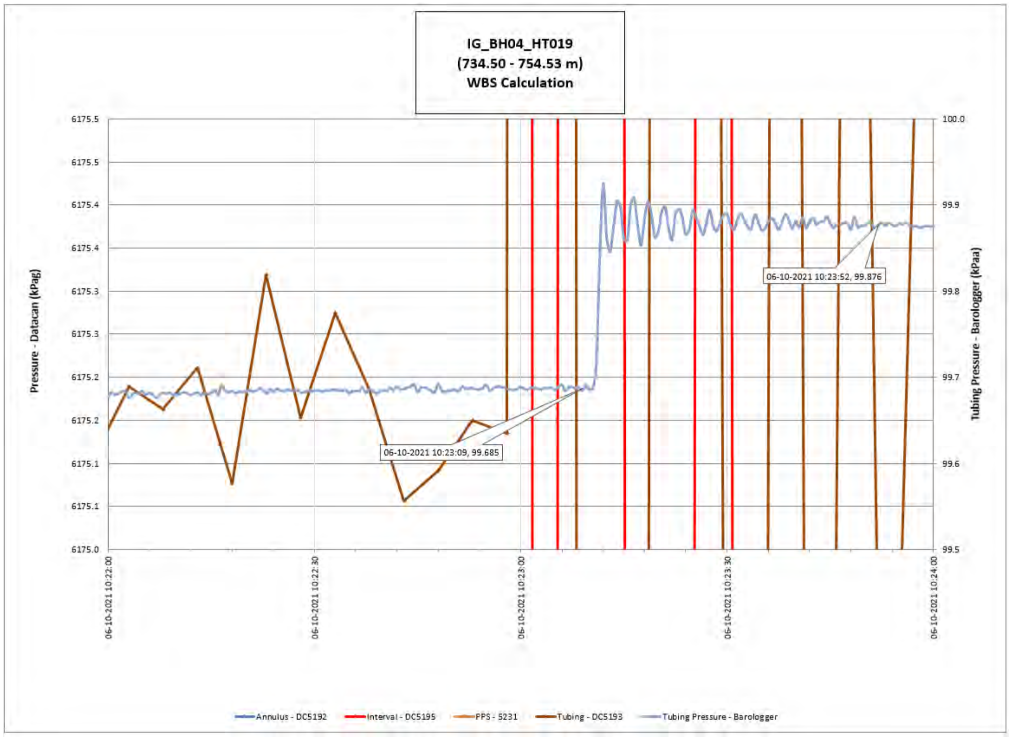

Figure 206: HT019 Tubing pressure during DHSIV activation. DHSIV Closed Wellbore Storage Estimate = 9E-11 m^3/Pa

Table 18: Summary of Analysis Results – HT019

	Formation conductivity	Skin zone conductivity	Static formation pressure	Formation specific storage	Radial thickness of skin	Flow dimension
	[m/s]	[m/s]	[kPa]	[1/m]	[m]	[–]
Best Fit	1.78E-13	1.6E-13	6531	4.4E-07	3.1E-03	2.5
Minimum	2.2E-15	1.6E-13	6451	1.8E-10	1.0E-03	1.3
Maximum	1.3E-11	7.6E-11	6572	9.5E-06	9.6E-01	3.0
Mean	6.8E-13	1.8E-12	6539	3.5E-07	2.1E-01	2.0
Median	3.7E-13	4.0E-13	6541	1.2E-07	1.2E-01	2.0
Geometric mean	3.5E-13	4.8E-13	6539	1.1E-07	9.9E-02	2.0

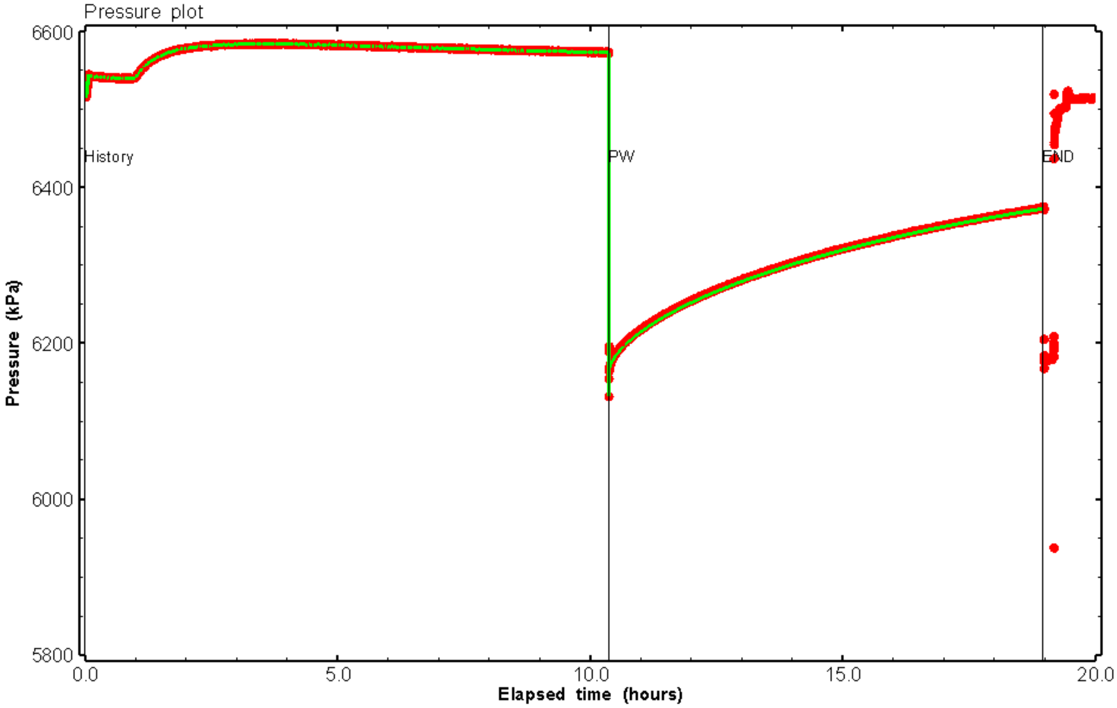

Figure 207: HT019 Pressure plot showing best-fit simulation and best fit results

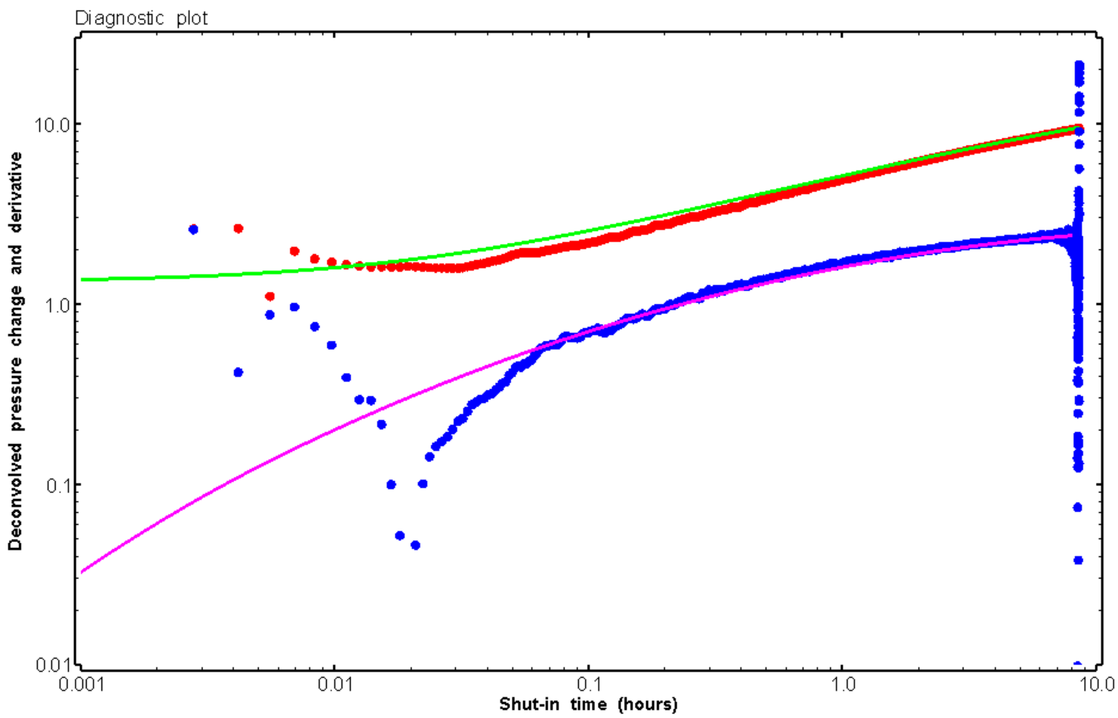

Figure 208: HT019 Deconvolved pressure change and derivative plot of the PW sequence showing best-fit simulation

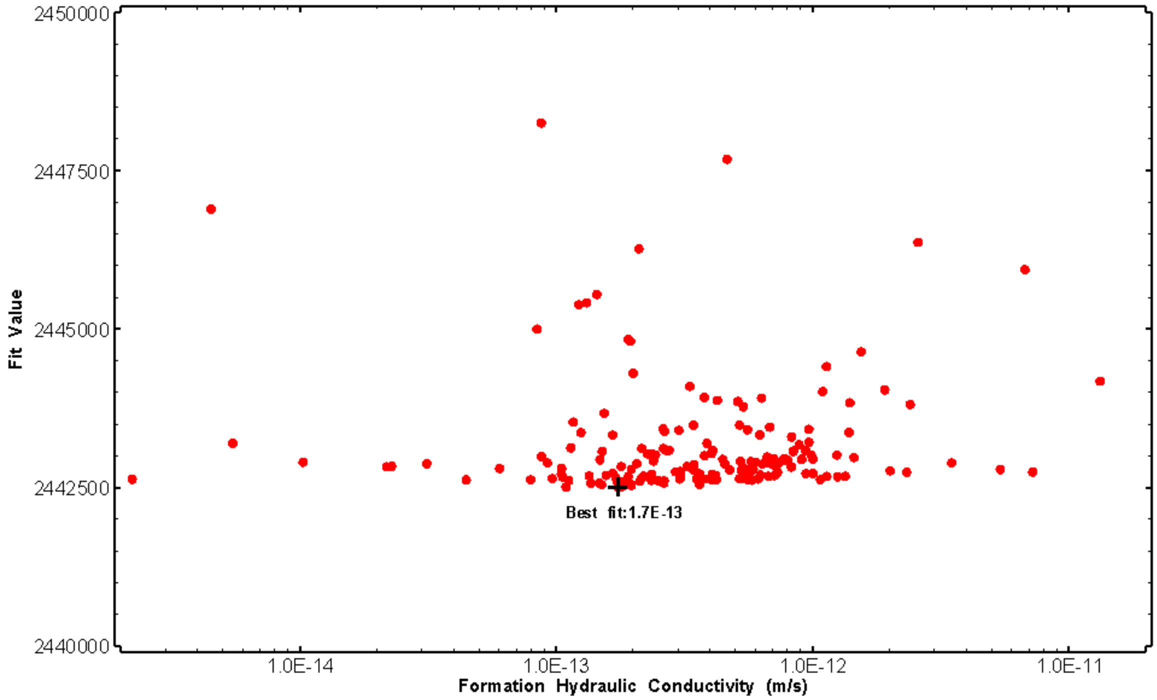

Figure 209: HT019 XY-scatter plot of formation hydraulic conductivity vs. fit value

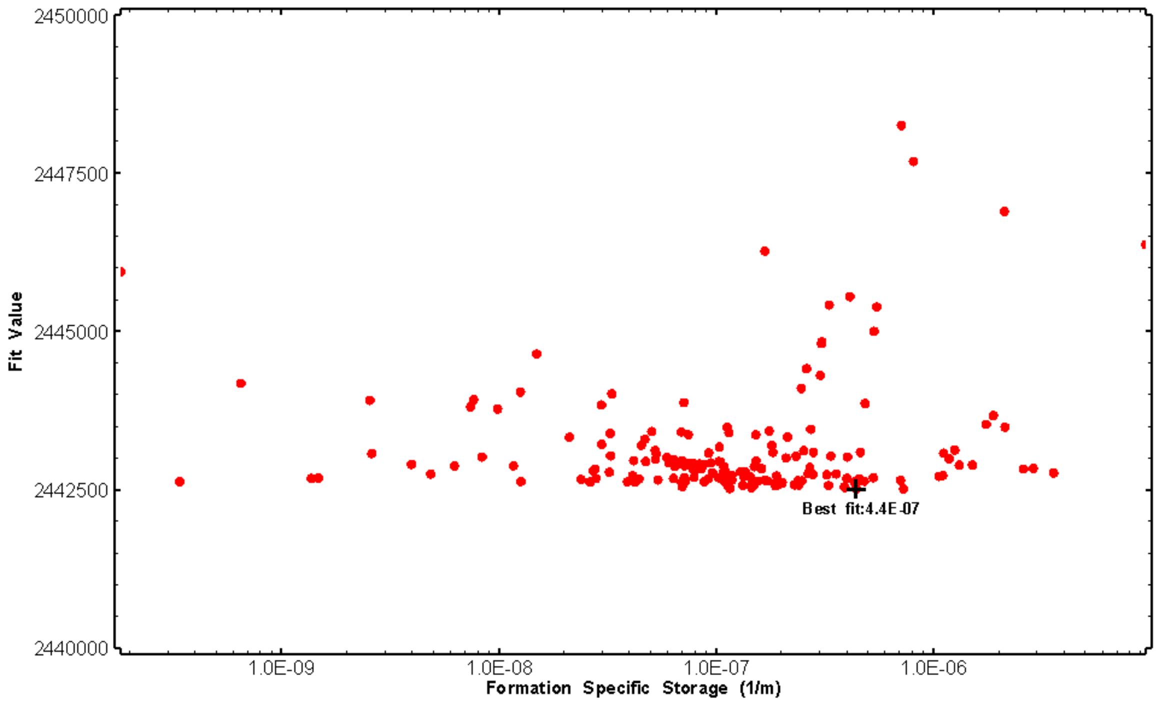

Figure 210: HT019 XY-scatter plot of formation specific storage vs. fit value

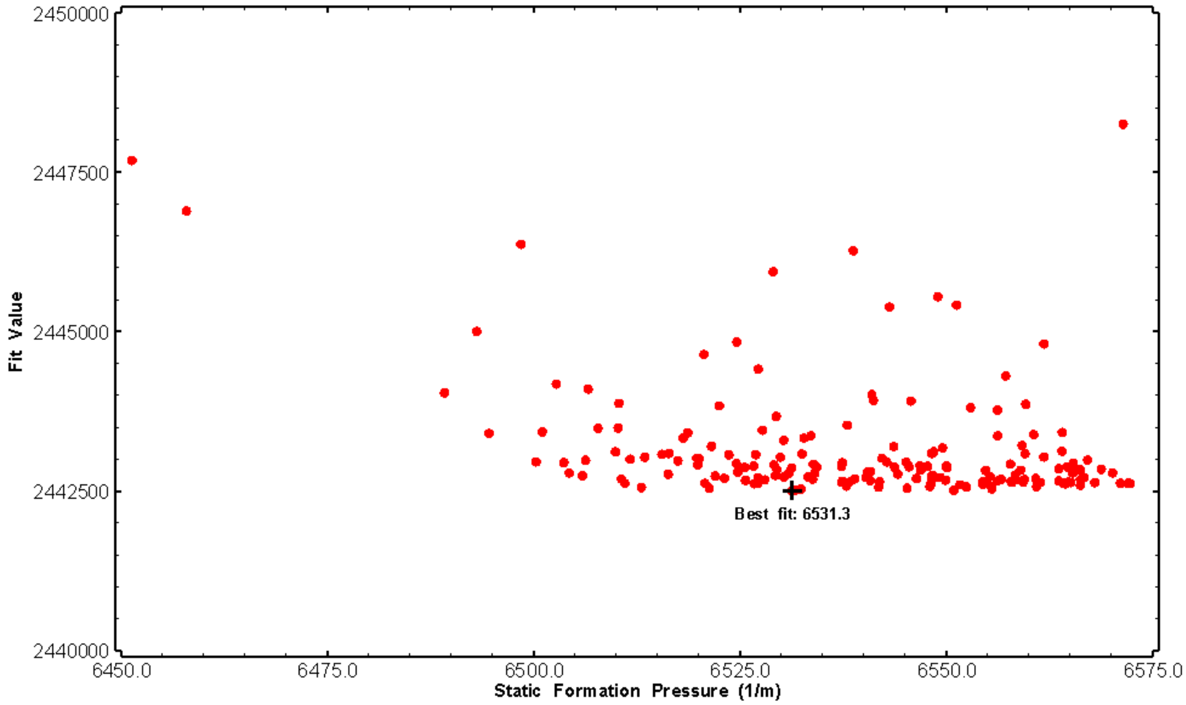

Figure 211: HT019 XY-scatter plot of static formation pressure vs. fit value

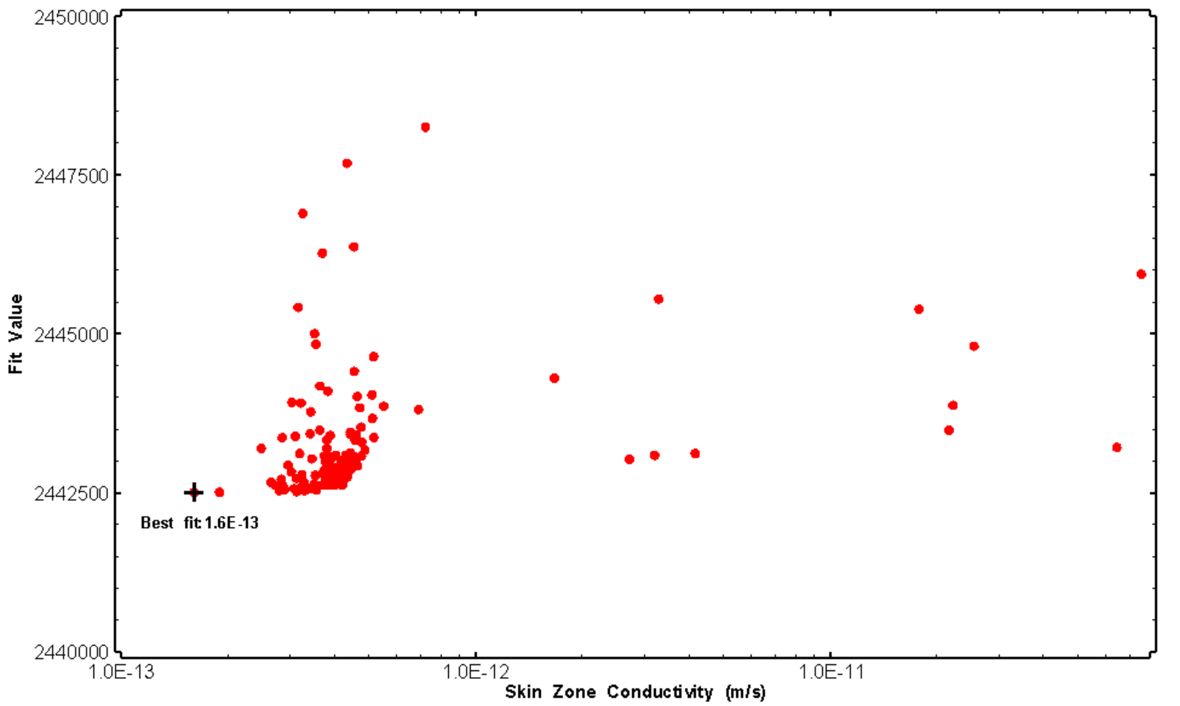

Figure 212: HT019 XY-scatter plot of skin zone conductivity vs. fit value

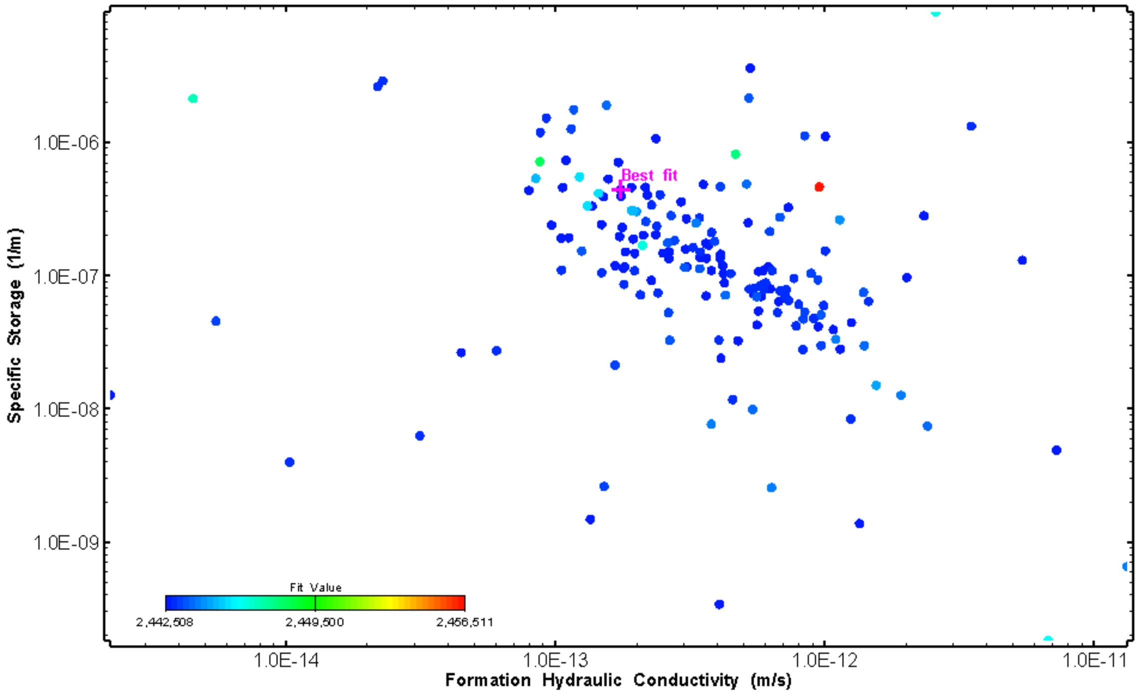

Figure 213: HT019 XY-scatter plot showing estimates of formation hydraulic conductivity and specific storage from perturbation analysis

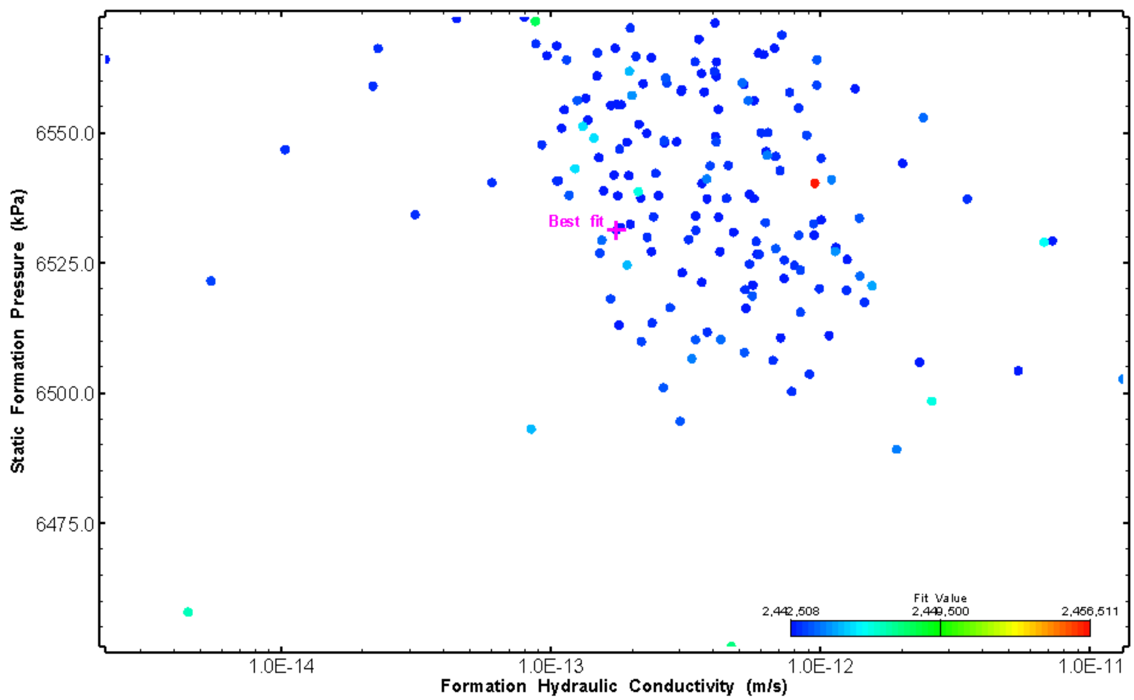

Figure 214: HT019 XY-scatter plot showing estimates of formation hydraulic conductivity and static formation pressure from perturbation analysis

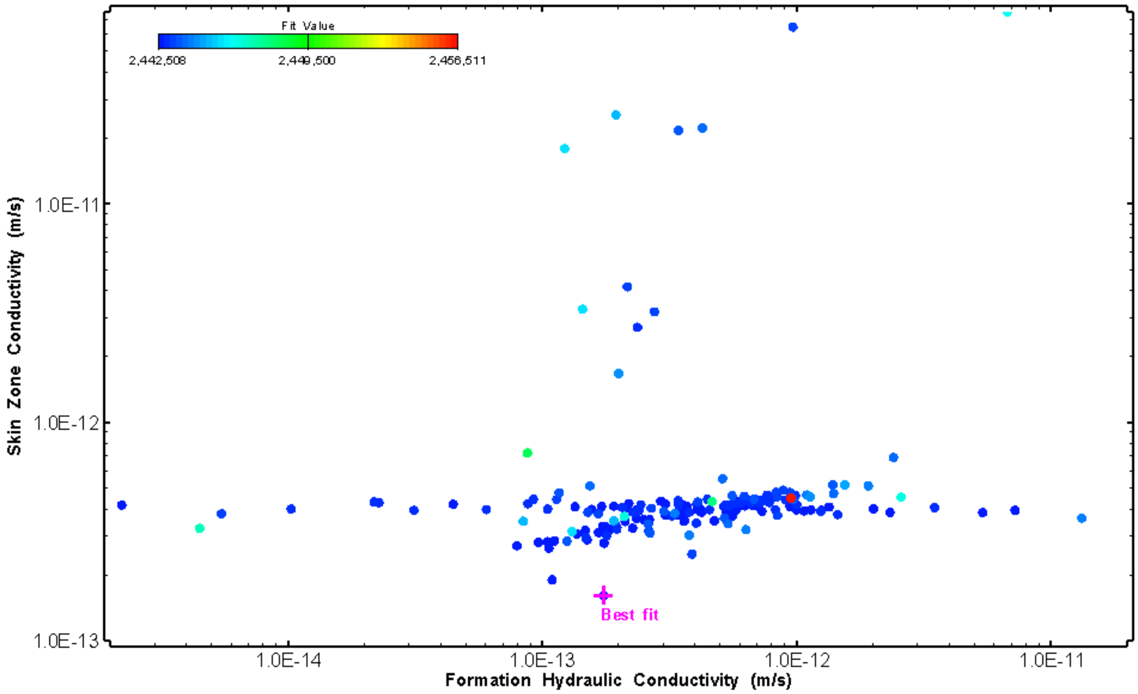

Figure 215: HT019 XY-scatter plot showing estimates of formation hydraulic conductivity and skin zone conductivity from perturbation analysis

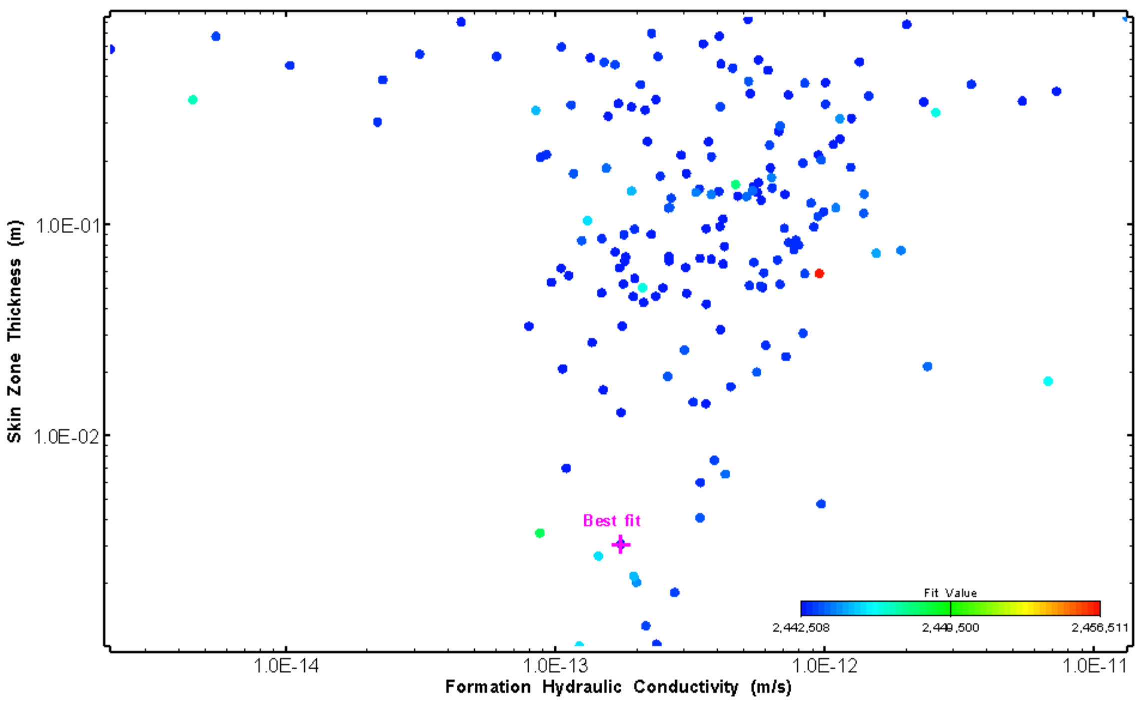

Figure 216: HT019 XY-scatter plot showing estimates of specific storage and static formation pressure from perturbation analysis

19.0 HT020 (754.25 – 774.28 M)

HT020 was selected to obtain continuous testing coverage from 600 to 800 m along hole. Zero broken fractures were observed in the core. No drill fluid parameter triggers were reached during drilling. A slight indication of flow was recorded during FFEC logging post-drilling.

The test was initiated with a shut-in pressure recovery phase (PSR). A pulse withdrawal test (PW) with a shut-in recovery was completed after the PSR phase.

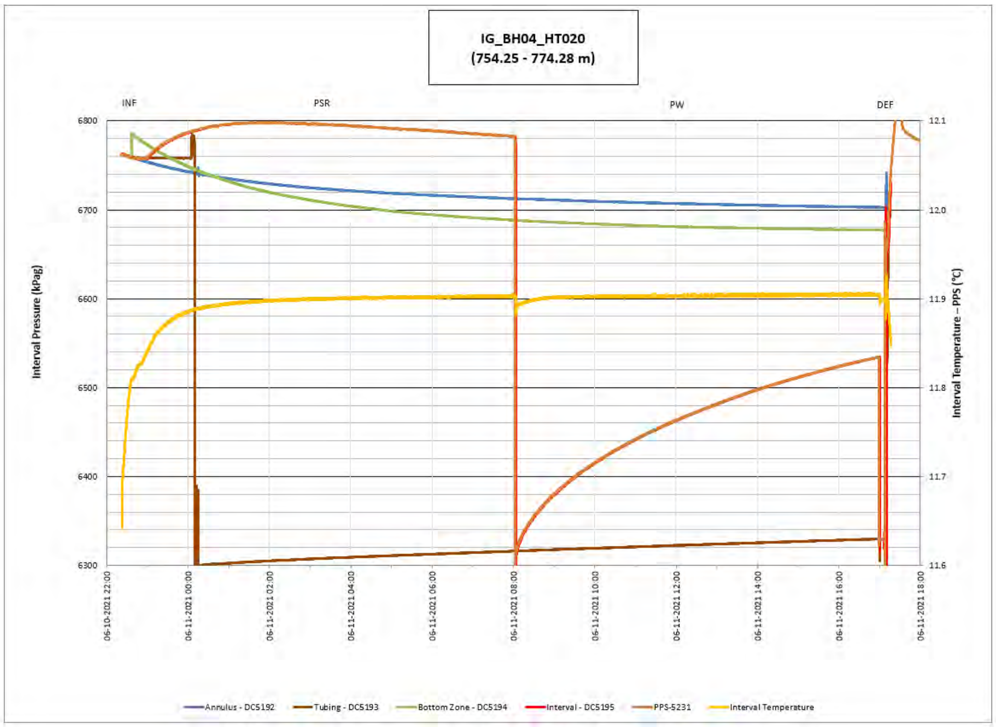

Figure 217: HT020 Annotated test plot showing monitored zone pressure and interval temperature.

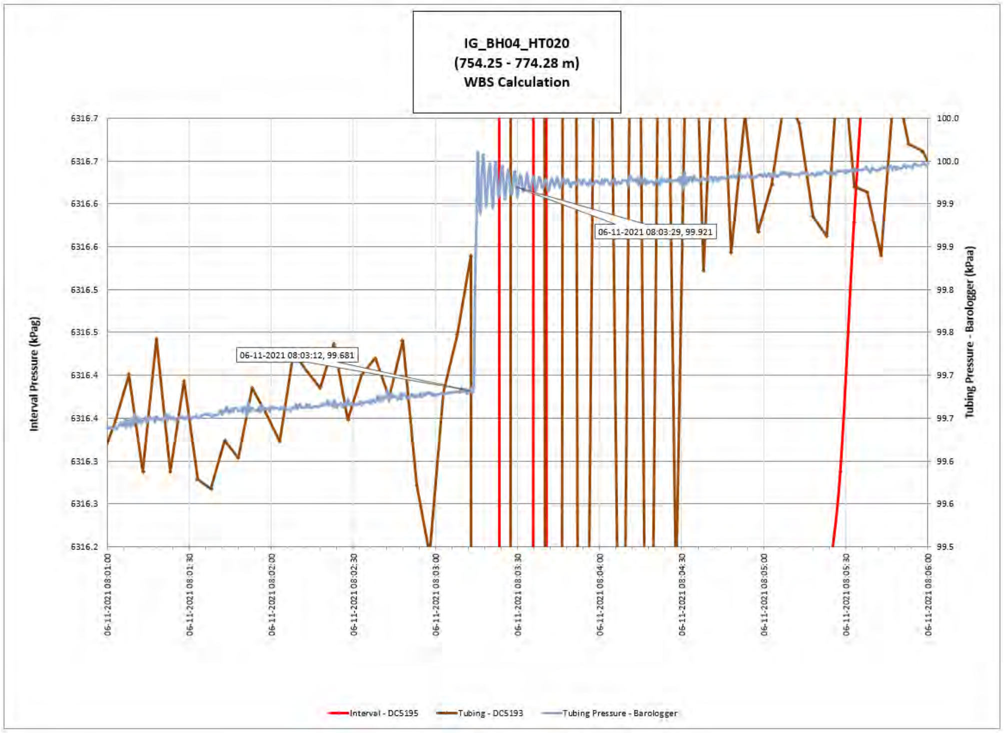

Figure 218: HT020 Tubing pressure during DHSIV activation. DHSIV Closed Wellbore Storage Estimate = 9E-11 m³/Pa

Table 19: Summary of Analysis Results – HT020

	Formation conductivity	Skin zone conductivity	Static formation pressure	Formation specific storage	Radial thickness of skin	Flow dimension
	[m/s]	[m/s]	[kPa]	[1/m]	[m]	[–]
Best Fit	1.9E-13	3.2E-14	6685	6.5E-07	1.0E-03	2.5
Minimum	1.0E-15	3.2E-14	6632	1.0E-09	1.0E-03	1.0
Maximum	9.8E-11	4.6E-11	7000	5.4E-06	9.8E-01	3.0
Mean	1.3E-12	1.6E-12	6730	6.9E-07	2.2E-01	1.9
Median	2.4E-13	4.7E-13	6698	1.8E-07	1.3E-01	1.8
Geometric mean	2.0E-13	4.7E-13	6729	2.1E-07	8.6E-02	1.8

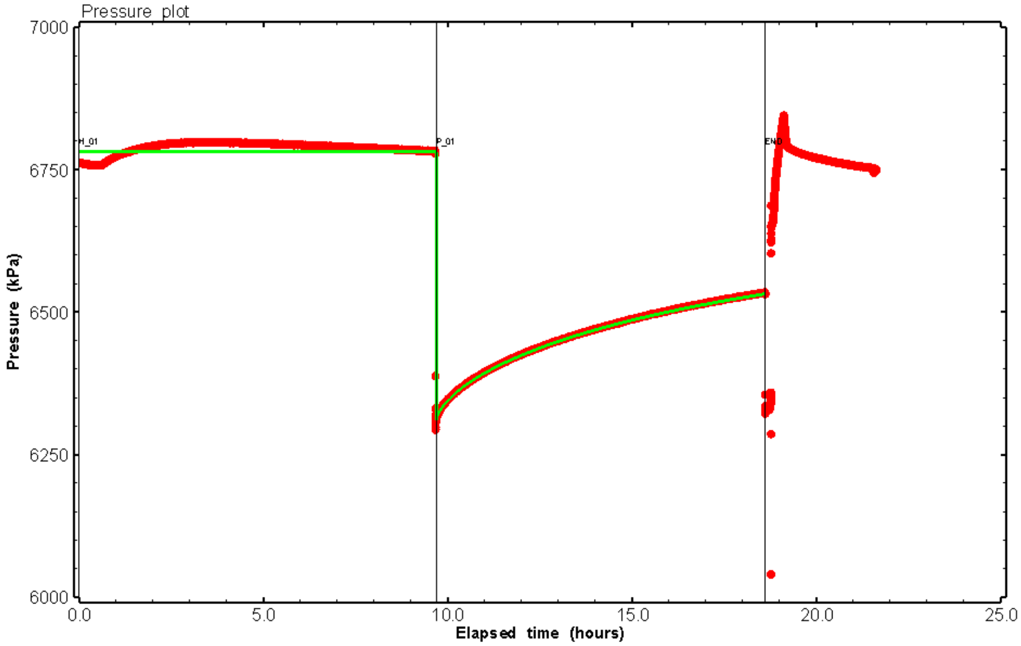

Figure 219: HT020 Pressure plot showing best-fit simulation and best fit results

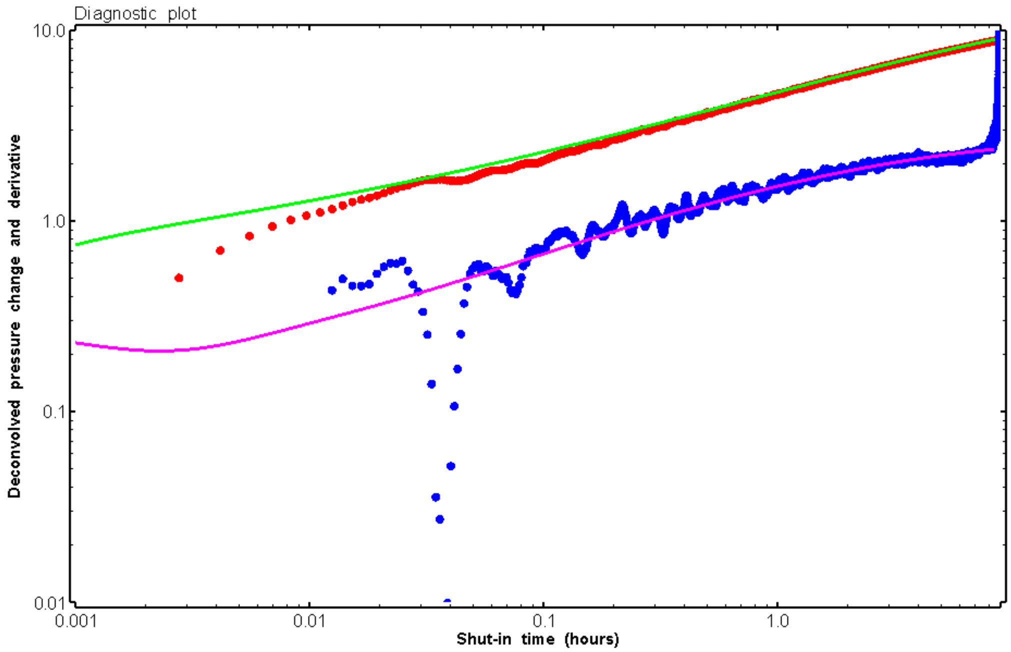

Figure 220: HT020 Deconvolved pressure change and derivative plot of the PW sequence showing best-fit simulation

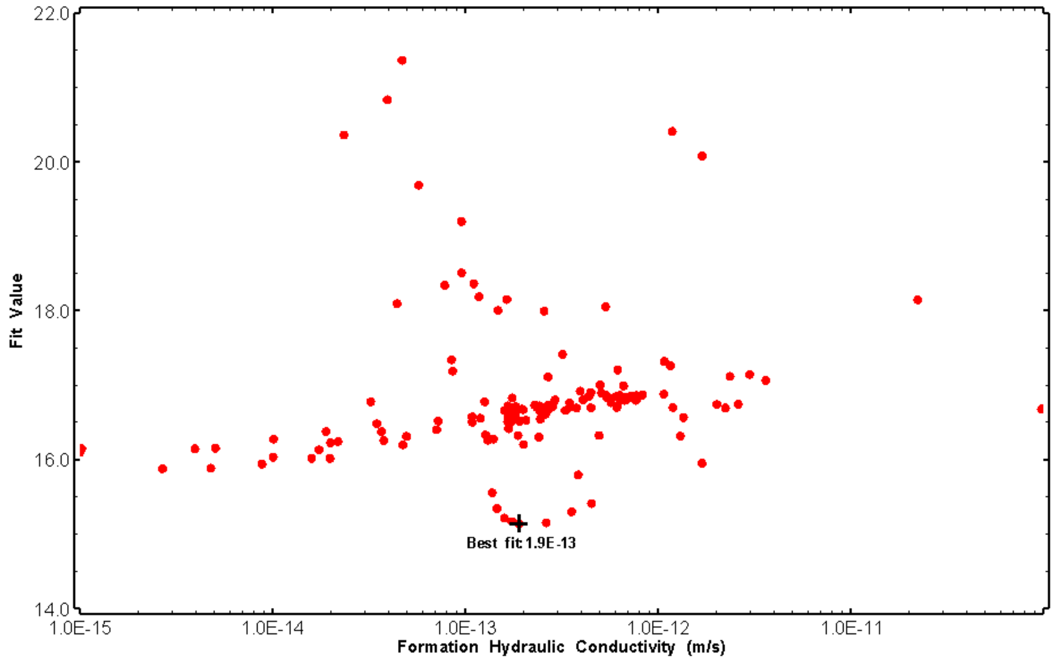

Figure 221: HT020 XY-scatter plot of formation hydraulic conductivity vs. fit value

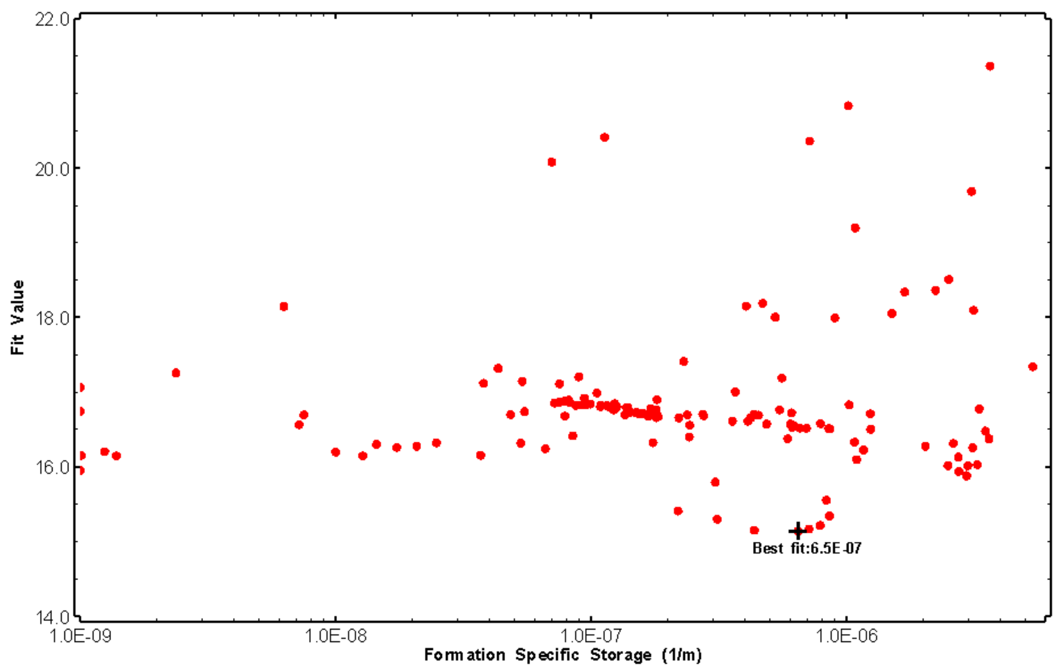

Figure 222: HT020 XY-scatter plot of formation specific storage vs. fit value

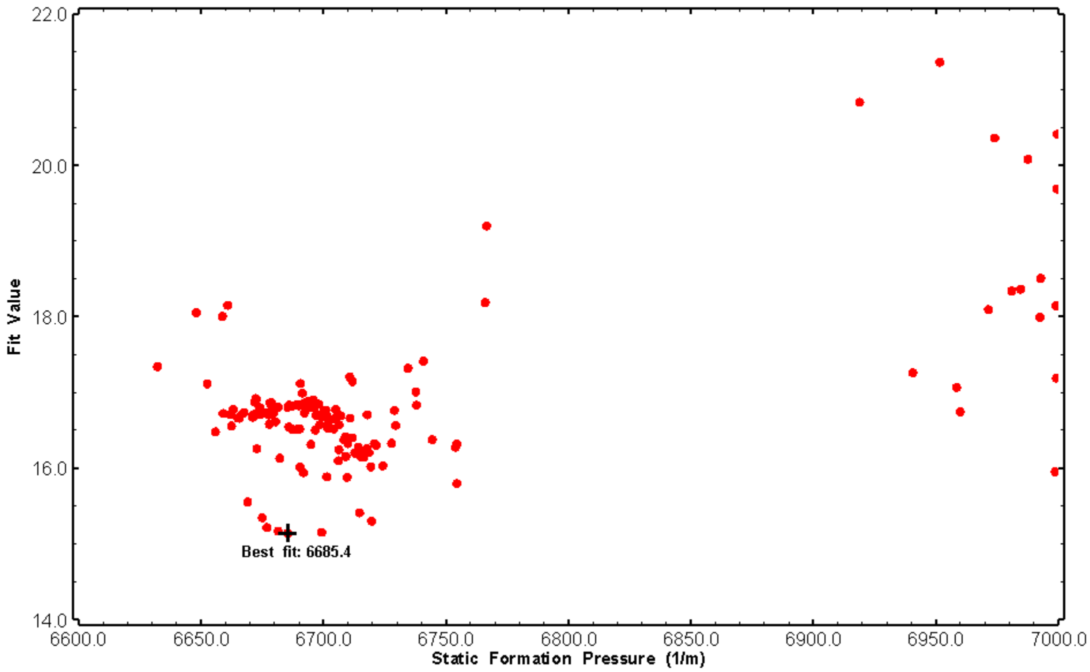

Figure 223: HT020 XY-scatter plot of static formation pressure vs. fit value

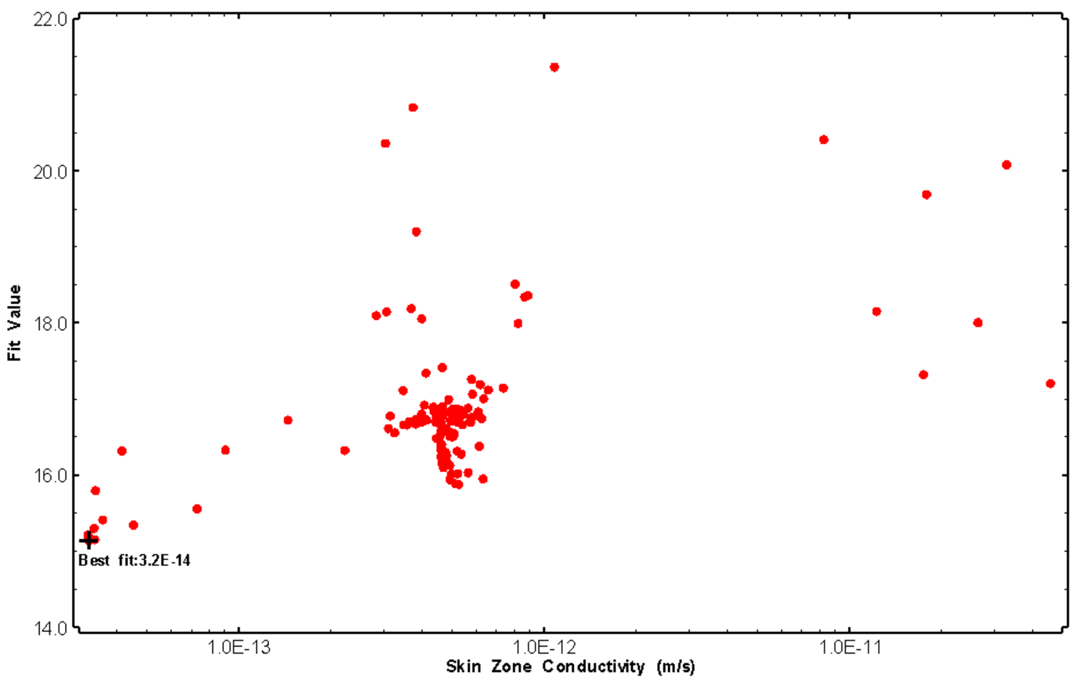

Figure 224: HT020 XY-scatter plot of skin zone conductivity vs. fit value

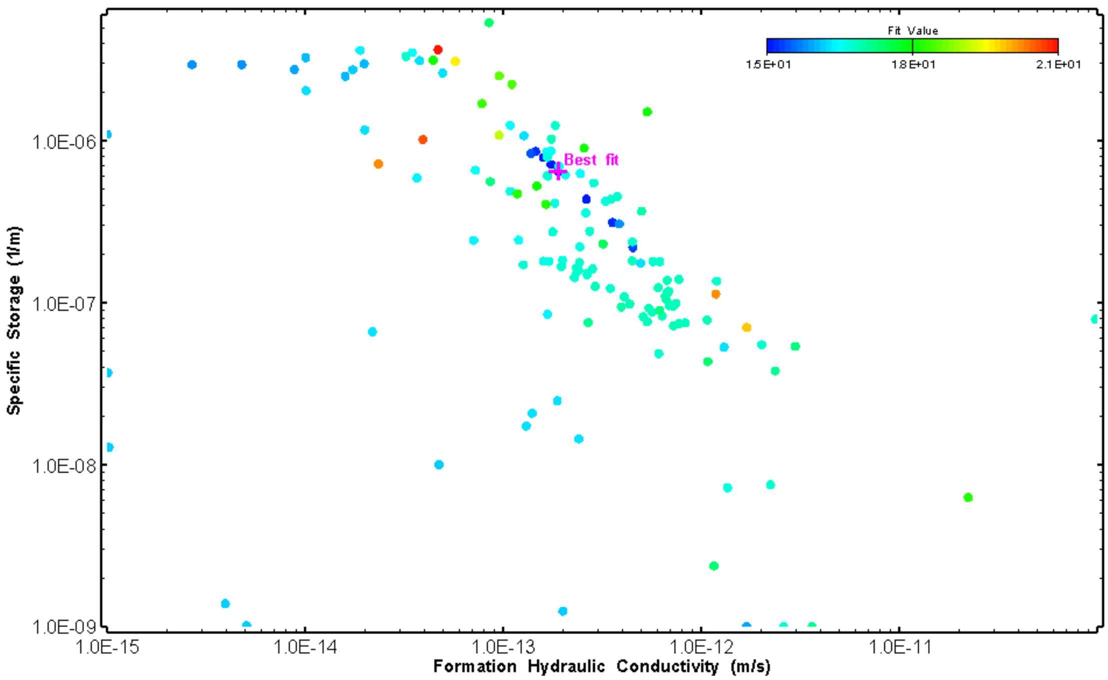

Figure 225: HT020 XY-scatter plot showing estimates of formation hydraulic conductivity and specific storage from perturbation analysis

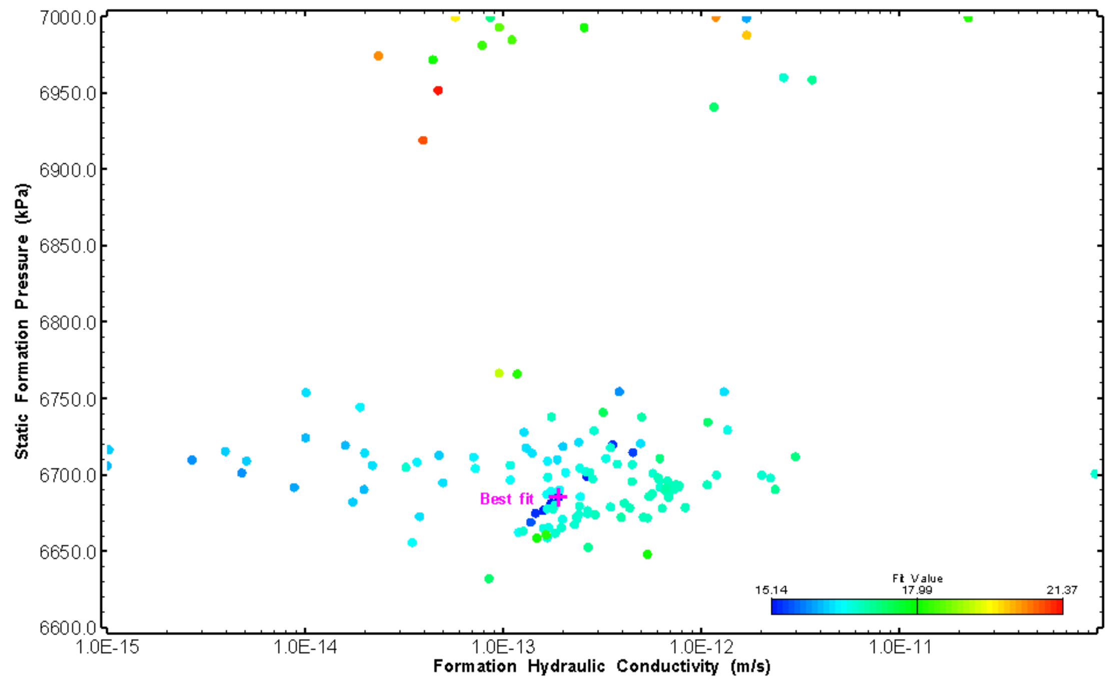

Figure 226: HT020 XY-scatter plot showing estimates of formation hydraulic conductivity and static formation pressure from perturbation analysis

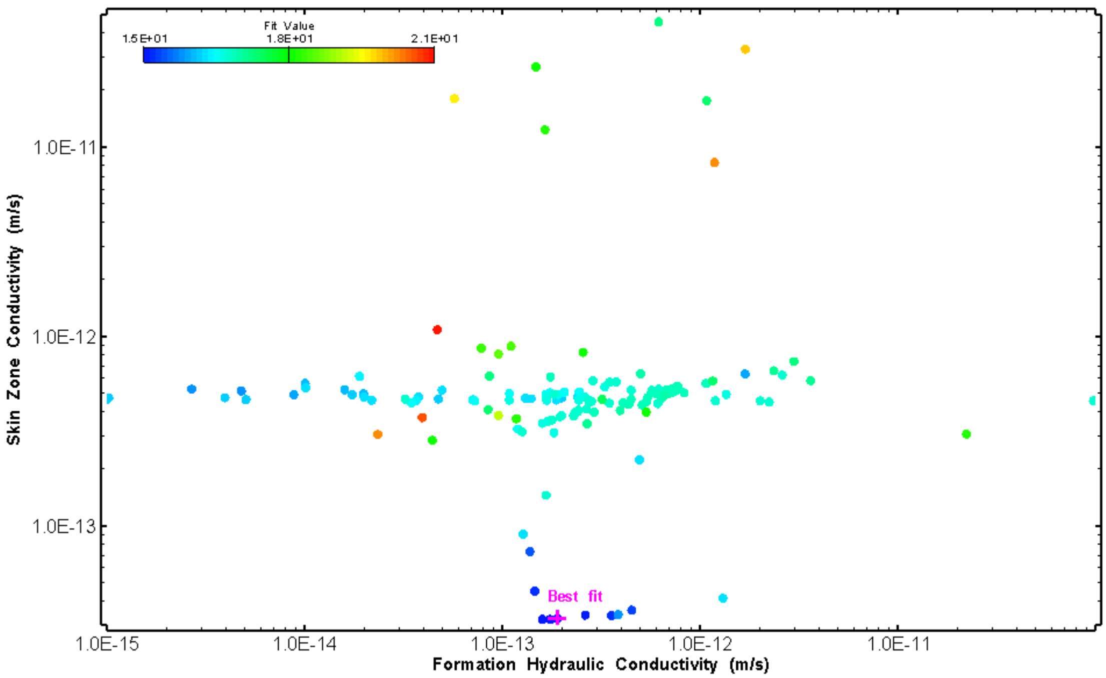

Figure 227: HT020 XY-scatter plot showing estimates of formation hydraulic conductivity and skin zone conductivity from perturbation analysis

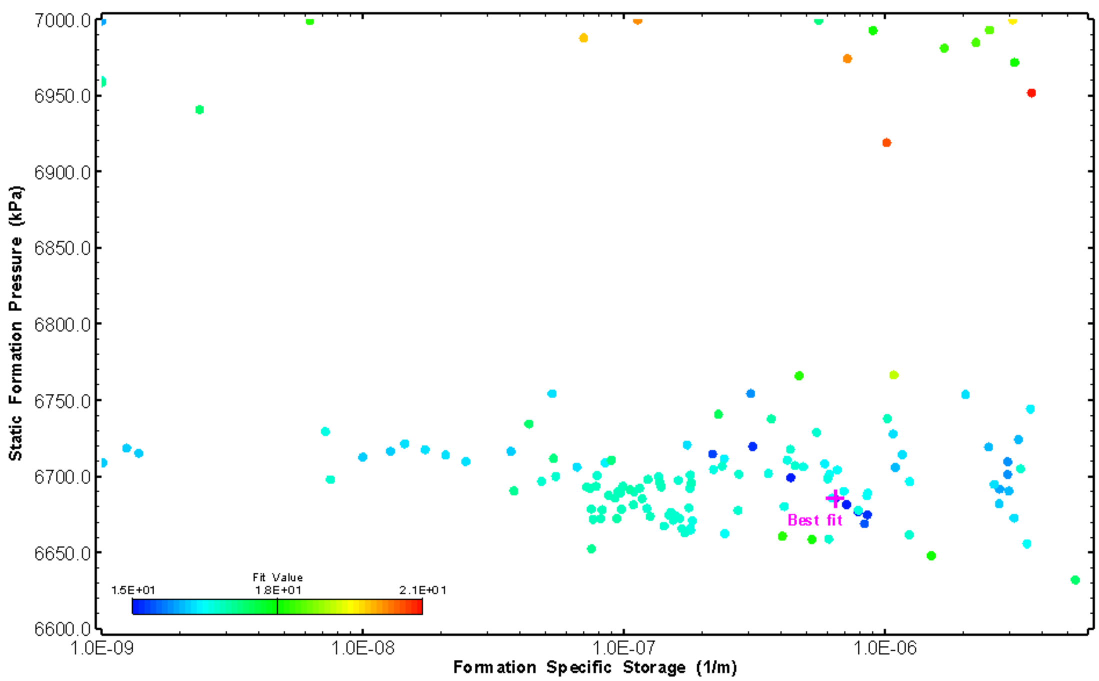

Figure 228: HT020 XY-scatter plot showing estimates of specific storage and static formation pressure from perturbation analysis

20.0 HT021 (774.00 – 794.03 M)

HT021 was selected to obtain continuous testing coverage from 600 to 800 m along hole. Zero broken fractures were observed in the core. A change in electrical conductivity of drilling fluid was observed in this interval. A slight indication of flow was recorded during FFEC logging post-drilling.

The test was initiated with a shut-in pressure recovery phase (PSR). A pulse withdrawal test (PW) with a shut-in recovery was completed after the PSR phase.

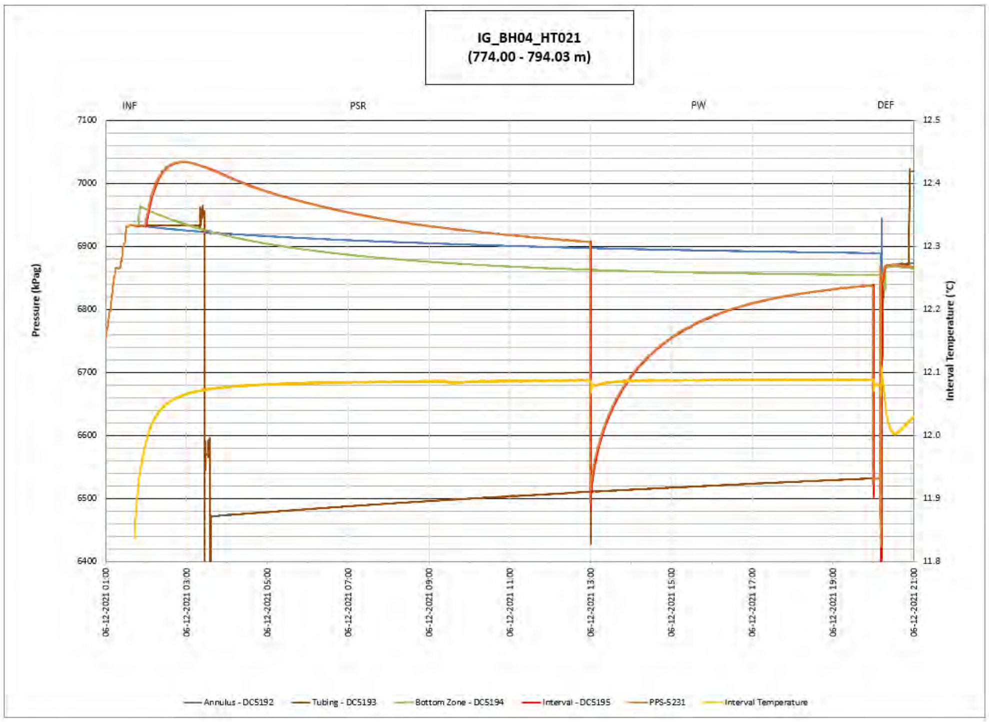

Figure 229: HT021 Annotated test plot showing monitored zone pressure and interval temperature.

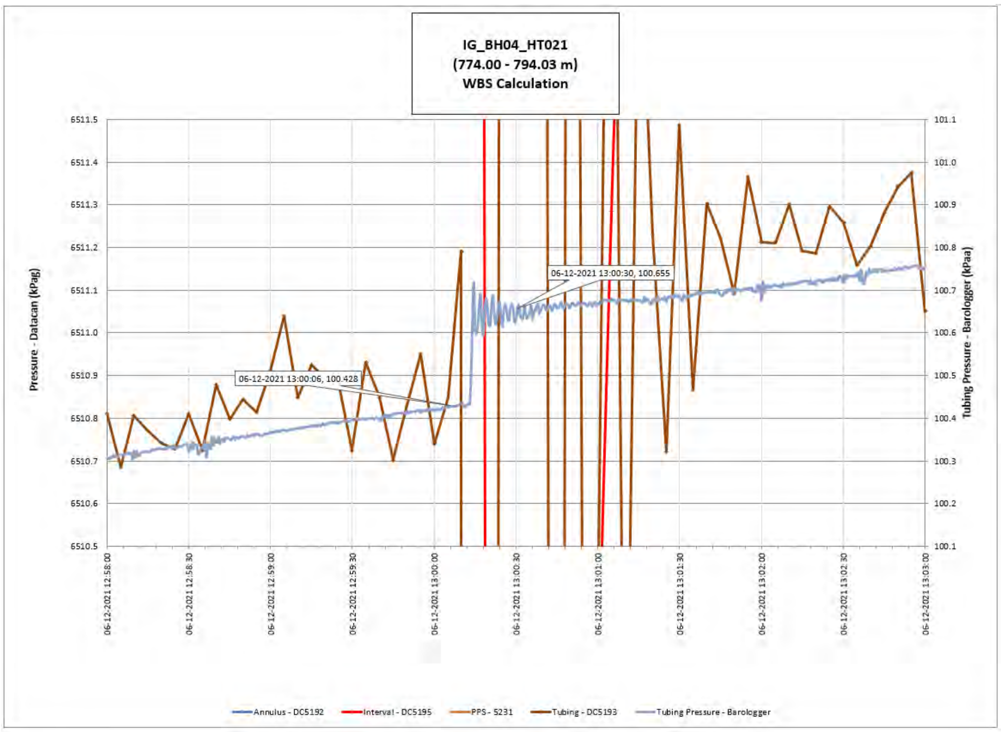

Figure 230: HT021 Tubing pressure during DHSIV activation. DHSIV Closed Wellbore Storage Estimate = 1E-10 m^3/Pa

Table 20: Summary of Analysis Results – HT021

	Formation conductivity	Skin zone conductivity	Static formation pressure	Formation specific storage	Radial thickness of skin	Flow dimension
	[m/s]	[m/s]	[kPa]	[1/m]	[m]	[–]
Best Fit	5.2E-14	6.1E-12	7124	8.3E-07	9.4E-01	1.5
Minimum	1.0E-14	9.3E-13	6861	1.0E-09	1.0E-02	1.0
Maximum	8.3E-11	7.9E-11	7381	9.9E-06	9.9E-01	2.8
Mean	6.7E-12	5.9E-12	6893	9.0E-07	1.5E-01	1.9
Median	2.5E-12	5.1E-12	6867	1.9E-07	4.6E-02	1.9
Geometric mean	2.7E-12	4.9E-12	6892	2.1E-07	5.9E-02	1.8

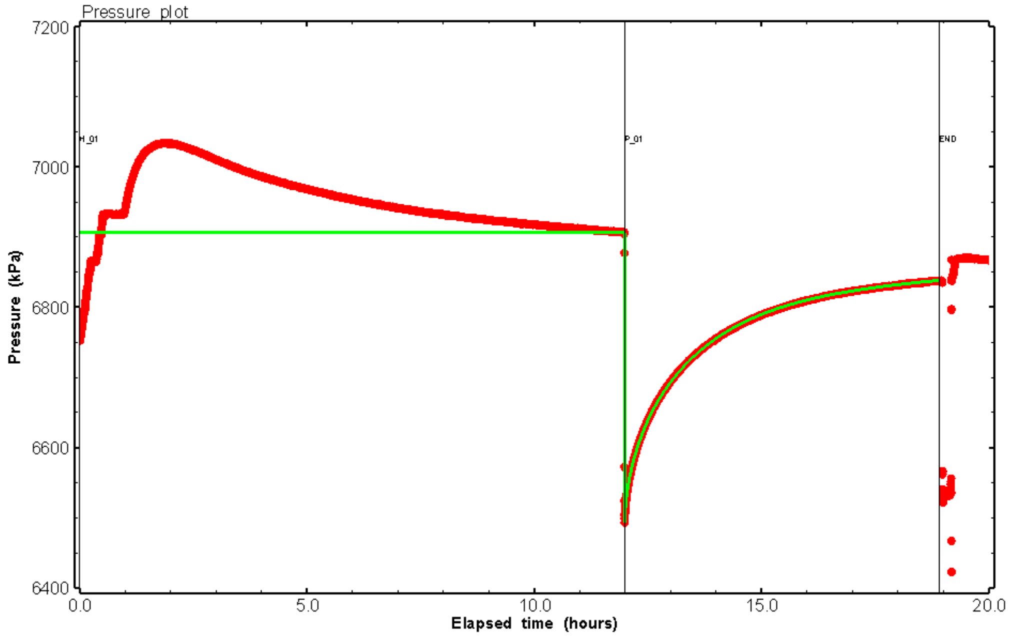

Figure 231: HT021 Pressure plot showing best-fit simulation and best fit results

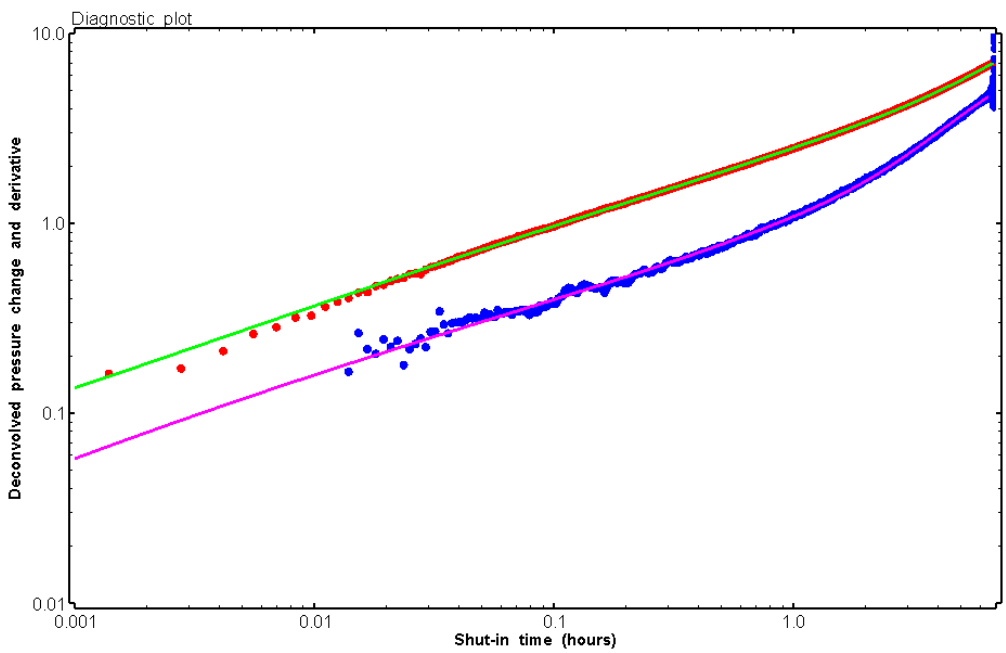

Figure 232: HT021 Deconvolved pressure change and derivative plot of the PW sequence showing best-fit simulation

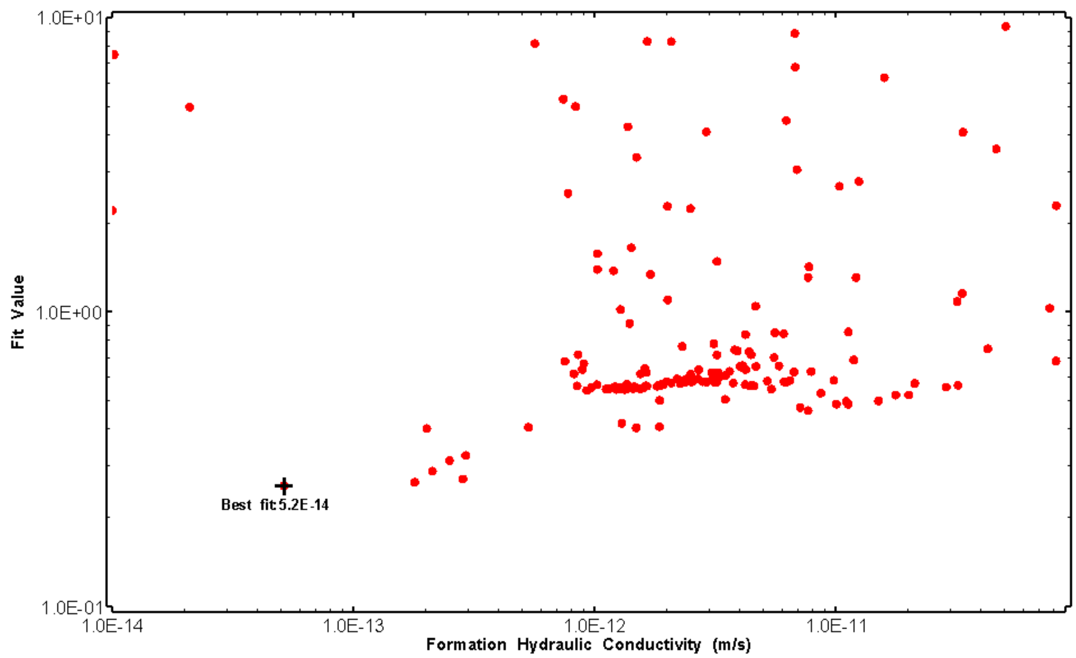

Figure 233: HT021 XY-scatter plot of formation hydraulic conductivity vs. fit value

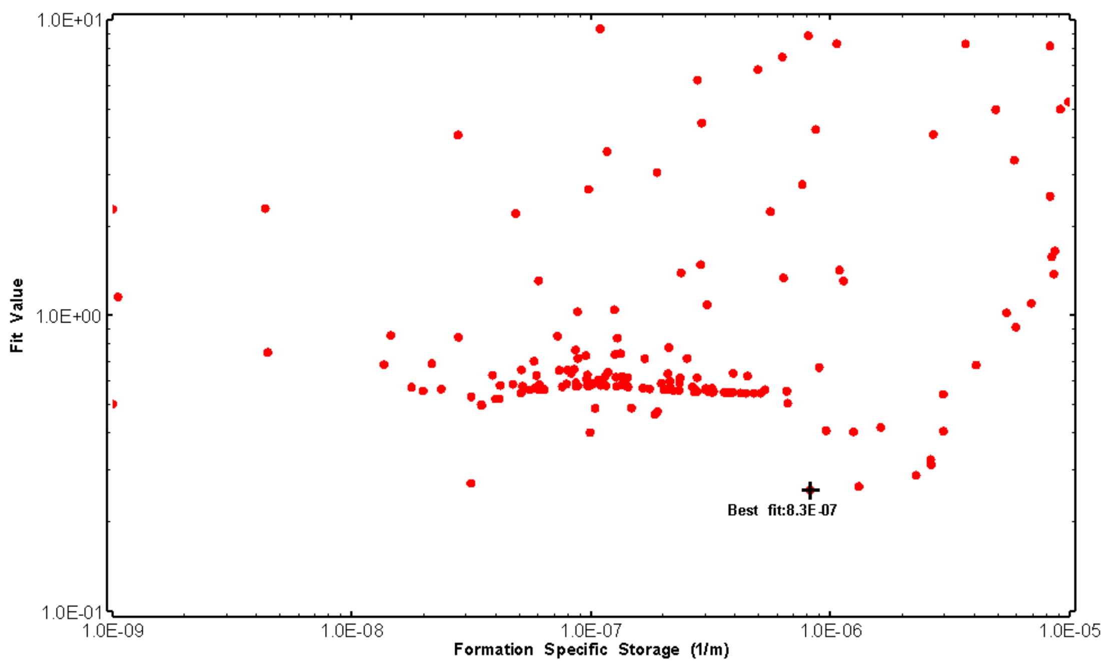

Figure 234: HT021 XY-scatter plot of formation specific storage vs. fit value

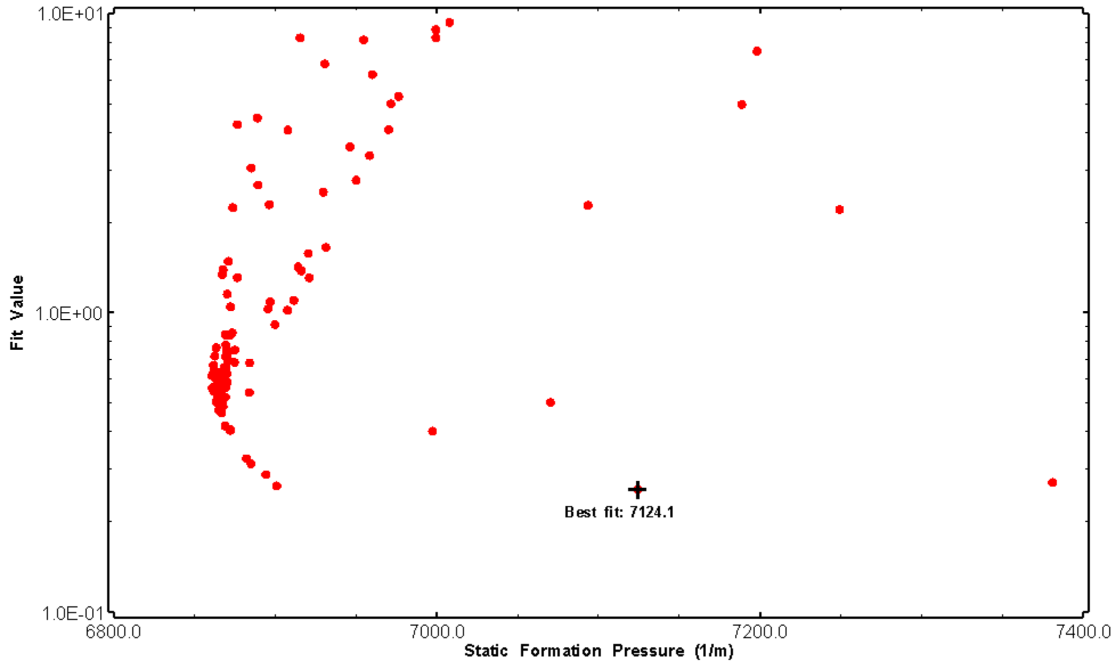

Figure 235: HT021 XY-scatter plot of static formation pressure vs. fit value

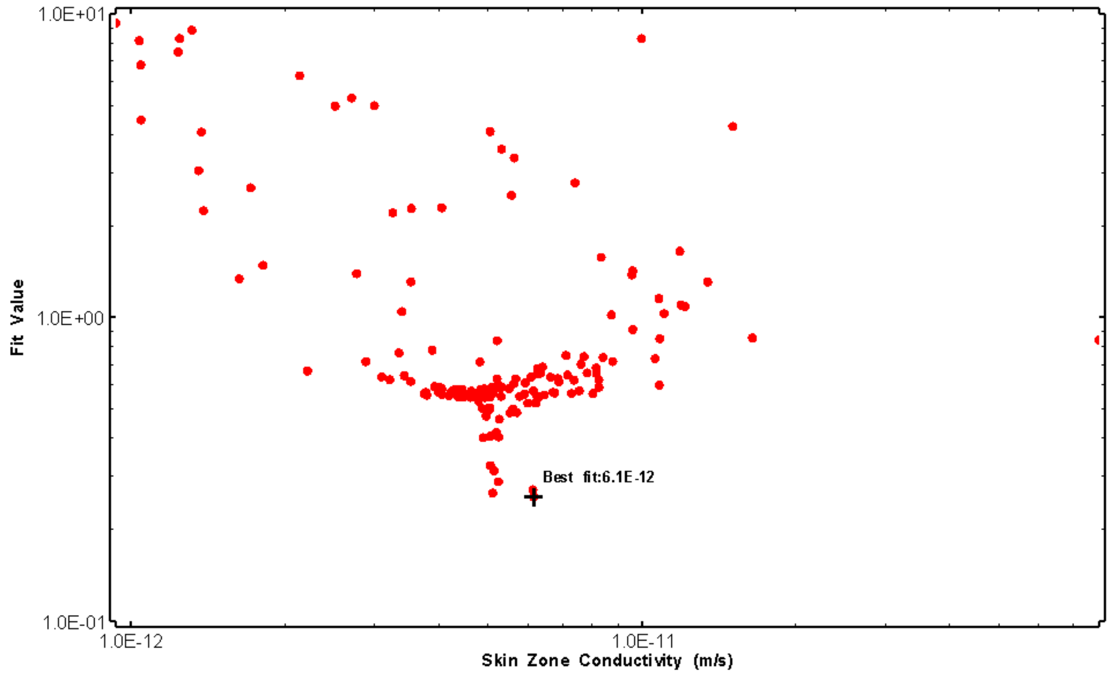

Figure 236: HT021 XY-scatter plot of skin zone conductivity vs. fit value

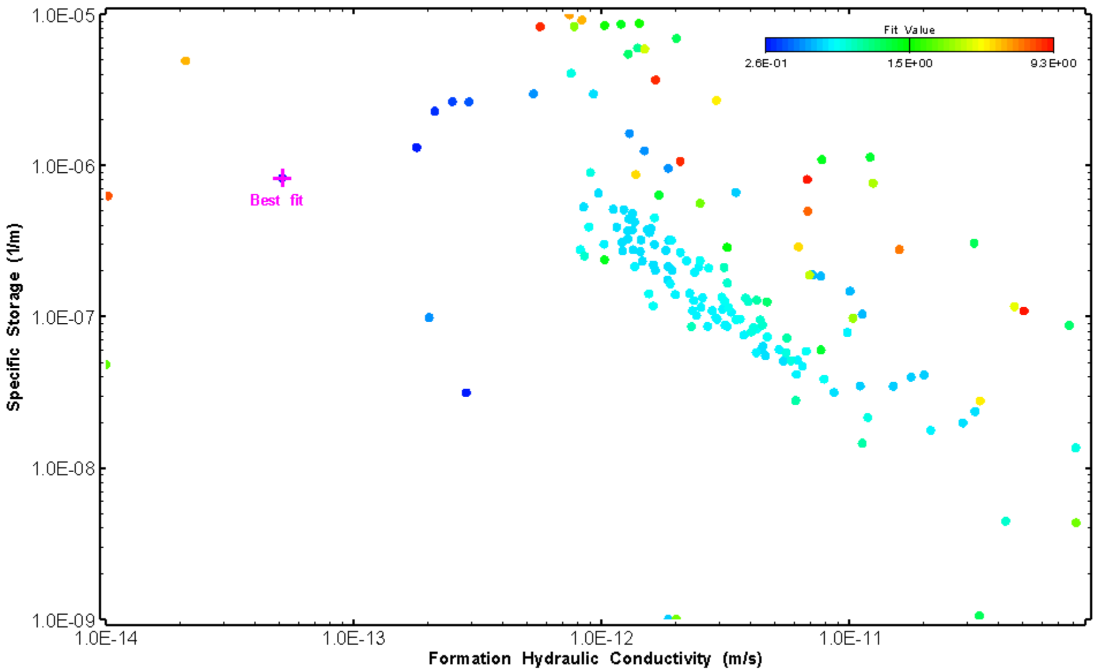

Figure 237: HT021 XY-scatter plot showing estimates of formation hydraulic conductivity and specific storage from perturbation analysis

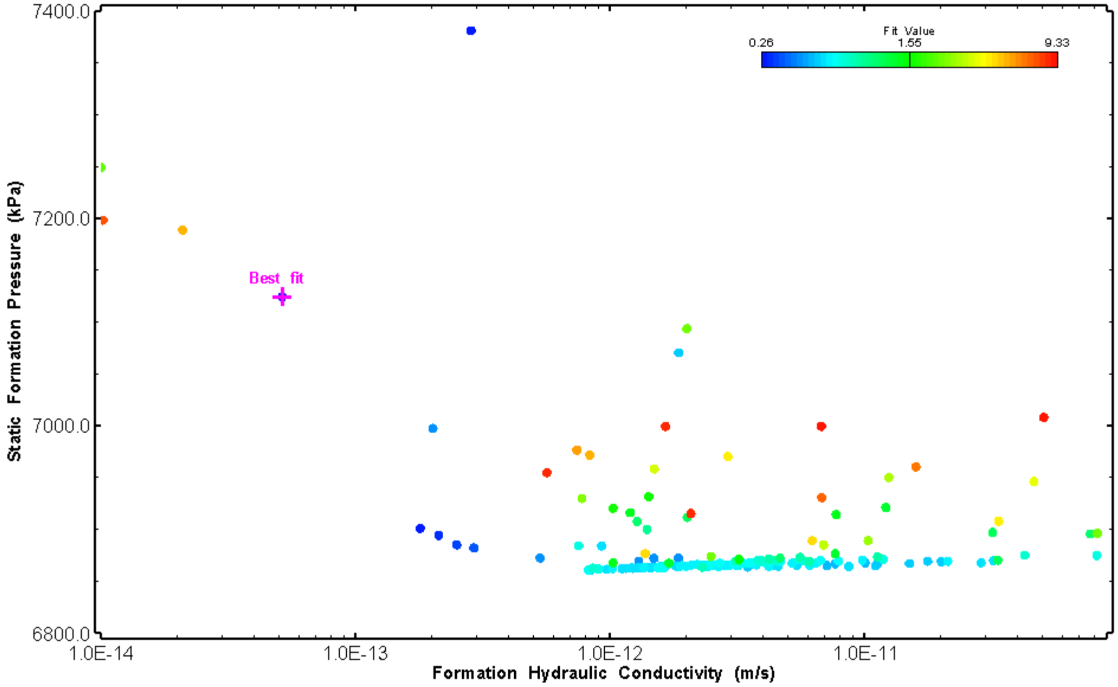

Figure 238: HT021 XY-scatter plot showing estimates of formation hydraulic conductivity and static formation pressure from perturbation analysis

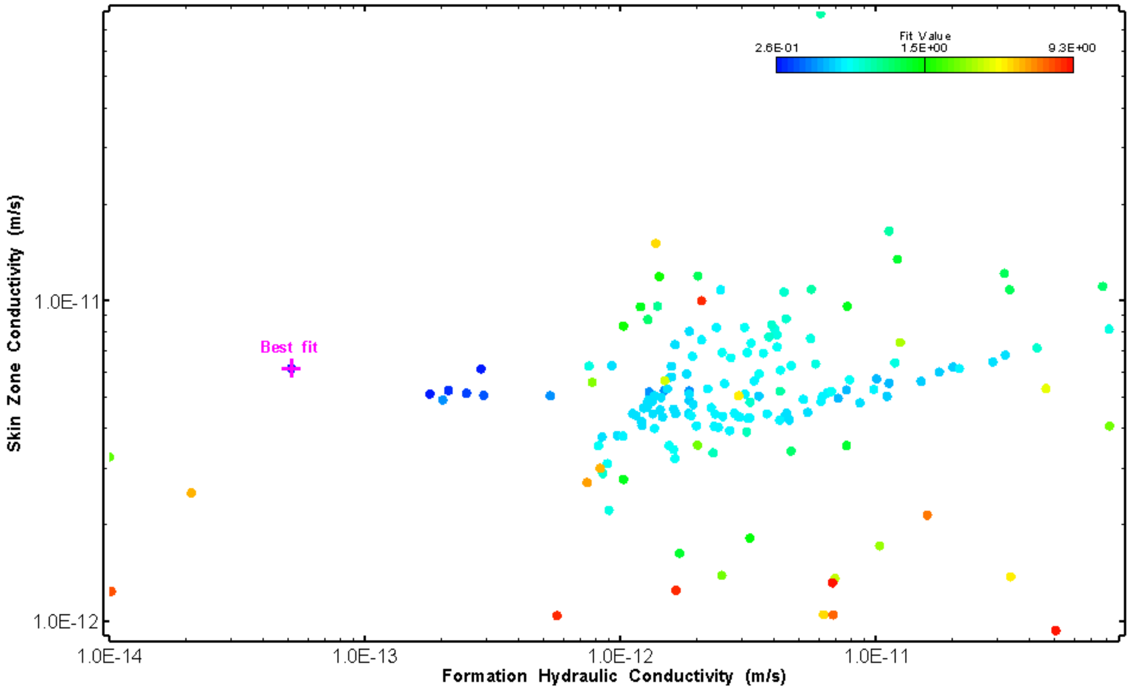

Figure 239: HT021 XY-scatter plot showing estimates of formation hydraulic conductivity and skin zone conductivity from perturbation analysis

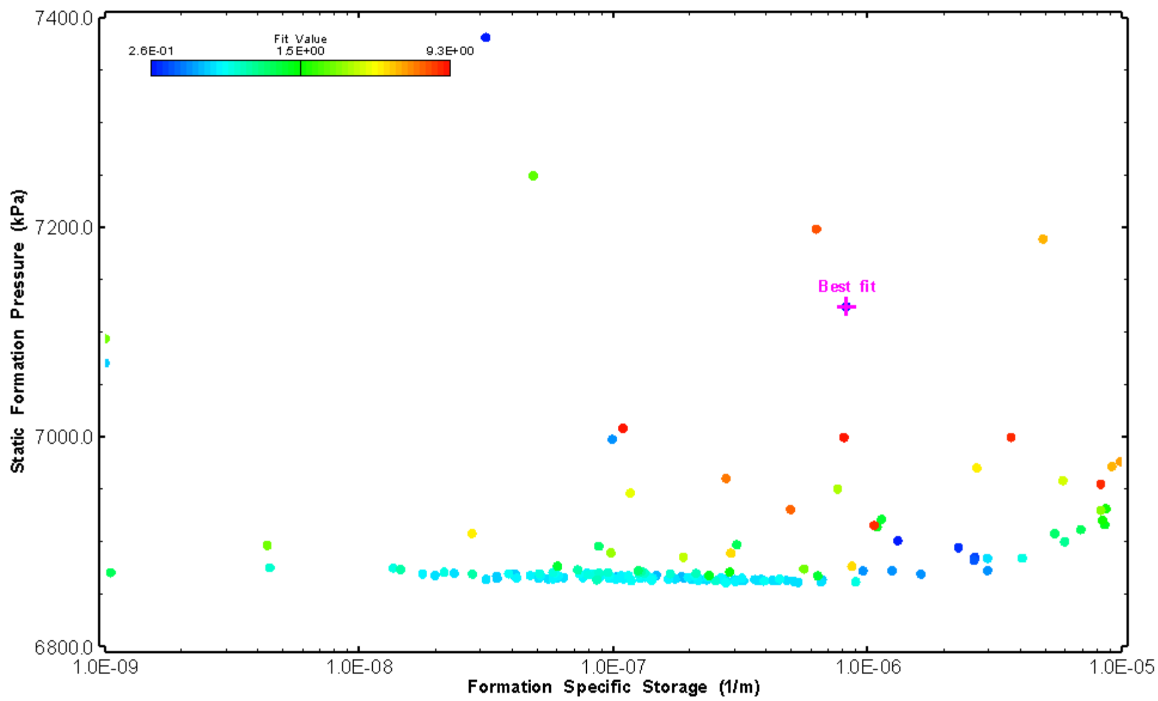

Figure 240: HT021 XY-scatter plot showing estimates of specific storage and static formation pressure from perturbation analysis

21.0 HT022 (793.14 – 813.17 M)

HT022 was selected to obtain continuous testing coverage from 600 to 800 m along hole. One broken fracture was observed in the core. A loss of drilling fluid was observed in this interval during drilling. A slight indication of flow was recorded during FFEC logging post-drilling.

The test was initiated with a shut-in pressure recovery phase (PSR). A pulse withdrawal test (PW) with a shut-in recovery was completed after the PSR phase.

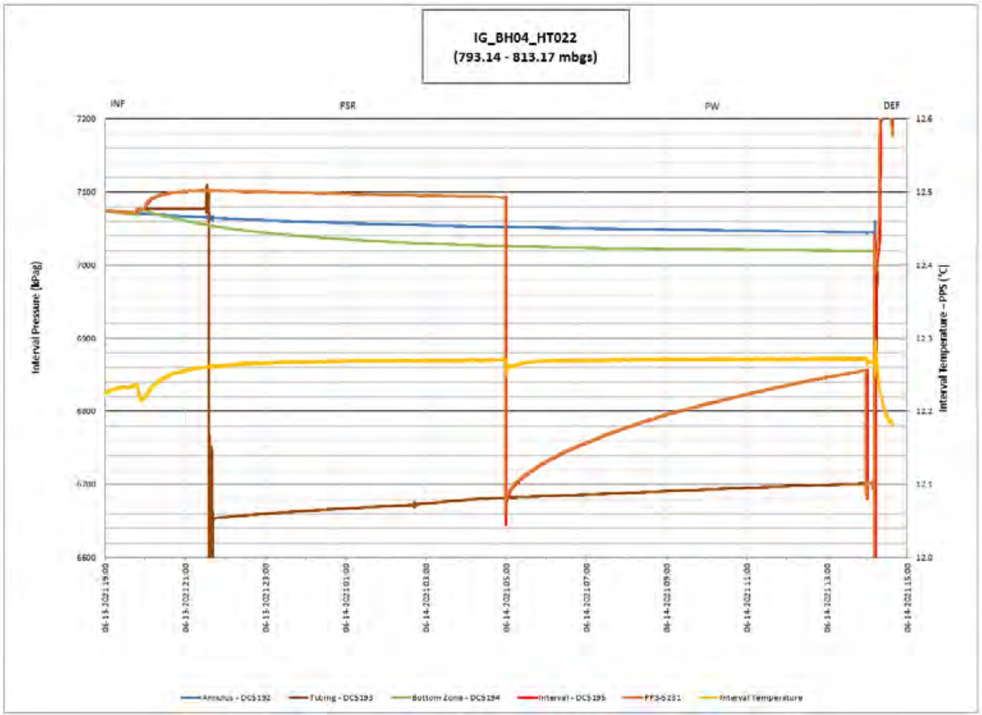

Figure 241: HT022 Annotated test plot showing monitored zone pressure and interval temperature.

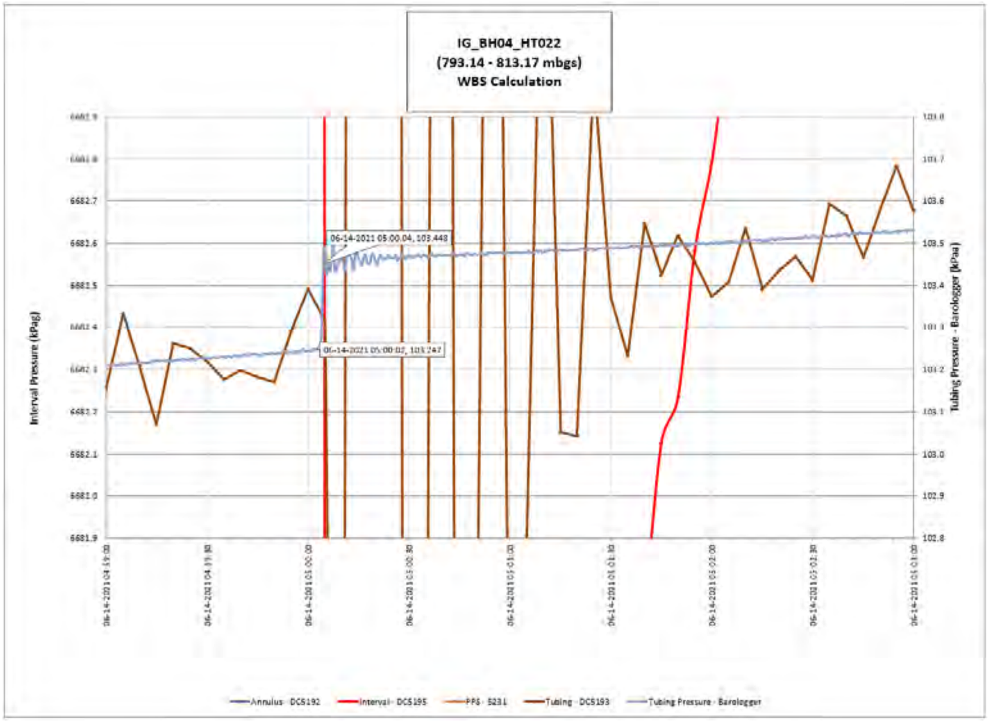

Figure 242: HT022 Tubing pressure during DHSIV activation. DHSIV Closed Wellbore Storage Estimate = 9E-11 m^3/Pa

Table 21: Summary of Analysis Results – HT022

	Formation conductivity	Skin zone conductivity	Static formation pressure	Formation specific storage	Radial thickness of skin	Flow dimension
	[m/s]	[m/s]	[kPa]	[1/m]	[m]	[–]
Best Fit	1.5E-12	8.5E-11	7104	8.3E-09	4.1E-02	1.5
Minimum	1.0E-14	3.3E-13	6648	1.0E-09	1.0E-02	1.0
Maximum	7.7E-12	1.0E-10	7557	5.5E-06	1.0E+00	3.0
Mean	4.9E-13	2.0E-11	7094	5.6E-07	7.0E-02	1.8
Median	2.4E-13	3.8E-12	7063	9.0E-08	3.4E-02	1.8
Geometric mean	2.1E-13	4.9E-12	7090	1.1E-07	3.9E-02	1.7

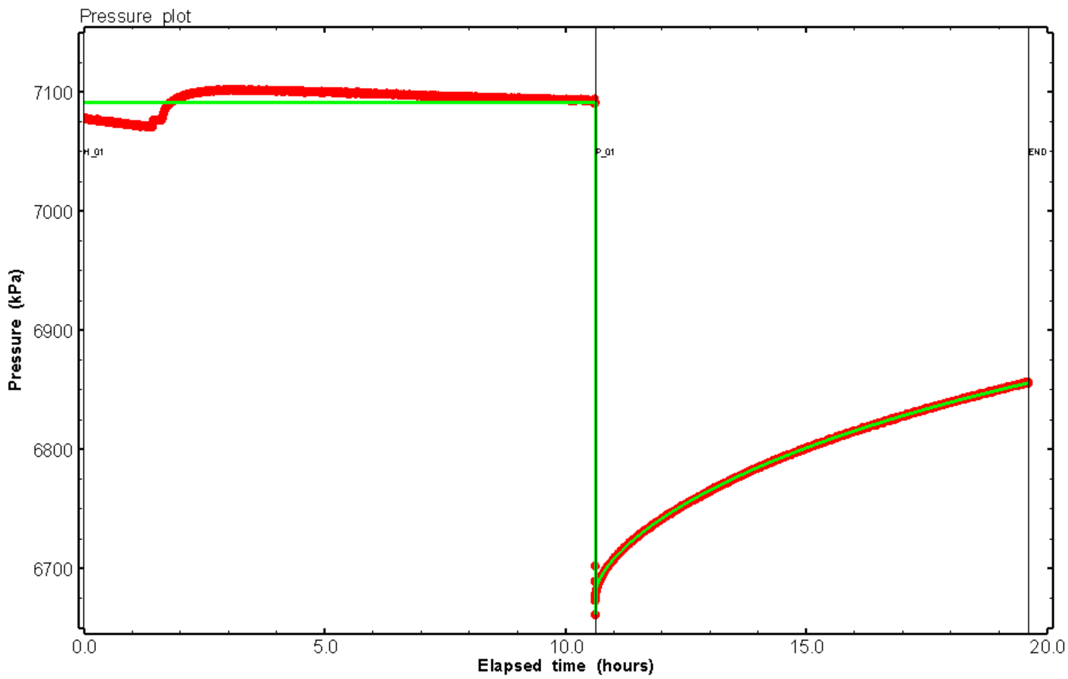

Figure 243: HT022 Pressure plot showing best-fit simulation and best fit results

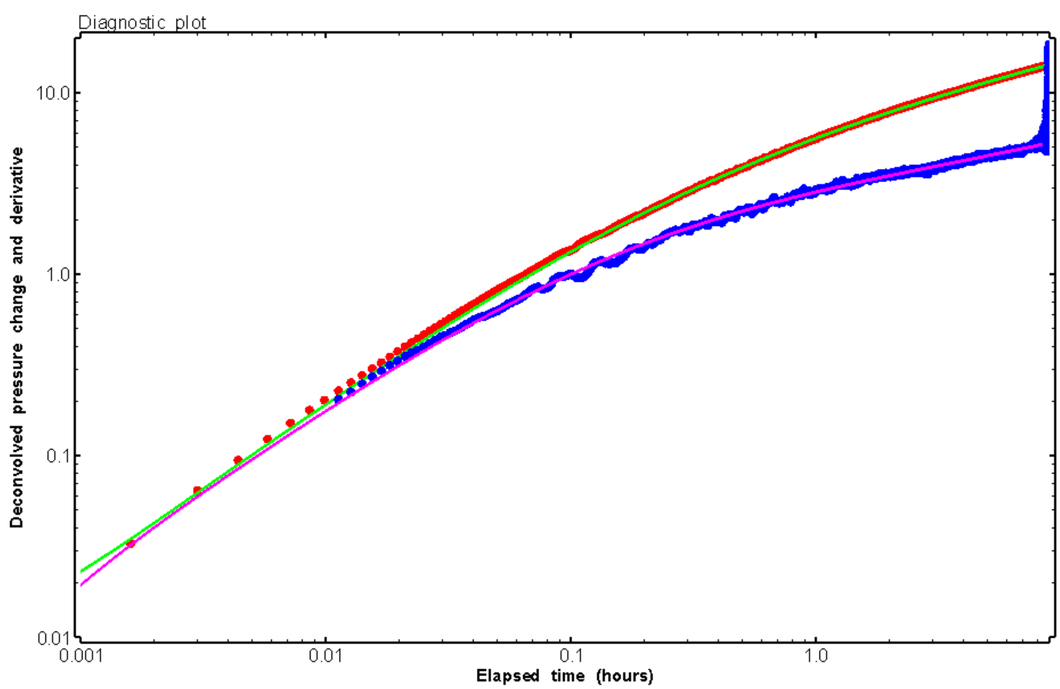

Figure 244: HT022 Deconvolved pressure change and derivative plot of the PW sequence showing best-fit simulation

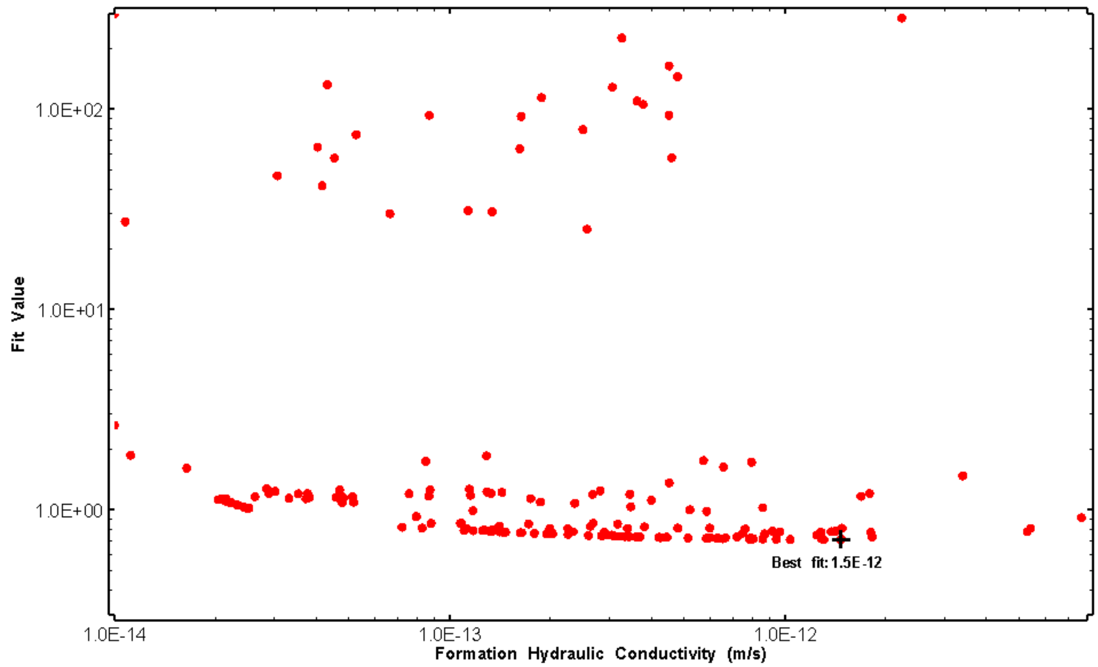

Figure 245: HT022 XY-scatter plot of formation hydraulic conductivity vs. fit value

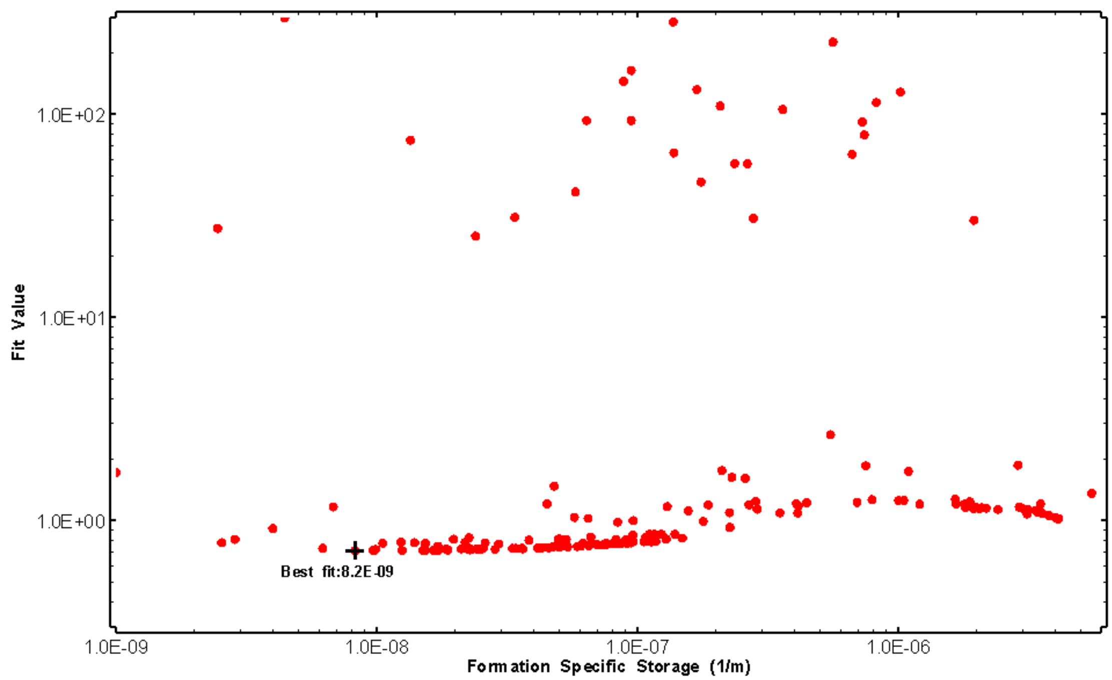

Figure 246: HT022 XY-scatter plot of formation specific storage vs. fit value

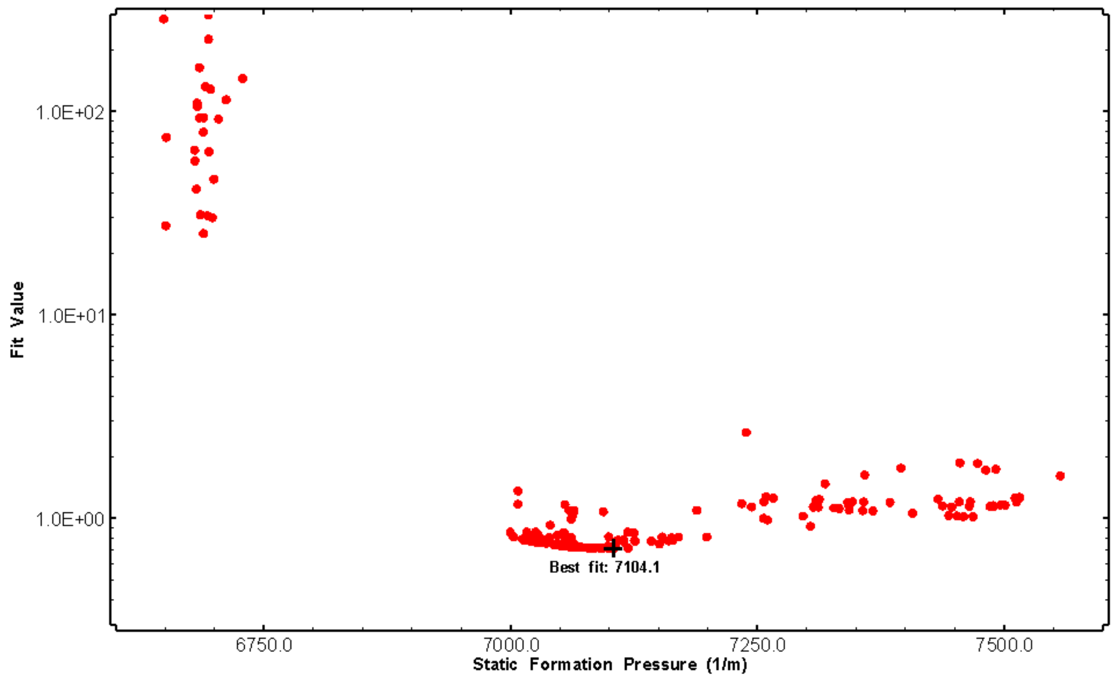

Figure 247: HT022 XY-scatter plot of static formation pressure vs. fit value

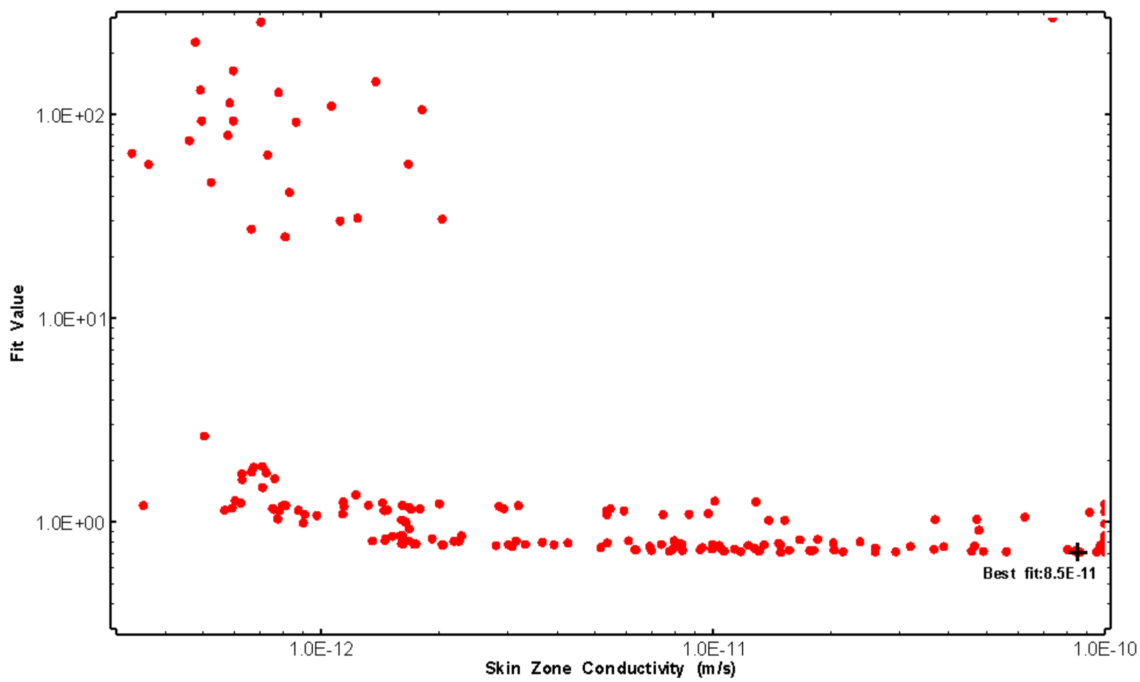

Figure 248: HT022 XY-scatter plot of skin zone conductivity vs. fit value

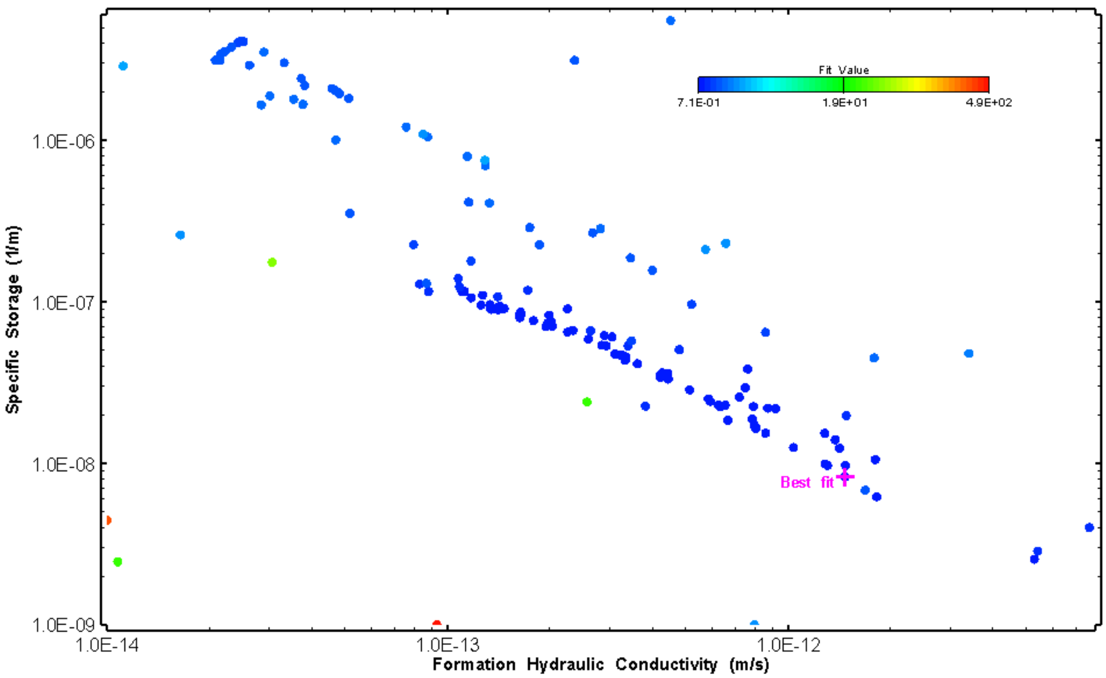

Figure 249: HT022 XY-scatter plot showing estimates of formation hydraulic conductivity and specific storage from perturbation analysis

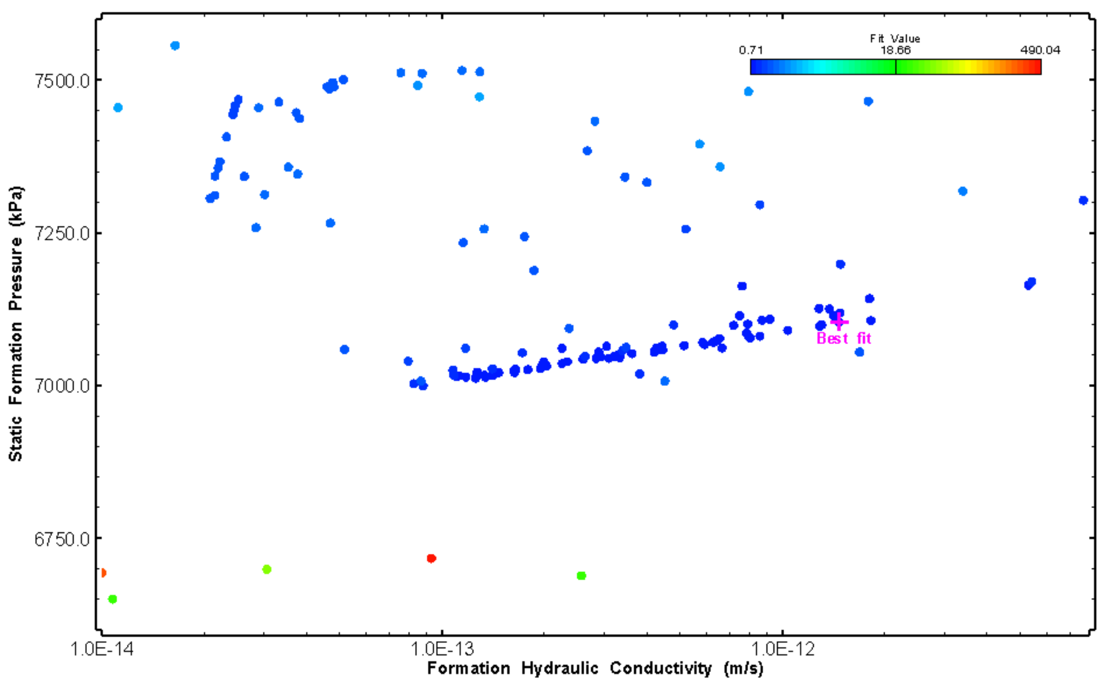

Figure 250: HT022 XY-scatter plot showing estimates of formation hydraulic conductivity and static formation pressure from perturbation analysis

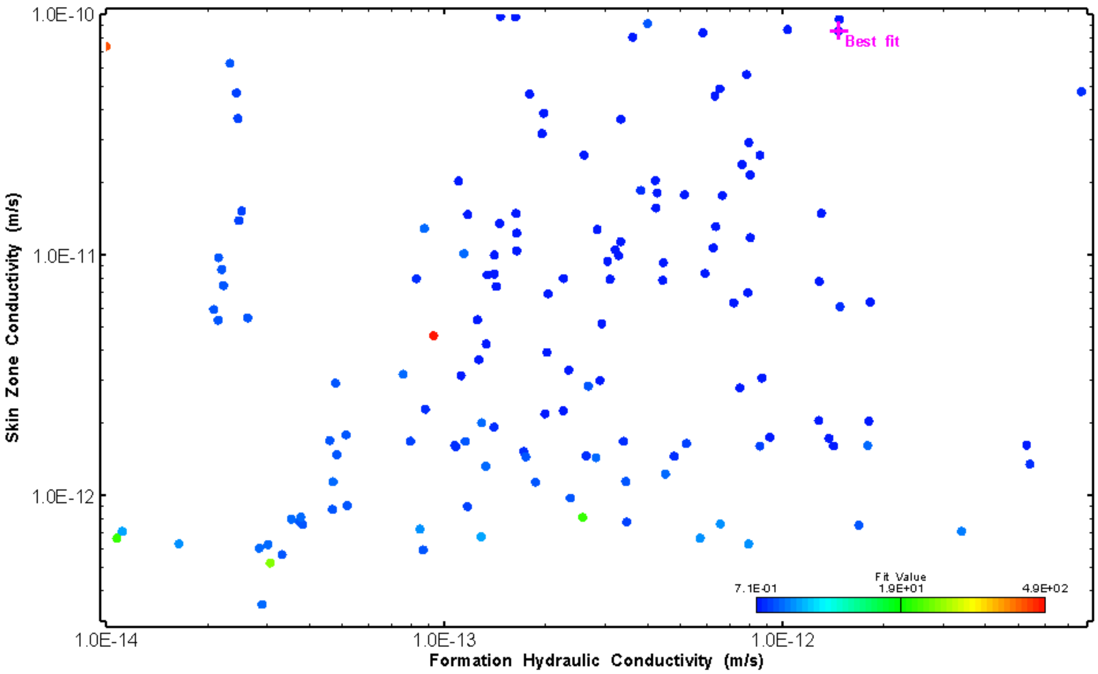

Figure 251: HT022 XY-scatter plot showing estimates of formation hydraulic conductivity and skin zone conductivity from perturbation analysis

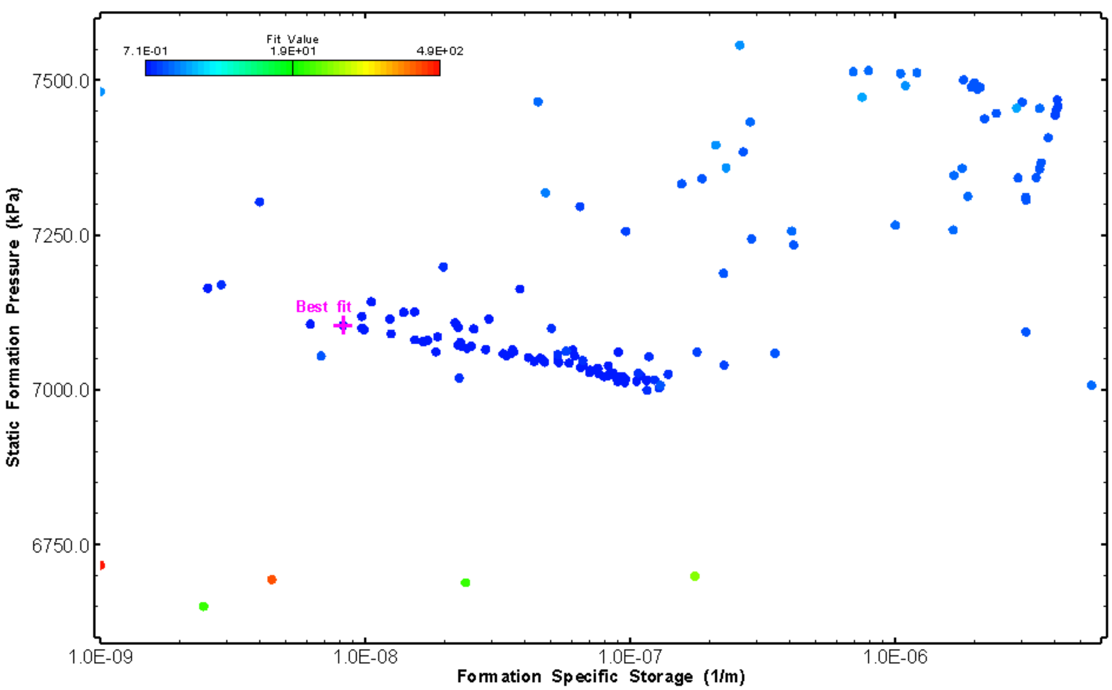

Figure 252: HT022 XY-scatter plot showing estimates of specific storage and static formation pressure from perturbation analysis

22.0 HT024 (849.93 – 869.96 M)

HT024 was selected to test an intact interval with a dyke. Zero broken fractures were observed in the core. A loss of drilling fluid was observed in this interval during drilling. An indication of flow was recorded during FFEC logging post-drilling.

The test was initiated with a shut-in pressure recovery phase (PSR). A pulse withdrawal test (PW) with a shut-in recovery was completed after the PSR phase.

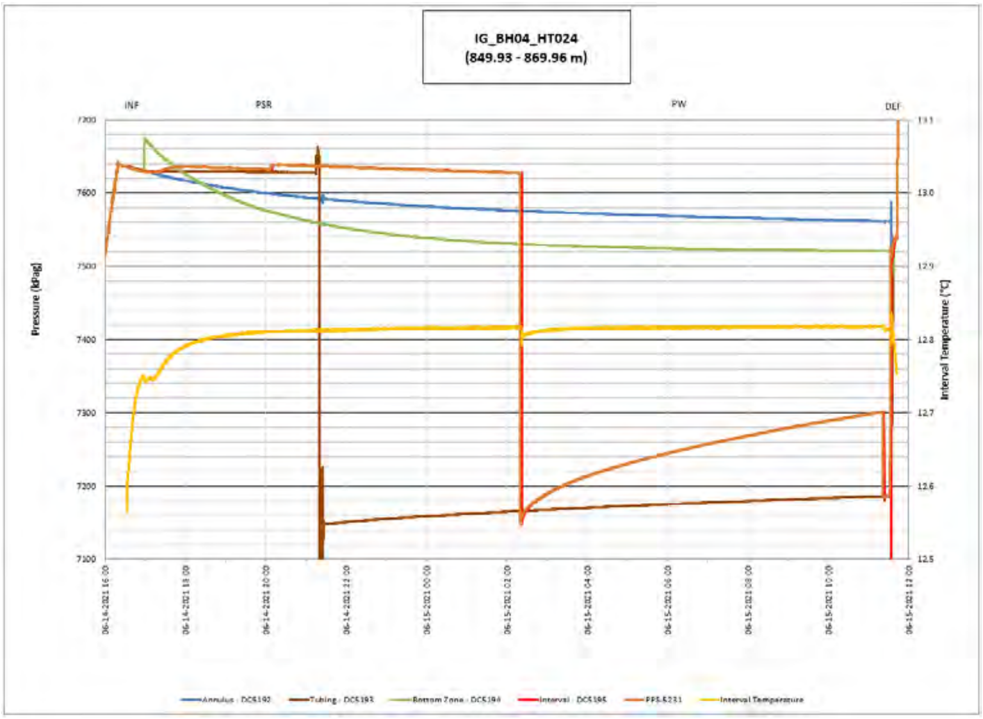

Figure 253: HT024 Annotated test plot showing monitored zone pressure and interval temperature.

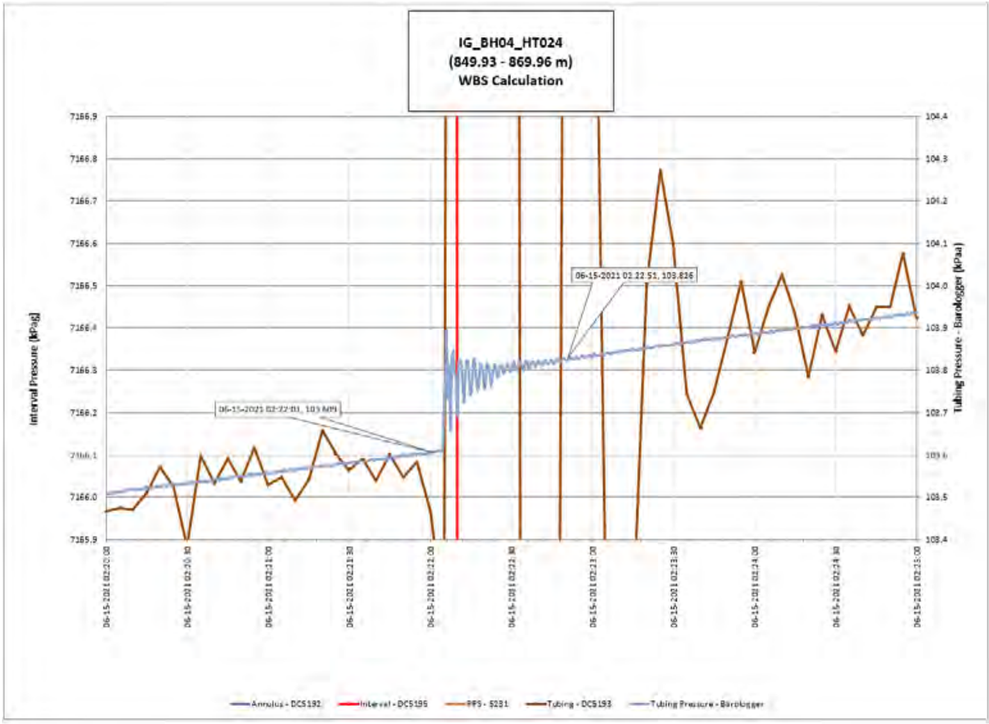

Figure 254: HT024 Tubing pressure during DHSIV activation. DHSIV Closed Wellbore Storage Estimate = 7E-11 m³/Pa

Table 22: Summary of Analysis Results – HT024

	Formation conductivity	Skin zone conductivity	Static formation pressure	Formation specific storage	Radial thickness of skin	Flow dimension
	[m/s]	[m/s]	[kPa]	[1/m]	[m]	[–]
Best Fit	3.4E-11	1.9E-13	7856	7.8E-09	2.9E-01	1.0
Minimum	1.0E-15	8.4E-14	7515	1.0E-09	9.9E-03	1.0
Maximum	9.6E-11	9.5E-11	7999	9.8E-06	9.6E-01	3.0
Mean	4.4E-12	1.3E-12	7813	7.6E-07	1.4E-01	1.6
Median	7.0E-14	1.5E-13	7836	1.9E-07	5.4E-02	1.5
Geometric mean	1.7E-13	2.0E-13	7812	1.0E-07	7.5E-02	1.5

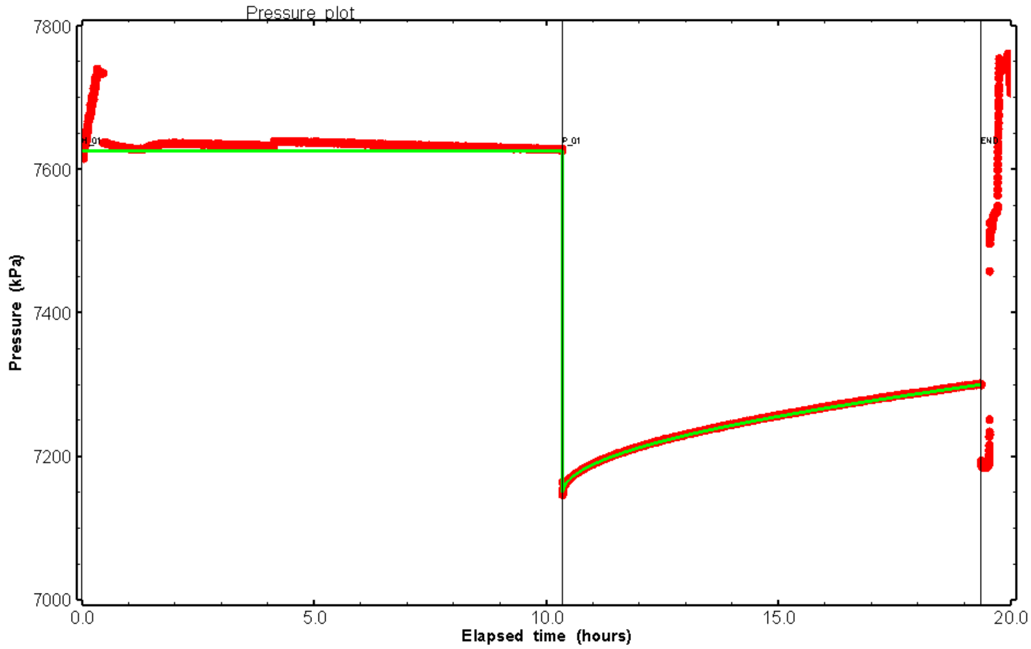

Figure 255: HT024 Pressure plot showing best-fit simulation and best fit results

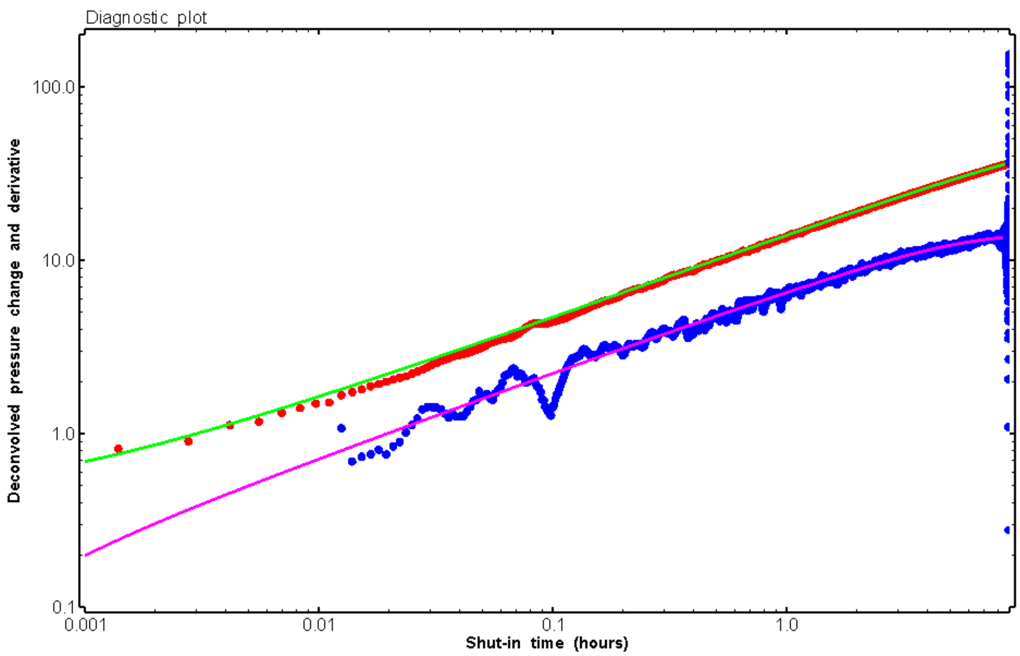

Figure 256: HT024 Deconvolved pressure change and derivative plot of the PW sequence showing best-fit simulation

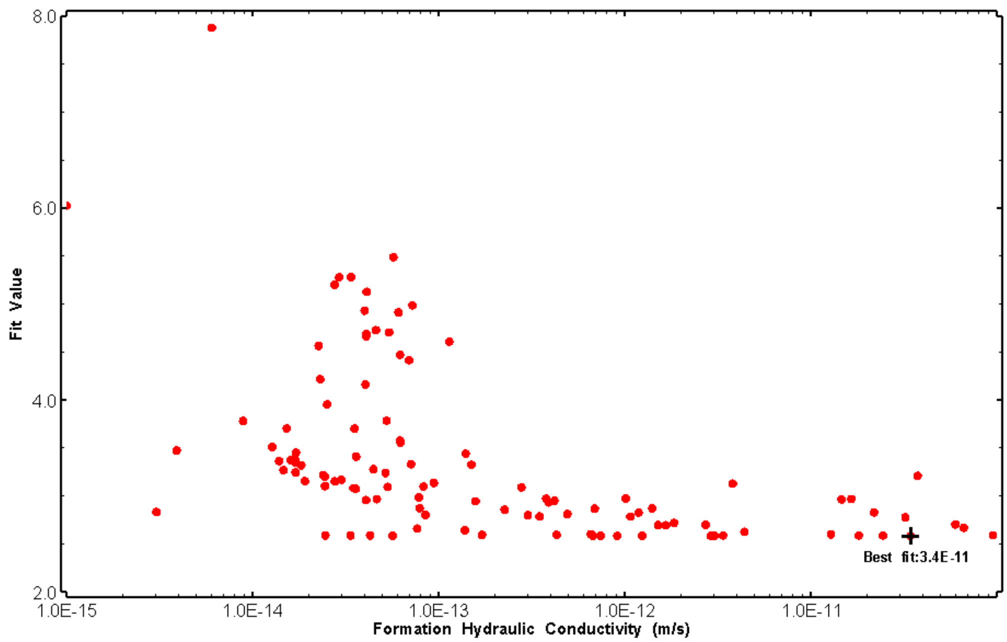

Figure 257: HT024 XY-scatter plot of formation hydraulic conductivity vs. fit value

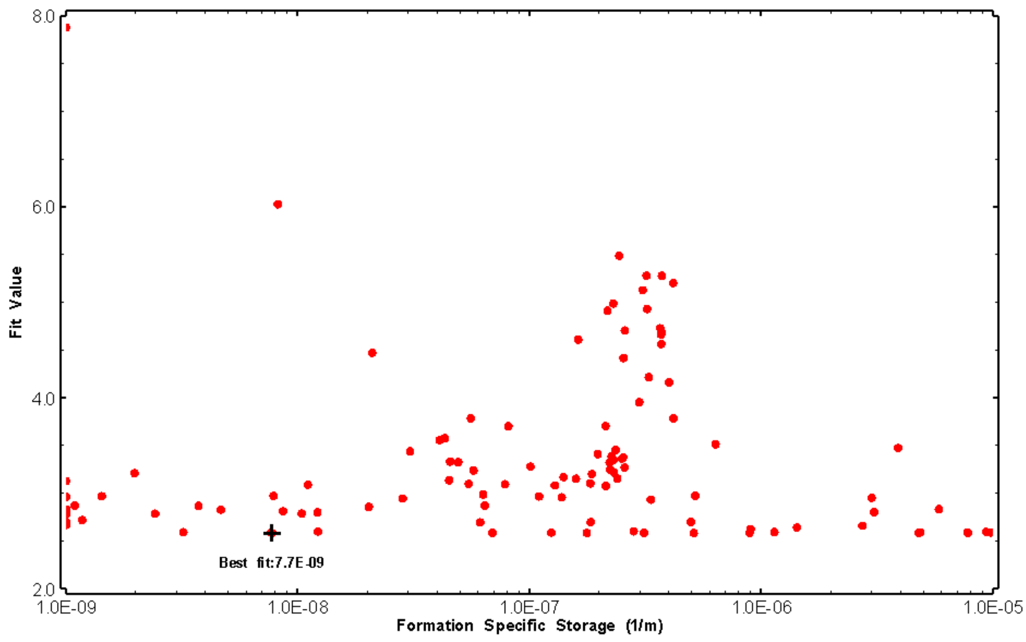

Figure 258: HT024 XY-scatter plot of formation specific storage vs. fit value

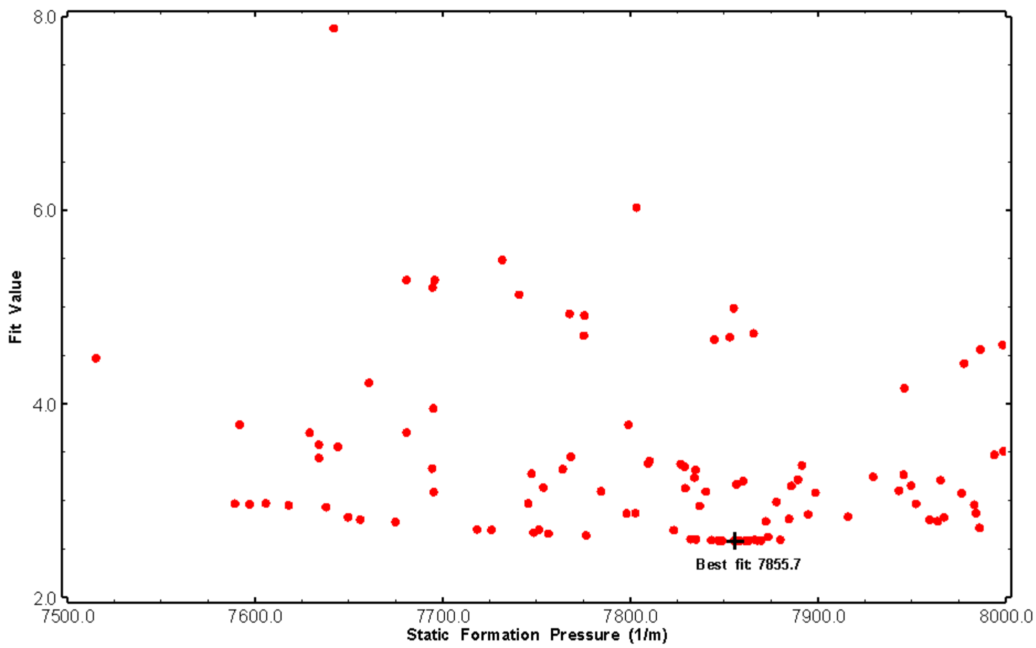

Figure 259: HT024 XY-scatter plot of static formation pressure vs. fit value

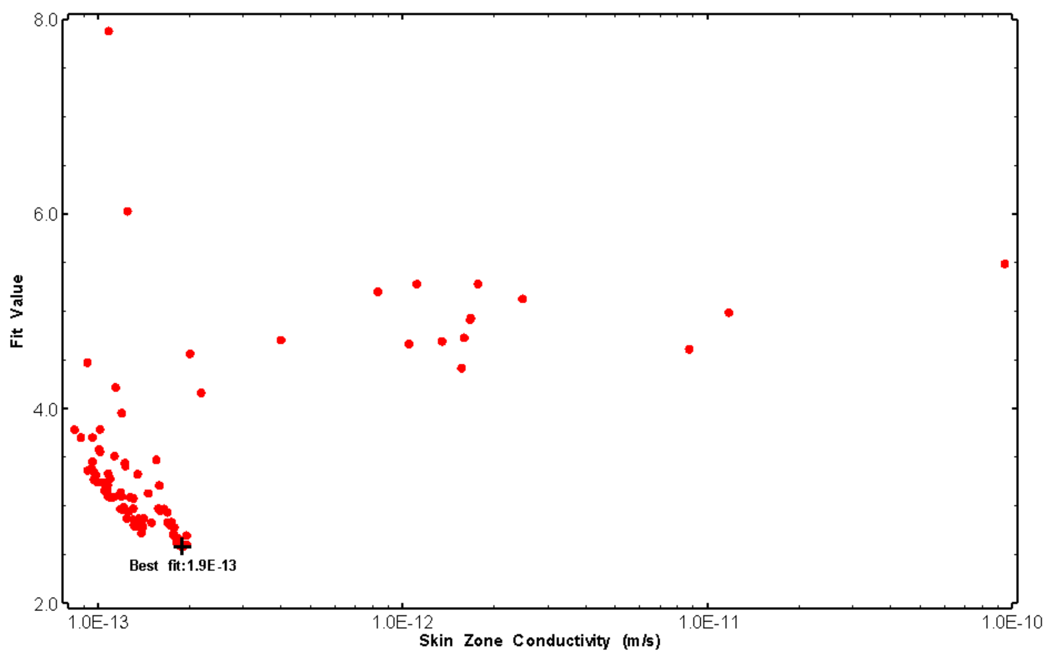

Figure 260: HT024 XY-scatter plot of skin zone conductivity vs. fit value

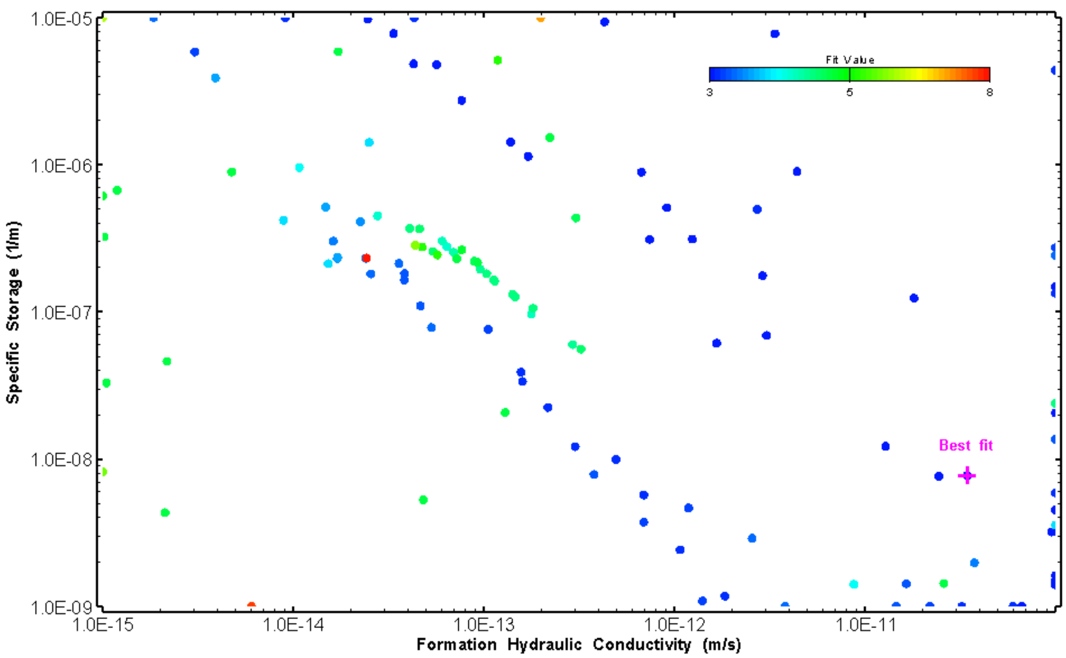

Figure 261: HT024 XY-scatter plot showing estimates of formation hydraulic conductivity and specific storage from perturbation analysis

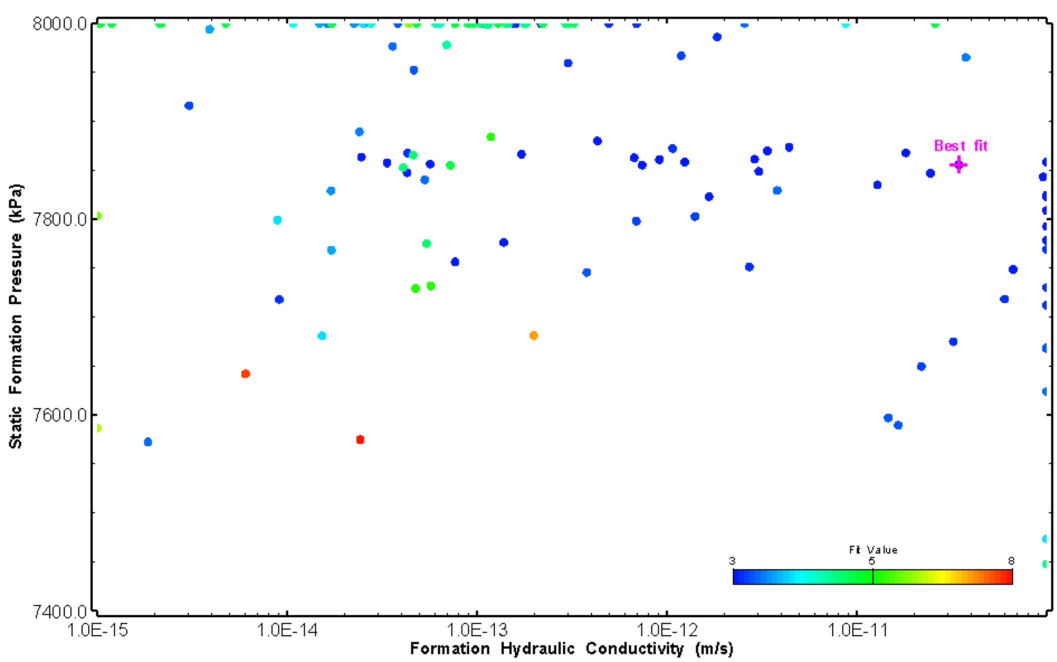

Figure 262: HT024 XY-scatter plot showing estimates of formation hydraulic conductivity and static formation pressure from perturbation analysis

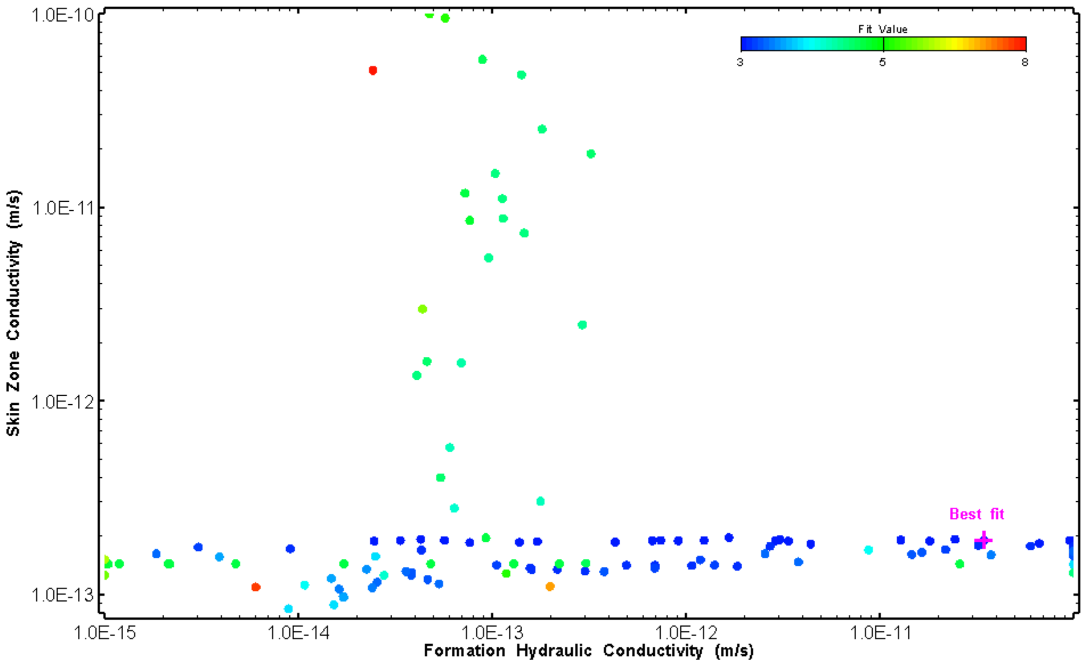

Figure 263: HT024 XY-scatter plot showing estimates of formation hydraulic conductivity and skin zone conductivity from perturbation analysis

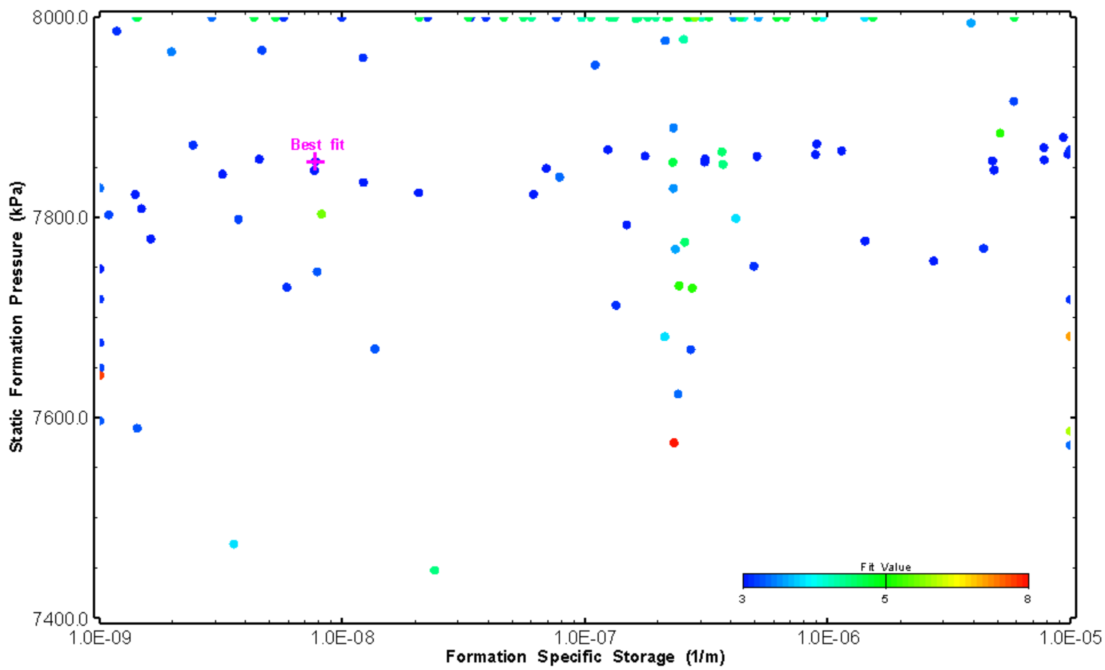

Figure 264: HT024 XY-scatter plot showing estimates of specific storage and static formation pressure from perturbation analysis

23.0 HT025 (881.24 – 901.27 M)

HT025 was selected to test a geological transition zone with a dyke. Seven broken fractures were observed in the core. A loss of drilling fluid was observed in this interval during drilling. A slight indication of flow was recorded during FFEC logging post-drilling.

The test was initiated with a shut-in pressure recovery phase (PSR). A pulse withdrawal test (PW) with a shut-in recovery was completed after the PSR phase.

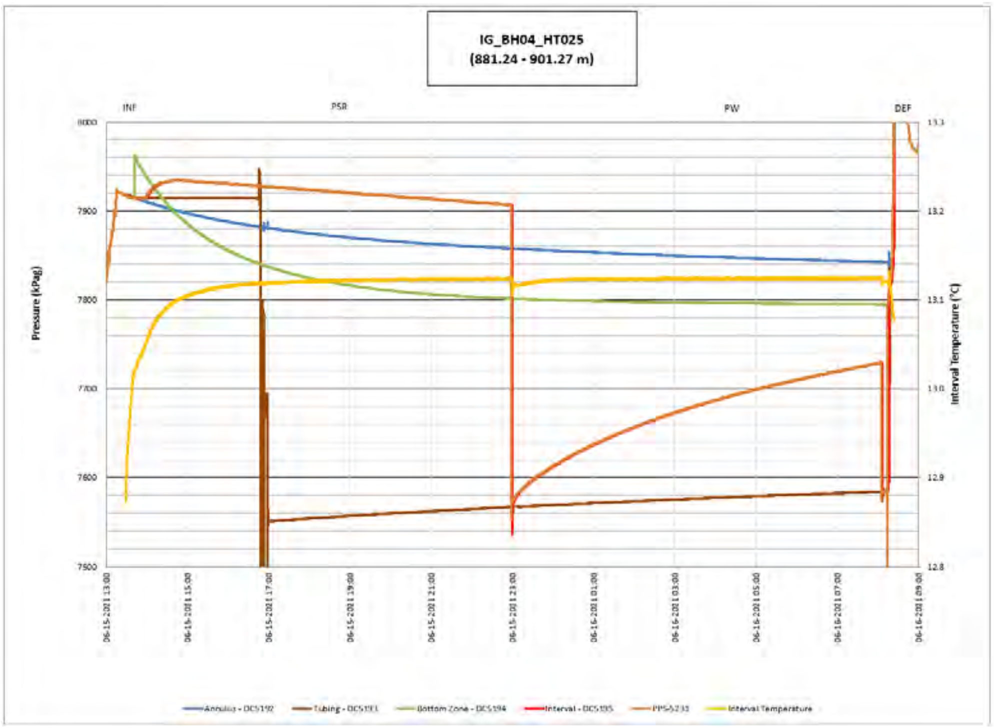

Figure 265: HT025 Annotated test plot showing monitored zone pressure and interval temperature.

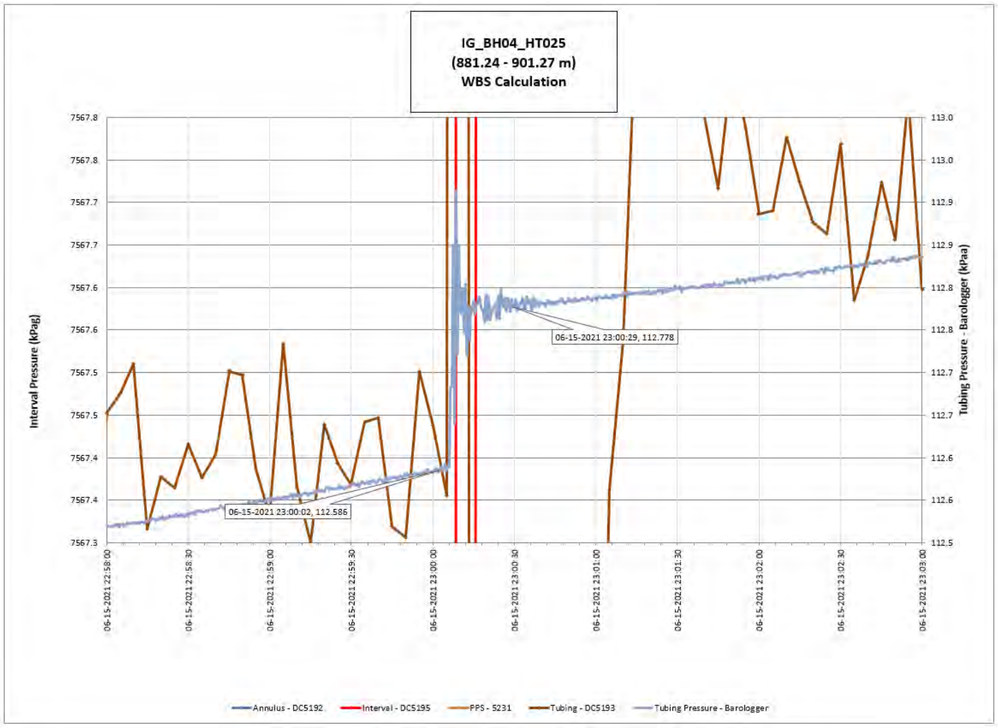

Figure 266: HT025 Tubing pressure during DHSIV activation. DHSIV Closed Wellbore Storage Estimate = 1E-10 m^3/Pa

Table 23: Summary of Analysis Results – HT025

	Formation conductivity	Skin zone conductivity	Static formation pressure	Formation specific storage	Radial thickness of skin	Flow dimension
	[m/s]	[m/s]	[kPa]	[1/m]	[m]	[–]
Best Fit	1.8E-13	2.7E-13	7879	8.1E-08	2.0E-01	2.3
Minimum	1.5E-15	1.1E-13	7793	1.3E-09	1.1E-03	1.1
Maximum	1.5E-11	5.0E-11	7906	9.9E-06	1.0E+00	3.0
Mean	6.1E-13	8.5E-13	7872	4.3E-07	2.0E-01	2.1
Median	3.2E-13	3.1E-13	7874	2.2E-07	1.0E-01	2.1
Geometric mean	3.1E-13	3.5E-13	7872	1.8E-07	1.0E-01	2.1

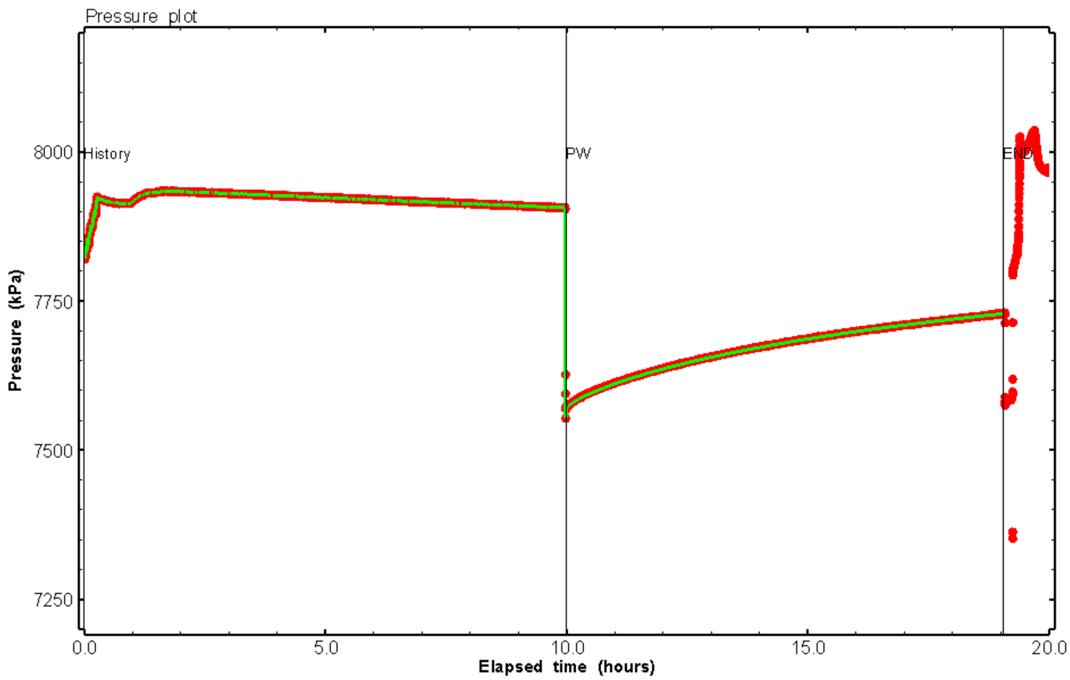

Figure 267: HT025 Pressure plot showing best-fit simulation and best fit results

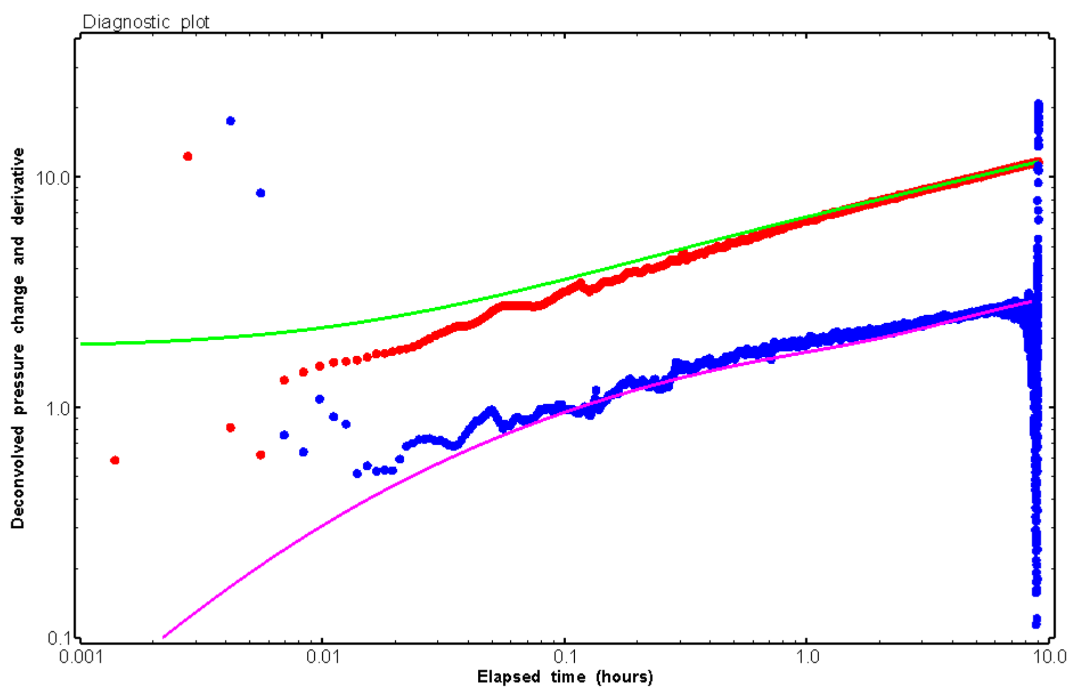

Figure 268: HT025 Deconvolved pressure change and derivative plot of the PW sequence showing best-fit simulation

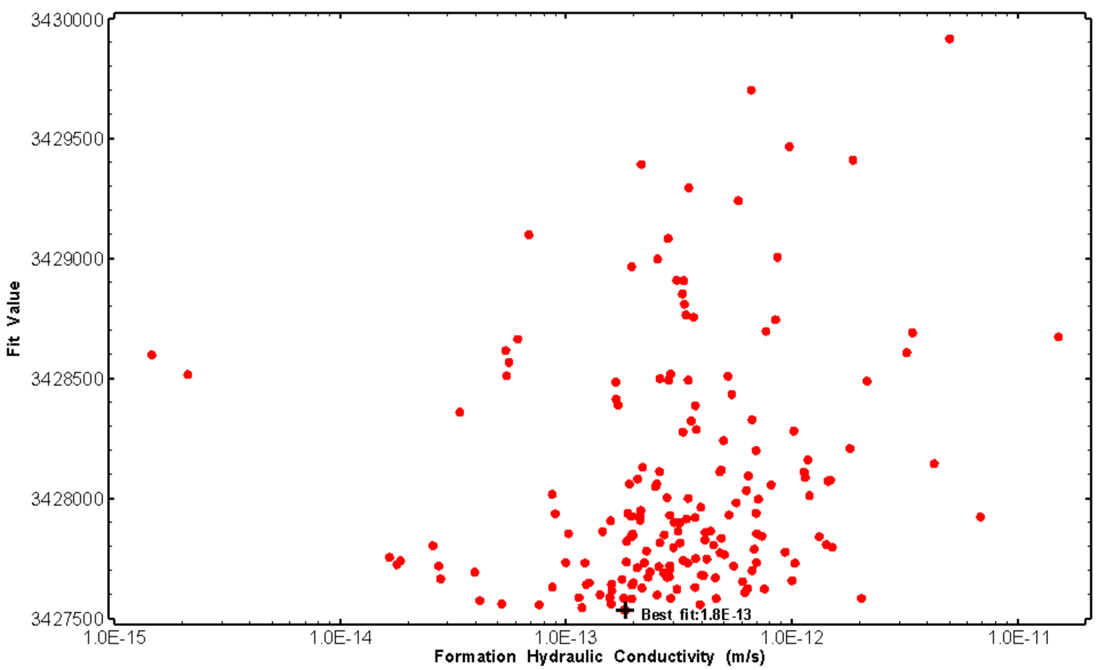

Figure 269: HT025 XY-scatter plot of formation hydraulic conductivity vs. fit value

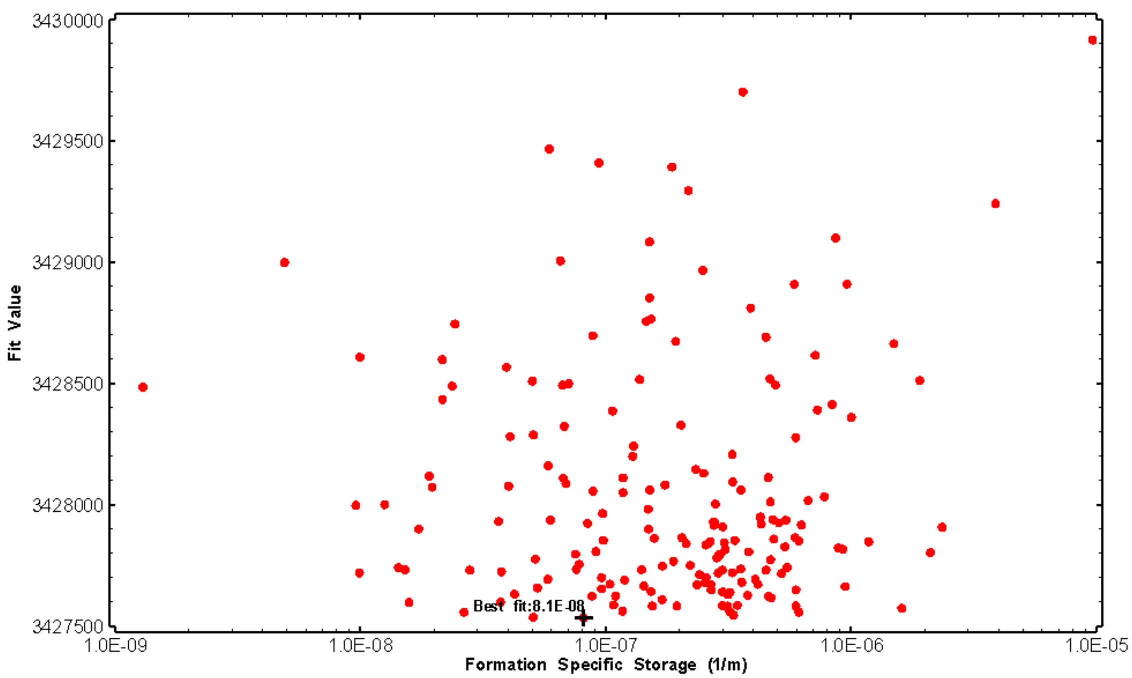

Figure 270: HT025 XY-scatter plot of formation specific storage vs. fit value

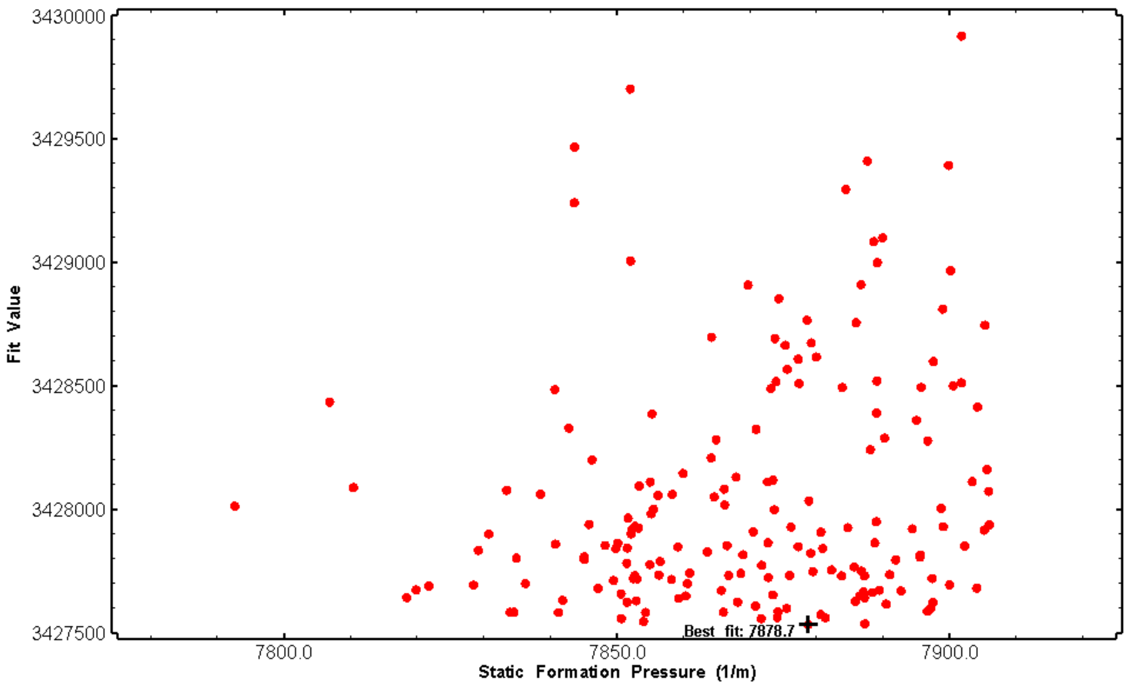

Figure 271: HT025 XY-scatter plot of static formation pressure vs. fit value

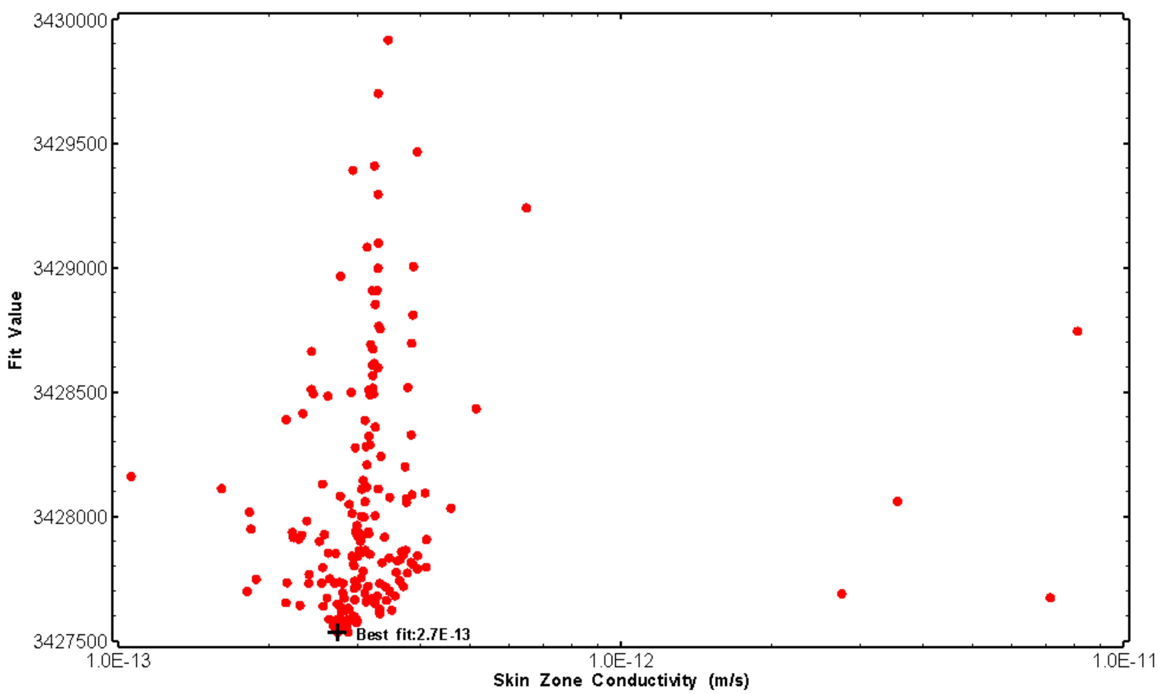

Figure 272: HT025 XY-scatter plot of skin zone conductivity vs. fit value

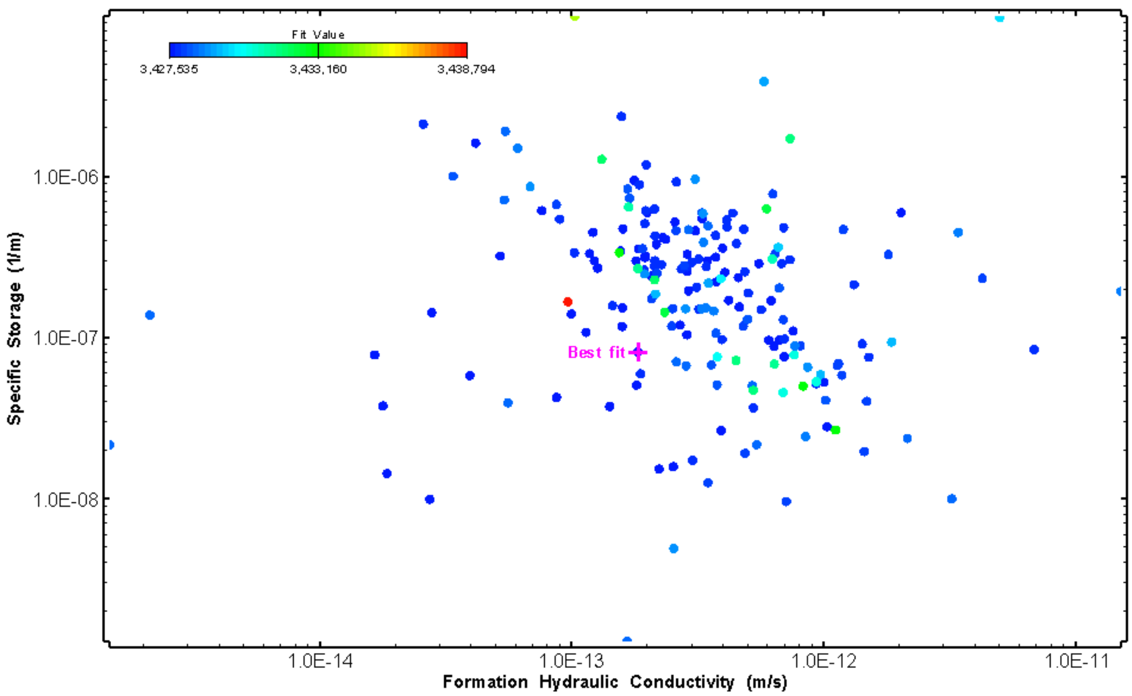

Figure 273: HT025 XY-scatter plot showing estimates of formation hydraulic conductivity and specific storage from perturbation analysis

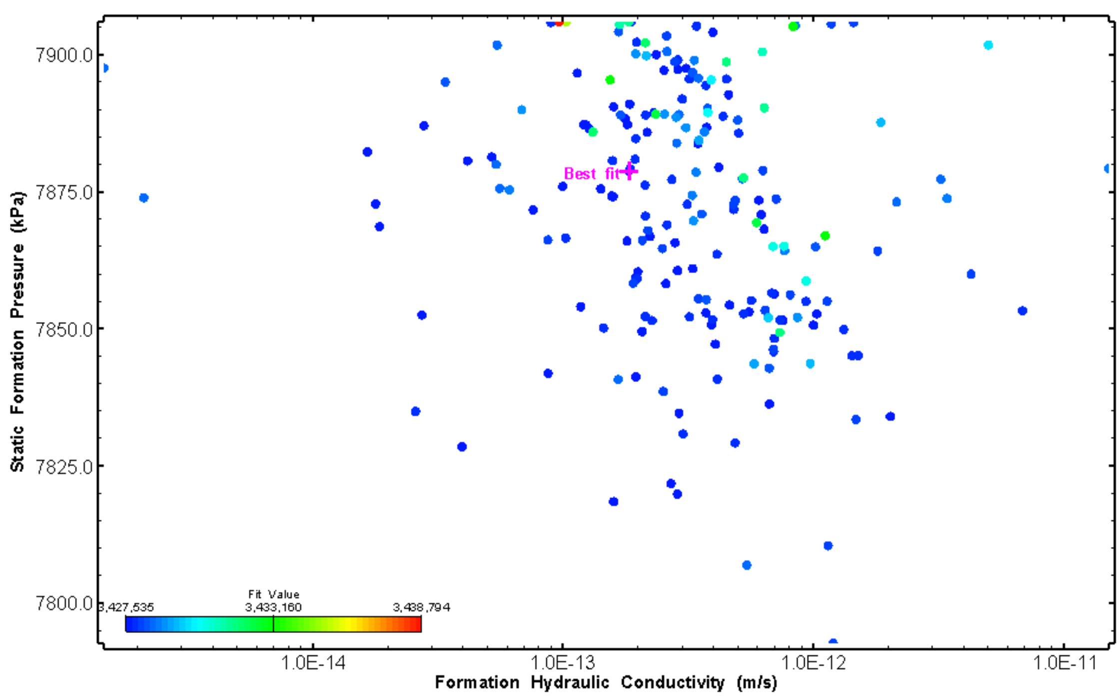

Figure 274: HT025 XY-scatter plot showing estimates of formation hydraulic conductivity and static formation pressure from perturbation analysis

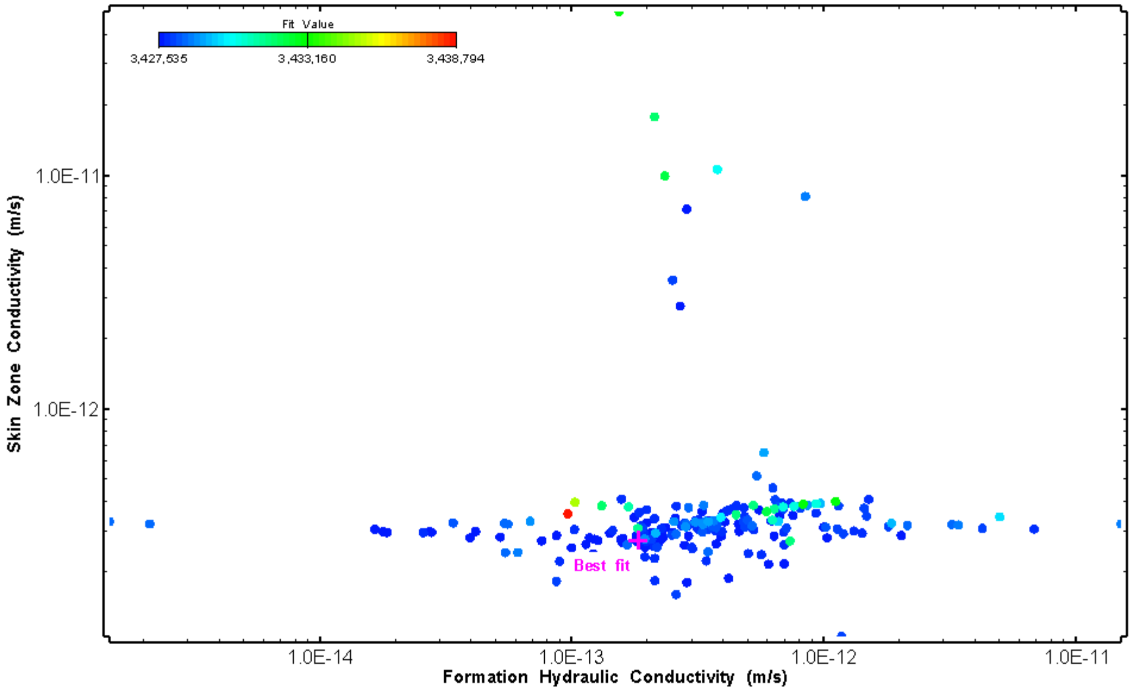

Figure 275: HT025 XY-scatter plot showing estimates of formation hydraulic conductivity and skin zone conductivity from perturbation analysis

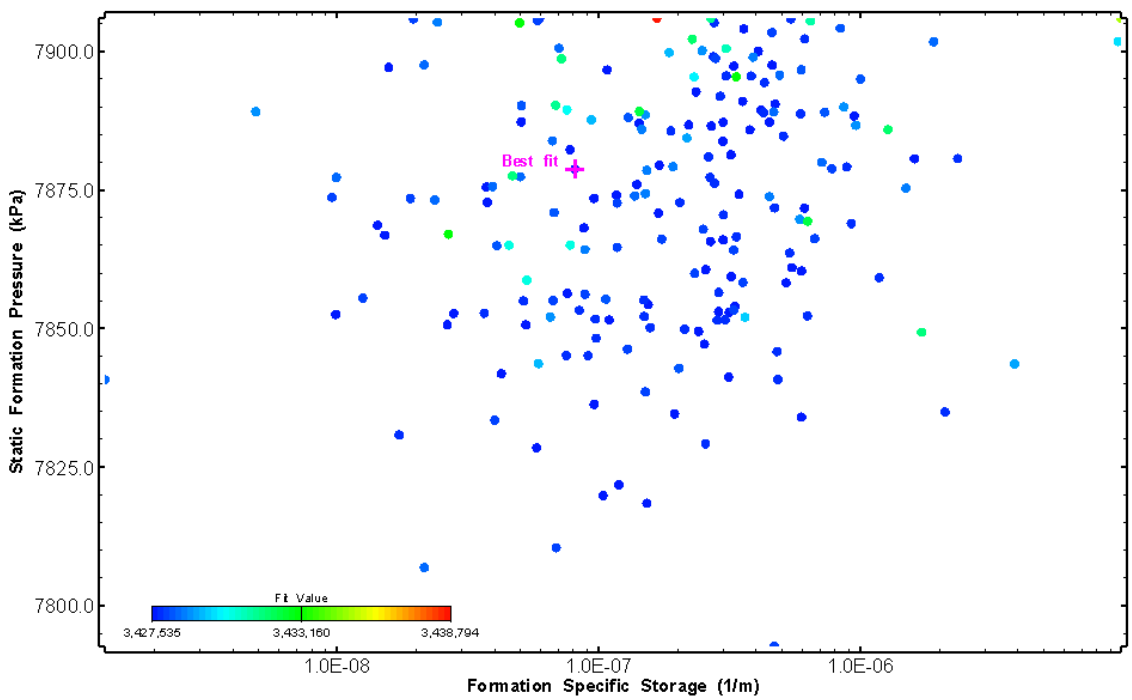

Figure 276: HT025 XY-scatter plot showing estimates of specific storage and static formation pressure from perturbation analysis

24.0 HT026 (902.64 – 922.67 M)

HT026 was selected to test an amphibolite dyke. Seven broken fractures were observed in the core. A loss of drilling fluid was observed in this interval during drilling. A slight indication of flow was recorded during FFEC logging post-drilling.

The test was initiated with a shut-in pressure recovery phase (PSR). A pulse withdrawal test (PW) with a shut-in recovery was completed after the PSR phase.

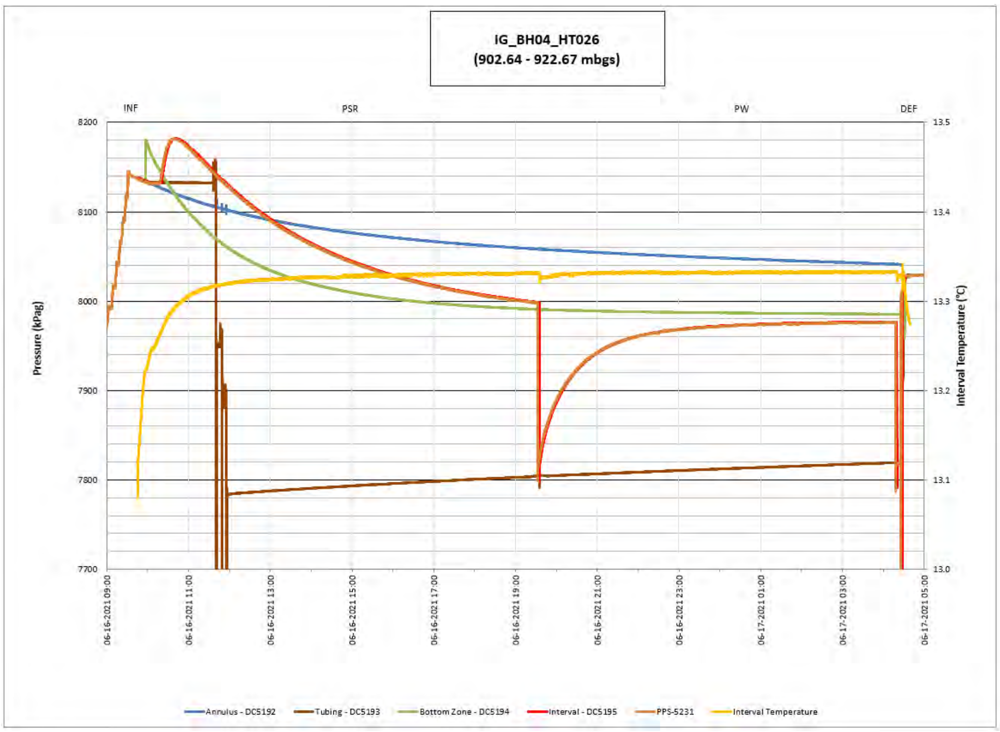

Figure 277: HT026 Annotated test plot showing monitored zone pressure and interval temperature.

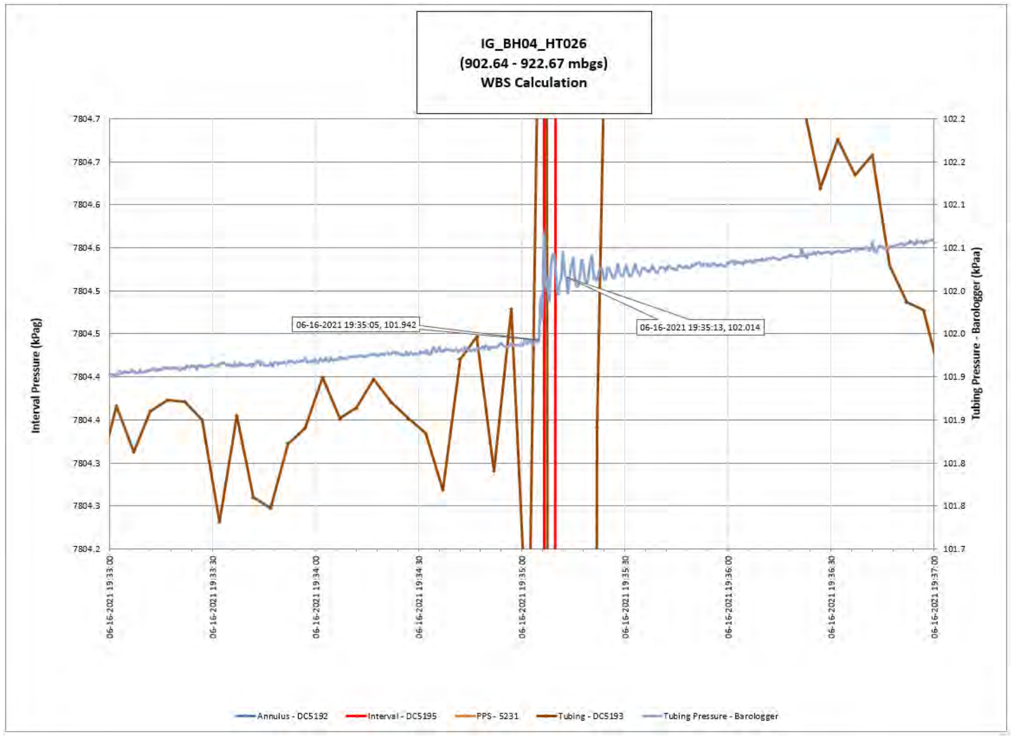

Figure 278: HT026 Tubing pressure during DHSIV activation. DHSIV Closed Wellbore Storage Estimate = 7E-11 m^3/Pa

Table 24: Summary of Analysis Results – HT026

	Formation conductivity	Skin zone conductivity	Static formation pressure	Formation specific storage	Radial thickness of skin	Flow dimension
	[m/s]	[m/s]	[kPa]	[1/m]	[m]	[–]
Best Fit	4.7E-12	1.9E-12	7978	1.9E-07	3.6E-02	2.1
Minimum	2.3E-14	1.1E-13	7975	1.3E-09	1.0E-03	1.5
Maximum	9.9E-12	9.2E-11	7991	5.4E-06	6.6E-01	3.0
Mean	4.0E-12	4.2E-12	7978	3.4E-07	6.7E-02	2.2
Median	3.9E-12	2.1E-12	7978	9.5E-08	2.1E-02	2.2
Geometric mean	3.3E-12	1.9E-12	7978	8.4E-08	2.0E-02	2.2

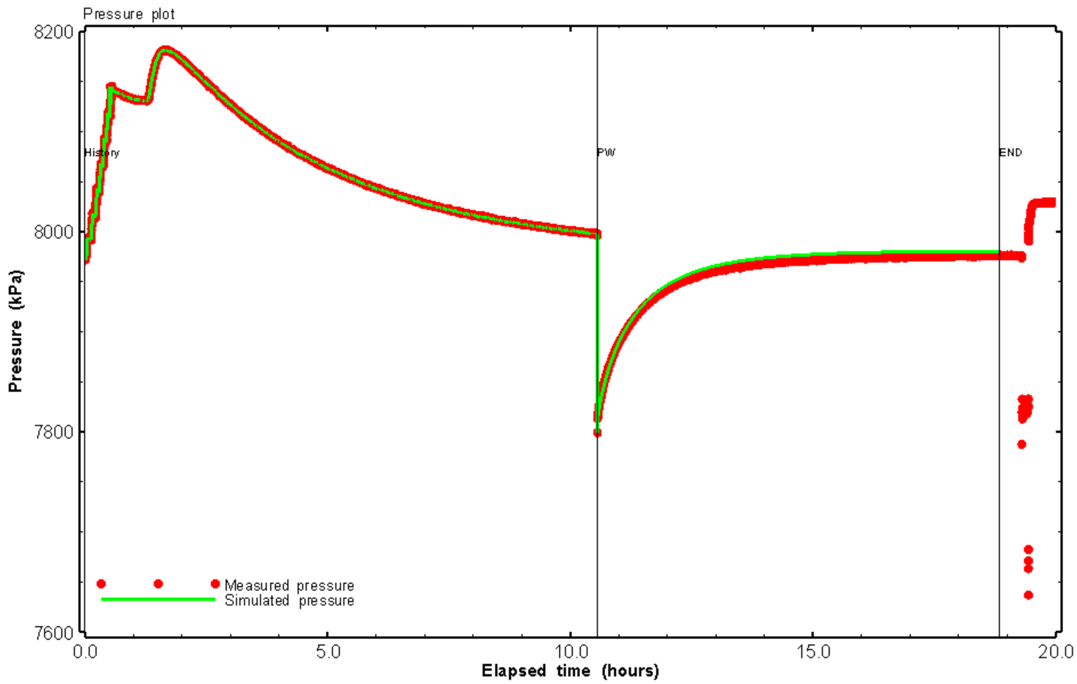

Figure 279: HT026 Pressure plot showing best-fit simulation and best fit results

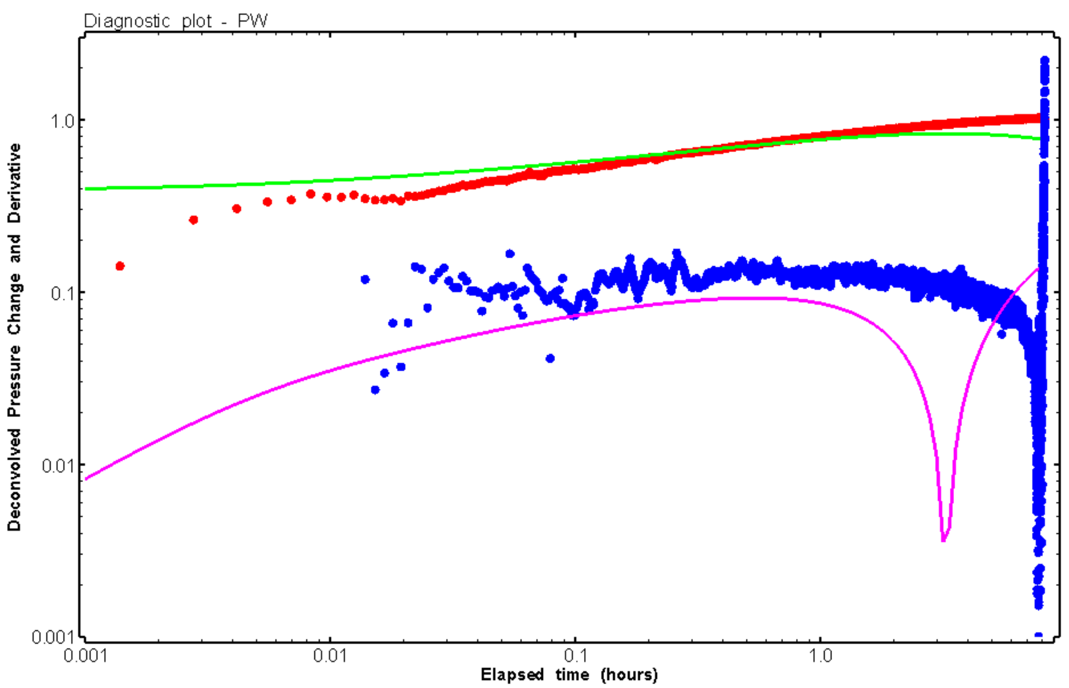

Figure 280: HT026 Deconvolved pressure change and derivative plot of the PW sequence showing best-fit simulation

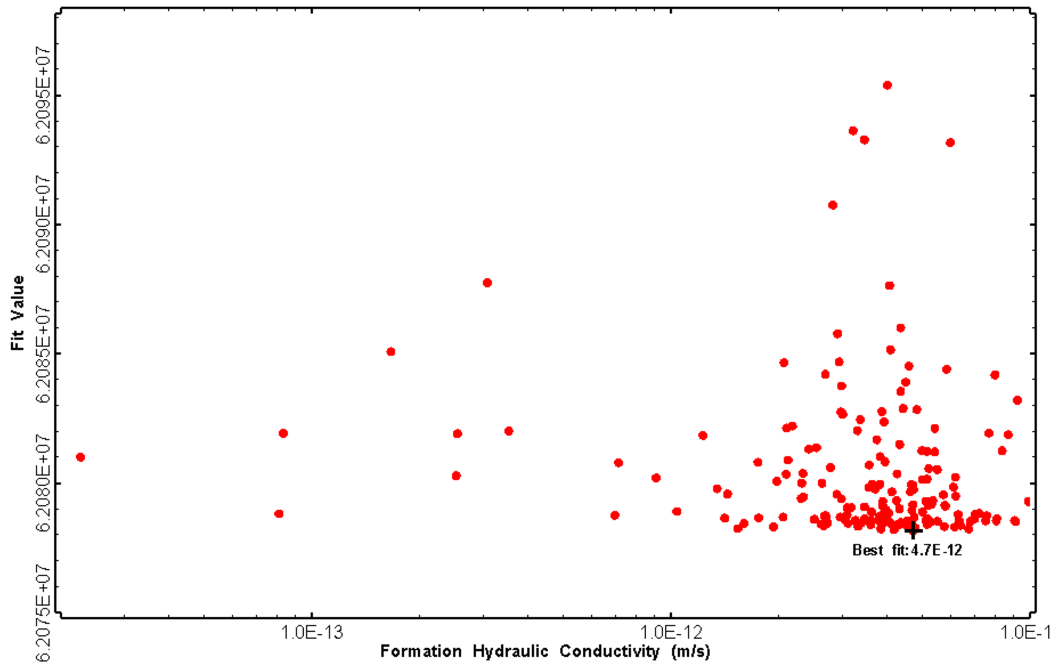

Figure 281: HT026 XY-scatter plot of formation hydraulic conductivity vs. fit value

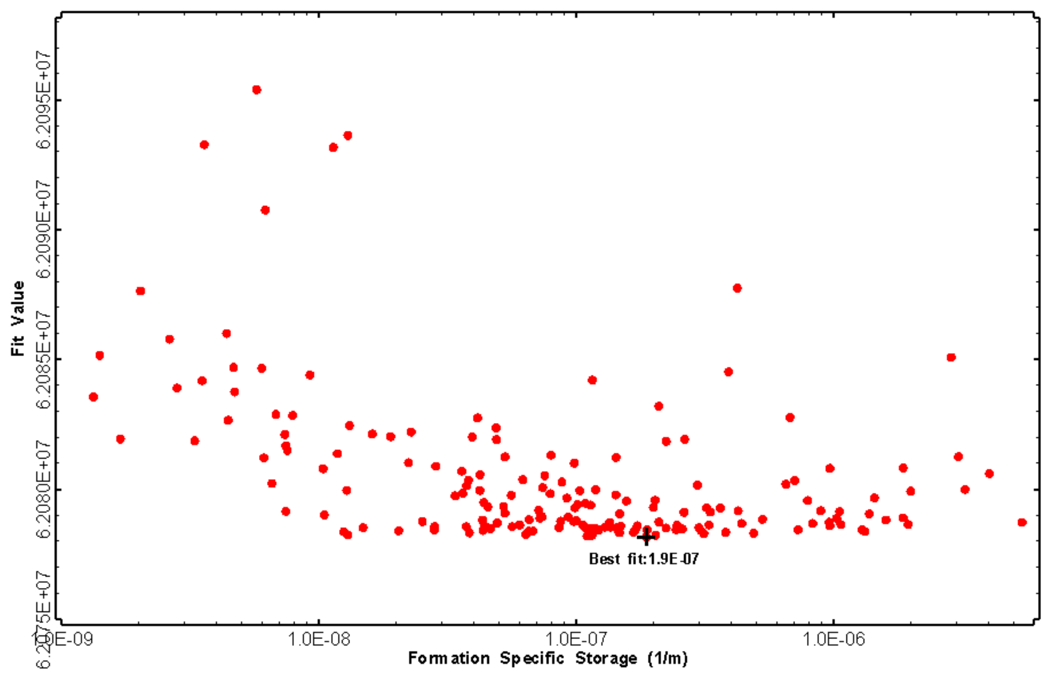

Figure 282: HT026 XY-scatter plot of formation specific storage vs. fit value

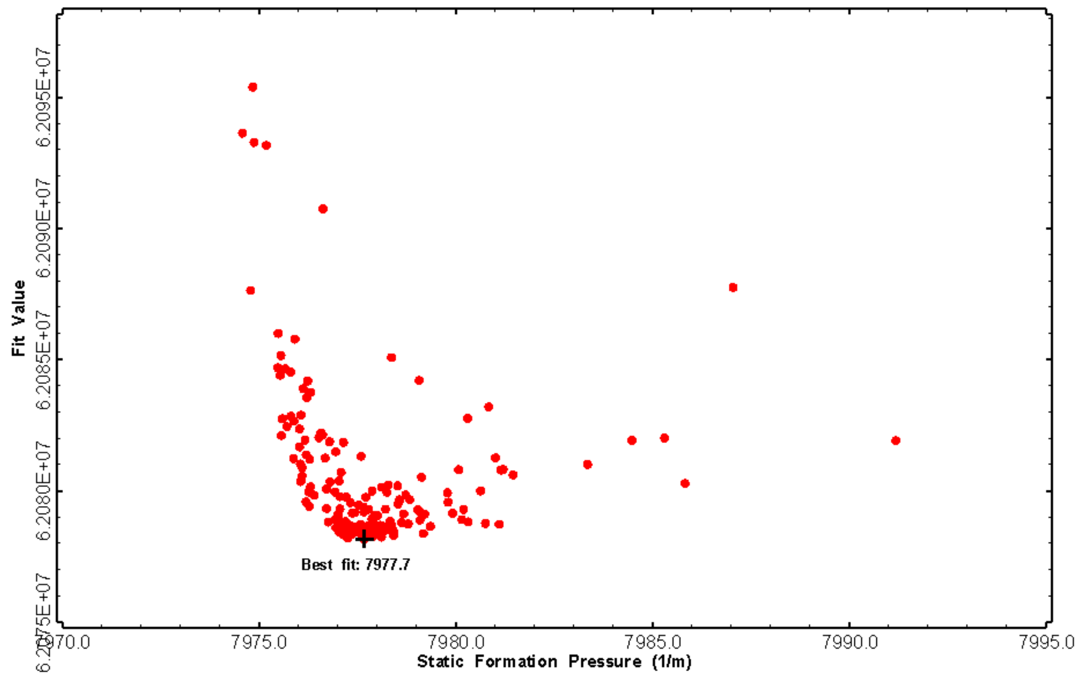

Figure 283: HT026 XY-scatter plot of static formation pressure vs. fit value

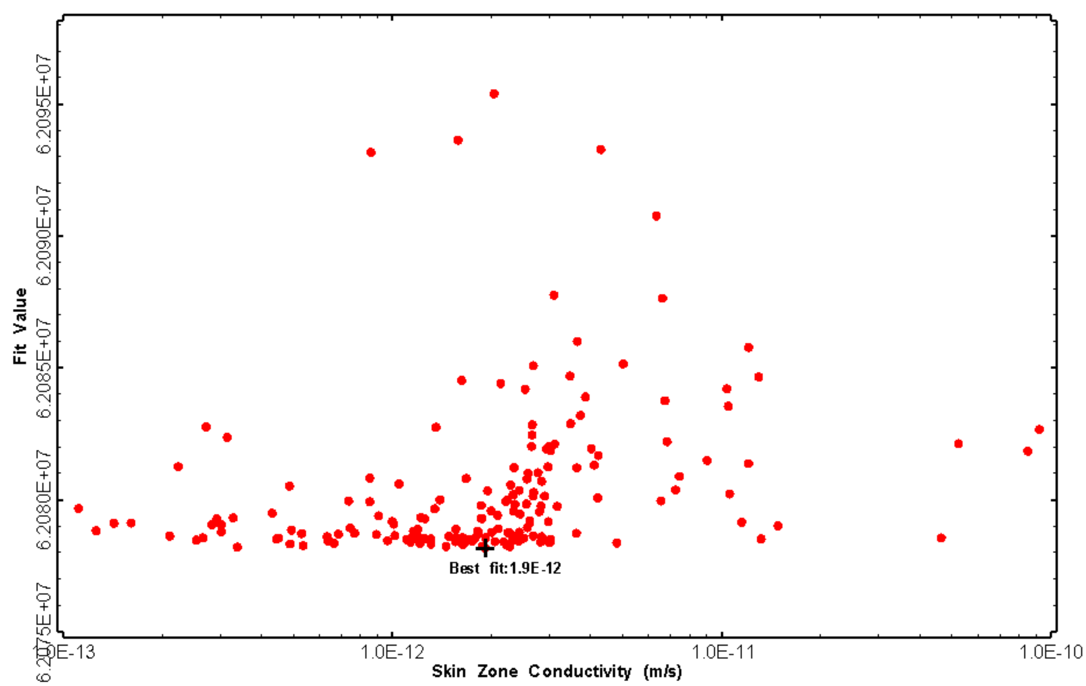

Figure 284: HT026 XY-scatter plot of skin zone conductivity vs. fit value

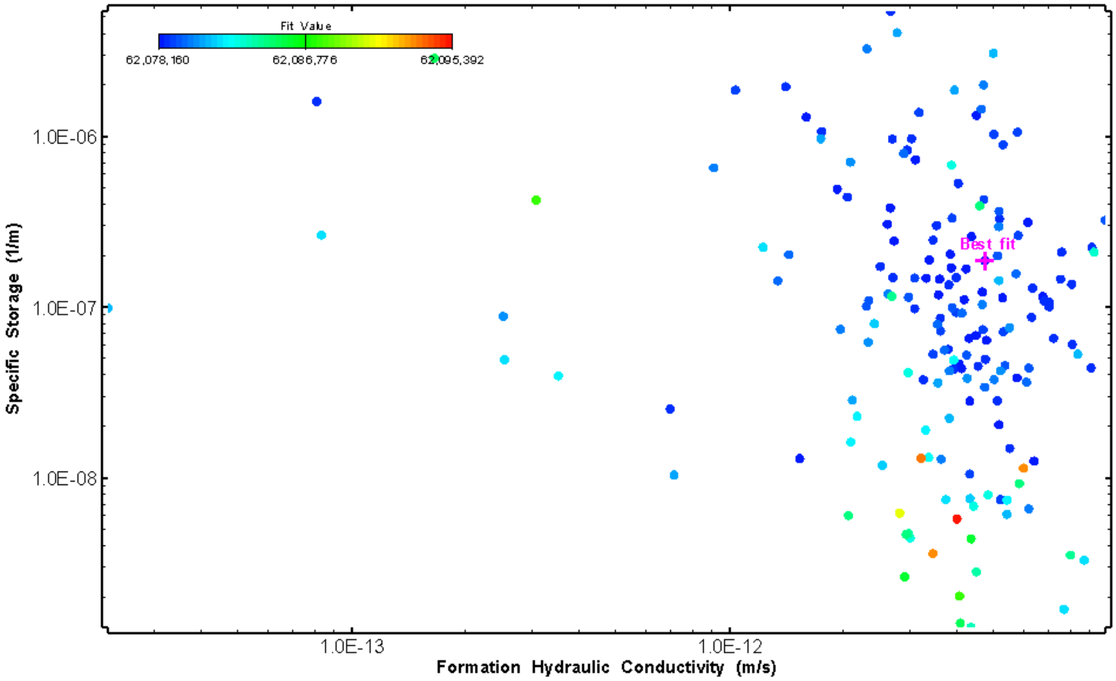

Figure 285: HT026 XY-scatter plot showing estimates of formation hydraulic conductivity and specific storage from perturbation analysis

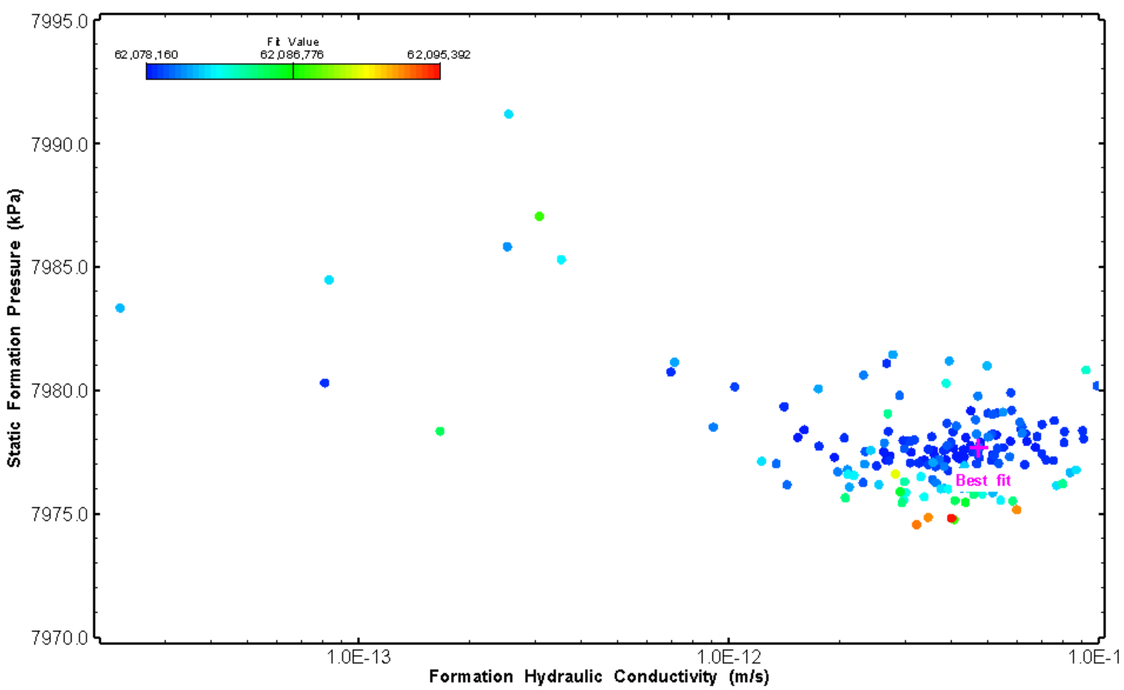

Figure 286: HT026 XY-scatter plot showing estimates of formation hydraulic conductivity and static formation pressure from perturbation analysis

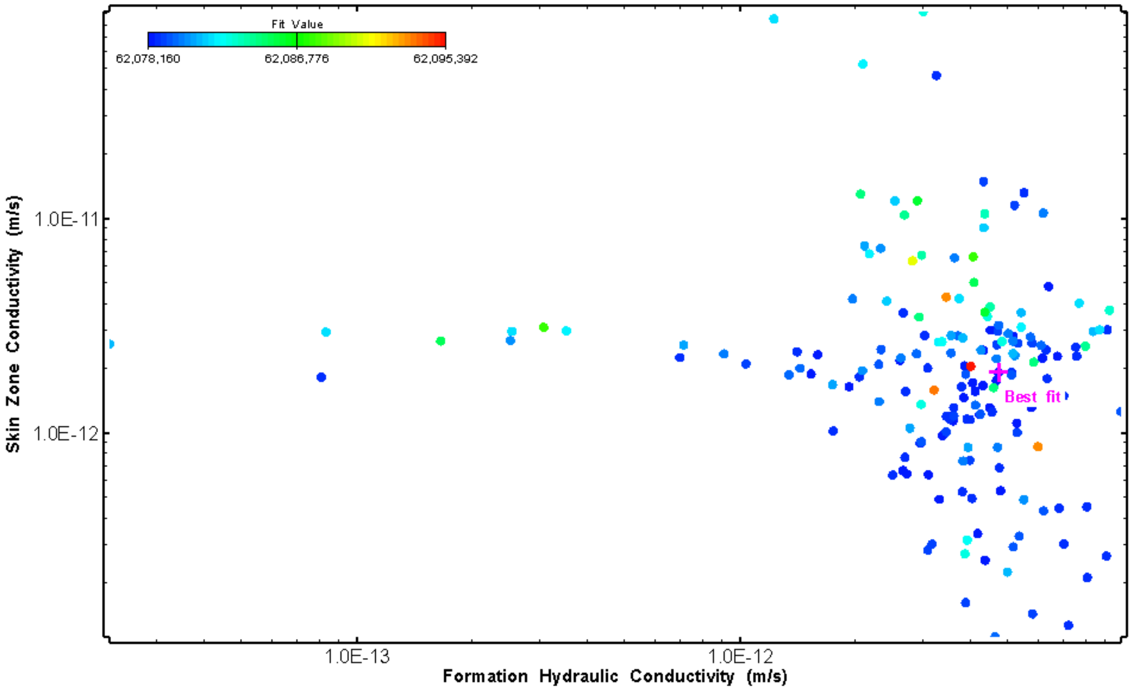

Figure 287: HT026 XY-scatter plot showing estimates of formation hydraulic conductivity and skin zone conductivity from perturbation analysis

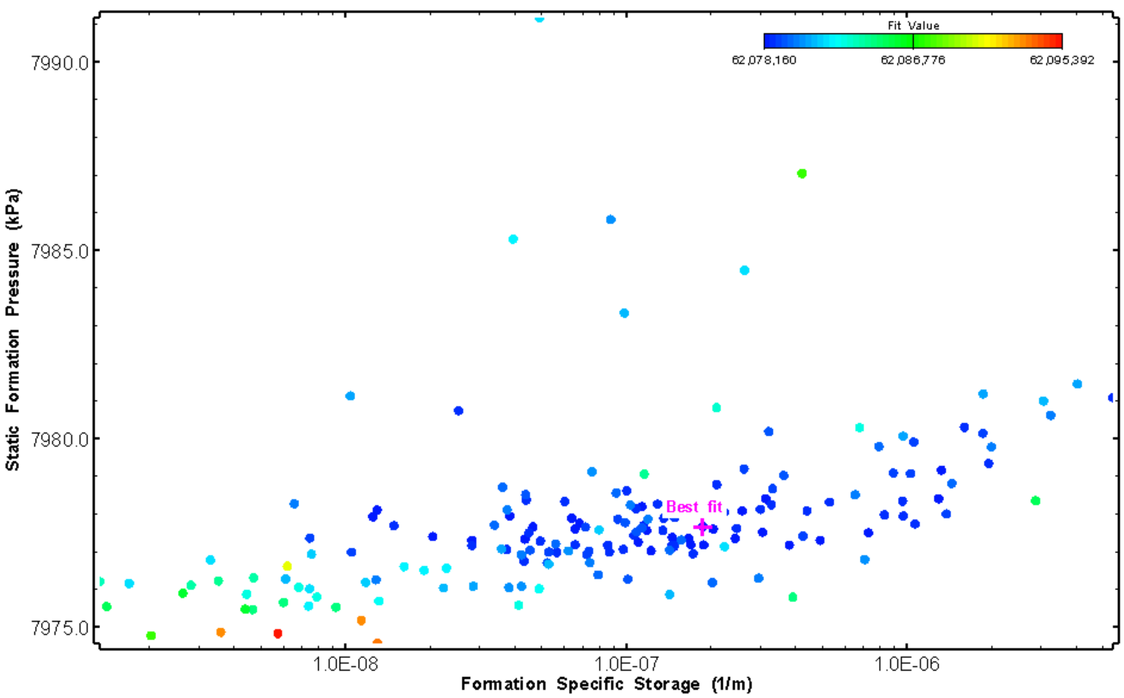

Figure 288: HT026 XY-scatter plot showing estimates of specific storage and static formation pressure from perturbation analysis

25.0 HT027 (923.00 – 943.03 M)

HT027 was selected to test a deep fractured interval. 14 broken fractures were observed in the core. A loss of drilling fluid was observed in this interval during drilling. No indication of flow was recorded during FFEC logging post-drilling.

The test was initiated with a shut-in pressure recovery phase (PSR). A pulse withdrawal test (PW) with a shut-in recovery was completed after the PSR phase.

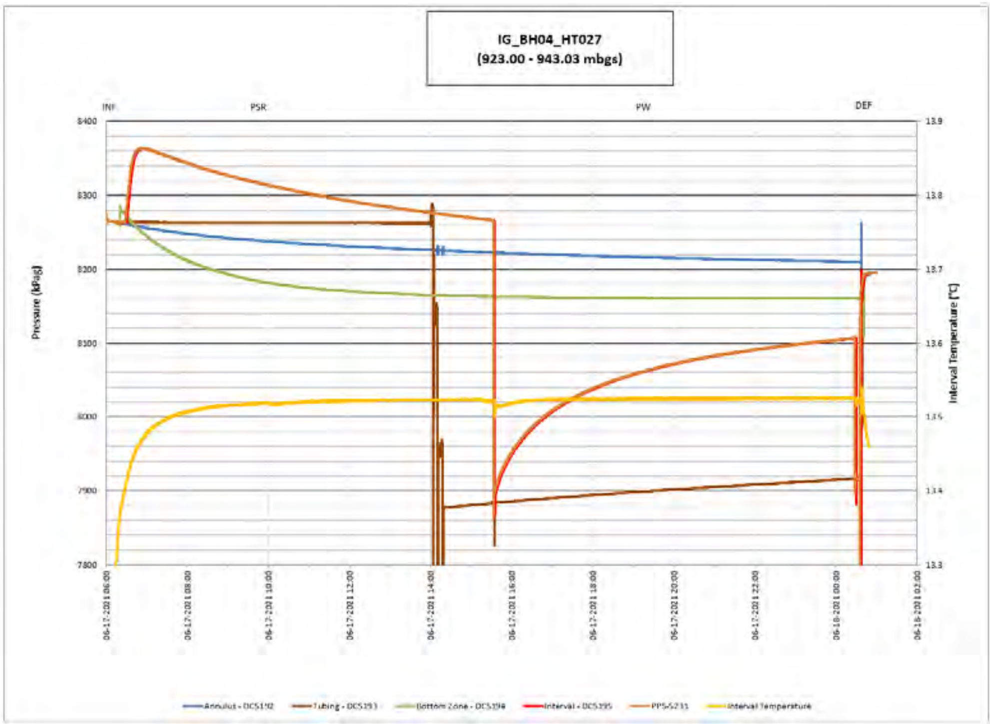

Figure 289: HT027 Annotated test plot showing monitored zone pressure and interval temperature.

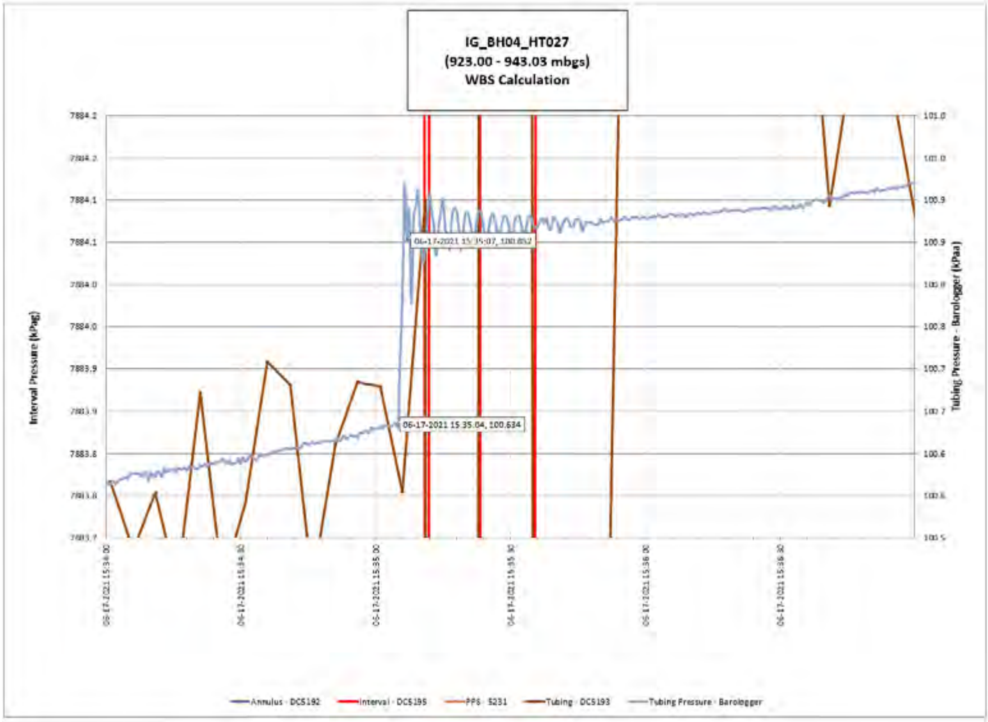

Figure 290: HT027 Tubing pressure during DHSIV activation. DHSIV Closed Wellbore Storage Estimate = 1E-10 m^3/Pa

Table 25: Summary of Analysis Results – HT027

	Formation conductivity	Skin zone conductivity	Static formation pressure	Formation specific storage	Radial thickness of skin	Flow dimension
	[m/s]	[m/s]	[kPa]	[1/m]	[m]	[–]
Best Fit	5.0E-14	1.4E-12	8754	8.5E-08	3.0E-01	1.7
Minimum	1.0E-15	2.7E-13	8146	1.0E-09	2.9E-03	1.0
Maximum	9.1E-11	9.1E-11	8799	6.1E-06	9.4E-01	2.7
Mean	1.7E-12	2.5E-12	8440	5.8E-07	2.5E-01	1.8
Median	8.3E-14	1.3E-12	8429	1.1E-07	2.6E-01	1.8
Geometric mean	1.2E-13	1.3E-12	8438	1.0E-07	1.9E-01	1.7

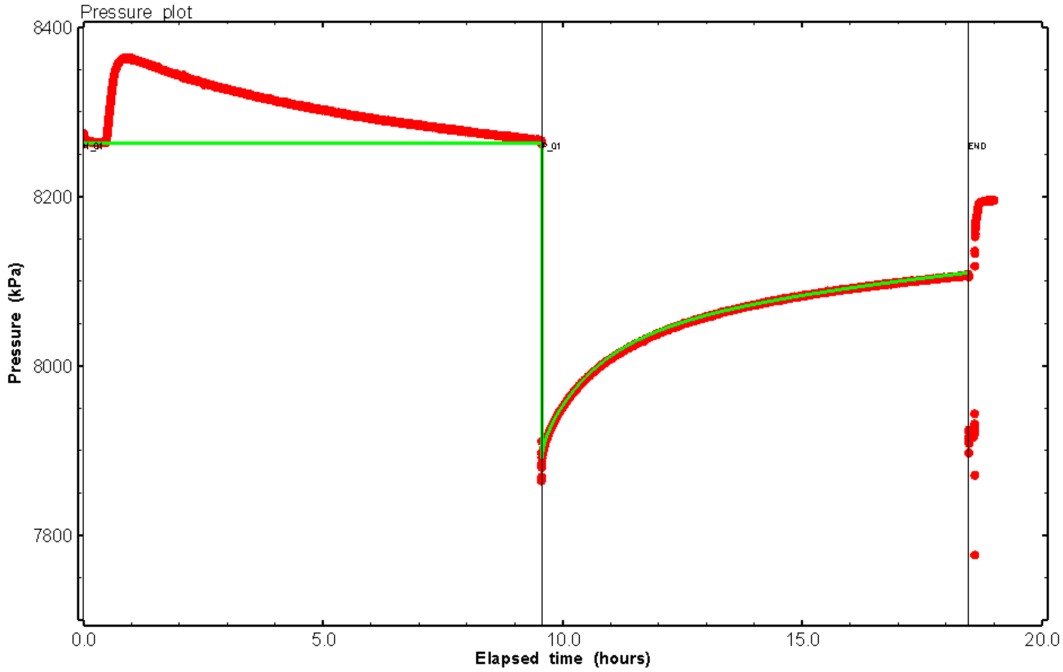

Figure 291: HT027 Pressure plot showing best-fit simulation and best fit results

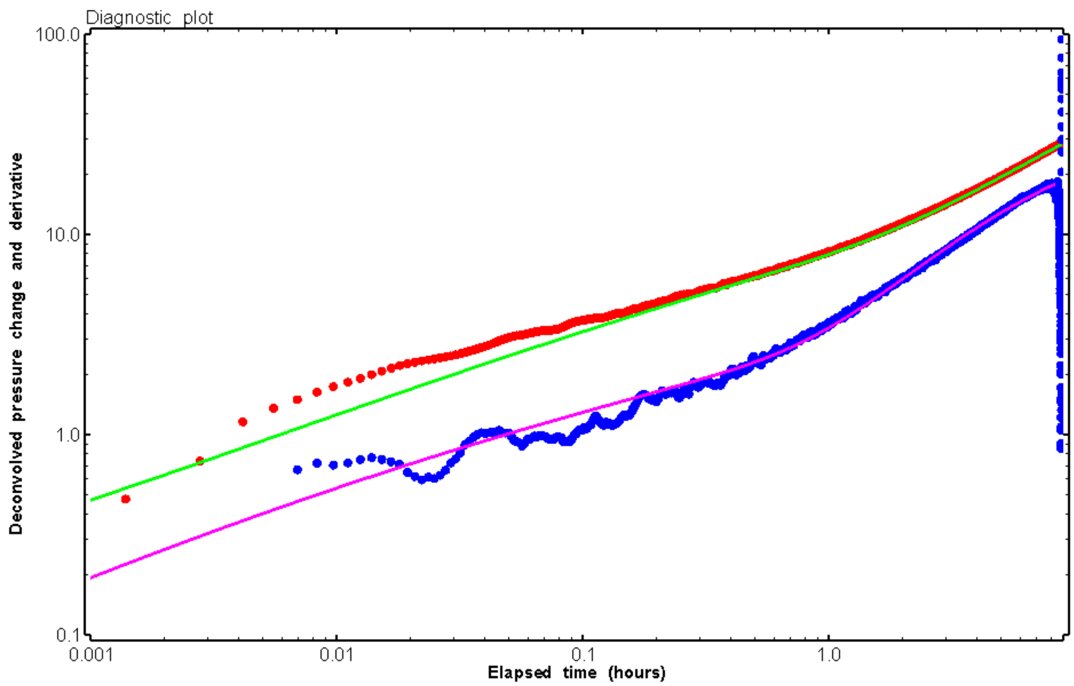

Figure 292: HT027 Deconvolved pressure change and derivative plot of the PW sequence showing best-fit simulation

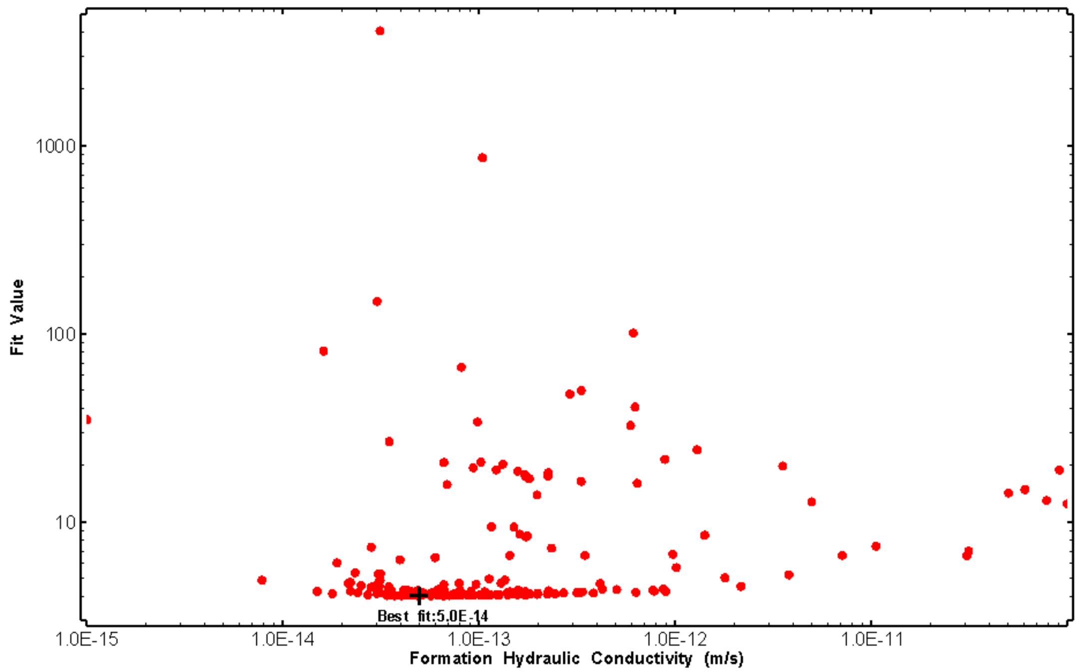

Figure 293: HT027 XY-scatter plot of formation hydraulic conductivity vs. fit value

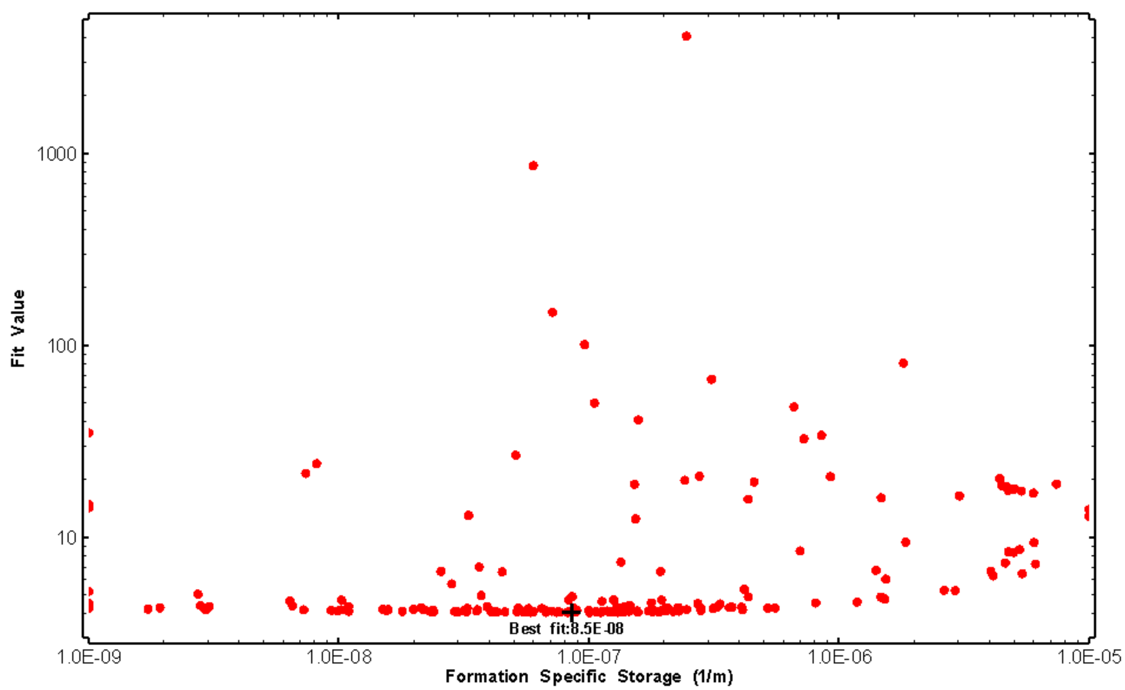

Figure 294: HT027 XY-scatter plot of formation specific storage vs. fit value

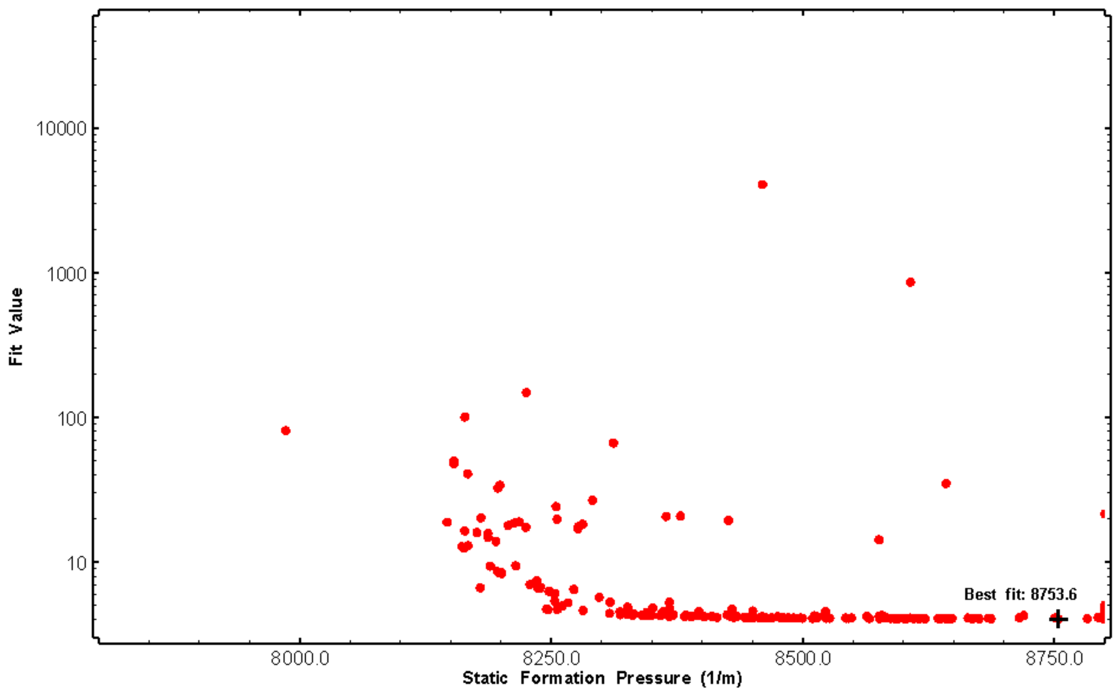

Figure 295: HT027 XY-scatter plot of static formation pressure vs. fit value

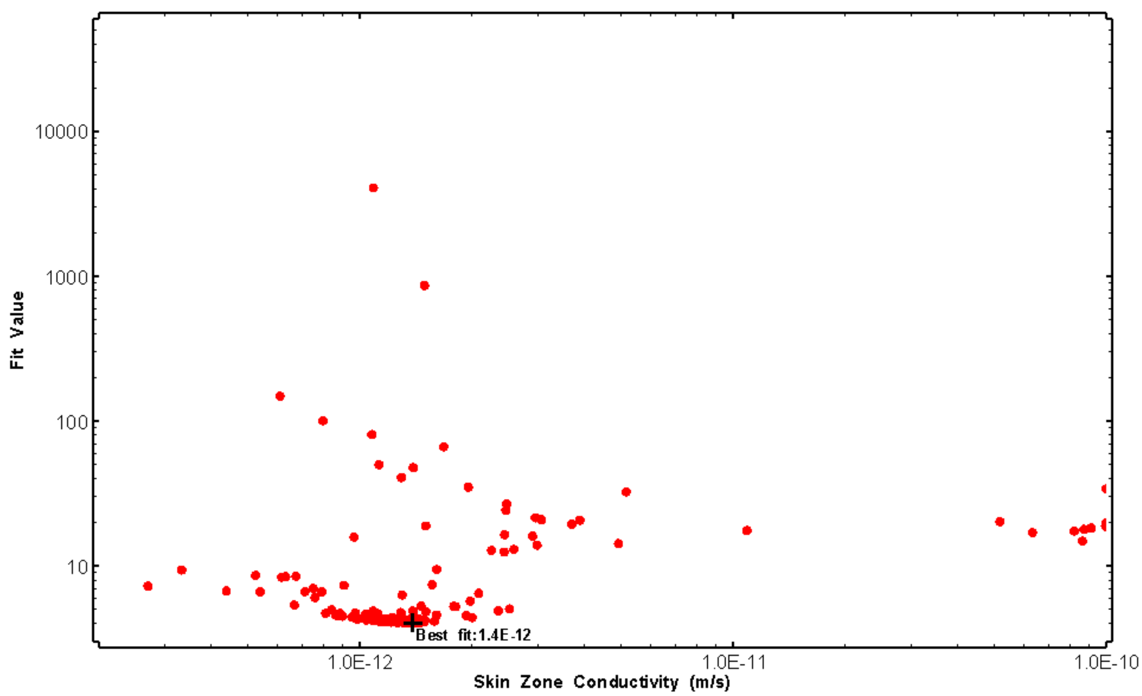

Figure 296: HT027 XY-scatter plot of skin zone conductivity vs. fit value

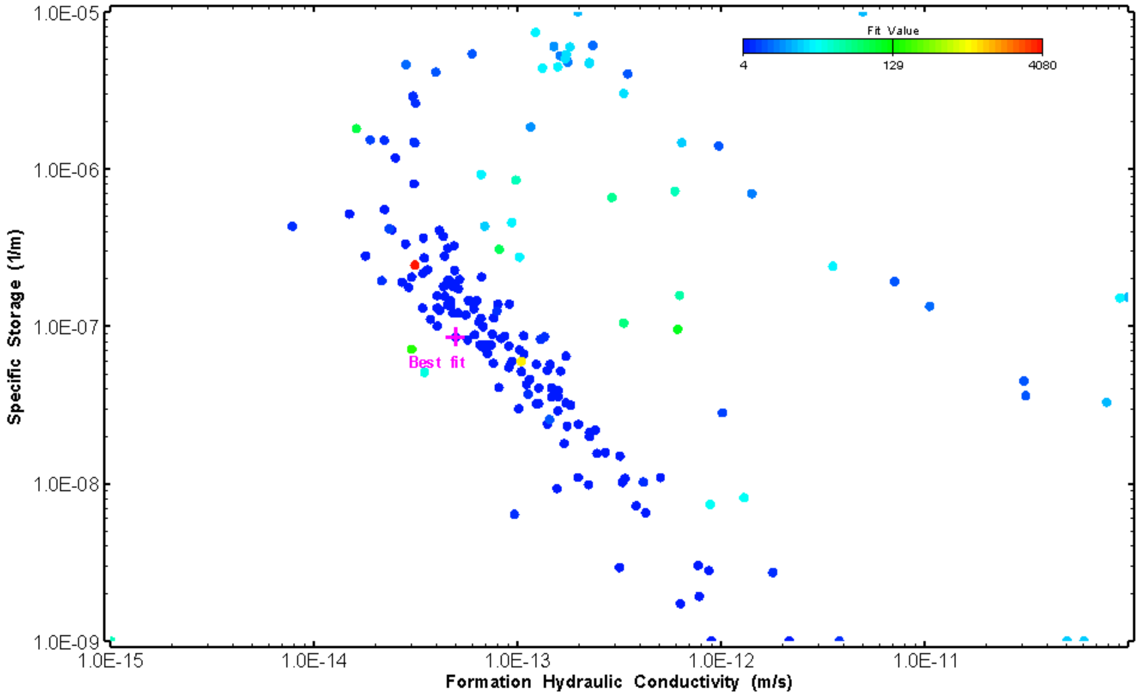

Figure 297: HT027 XY-scatter plot showing estimates of formation hydraulic conductivity and specific storage from perturbation analysis

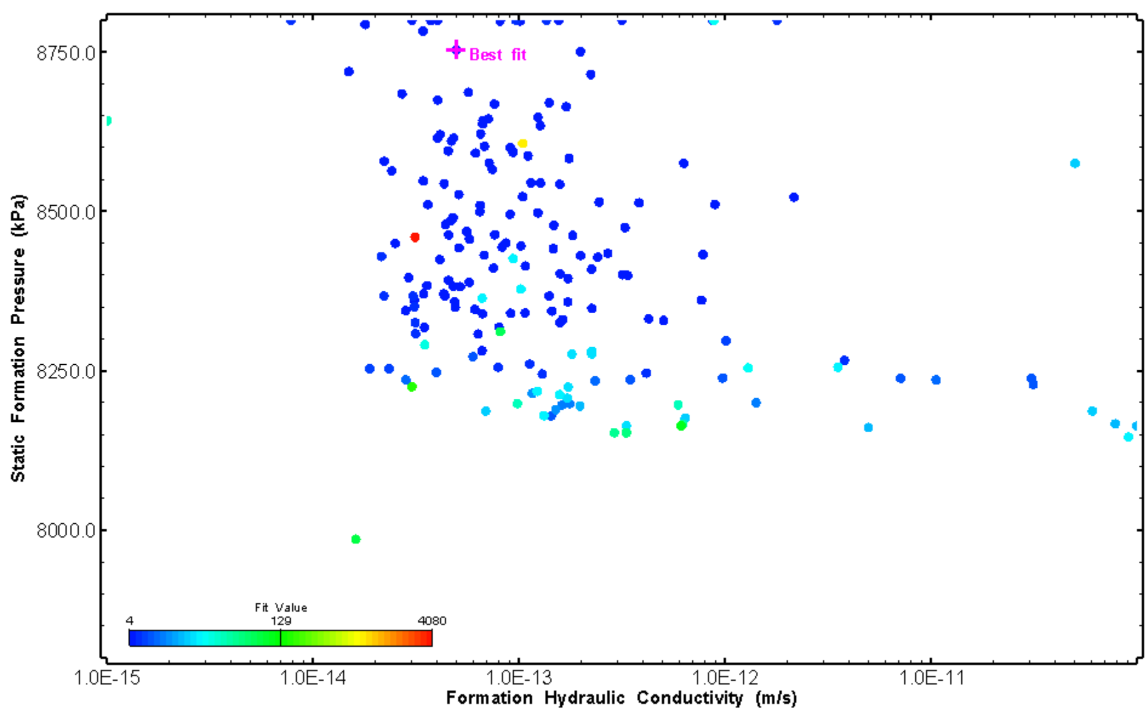

Figure 298: HT027 XY-scatter plot showing estimates of formation hydraulic conductivity and static formation pressure from perturbation analysis

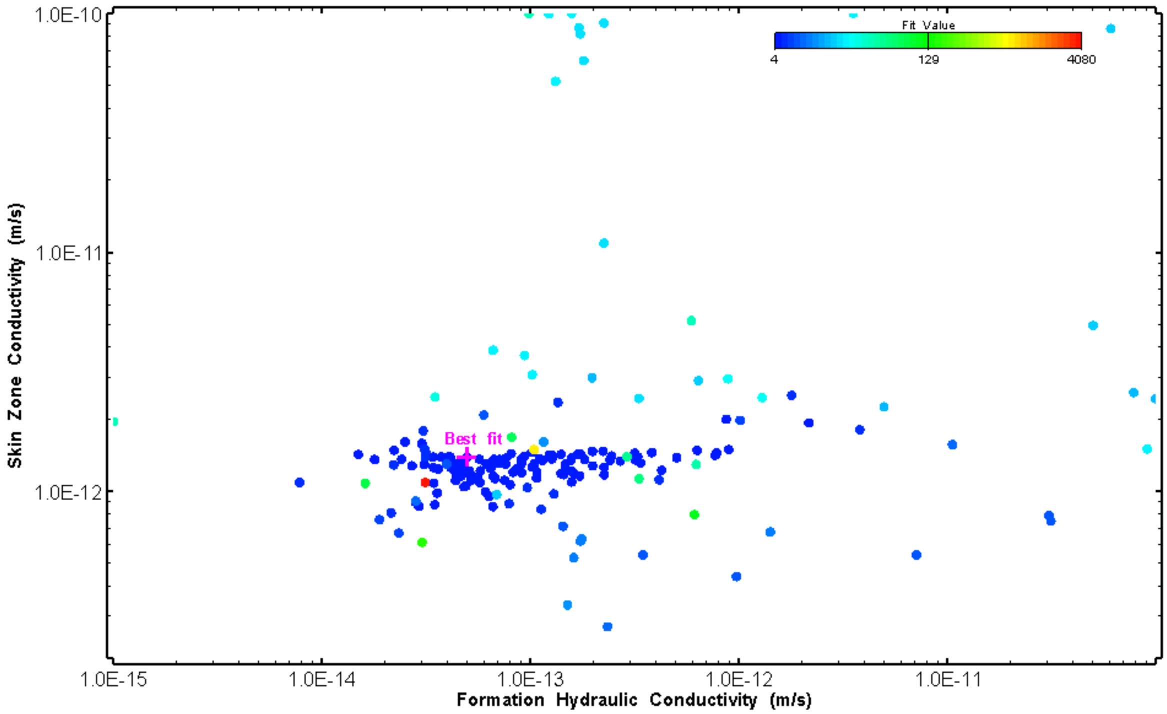

Figure 299: HT027 XY-scatter plot showing estimates of formation hydraulic conductivity and skin zone conductivity from perturbation analysis

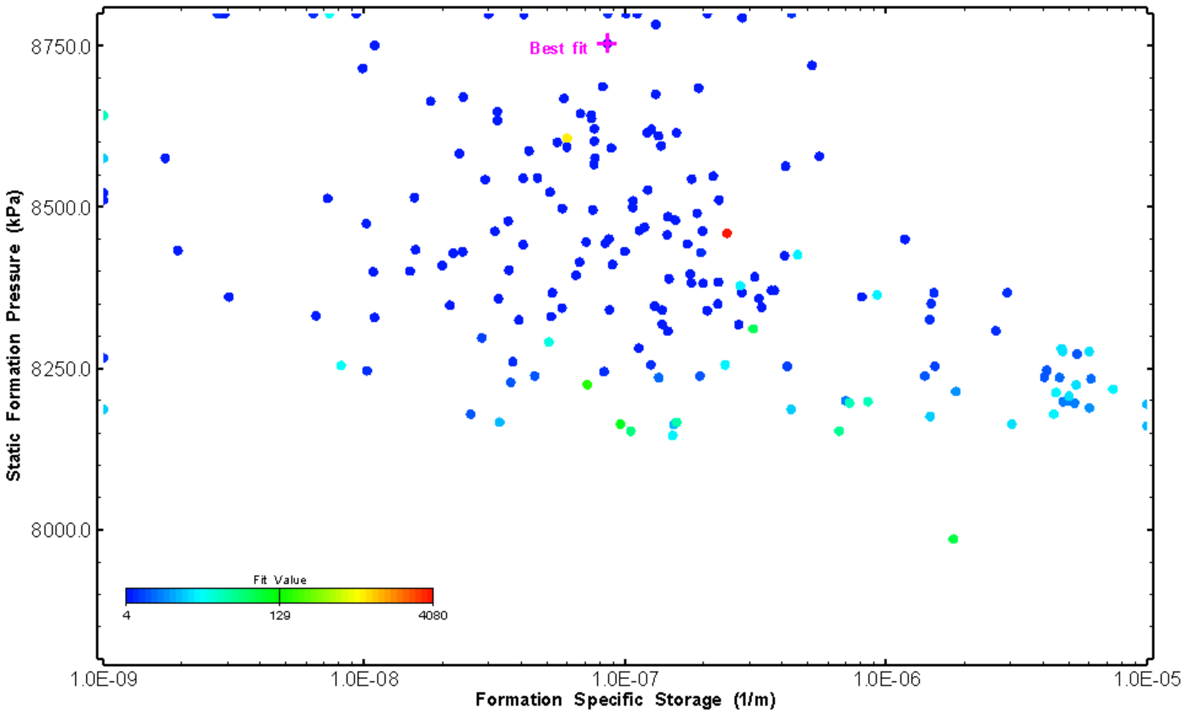

Figure 300: HT027 XY-scatter plot showing estimates of specific storage and static formation pressure from perturbation analysis

26.0 HT028 (938.50 – 958.53 M)

HT028 was selected to test a deep fractured interval with an amphibolite dyke. 25 broken fractures were observed in the core. A loss of drilling fluid was observed in this interval during drilling. No indication of flow was recorded during FFEC logging post-drilling.

The test was initiated with a shut-in pressure recovery phase (PSR). A pulse withdrawal test (PW) with a shut-in recovery was completed after the PSR phase.

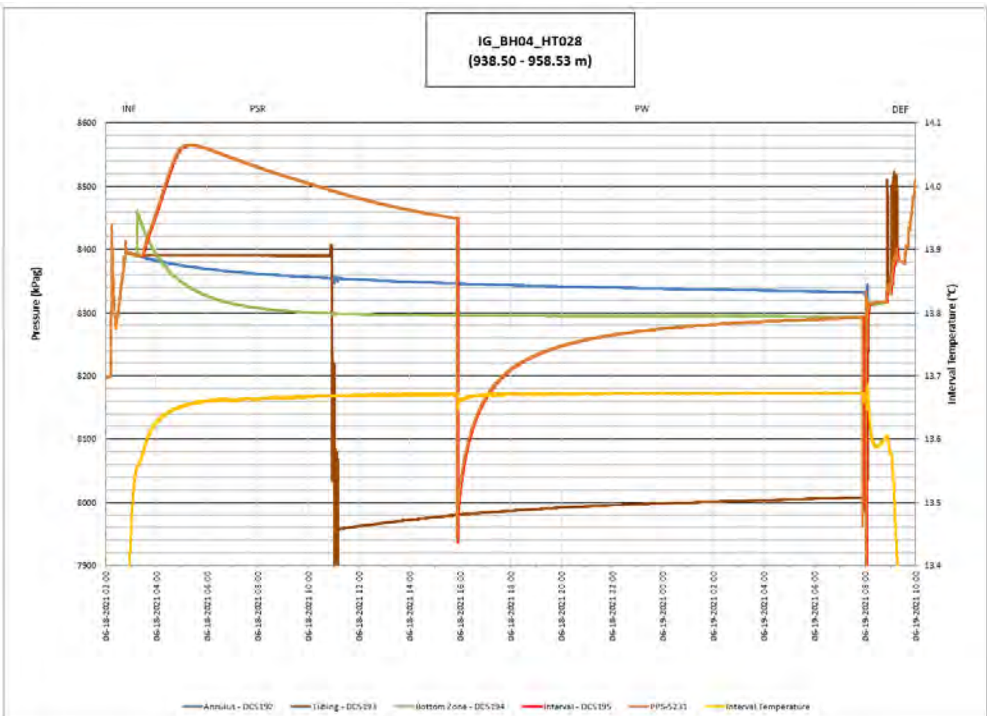

Figure 301: HT028 Annotated test plot showing monitored zone pressure and interval temperature.

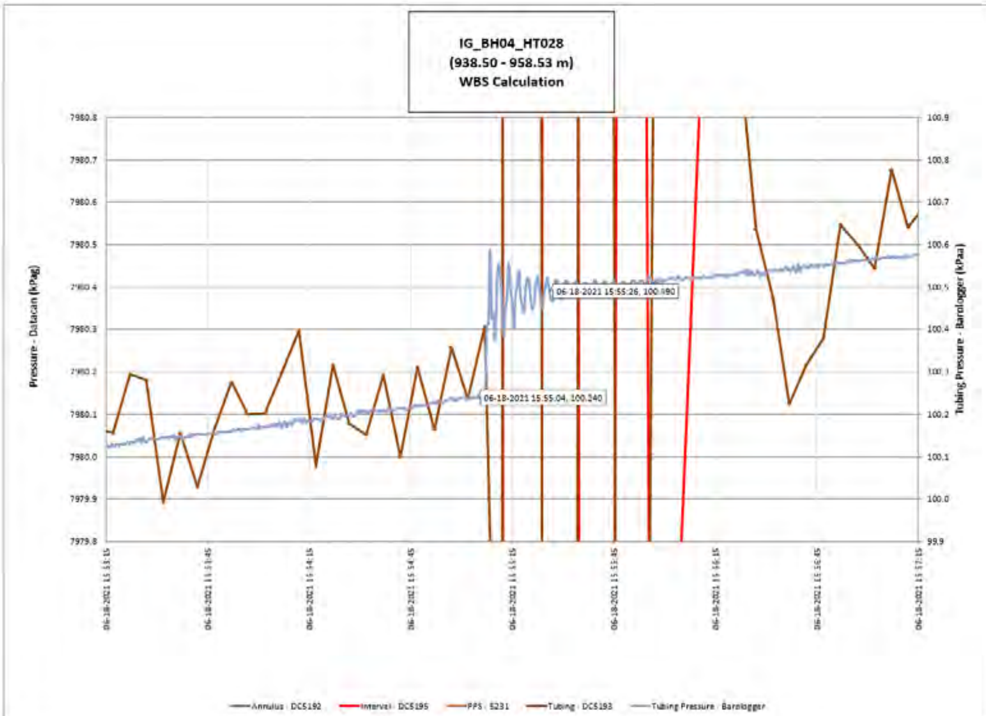

Figure 302: HT028 Tubing pressure during DHSIV activation. DHSIV Closed Wellbore Storage Estimate = 1E-10 m^3/Pa

Table 26: Summary of Analysis Results – HT028

	Formation conductivity	Skin zone conductivity	Static formation pressure	Formation specific storage	Radial thickness of skin	Flow dimension
	[m/s]	[m/s]	[kPa]	[1/m]	[m]	[–]
Best Fit	2.6E-12	6.0E-12	8596	3.3E-09	8.7E-01	1.3
Minimum	1.1E-14	1.1E-12	8320	1.0E-09	1.3E-01	1.1
Maximum	1.2E-11	8.9E-12	8599	5.3E-06	9.9E-01	2.8
Mean	1.3E-12	4.7E-12	8492	5.9E-07	6.3E-01	1.5
Median	2.1E-13	5.1E-12	8518	8.5E-08	6.7E-01	1.3
Geometric mean	2.5E-13	4.2E-12	8492	6.9E-08	5.8E-01	1.5

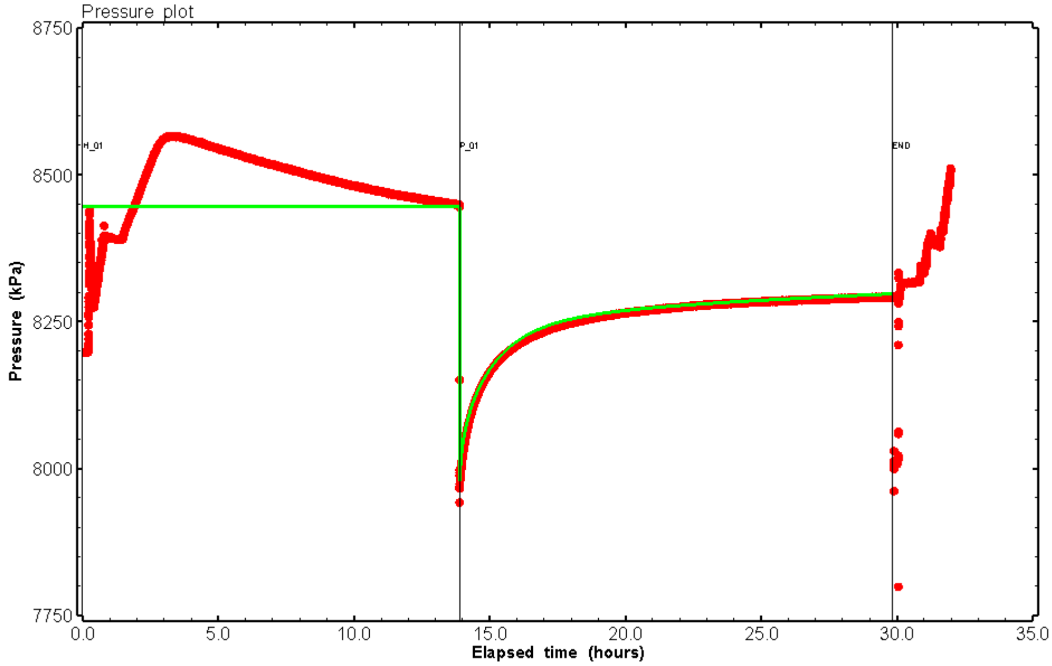

Figure 303: HT028 Pressure plot showing best-fit simulation and best fit results

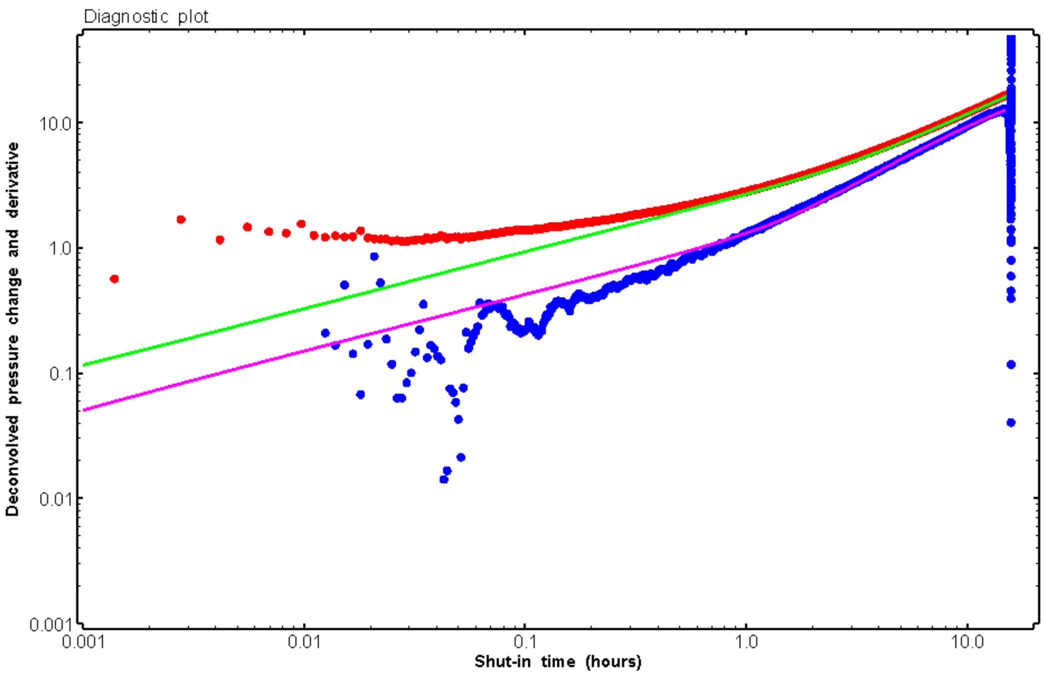

Figure 304: HT028 Deconvolved pressure change and derivative plot of the PW sequence showing best-fit simulation

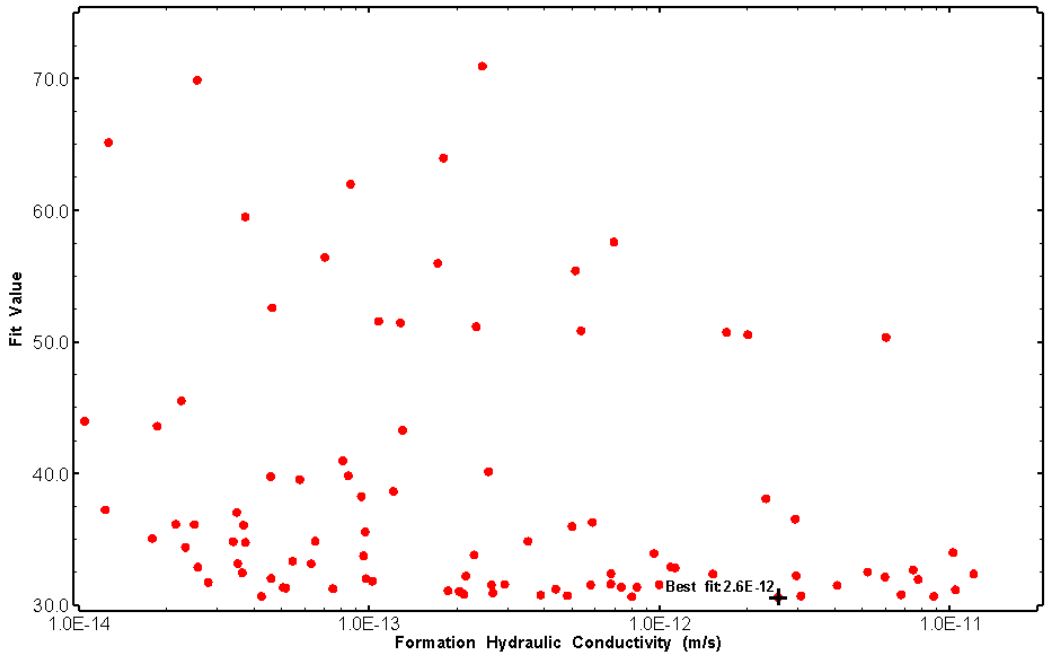

Figure 305: HT028 XY-scatter plot of formation hydraulic conductivity vs. fit value

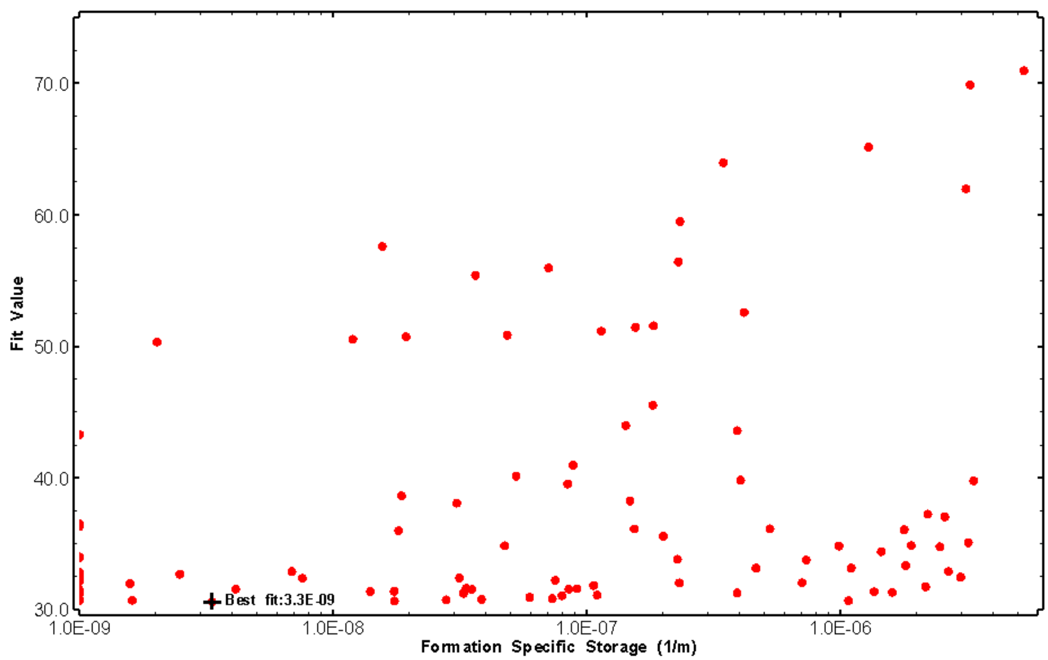

Figure 306: HT028 XY-scatter plot of formation specific storage vs. fit value

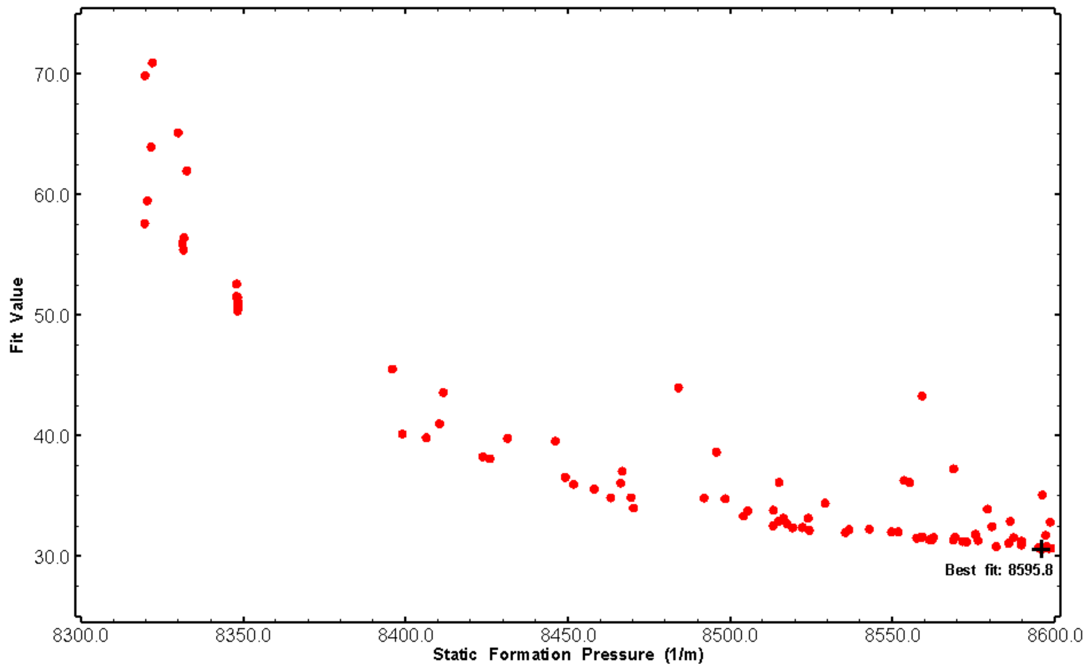

Figure 307: HT028 XY-scatter plot of static formation pressure vs. fit value

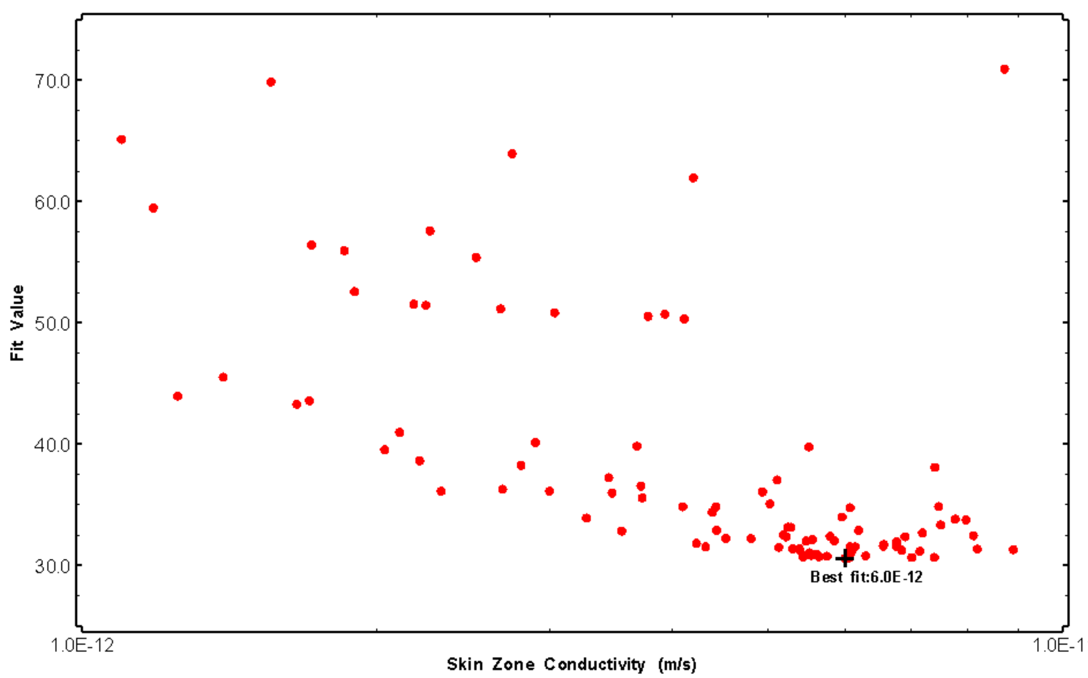

Figure 308: HT028 XY-scatter plot of skin zone conductivity vs. fit value

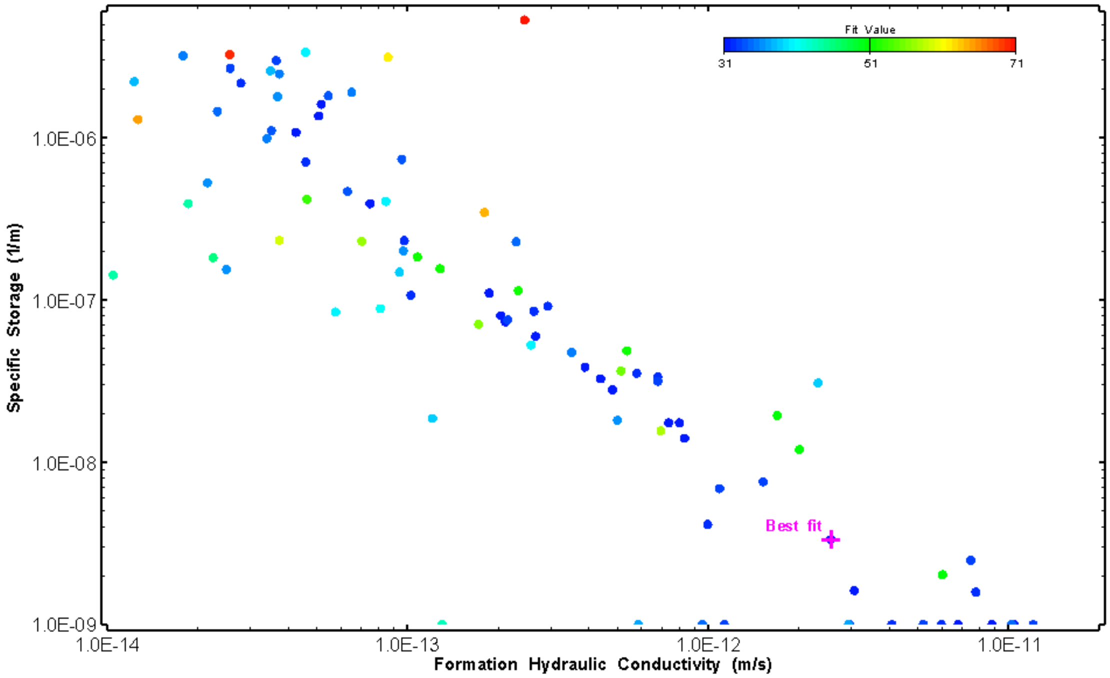

Figure 309: HT028 XY-scatter plot showing estimates of formation hydraulic conductivity and specific storage from perturbation analysis

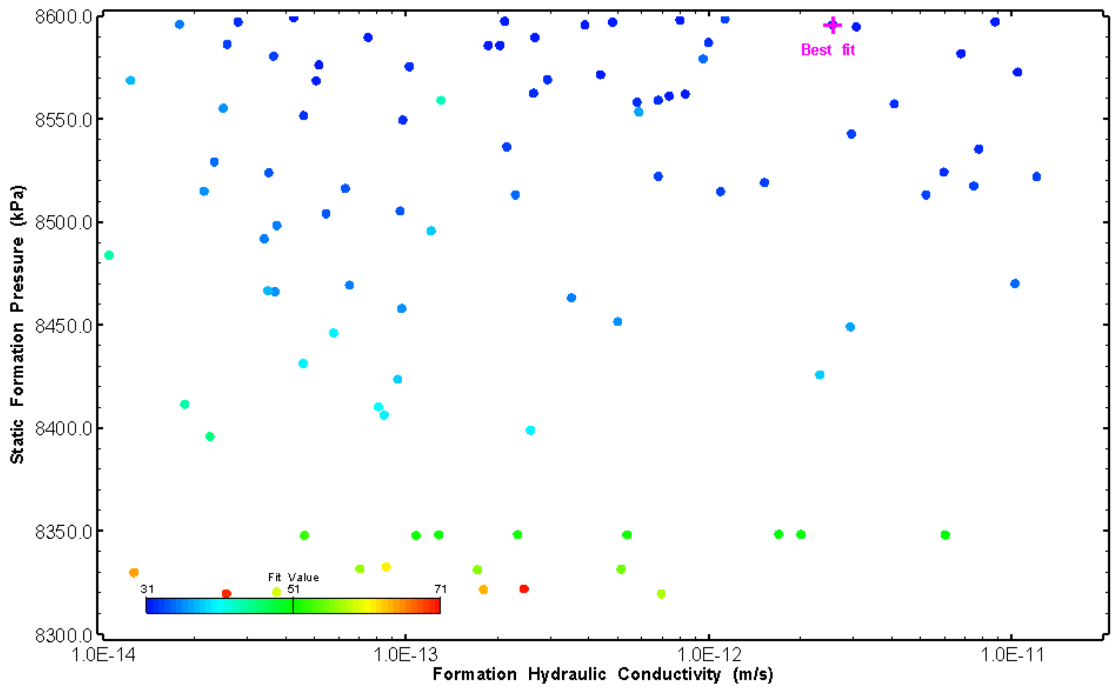

Figure 310: HT028 XY-scatter plot showing estimates of formation hydraulic conductivity and static formation pressure from perturbation analysis

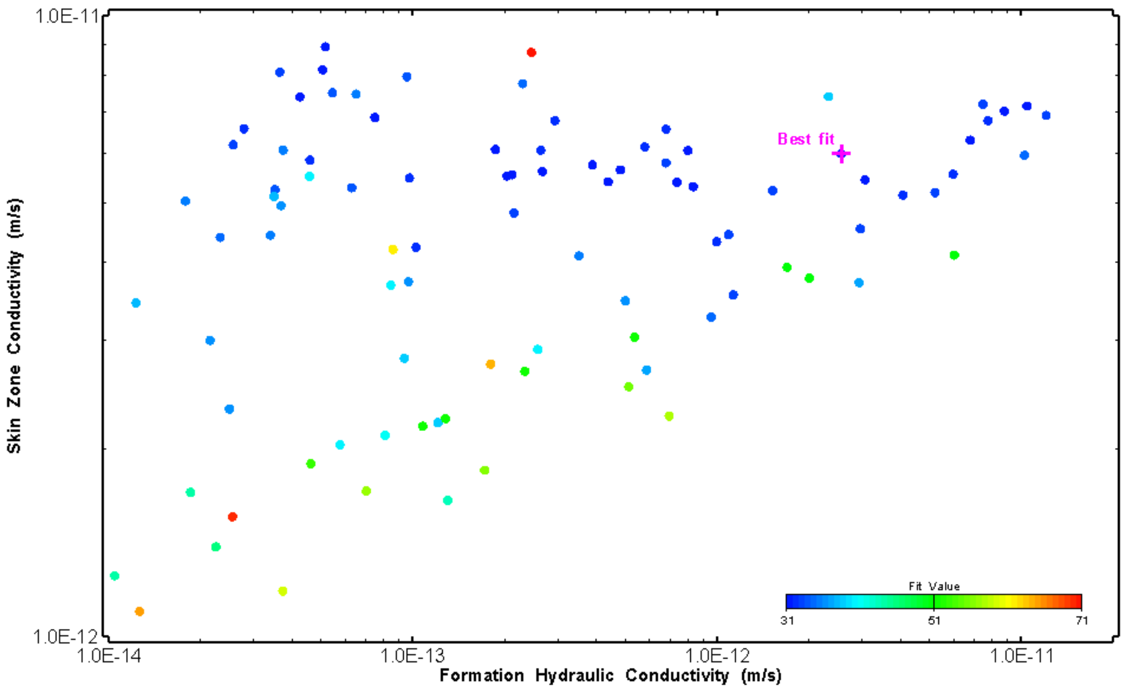

Figure 311: HT028 XY-scatter plot showing estimates of formation hydraulic conductivity and skin zone conductivity from perturbation analysis

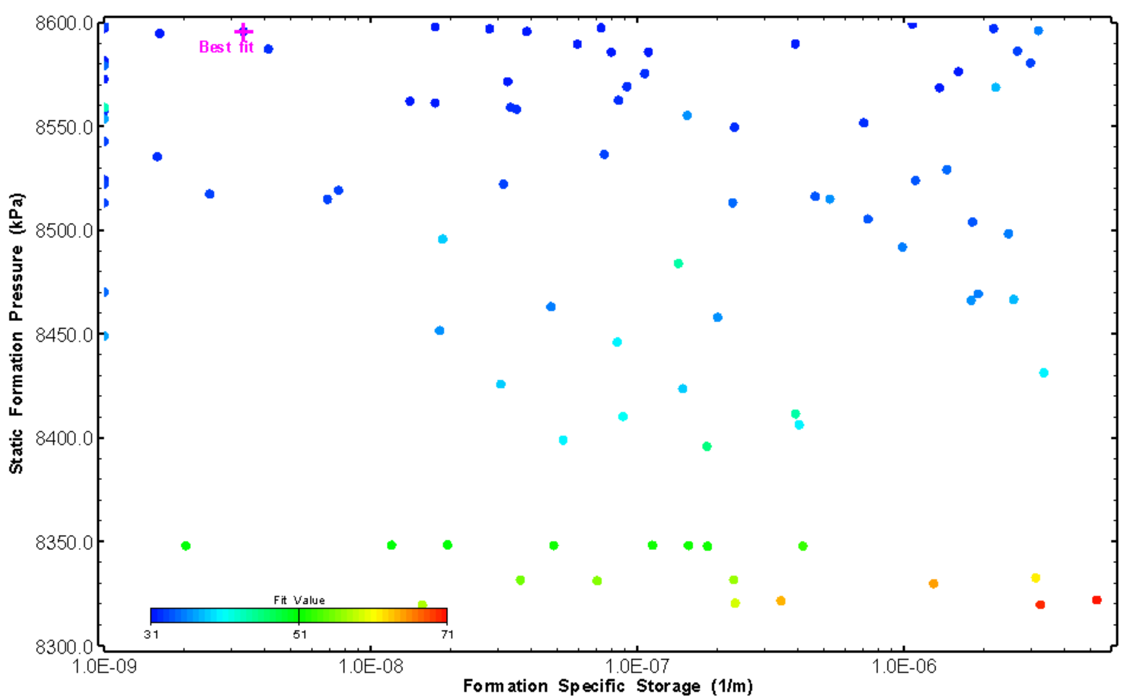

Figure 312: HT028 XY-scatter plot showing estimates of specific storage and static formation pressure from perturbation analysis

27.0 HT030 (959.65 – 1000.20 M)

HT030 was selected to test the bottom of the borehole. 54 broken fractures were observed in the core. A loss of drilling fluid was observed in this interval during drilling. No indication of flow was recorded during FFEC logging post-drilling.

The test was initiated with a shut-in pressure recovery phase (PSR). A pulse withdrawal test (PW) with a shut-in recovery was completed after the PSR phase.

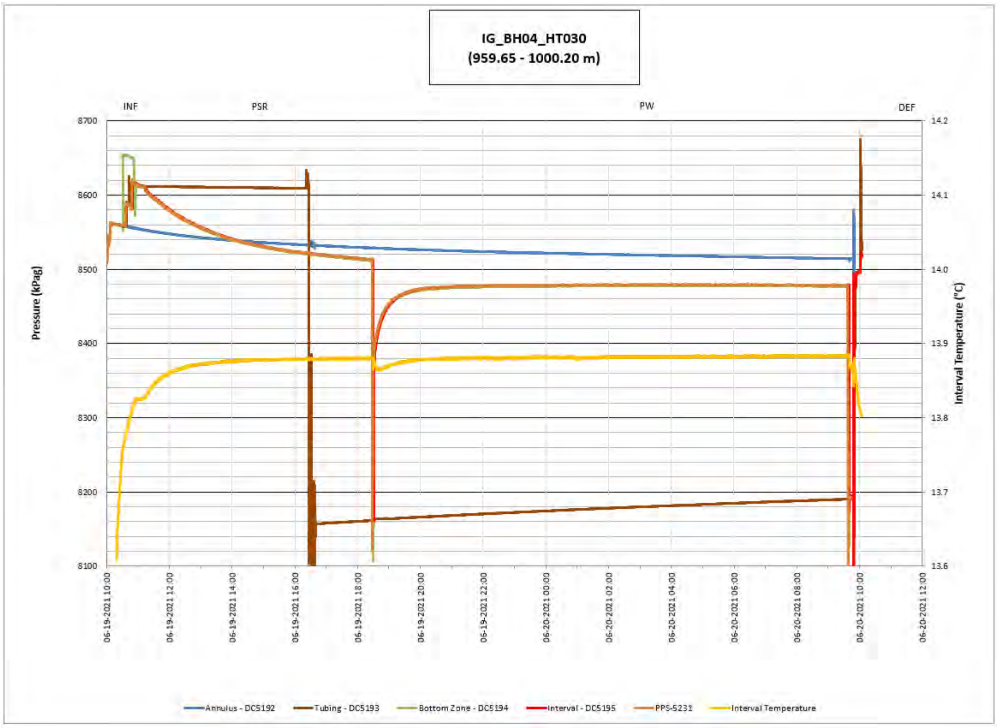

Figure 313: HT030 Annotated test plot showing monitored zone pressure and interval temperature.

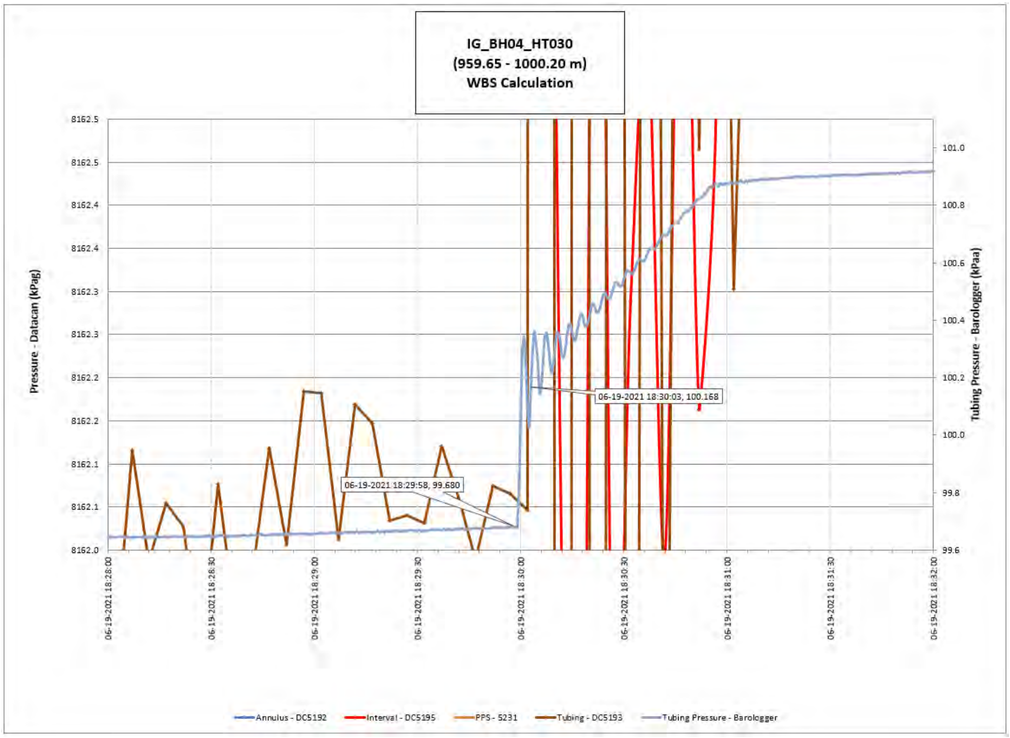

Figure 314: HT030 Tubing pressure during DHSIV activation. DHSIV Closed Wellbore Storage Estimate = 3E-10 m^3/Pa

Table 27: Summary of Analysis Results – HT030

	Formation conductivity	Skin zone conductivity	Static formation pressure	Formation specific storage	Radial thickness of skin	Flow dimension
	[m/s]	[m/s]	[kPa]	[1/m]	[m]	[–]
Best Fit	3.6E-12	2.1E-10	8477	3.7E-08	2.3E-01	2.7
Minimum	9.7E-13	5.0E-11	8470	1.0E-09	1.2E-01	1.2
Maximum	9.9E-11	9.5E-09	8477	9.6E-06	9.5E-01	3.0
Mean	1.9E-11	8.7E-10	8474	9.3E-07	3.6E-01	1.9
Median	1.1E-11	5.3E-10	8474	2.6E-07	3.4E-01	1.9
Geometric mean	1.2E-11	6.0E-10	8474	2.6E-07	3.4E-01	1.9

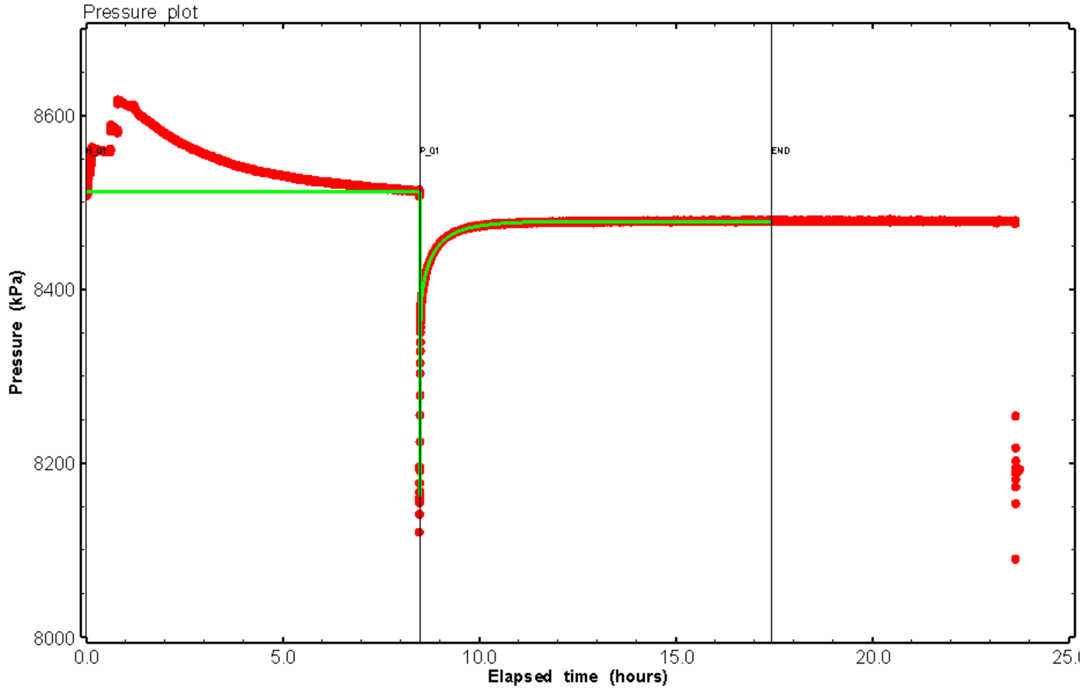

Figure 315: HT030 Pressure plot showing best-fit simulation and best fit results

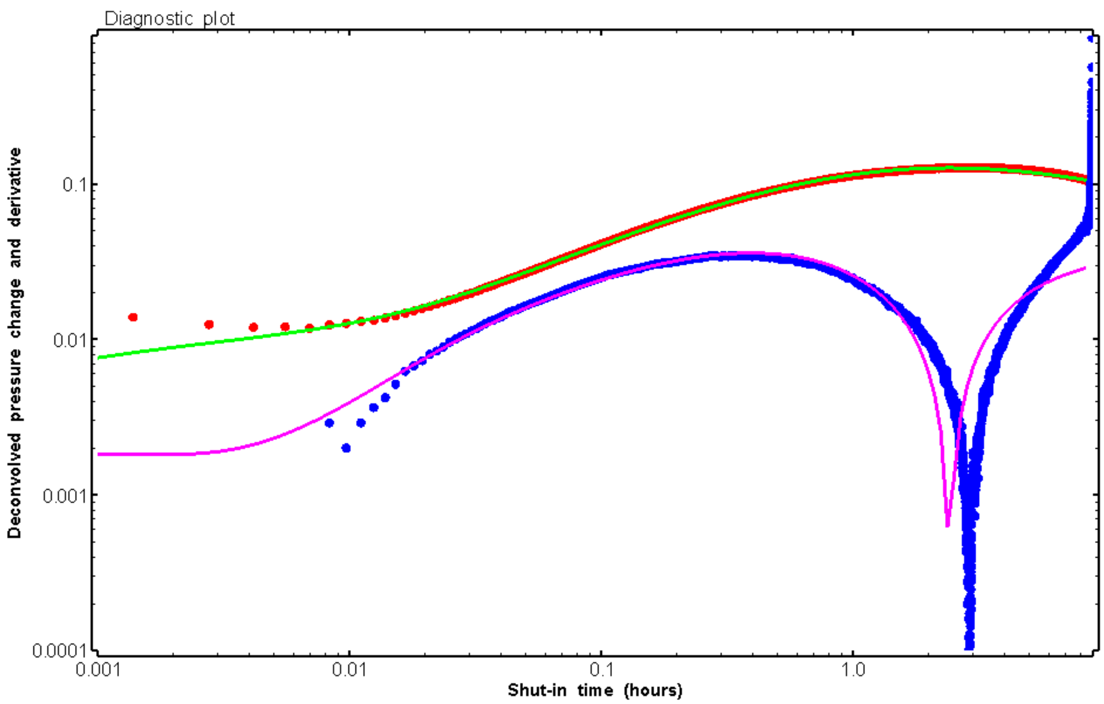

Figure 316: HT030 Deconvolved pressure change and derivative plot of the PW sequence showing best-fit simulation

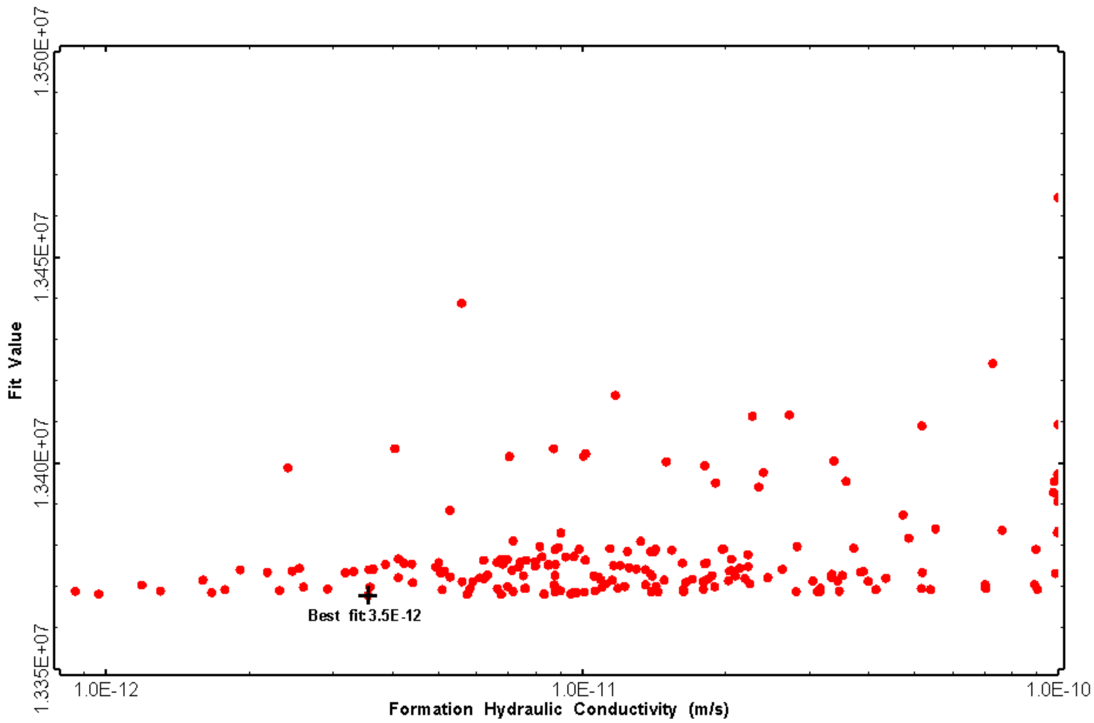

Figure 317: HT030 XY-scatter plot of formation hydraulic conductivity vs. fit value

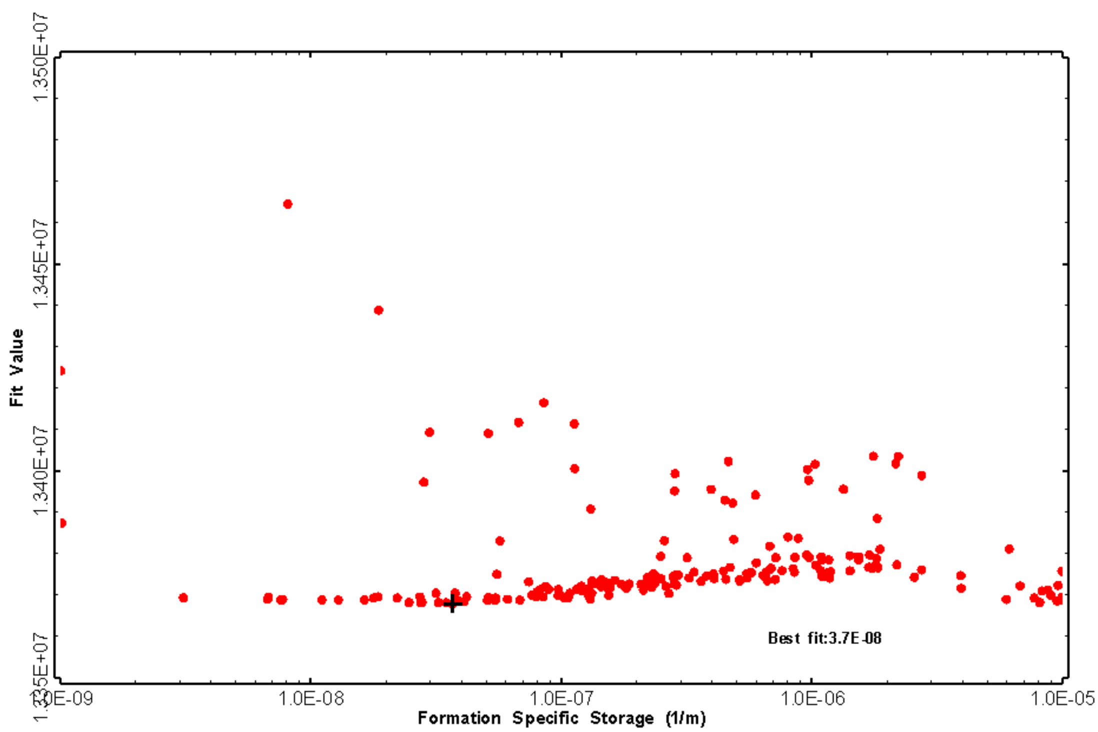

Figure 318: HT030 XY-scatter plot of formation specific storage vs. fit value

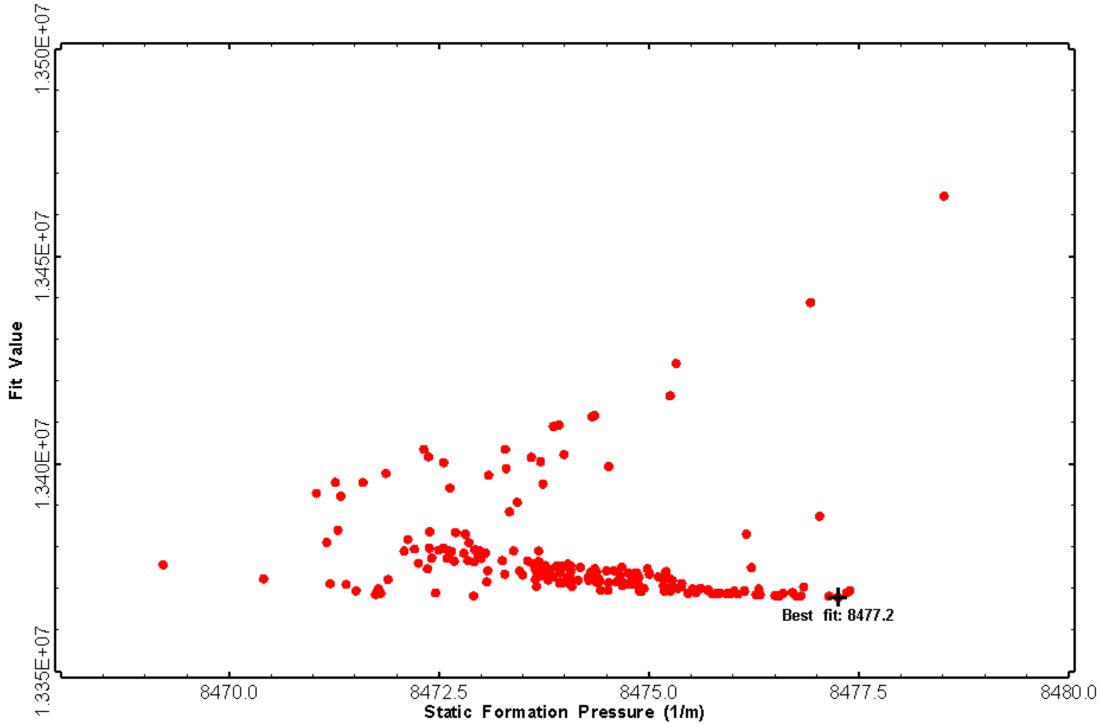

Figure 319: HT030 XY-scatter plot of static formation pressure vs. fit value

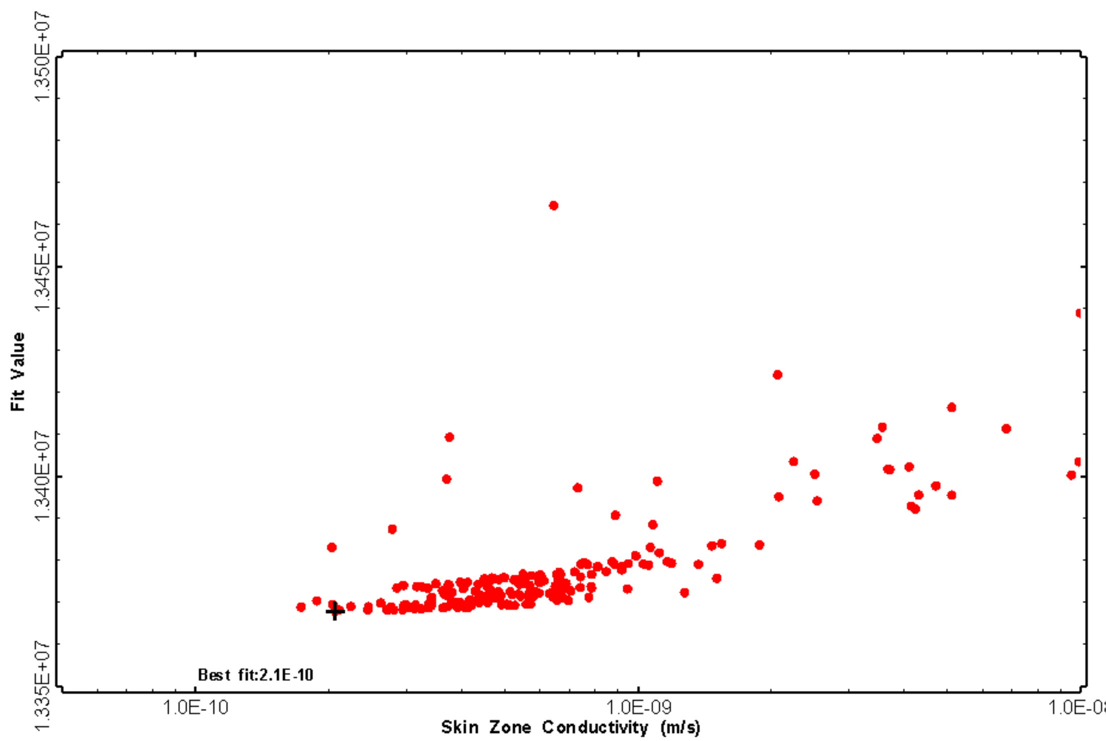

Figure 320: HT030 XY-scatter plot of skin zone conductivity vs. fit value

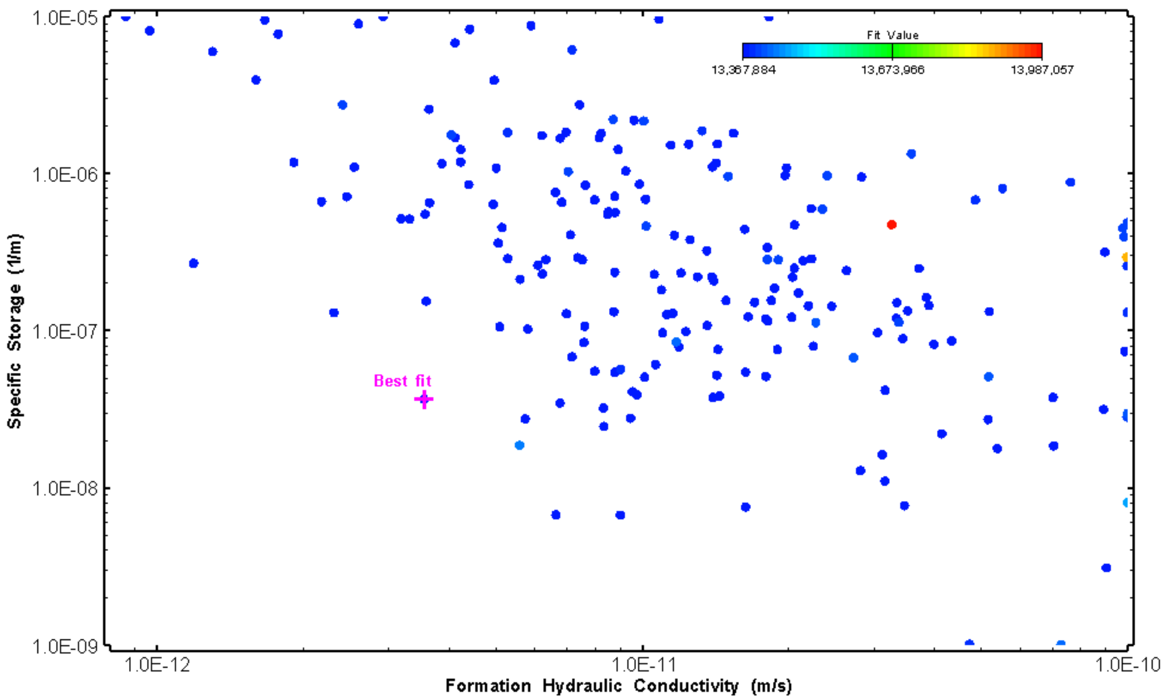

Figure 321: HT030 XY-scatter plot showing estimates of formation hydraulic conductivity and specific storage from perturbation analysis

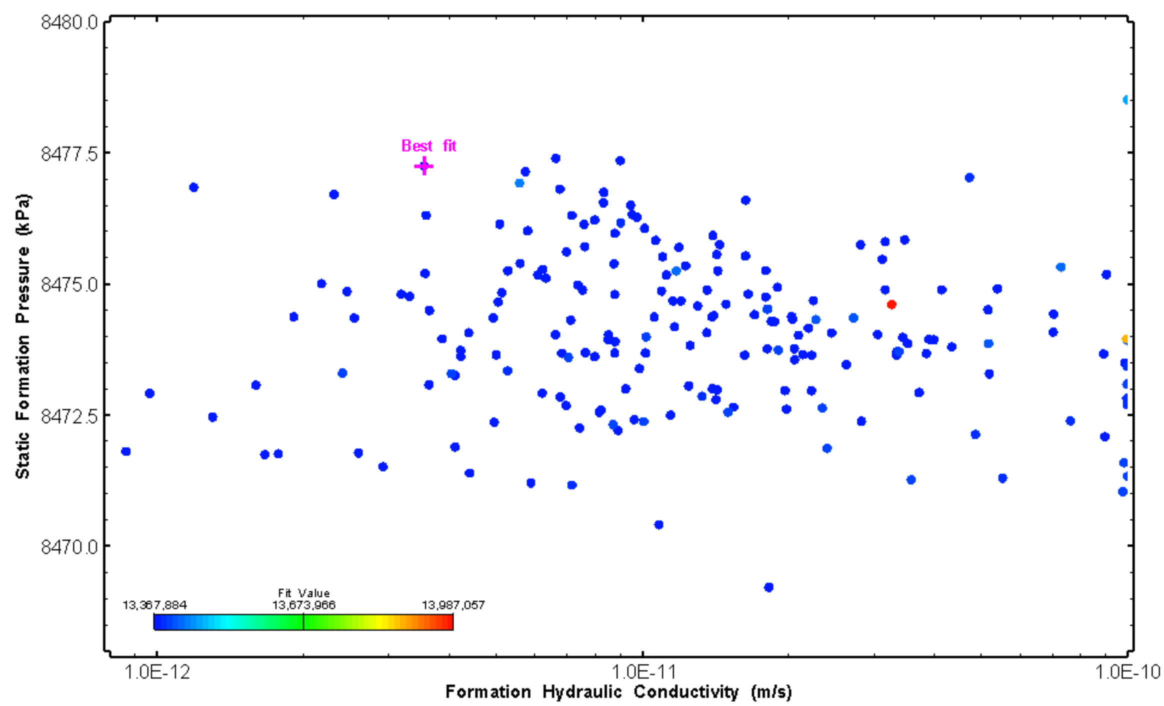

Figure 322: HT030 XY-scatter plot showing estimates of formation hydraulic conductivity and static formation pressure from perturbation analysis

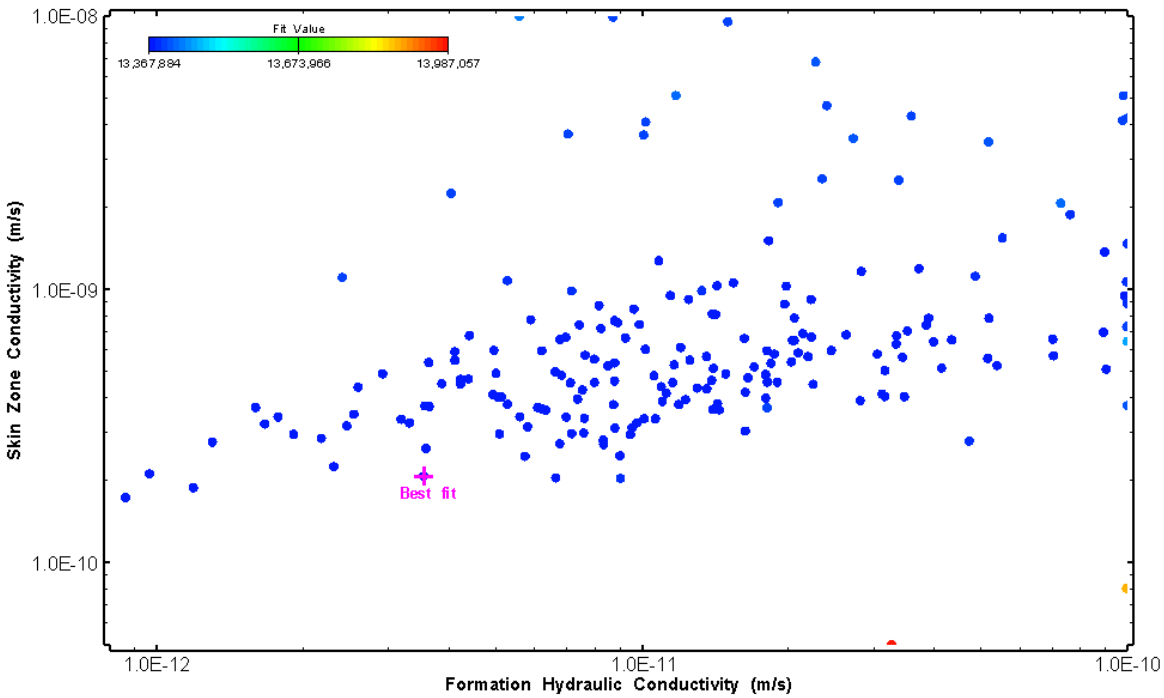

Figure 323: HT030 XY-scatter plot showing estimates of formation hydraulic conductivity and skin zone conductivity from perturbation analysis

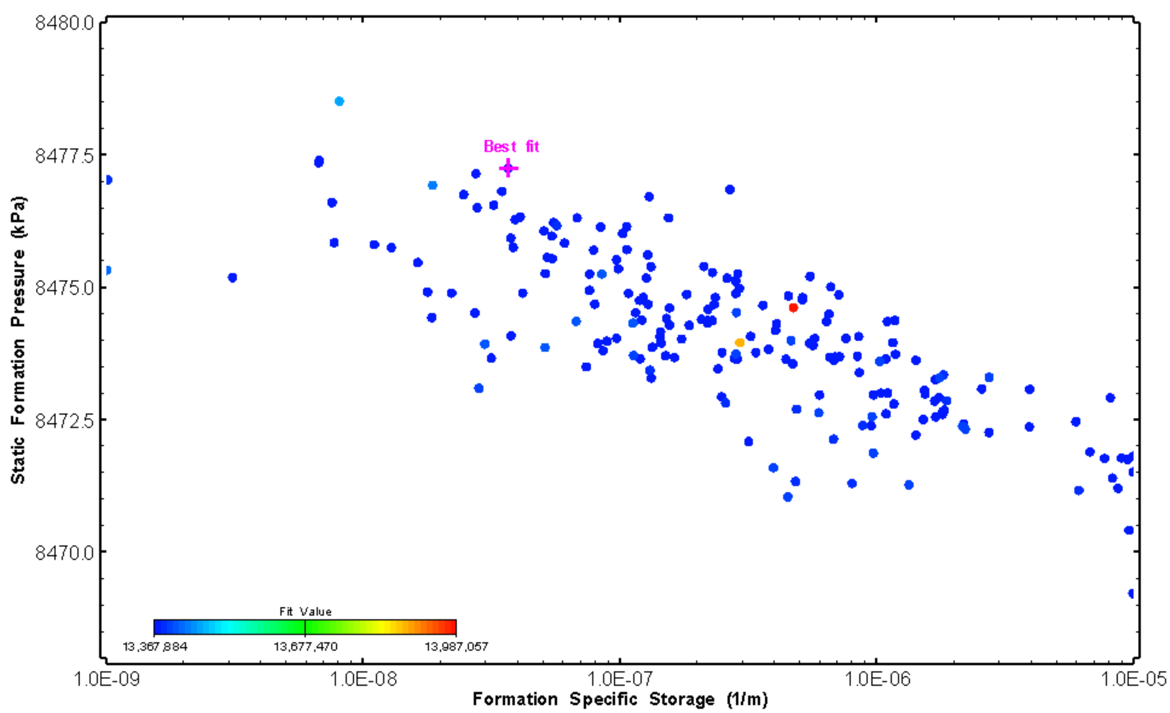

Figure 324: HT030 XY-scatter plot showing estimates of specific storage and static formation pressure from perturbation analysis

28.0 LT001 (74.58 – 94.61 M)

LT001 was completed to confirm that the tool performance met the project's requirement of accurately measuring test interval hydraulic conductivity down to 10^{-13} m/sec. LT001 was conducted within the well surface casing.

The test was initiated with a shut-in pressure recovery phase (PSR). A slug withdrawal test (SW) followed by a slug withdrawal shut-in (SWS) phase were completed after the PSR phase.

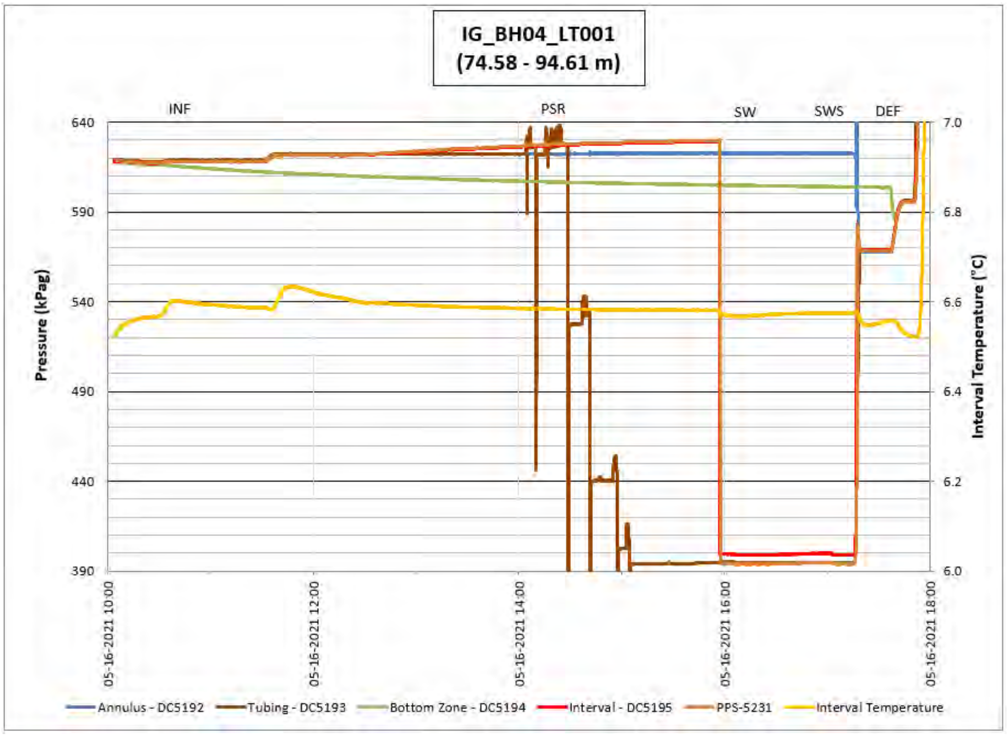

Figure 325: LT001 Annotated test plot showing monitored zone pressure and interval temperature.

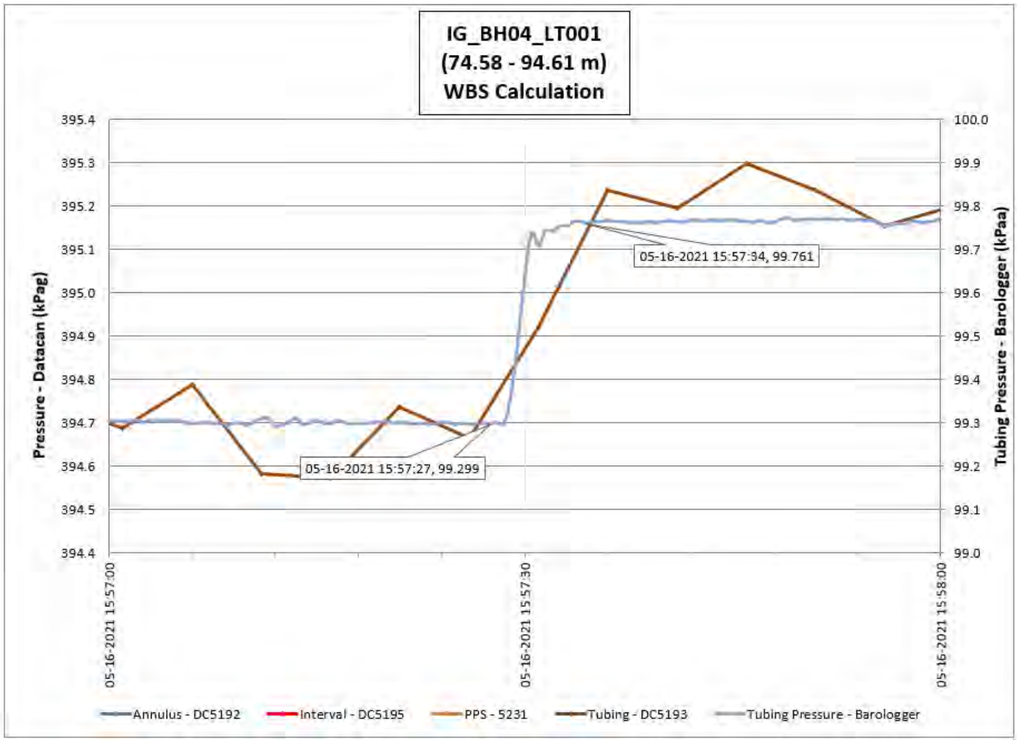

Figure 326: LT001 Tubing pressure during DHSIV activation. DHSIV Closed Wellbore Storage Estimate = 4E-10 m3/Pa

Table 2: Summary of Analysis Results – LT001

	Formation conductivity	Skin zone conductivity	Static formation pressure	Formation specific storage	Radial thickness of skin	Flow dimension
	[m/s]	[m/s]	[kPa]	[1/m]	[m]	[–]
Best Fit	1.6E-14	1.2E-12	617	2.8E-09	1.5E-01	2.5
Minimum	6.4E-15	2.1E-14	609	1.1E-09	4.4E-03	1.4
Maximum	9.5E-13	1.3E-12	647	1.4E-07	7.6E-01	2.7
Mean	3.0E-13	1.3E-13	631	2.4E-08	1.9E-01	2.0
Median	2.3E-13	9.0E-14	631	1.2E-08	1.4E-01	2.0
Geometric mean	2.2E-13	9.2E-14	631	1.3E-08	1.2E-01	2.0

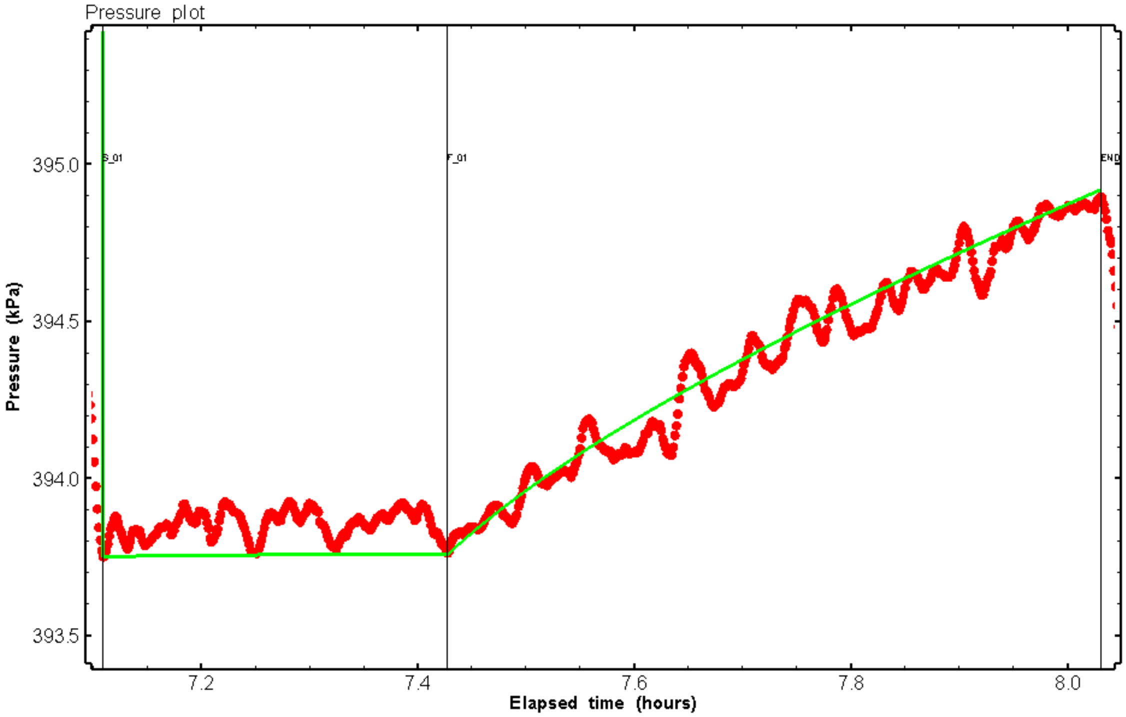

Figure 327: LT001 Pressure plot showing best-fit simulation and best fit results

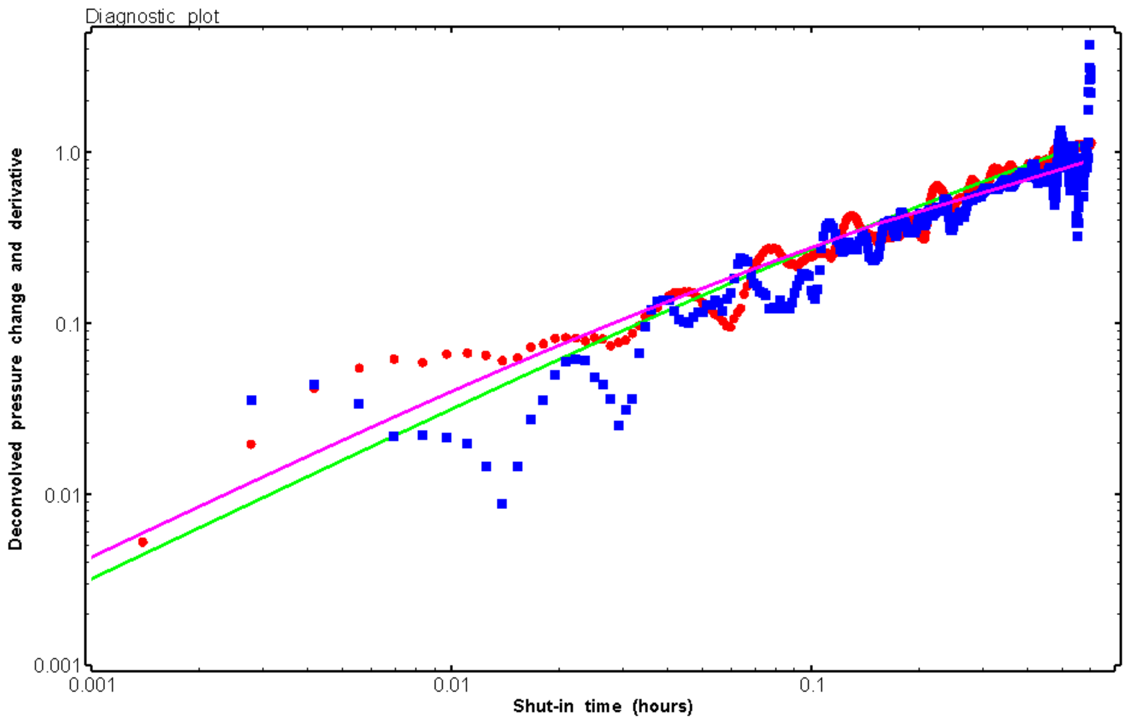

Figure 328: LT001 Deconvolved pressure change and derivative plot

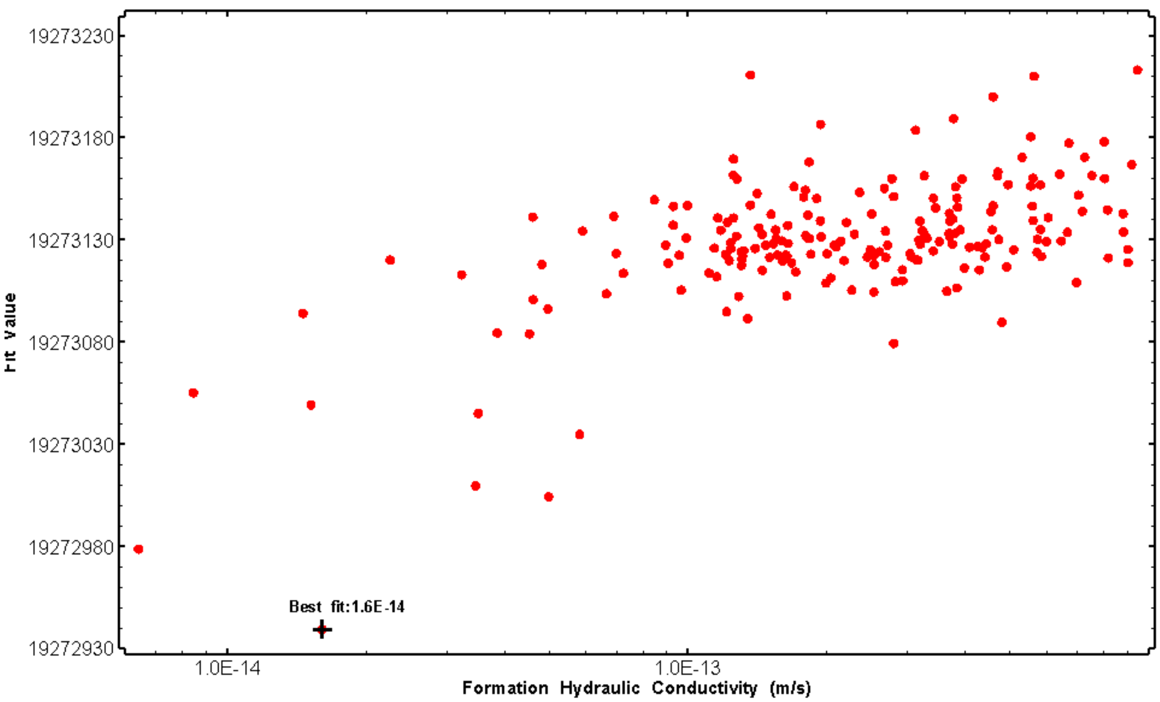

Figure 329: LT001 XY-scatter plot of formation hydraulic conductivity vs. fit value

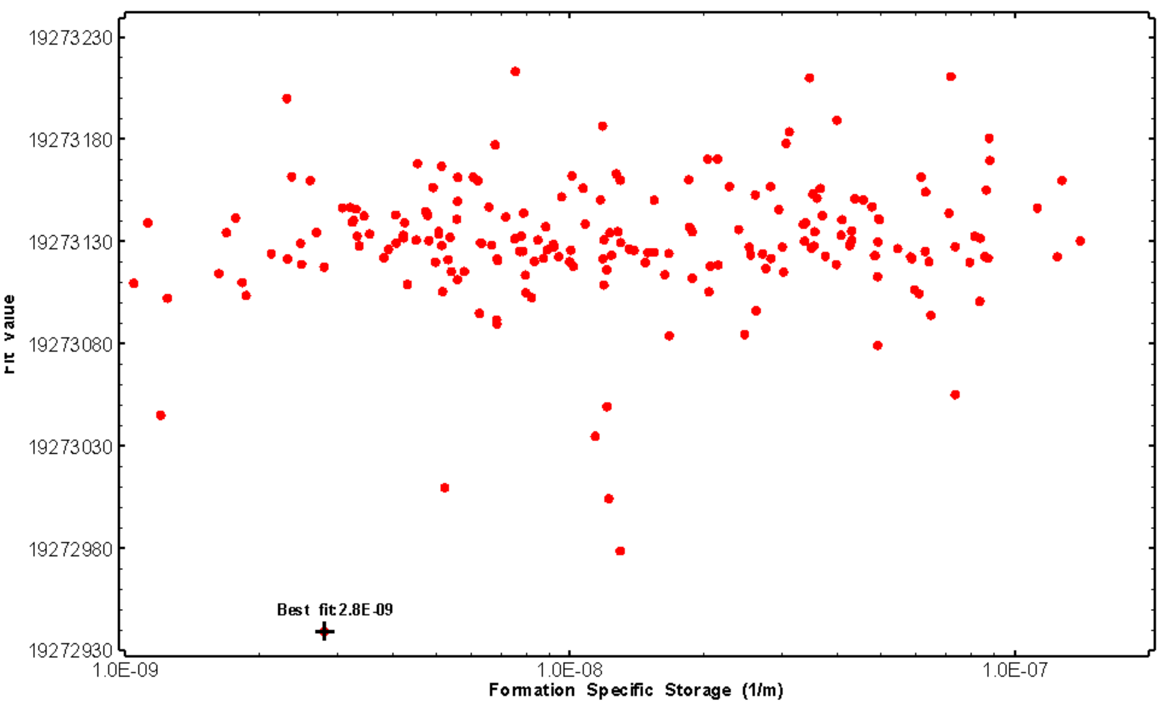

Figure 330: LT001 XY-scatter plot of formation specific storage vs. fit value

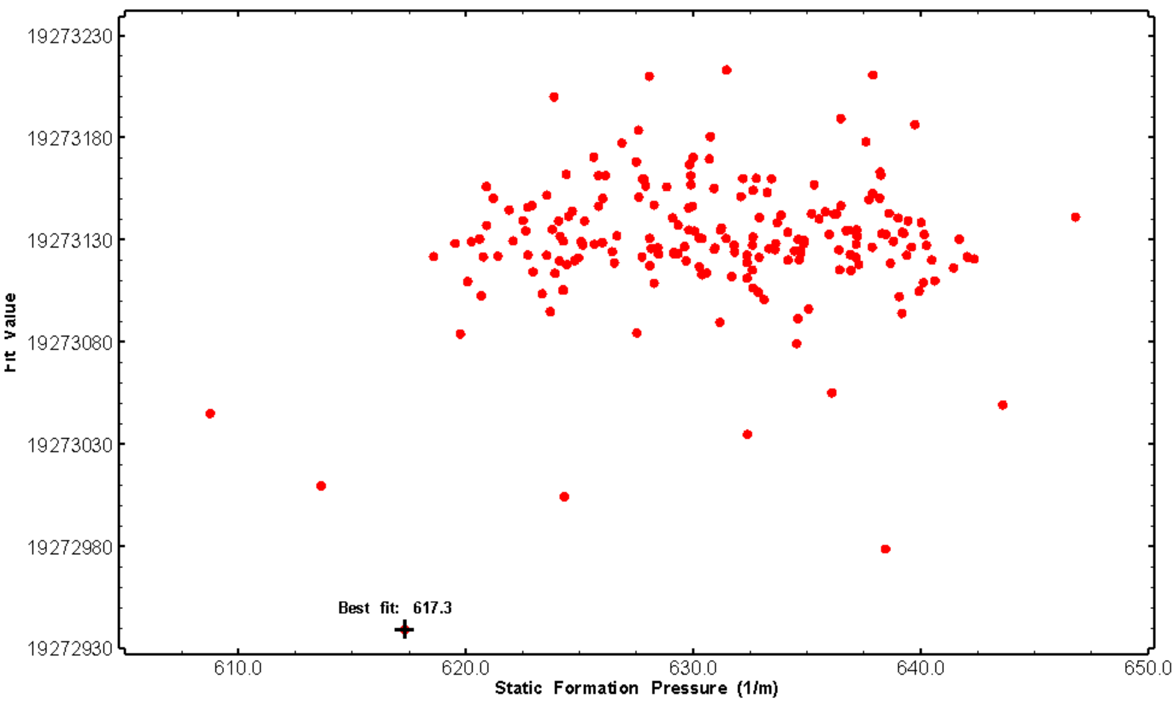

Figure 331: LT001 XY-scatter plot of static formation pressure vs. fit value

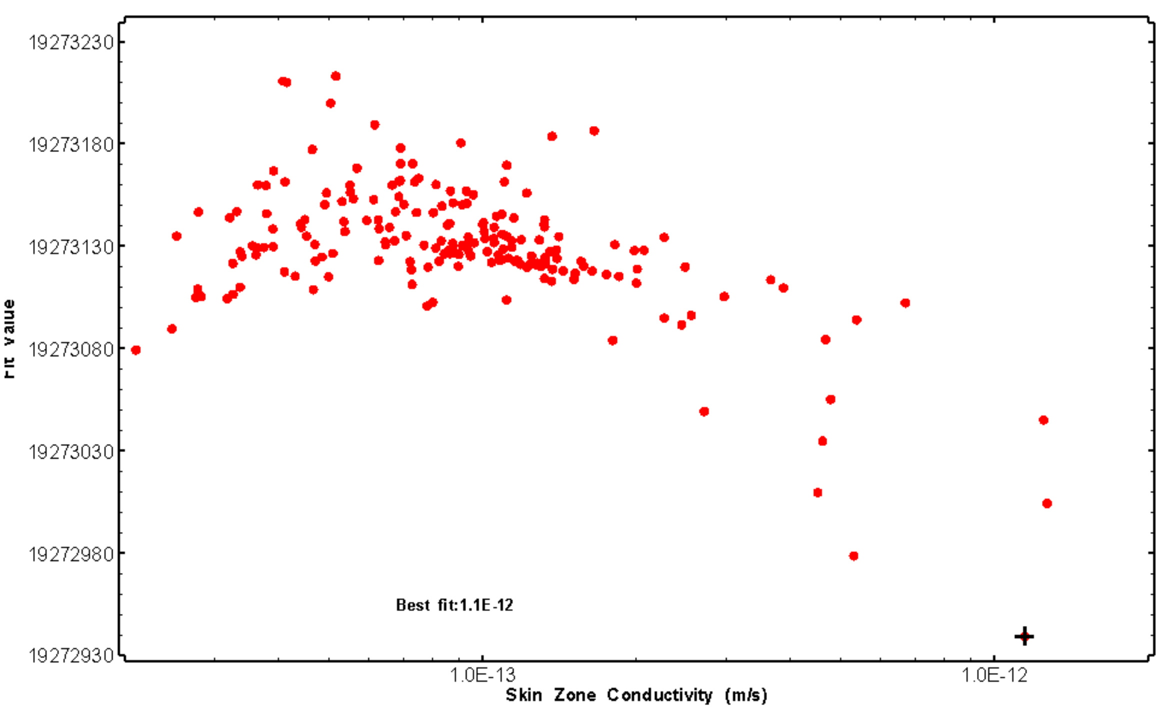

Figure 332: LT001 XY-scatter plot of skin zone conductivity vs. fit value

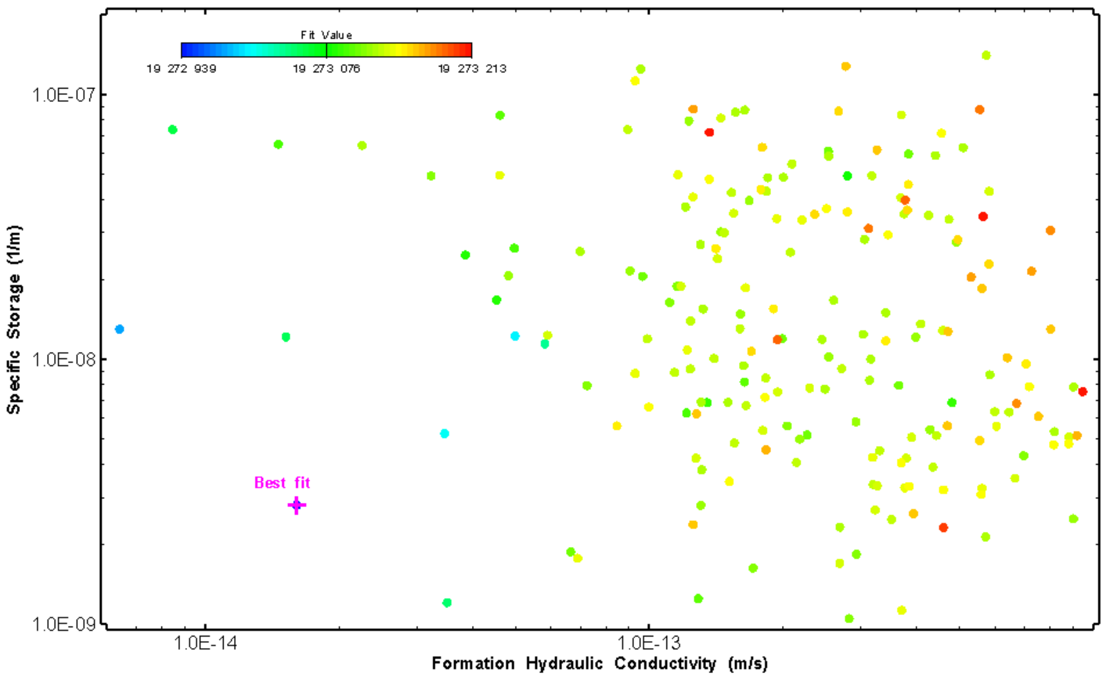

Figure 333: LT001 XY-scatter plot showing estimates of formation hydraulic conductivity and specific storage from perturbation analysis

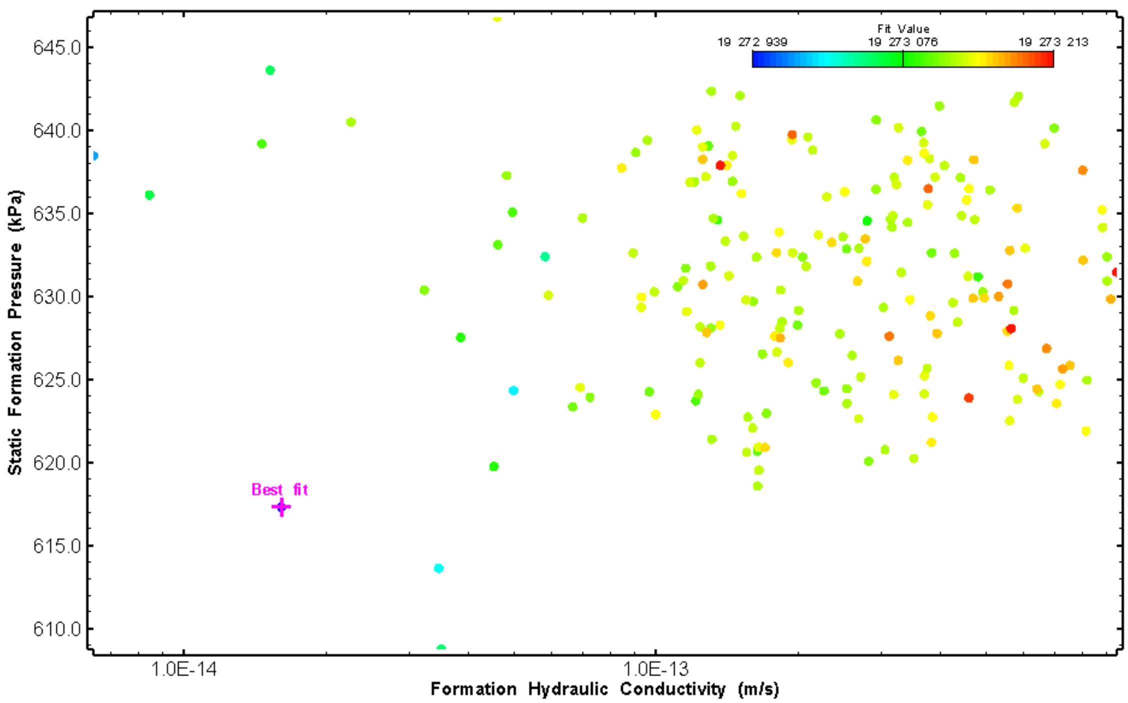

Figure 334: LT001 XY-scatter plot showing estimates of formation hydraulic conductivity and static formation pressure from perturbation analysis

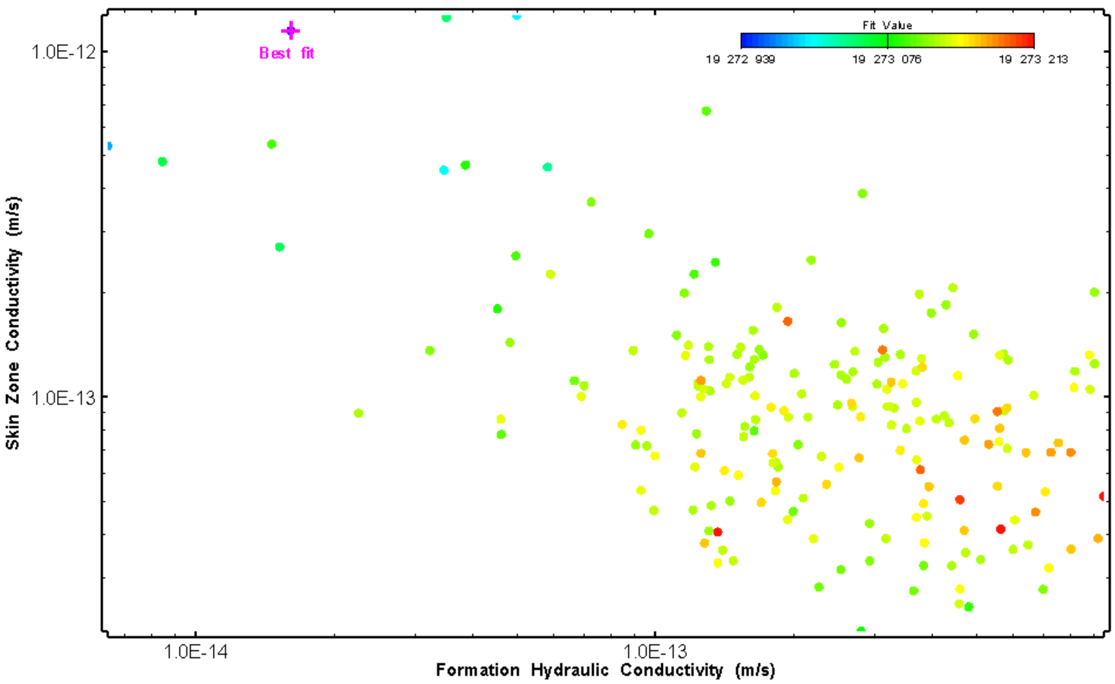

Figure 335: LT001 XY-scatter plot showing estimates of formation hydraulic conductivity and skin zone conductivity from perturbation analysis

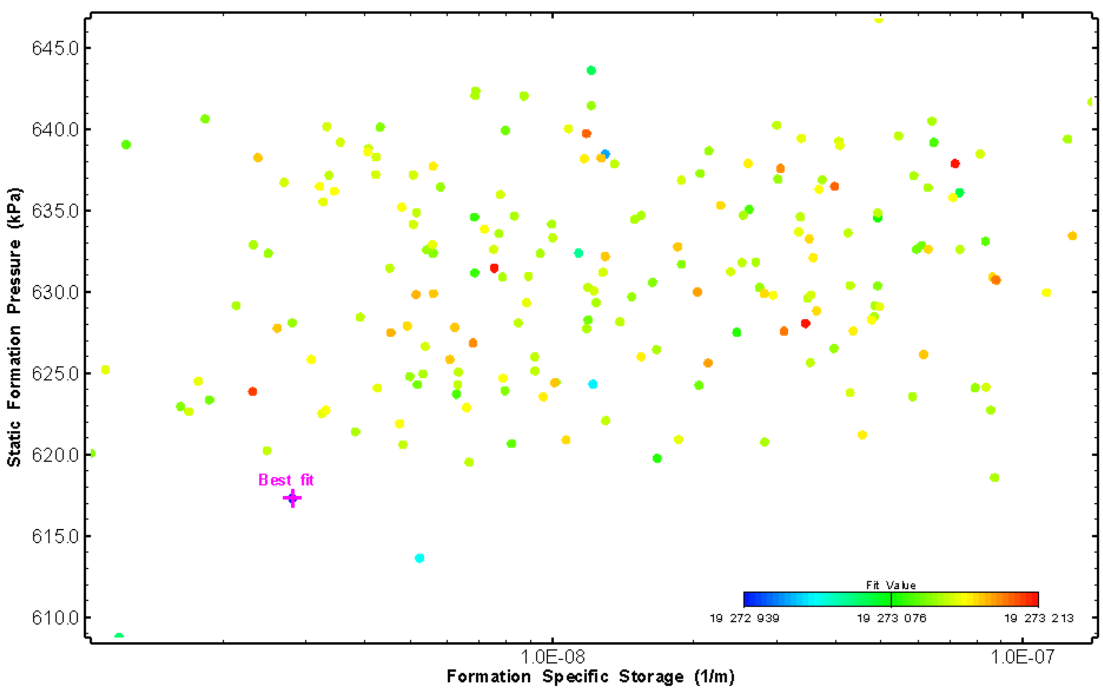

Figure 336: LT001 XY-scatter plot showing estimates of specific storage and static formation pressure from perturbation analysis

29.0 LT002 (74.62 – 94.65 M)

LT002 was completed to confirm that the tool performance met the project's requirement of accurately measuring test interval hydraulic conductivity down to 10^{-13} m/sec. LT002 was conducted within the well surface casing.

The test was initiated with a shut-in pressure recovery phase (PSR). A slug withdrawal test (SW) followed by a slug withdrawal shut-in (SWS) phase were completed after the PSR phase.

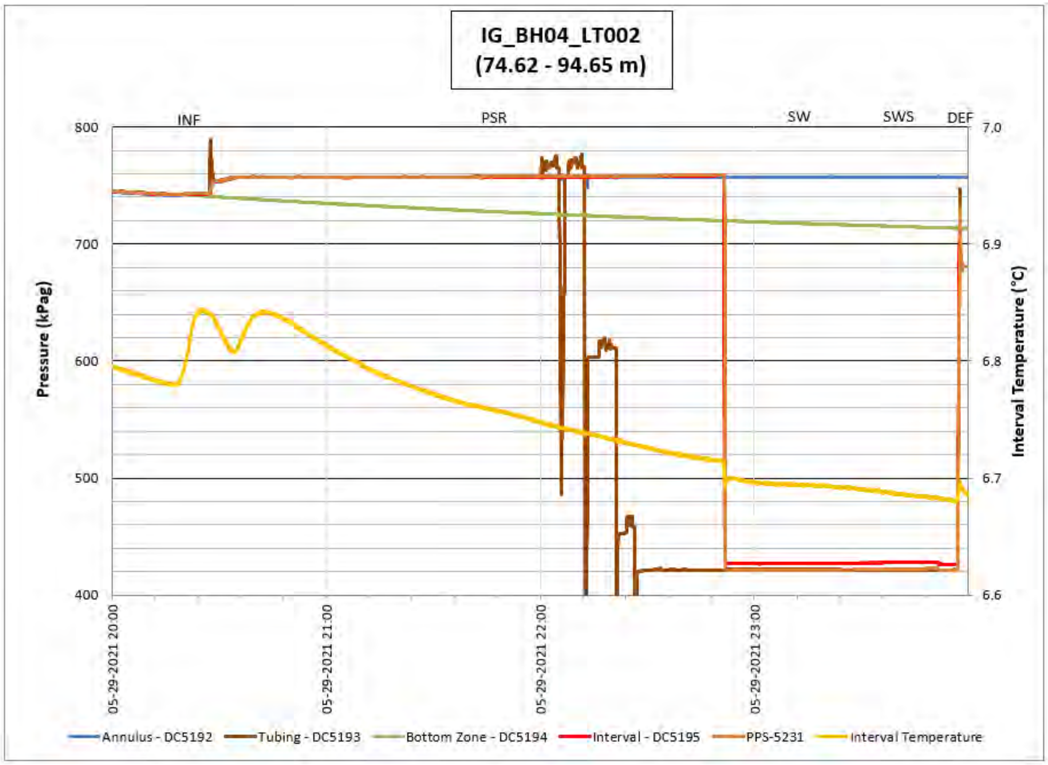

Figure 337: LT002 Annotated test plot showing monitored zone pressure and interval temperature.

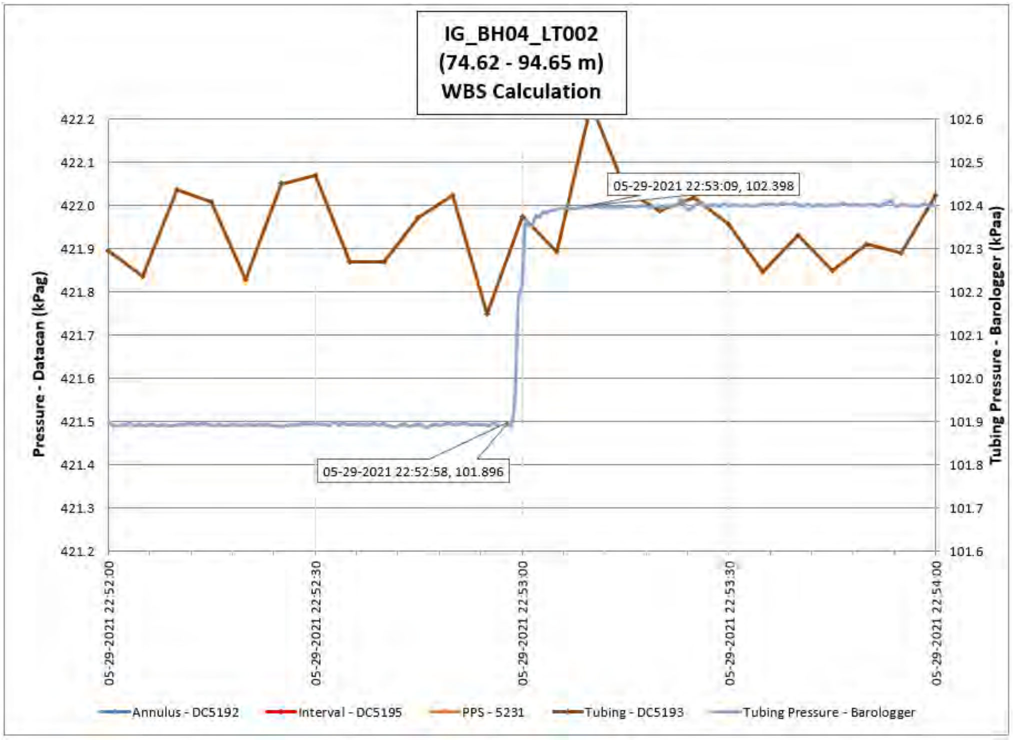

Figure 338: LT002 Tubing pressure during DHSIV activation. DHSIV Closed Wellbore Storage Estimate = 3E-10 m3/Pa

Table 3: Summary of Analysis Results – LT002

	Formation conductivity	Skin zone conductivity	Static formation pressure	Formation specific storage	Radial thickness of skin	Flow dimension
	[m/s]	[m/s]	[kPa]	[1/m]	[m]	[–]
Best Fit	7.4E-15	1.8E-11	777	4.3E-09	2.8E-01	2.4
Minimum	1.8E-15	1.2E-12	671	1.2E-09	1.7E-01	1.4
Maximum	5.0E-14	9.9E-09	797	2.8E-07	8.5E-01	2.6
Mean	1.1E-14	1.1E-09	757	3.3E-08	3.9E-01	2.0
Median	7.7E-15	1.8E-10	759	1.6E-08	3.7E-01	2.0
Geometric mean	8.3E-15	2.2E-10	756	1.7E-08	3.8E-01	2.0

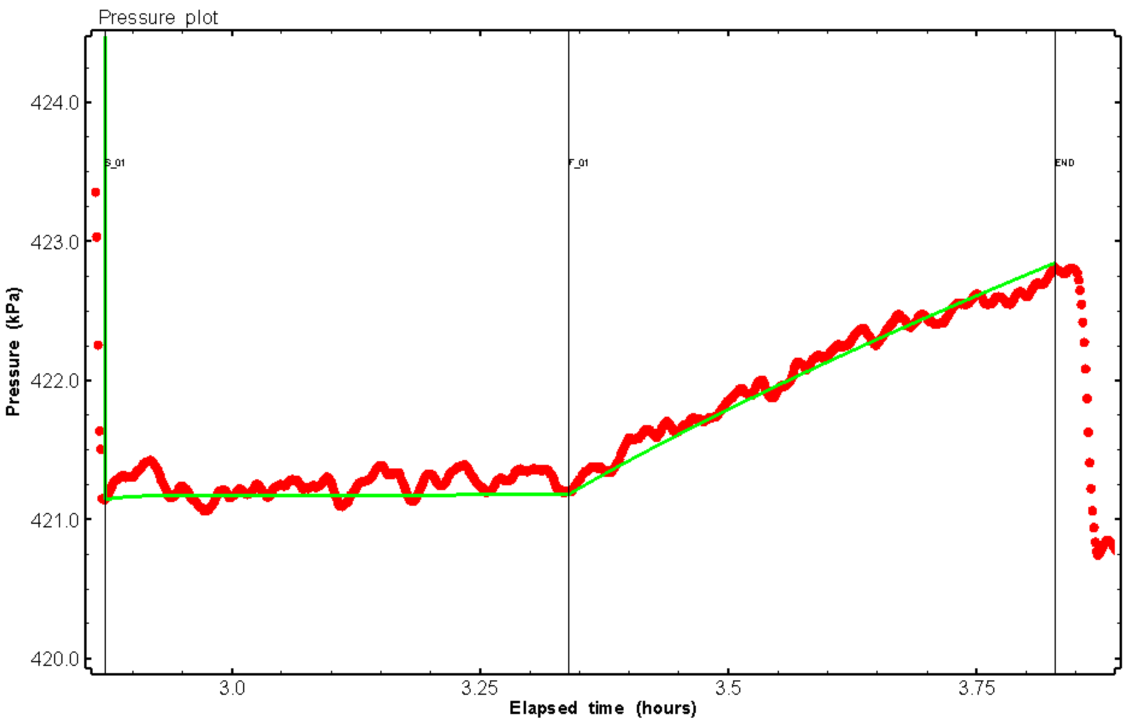

Figure 339: LT002 Pressure plot showing best-fit simulation and best fit results

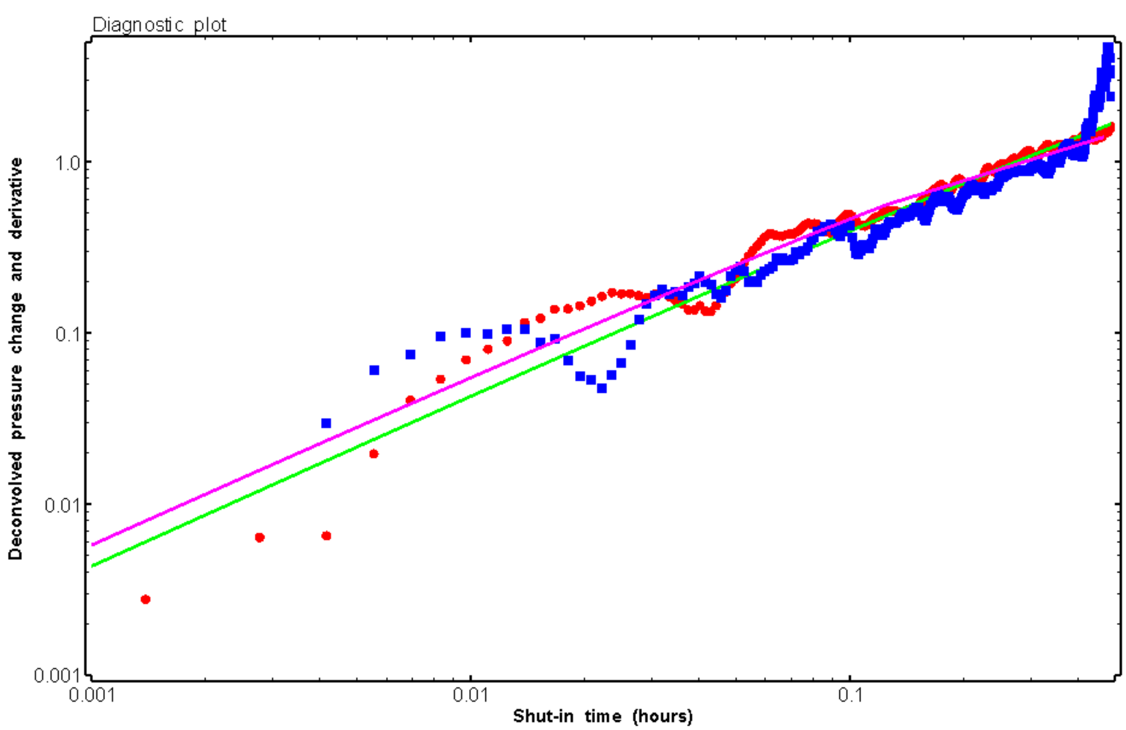

Figure 340: LT002 Deconvolved pressure change and derivative plot

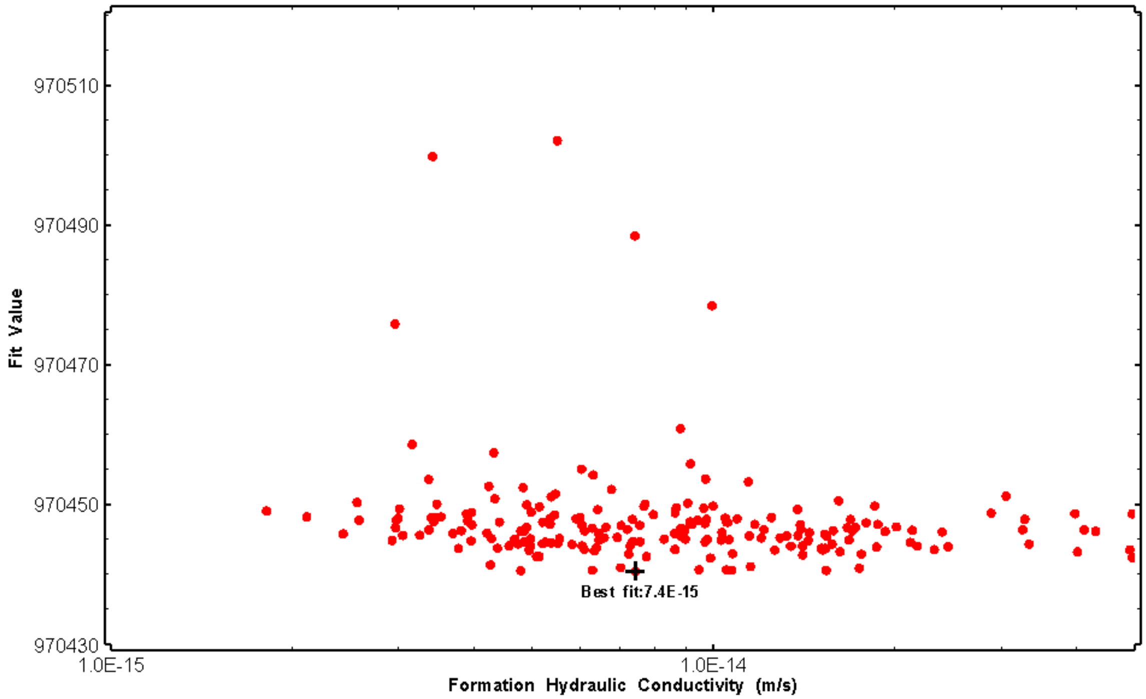

Figure 341: LT002 XY-scatter plot of formation hydraulic conductivity vs. fit value

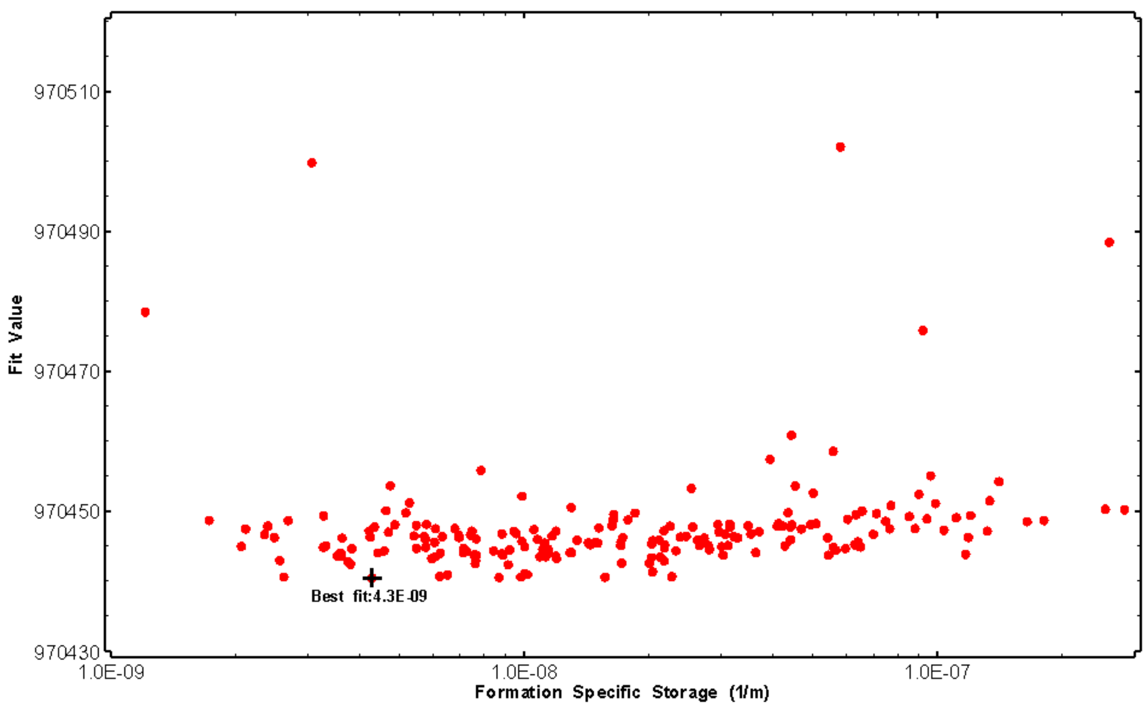

Figure 342: LT002 XY-scatter plot of formation specific storage vs. fit value

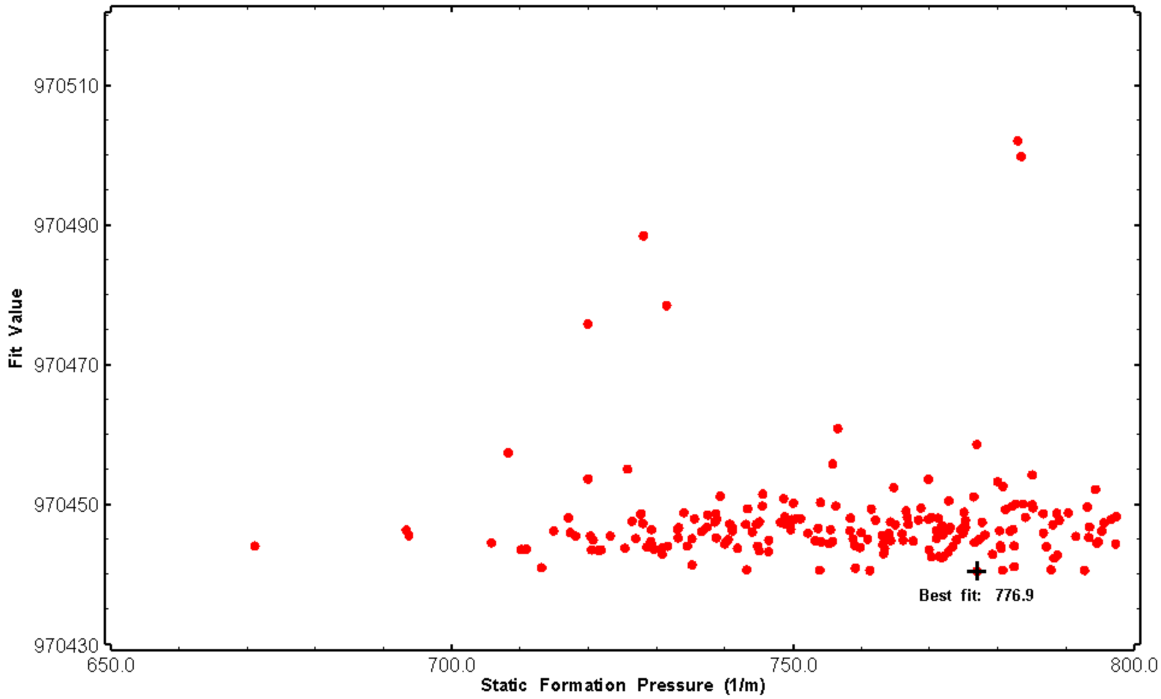

Figure 343: LT002 XY-scatter plot of static formation pressure vs. fit value

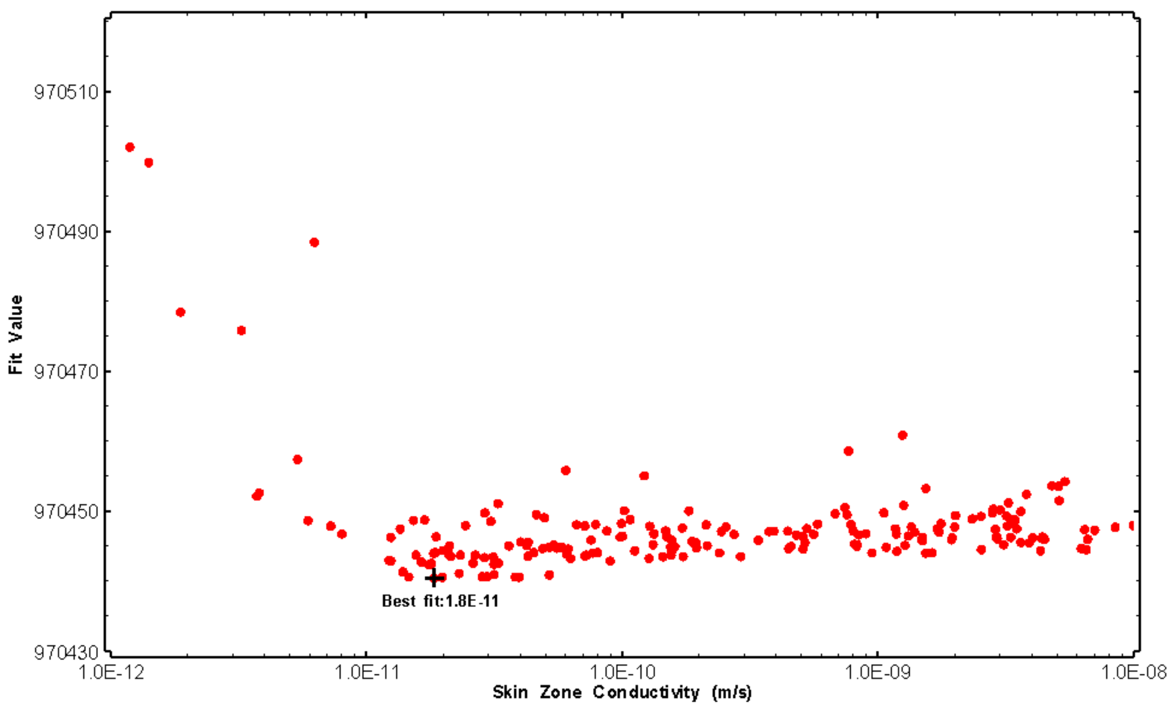

Figure 344: LT002 XY-scatter plot of skin zone conductivity vs. fit value

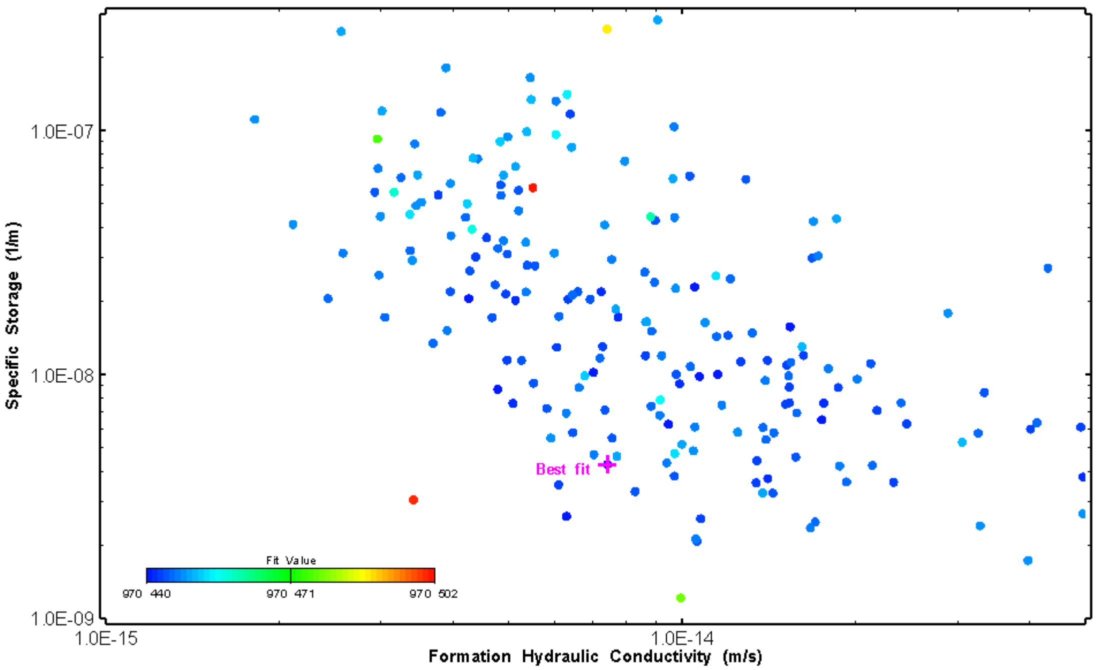

Figure 345: LT002 XY-scatter plot showing estimates of formation hydraulic conductivity and specific storage from perturbation analysis

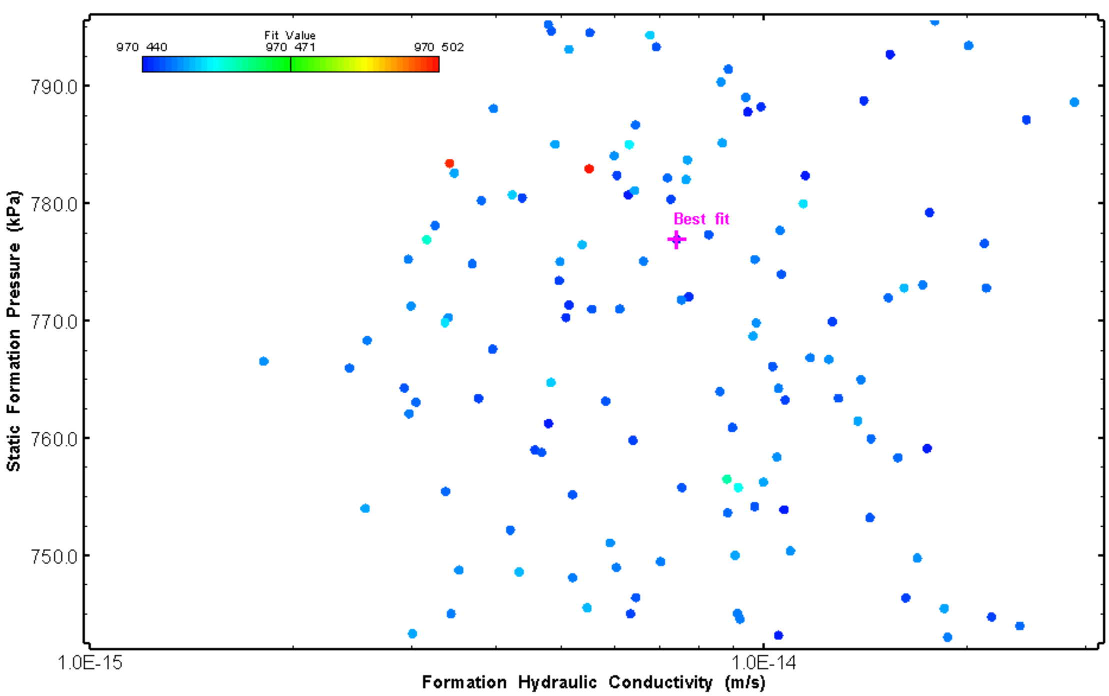

Figure 346: LT002 XY-scatter plot showing estimates of formation hydraulic conductivity and static formation pressure from perturbation analysis

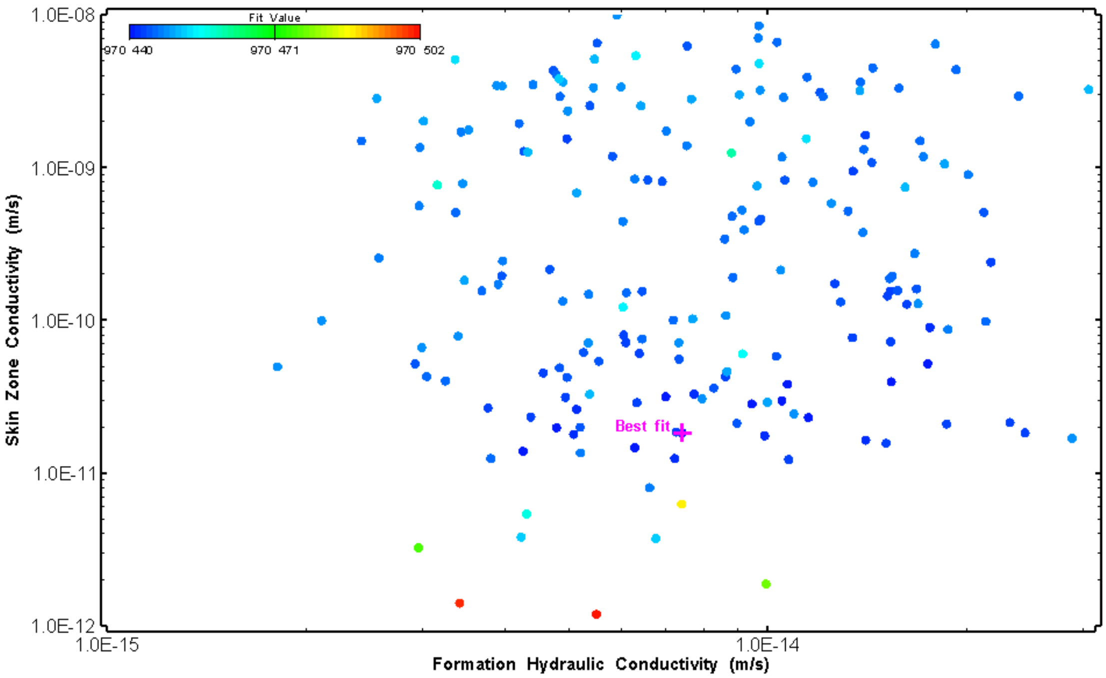

Figure 347: LT002 XY-scatter plot showing estimates of formation hydraulic conductivity and skin zone conductivity from perturbation analysis

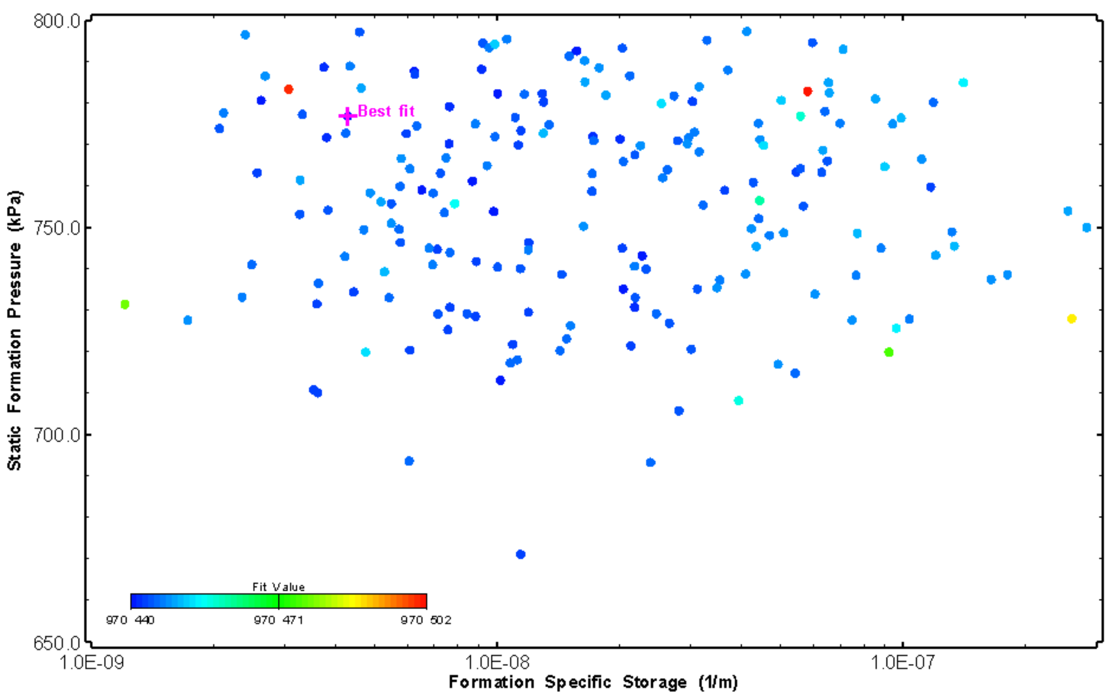

Figure 348: LT002 XY-scatter plot showing estimates of specific storage and static formation pressure from perturbation analysis

30.0 LT003 (74.61 – 94.64 M)

LT003 was completed to confirm that the tool performance met the project's requirement of accurately measuring test interval hydraulic conductivity down to 10^{-13} m/sec. LT003 was conducted within the well surface casing.

The test was initiated with a shut-in pressure recovery phase (PSR). A slug withdrawal test (SW) followed by a slug withdrawal shut-in (SWS) phase were completed after the PSR phase.

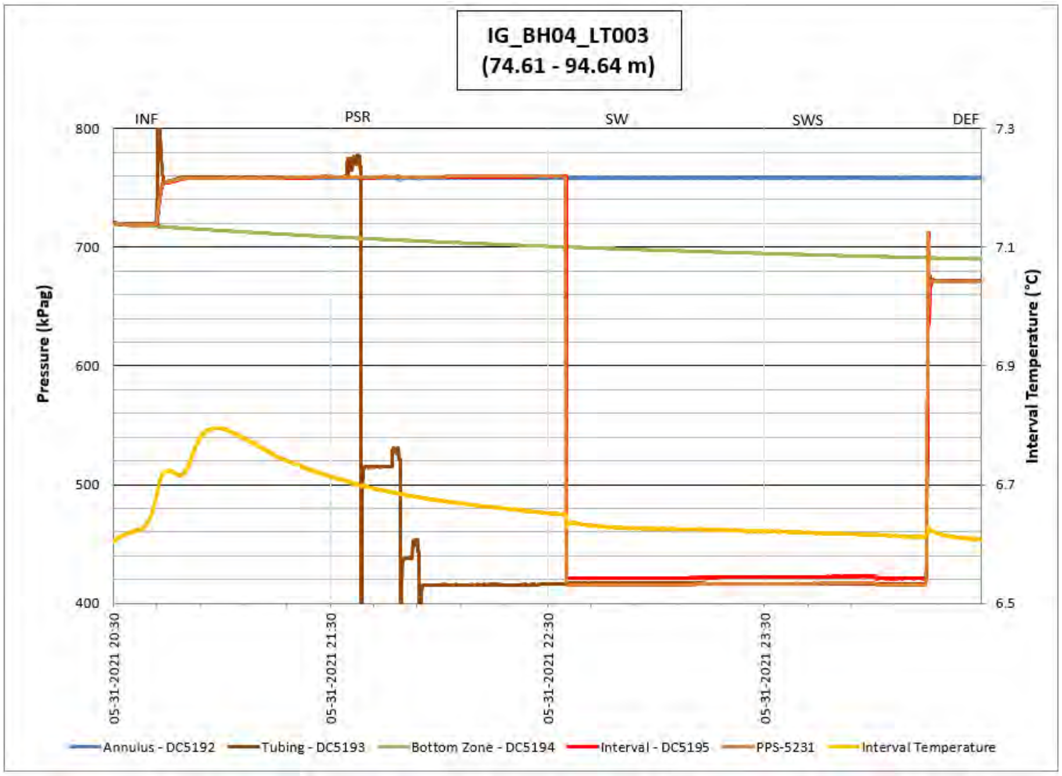

Figure 349: LT003 Annotated test plot showing monitored zone pressure and interval temperature.

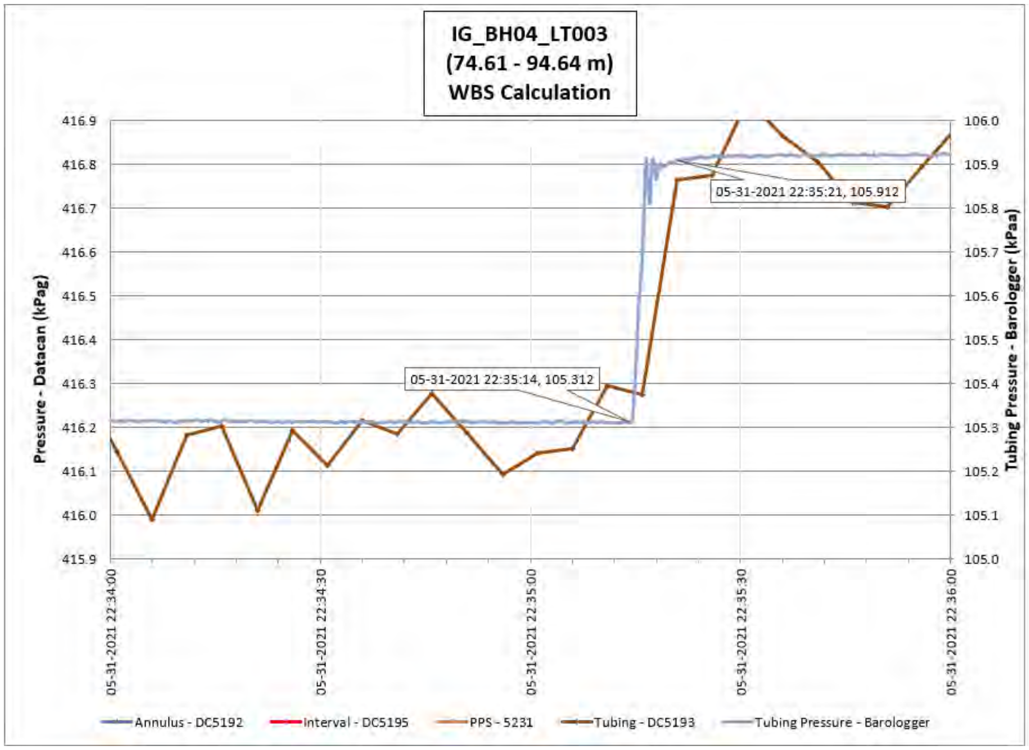

Figure 350: LT003 Tubing pressure during DHSIV activation. DHSIV Closed Wellbore Storage Estimate = 3E-10 m3/Pa

Table 4: Summary of Analysis Results – LT003

	Formation conductivity	Skin zone conductivity	Static formation pressure	Formation specific storage	Radial thickness of skin	Flow dimension
	[m/s]	[m/s]	[kPa]	[1/m]	[m]	[–]
Best Fit	2.7E-15	2.4E-12	765	2.8E-07	2.4E-01	1.6
Minimum	1.1E-15	3.5E-14	759	1.4E-09	1.1E-03	1.0
Maximum	2.1E-14	8.1E-11	770	9.5E-06	8.2E-01	2.8
Mean	3.6E-15	6.8E-12	767	1.7E-06	1.7E-01	1.9
Median	2.7E-15	1.7E-12	767	1.4E-06	8.4E-02	1.9
Geometric mean	2.9E-15	1.5E-12	767	1.0E-06	1.0E-01	1.9

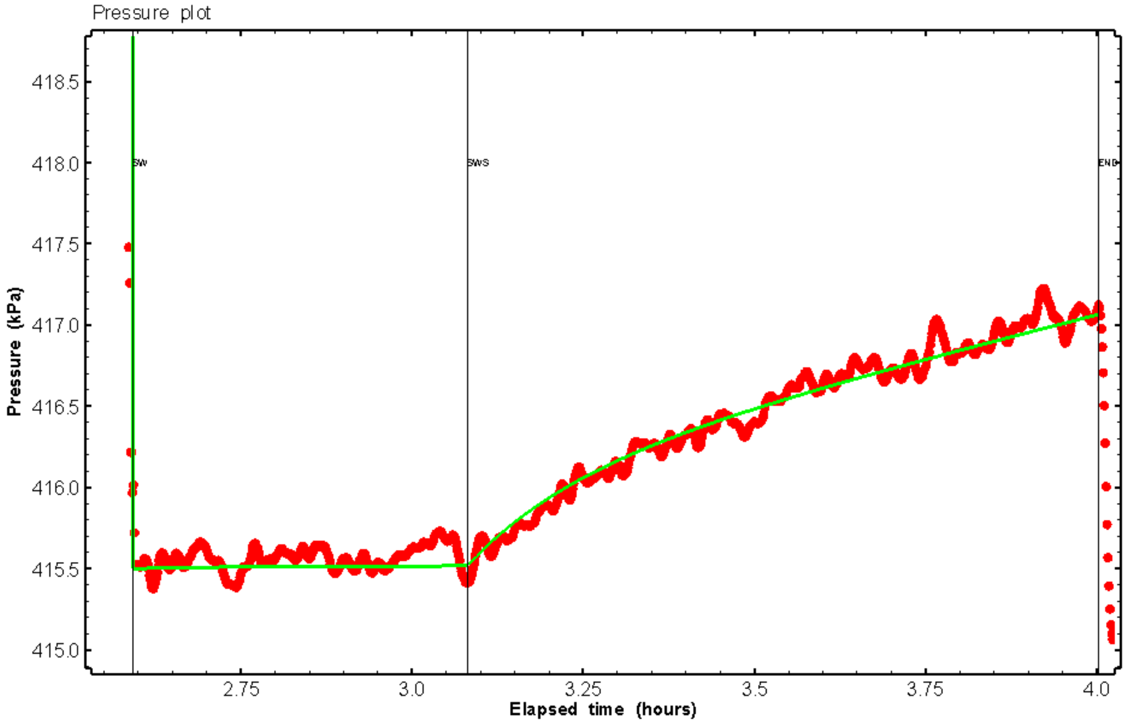

Figure 351: LT003 Pressure plot showing best-fit simulation and best fit results

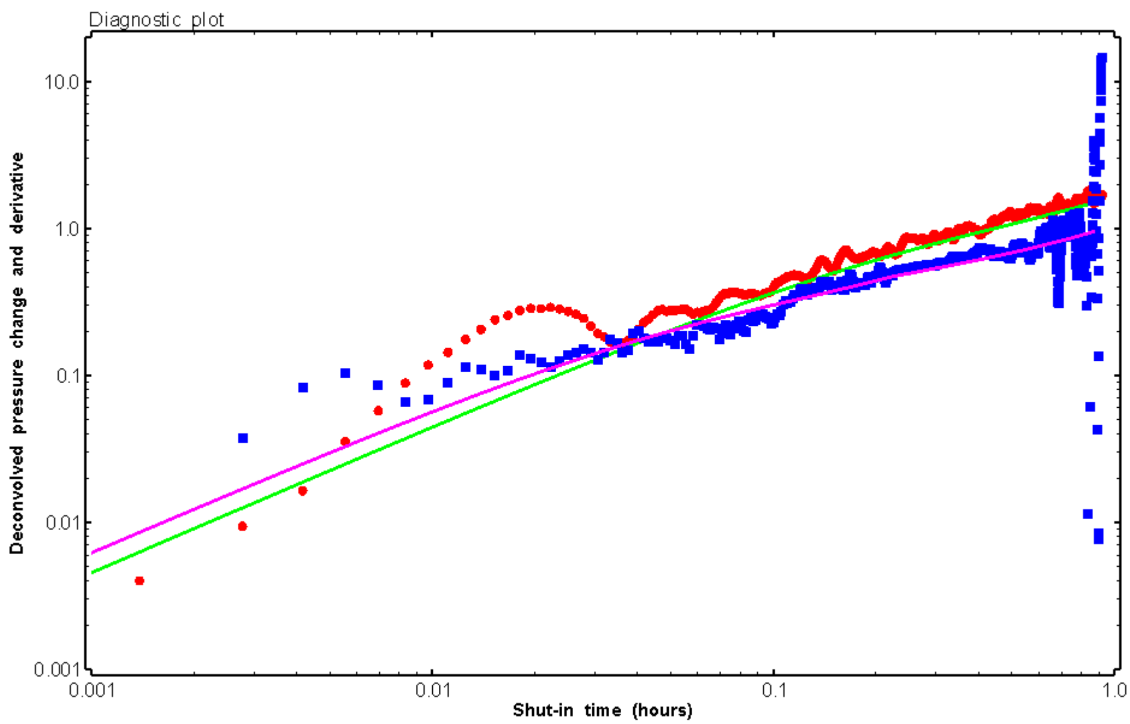

Figure 352: LT003 Deconvolved pressure change and derivative plot

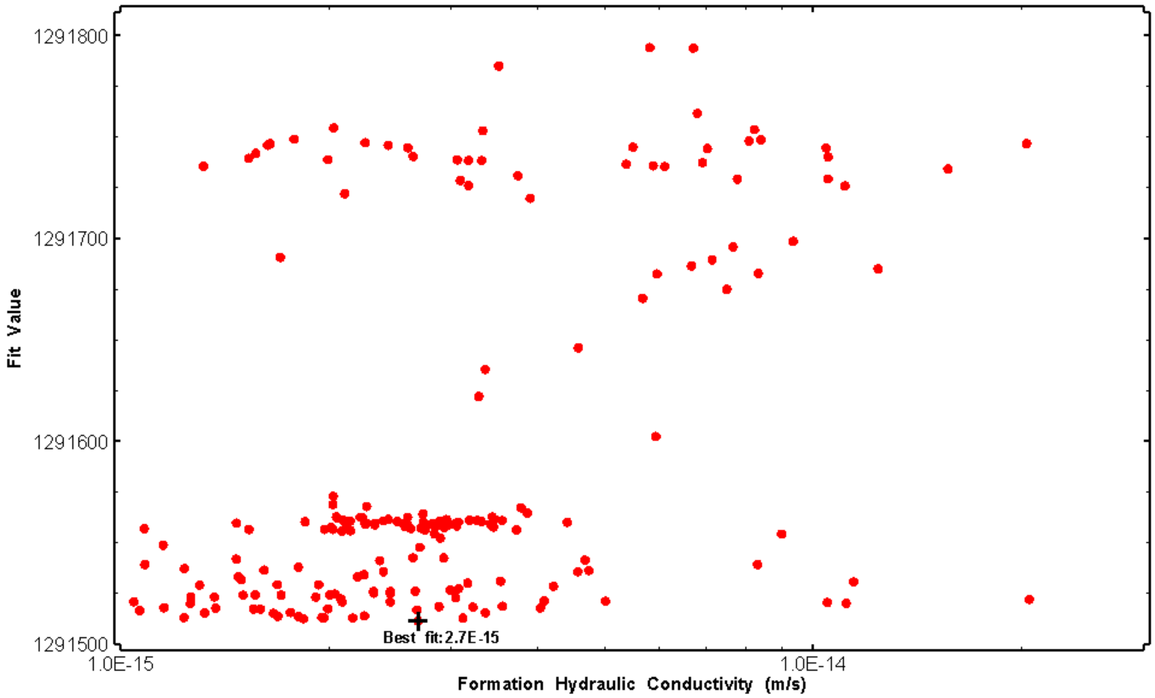

Figure 353: LT003 XY-scatter plot of formation hydraulic conductivity vs. fit value

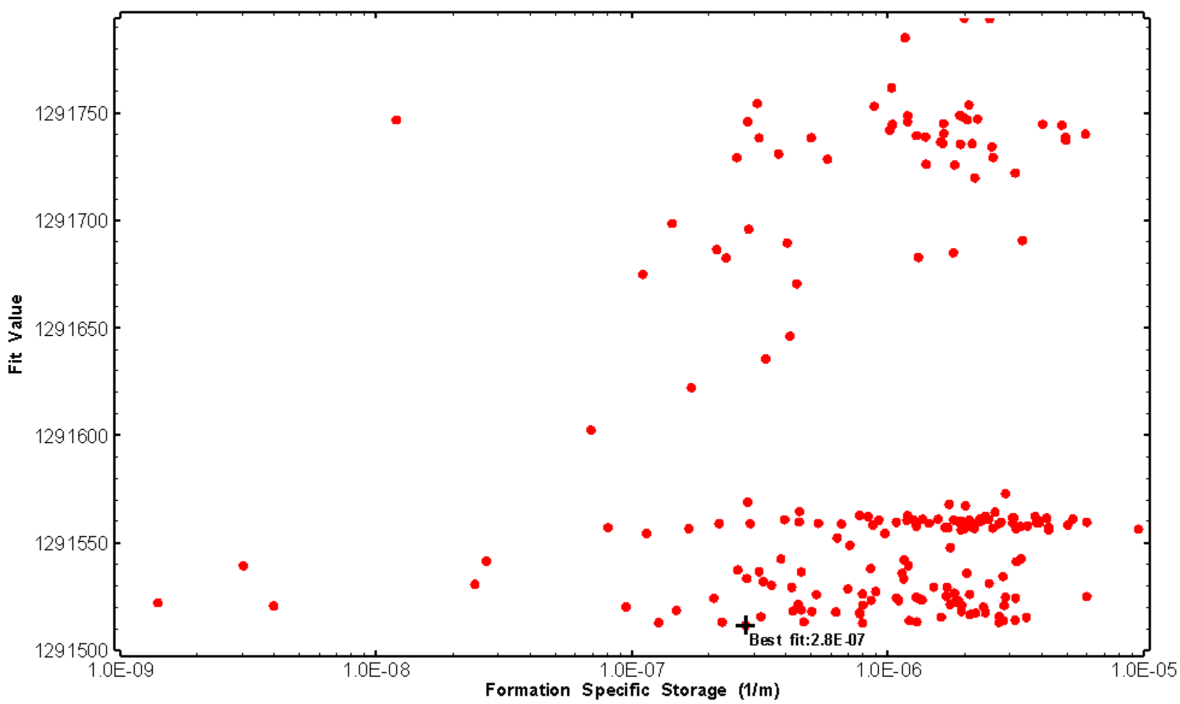

Figure 354: LT003 XY-scatter plot of formation specific storage vs. fit value

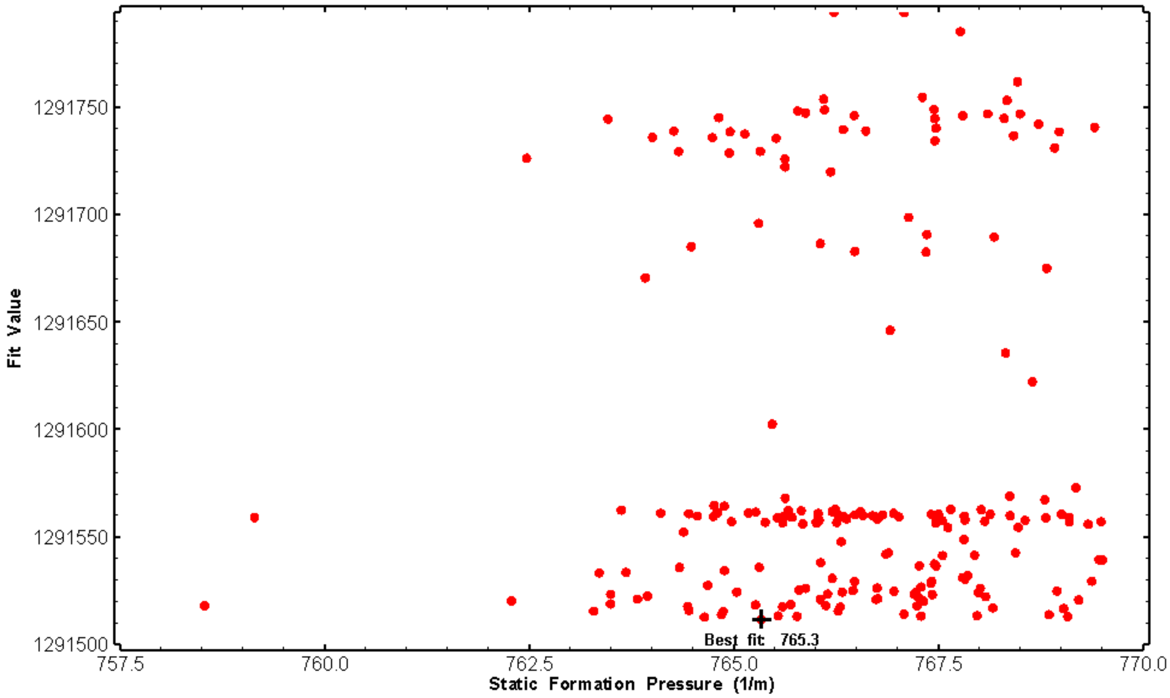

Figure 355: LT003 XY-scatter plot of static formation pressure vs. fit value

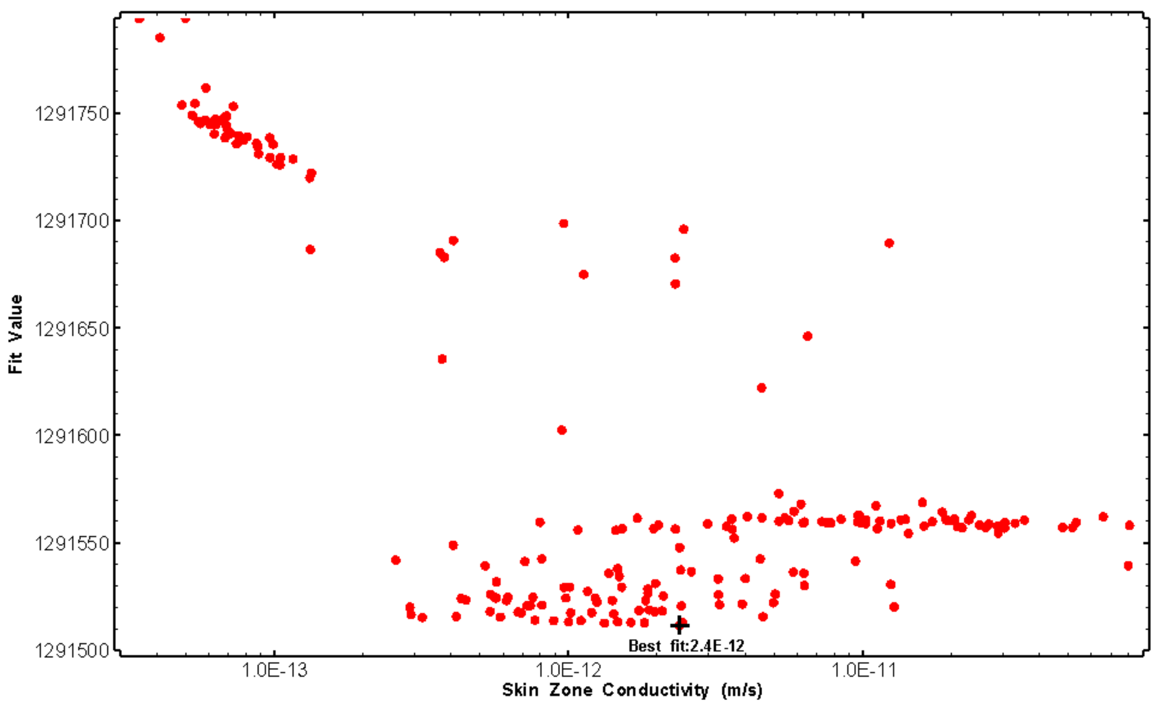

Figure 356: LT003 XY-scatter plot of skin zone conductivity vs. fit value

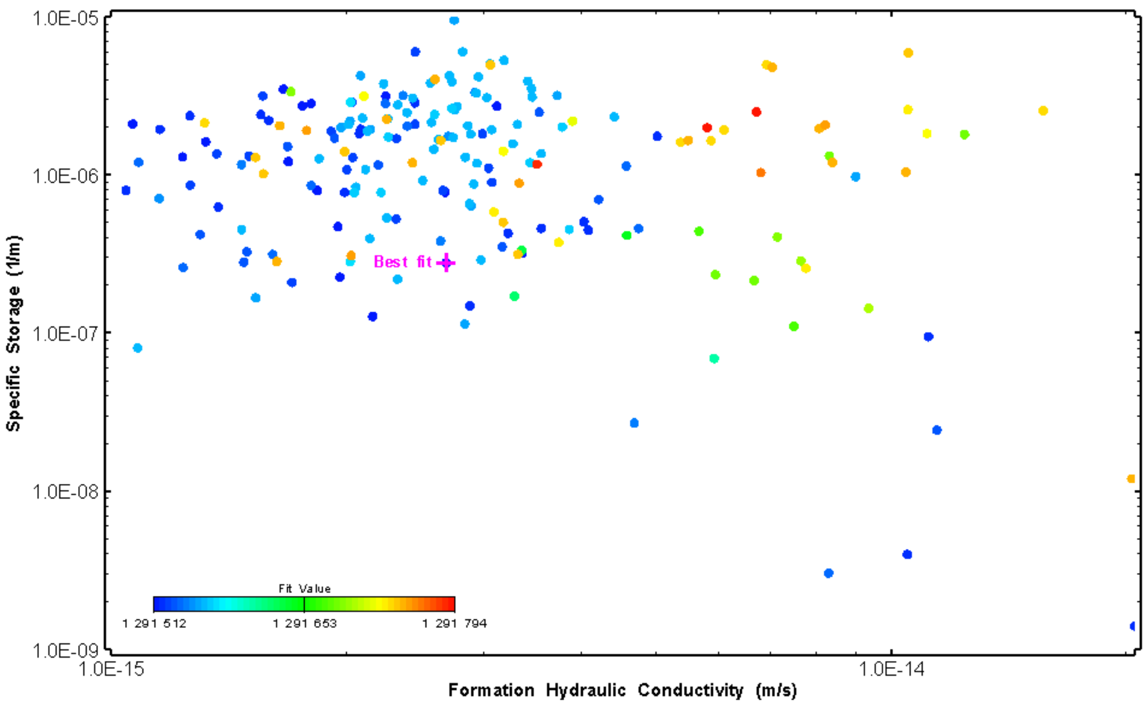

Figure 357: LT003 XY-scatter plot showing estimates of formation hydraulic conductivity and specific storage from perturbation analysis

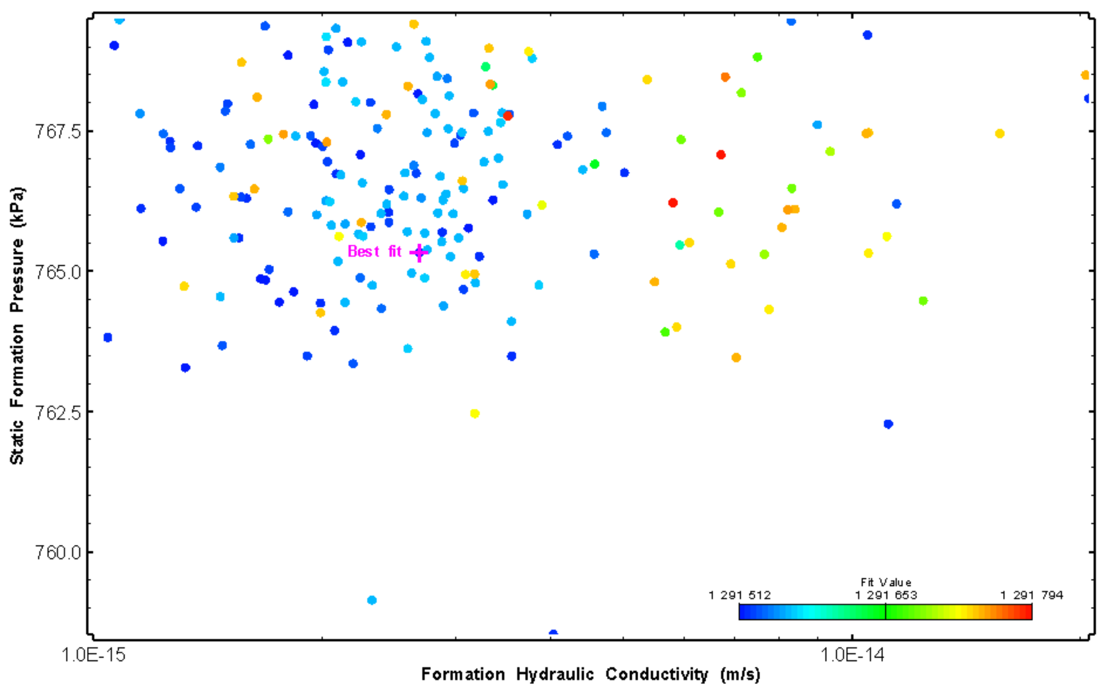

Figure 358: LT003 XY-scatter plot showing estimates of formation hydraulic conductivity and static formation pressure from perturbation analysis

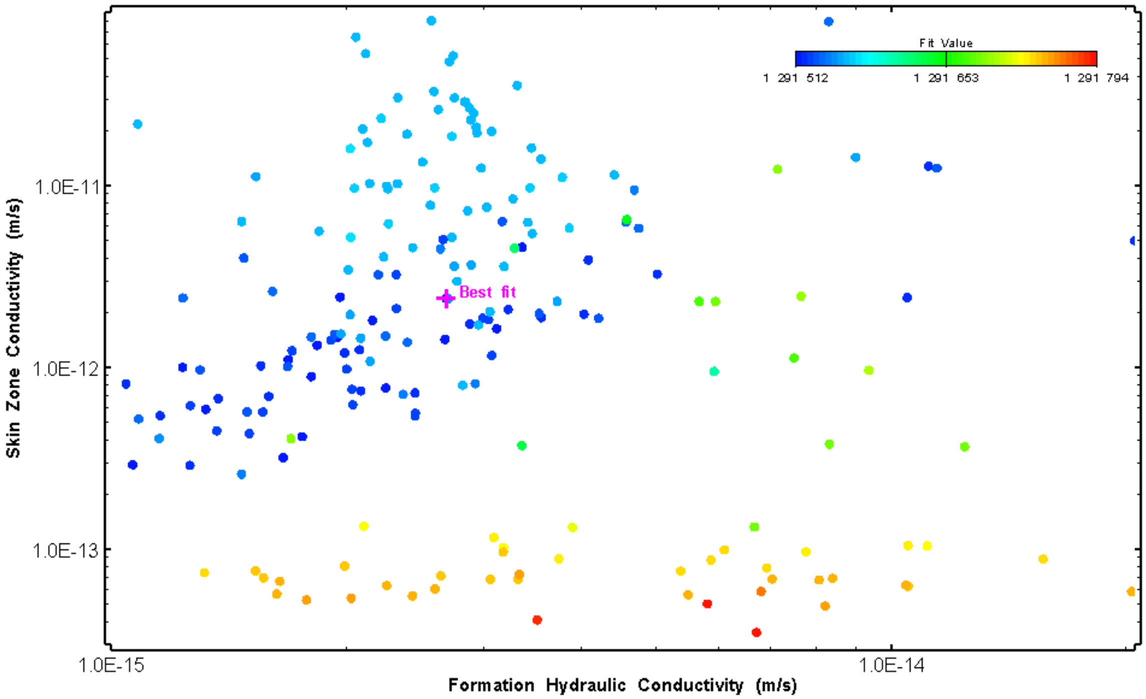

Figure 359: LT003 XY-scatter plot showing estimates of formation hydraulic conductivity and skin zone conductivity from perturbation analysis

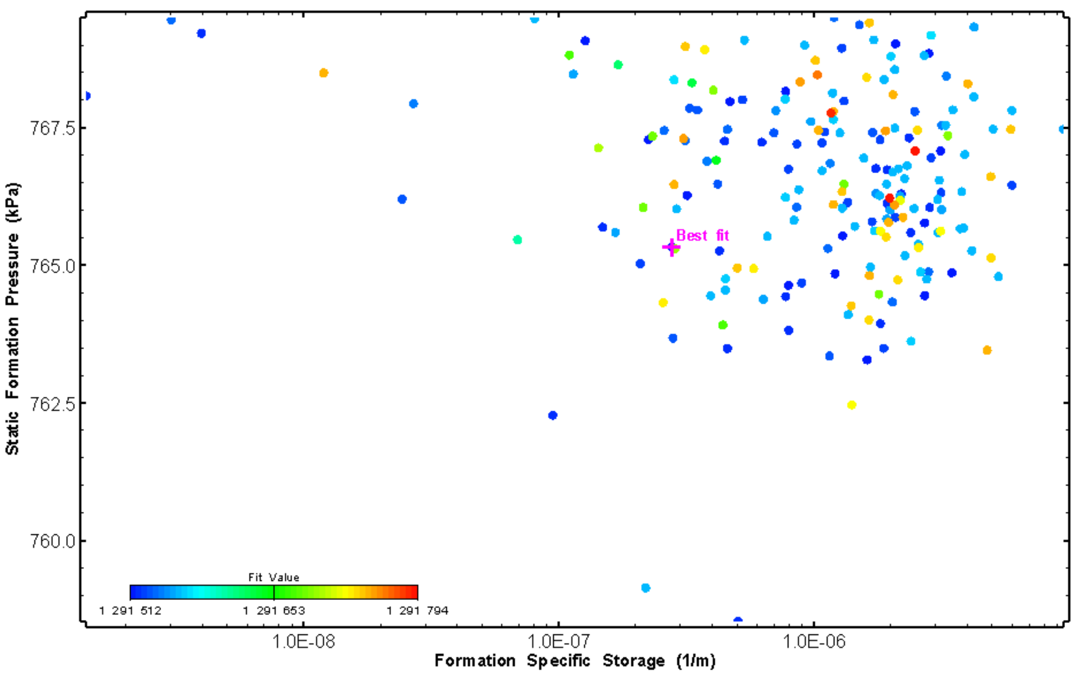

Figure 360: LT003 XY-scatter plot showing estimates of specific storage and static formation pressure from perturbation analysis

31.0 LT004 (74.60 – 94.63 M)

LT004 was completed to confirm that the tool performance met the project's requirement of accurately measuring test interval hydraulic conductivity down to 10^{-13} m/sec. LT004 was conducted within the well surface casing.

The test was initiated with a shut-in pressure recovery phase (PSR). A slug withdrawal test (SW) followed by a slug withdrawal shut-in (SWS) phase were completed after the PSR phase.

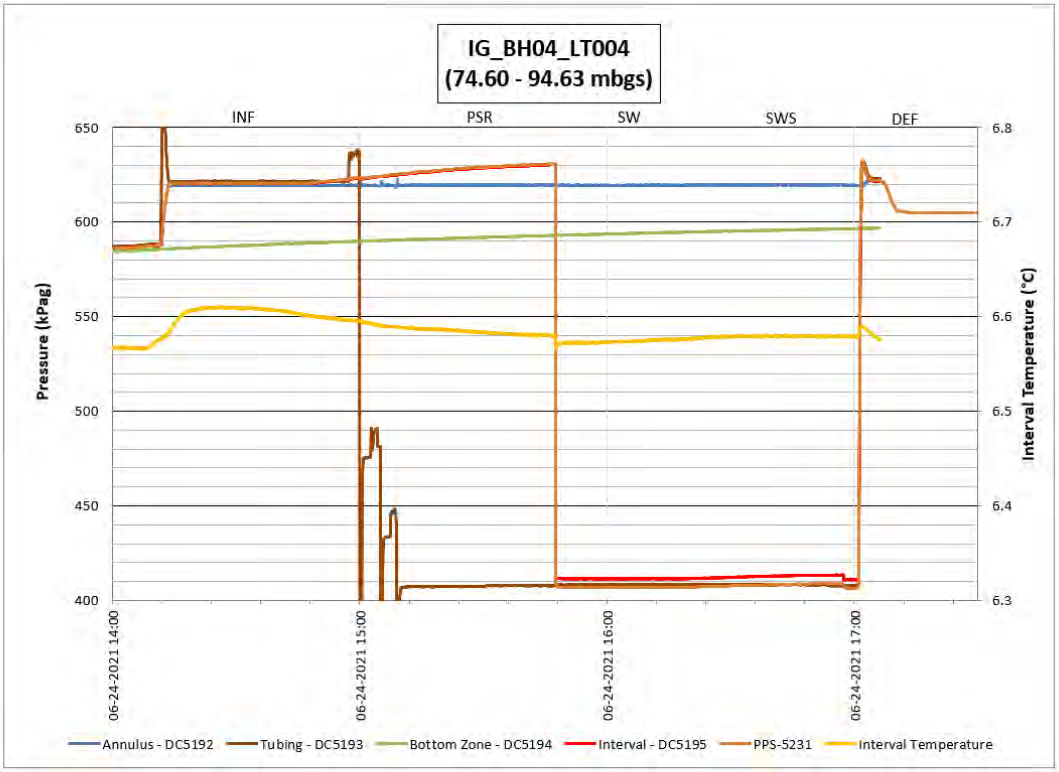

Figure 361: LT004 Annotated test plot showing monitored zone pressure and interval temperature.

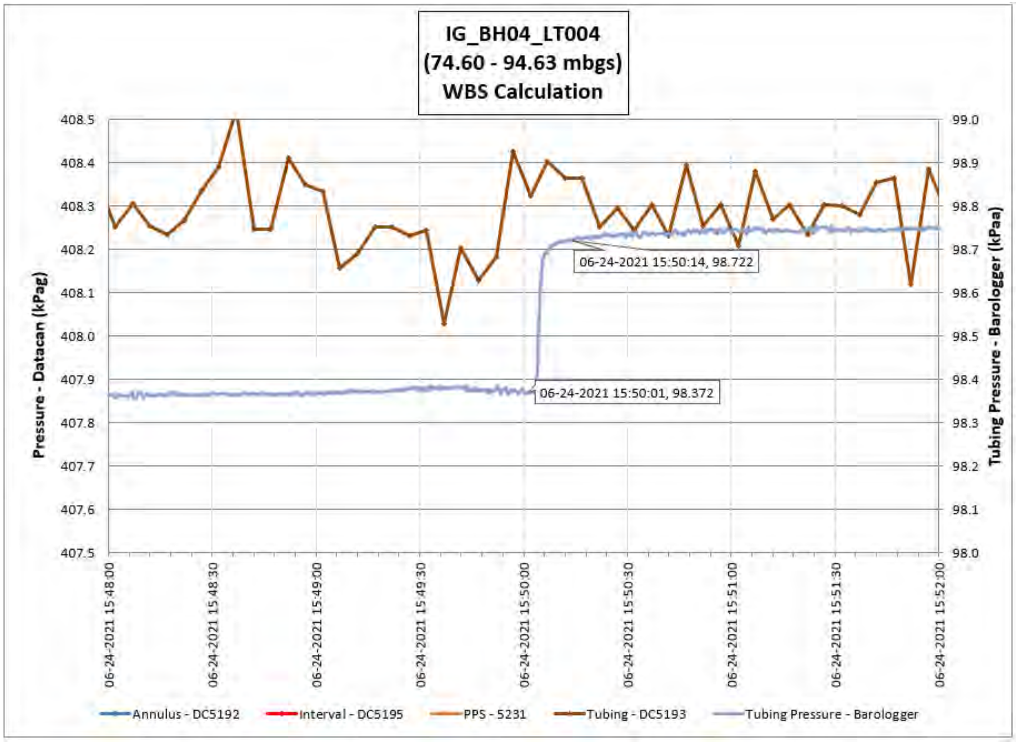

Figure 362: LT004 Tubing pressure during DHSIV activation. DHSIV Closed Wellbore Storage Estimate = 3E-10 m3/Pa

Table 5: Summary of Analysis Results – LT004

	Formation conductivity	Skin zone conductivity	Static formation pressure	Formation specific storage	Radial thickness of skin	Flow dimension
	[m/s]	[m/s]	[kPa]	[1/m]	[m]	[–]
Best Fit	2.6E-14	7.4E-13	619	1.1E-08	2.5E-01	2.0
Minimum	5.6E-15	2.3E-13	587	2.1E-09	2.5E-02	1.4
Maximum	2.7E-13	7.8E-11	649	2.3E-07	6.4E-01	2.5
Mean	3.6E-14	9.6E-12	631	3.6E-08	2.3E-01	2.0
Median	2.9E-14	1.9E-12	631	1.8E-08	2.2E-01	2.0
Geometric mean	2.8E-14	2.9E-12	631	2.0E-08	2.1E-01	2.0

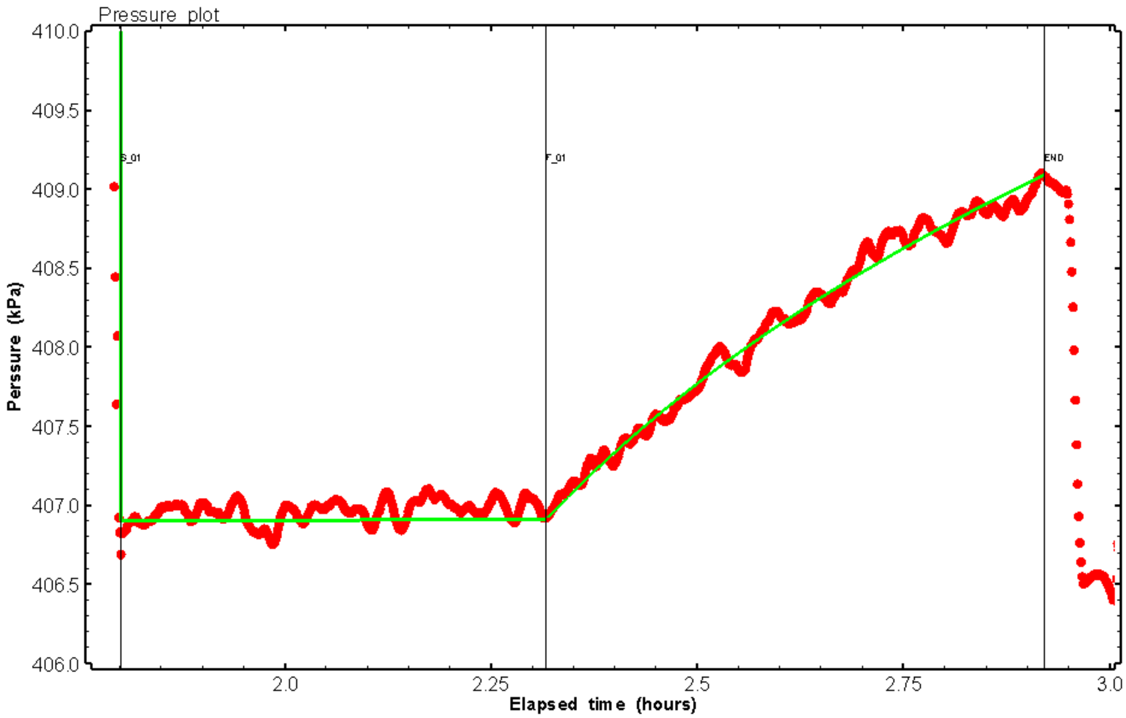

Figure 363: LT004 Pressure plot showing best-fit simulation and best fit results

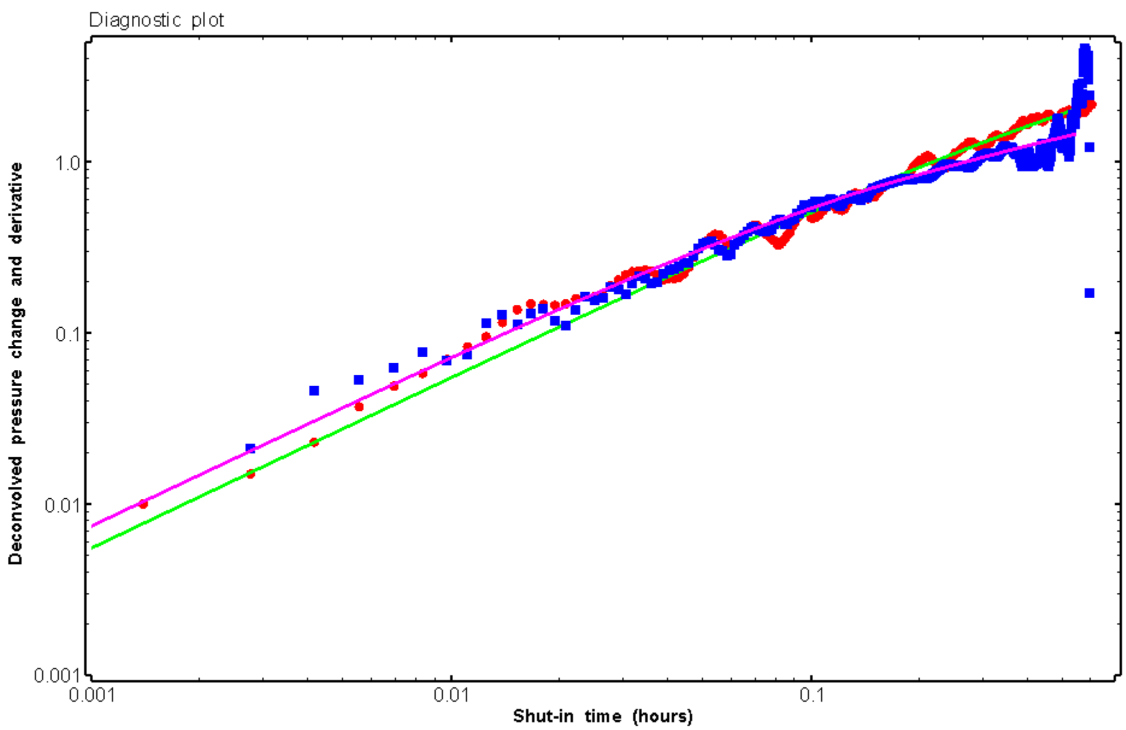

Figure 364: LT004 Deconvolved pressure change and derivative plot

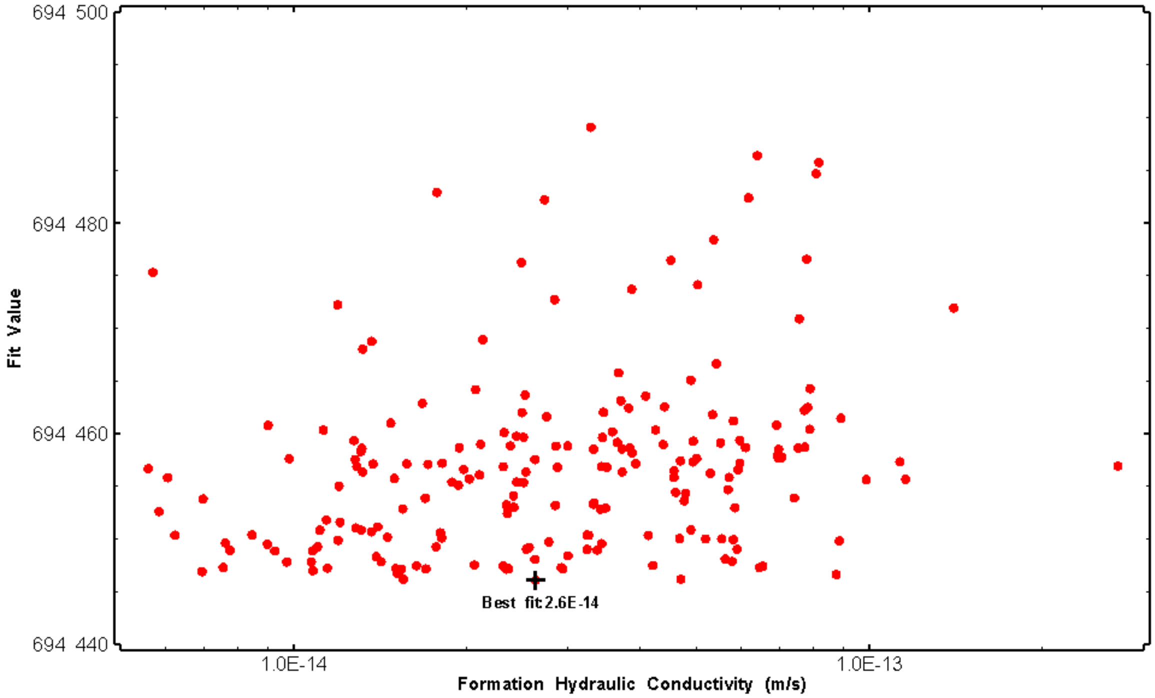

Figure 365: LT004 XY-scatter plot of formation hydraulic conductivity vs. fit value

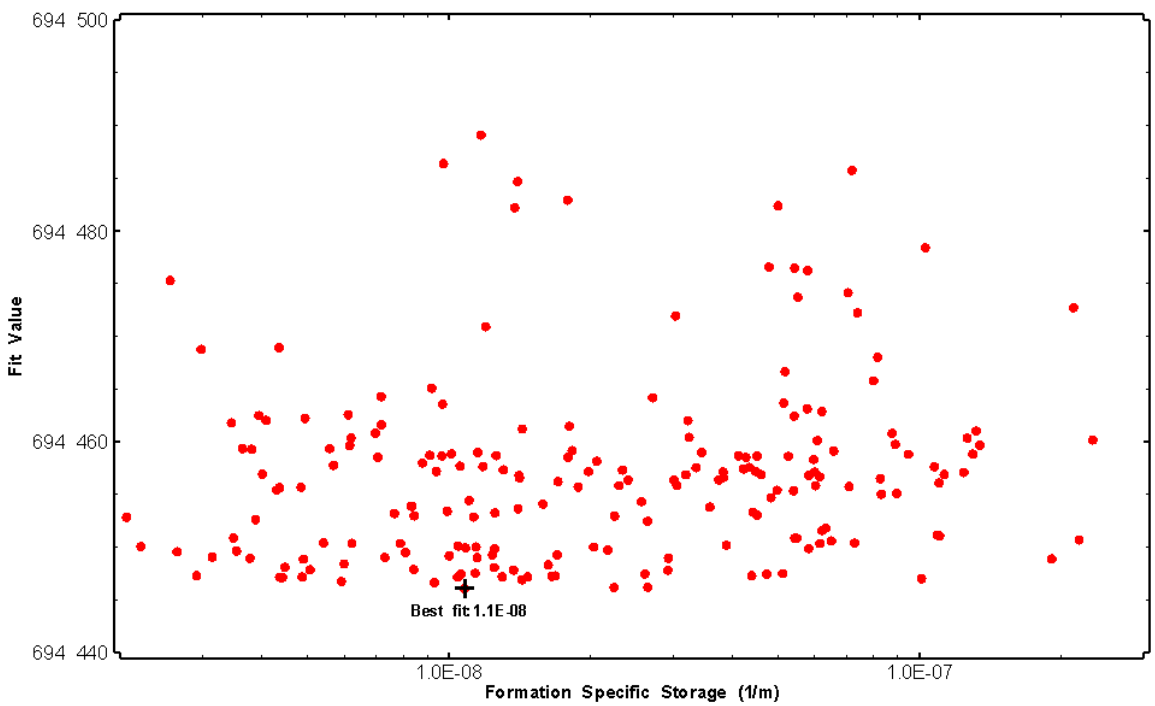

Figure 366: LT004 XY-scatter plot of formation specific storage vs. fit value

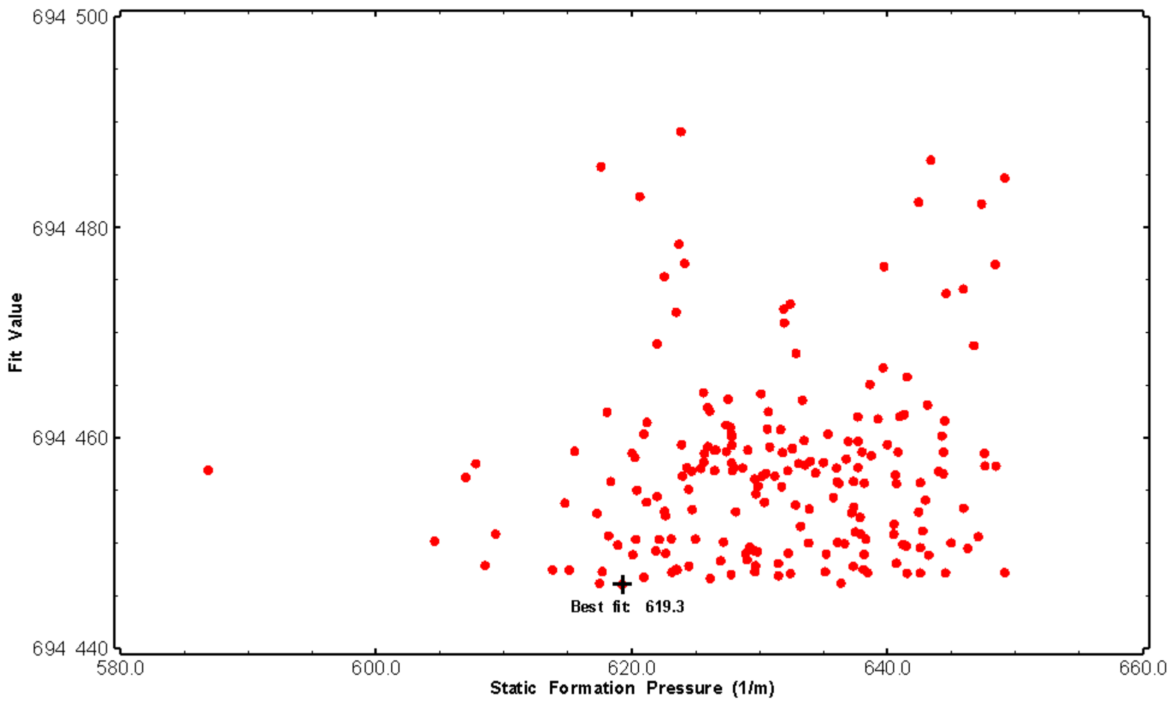

Figure 367: LT004 XY-scatter plot of static formation pressure vs. fit value

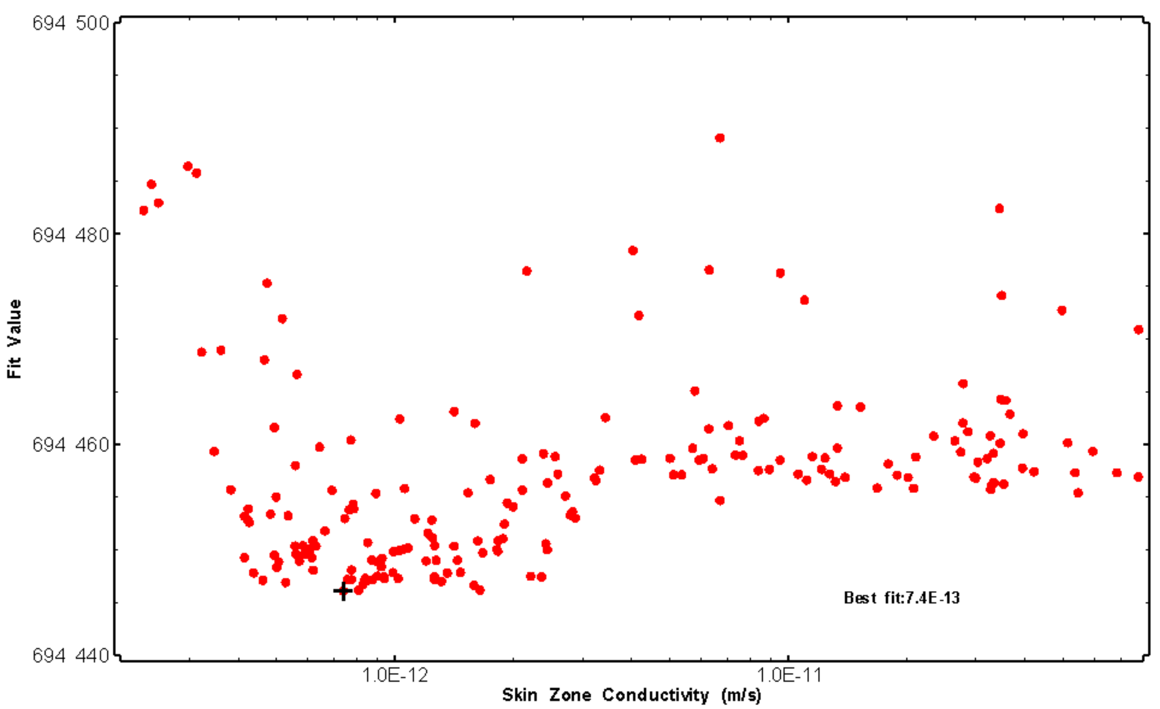

Figure 368: LT004 XY-scatter plot of skin zone conductivity vs. fit value

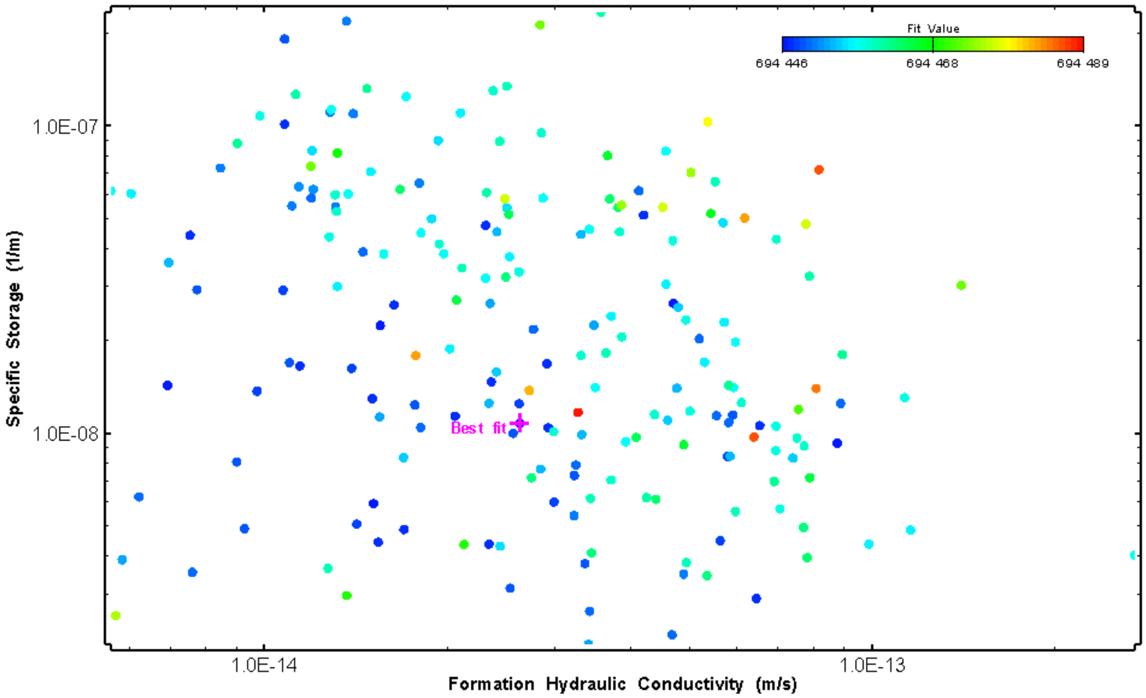

Figure 369: LT004 XY-scatter plot showing estimates of formation hydraulic conductivity and specific storage from perturbation analysis

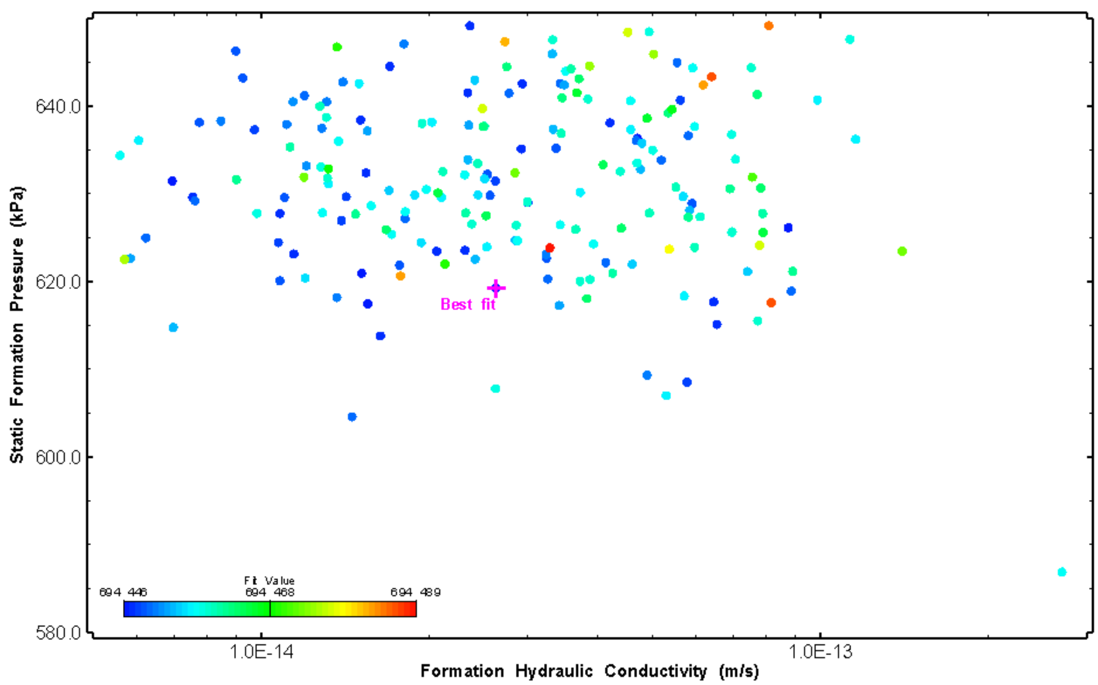

Figure 370: LT004 XY-scatter plot showing estimates of formation hydraulic conductivity and static formation pressure from perturbation analysis

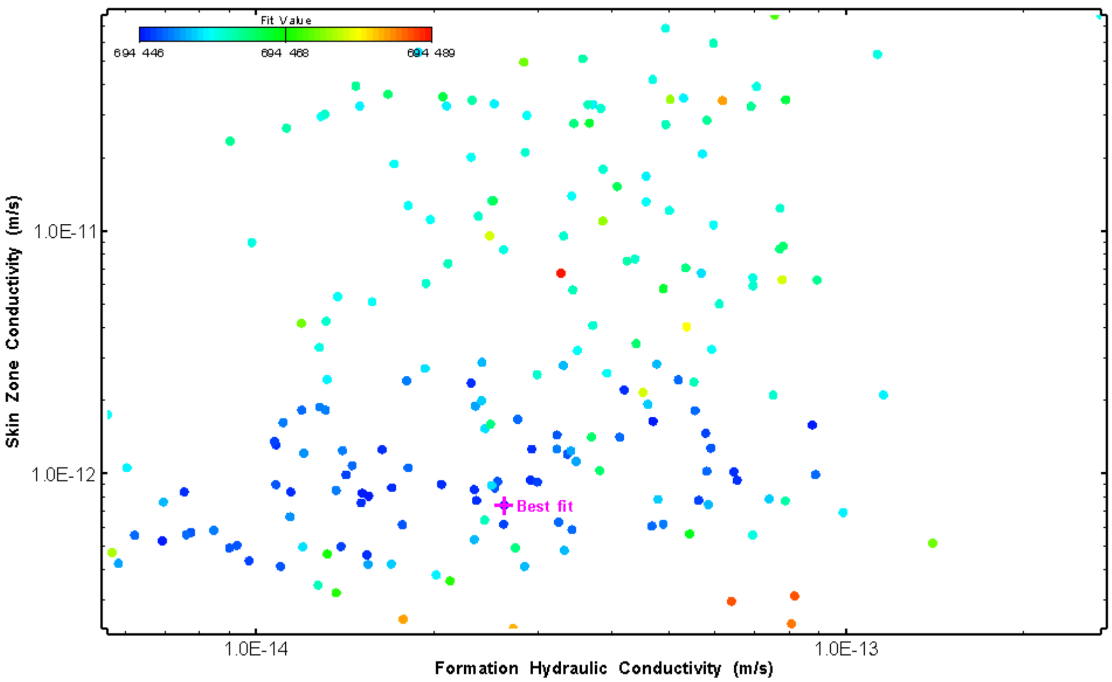

Figure 371: LT004 XY-scatter plot showing estimates of formation hydraulic conductivity and skin zone conductivity from perturbation analysis

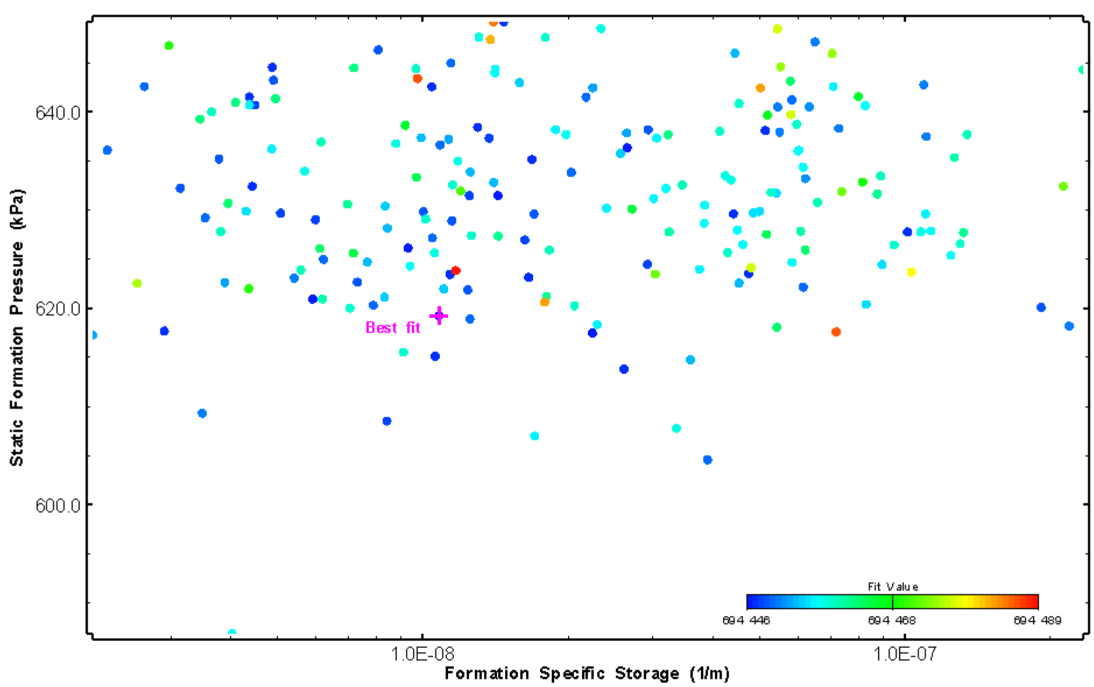

Figure 372: LT004 XY-scatter plot showing estimates of specific storage and static formation pressure from perturbation analysis

wsp.com